1.9.3.

NATIONAL AERONAUTICS AND SPACE ADMINISTRATION

Copy No.
MSC-A-R-66-5

POSTLAUNCH REPORT FOR MISSION AS-202

(Apollo Spacecraft 011)

MANNED SPACECRAFT CENTER
HOUSTON, TEXAS

October 12, 1966

APOLLO SPACECRAFT FLIGHT HISTORY

Mission	Spacecraft	Description	Launch date	Launch site
PA-1	BP-6	First pad abort	Nov. 7, 1963	White Sands Missile Range, N. Mex.
A-001	BP-12	Transonic abort	May 13, 1964	White Sands Missile Range, N. Mex.
AS-101	BP-13	Nominal launch and exit environment	May 28, 1964	Cape Kennedy, Fla.
AS-102	BP-15	Nominal launch and exit environment	Sept. 18, 1964	Cape Kennedy, Fla.
A-002	BP-23	Maximum dynamic pressure abort	Dec. 8, 1964	White Sands Missile Range, N. Mex.
AS-103	BP-16	Micrometeoroid experiment	Feb. 16, 1965	Cape Kennedy, Fla.
A-003	BP-22	Low-altitude abort (planned high-altitude abort)	May 19, 1965	White Sands Missile Range, N. Mex.
AS-104	BP-26	Micrometeoroid experiment and service module RCS launch environment	May 25, 1965	Cape Kennedy, Fla.
PA-2	BP-23A	Second pad abort	June 29, 1965	White Sands Missile Range, N. Mex.
AS-105	BP-9A	Micrometeoroid experiment and service module RCS launch environment	July 30, 1965	Cape Kennedy, Fla.
A-004	SC-002	Power-on tumbling boundary abort	Jan. 20, 1966	White Sands Missile Range, N. Mex.
AS-201	SC-009	Supercircular re-entry with high heat rate	Feb. 26, 1966	Cape Kennedy, Fla.
AS-202	SC-011	Supercircular re-entry with high heat load	Aug. 25, 1966	Cape Kennedy, Fla.

MSC-A-R-66-5

POSTLAUNCH REPORT FOR MISSION AS-202 (APOLLO SPACECRAFT 011)

Comment Sheet

In keeping with the President's policy on cost reduction and in order to update the distribution of this document, please detach, fill in, and return to MSC-PM4. If this document is no longer needed, please destroy or, if at MSC, return to PM4.

To: PM4
National Aeronautics and Space Administration
Manned Spacecraft Center
Houston, Texas 77058

Subject: Comments - AS-202 Distribution - Postlaunch Report for Mission AS-202 Apollo Spacecraft 011 - MSC-A-R-66-5.

1. This office has received_____copies of the AS-202 Postlaunch Report (MSC-A-R-66-5).

2. This office_____(does or does not) have need of this document and _____(does or does not) wish to receive future Postlaunch Reports on Apollo flights.

3. Distribution changes (please show present recipient and address according to current distribution list).

   a. Change quantity from_____copies to_____copies.

      Name_____
      (present recipient)

      Mailing Information_____

      _____

      _____

   b. Add_____copies for:

      Name_____
      (additional distribution)

      Complete mailing address_____

      _____

      _____

_____ _____
Signed Date

MSC-A-R-66-5

POSTLAUNCH REPORT FOR

APOLLO MISSION AS-202

(APOLLO SPACECRAFT 011)

Approved for Distribution:

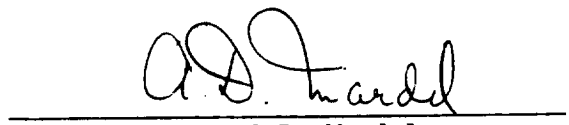

Alfred D. Mardel
Chief, Mission Support Division

NATIONAL AERONAUTICS AND SPACE ADMINISTRATION

MANNED SPACECRAFT CENTER

HOUSTON, TEXAS

October 12, 1966

NOTICE

Unless otherwise specified, zero time (T-0) for all data in this report is referenced to "Range zero" which is the first integral second of Range time prior to "lift-off." Lift-off is the instant of Saturn Instrument Unit umbilical disconnect.

NASA-S-66-10220

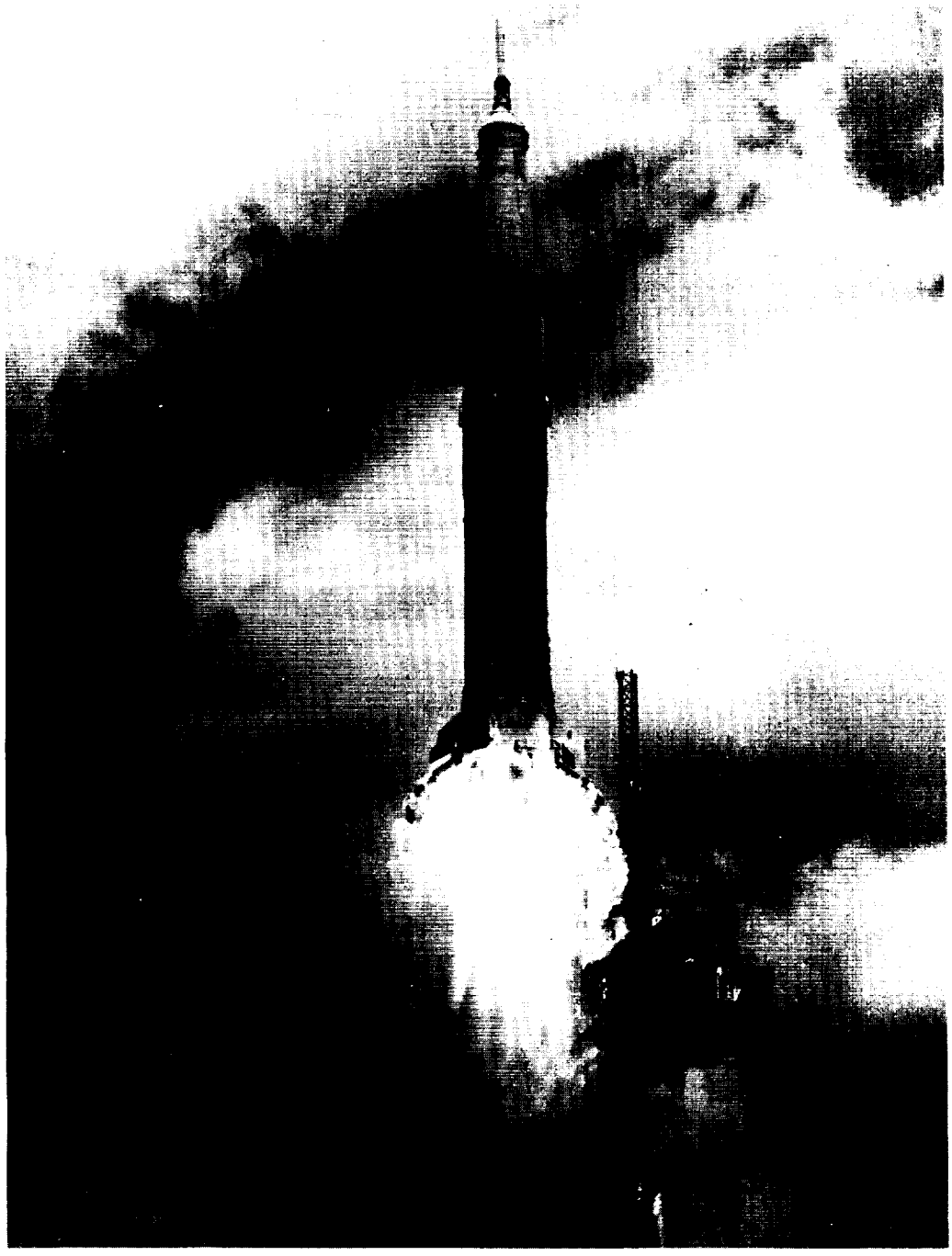

Lift-off, Mission AS-202.

CONTENTS

TABLES

FIGURES

ABBREVIATIONS AND SYMBOLS

Abbreviations

ACE	automatic checkout equipment
ACS	attitude control subsystem
AFETR	Air Force Eastern Test Range
AGAP	attitude gyro accelerometer package
AGC	Apollo guidance computer
AGCU	attitude gyro coupling unit
AOA	angle of attack
AOS	acquisition of signal
ARA	auxiliary recovery antenna
ASC	Ascension
AS/GPI	attitude set and gimbal position indicator
AUX ECA	auxiliary electronic control assembly
BDA	Bermuda
BECO	booster engine cutoff
BEPP	best estimate propulsion parameters
BER	bit error rate
BMAG	body-mounted attitude gyro
BPC	boost protective cover
CDU	coupling data unit
CDU	coupling display unit
CFE	contractor furnished equipment

c.g.	center of gravity
CM	command module
CSM	command and service modules
CSQ	Coastal Sentry Quebec
CRO	Carnarvon
CTE	central timing equipment
CYI	Grand Canary Island
DAC	digital to analog converter
D & C	displays and controls
DDP	digital data processing
DOD	Department of Defense
DPDM	differentiated pulse duration modulation
DSE	data storage equipment
DSKY	display and keyboard
ECA	electronic control assembly
ECS	environmental control subsystem
EDS	emergency detection subsystem
ELS	earth landing subsystem
ELSC	earth landing sequence controller
EPS	electrical power subsystem
FCSM	flight combustion stability monitor
FDAI	flight director attitude indicator
FDS	fluid distribution system

FIDO	flight dynamics officer
FQ	flight qualification
FQTR	flight qualification tape recorder
GCS	guidance and control subsystem
GFE	government furnished equipment
G & N	guidance and navigation
GOSS	ground operational support specification
GSE	ground support equipment
GSFC	Goddard Space Flight Center
IF	intermediate frequency
IMU	inertial measuring unit
IECO	inboard engine cutoff
IP	impact point
IRIG	inertial rate integrating gyros
ISS	input subsystem
IU	instrument unit
KSC	Kennedy Space Center
LARC	lighter, amphibious, resupply, carrier
LCU	landing craft, utility
L/D	lift-to-drag ratio
LES	launch-escape subsystem
LET	launch-escape tower
LL	low level
LM	lunar module

LORAN	long rate navigation
LOS	loss of signal
LOX	liquid oxygen
LVTR	landing vehicle, tracked, reconnaisance
MCC-H	Mission Control Center, Houston
MCC-K	Mission Control Center, Cape Kennedy
MCP	mission control programmer
MDC	main display console
MERU	milli-earth rate unit (0.015 deg/hr)
MESC	master events sequence controller
MILA	Merritt Island launch area
MSFC	Marshall Space Flight Center
MFSN	Manned Space Flight Network
OCDU	optics coupling display unit
OCP	operational checkout procedures
OECO	outboard engine cutoff
PA	power amplifier
PAM	parts and material
PCM	pulse code modulation
PCVB	pyro continuity verification box
PDM	pulse duration modulation
PIPA	pulse integrating pendulous accelerometer
PM	pulse modulation
PMP	premodulation processor
PRN	pseudo-random noise

PSA	power and servo assembly
PSK	phase shift keying
PUGS	propellant utilization and gaging system
RCS	reaction control subsystem
RCSC	reaction control subsystem controller
RF	radio frequency
RGP	rate gyro package position indicator
RKV	Rose Knot Victor
rms	root mean square
RSDP	remote site data processor
RTC	real-time command
RTCC	real-time computer complex
SARAH	search, range, and homing beacon
SCE	signal conditioning equipment
SCS	stabilization and control subsystem
SECS	sequential events control subsystem
SEP	spacecraft electronic package
SFC	specific fuel consumption
SI	system integration
SLA	spacecraft lunar-module adapter
SM	service module
SMJC	service module jettison controller
SPE	service propulsion engine
SPL	sound pressure level

SPS	service propulsion subsystem
SRS	simulated remote site
TDP	tracking data processor
TM	telemetry
UDL	up-data link
USB	unified S-band
USBE	unified S-band equipment
VCO	voltage controlled oscillation
VSWR	voltage standing wave ratio
W/G	water/glycol
WSMR	White Sands Missile Range
WSTF	White Sands Test Facility

1.0 MISSION SUMMARY

Mission AS-202 was successfully accomplished using Apollo spacecraft 011 and an uprated Saturn I launch vehicle. The unmanned spacecraft was launched from launch complex 34, Cape Kennedy, Florida, on August 25, 1966, at 12:15 p.m. e.s.t.

Apollo spacecraft 011 was essentially a Block I type configuration, consisting of a spacecraft lunar-module adapter (SLA), a service module (SM), a command module (CM), and a launch-escape subsystem (LES). The major differences between spacecraft 011 and the Block I configuration were: the omission of couches, crew equipment, and cabin postlanding ventilation; and the addition of three auxiliary batteries, mission control programmer, four cameras, and flight qualification instrumentation.

The uprated Saturn I two stage launch vehicle, consisting of stages S-IB and S-IVB and an instrument unit, performed satisfactorily. First-stage ignition, lift-off, programmed roll and pitch, and cutoff were executed as planned. Separation and second-stage ignition were as planned, followed by a nominal launch-escape tower and boost protective cover jettison at T+170.5 seconds.

Second-stage cutoff occurred at T+588.5 seconds, 13.8 seconds earlier than predicted. Command and service module (CSM)/SLA/S-IVB separation occurred successfully at T+598.7 seconds. The trajectory at separation was near nominal with only minor deviations.

The spacecraft structure performed as required during the launch phase and throughout the remainder of the mission, with no adverse structural vibrations or structural loadings occurring.

The unified S-band (USB) spacecraft - Manned Space Flight Network signal levels were lower than predicted, especially at the Merritt Island launch area site. As a result, USB did not provide continuous telemetry and voice data during the initial powered phase. Ground station problems also resulted in partial loss of data at Carnarvon.

Following separation, the guidance and navigation subsystem (G & N) oriented the spacecraft for the first service propulsion subsystem (SPS) burn, which was initiated at T+609.7 seconds. Upon attainment of the proper velocity increment, the first burn was terminated at 825.6 seconds. Following engine cutoff the spacecraft was reoriented with the CM apex toward the earth (local vertical) and maintained this attitude for approximately 2000 seconds. During this coast period, an apogee of 617 nautical miles was attained at T+2474 seconds.

Following the coast period, the spacecraft was reoriented for the second SPS burn, which was initiated at T+3956.1 seconds. Upon achievement of the proper trajectory conditions, the second burn was terminated by the G & N at T+4044.5 seconds. Two additional burns of 3-second duration, initiated at T+4054.5 seconds and T+4067.5 seconds, were accomplished as planned.

The environmental control subsystem (ECS), as installed in spacecraft 011, performed satisfactorily with the exception of the glycol evaporator. The evaporator did not function from T+840 to T+4080 seconds, thereby allowing the outlet temperature to exceed 75° F. No other spacecraft equipment was affected adversely by this condition.

The electrical power subsystem (EPS) performed satisfactorily throughout the mission, with the exception that the condenser exhaust temperature on the fuel cells approached maximum limits.

Orientation of the spacecraft for CM/SM separation was initiated at T+4188.2 seconds and separation occurred at T+4264.0 seconds. Although no physical separation indication was received by ground stations, separation did occur satisfactorily.

Following separation, the CM was oriented to the entry attitude. Entry was initiated with a space-fixed velocity of 28 512 ft/sec at T+4348.0 seconds. Spacecraft communications blackout began at T+4416.0 seconds and lasted until T+5008.0 seconds.

During entry, spacecraft attitude was controlled to provide a skip trajectory resulting in a double-peak heating-rate history. The CM was subjected to an initial maximum heating rate of 83 $Btu/ft^2/sec$ followed by cooling to 19 $Btu/ft^2/sec$, and a second peak of 43 $Btu/ft^2/sec$. The entry heat load was approximately 20 000 Btu/ft^2 as planned. The CM structure and heat shields performed adequately in the entry environment with no adverse effects.

Forward heat shield jettison, drogue parachute deployment, and main parachute deployment occurred as planned. The CM landed undamaged, upright in the stable I attitude at T+5582.2 seconds, 7.5 seconds later than the preflight prediction.

Upon landing, the main parachutes were disconnected, and the recovery aids deployed and operated satisfactorily.

The point of splashdown was 16°07'N latitude and 168°54'E longitude, approximately 200 miles uprange southwest of the recovery ship,

due to lower spacecraft lift-to-drag ratio and steeper reentry flight-path angle than predicted. The spacecraft was sighted at 2:24 p.m. e.s.t. by recovery aircraft. The spacecraft was aboard the recovery ship at 10:17 p.m. e.s.t. (10 hours 2 minutes after lift-off).

Postflight tests were conducted for the evaluation of subsystem performance and for the resolution of mission anomalies.

Spacecraft anomalies which occurred during the flight had no adverse effect upon the accomplishment of the mission. The Mission AS-202 spacecraft test objectives for the ECS, EPS fuel cell temperature control, and USB communications subsystem were not completely satisfied. All other spacecraft test objectives were successfully accomplished.

There were no experiments flown on Apollo Mission AS-202.

2.0 INTRODUCTION

Mission AS-202 (Apollo spacecraft 011) was the second flight test of a production Apollo Block I type spacecraft utilizing the uprated Saturn I launch vehicle. This was an unmanned suborbital flight. Lift-off from launch complex 34, Cape Kennedy, Florida, occurred at 12:15 p.m. e.s.t. (17:15 G.m.t.) August 25, 1966. The spacecraft command module (CM) landed safely in the primary landing area in the southwest Pacific near Wake Island, approximately 1 hour 33 minutes later (18:48 G.m.t.), and was recovered as planned.

The major spacecraft mission objectives were to demonstrate the structural integrity and compatibility of the spacecraft/uprated Saturn I configuration, to verify subsystem operation, and to evaluate the spacecraft heat shield performance during a high heat load reentry. The complete test objectives and the degree of accomplishment are presented in section 3.0 of this report. The times of major mission events are given in table 2.0-I, and the mission profile is presented in figure 2.0-1.

This report includes an evaluation of the mission, a summary of the launch vehicle performance, and an analysis of the spacecraft performance on the basis of flight test data and results of completed postflight tests. Results of analyses and postflight testing not available for this report will be contained in a supplement.

Prior to Mission AS-202, two other production-type spacecraft and 10 boilerplate-type spacecraft had been flight tested (see inside front cover); all were unmanned. The results of the missions, which included functioning spacecraft subsystems, have been presented in mission or postlaunch reports (refs. 1 to 9).

Unless otherwise specified, zero time (T-0) for all data in this report is referenced to range zero, which is the first integral second before lift-off. (Lift-off is the instant of umbilical disconnect of the launch vehicle instrument unit.)

In this report, the mission phase between insertion and reentry is described as "suborbital flight" or the "suborbital flight phase" of the mission, since, with the combination of true orbital apogee and perigee neither planned nor achieved for this mission, the term "suborbital flight" applies rather than "orbital phase."

TABLE 2.0-I.- MISSION EVENTS

Event	Range time, sec		Difference, (actual minus nominal), sec
	Nominal	Actual	
Range zero 17:15:32 G.m.t.			
First motion	0.5	0.7	0.2
Lift-off	0.7	0.9	0.2
OECO	144.6	143.5	-1.1
S-IB/S-IVB separation	145.2	144.2	-1.0
S-IVB ignition	146.7	145.6	-1.1
LES jettison	170.7	170.5	-0.2
S-IVB cutoff	602.3	588.5	-13.8
RCS direct ullage on	610.8	597.0	-13.8
S-IVB/CSM separation	612.5	598.7	-13.8
+X translation on	613.3	600.0	-13.3
Start maneuver for first SPS burn	616.0	603.6	-12.4
SPS on (first burn)	623.3	609.7	-13.6
SPS off (first burn)	841.1	825.6	-15.5
Start maneuver to local vertical	848.9	837.1	-11.8
Apogee	2478.0	2474.0	-4.0
+X translation on	3941.6	3926.1	-15.5
SPS on (second burn)	3971.6	3956.1	-15.5
SPS off (second burn)	4061.2	4044.5	-16.7
SPS on (third burn)	4071.2	4054.5	-16.7
SPS off (third burn)	4074.2	4057.5	-16.7
SPS on (fourth burn)	4084.2	4067.5	-16.7
SPS off (fourth burn)	4087.2	4070.5	-16.7
Start maneuver to CM/SM separation attitude	4203.2	4188.2	-15.0
CM/SM separation	4273.4	4264.0	-9.4
Start maneuver to entry attitude	4280.8	4272.2	-8.6
Entry	4358.4	4348.0	-10.4
Begin blackout	4418.7	4416.0	-2.7
0.05g	4435.1	4426.9	-8.2
End blackout	5010.8	5008.0	-2.8
Forward heat shield jettison	5196.1	5218.3	22.2
Drogue parachute deployment	5197.1	5219.9	22.8
Main parachute deployment	5247.8	5268.2	20.4
Splashdown	5574.7	5582.2	7.5

NASA-S-66-9956

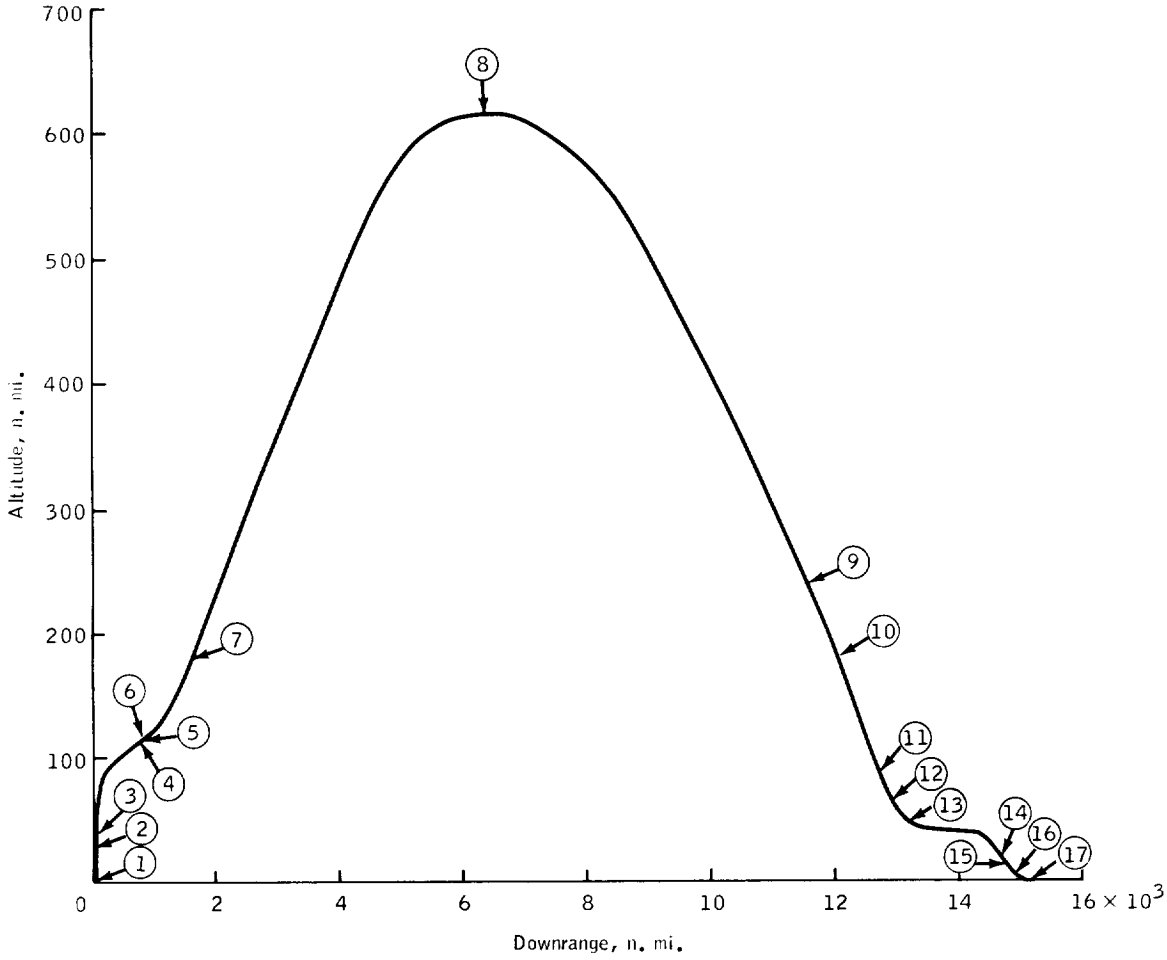

1. Lift-off (12:15:32 p.m. e.s.t.)
2. OECO
3. LES jettison
4. S-IVB cutoff
5. S-IVB/CSM separation
6. 1st SPS burn on
7. 1st SPS burn off
8. Apogee
9. 2nd SPS burn on
10. 4th SPS burn off
11. CM/SM separation
12. Entry
13. Begin blackout
14. End blackout
15. Drogue parachute deployment
16. Main parachute deployment
17. Splashdown

Figure 2.0-1.- Sequence of major events, Mission AS-202.

3.0 TEST OBJECTIVES*

The spacecraft objectives for Mission AS-202 are listed below. The degree of accomplishment for each objective is indicated in the listing of the detailed test objectives.

General test objectives.-

Primary test objectives:

(a) Demonstrate structural integrity and compatibility of the launch vehicle and spacecraft and confirm launch loads.

(b) Demonstrate separation of the S-IVB/IU from the S-IB, the LES and boost protective cover from the CSM/SLA/LV (nominal mode), the CSM from the S-IVB/IU/SLA, and the CM from the SM.

(c) Verify operation of the following subsystems:

(1) Launch vehicle: propulsion, guidance and control, and electrical subsystems.

(2) Spacecraft: CM heat shield (adequacy for entry from low earth orbit), service propulsion subsystem (SPS) (including multiple restart), guidance and navigation (G & N), environmental control subsystem (ECS) (pressure and temperature control), communications (partial), CM reaction control subsystem (RCS), SM RCS, stabilization and control subsystem (SCS), earth landing subsystem (ELS), and electrical power subsystem (EPS).

(d) Evaluate the space vehicle emergency detection subsystem (EDS) in closed-loop configuration.

(e) Evaluate the heat shield at high heat load during entry at approximately 28 000 ft/sec.

(f) Demonstrate the mission support facilities required for launch, mission operations, and CM recovery.

Secondary test objective: The secondary test objective for AS-202 is to determine subsystem performance other than the minimum required to demonstrate manned orbital capability.

---

*See update of Mission Requirements for AS-202, Memo No. PM2-M158 dated August 22, 1966.

Detailed test objectives.-

Primary test objectives:	Mission accomplishments:
(a) Demonstrate structural integrity and compatibility of the launch vehicle and spacecraft, and confirm launch loads, including:	
(1) Demonstrate compatibility and structural integrity of CSM-Saturn IB.[1]	Satisfactorily demonstrated; objective accomplished.
(2) Determine structural loading of the spacecraft adapter when subjected to the Saturn IB[1] launch environment.	Loading determined; objective accomplished.
(b) Demonstrate separation of the S-IVB/IU from the S-IB, the LES and BPC from the CSM/SLA/LV (nominal mode), the CSM from the S-IVB/IU/SLA, and the CM from the SM.	Satisfactorily demonstrated; objective accomplished.
(c) Verify operation of the following spacecraft subsystems: CM heat shield (adequacy for entry from low earth orbit), SPS (including multiple restart), G & N, ECS (pressure and temperature control), communications (partial), CM RCS, SM RCS, SCS, ELS, and EPS, including:	
(1) Determine CM adequacy for manned entry from low earth orbit.	Adequacy determined; objective accomplished.
(2) Demonstrate multiple SPS restart (at least 3 burns of at least 3-second duration at 10-second intervals).	Multiple restart demonstrated; objective accomplished.
(3) Determine performance of G & N subsystem, SCS, ECS (pressure and temperature control), EPS, CM RCS, SM RCS,	Satisfactory performance and adequacy for a manned orbital mission

[1]Saturn IB refers to the uprated Saturn I launch vehicle.

Primary test objectives:	Mission accomplishments:
communications (partial), and their adequacy for a manned orbital mission.	were determined for the G & N subsystem, SCS, CM RCS, SM RCS, communications, and for the EPS except for the high fuel cell condenser outlet temperatures. prior to Mission AS-202, the equipment and system associated with the problems encountered with the ECS and fuel cell temperature control were superseded by newer designs for Mission AS-202. Objective partially accomplished.
(4) Demonstrate operation of the parachute recovery subsystem and recovery aids following entry.	Satisfactorily demonstrated; objective accomplished.
(5) Evaluate G & N performance during boost and closed-loop entry.	Performance evaluated; objective accomplished.
(6) Verify S-band communications operations for turnaround ranging mode and downlink modes (PCM telemetry and simulated voice).	General unified S-band (USB) spacecraft - Manned Space Flight Network subsystem operation was verified. Detailed performance evaluation was only partially accomplished due to low signal strengths during initial powered flight phase and ground station operational problems at Carnarvon.
(7) Verify SPS standpipe fix (minimum of 198 seconds of SPS burn required).	Standpipe fix verified; objective accomplished.
(8) Verify astrosextant thermal protection subsystem.	Subsystem verified; objective accomplished.

Primary objectives:	Mission accomplishments:
(d) Evaluate the space vehicle EDS in closed-loop configuration.	Subsystem evaluated; objective accomplished.
(e) Evaluate the heat shield at high heat load during entry at approximately 28 000 ft/sec, including the thermal performance of the CM heat shield ablator during a high heat load (20 000 Btu/sq ft) entry.	Heat shield performance during 20 000 Btu/sq ft entry evaluated; objective accomplished.
(f) Demonstrate the mission support facilities required for launch, mission operations, and CM recovery.	Satisfactorily demonstrated; objective accomplished.
Secondary test objective:	Mission accomplishments:
The detailed secondary test objective for Mission AS-202 is to determine subsystem performance other than the minimum required to demonstrate manned orbital capability including:	
(a) Determine long duration (approximately 200 seconds) SPS performance, including shutdown characteristics.	Performance and shutdown characteristics determined satisfactorily; objective accomplished.
(b) Obtain data on SPS engine burn stability.	Satisfactory data obtained; objective accomplished.

4.0 SPACE VEHICLE DESCRIPTION

The AS-202 space vehicle consisted of an uprated Saturn I launch vehicle and an Apollo Block I type spacecraft. The launch configuration is indicated in figure 4.0-1.

NASA-S-66-9957

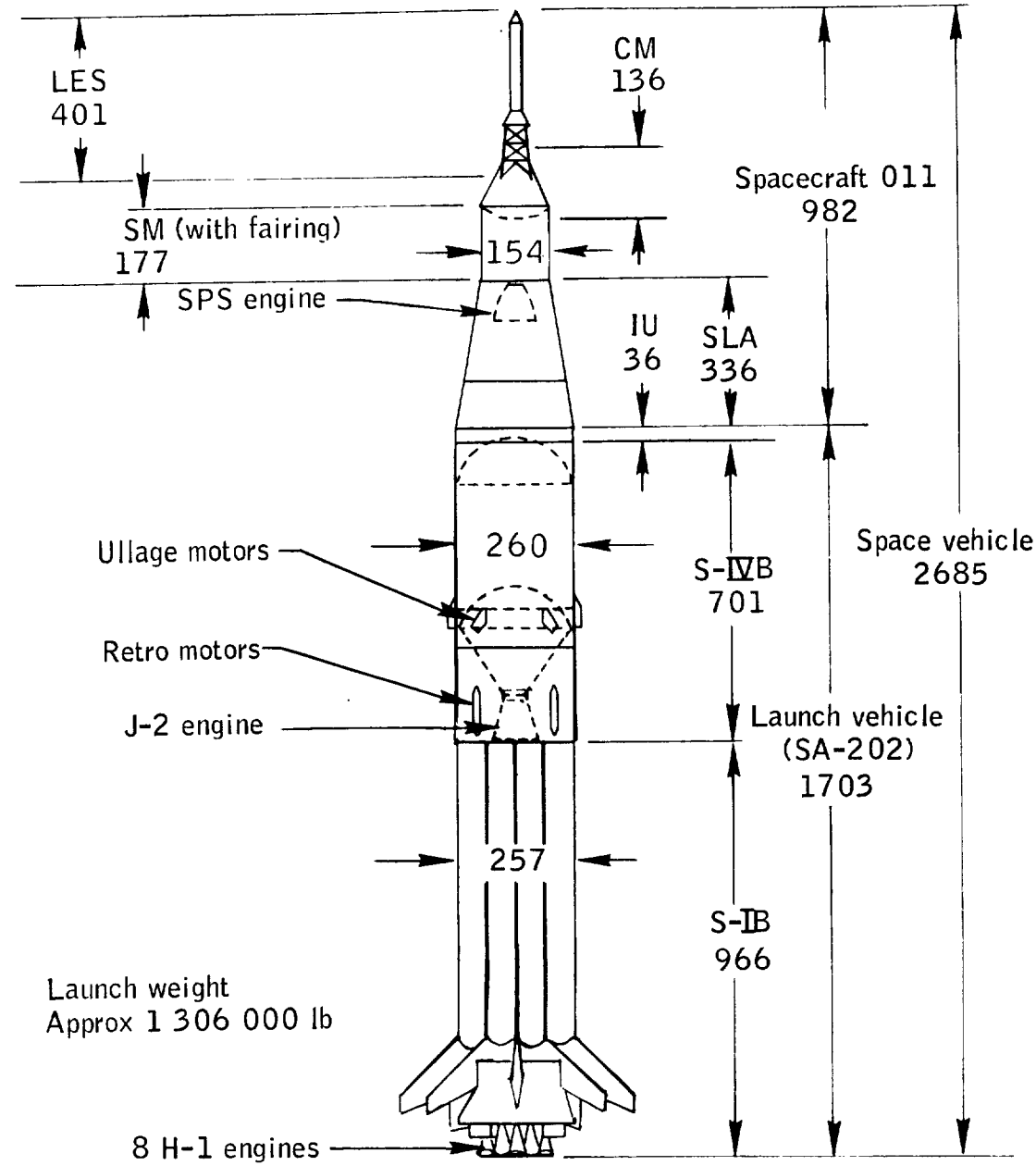

Notes: All dimensions are in inches
All dimensions are approximate
Drawing not to scale

Figure 4.0-1.- Space vehicle, Mission AS-202.

4.1 Spacecraft Description and Mass Properties

Spacecraft description.- Apollo spacecraft command and service module (CSM) 011 was a Block I unmanned configuration consisting of a launch escape subsystem (LES), command module (CM), service module (SM), and spacecraft lunar module adapter (SLA) as indicated in figure 4.1-1. Detailed spacecraft design requirements and configuration are set forth in references 10 and 11. A brief description of these modules is provided below.

Launch-escape subsystem: The LES provided abort capability to remove the CM from the space vehicle for any abort required from the launch pad through launch vehicle second-stage thrust stabilization. The LES was jettisoned and propelled from the space vehicle during the mission launch phase on command from the launch vehicle.

The LES consisted of solid propellant rocket motors, associated structural attachments, and release devices. It also contained a boost protective cover to protect the exterior CM surface from boost heating and a Q-ball to provide flight safety aerodynamic data to the space vehicle emergency detection subsystem (EDS).

Command module: The CM provided a habitable environment for a spacecraft crew in all mission phases and contained equipment for controlling the execution of all spacecraft functions and maneuvers. CSM 011 was unmanned and sequences were performed by an onboard mission control programmer (MCP).

The CM consisted of an inner pressurized compartment surrounded by a conical ablative heat shield. The pressurized compartment contained life support and cooling equipment; guidance, navigation, and stabilization controls; electrical power, communications, and instrumentation equipment; and displays and controls for all spacecraft subsystems. The area between the heat shield and pressure compartment contained a thruster system for entry attitude control and a parachute subsystem for controlling CM descent velocity.

Service module: The SM provided a reservoir of energy for spacecraft propulsive maneuvers and electrical power prior to entry. It contained a rocket propulsion subsystem for major delta V maneuvers, a thruster subsystem for spacecraft attitude control, an electrical power generation subsystem (fuel cells and reactants), and radiators for spacecraft equipment heat rejection. The SM was separated from the CM prior to the mission entry phase.

Spacecraft lunar module adapter: The SLA provided a structural transition between the CSM and launch vehicle, and would support the lunar module (LM) during the mission launch phase. Mission AS-202 did not include an LM, and bracing was used in its place to maintain SLA structural rigidity.

The SLA was a truncated conical shell composed of four panels hinged at the base. At CSM/SLA separation, these panels were separated by explosive charges and forced outward.

CSM 011 configuration differences: The differences between the CSM 011 and the Block I manned spacecraft were due primarily to the CSM 011 being unmanned. The significant differences were:

(a) Omission of couches and crew equipment/instrumentation.

(b) Omission of certain waste management items.

(c) Omission of postlanding ventilation valves.

(d) Addition of three auxiliary batteries.

(e) Addition of mission control programmer.

(f) Addition of four CM motion picture cameras and an SLA television camera.

(g) Addition of flight qualification instrumentation.

CSM 011 first flight-test items: The following subsystems and major components were included on a flight test for the first time:

(a) Guidance and navigation subsystem

(b) Fuel cells and reactants subsystem

(c) Mission control programmer (different from AS-201)

(d) Service propulsion propellant gaging subassembly

(e) Modified service propulsion propellant-tank standpipes

(f) Dual mode LES separation subsystem (frangible nut)

(g) Augmented forward heat shield separation subsystem (drag parachute)

(h) Astrosextant passive thermal protection subsystem

(i) S-band communications equipment

(j) Gas chromatograph and carbon-dioxide sensor

(k) Closed-loop emergency detection subsystem

(l) Flight director attitude indicator (FDAI)

(m) Electrical power subsystem (EPS) and environmental control subsystem (ECS) radiators

Mass properties.- Mass properties for spacecraft 011 for Mission AS-202 are summarized in table 4.1-I. Weights and centers of gravity for each module were measured prior to stacking. Changes accomplished prior to launch were monitored and measured data revised as required. The mass properties of the ring retained with the SM following separation from the adapter were calculated. The weight and centers of gravity of the complete adapter were measured.

Spacecraft mass properties at launch shown in table 4.1-I did not vary significantly from the predicted values used for trajectory calculations. Command module weight was increased as a result of a camera system installation, astrosextant door modifications, forward heat shield drogue parachute installation, and other minor changes. Propellant requirements were reduced consistent with the decision to load the sump tanks only. Additional minor changes in SM and tanked propellant weights resulted from detailed definition of weights and locations of trapped and residual propellant. Some fuel was inadvertently loaded in the storage tank, of which approximately 22 pounds could not be removed prior to launch. Other expendable loadings did not vary from the predicted values; however, the CM ECS potable water tank was drained during the countdown procedure. As a result, the actual amount of water in the tank at launch and during the flight was less than predicted.

Postrecovery weight and balance tests were performed to verify the accuracy of the CM center-of-gravity locations as a process of investigation of factors that could have contributed to a low lift-to-drag ratio. The weight and center-of-gravity locations of the CM were measured at the contractor's Downey facility.

Spacecraft body axes are indicated in figure 4.1-2 (also see ref. 12).

4.2 Launch Vehicle Description

The uprated Saturn I launch vehicle consisted of an S-IB stage, S-IVB stage, and instrument unit.

S-IB stage: The S-IB stage consisted of a tail section, a propellant container section, and a spider beam assembly.

The tail section supported the vehicle on the launch pedestal and contained eight H-1 engines uprated to 200 000 pounds of thrust. It consisted of a thrust structure, eight fins, a shroud, actuation controls, and the eight H-1 engines. Eight fins were spaced 45 degrees apart around the circumference of the shroud. The four inboard engines were installed in the pitch and yaw planes of the vehicle and were canted 3 degrees radially outboard. The four outboard engines are installed in planes 45 degrees from the pitch and yaw axis of the vehicle and are canted 6 degrees radially outboard and gimbal ± 8 degrees to provide thrust vector control for trajectory guidance.

The propellant container section consisted of nine propellant tanks. Eight of these were 70 inches in diameter and were mounted in a circular pattern around a 105-inch-diameter liquid oxygen (LOX) tank. Four of the eight 70-inch tanks contained LOX and the others contained fuel (RP-1) arranged alternately.

The spider beam assembly consisted of eight aluminum I beams radiating from a central hub and an outer ring to stabilize the radial beams. It provided forward attachment points for the propellant tanks, structural integrity for the forward portion of the S-IB stage, mounting for high-pressure nitrogen and helium storage spheres, and for a field splice to the S-IB/S-IVB interstage.

S-IVB stage: The S-IVB stage included an aft interstage, an aft skirt, a divided propellant container, and a forward skirt.

The aft interstage provided structural attachment between the S-IB and S-IVB, and provided mounting for the four solid propellant retro-motors.

The aft skirt structure was attached to the aft end of the propellant container and provided mounting hardware for the three solid propellant ullage motors to settle propellants for the J-2 engine start. It also included two attitude control modules, each of which contained three 150-pound thrust hypergolic rocket engines.

The propellant container was an internally insulated cylinder with hemispherical bulkheads at each end. An internal hemispherical bulkhead with the concave side facing aft divided the propellant container into an aft section for LOX storage and a forward section for liquid hydrogen storage.

The forward skirt was a cylindrical structure which was attached to the forward end of the propellant container and supported the instrument unit and the Apollo spacecraft payload.

A single J-2 rocket engine of 200 000-pound nominal vacuum thrust was mounted on the thrust structure on the centerline of the S-IVB stage. The engine could gimbal ± 7 degrees in a square pattern to provide thrust vector control.

Instrument unit: The instrument unit was a cylindrical structure which provided for systems hardware support and transmitted the flight loads between the Apollo spacecraft and the S-IVB stage. Systems contained within the instrument unit included command guidance and control, tracking, telemetry, power supply and distribution, and environmental control.

TABLE 4.1-I.- MASS PROPERTIES AT LAUNCH, MISSION AS-202

	Control weight, lb (a)	Final trajectory weight, lb (b)	Actual weight, lb	Center of gravity, in. (c)			Moments of inertia, slug-ft^2 (d)		
				X	Y	Z	I_{xx}	I_{yy}	I_{zz}
Command module	11 893	12 061	12 061	1 040.3	0.6	5.2	6 194	5 654	4 841
Service module[e]	9 770	9 823	9 845	913.6	0.3	0.0	6 311	10 591	10 177
SLA attachment ring	87	91	91	837.0	0.6	-1.8	113	58	56
Total, less propellant	21 750	21 975	21 997	982.8	0.4	2.8	12 650	35 613	34 352
Propellant tanked[f]	22 769	22 410	22 483	912.8	27.2	-11.6	7 388	11 349	12 438
Total with propellant	44 519	44 385	44 480	946.6	14.0	-4.5	22 411	60 495	61 564
Adapter, less ring	3 713	3 725	3 725	640.1	1.1	-2.6	9 296	12 793	12 546
Total injected	48 232	48 110	48 205	923.0	13.1	-4.3	31 834	143 249	144 240
Launch escape system	8 601	8 611	8 611	1 302.2	-0.5	2.1	662	24 730	24 708
Total launch	56 833	56 721	56 861	980.3	11.0	-3.4	32 849	395 241	396 434

[a] Used preflight for operational and references trajectory calculations.

[b] Revised data for preflight operational trajectory calculations.

[c] Centers of gravity are in the NASA reference system. The longitudinal reference has an origin 1000 inches below the tangency line of the command module substructure mold line.

[d] Moments of inertia are measured about the individual centers of gravity.

[e] Includes propellants trapped in the engine and lines external of the tanks.

[f] Includes trapped and residual propellants in the tanks.

NASA-S-66-9958

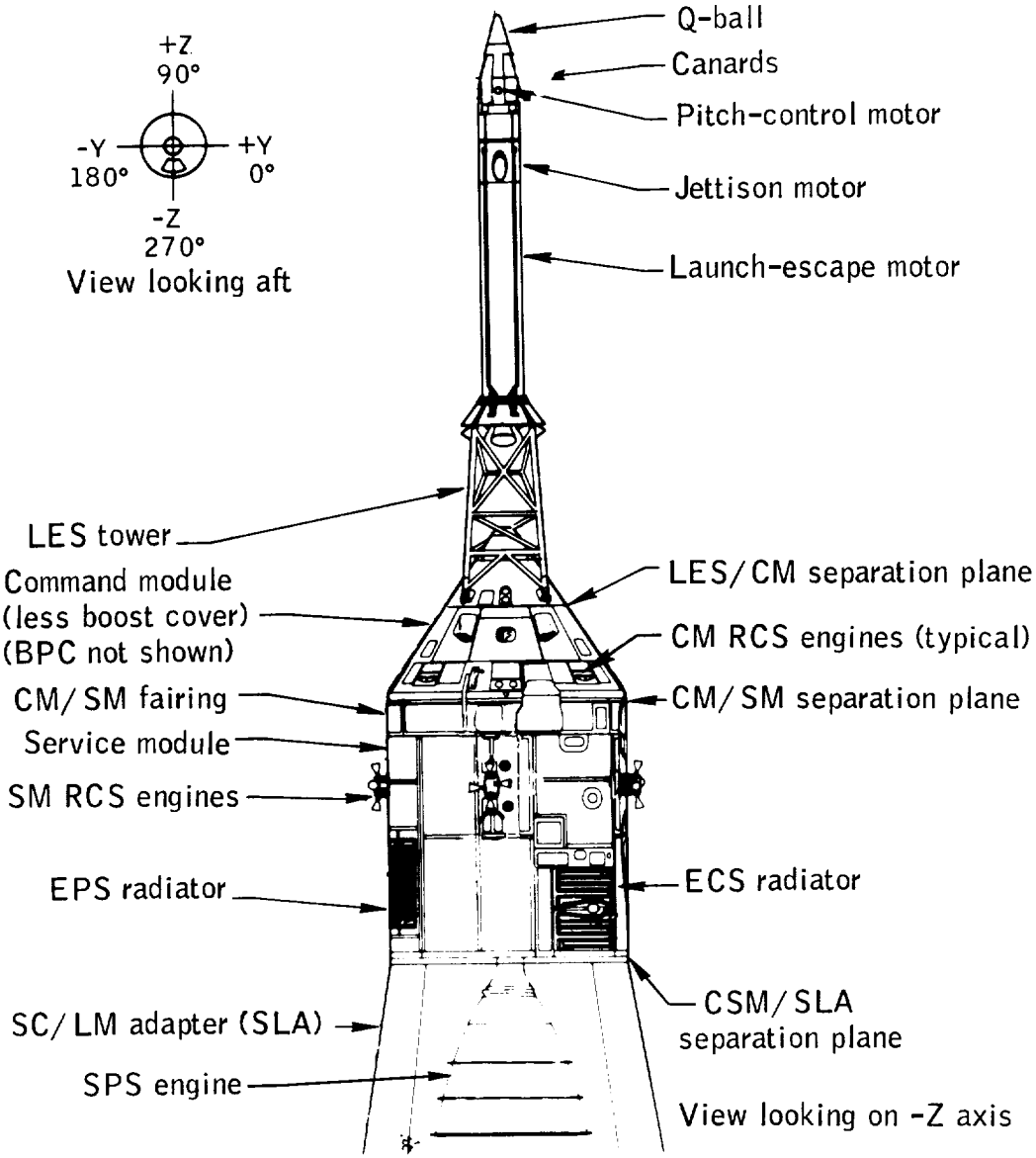

Figure 4.1-1.- Apollo spacecraft 011, Mission AS-202.

NASA-S-66-9959

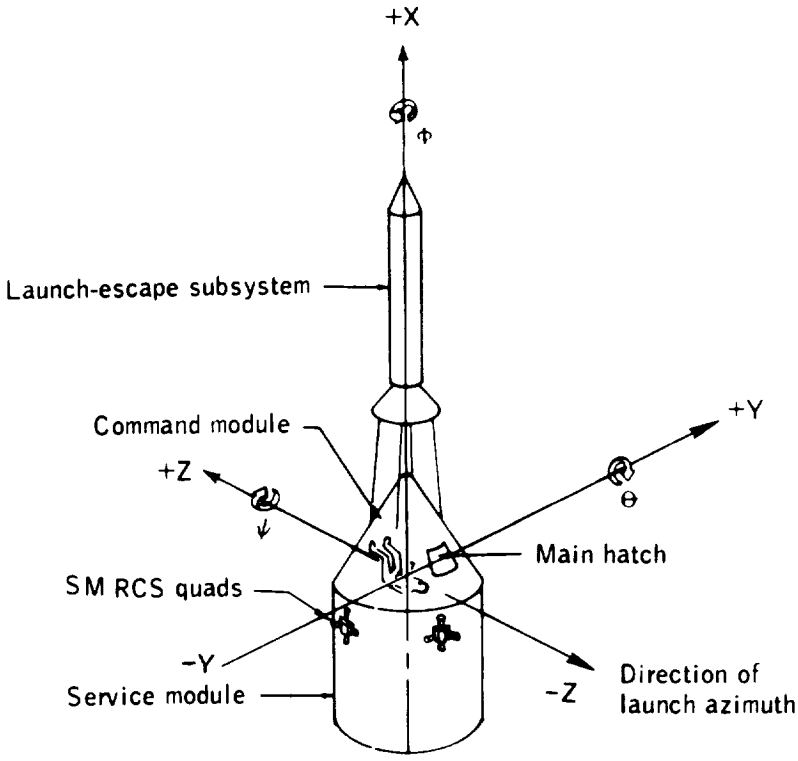

Direction	Axis	Moment	Positive direction	Spacecraft maneuver & symbol	Linear velocity	Angular velocity
Longitudinal	X	L	Y to Z	Roll Φ	u	p
Lateral	Y	M	Z to X	Pitch Θ	v	q
Vertical	Z	N	X to Y	Yaw Ψ	w	r

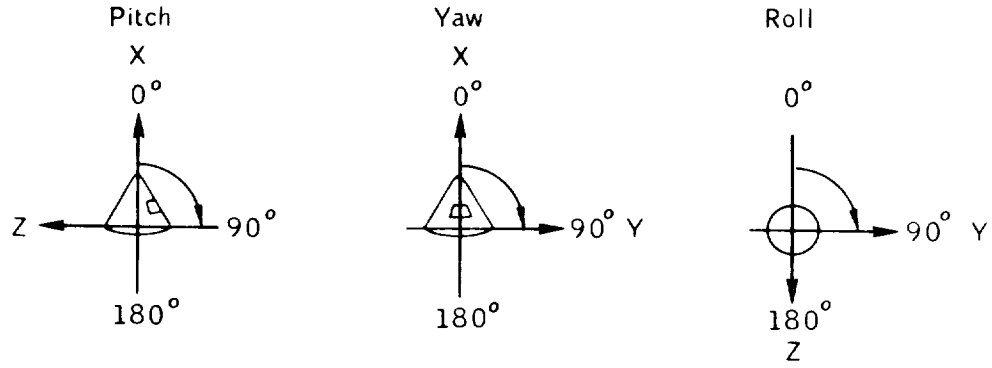

Figure 4.1-2.- Apollo spacecraft body axis system.

5.0 FLIGHT TRAJECTORY

5.1 Summary of the AS-202 Flight Trajectory Profile

The trajectory of AS-202 was essentially as planned with the exception of the entry phase. Targeted parameters were met by the launch vehicle and command and service module first and second service propulsion system burns (section 7.11). The event times were earlier than planned, as the spacecraft timing sequence was initiated by S-IVB separation command which occurred 13.8 seconds early due to higher than expected performance of the launch vehicle. This overperformance was caused by a fuel-oxidizer ratio shift in the S-IVB which occurred later than planned. Based on the aircraft long range navigation (LORAN) fix (section 9.3), the spacecraft landed 205 nautical miles uprange from the planned point. This is attributed to a lift-to-drag ratio of 0.28 (section 6.0), as compared with the planned ratio of 0.33 ± 0.04, and a slightly steeper than planned flight-path angle (γ_i) at entry interface ($\gamma_i = -3.53$ versus the planned value of -3.48).

Comparisons of actual data with planned data for significant events are presented in table 5.1-I. Figure 5.1-1 is a ground track of the AS-202 trajectory. Figures 5.1-2 through 5.1-5 present comparisons of time histories of selected parameters for the launch, midcourse, and entry phases of the flight.

TABLE 5.1-I.- COMPARISON OF PLANNED AND ACTUAL TRAJECTORY PARAMETERS,

Mission AS-202

Condition	Planned	Actual
S-IB outboard engine cutoff		
Time from range zero, sec	144.6	143.5
Time from range zero, min:sec	2:24.6	2:23.5
Geodetic latitude, deg:min North	28:23	28:24
Longitude, deg:min West	79:59	80:00
Altitude, ft	182 511	191 059
Altitude, n. mi.	30.0	31.4
Range, n. mi.	30.0	30.4
Space-fixed velocity, ft/sec	7 249	7 317
Space-fixed flight-path angle, deg	25.54	26.43
Space-fixed heading angle, deg East of North	102.14	101.83
LES jettison		
Time from range zero, sec	170.7	170.5
Time from range zero, min:sec	2:50.7	2:50.5
Geodetic latitude, deg:min North	28:17	28:17
Longitude, deg:min West	79:34	79:34
Altitude, ft	256 764	271 400
Altitude, n. mi.	42.3	44.7
Range, n. mi.	52.9	54.2
Space-fixed velocity, ft/sec	7 411	7 494
Space-fixed flight-path angle, deg	20:76	21.44
Space-fixed heading angle, deg East of North	102.54	102.30

TABLE 5.1-I.- COMPARISON OF PLANNED AND ACTUAL TRAJECTORY PARAMETERS, MISSION AS-202 - Continued

Condition	Planned	Actual
S-IVB cutoff		
Time from range zero, sec	602.3	588.5
Time from range zero, min:sec	10:02.3	9:48.5
Geodetic latitude, deg:min North	23:39	23:47
Longitude, deg:min West	65:31	65:53
Altitude, ft	712 966	712 708
Altitude, n. mi.	117.3	117.3
Range, n. mi.	861.4	840.7
Space-fixed velocity, ft/sec	22 308	22 310
Space-fixed flight-path angle, deg	4.00	3.99
Space-fixed heading angle, deg East of North	111.99	111.84
S-IVB/CSM separation		
Time from range zero, sec	612.5	598.7
Time from range zero, min:sec	10:12.5	9:58.7
Geodetic latitude, deg:min North	23:26	23:33
Longitude, deg:min West	64:58	65:19
Altitude, ft	728 412	728 094
Altitude, n. mi.	119.9	119.8
Range, n. mi.	895.6	874.8
Space-fixed velocity, ft/sec	22 305	22 310
Space-fixed flight-path angle, deg	3.83	3.82
Space-fixed heading angle, deg East of North	112.24	112.08

TABLE 5.1-I.- COMPARISON OF PLANNED AND ACTUAL TRAJECTORY PARAMETERS, MISSION AS-202 - Continued

Condition	Planned	Actual
First SPS ignition		
Time from range zero, sec	623.3	609.7
Time from range zero, min:sec	10:23:3	10:09.7
Geodetic latitude, deg:min North	23:11	23:19
Longitude, deg:min West	64:23	64:43
Altitude, ft	743 793	744 311
Altitude, n. mi.	122.4	122.5
Range, no. mi.	--	--
Space-fixed velocity, ft/sec	22 287	22 297
Space-fixed flight-path angle, deg	3.64	3.58
Space-fixed heading angle, deg East of North	112.48	112.35
First SPS cutoff (+0.8 sec for tailoff)		
Time from range zero, sec	841.9	826.4
Time from range zero, min:sec	14:01.9	13:46.4
Geodetic latitude, deg:min North	17:27	17:42
Longitude, deg:min West	52:05	52:32
Altitude, ft	1 113 685	1 110 106
Altitude, n. mi.	183.3	182.7
Range, n. mi.	--	--
Space-fixed velocity, ft/sec	25 492	25 501
Space-fixed flight-path angle, deg	5.68	5.71
Space-fixed heading angle, deg East of North	116.67	116.42

TABLE 5.1-1.- COMPARISON OF PLANNED AND ACTUAL TRAJECTORY PARAMETERS, MISSION AS-202 - Continued

Condition	Planned	Actual
Apogee		
Time from range zero, sec	2 478	2 474
Time from range zero, min:sec	41:18	41:14
Geodetic latitude, deg:min South	26:38	26:35
Longitude, deg:min East	26:21	26:28
Altitude, ft	3 727 322	3 749 571
Altitude, n. mi.	613.4	617.1
Range, n. mi.	--	--
Space-fixed velocity, ft/sec	22 681	22 664
Space-fixed flight-path angle, deg	0.00	0.00
Space-fixed heading angle, deg East of North	107.58	107.55
Second SPS ignition		
Time from range zero, sec	3 971.6	3 956.1
Time from range zero, hr:min:sec	1:06:11.6	1:05:56.1
Geodetic latitude, deg:min South	18:18	18:37
Longitude, deg:min East	112:50	112:12
Altitude, ft	1 478 215	1 500 586
Altitude, n. mi.	243.3	247.0
Range, n. mi.	--	--
Space-fixed velocity, ft/sec	25 092	25 071
Space-fixed flight-path angle, deg	-5.75	-5.84
Space-fixed heading angle, deg East of North	63.92	64.11

TABLE 5.1-I.- COMPARISON OF PLANNED AND ACTUAL TRAJECTORY PARAMETERS, MISSION AS-202 - Continued

Condition	Planned	Actual
Second SPS cutoff (+0.8 sec for tailoff)		
Time from range zero, sec	4 062.0	4 045.3
Time from range zero, hr:min:sec	1:07:12	1:07:25.3
Geodetic latitude, deg:min South	15:33	15:55
Longitude, deg:min East	118:06	117:28
Altitude, ft	1 212 819	1 226 211
Altitude, n. mi.	198.0	201.8
Range, n. mi.	--	--
Space-fixed velocity, ft/sec	27 482	27 443
Space-fixed flight-path angle, deg	-7.31	-7.35
Space-fixed heading angle, deg East of North	62.31	62.62
Third SPS ignition		
Time from range zero, sec	4 071.2	4 054.5
Time from range zero, hr:min:sec	1:07:51.2	1:07:34.5
Geodetic latitude, deg:min South	15:14	15:39
Longitude, deg:min East	118.40	117.57
Altitude, ft	1 171 000	1 198 083
Altitude, n. mi.	192.7	197.2
Range, n. mi.	--	--
Space-fixed velocity, ft/sec	27 520	27 477
Space-fixed flight-path angle, deg	-7.21	-7.27
Space-fixed heading angle, deg East of North	62.15	62.48

TABLE 5.1-I.- COMPARISON OF PLANNED AND ACTUAL TRAJECTORY PARAMETERS,

MISSION AS-202 - Continued

Condition	Planned	Actual
Third SPS cutoff (+0.8 sec for tailoff)		
Time from range zero, sec	4 075.0	4 058.3
Time from range zero, hr:min:sec	1:07:55.0	1:07:38.3
Geodetic latitude, deg:min South	15:07	15:31
Longitude, deg:min East	118.54	118.11
Altitude, ft	1 157 703	1 184 059
Altitude, n. mi.	190.5	194.9
Range, n. mi.	--	--
Space-fixed velocity, ft/sec	27 618	27 576
Space-fixed flight-path angle, deg	-7.22	-7.29
Space-fixed heading angle, deg East of North	62.09	62.41
Fourth SPS ignition		
Time from range zero, sec	4 084.2	4 067.5
Time from range zero, hr:min:sec	1:08:04.2	1:07:47.5
Geodetic latitude, deg:min South	14:47	15:11
Longitude, deg:min East	119.29	118:48
Altitude, ft	1 124 626	1 149 105
Altitude, n. mi.	185.1	189.1
Range, n. mi.	--	--
Space-fixed velocity, ft/sec	27 656	27 624
Space-fixed flight-path angle, deg	-7.12	-7.18
Space-fixed heading angle, deg East of North	61.93	62.24

TABLE 5.1-I.- COMPARISON OF PLANNED AND ACTUAL TRAJECTORY PARAMETERS,

MISSION AS-202 - Continued

Condition	Planned	Actual
Fourth SPS cutoff (+0.8 sec for tailoff)		
Time from range zero, sec	4 088.0	4 071.3
Time from range zero, hr:min:sec	1:08:08.0	1:07:81.3
Geodetic latitude, deg:min South	14:41	15:04
Longitude, deg:min East	119:41	119:03
Altitude, ft	1 112 903	1 135 166
Altitude, n. mi.	183.2	186.8
Range, n. mi.	--	--
Space-fixed velocity, ft/sec	27 755	27 719
Space-fixed flight-path angle, deg	-7.11	-7.19
Space-fixed heading angle, deg East of North	61.90	62.17
CM/SM separation		
Time from range zero, sec	4 273.4	4 264
Time from range zero, hr:min:sec	1:11:13.4	1:11:04
Geodetic latitude, deg:min South	7:52	8:08
Longitude, deg:min East	131:07	130:49
Altitude, ft	570 838	571 949
Altitude, n. mi.	94.0	94.1
Range, n. mi.	--	--
Space-fixed velocity, ft/sec	28 329	28 315
Space-fixed flight-path angle, deg	-4.68	-4.71
Space-fixed heading angle, deg East of North	59.47	59.64

TABLE 5.1-I.- COMPARISON OF PLANNED AND ACTUAL TRAJECTORY PARAMETERS, MISSION AS-202 - Concluded

Condition	Planned	Actual
Entry interface		
Time from range zero, sec	4 358.4	4 348
Time from range zero, hr:min:sec	1:12:58.4	1:12:28
Geodetic latitude, deg:min South	4:36	4:50
Longitude, deg:min East	136:15	136:00
Altitude, ft	400 000	400 000
Altitude, n. mi.	65.8	65.8
Range, n. mi.	--	--
Space-fixed velocity, ft/sec	28 513	28 512
Space-fixed flight-path angle, deg	-3.48	-3.53
Space-fixed heading angle, deg East of North	58.87	59.01

TABLE 5.0-III.- COMPARISON OF PLANNED AND ACTUAL TRAJECTORY PARAMETERS, COMMAND MODULE IMPACT, MISSION AS-202

Condition	Planned	Actual[a]	Recovered[b]
Time from range zero, sec	5575	5582	--
Time from range zero, hr:min:sec	1:32:55	1:33:02	10:02:00
Geodetic latitude, deg:min North	17:52	16:07	16:05
Longitude, deg:min East	171:52	168:54	168:39

[a]Based on aircraft LORAN fix.

[b]CM position at time of shipboard recovery

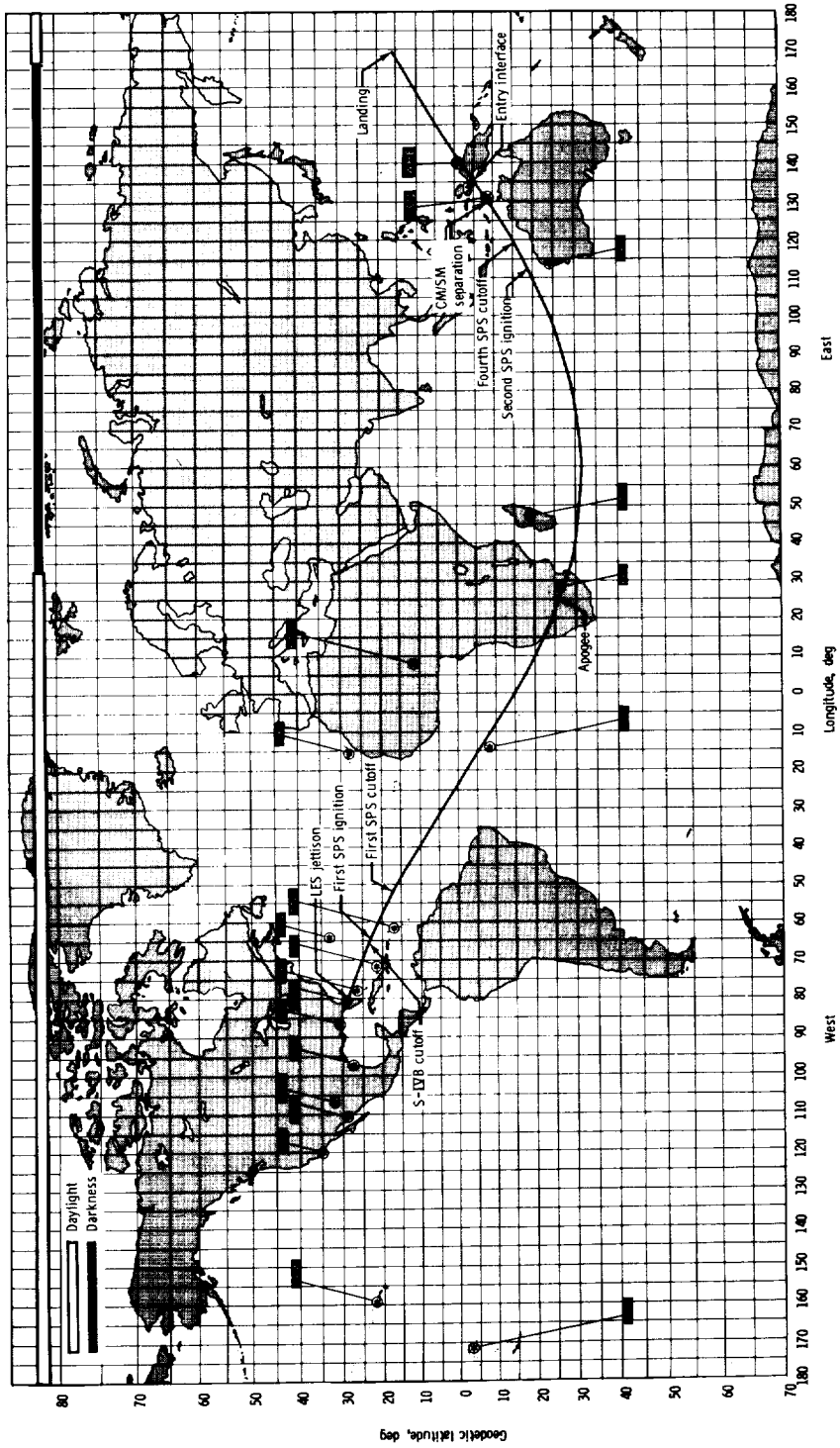

Figure 5.1-1.- Ground track for Mission AS-202.

NASA-S-66-9960

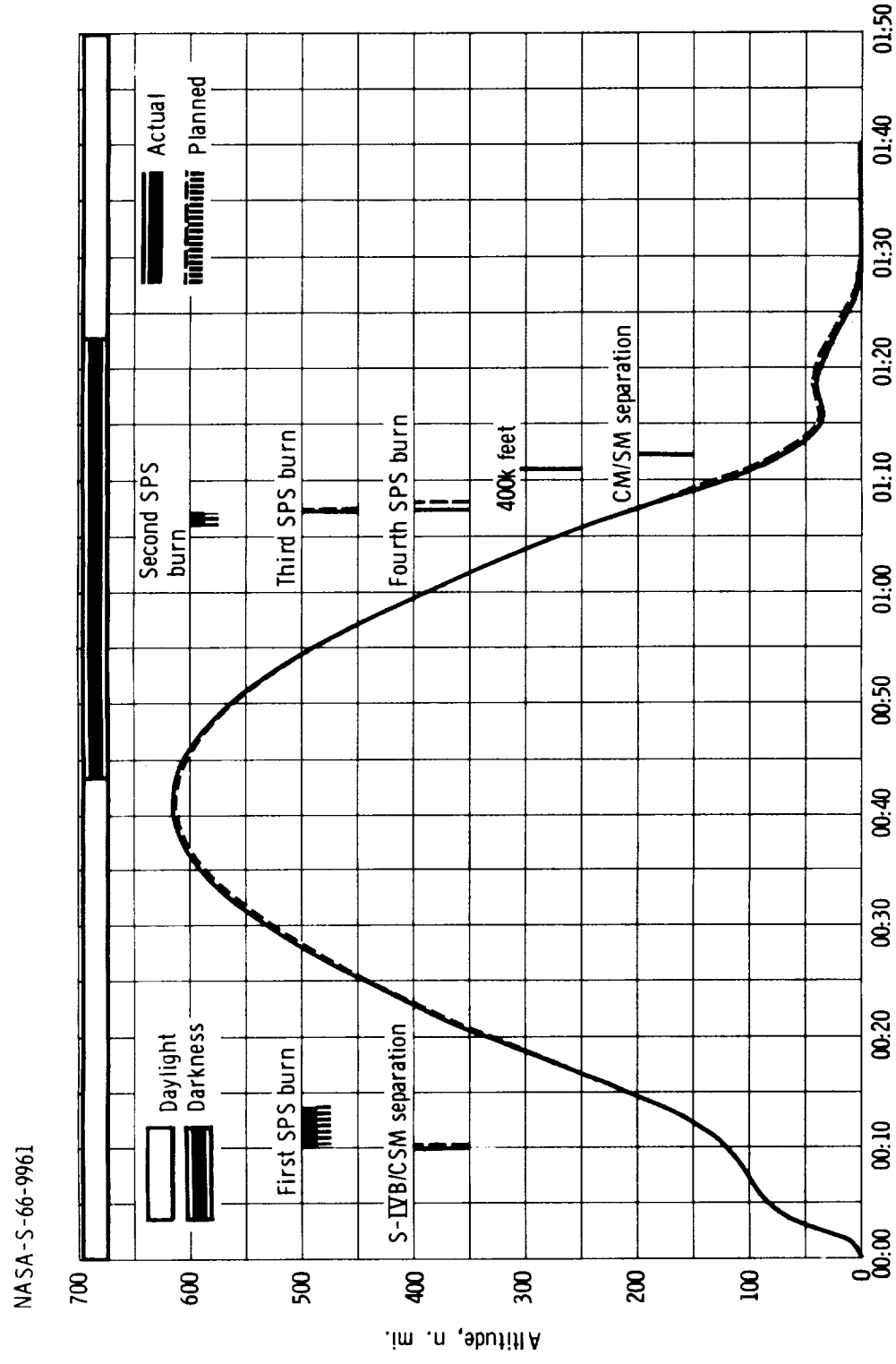

Figure 5.1-2. - Time history of altitude, Mission AS-202.

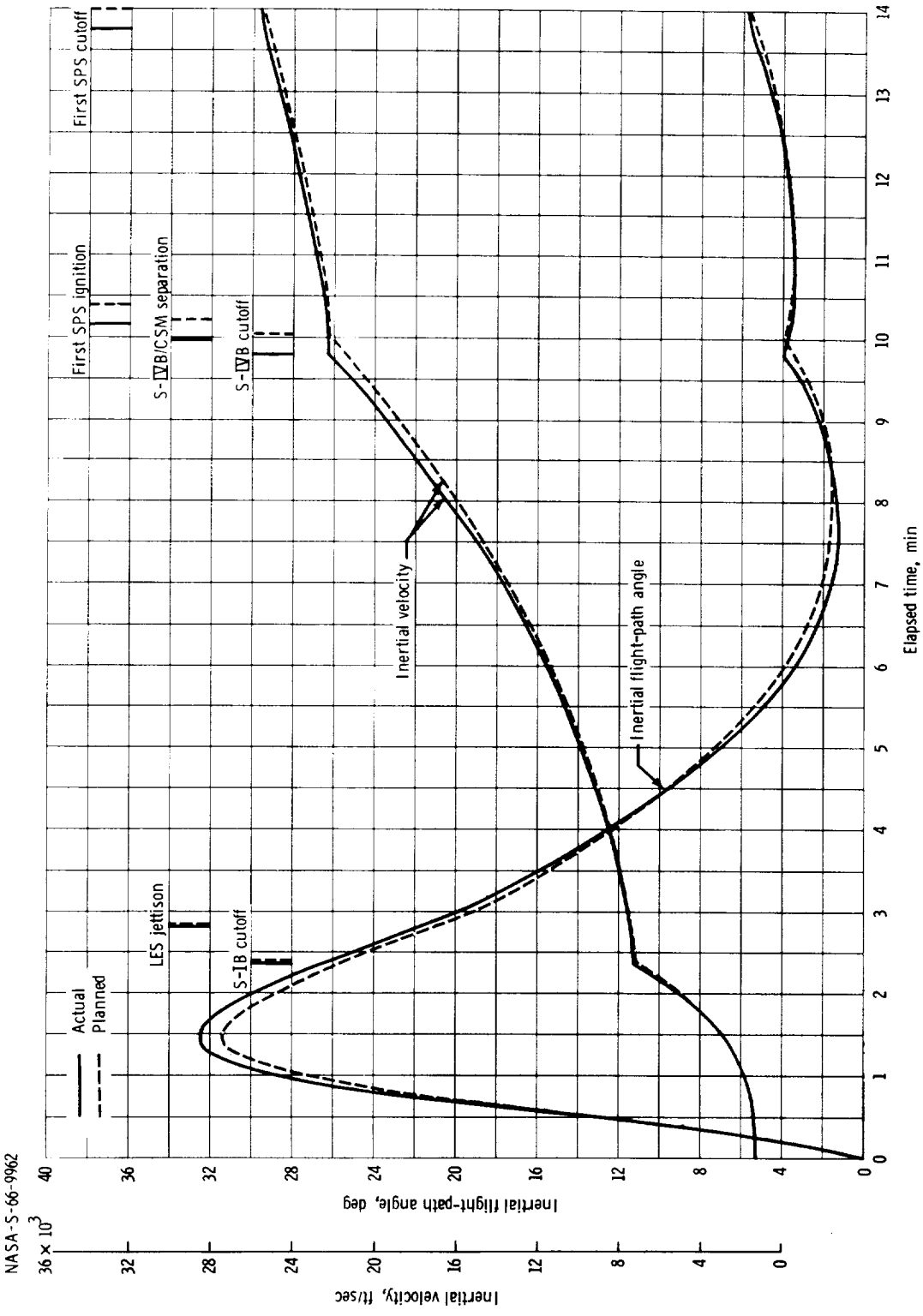

(a) Inertial velocity and inertial flight-path angle.

Figure 5.1-3.- Time histories of trajectory parameters for Mission AS-202 launch phase.

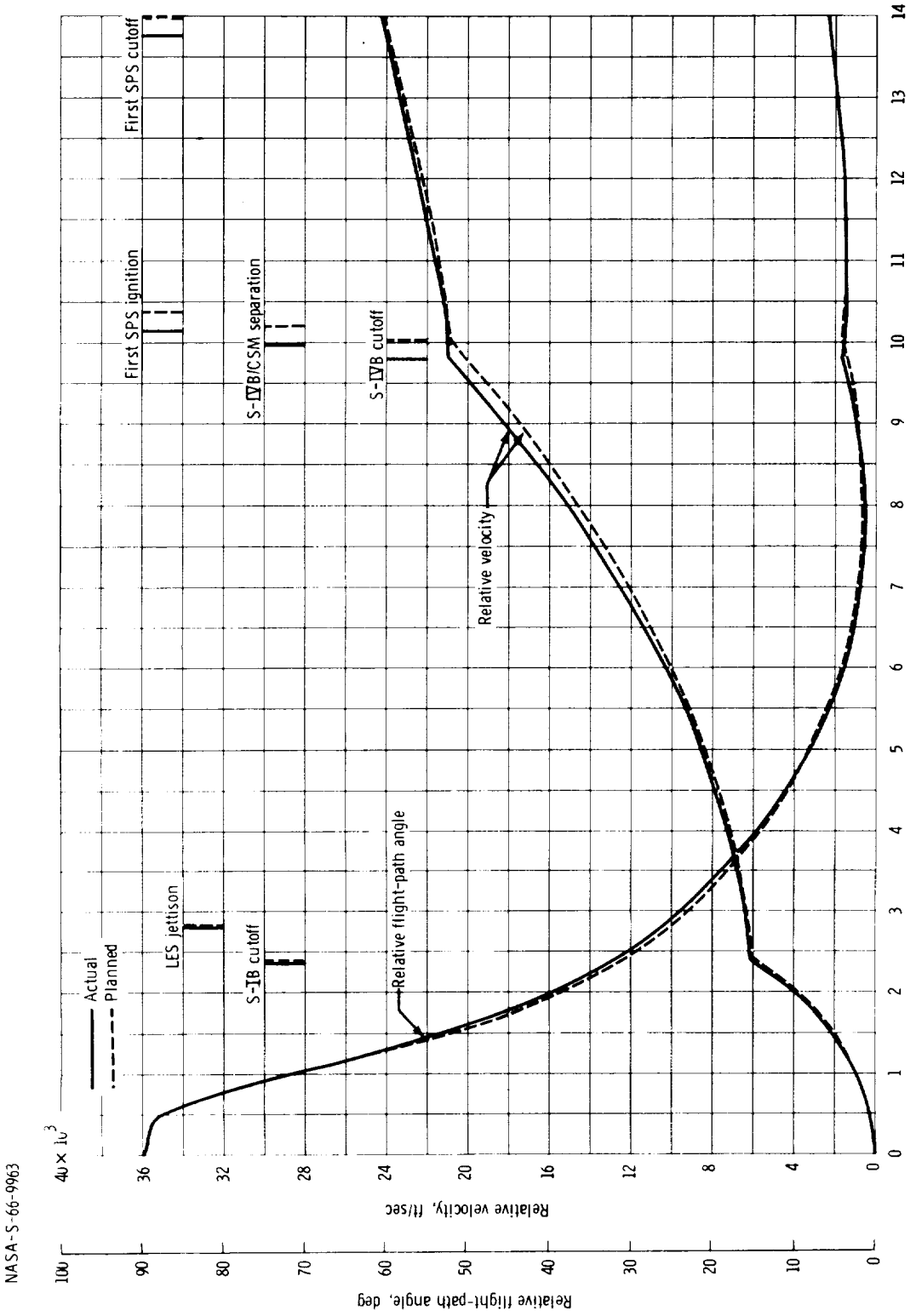

(b) Relative velocity and relative flight-path angle.

Figure 5.1-3. - Continued.

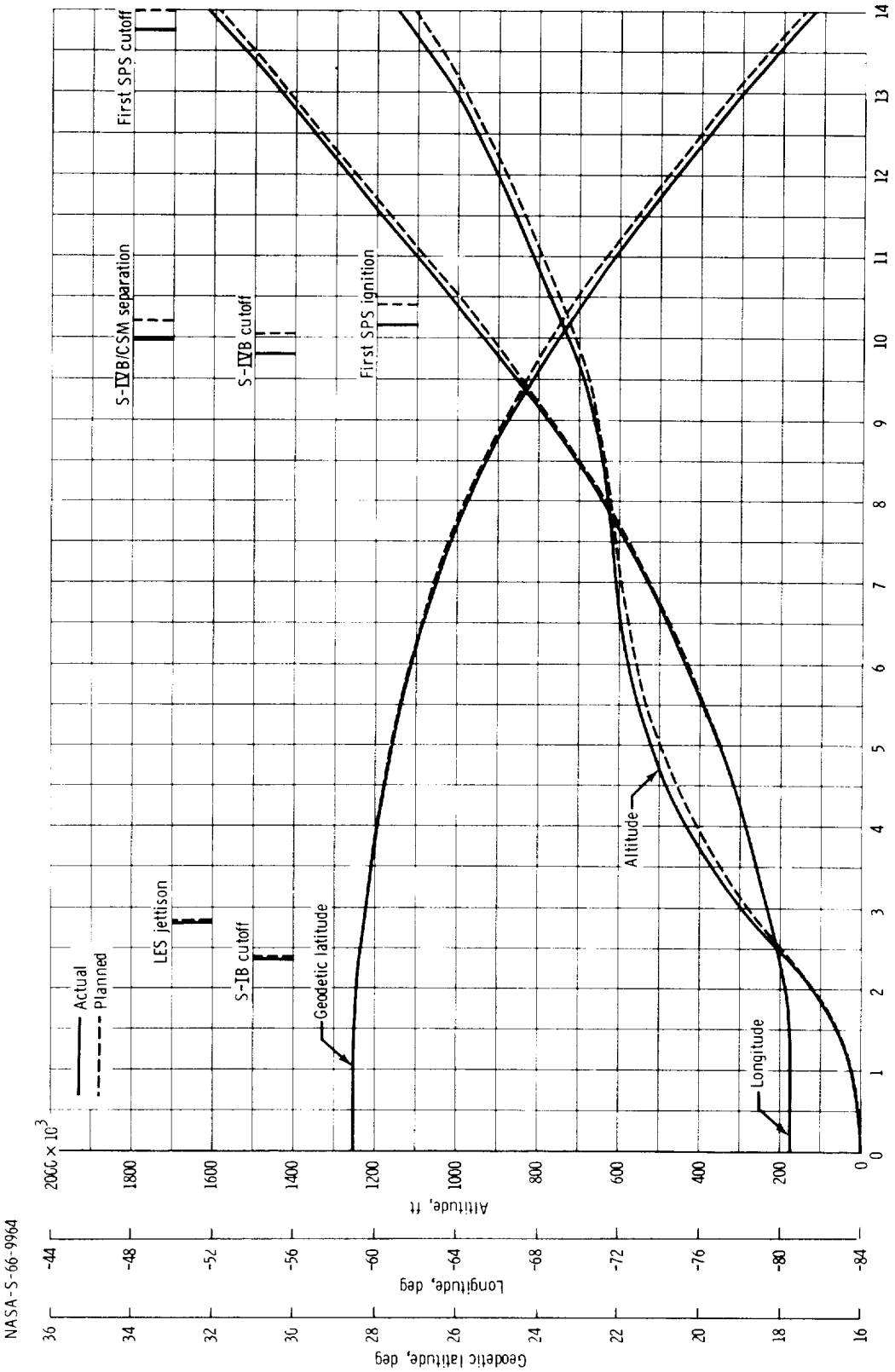

(c) Altitude, longitude and geodetic latitude.

Figure 5.1-3.- Continued.

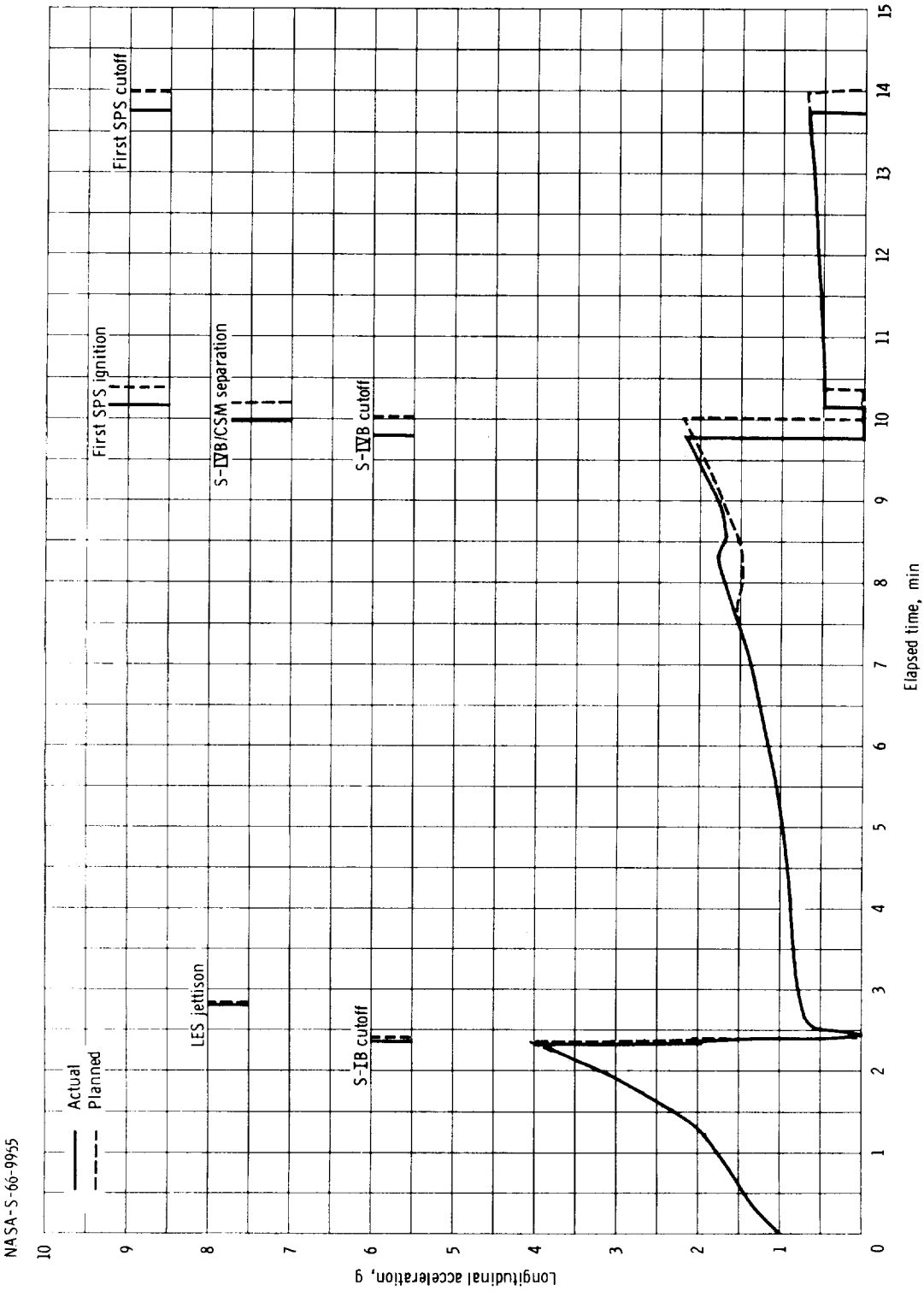

(d) Longitudinal acceleration.

Figure 5.1-3.- Continued.

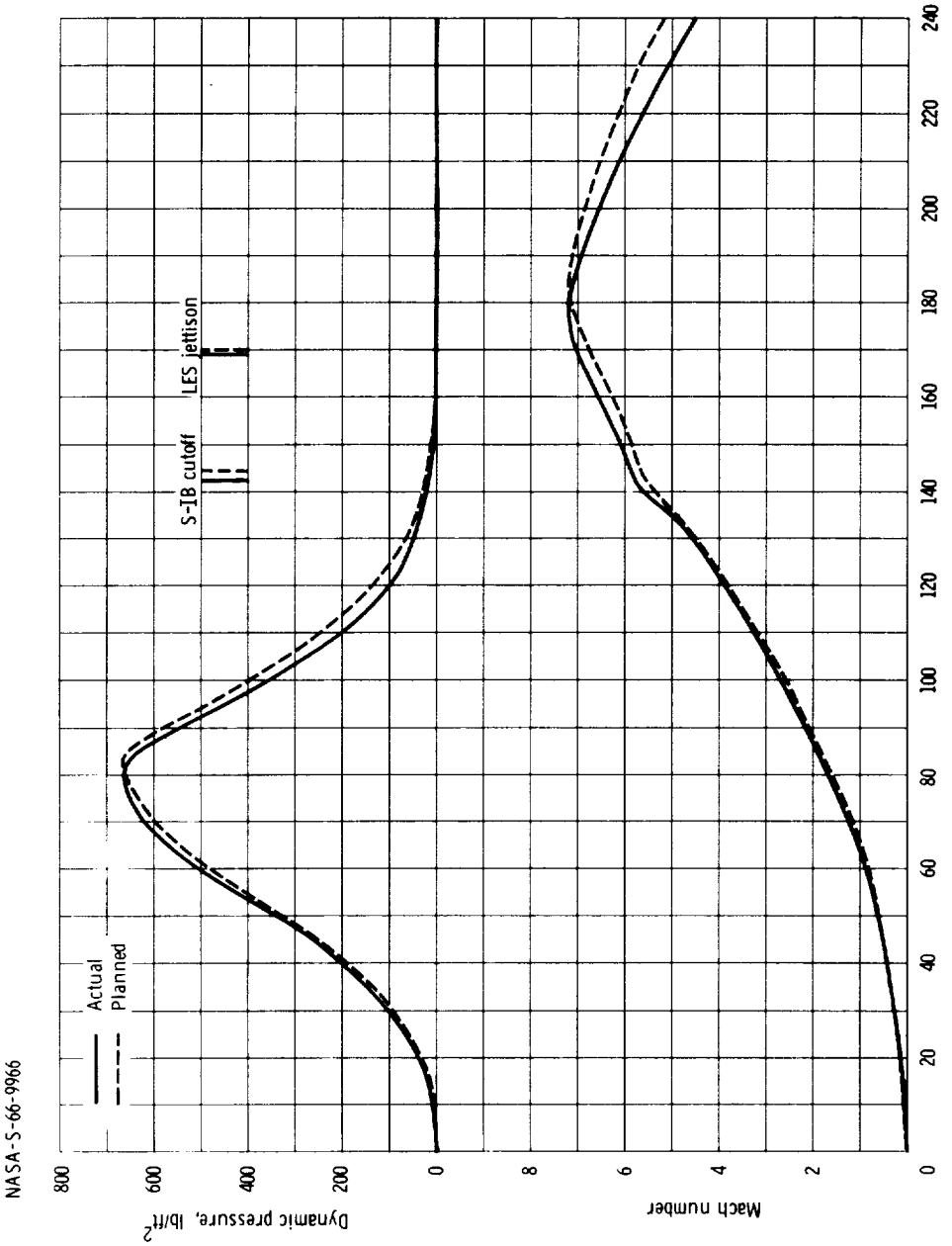

(e) Mach number and dynamic pressure.

Figure 5.1-3. - Concluded.

NASA-S-66-9967

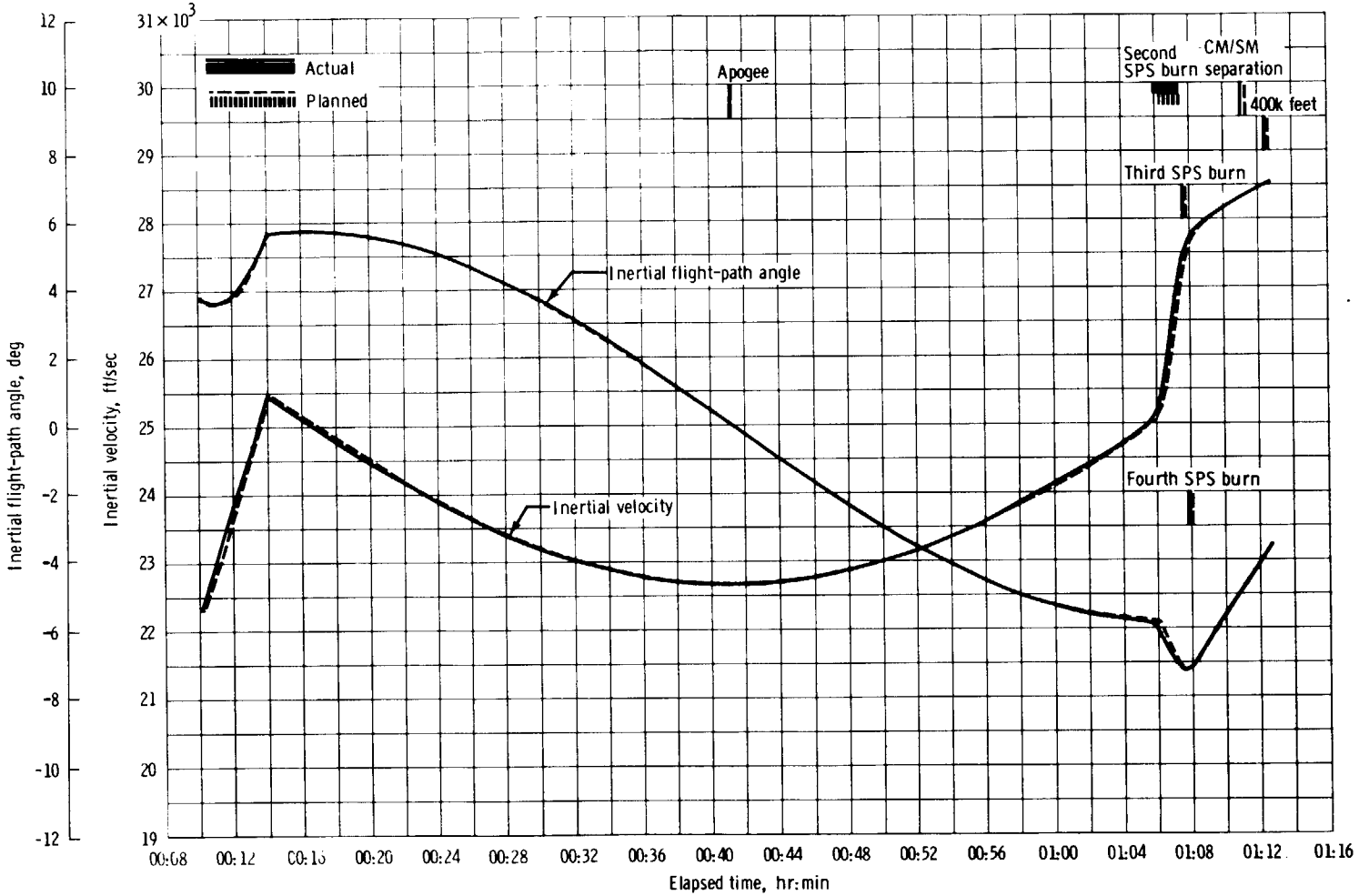

(a) Inertial velocity and inertial flight-path angle.

Figure 5.1-4. - Time histories of trajectory parameters for Mission AS-202 midcourse phase.

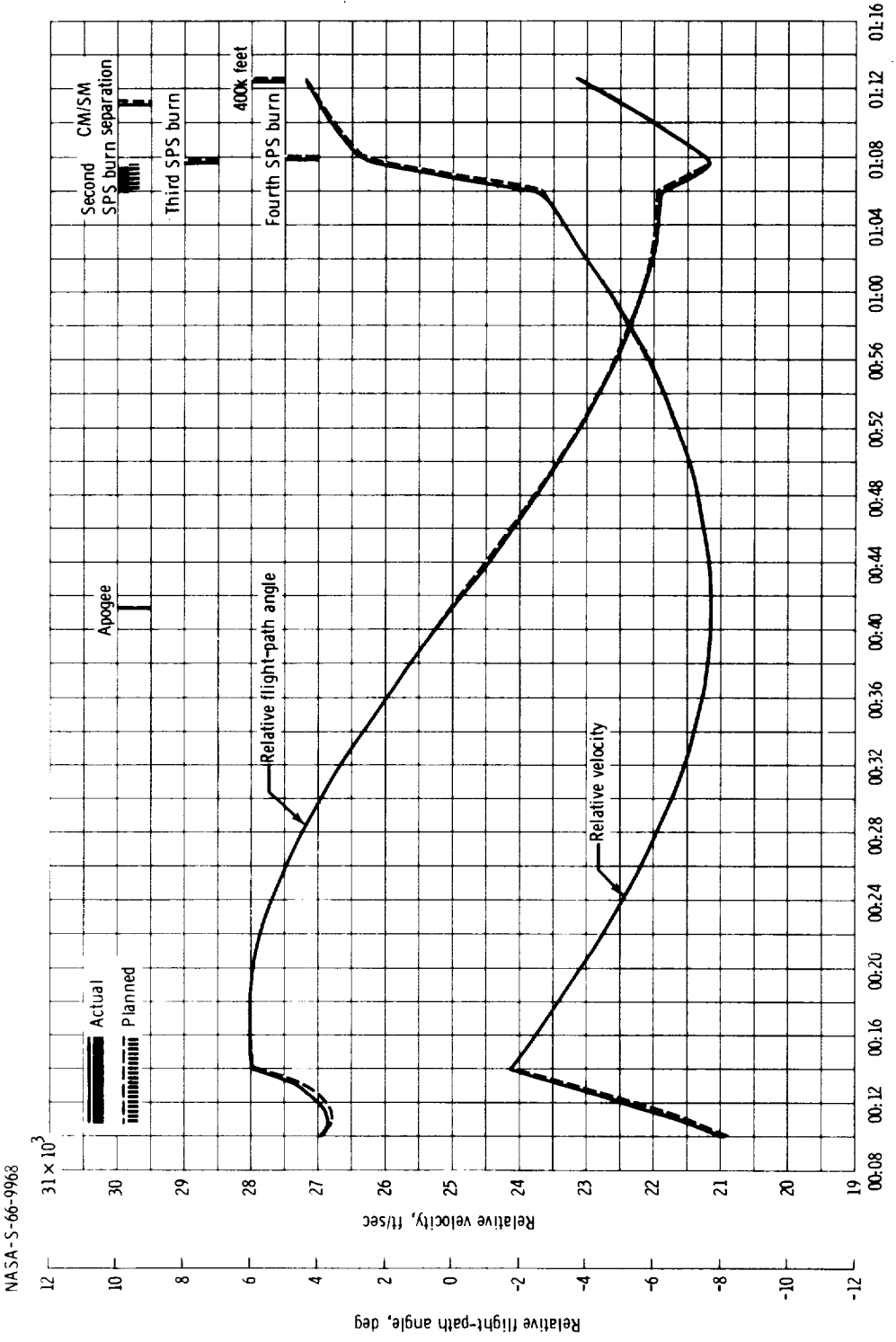

(b) Relative velocity and relative flight-path angle.

Figure 5.1-4. - Continued.

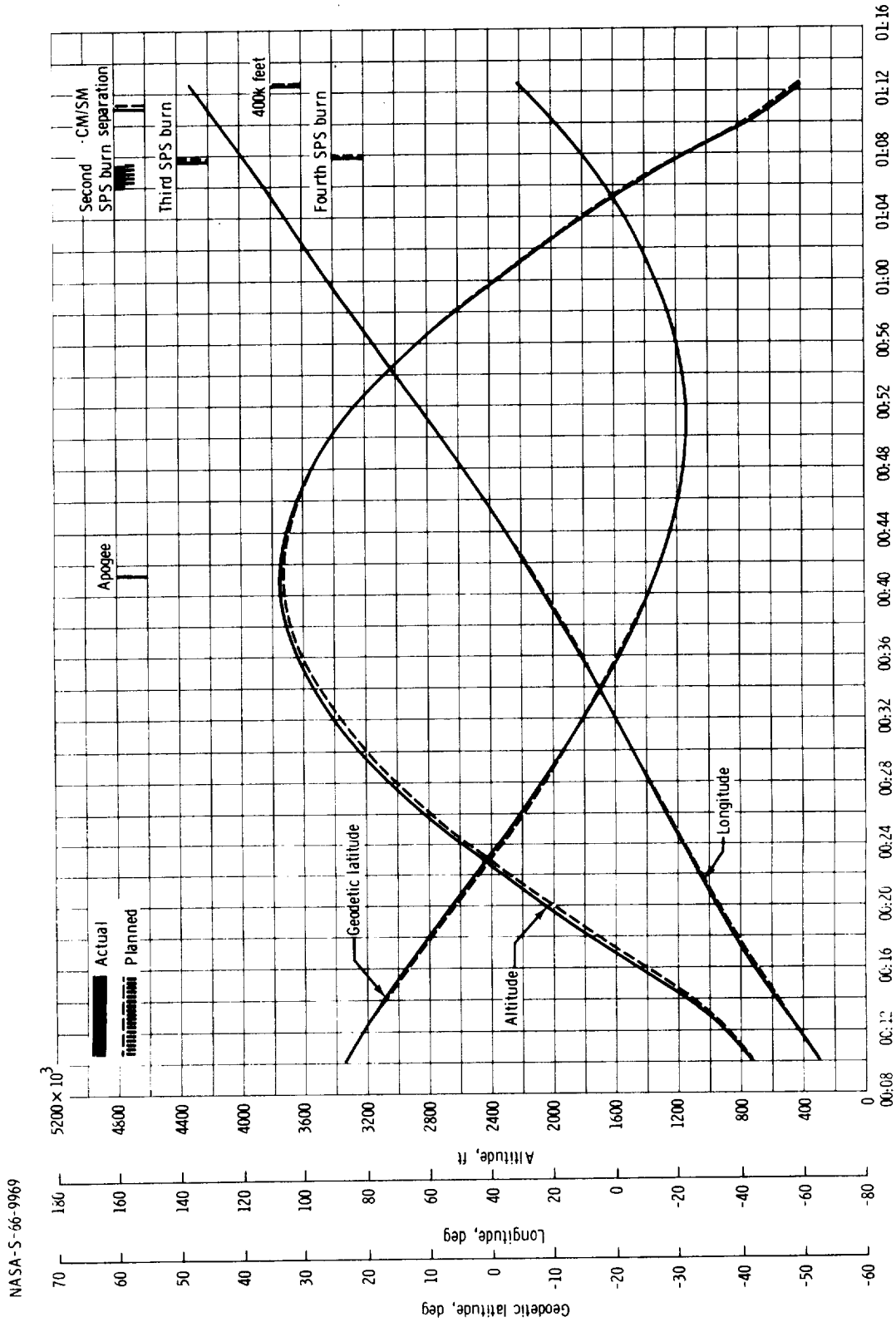

(c) Altitude, longitude and geodetic latitude.

Figure 5.1-4. - Concluded.

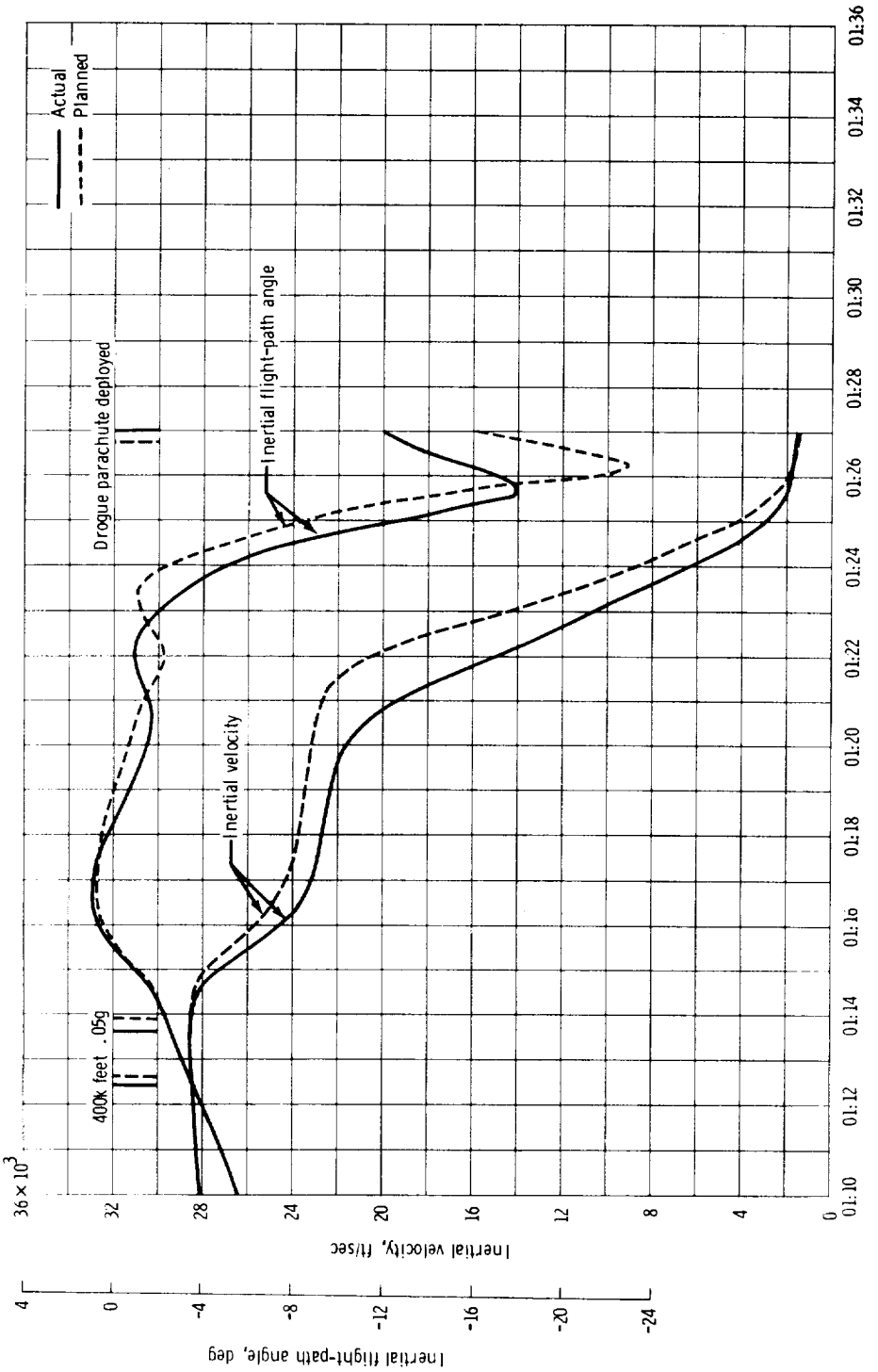

NASA-S-66-9970

(a) Inertial velocity and inertial flight-path angle.

Figure 5.1-5. - Time histories of trajectory parameters for Mission AS-202 reentry phase.

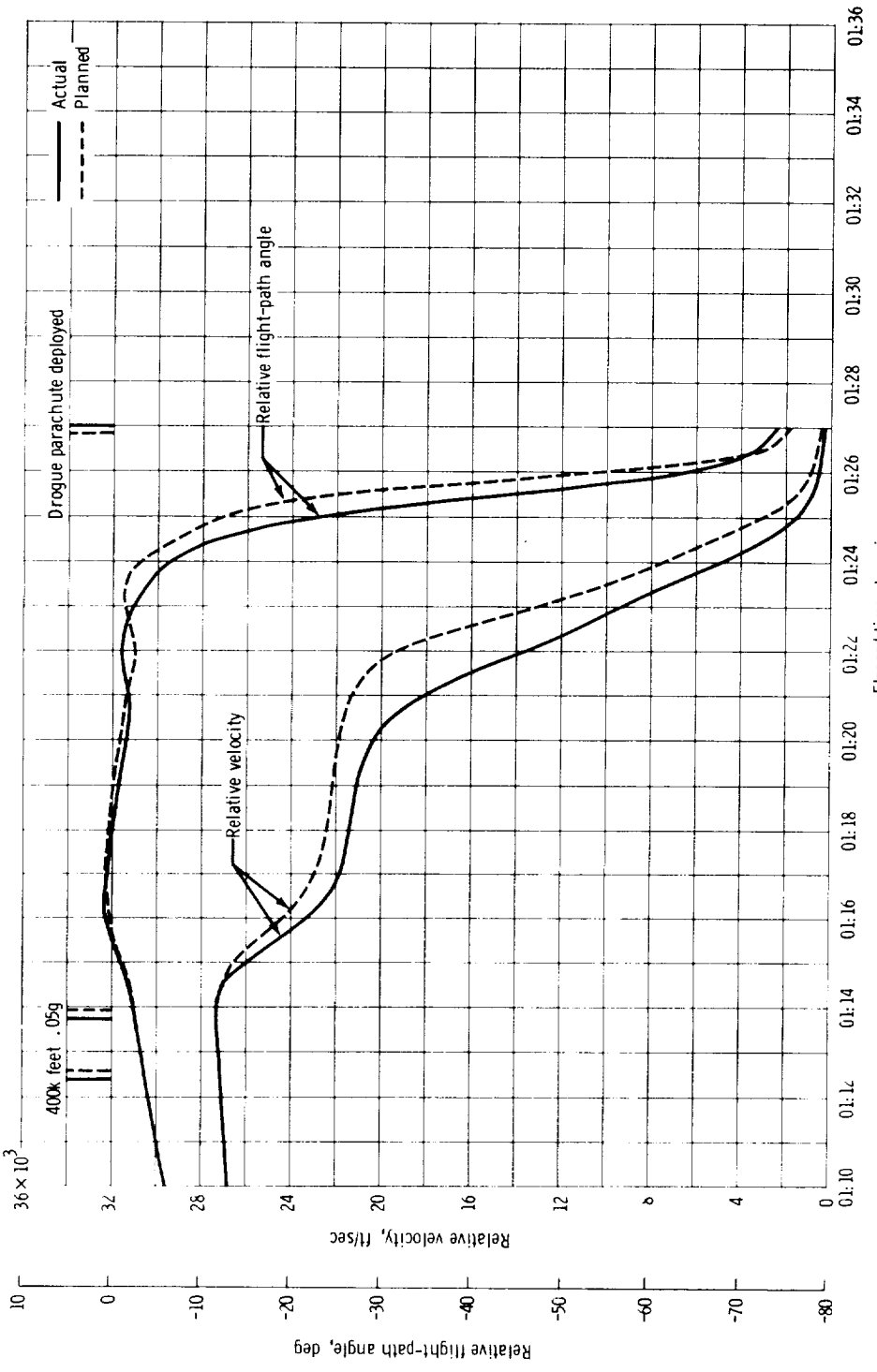

NASA-S-66-9971

(b) Relative velocity and relative flight-path angle.

Figure 5.1-5. - Continued.

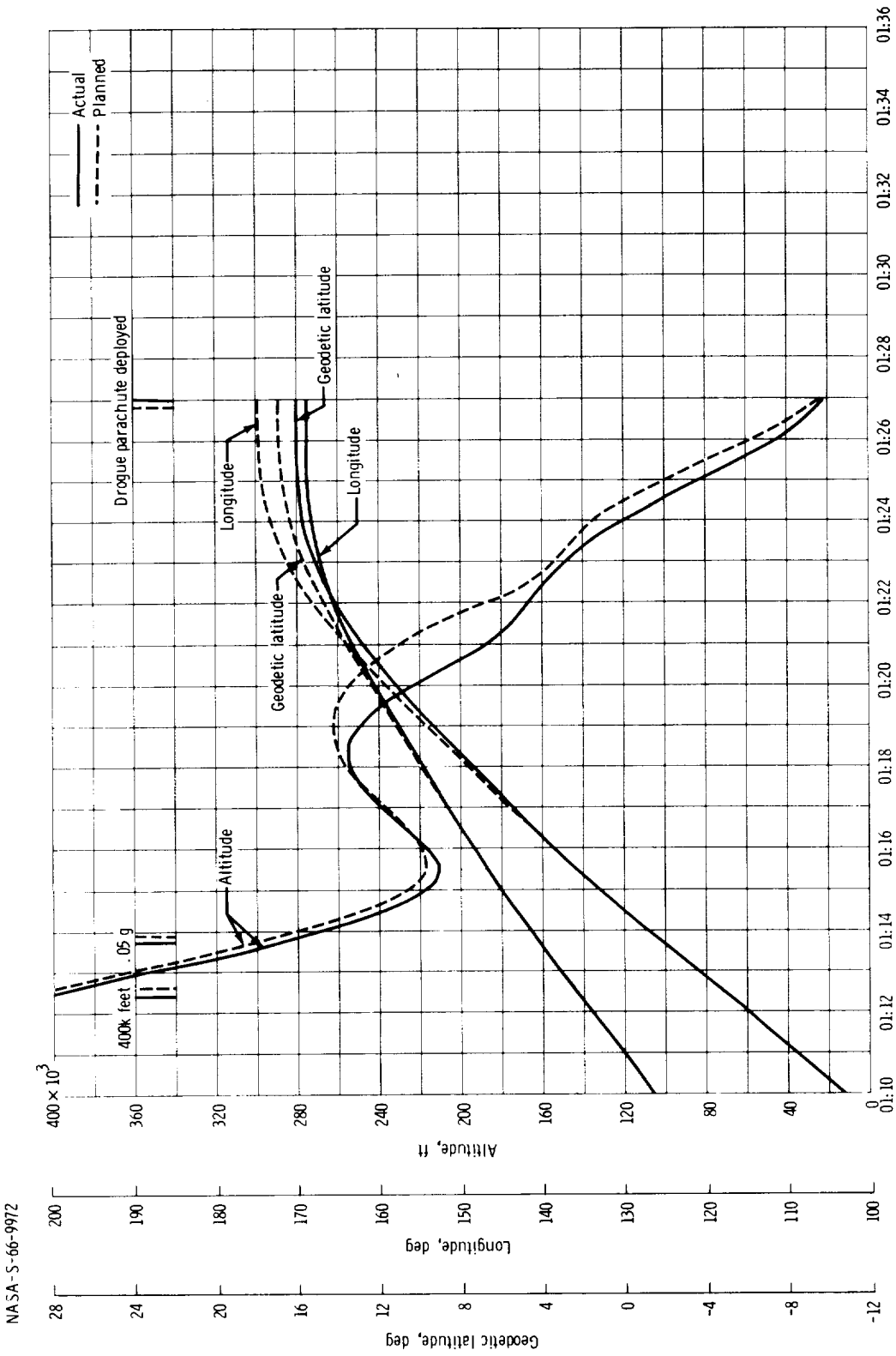

(c) Altitude, longitude and geodetic latitude.

Figure 5.1-5. - Continued.

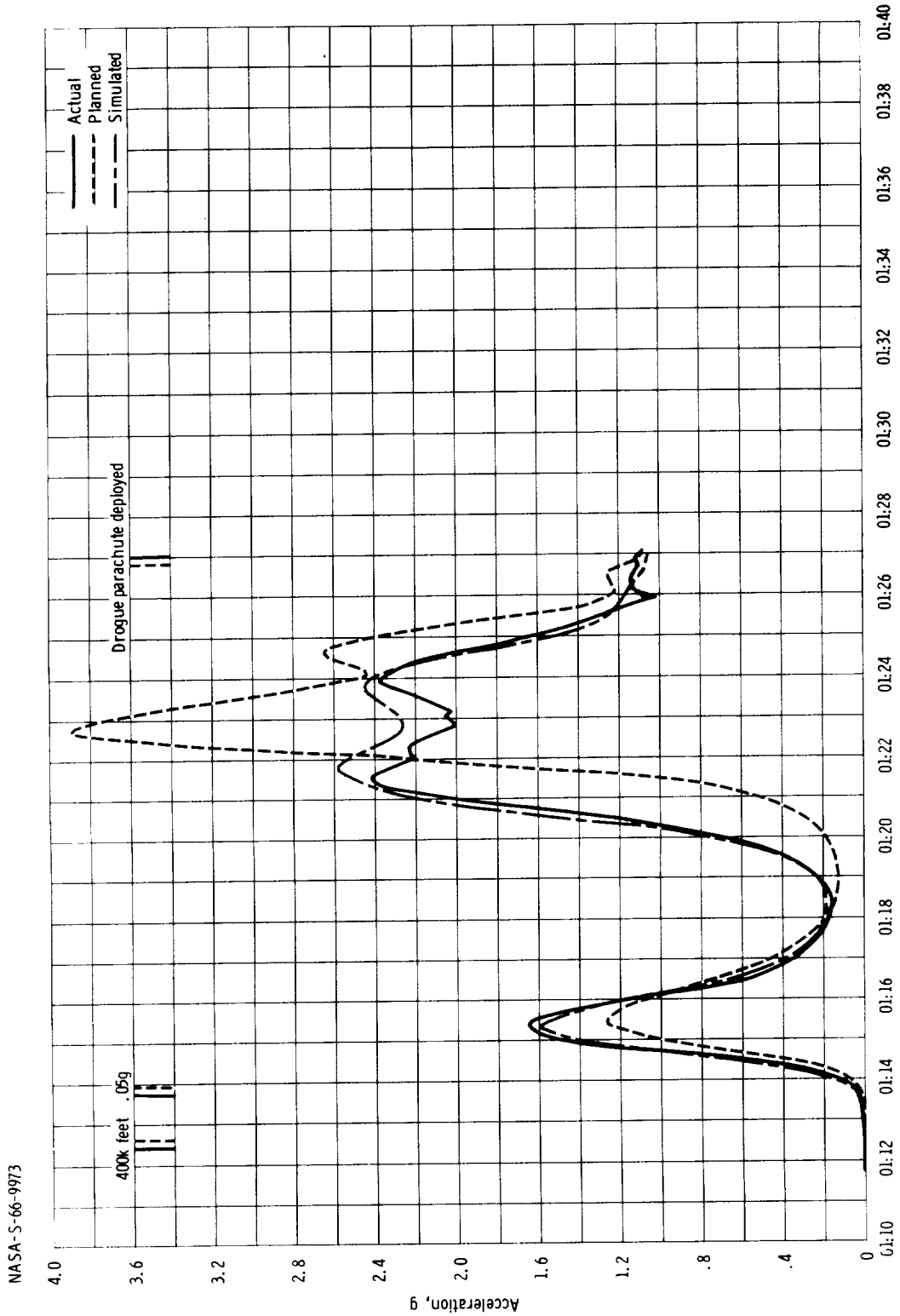

(d) Acceleration.

Figure 5.1-5. - Continued.

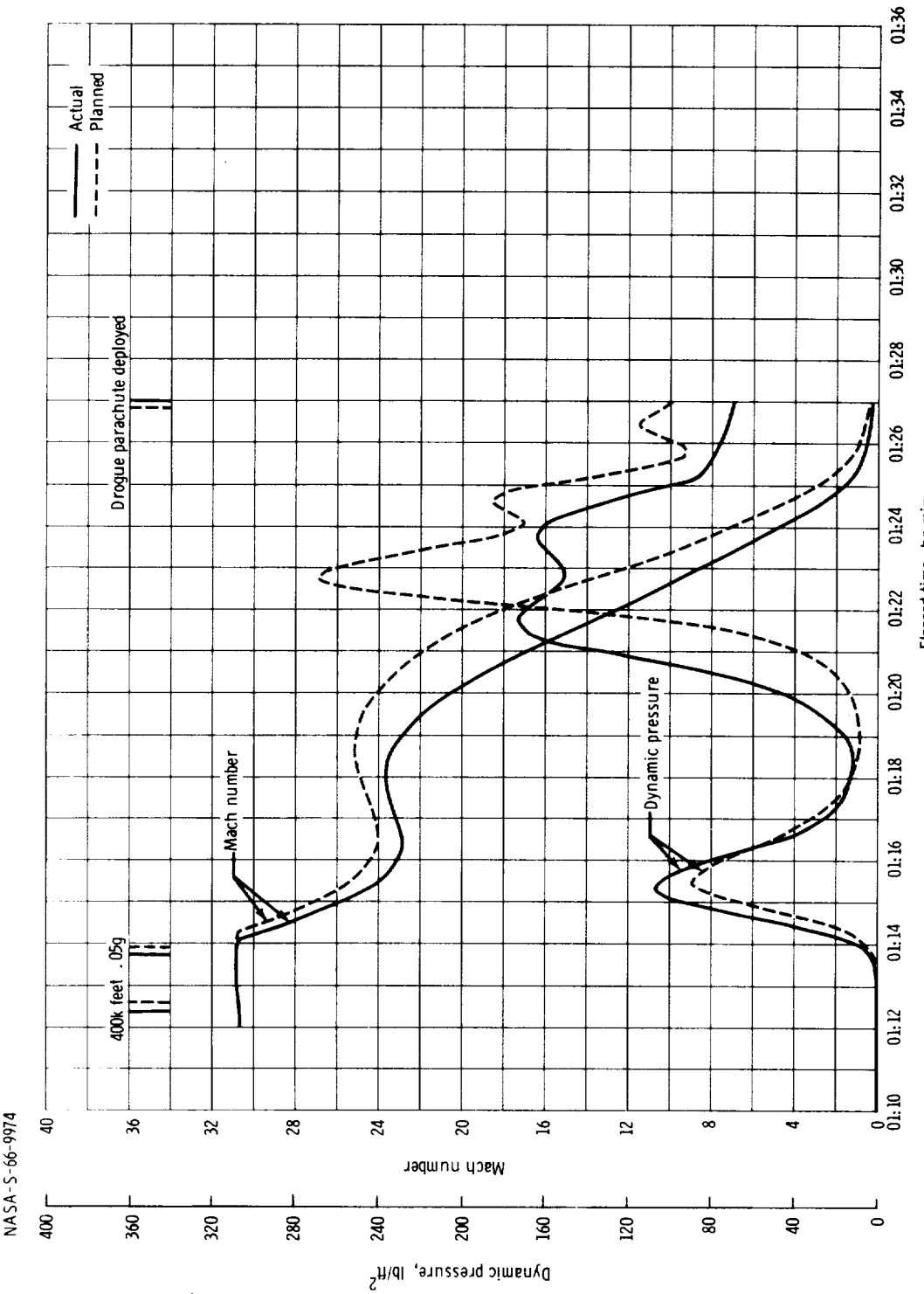

(e) Mach number and dynamic pressure.

Figure 5.1-5. - Concluded.

5.2 Nominal Data Description

The nominal or planned data presented in this report are taken from the T-3 day update to the "AS-202 Operational Spacecraft Flight Trajectory" as prepared by Mission Planning and Analysis Division, MSC, and the "AS-202 Launch Vehicle Operational Flight Trajectory," dated June 3, 1966, published by Marshall Space Flight Center.

5.3 Actual Data Description

The actual trajectory data presented in this report were generated by the following methods:

Segment one.- The launch trajectory from lift-off to S-IVB/CSM separation was prepared by MSFC using their "Observed Mass Point Trajectory (OMPT) Program" and is their final best estimate trajectory (BET).

Segment two.- The CSM powered-flight trajectory from S-IVB/CSM separation to the first SPS cutoff was simulated using the operational trajectory design program. The trajectory parameters for this simulation were derived from segment three data. The thrust level was modified to yield the correct burn time as determined from SPS bilevel sequence of event data.

Segment three.- The CSM free-flight trajectory from first SPS cutoff to second SPS ullage ignition was based upon a least-squares curve fit of C-band radar data from Ascension, Antigua, Pretoria, and Carnarvon, and is a BET. The root mean square (rms) radar residuals from each tracker for this fit are presented in table 5.3-I. These rms values are based upon estimates of the noise on the data and do not account for possible systematic errors such as station location errors, timing biases, etc., that may be present. Therefore, one sigma estimates of position and velocity errors of 300 feet and 1 ft/sec, respectively, are assigned and are based upon prior knowledge of the capability of the tracking network.

Segment four.- The powered-flight trajectory from second SPS ullage ignition to the fourth SPS cutoff, and the free-flight trajectory to entry interface, were generated by starting with a state vector (time, position, and velocity) from segment three data and integrating through the thrust periods using the pulse integrating pendulous accelerometer (PIPA) data corrected for a Y-axis platform misalignment of 400 seconds of arc toward Z, and an X-axis accelerometer misalignment error of 53 seconds of arc toward Z. At the entry interface, the maximum expected error is 20 ft/sec in the vertical direction and 10 ft/sec

along the flight azimuth. The maximum expected position error is 2.0 minutes of latitude and 2.0 minutes of longitude.

Segment five.- The entry trajectory was simulated using the actual impact point, the actual coupling data unit (CDU) angles, a lift-to-drag ratio of 0.28, the U.S. standard atmosphere of 1962, and a real-time computer complex (RTCC) state vector at 400 000 feet as an anchor point. The program was allowed to solve for flight-path angle (γ_i) at 400 000 feet, and converged on $(\gamma_i = -3.53)$ which is also the value of (γ_i) derived by the independent method used in generating the data for segment four of the trajectory.

The acceleration profile which results from the simulation is in good agreement with onboard data [fig. 5.1-5(d)] and is thus considered to be a good representation of the actual trajectory flown.

Further trajectory refinement is in progress.

TABLE 5.3-I.- RADAR RESIDUALS FOR FREE FLIGHT DATA

Station	Number of data points	rms radar residuals		
		Range, ft	Azimuth, deg	Elevation, deg
Antigua	20	8	0.008	0.013
Ascension	150	89	0.011	0.009
Pretoria	150	52	0.010	0.012
Carnarvon	50	26	0.004	0.006

6.0 AERODYNAMICS

6.1 Summary

Several methods were used to obtain reentry flight aerodynamic characteristics for comparison with preflight data. These included utilization of guidance and navigation measurements from the Apollo guidance computer and the inertial measuring unit, postflight trajectory simulations, body-mounted structure accelerometer data, and related aerothermodynamic data.

The conclusions reached from analysis of the data presented herein indicate that the preflight estimate of the force coefficient data was good (with the exception of the method used to determine effective heat shield cant angle); the trim angle of attack was lower than nominal; and the lift-to-drag ratio was correspondingly low. On the basis of an analysis of the flight data it is estimated that for the Mach number region above M = 6, the trimmed lift-to-drag (L/D) ratio is L/D = 0.28 $\pm$ 0.2.

6.2 Preflight Aerodynamic Data

Preflight trimmed wind-tunnel data are shown in figure 6.2-1(a) as a function of Mach number and are based on the center-of-gravity (c.g.) position that was determined prior to launch (section 4.1). The estimated uncertainty in the trimmed lift-to-drag ratio, $(L/D)_{trim}$, is indicated by the dashed lines about the nominal value and is based on the uncertainties of the wind-tunnel measurement system as well as c.g. dispersions.

L/D is presented as a function of the c.g. position in figure 6.2-1(b) for the Mach number range of M = 6 to M = 25, where these flight conditions exist for nearly 80 percent of the reentry time. The nominal c.g. value is indicated in the figure with uncertainties in determination of the nominal shown as a cross-hatched area.

Correction to preflight aerodynamic data for effective aft heat shield cant.- The method for determining the effective aft heat shield cant has been revised, and the revision resulted in a significant reduction of L/D_{trim} from that presented as preflight data. Analysis of the former method has determined that the method did not consider the difference in ablator thickness between the windward and leeward corner edges of the heat shield. Consideration of this difference was important in that it shifted the center of the heat shield farther

off the afterbody centerline than previously calculated, and also resulted in a change of the effective cant angle from 0.312 degree to 0.195 degree. When applied to the M = 6 to M = 25 aerodynamic data, this correction resulted in an L/D_{trim} approximately 0.015 degree lower than that predicted by preflight data which are shown in figures 6.2-1(a) and 6.2-1(b). This information was determined postflight and therefore does not appear on the preflight values.

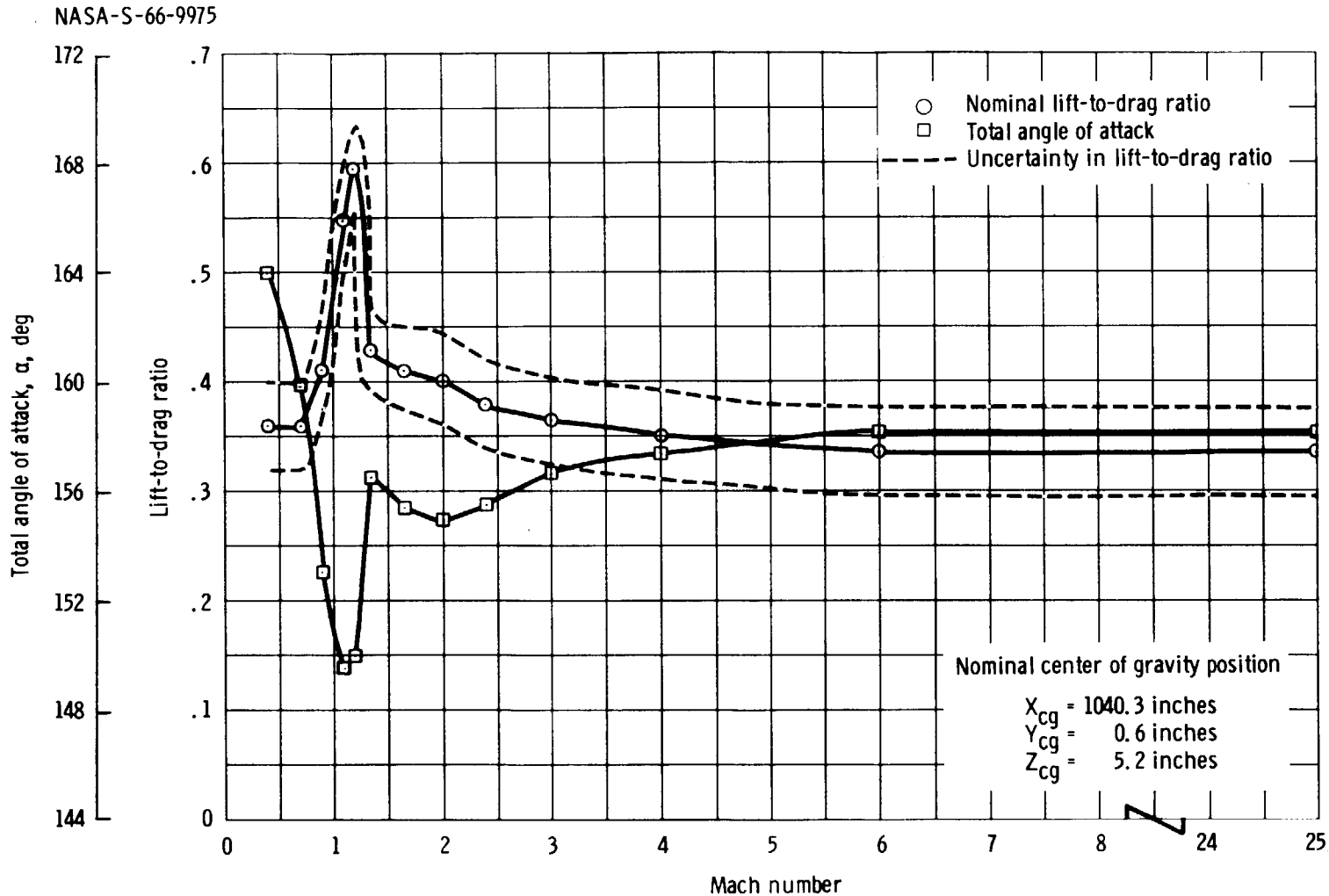

(a) Trimmed values of lift-to-drag ratio and total angle of attack as a function of Mach number.

Figure 6.2-1. - Preflight aerodynamic data for the reentry configuration, Mission AS-202.

NASA-S-66-9976

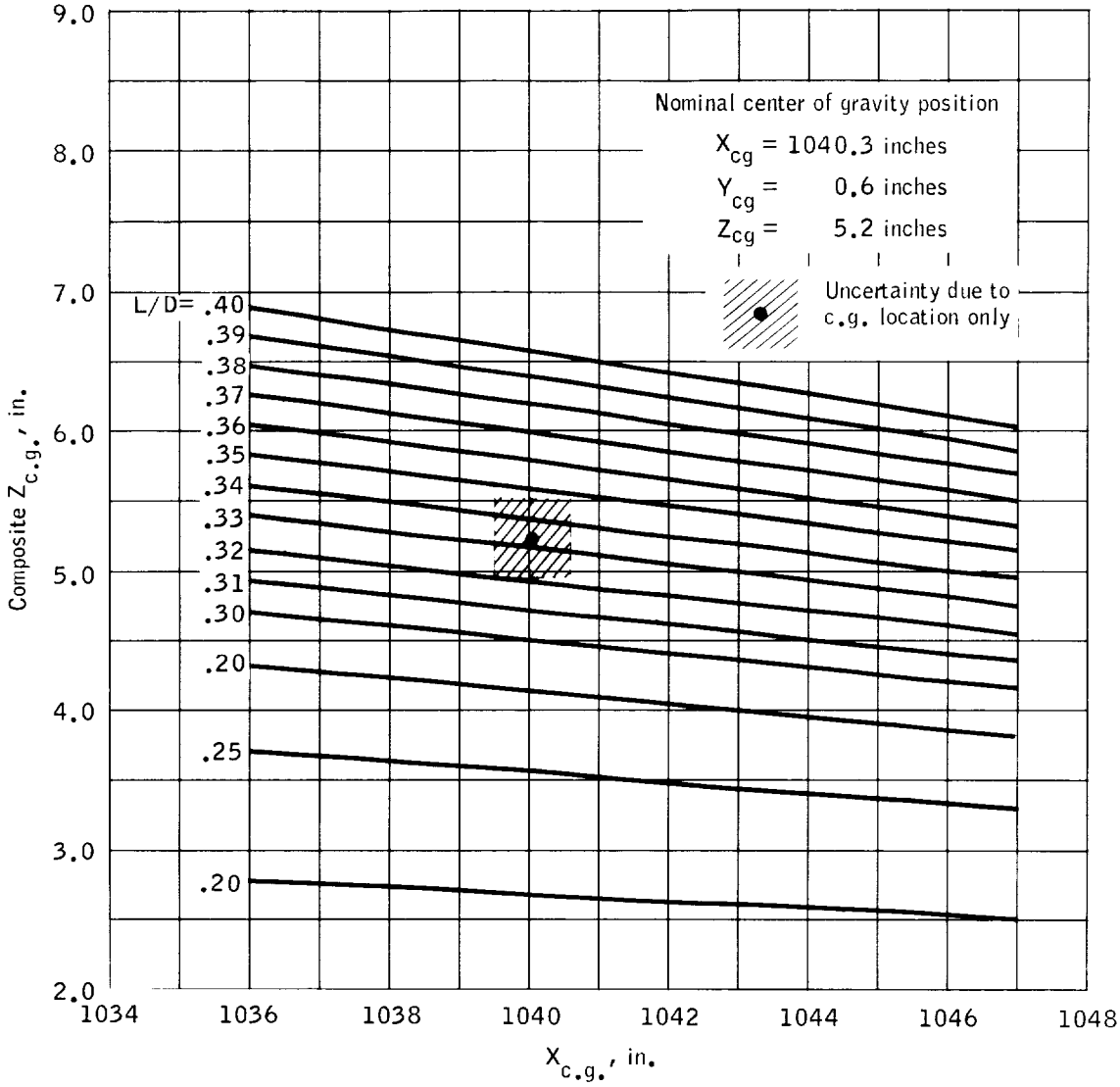

(b) Command module L/D trim as a function of center of gravity location using M = 6 to 25 wind tunnel data, heat shield cant is 0.3120 deg, composite $Z_{cg} = \sqrt{(Y_{cg})^2 + (Z_{cg})^2}$.

Figure 6.2-1.- Concluded.

6.3 Atmospheric Data

Atmospheric data were obtained in the reentry area (Eniwetok Atoll, Marshall Islands) in the form of Rawindsonde data up to 115 000 feet and Arcasonde data to 180 000 feet. These data were analyzed and then extrapolated to 400 000 feet to obtain the pressure, density, temperature, and speed of sound variations, shown in figure 6.3-1 as percentages of the 1962 Standard Atmosphere.

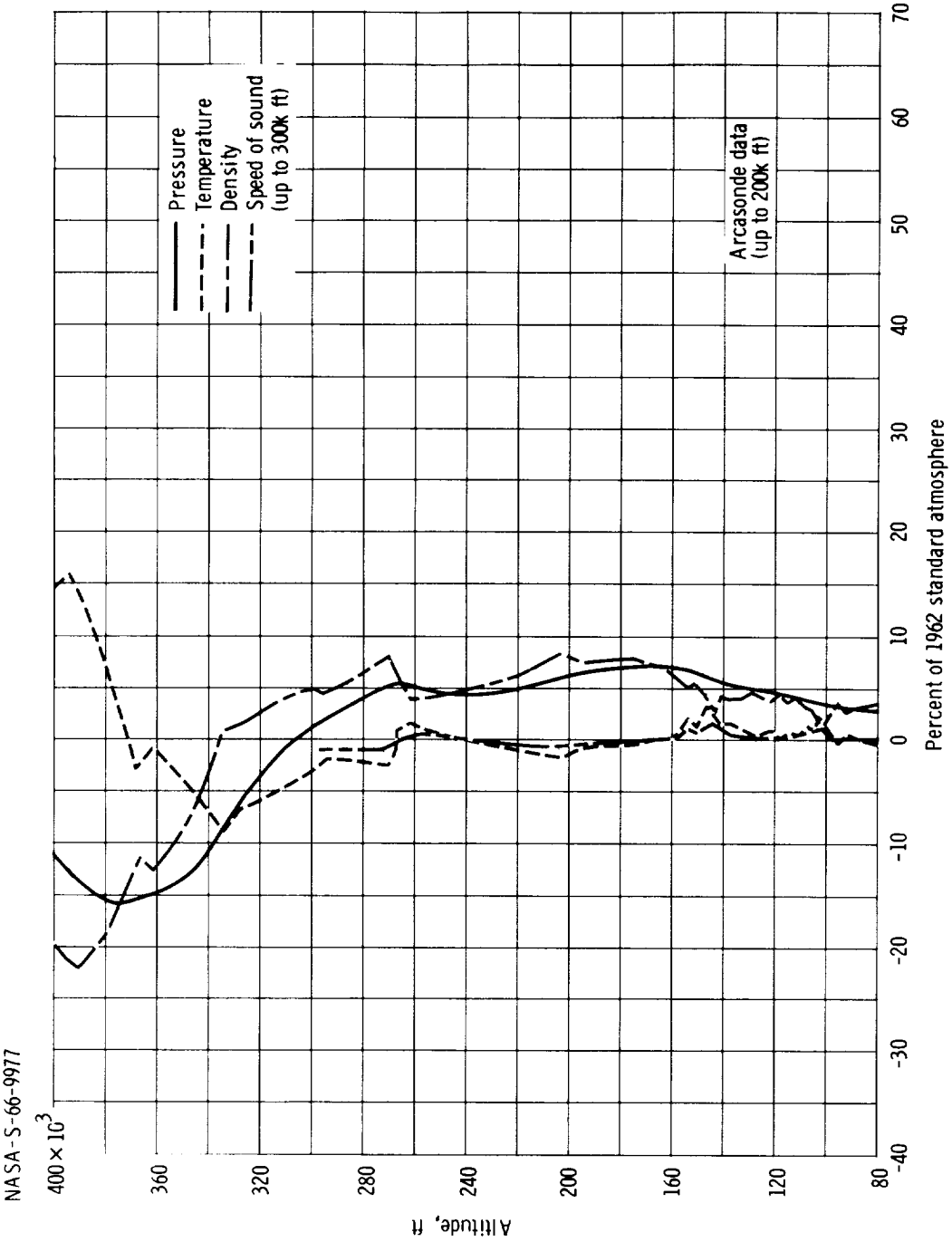

Figure 6.3-1.- Extrapolated postflight reentry atmospheric data, Mission AS-202.

6.4 Flight Aerodynamic Data From Guidance And Navigation Measurements

The Apollo guidance computer (AGC) downlink word list, as recorded on the data storage equipment (DSE) during reentry, was used to reconstruct a preliminary trajectory compatible with the inertial measuring unit (IMU) accelerations. The resulting data shown in figure 6.4-1 in three parts: (a) a definition of the aerodynamic angles related to the body axis system, (b) a time history of the total angle of attack, and (c) a time history of L/D. The values of L/D are averaged values over a 2-second interval. Their reliability decreases near the end of the reentry because of the uncertainty in the direction and magnitude of the earth relative velocity vector. The calculated values of L/D also show large scatter where the deceleration level is low [see figure 5.1-5(d)].

NASA-S-66-9978

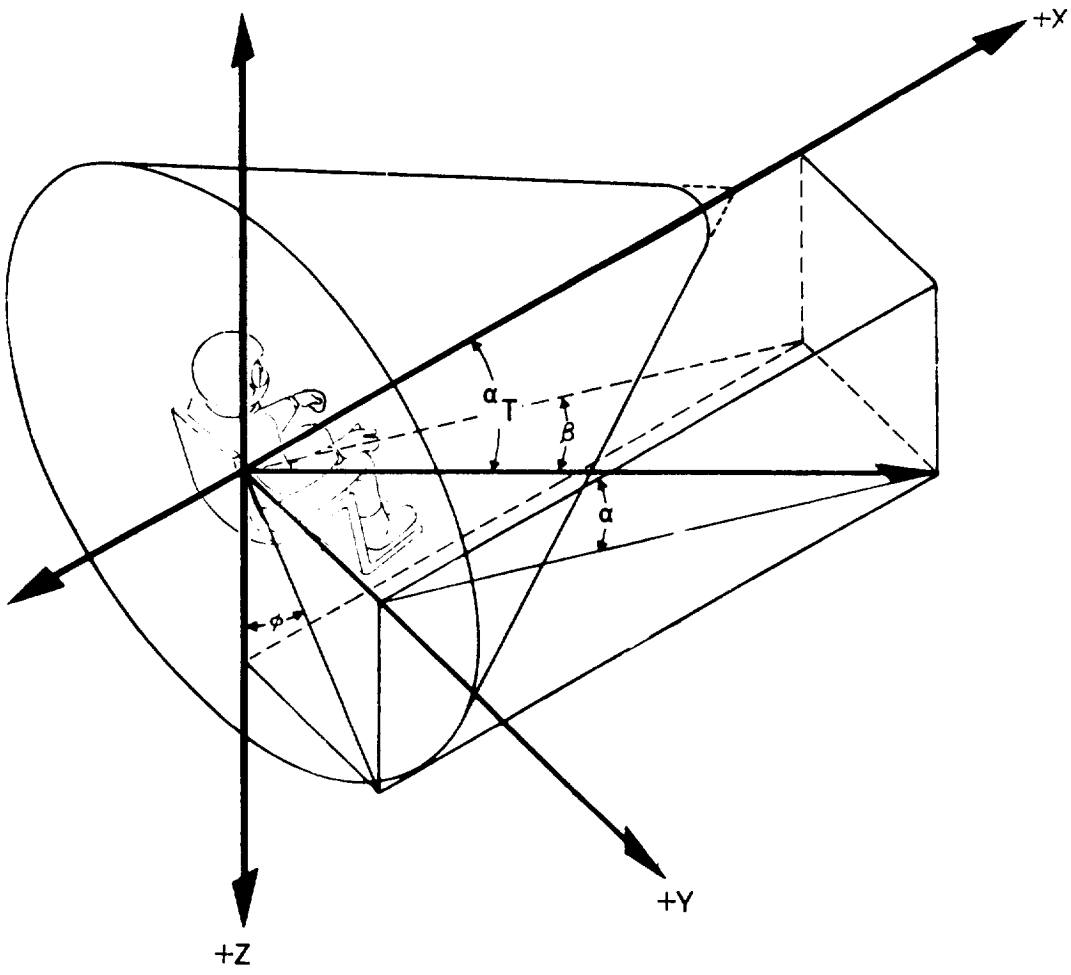

(a) Aerodynamic angle definitions.

Figure 6.4-1.- Flight aerodynamic characteristics from guidance and navigation data, Mission AS-202.

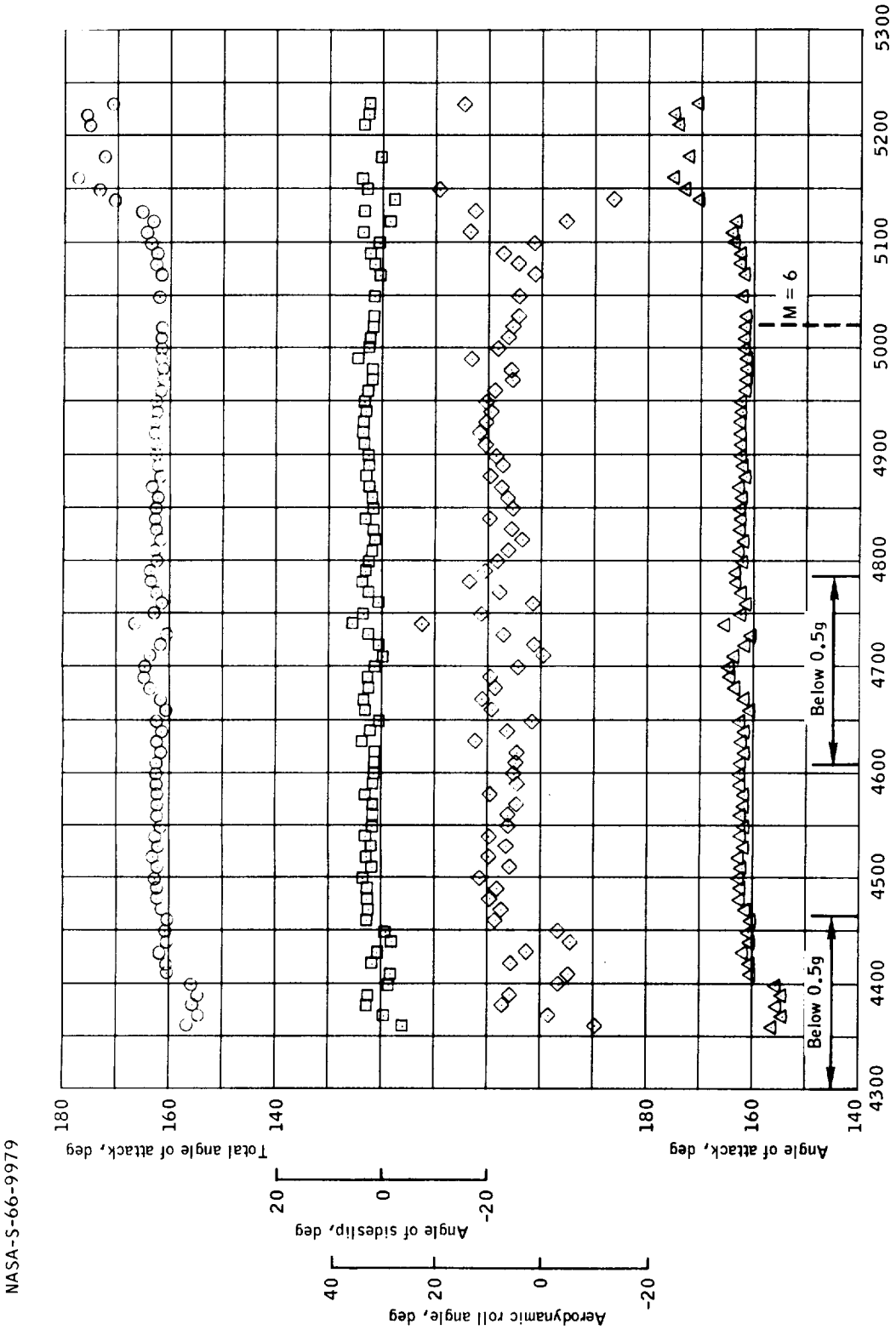

(b) Aerodynamic angles.

Figure 6.4-1.- Continued.

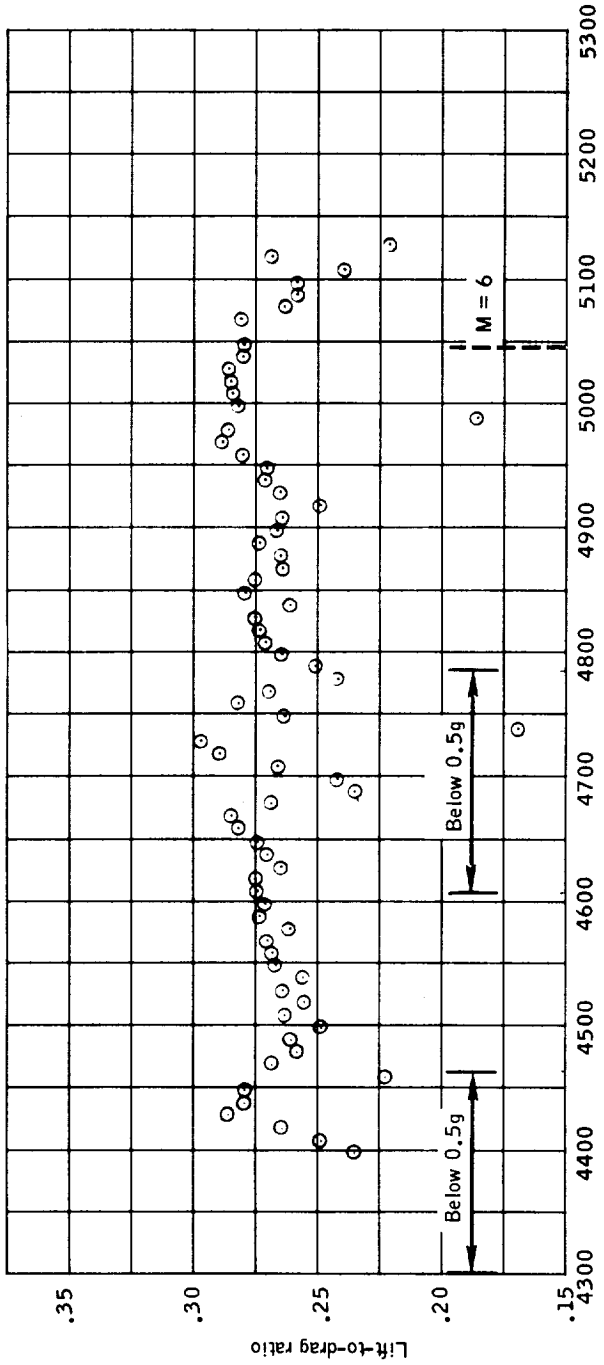

(c) Lift-to-drag ratio.

Figure 6.4-1.- Concluded.

NASA-S-66-9980

6.5 Flight Aerodynamic Data From Body-Mounted Accelerometers

Measurements CK0004A, CK0005A, and CK0006A from the linear accelerometers, which are aligned along the structure X-, Y-, and Z-axes respectively, were used to obtain values of normal force coefficient to axial force coefficient ratio, C_N/C_A, as presented in figure 6.5-1. These data are compared with the preflight aerodynamics, where ratios are presented for both the preflight trim predictions and for coefficients corresponding to α for L/D = 0.28. The data appear to show closer correlation to the predicted aerodynamics; however, considering that the purpose of this instrumentation was to measure the gross structural loads, it is felt that the end-to-end accuracy precludes any firm conclusions from these data. The scatter in the measurements alone is shown in figure 6.5-1.

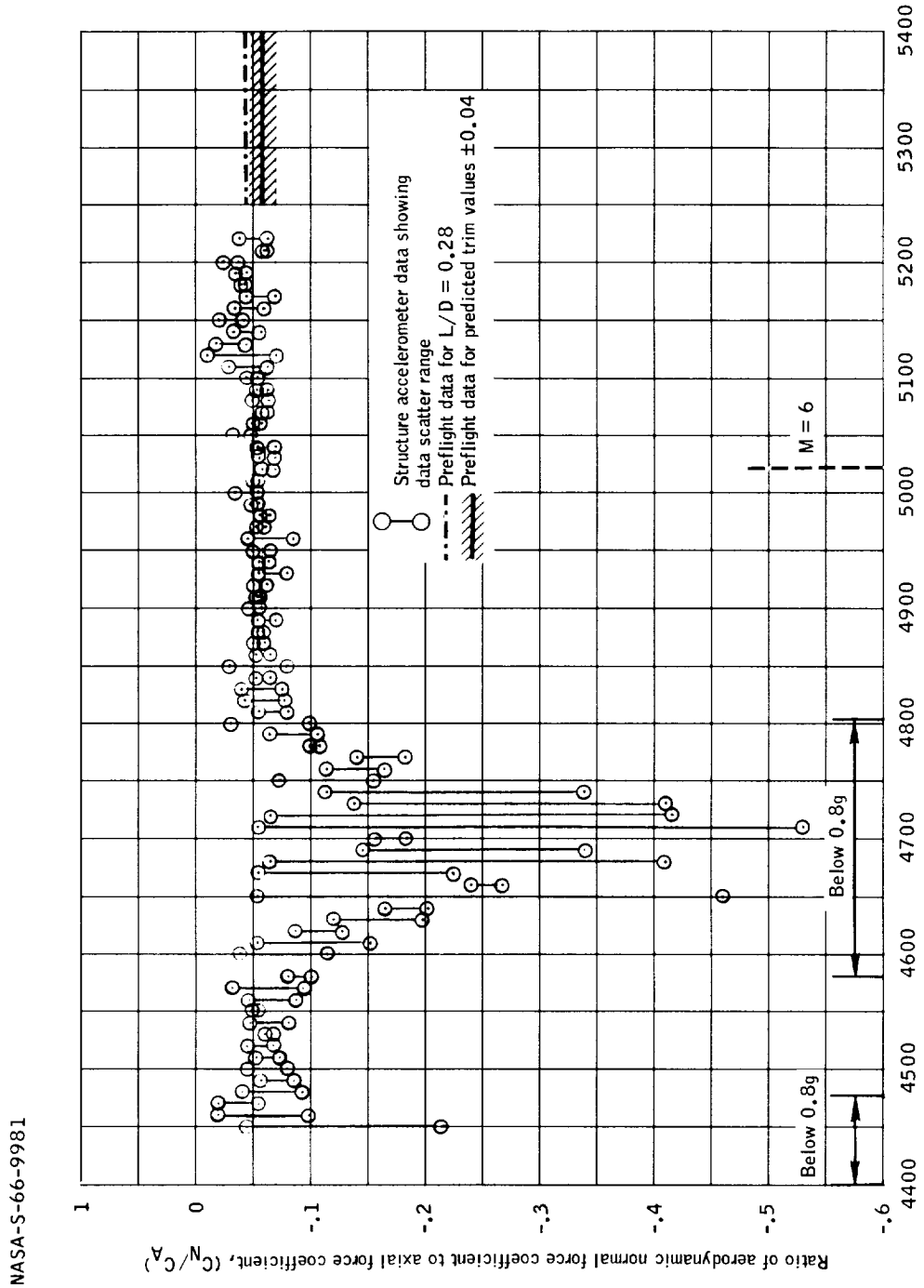

NASA-S-66-9981

Figure 6.5-1.- Flight aerodynamic data from structure accelerometers, Mission AS-202.

6.6 Aerothermodynamic Related Indications

Pressure measurements on the aft heat shield in the form of pressure ratios were compared with numerical calculations of pressure distributions for a flow field program based on angle of attack (section 7.3). Data were chosen for Mach numbers greater than 10, and indicated a trim angle-of-attack range of 160 degrees $\pm$ 2.

Further comparison of flight peak pressure data at a point on the spacecraft with theoretical calculations based on the L/D = 0.28 reentry profile of section 5.0 also show good agreement down to a Mach number of approximately M = 15.5.

6.7 Concluding Remarks

Aerodynamic data from preflight investigations, flight measurements, and postflight simulations are summarized in table 6.7-I and in figure 6.7-1. These data represent the Mach number range of M = 6 to M = 25, and, as shown in figure 5.1-5(e), cover most of the reentry.

Flight and postflight data analyses point to a lift-to-drag ratio that is lower than preflight estimates. Based on these findings and on experience with Gemini aerodynamics trim angle-of-attack coefficient data, it is believed that the preflight measurements of force data with angle of attack was good. A correction of the method used to determine the effective heat shield cant angle lowers the predicted preflight values of L/D by about 0.015 degree, however, the angle of attack at which the reentry configuration trims is considered to be the primary cause of the low L/D indications. This could result from either a poor determination of the vehicle c.g. location or from poor determination of the aerodynamic reentry moments.

The c.g. determination has been established as accurate. As a result an investigation into the latter cause, and a determination of requirements for additional wind-tunnel testing are being made.

The L/D_{trim} is estimated to be L/D = 0.28 $\pm$ 0.02 with corresponding values of α trim = 161.8 degrees $\pm$ 1.4 for the Mach number region of M = 6 to M = 25.

TABLE 6.7-I.- AERODYNAMIC CHARACTERISTICS SUMMARY FOR MACH NUMBERS GREATER THAN 6.0

Source	Lift-to-drag ratio			Total angle of attack, deg			Remarks
	Maximum	Nominal	Minimum	Minimum	Nominal	Maximum	
Preflight aerodynamics	0.375	0.335	0.295	[a](155.4)	158.2	(160.8)	These data should be reduced in L/D by 0.015 degree due to a revision of the effective heat shield cant angle.
G & N data	0.288	0.27	0.249	161.1	162	162.9	Data for decelerations greater than 0.5g. No data used after T+5022 sec.
Trajectory simulations	--	0.28	--	--	(161.8)	--	L/D used as a constant for entire reentry phase
Structure accelerometer data	(0.446)	(0.322)	(0.232)	(150.2)	(159)	(165.1)	Data inconclusive due to poor instrumentation accuracy. Data above 0.8g used.
Aerothermodynamic data	(0.336)	(0.306)	(0.284)	158	160	162	In section 7.3, angle of attack is referred to the center of the aft heat shield.
Current estimates	0.30	0.28	0.26	(160.4)	(161.8)	(163.2)	To be updated with a revision to the Apollo Mission Data Specification documents.

[a]Data in parentheses were obtained using figure 6.7-1.

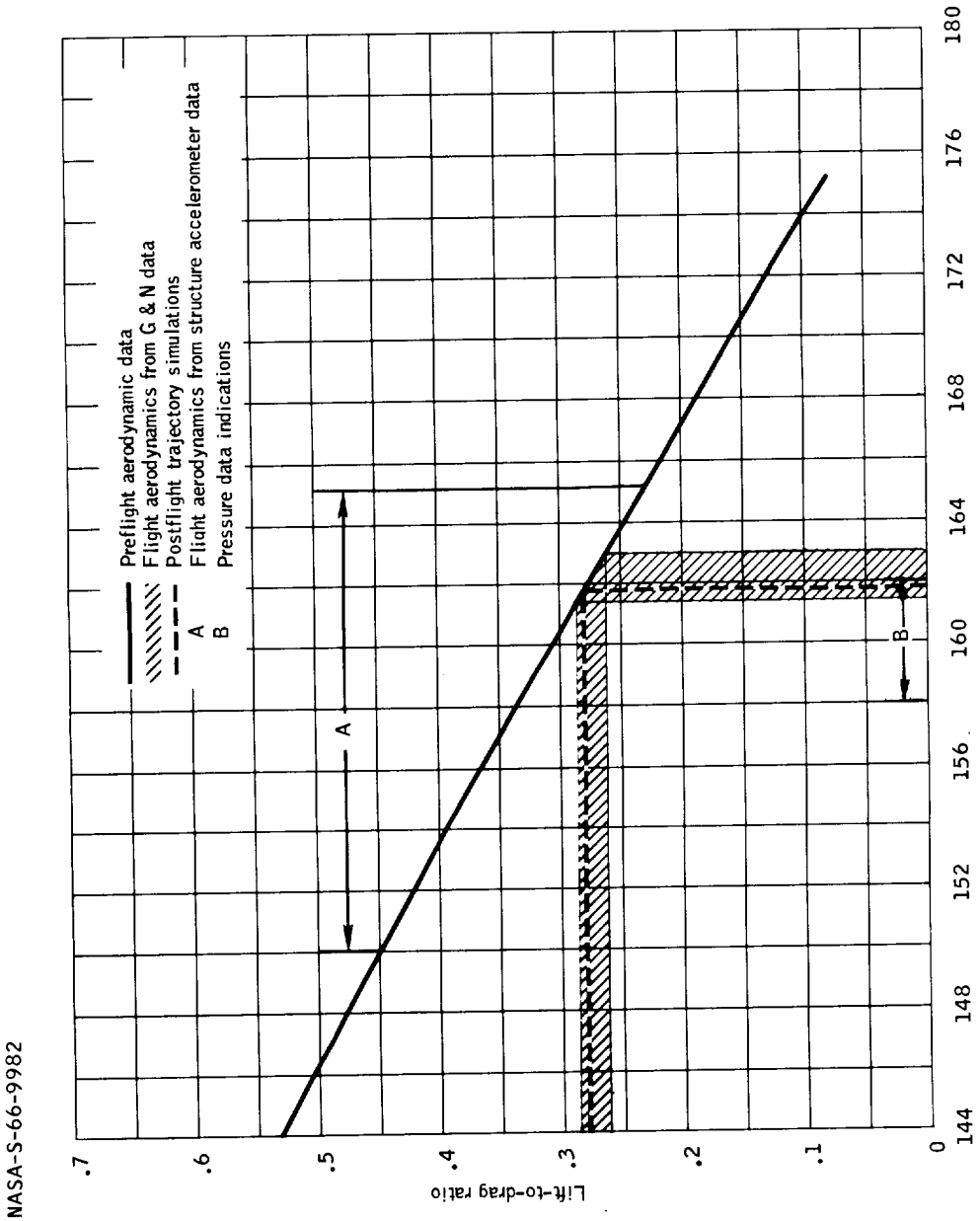

NASA-S-66-9982

Figure 6.7-1.- Summary of reentry aerodynamic characteristics for Mach numbers greater than 6.0, Mission AS-202.

7.0 SPACECRAFT SUBSYSTEMS

7.1 Structural Dynamics

Summary.- The spacecraft vibration data indicated that the spacecraft structure performed as required in the launch environment.

During lift-off, the command module (CM) longitudinal vibration reached a maximum of 1.2g peak to peak. The predominant frequency of oscillation was approximately 10 cps, which corresponded closely to the experimentally determined test vehicle first longitudinal frequency of 9.7 cps. This oscillation damped out within 2 seconds. The structural loads resulting from this oscillation are discussed in section 7.2.

Maximum vibration of the CM inner structure occurred between T+84 and T+88 seconds. Vibration levels, corrected for dynamic pressure, were lower than the established Apollo vibration criteria. The display panel (DSKY) vibration was approximately 6 dB lower than its established criteria. During the launch and service propulsion subsystem (SPS) burn periods, the service module (SM) interior structure vibration data showed very small response. The SPS engine dome longitudinal vibration was between 15g and 25g peak to peak during steady state SPS burn, which is considered normal.

During lift-off, the spacecraft lunar module adapter (SLA) skin panel vibration levels compared very favorably to that of spacecraft 009 and the established vibration criteria.

Crew related dynamics and crew station acoustics are discussed in sections 7.18.3 and 7.18.4, respectively.

Low-frequency accelerations.-

X-axis acceleration: The spacecraft 011 CM was instrumented with an accelerometer, measurement CK0004A, to measure low-frequency accelerations in the X-axis of the vehicle. This measurement was ranged from -2g to +10g with the data recorded at a rate of 100 samples per second.

Figures 7.1-1 and 7.1-2 present the acceleration spectral density for the lift-off and supersonic periods of flight. Measurement CK0004A showed maximum oscillatory accelerations occurring at lift-off and during the period between T+84 and T+87 seconds (max. q). The maximum peak-to-peak values were 1.2g at lift-off and 2.0g between T+84 and T+87 seconds. The predominant frequency of vibration at lift-off was

approximately 10 cps, which corresponds closely to the experimentally determined test vehicle first longitudinal frequency of 9.7 cps. This oscillation was excited by the thrust buildup characteristics of the S-IB engine and subsequent release. The oscillation damped out completely within 2 seconds. An oscillograph record of this acceleration during the lift-off period is shown in figure 7.1-3.

Y-axis and Z-axis accelerations: The spacecraft 011 CM was instrumented with two accelerometers, measurements CK0005A and CK0006A, which measured low frequency accelerations in the Y-axis and Z-axis of the vehicle, respectively. These measurements were ranged $\pm$2g with the data recorded at a rate of 100 samples per second.

Maximum accelerations during the lift-off period were approximately 1.0g peak to peak for both Y- and Z-axes (section 7.2). The predominant frequencies of vibration at lift-off in the Y-axis were approximately 1.4, 2.25, and 4 cps. These correspond closely to the first three experimental bending frequencies of 1.34, 2.27, and 4.2 cps. An oscillation of 8 cps was also excited. The excitation of these frequencies is believed caused by the unsymmetric thrust buildup of the S-IB engines (fig. 7.1-4). Excitation of the second and third bending modes was also noted during the period between T+84 and T+87 seconds. During this period maximum oscillations (due to high wind shear) were 1.5g and 0.6g peak to peak for the Y- and Z-axes, respectively. Acceleration spectral density plots are shown in figures 7.1-5 through 7.1-8. Resulting loads during this period are discussed in section 7.2.

Command module vibrations.- The CM was instrumented with seven accelerometers, the details of which are given in table 7.1-I. Accelerometer CK0043D measured vibration in the Z direction of a cable tray, mounted on secondary structure within the lower equipment bay aft section. Accelerometers CK0501D, CK0502D, and CK0503D measured vibrations of the center and left-hand display panels. Accelerometers CG6001D, CG6002D, and CG6003D measured vibration of the guidance and navigation (G & N) navigation base.

Acceleration time histories in figures 7.1-9 through 7.1-15 show that maximum vibrations occurred between T+80 and T+90 seconds. This time period corresponds to a Mach number range of 1.67 to 2.15.

Comparison of the spectral distribution of measurement CK0043D with the spectral distribution for Mission AS-201 showed that the spacecraft 011 vibration level in the lower equipment bay was approximately one-half of the spacecraft 009 level due to lower response in the 150- to 300-cps frequency range. The spectral distributions for the display panel accelerometers showed considerably lower energy than had been anticipated based on the CM vibration criteria (fig. 7.1-16).

The spectral density plots for the navigation base accelerometers (figs. 7.1-17 through 7.1-19) give a good indication of the natural frequencies of the shock isolation system used to mount the navigation base to the CM.

Service module vibrations.- The SM was instrumented with nine accelerometers to measure vibrations of the aft helium tank mount in the longitudinal and radial directions, the aft bulkhead at the base of the sector II oxidizer tank in the directions of the X- , Y- , and Z-axes, radial beams 2 and 5 in the SM circumferential direction, and the SM engine dome in the longitudinal and radial directions. Details of instrument location, range, and frequency response are given in table 7.1-I.

Rms time histories of aft helium tank mount vibration are shown in figures 7.1-20 and 7.1-21 for the longitudinal and radial directions. Figures 7.1-22 and 7.1-23 present the acceleration spectral densities for these two measurements during lift-off. Although no vibration specification was available for the tank mount, the vibration energy appeared to be of the approximate level of the helium tank vibration criteria, with the exception of the large energy contents between 20 and 25 cps. No problems were encountered as a result of this vibration level; however, the helium tank had not been qualified to this input level. In order to insure that the tank would not be damaged as a result of this energy, a sinusoidal vibration qualification test in this frequency range or a detailed analysis should be considered.

Data from measurements SK0242A, SK0243A, and SK0244A, which measured aft bulkhead vibration in the directions of the X- , Y- , and Z-axes at the base of the sector II oxidizer tank, were not useable except at lift-off, between T+20 and T+30 seconds, and during transonic flight. These measurements recorded such small response during the remainder of the launch phase that data were within a factor of 2 of the telemetry channel noise, causing a degradation of the data. The low frequency response of the telemetry channels assigned to these measurements was a major cause of the small response measured, since the majority of vibratory energy was expected to occur at frequencies much higher than the available channel cutoff frequency of 59 cps. Acceleration spectral densities for lift-off are shown in figures 7.1-24 through 7.1-26. The 10-cps longitudinal oscillation noticed in the low frequency vibration data from CK0004A was also recorded by SK0242A.

Data from measurements SA0993D and SA0994D, which measured vibration of radial beams 2 and 5 in the SM circumferential direction, showed low response, with a maximum response of 4g rms occurring during transonic flight.

During the flight of spacecraft 002, abnormally high vibration levels were experienced on the inner cap of beam 5 after T+38 seconds. Studies indicated static failure of the lateral support braces due to the pressure differential during transonic flight. A transitory pressure differential was experienced in this flight regime due to reattachment of the aerodynamic flow at the shoulder of the spacecraft, and this phenomenon was characterized by the drop in fluctuating pressure and vibration levels at Mach 0.85. On spacecraft 011, a modification was made to the braces at $X_S 277$ to allow for SM expansion during transonic flight. A comparison of beam vibration levels for spacecraft 011 and spacecraft 002 is shown in figure 7.1-27, which indicated low levels for spacecraft 011 and that the modification was satisfactory.

Measurements SK0020D and SP1031D, which measured vibration of the SPS engine dome in the longitudinal and radial directions, respectively, showed ignition vibration of 100g and 94g peak to peak on the first burn, 162g and 100g peak to peak on the second burn, 175g and 87g peak to peak on the third burn, and 262g and 137g peak to peak on the fourth burn, respectively. The average steady state burn vibrations for the longitudinal and radial directions were 15g to 25g peak to peak and 13g to 15g peak to peak, respectively. Acceleration spectral density of the SPS steady state burn is shown in figures 7.1-28 and 7.1-29. No significant increase in CSM vibration was noted during the SPS burns. The vibration levels on the SPS engine were approximately the same as those experienced during ground tests and were considered normal.

In general, the magnitude of all vibration data in the SM was low during the transonic, supersonic, and SPS burn periods. No structural problems are anticipated from these low levels.

SLA vibrations.- Three accelerometers were located on the SLA to measure radial vibration of the skin panels. Measurement locations are given in table 7.1-I. These accelerometers, AK0250D, AK0251D, and AK0252D, were ranged $\pm$100g with frequency responses of 160, 220, and 330 cps, respectively.

A comparison of dynamic pressure, Mach number, and time for spacecraft 011 and spacecraft 009 is shown in figures 7.1-30 and 7.1-31. Although spacecraft 011 had slightly higher dynamic pressures than spacecraft 009, as shown in figures 7.1-30 and 7.1-31, the vibration levels were approximately the same for both flights. Acceleration spectral densities for spacecraft 011 SLA shell panel vibrations are

compared with spacecraft 009 data and vibration criteria in figures 7.1-32 and 7.1-33. These data were not corrected for the differences in dynamic pressure.

TABLE 7.1-I.- STRUCTURAL DYNAMIC MEASUREMENTS, MISSION AS-202

Measurement number	Measurement description	Range	Response	Location	Channel or track
Low frequency accelerations					
CK0004A	X-axis CM accelerometer	-2 to +10g	100 s/s	X_C78, Y0, Z21	PCM
CK0005A	Y-axis CM accelerometer	±2g	100 s/s	X_C78, Y0, Z21	PCM
CK0006A	Z-axis CM accelerometer	±2g	100 s/s	X_C78, Y0, Z21	PCM
Command module vibrations					
CK0043D	Lower equipment bay Z-axis	±75g	600 cps	X_C30.83, Y0.5, Z39.5	FQTR 7, 8
CK0501D	Center display panel, normal vibration	±75g	2500 cps	Center display panel	FQTR 5
CK0502D	Center display panel, 17 deg from Z-axis	±75g	2500 cps	Center display panel	FQTR 13
CK0503D	Left hand display panel, normal vibration	±75g	2500 cps	Left-hand display panel	FQTR 9
CG6001D	Navigation base, roll vibration	±50g	2500 cps	Navigation base	FQTR 2
CG6002D	Navigation base, yaw vibration	±50g	2500 cps	Navigation base	FQTR 4
CG6003D	Navigation base, pitch vibration	±50g	2500 cps	Navigation base	FQTR 6
Service module vibrations					
SK0020D	SPS engine dome, longitudinal vibration	±250g	5 kc	SPS engine dome	FQTR 1
SP1031D	SPS engine dome, radial vibration	±250g	5 kc	SPS engine dome	FQTR 3
SK0240D	Aft helium tank mount, X-axis vibration	±20g	110 cps	X_S286.5, 145°, R22	SMMK 11
SK0241D	Aft helium tank mount, radial vibration	±20g	81 cps	X_S286.5, 145° R22	SMMK 10
SK0242A	Aft bulkhead tank base, X-axis accelerometer	±20g	59 cps	X_S203, Y24, Z-6	SMMK 9
SK0243A	Aft bulkhead tank base, Y-axis accelerometer	±10g	45 cps	X_S203, Y24, Z-6	SMMK 8
SK0244A	Aft bulkhead tank base, Z-axis accelerometer	±10g	35 cps	X_S203, Y24, Z-6	SMMK 7
SA0993D	Radial beam 2, circumferential vibration	±250g	600 cps	X_S275, R22	SMMK 16
SA0994D	Radial beam 5, circumferential vibration	±250g	450 cps	X_S275, R22	SMMK 15
Spacecraft - LM adapter vibrations					
AK0250D	Skin panel, radial vibration	±100g	160 cps	X_A543.25, 304°	SMMK 12
AK0251D	Skin panel, radial vibration	±100g	220 cps	X_A657.5, 236°	SMMK 13
AK0252D	Skin panel, radial vibration	±100g	330 cps	X_A780, 304°	SMMK 14

NASA-S-66-9983

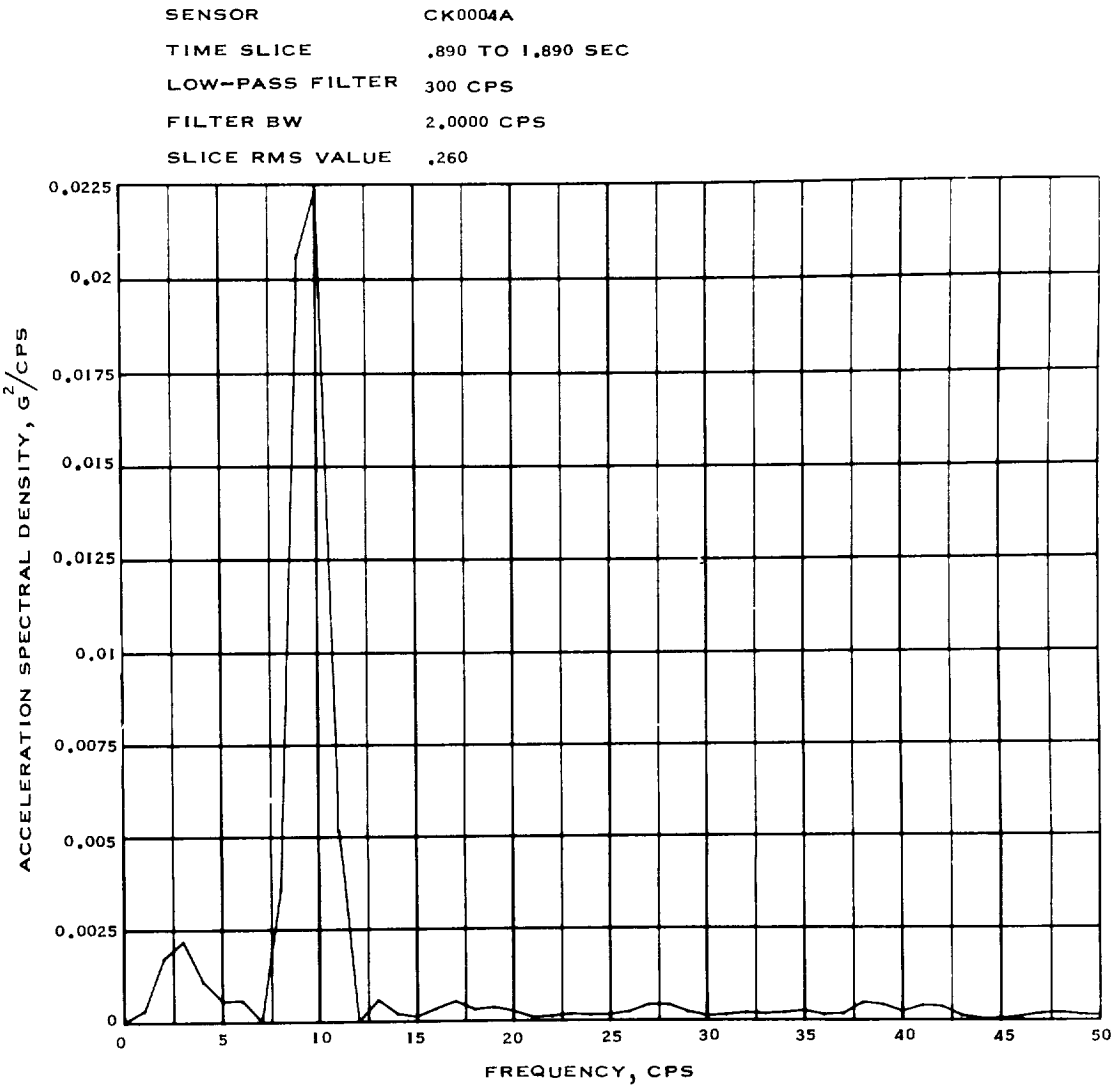

Figure 7.1-1.- Acceleration spectral density of CM X-axis acceleration at lift-off, measurement CK0004A, Mission AS-202.

NASA-S-66-9984

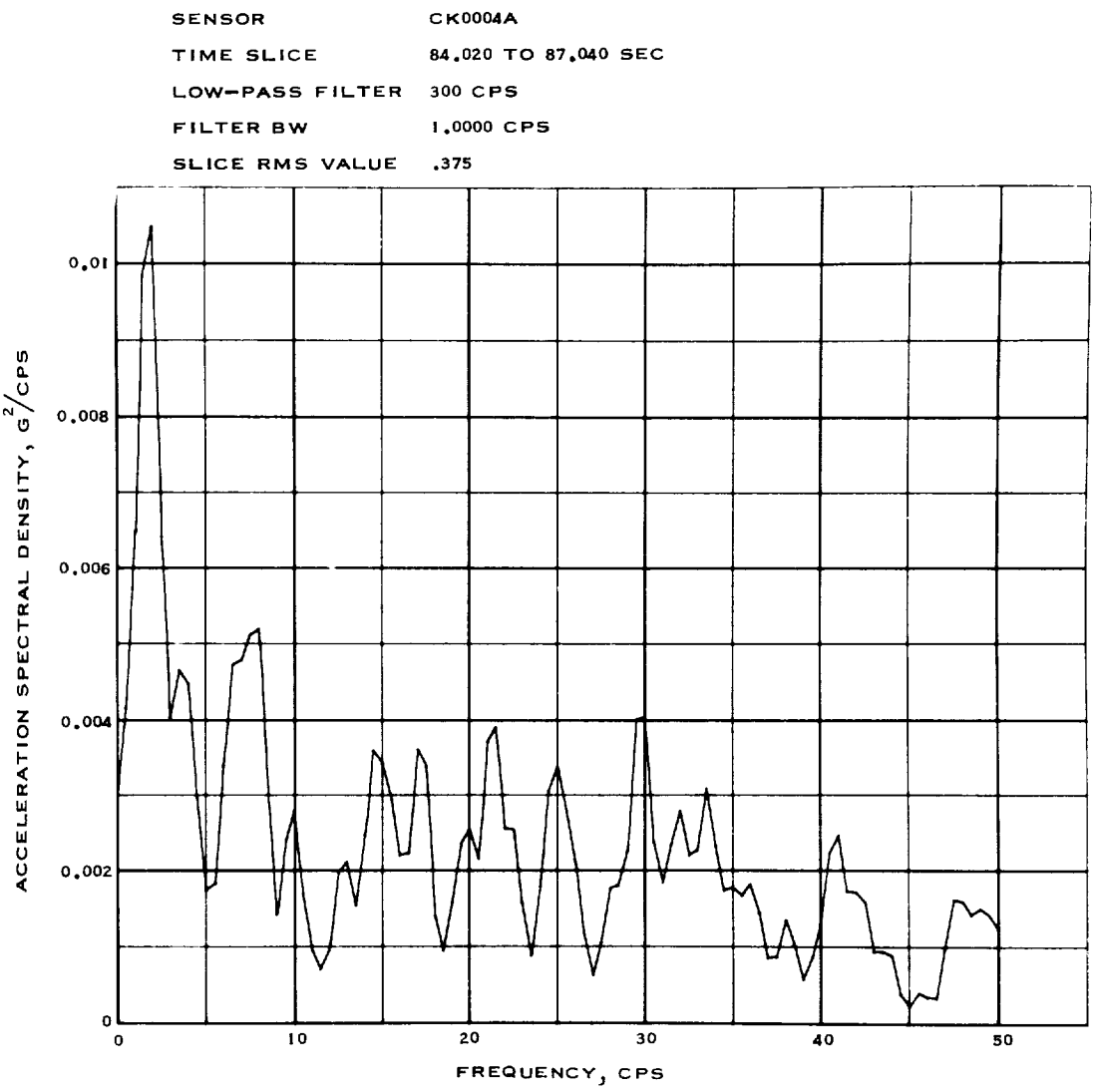

Figure 7.1-2.- Acceleration spectral density of CM X-axis acceleration during period of maximum response, measurement CK0004A, Mission AS-202.

NASA-S-66-9985

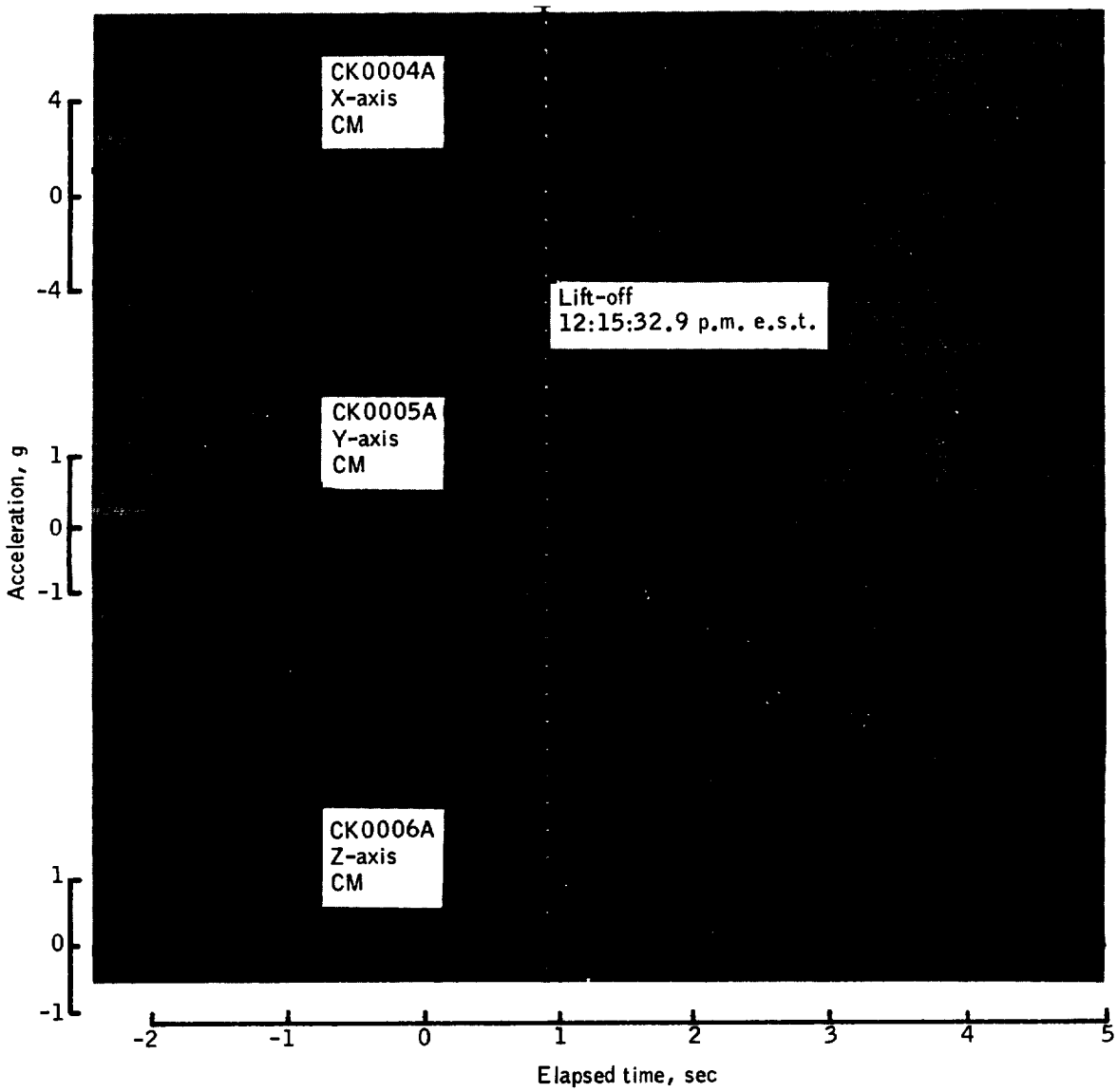

Figure 7.1-3.- CM lift-off accelerations, Mission AS-202.

NASA-S-66-9986

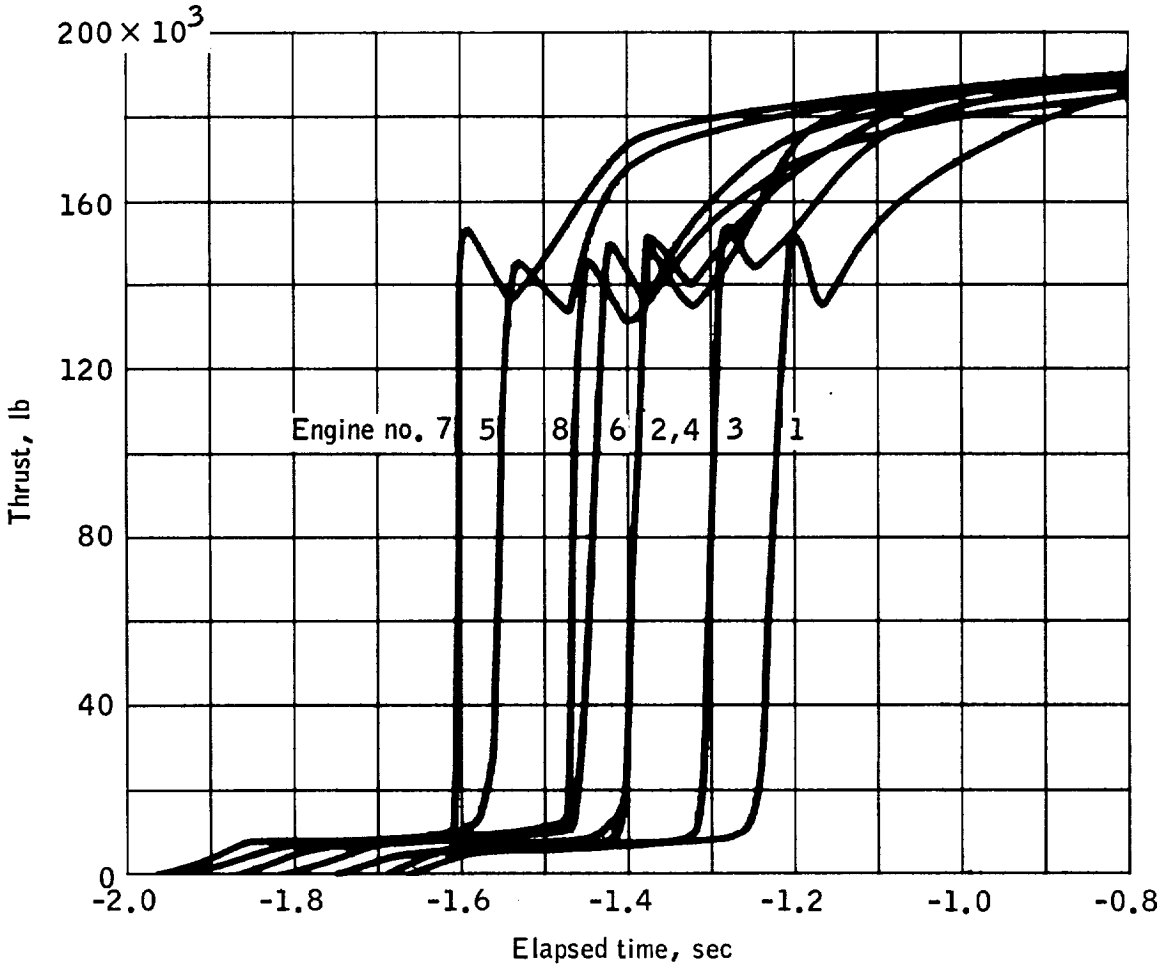

Figure 7.1-4.- S-IB engine thrust buildup, Mission AS-202.

NASA-S-66-9987

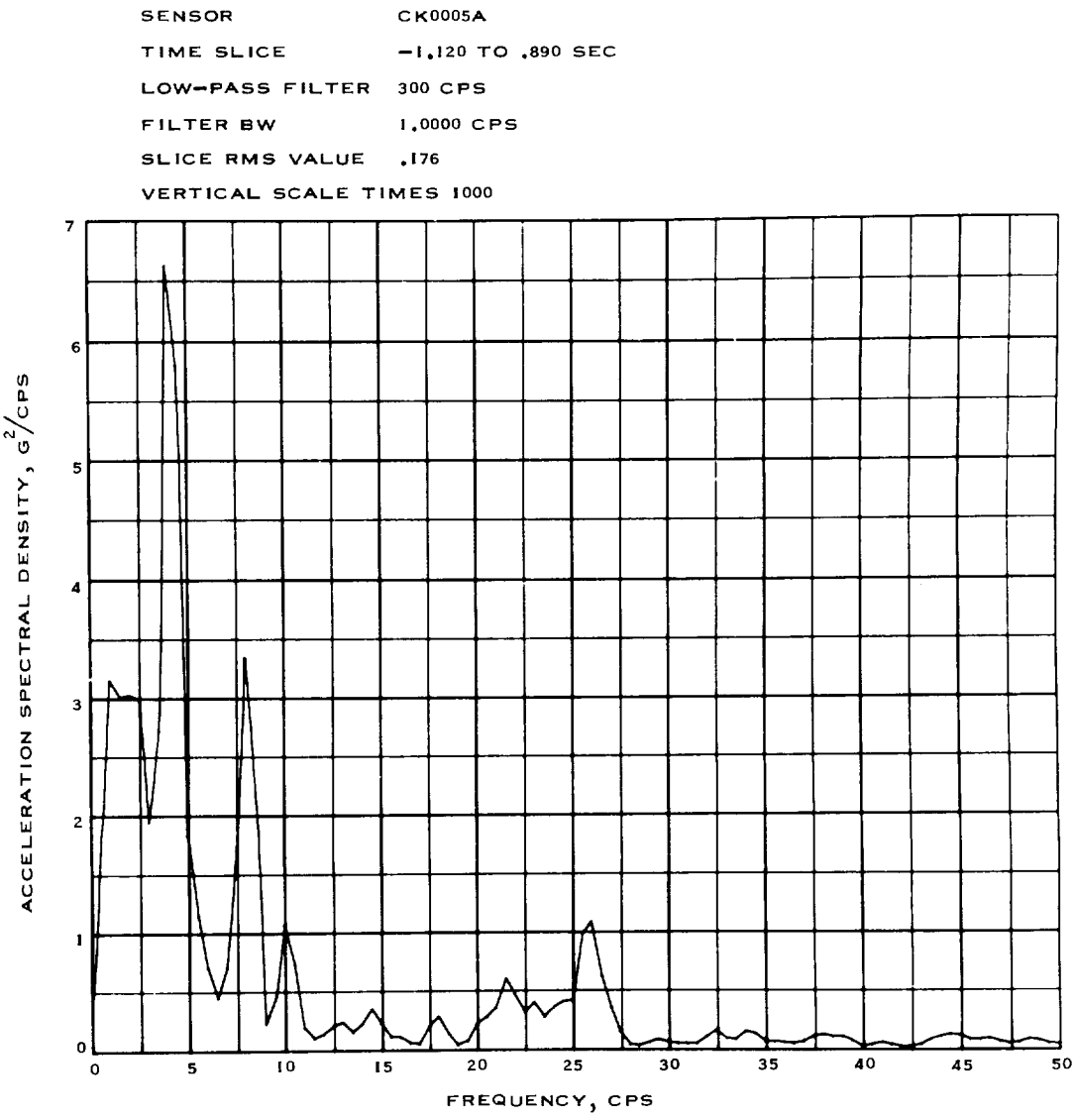

Figure 7.1-5.- Acceleration spectral density of CM Y-axis acceleration at lift-off, measurement CK0005A, Mission AS-202.

NASA-S-66-9988

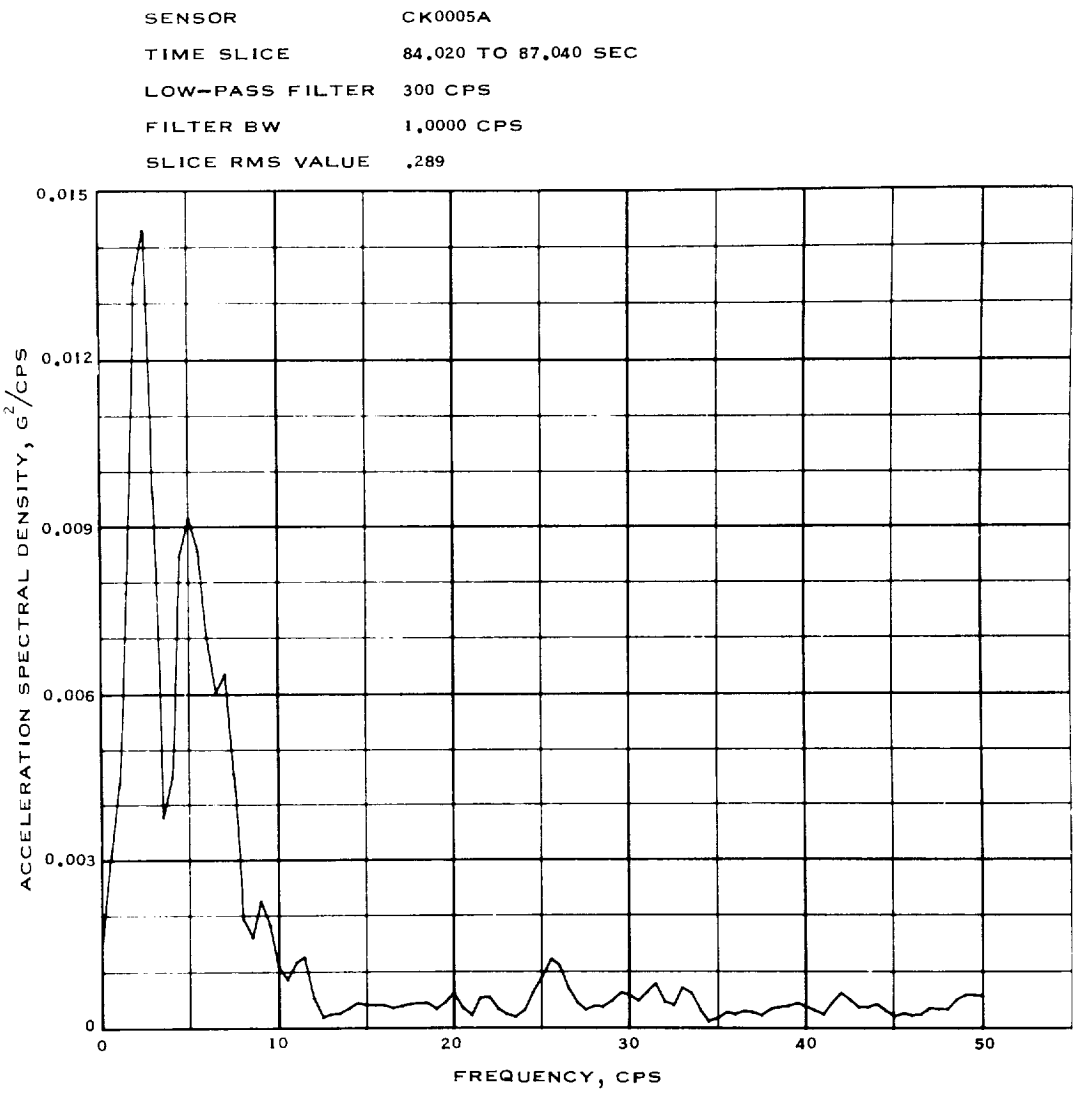

Figure 7.1-6.- Acceleration spectral density of CM Y-axis acceleration during period of maximum response, measurement CK0005A, Mission AS-202.

NASA-S-66-9989

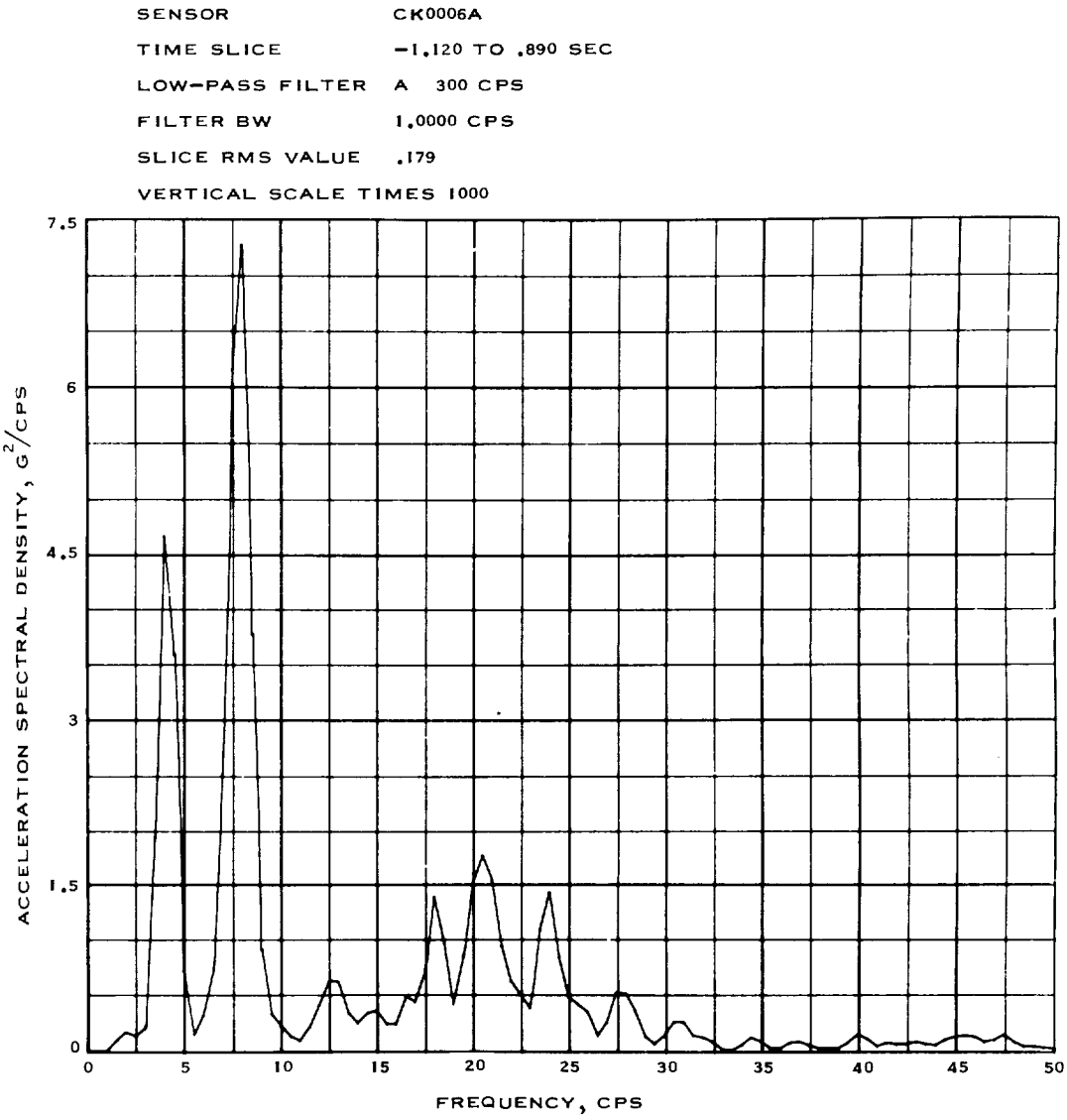

Figure 7.1-7.- Acceleration spectral density of CM Z-axis acceleration at lift-off, measurement CK0006A, Mission AS-202.

NASA-S-66-9990

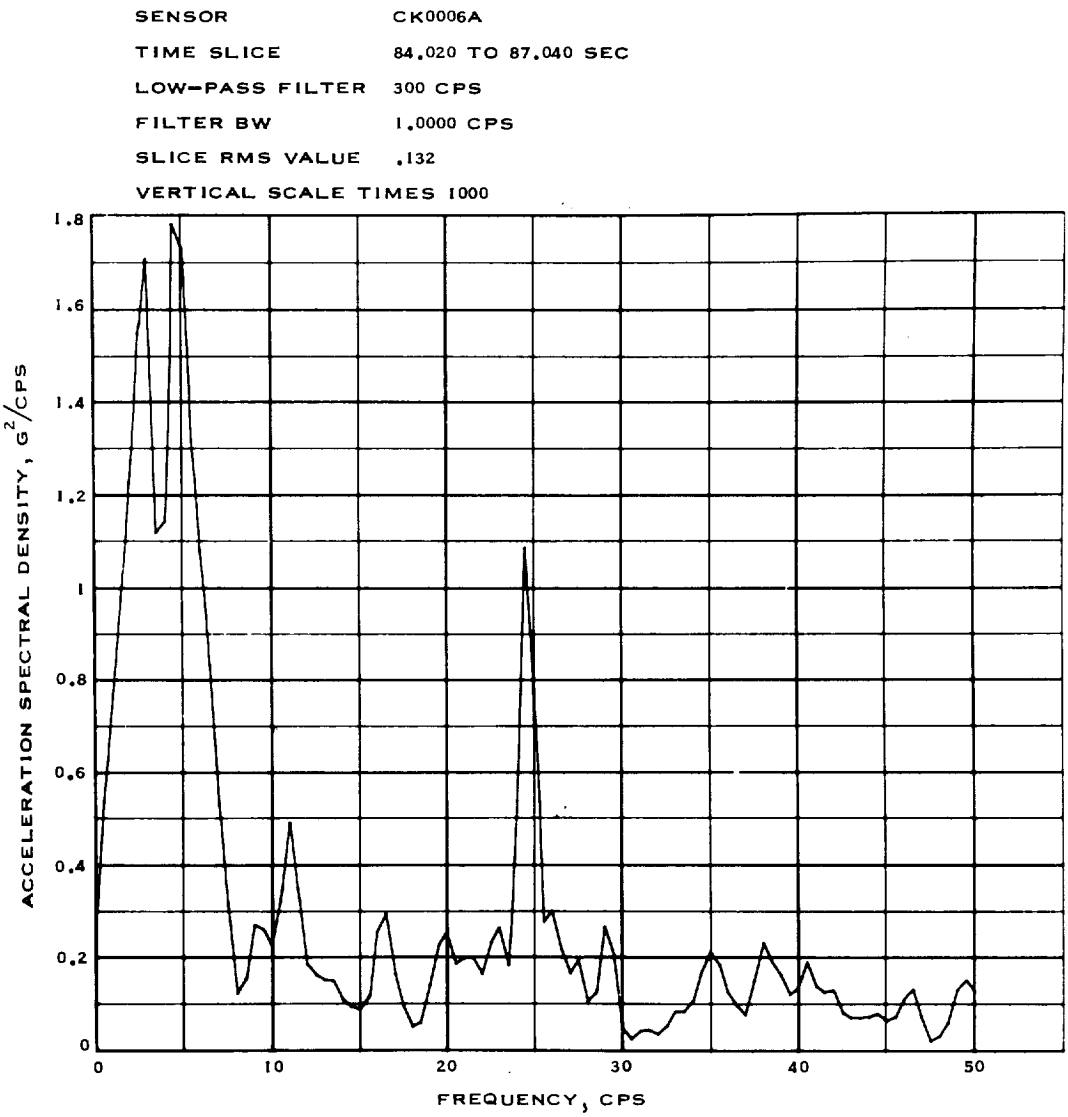

Figure 7.1-8.- Acceleration spectral density of CM Z-axis acceleration during period of maximum response, measurement CK0006A, Mission AS-202.

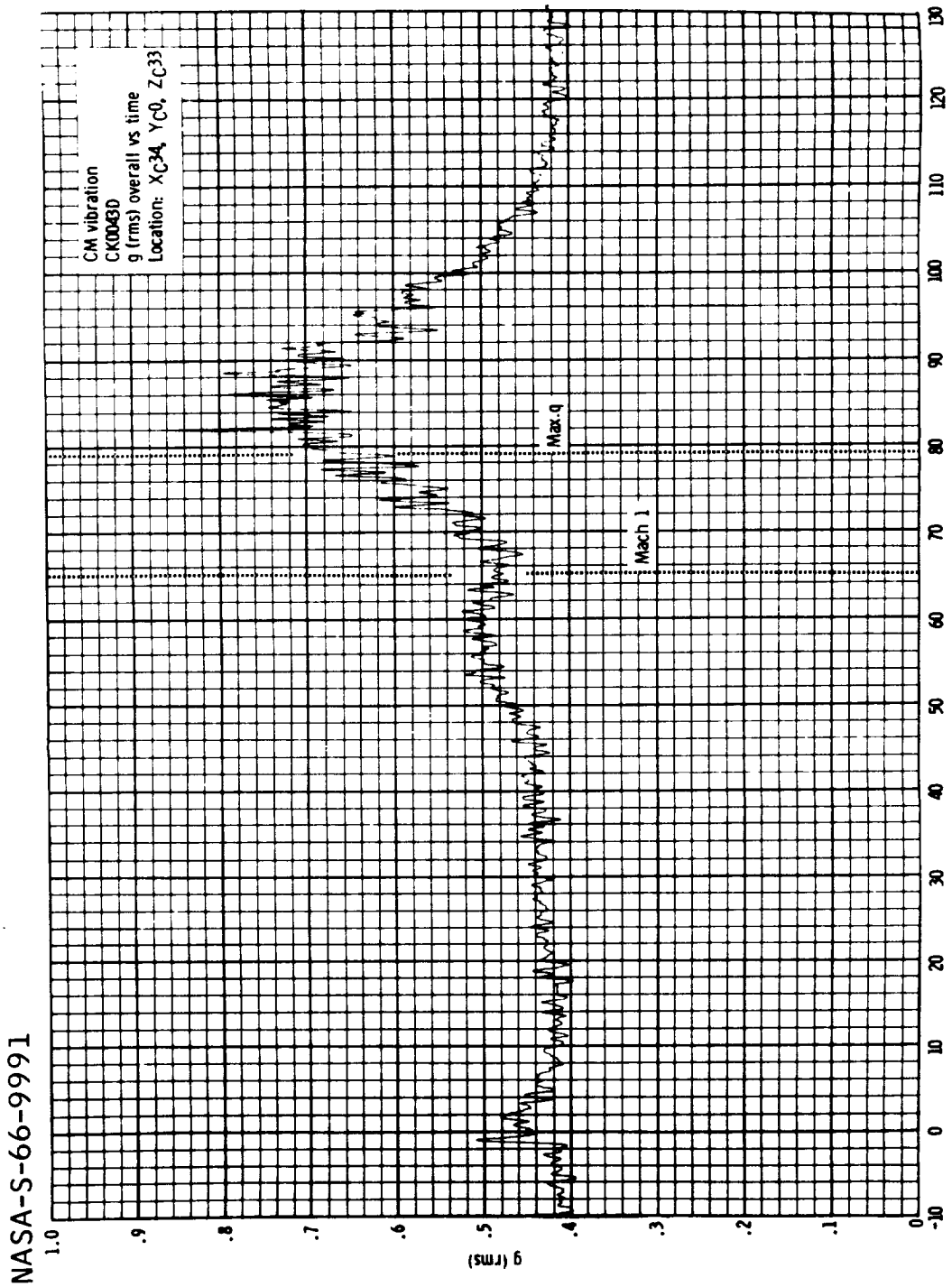

Figure 7.1-9.- Z-axis acceleration rms time history of lower equipment bay cable tray, Mission AS-202.

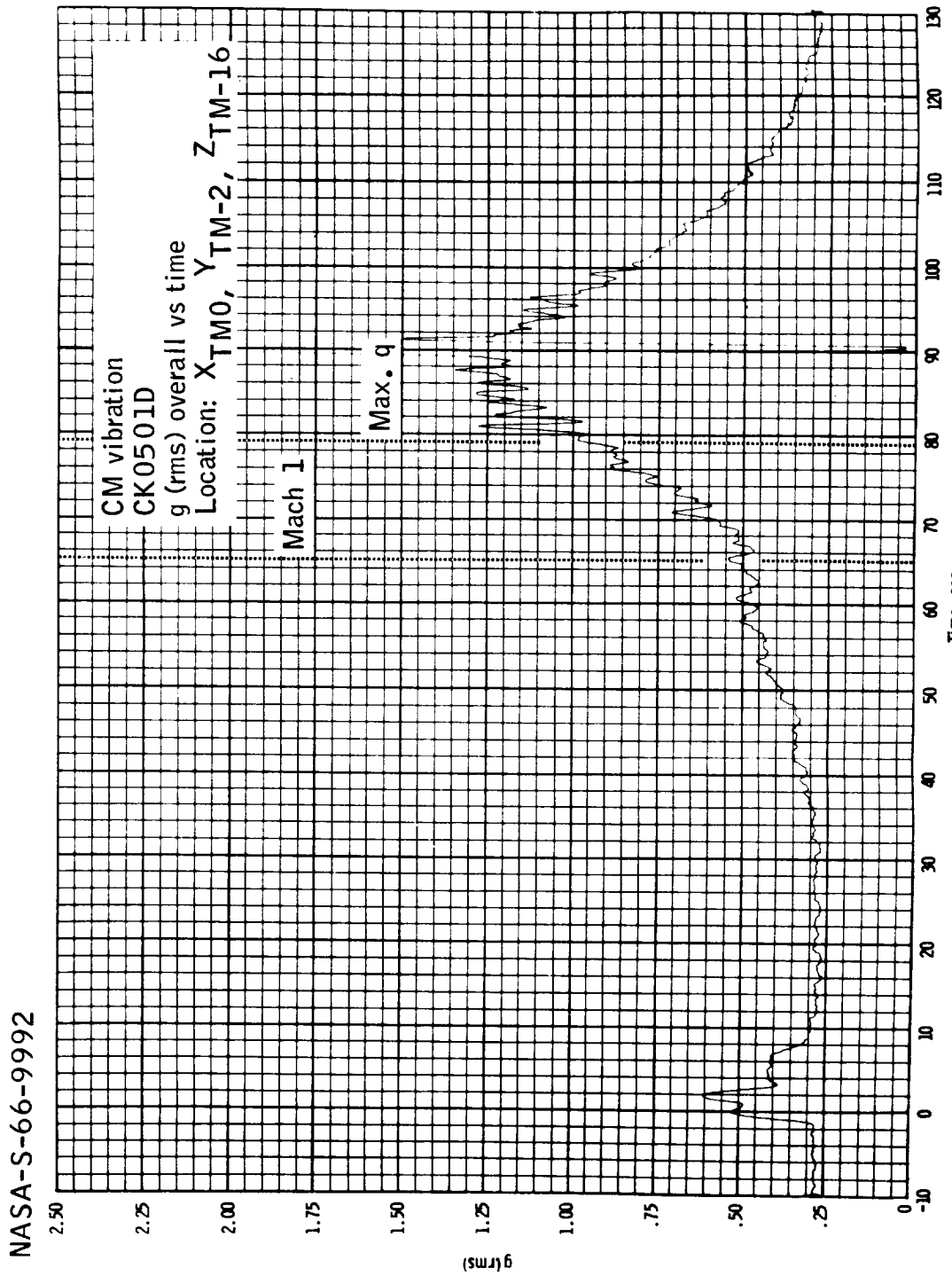

Figure 7.1-10.- Acceleration rms time history of center display panel normal vibration, Mission AS-202.

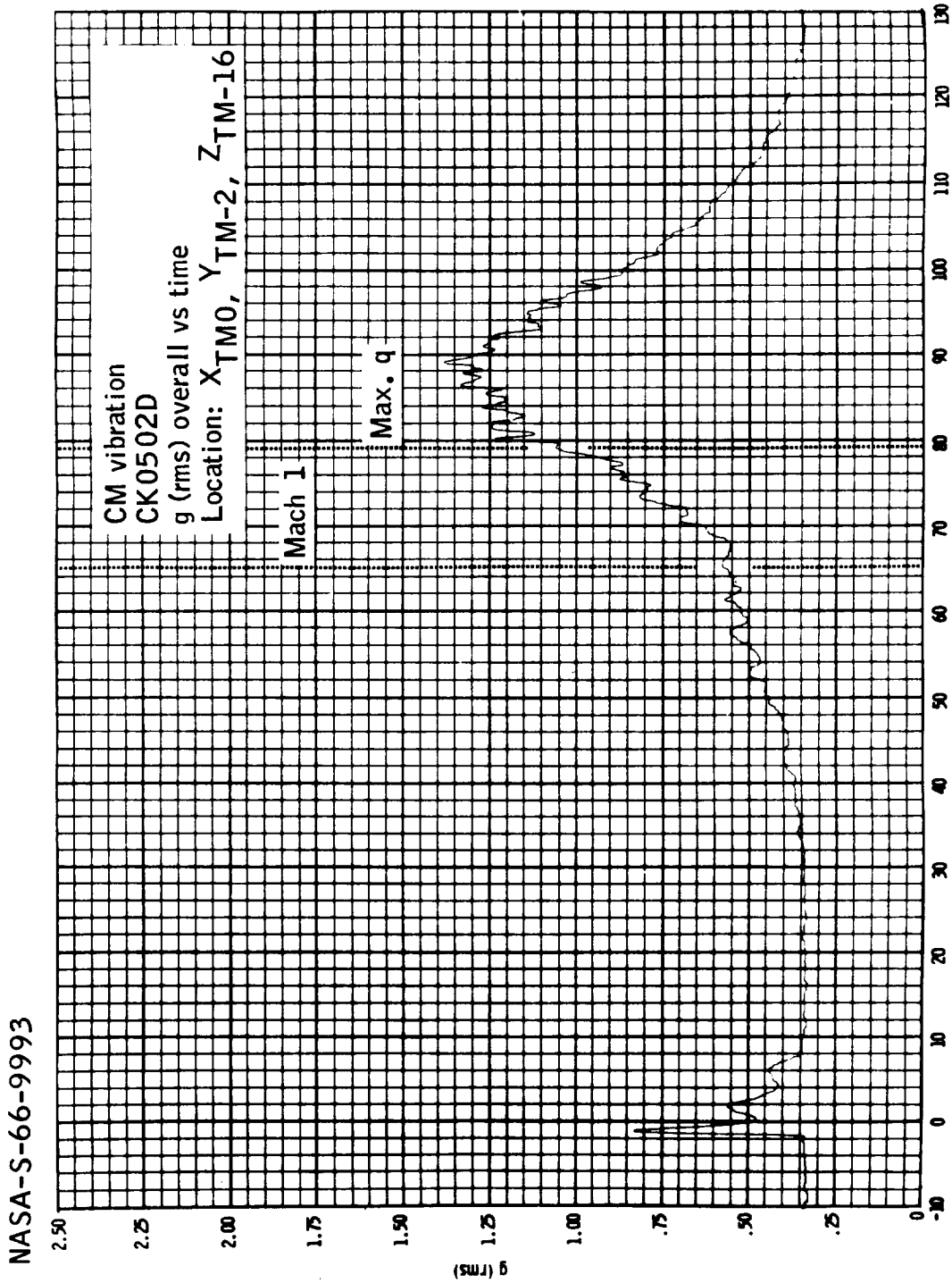

Figure 7.1-11.- Z-axis acceleration rms time history of center display panel, Mission AS-202.

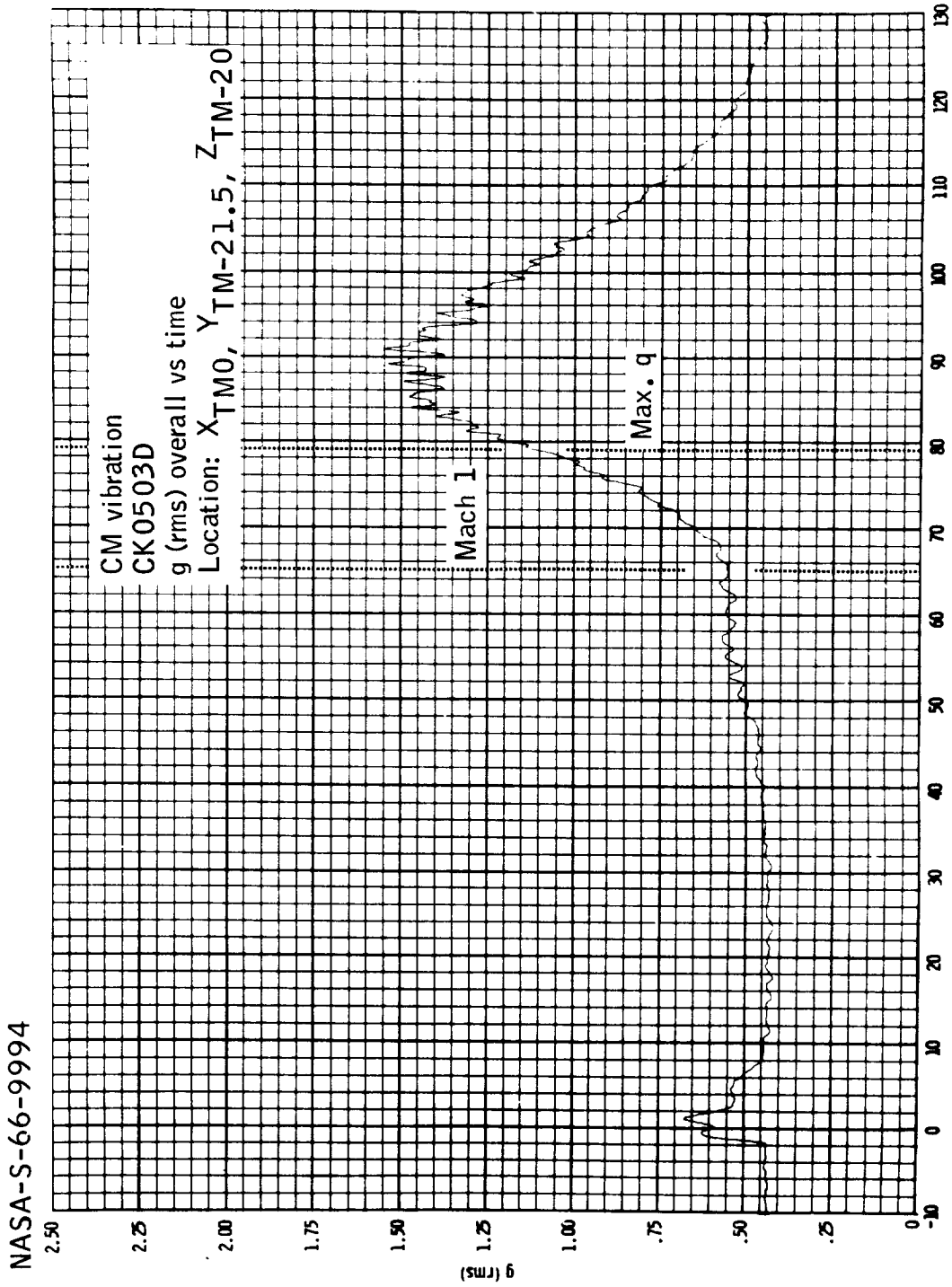

Figure 7.1-12.- Acceleration rms time history of left-hand display panel normal vibration, Mission AS-202.

NASA-S-66-9995

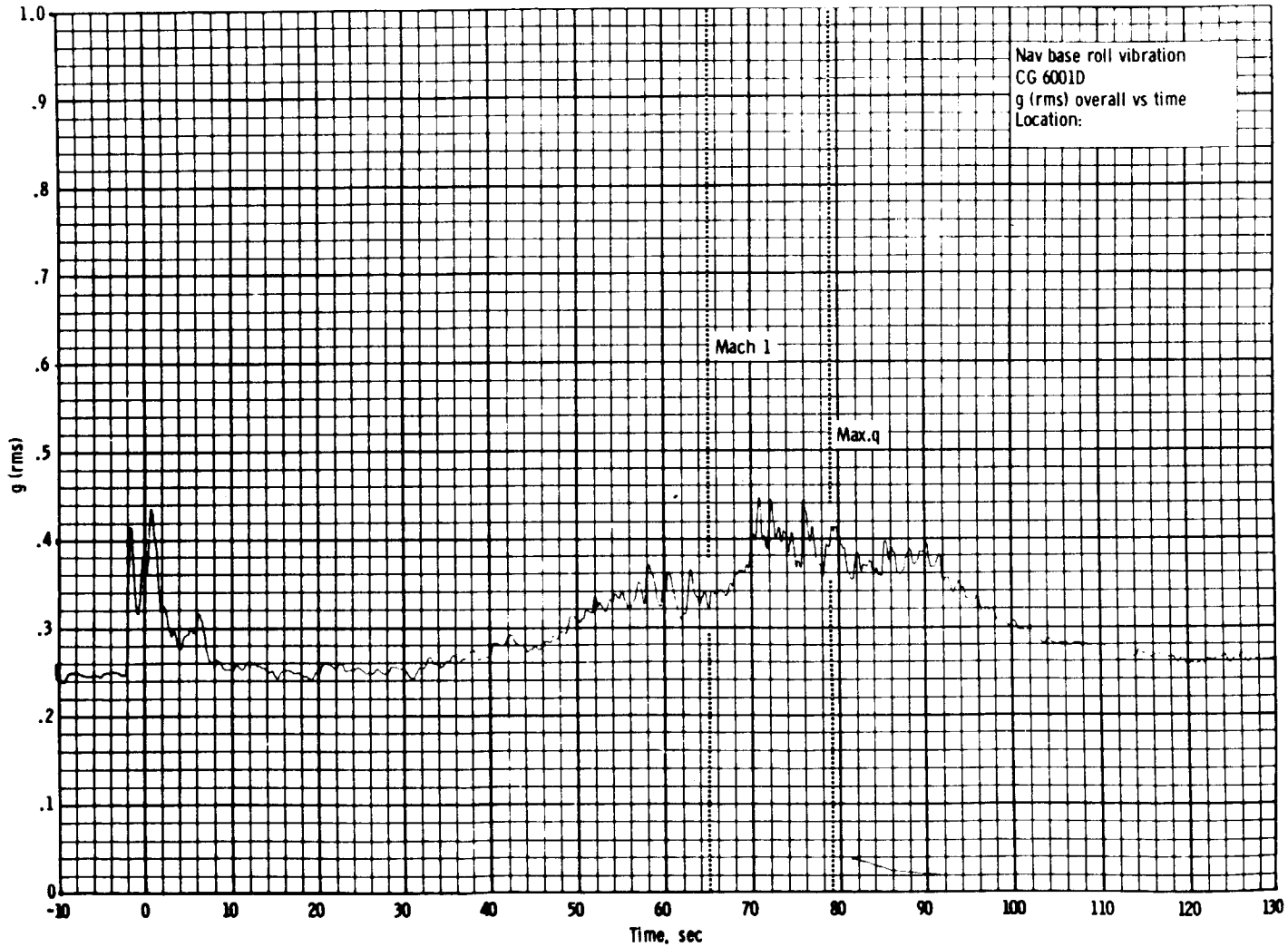

Figure 7.1-13.- Acceleration rms time history of roll axis navigation base vibration, Mission AS-202.

NASA-S-66-9996

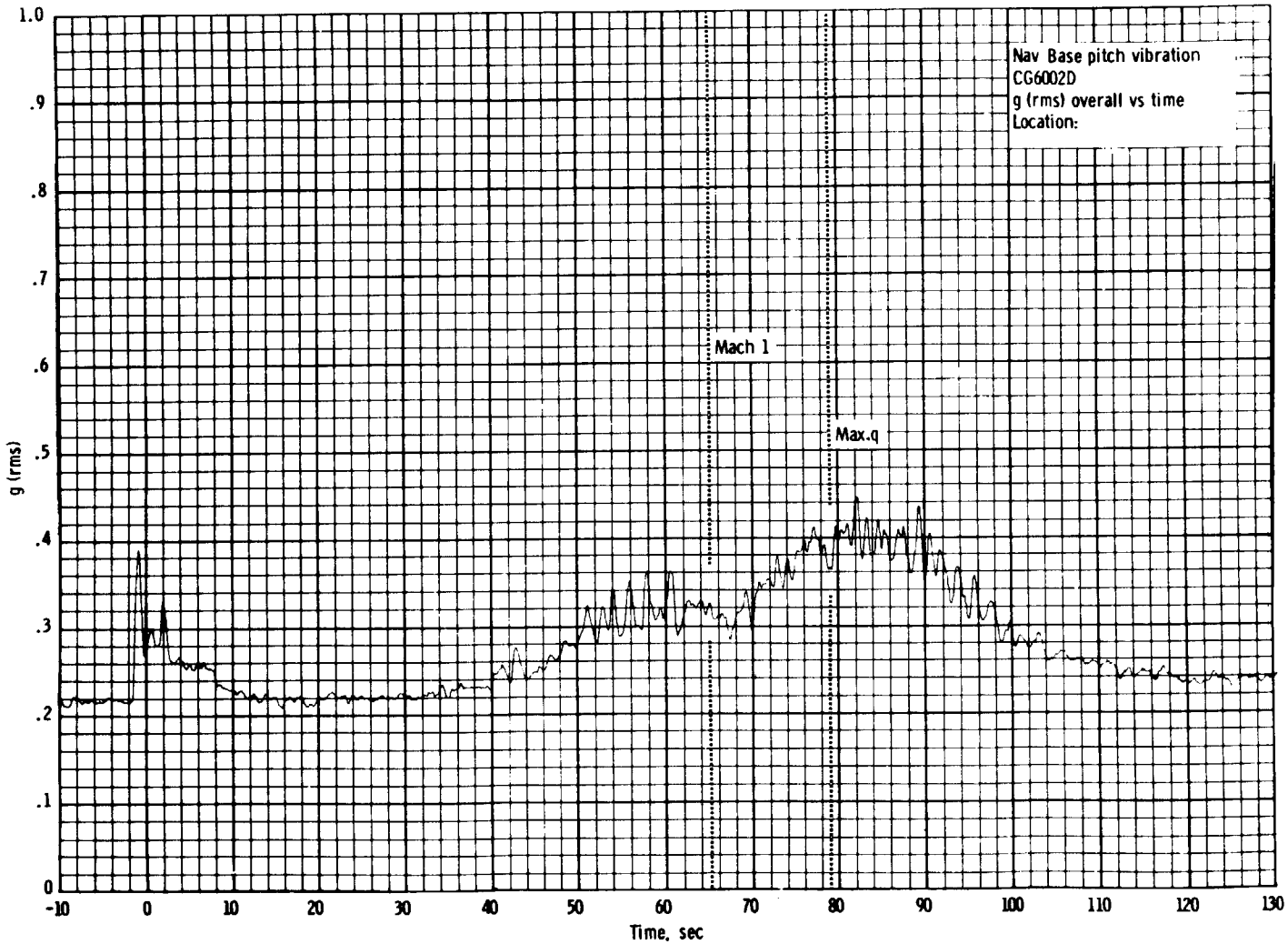

Figure 7.1-14.- Acceleration rms time history of pitch axis navigation base vibration, Mission AS-202.

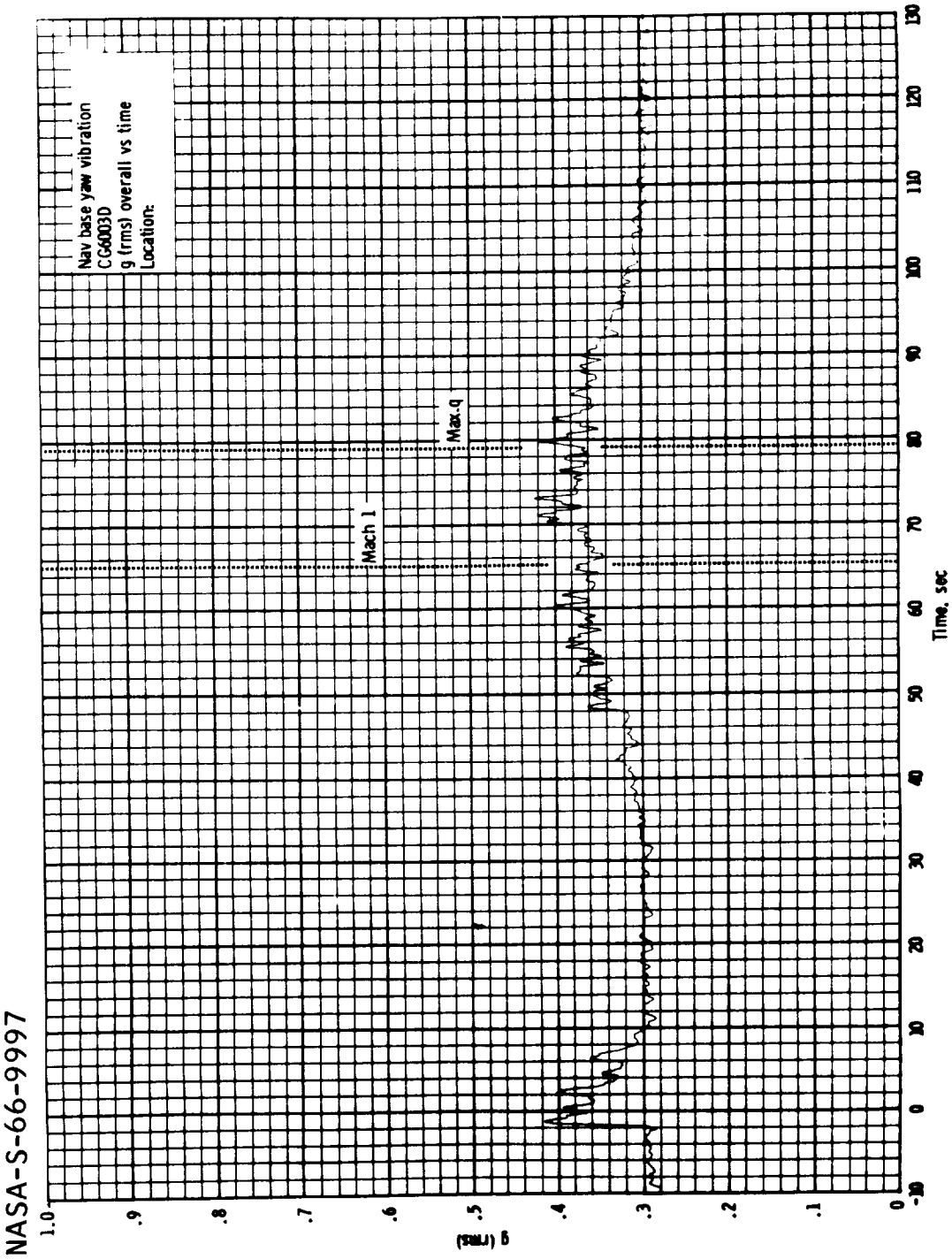

Figure 7.1-15.- Acceleration rms time history of yaw axis navigation base vibration, Mission AS-202.

NASA-S-66-9998

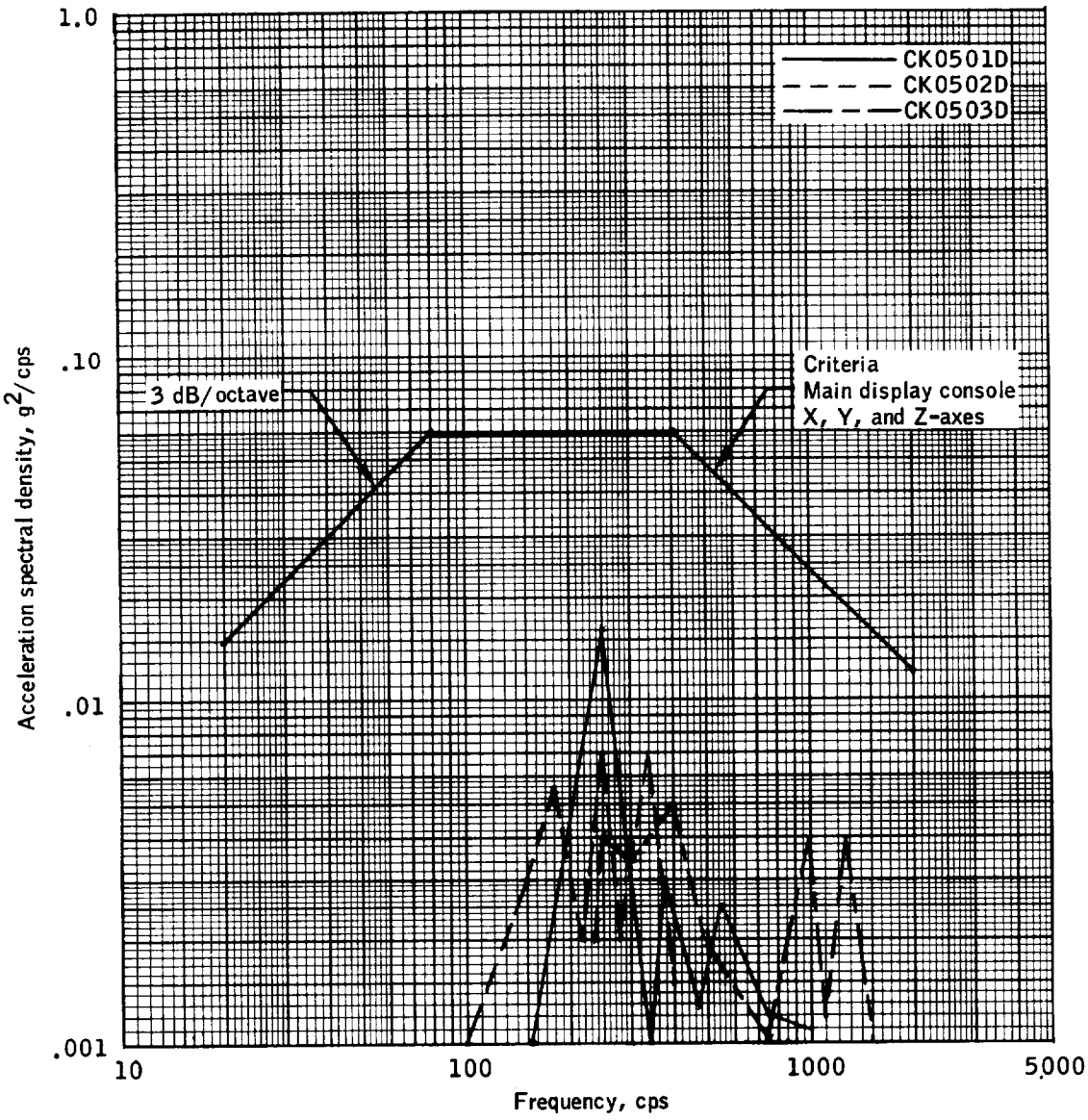

Figure 7.1-16.- Comparison of CM display panel vibration during a period of maximum response with criteria, Mission AS-202.

NASA-S-66-9999

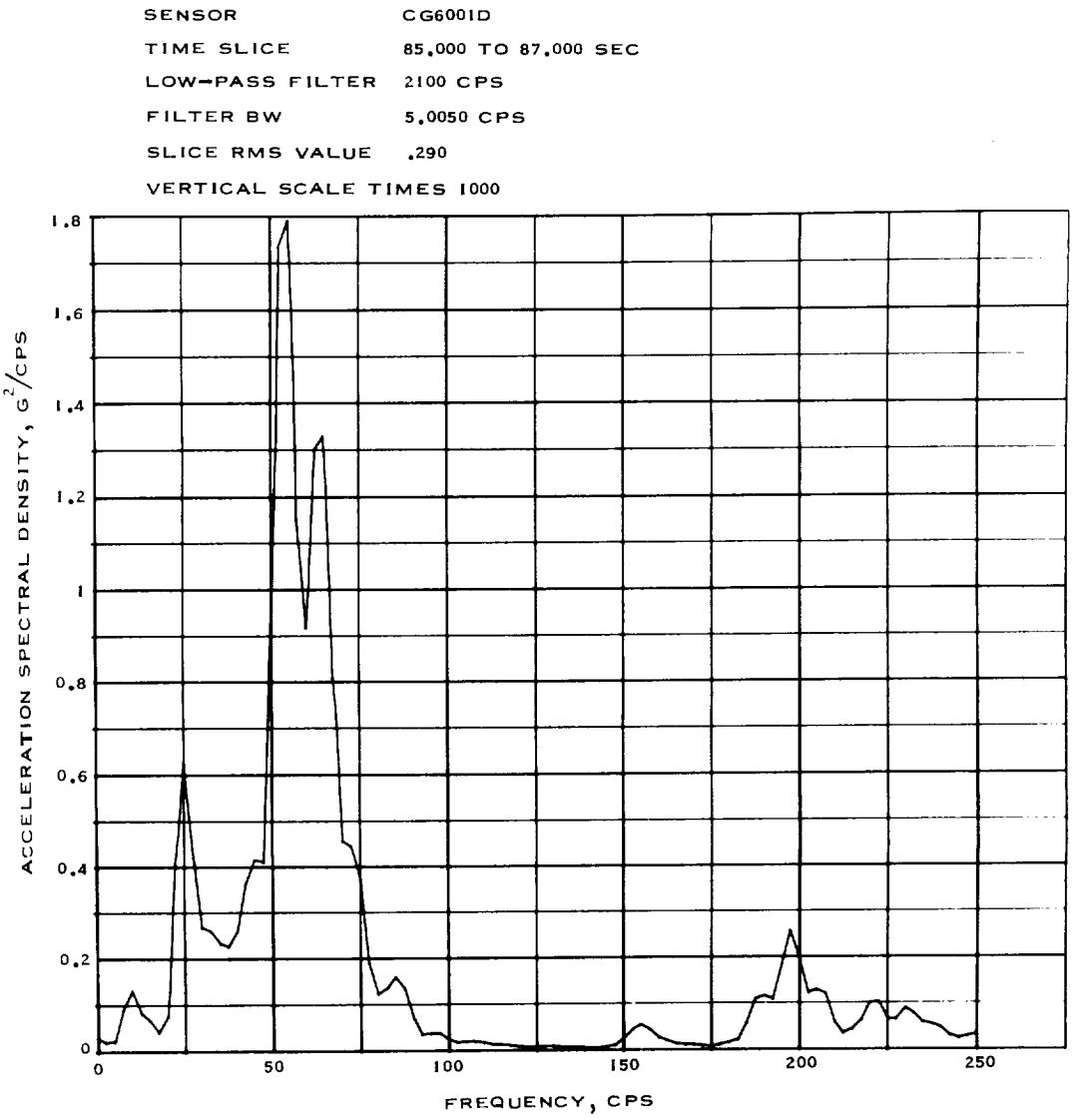

Figure 7.1-17.- Acceleration spectral density of roll axis navigation base vibration during period of maximum response, measurement CG6001D, Mission AS-202.

NASA-S-66-10000

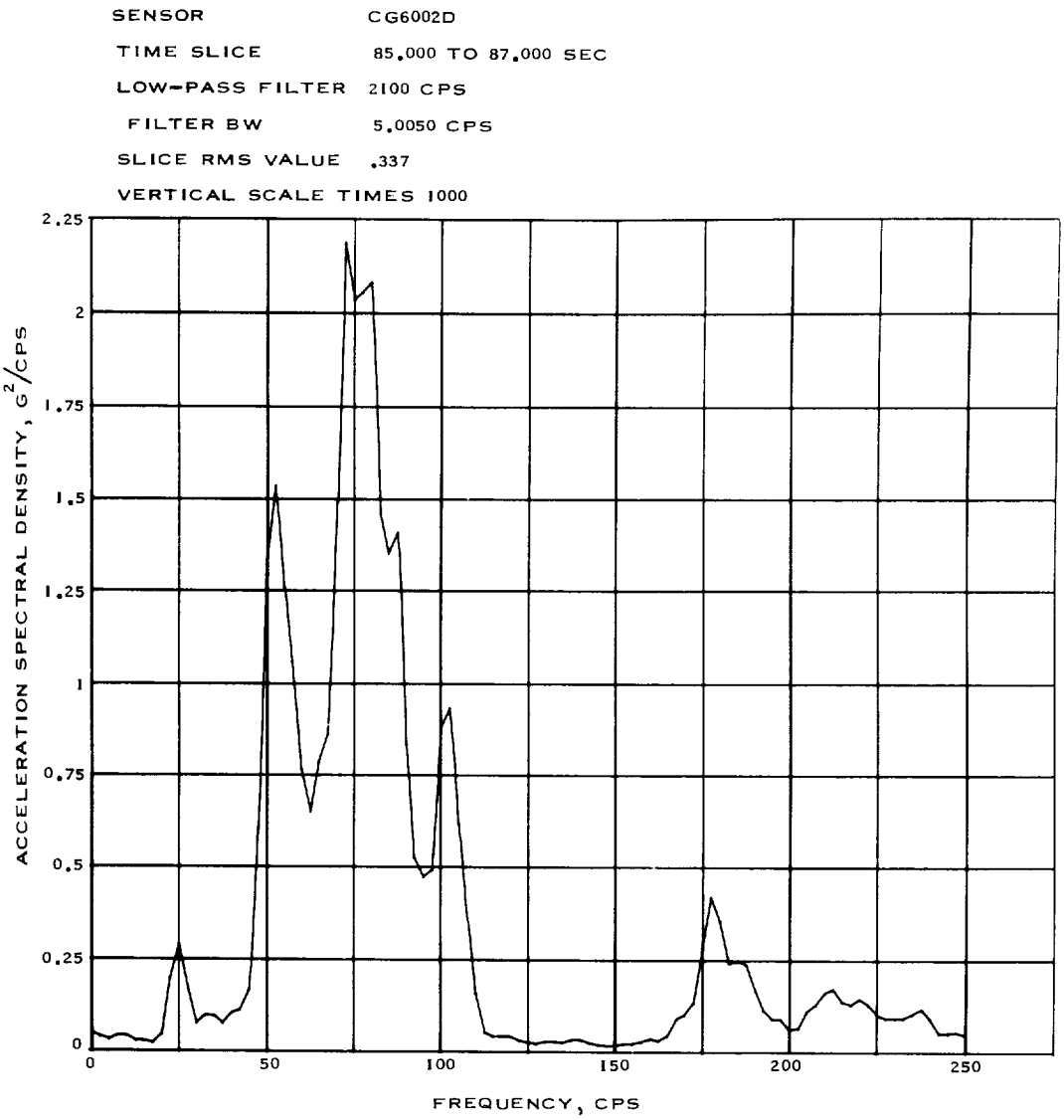

Figure 7.1-18.- Acceleration spectral density of pitch axis navigation base vibration during period of maximum response, measurement CG6002D, Mission AS-202.

NASA-S-66-10001

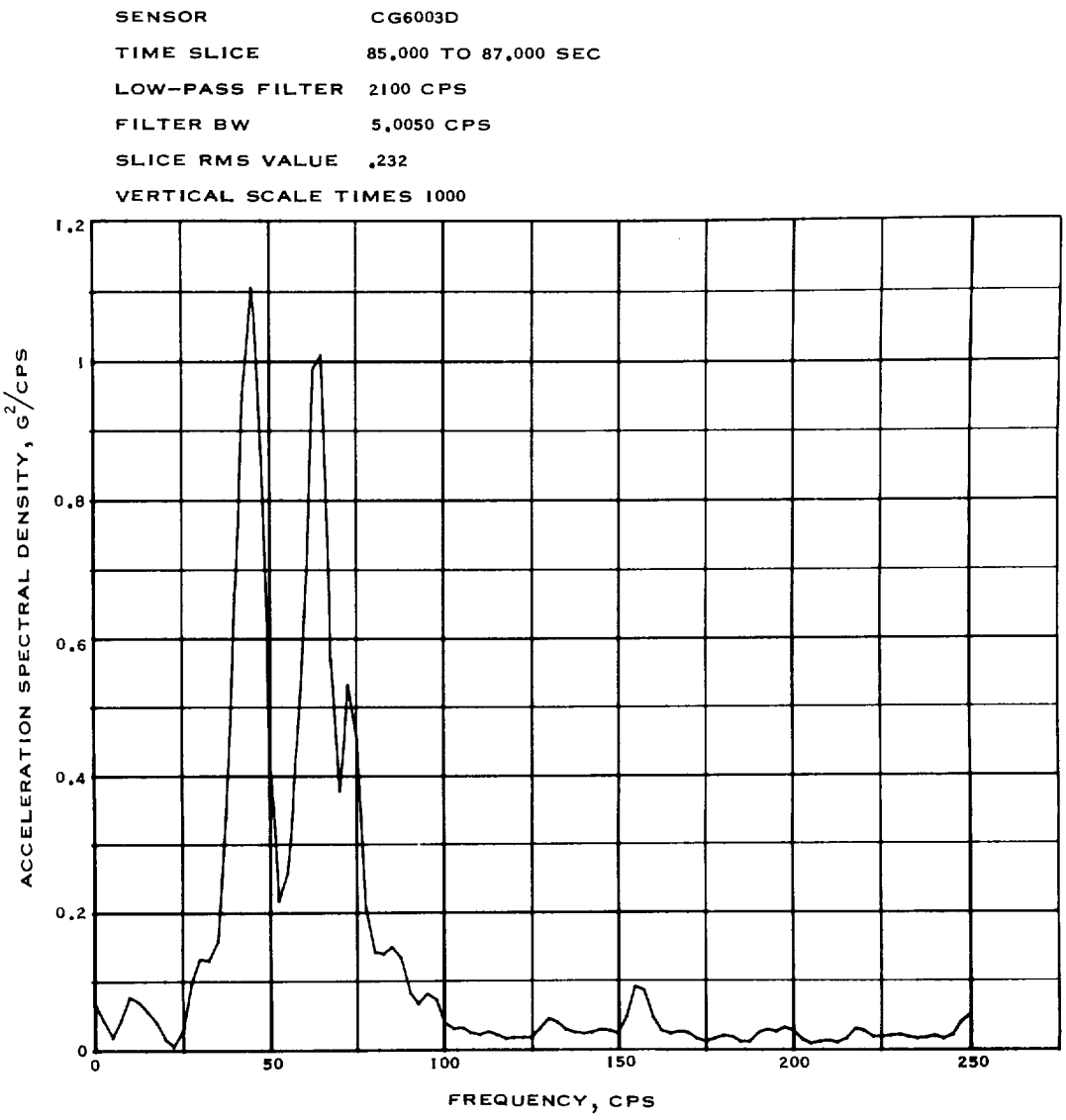

Figure 7.1-19.- Acceleration spectral density of yaw axis navigation base vibration during period of maximum response, measurement CG6003D, Mission AS-202.

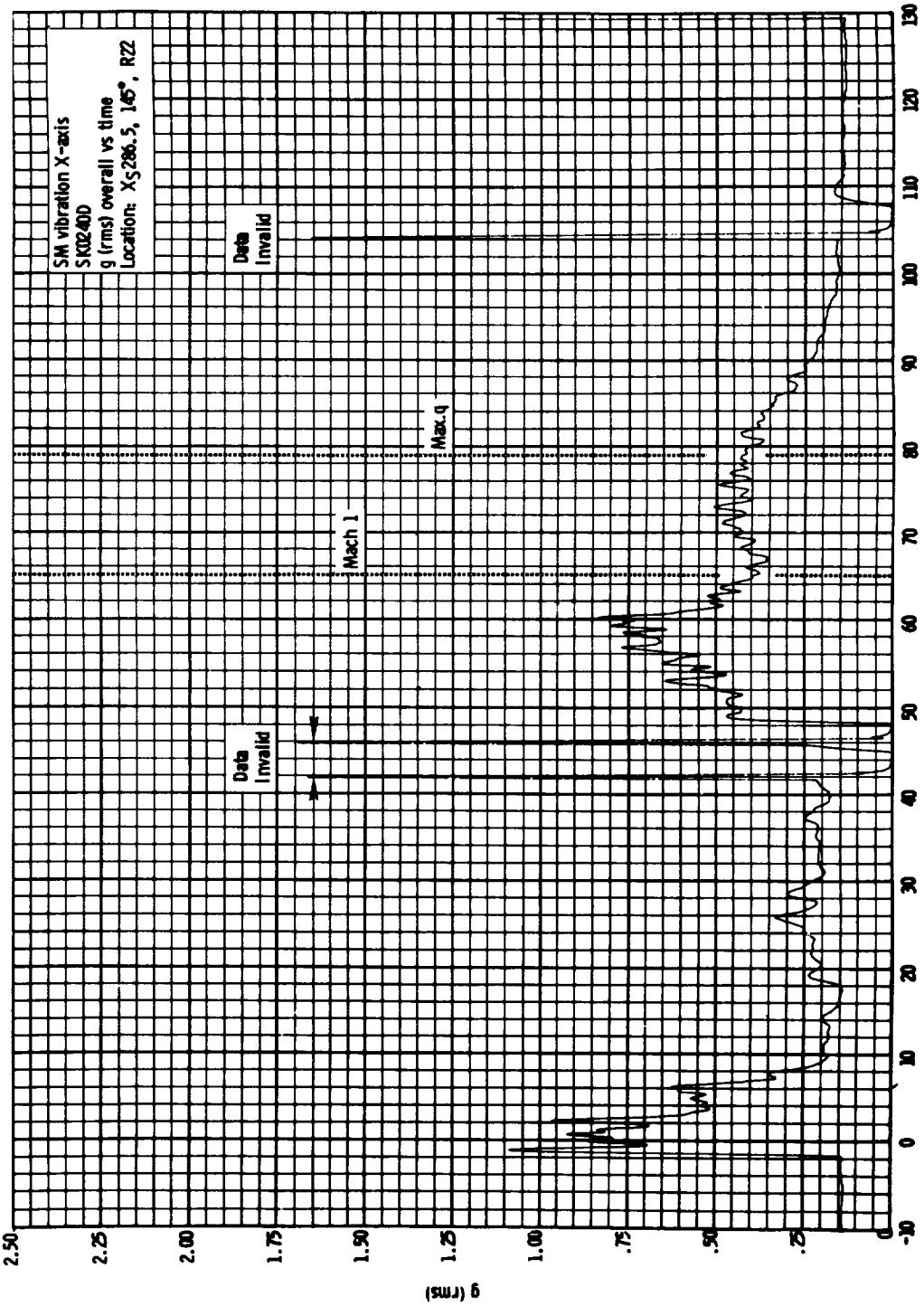

NASA-S-66-10002

Figure 7.1-20.- X-axis acceleration rms time history of aft helium tank mount, Mission AS-202.

NASA-S-66-10003

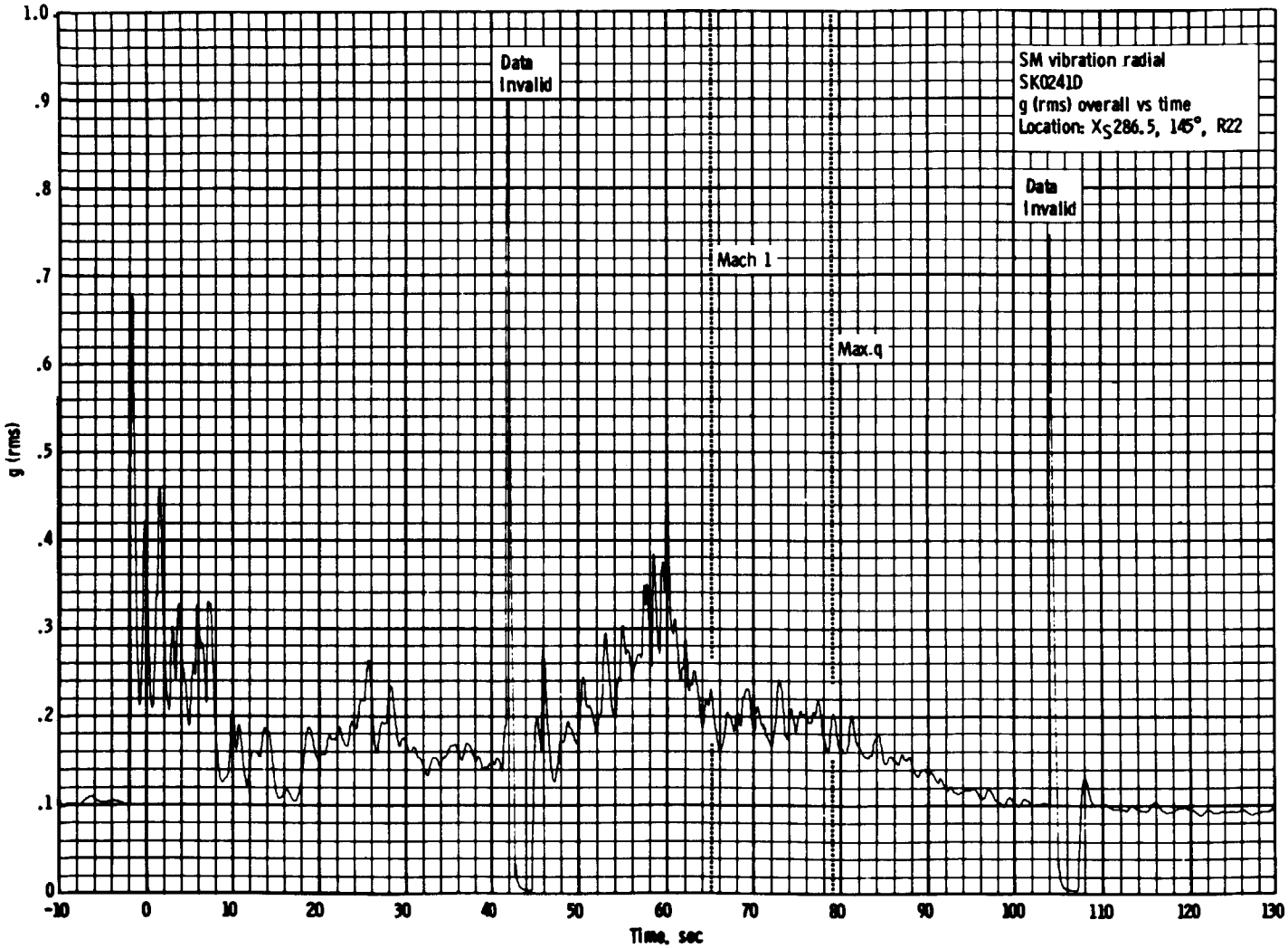

Figure 7.1-21.- Acceleration rms time history of aft helium tank mount radial direction vibration, Mission AS-202.

NASA-S-66-10004

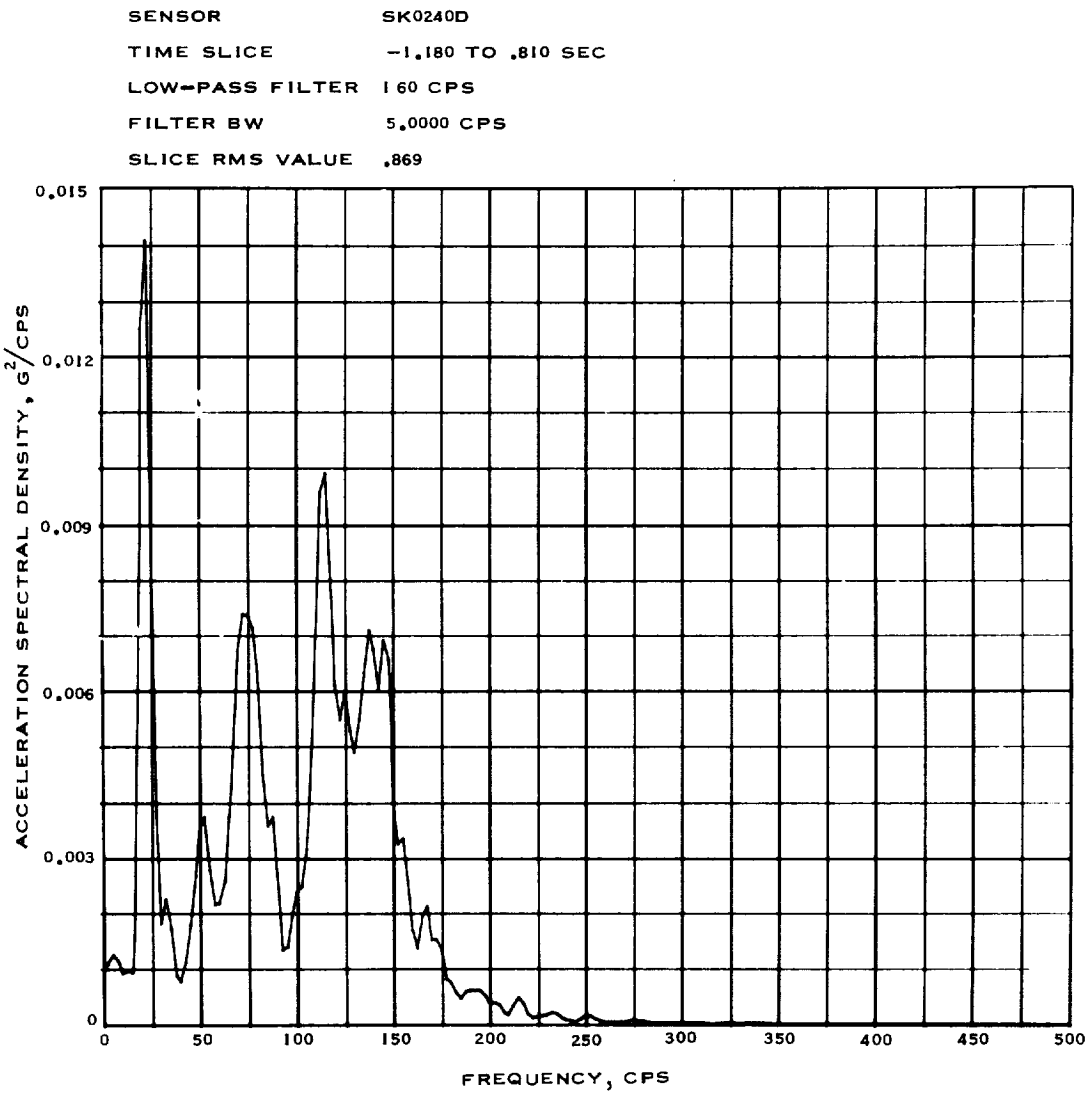

Figure 7.1-22.- Acceleration spectral density of aft helium tank mount X-axis vibration at lift-off, measurement SK0240D, Mission AS-202.

NASA-S-66-10005

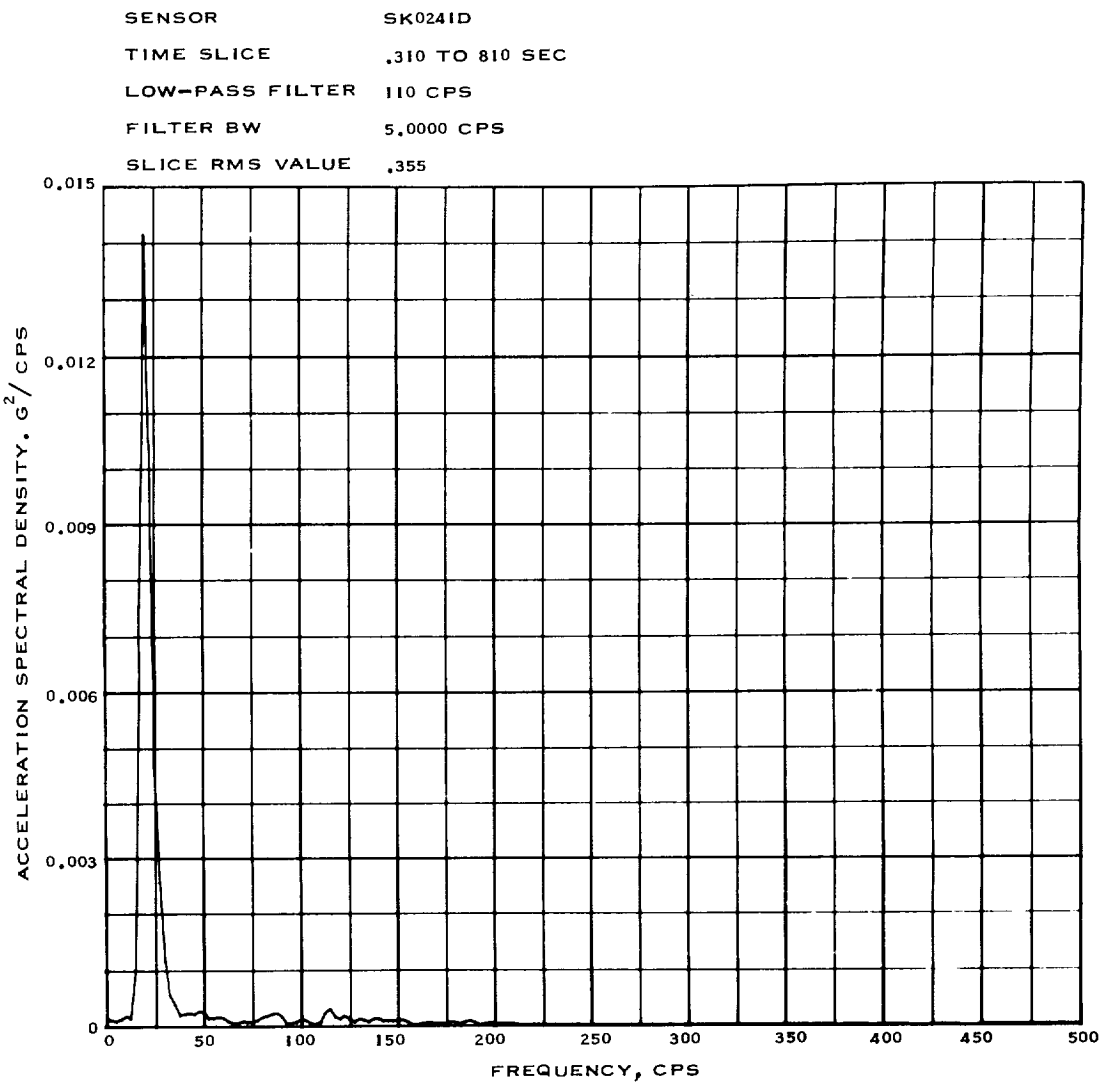

Figure 7.1-23.- Acceleration spectral density of aft helium tank mount radial vibration at lift-off, Mission AS-202.

NASA-S-66-10006

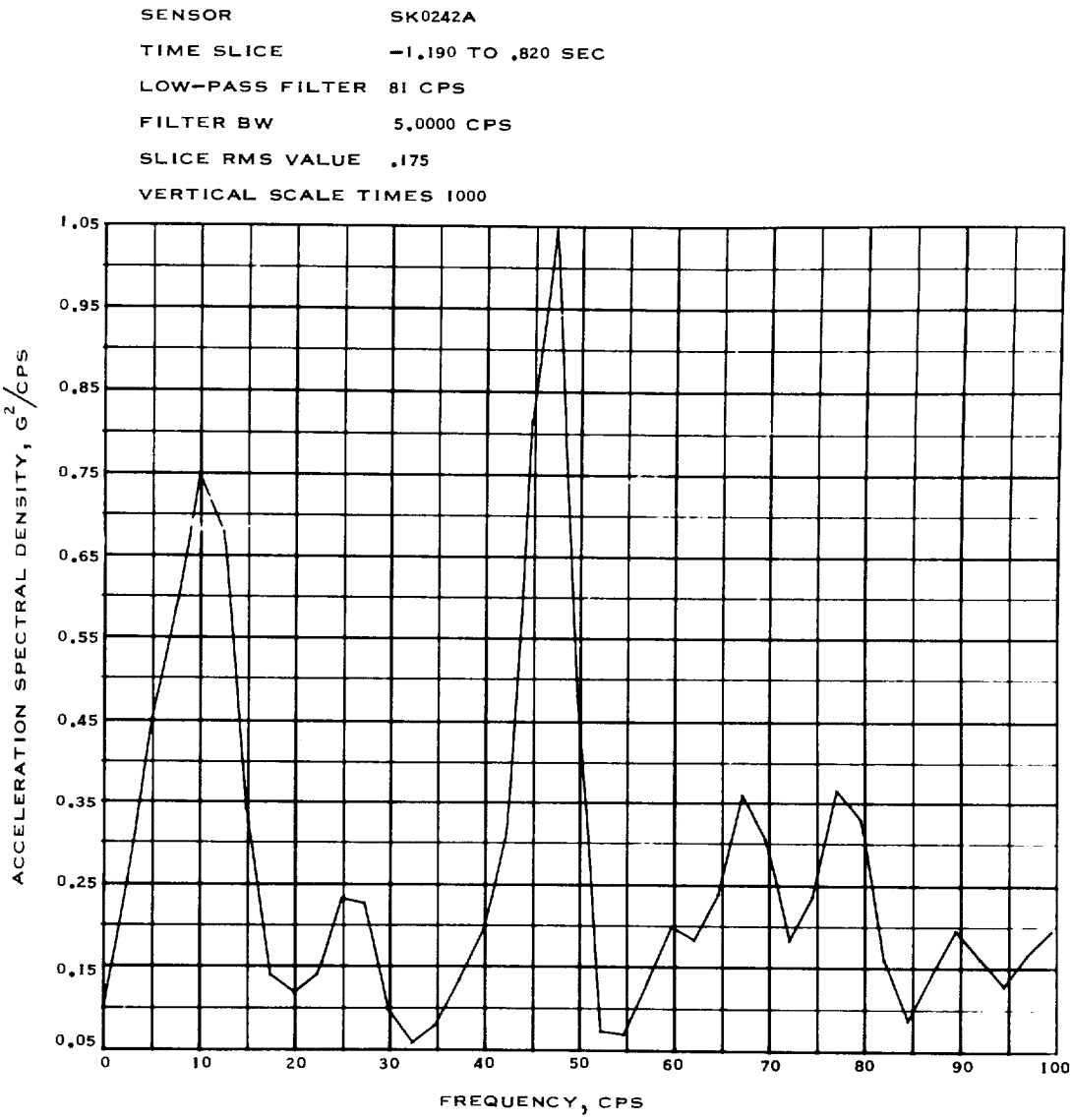

Figure 7.1-24.- Acceleration spectral density of aft bulkhead X-axis vibration at lift-off, measurement SK0242A, Mission AS-202.

NASA-S-66-10007

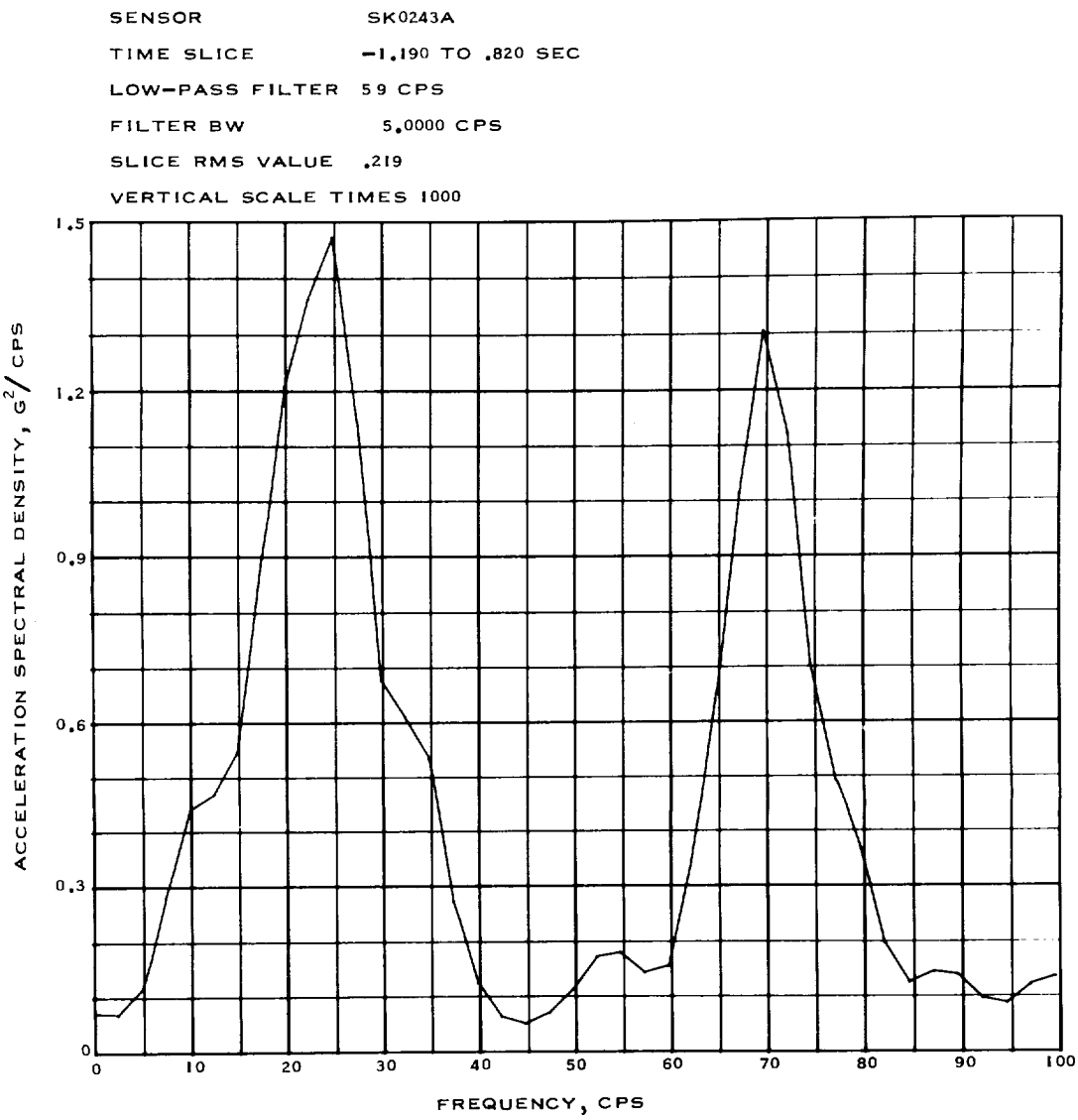

Figure 7.1-25.- Acceleration spectral density of aft bulkhead Y-axis vibration at lift-off, measurement SK0243A, Mission AS-202.

NASA-S-66-10008

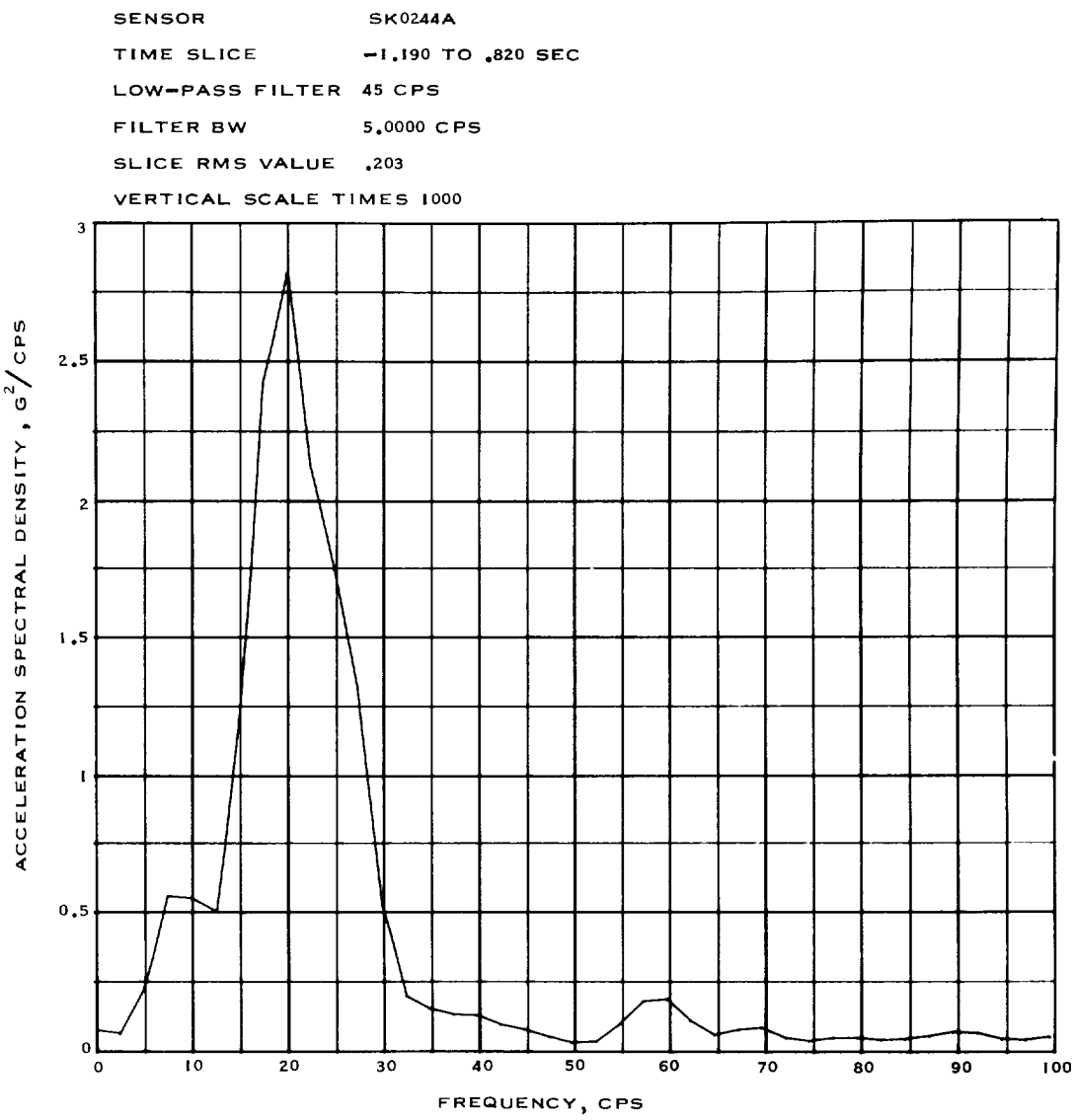

Figure 7.1-26.- Acceleration spectral density of aft bulkhead Z-axis vibration at lift-off, measurement SK0244A, Mission AS-202.

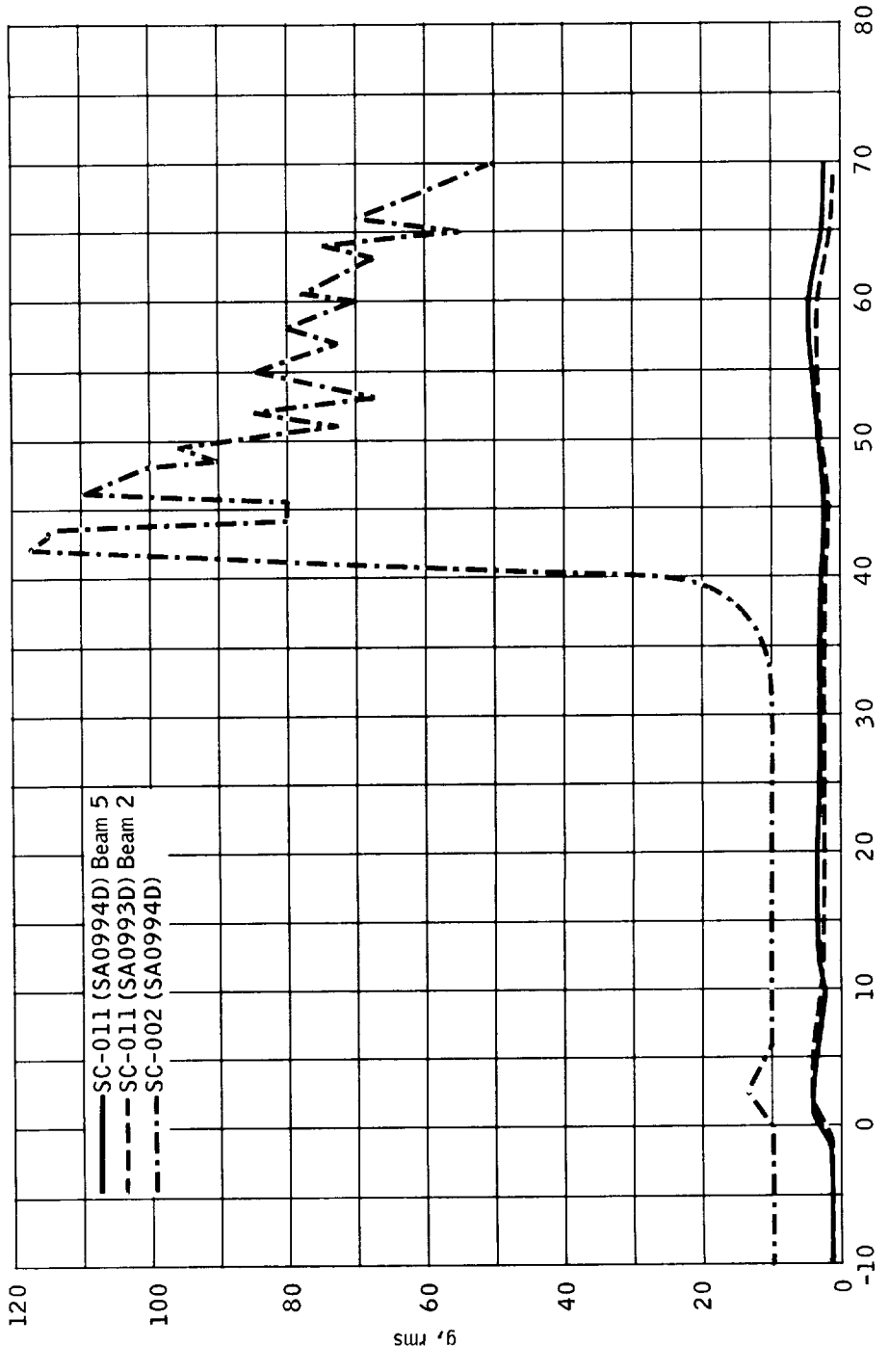

NASA-S-66-10009

Figure 7.1-27.- Comparison of SM radial beam vibration for Missions AS-202 and A-004.

NASA-S-66-10010

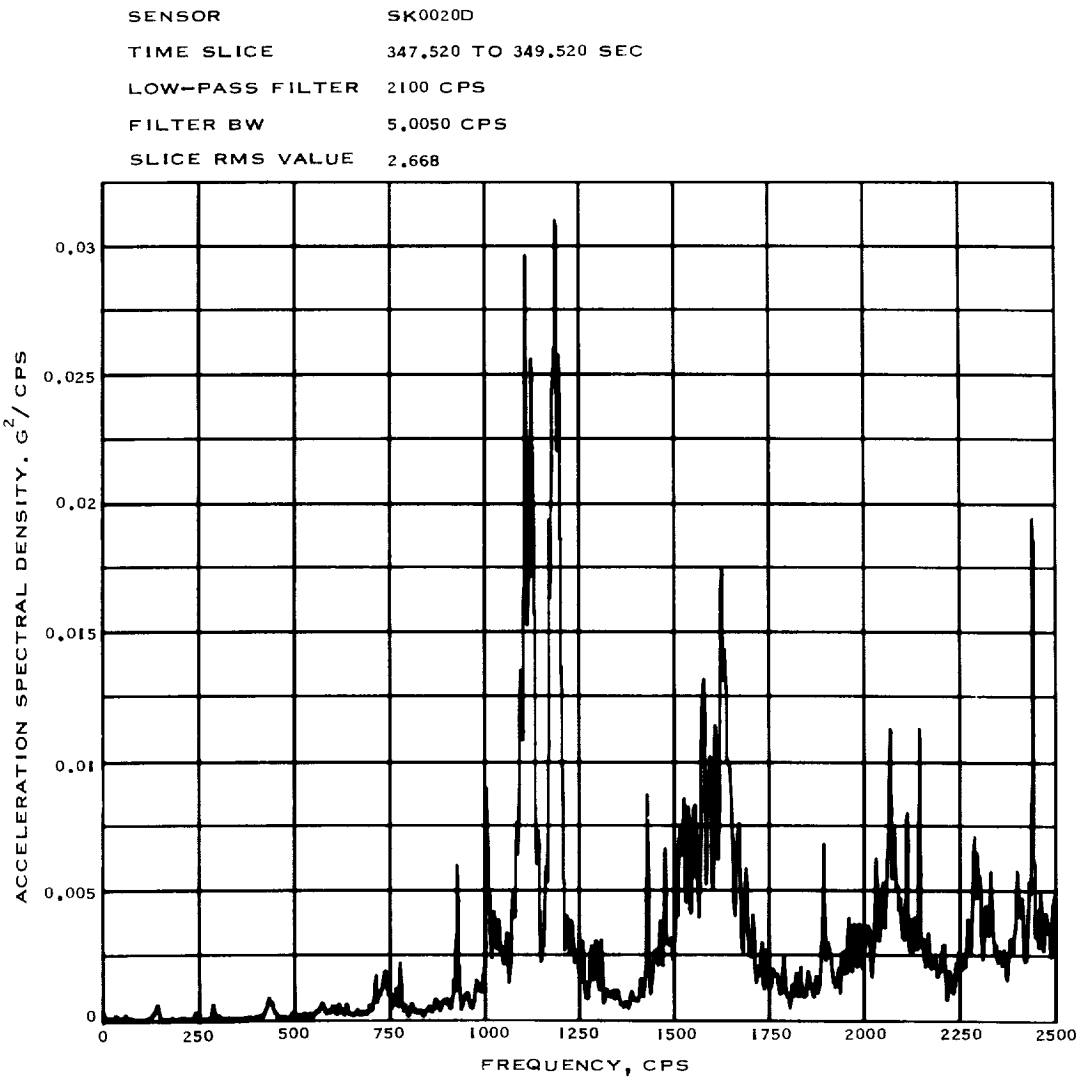

Figure 7.1-28.- Acceleration spectral density of SPS engine dome, X-axis acceleration measurement SK0020D, Mission AS-202.

NASA-S-66-10011

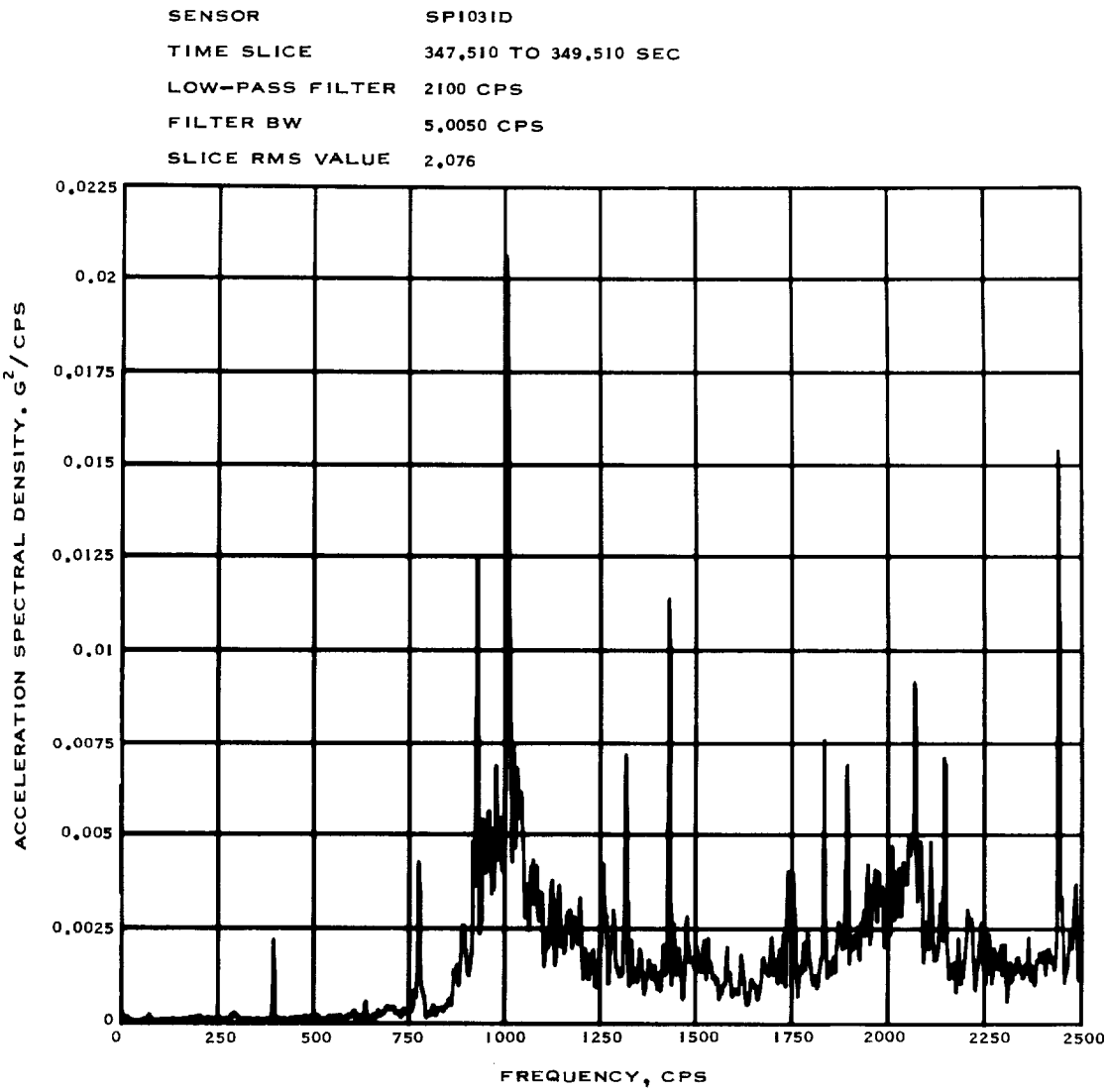

Figure 7.1-29.- Acceleration spectral density of SPS engine dome acceleration, radial direction, measurement SP1031D, Mission AS-202.

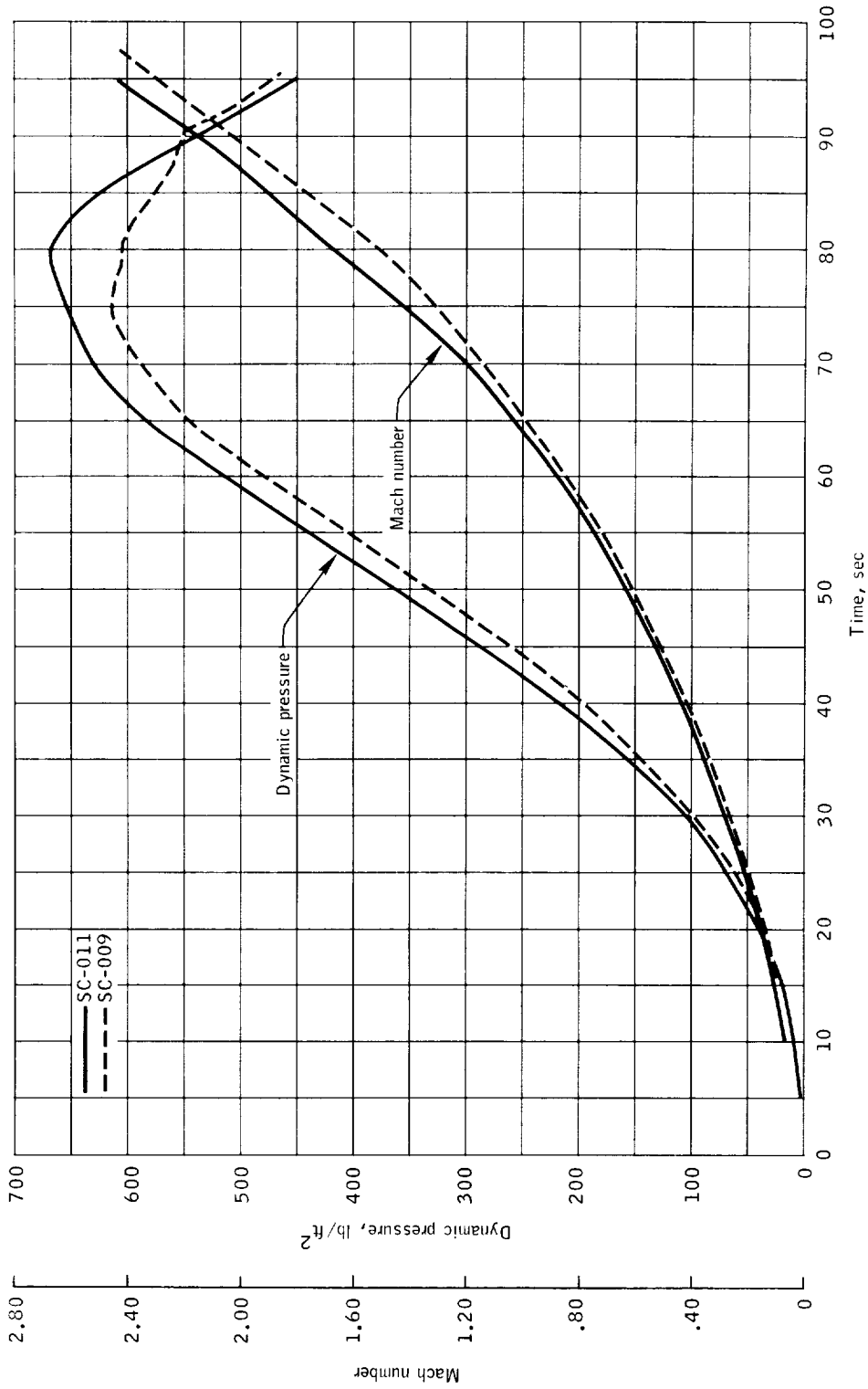

Figure 7.1-30.- Comparison of dynamic pressure and Mach number plotted against time for SC-011 and SC-009.

NASA-S-66-10013

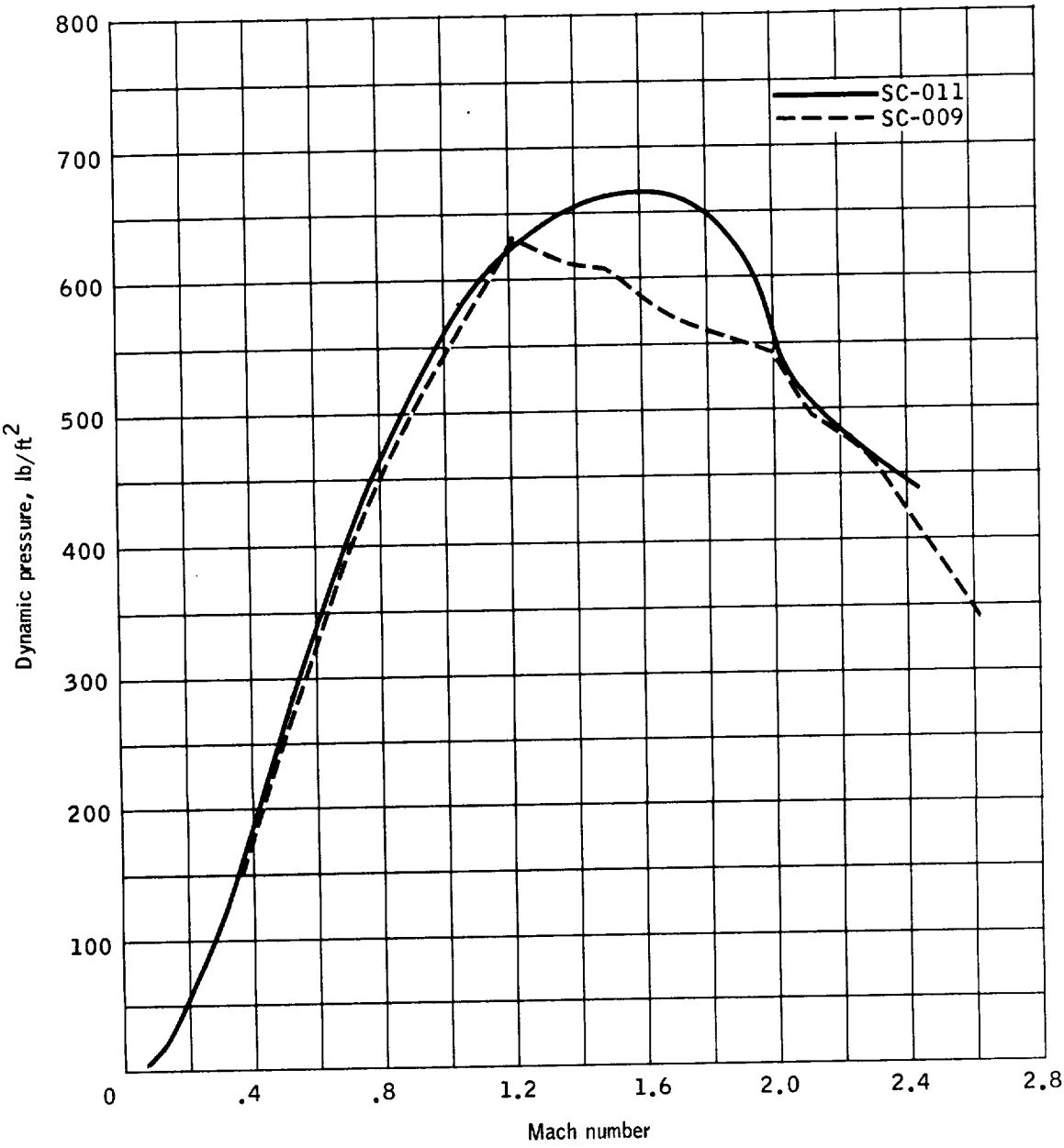

Figure 7.1-31.- Comparison of dynamic pressure plotted against Mach number for SC-011 and SC-009.

NASA-S-66-10014

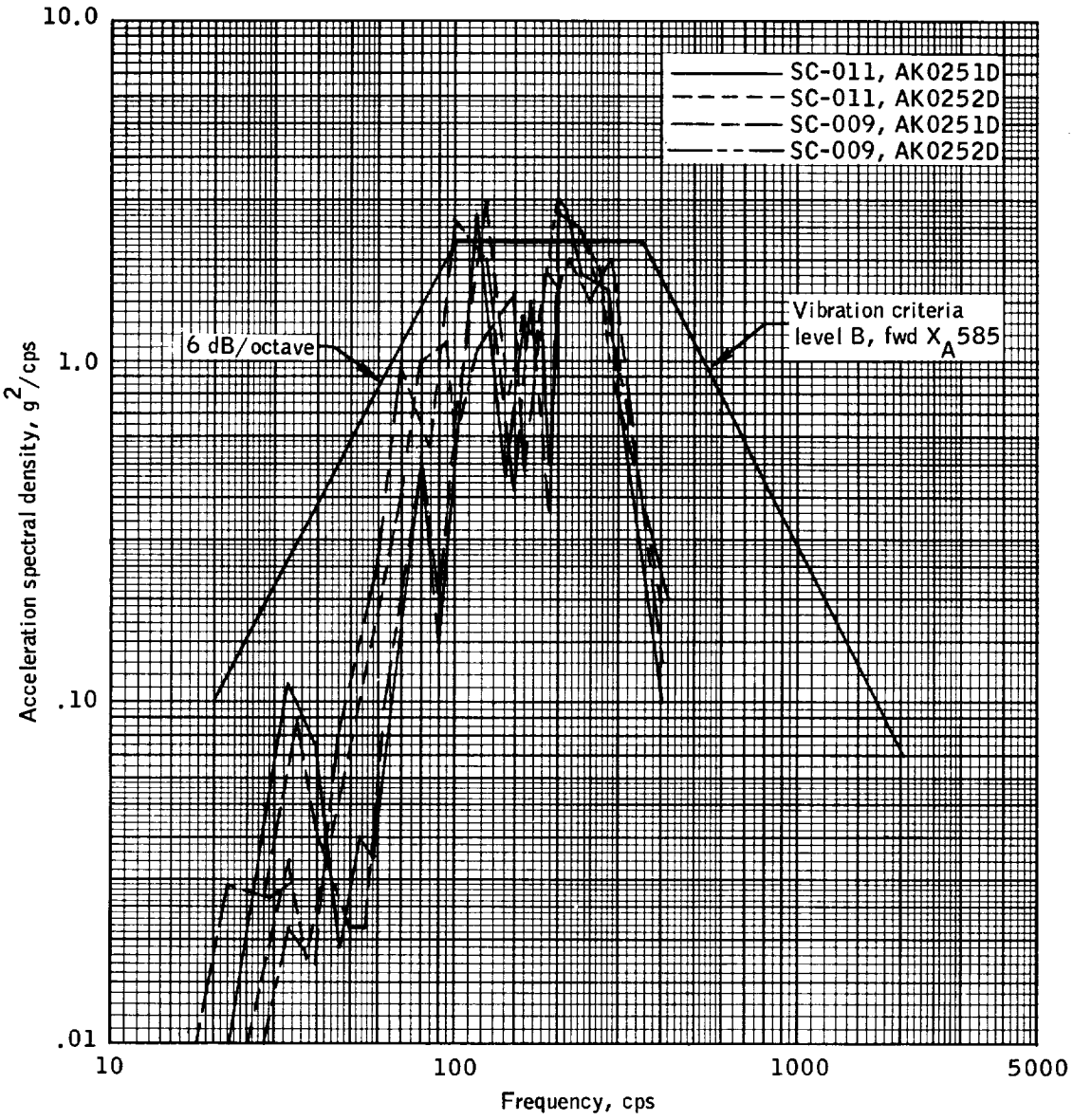

Figure 7.1-32.- Comparison of SLA shell panel vibration at lift-off with criteria for Missions AS-201 and AS-202. (Fwd X_A585).

NASA-S-66-10015

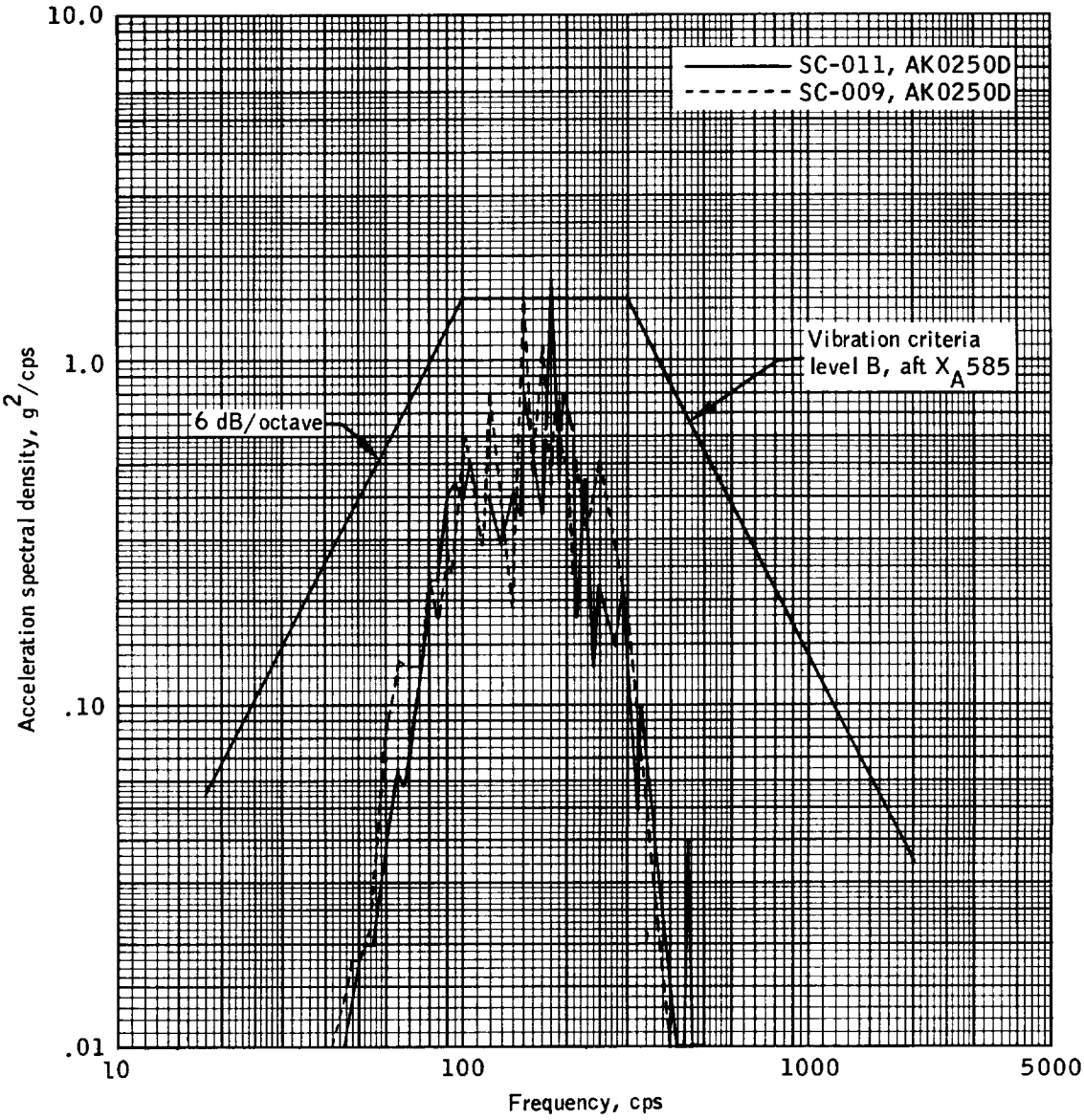

Figure 7.1-33.- Comparison of SLA shell panel vibration at lift-off with criteria for Missions AS-201 and AS-202. (Fwd X_A585).

7.2 Structural Loads

Mission AS-202 was the second flight test of the Apollo Block I spacecraft structure under the uprated Saturn I launch environment, SPS operation, and reentry loading conditions. Critical loading conditions and body loads at the spacecraft structural interface for the mission are summarized in table 7.2-I(a), and are compared with the design loads of reference 13. Stresses in the CM, SM, and SLA were determined from strain gage readings and were compared with the allowable stresses.

Description.- The spacecraft 011 structure included Block I type launch escape subsystem (LES), CM, SM, and SLA.

Launch escape subsystem: The Block I type LES was identical to that used on Mission AS-201 (ref. 9) except for the following differences:

(a) The tower leg fitting was changed from a casting to a die forging.

(b) The CM to tower leg attachment was changed from single mode bolt to a dual mode separation system utilizing a frangible nut.

Command module: The Block I type CM structure was similar to that used on Mission AS-201 (ref. 9) with the following exceptions:

(a) The astrosextant passive thermal protection system was provided instead of moveable doors.

(b) The aft side wall outer skin thickness was changed from 0.016 to 0.035 inch.

(c) A doubler under the parachute retention bracket was added to spacecraft 011.

(d) Spacecraft 011 had integral variations in the aft heat shield skin gage, whereas spacecraft 009 had bonded doublers.

(e) Spacecraft 011 had honeycomb edge member material of 17-4 H 1150M stainless steel, while spacecraft 009 used 17-4 H 1150 stainless steel. Along with this change of material, some edge members were resized, and adjacent honeycomb core was increased in density.

(f) A parachute and deploy mortar were added to the forward heat shield apex cover to assist separation from the CM.

(g) The pitch and yaw engine attach plate was integral with the honeycomb shell structure.

Boost protective cover: The spacecraft 011 boost protective cover (BPC), was similar to that of spacecraft 009 (ref. 9) except for the following additions:

(a) The astrosextant door cover panel.

(b) The Block I type latching mechanism on the outer hatch.

Service module: The spacecraft 011 SM was similar to that of spacecraft 009 (ref. 9).

Spacecraft - lunar module adapter: The spacecraft 011 SLA was identical to that of spacecraft 009 except that the hinge backup structure was strengthened for this mission.

Body loads.- Loads were derived at the CM/SM structural interface for the critical loading condition of launch release, and at the CM/SM, SM/SLA, and SLA/instrument unit (IU) structural interfaces for the maximum dynamic pressure region and S-IB end of boost loading condition. For each of these conditions, calculated loads were compared to design loads (ref. 13). Preflight predicted loads were also included for the maximum dynamic pressure region.

Launch release: CM/SM interface lateral loads during thrust buildup are caused by the steady drag load from ground winds and vehicle dynamic excitation from wind gusts, vortex shedding, and unsymmetric S-IB engine thrust buildup. These excitations also result in a large constraining shear and moment at the base of the launch vehicle. CM/SM interface lateral loads after lift-off are caused primarily by the sudden release of this constraining shear and moment. Typically large axial dynamic oscillations result primarily from the release of tension in the launch vehicle hold-down arms.

Prior to AS-202 lift-off, significant lateral accelerations were caused primarily by the S-IB unsymmetric thrust buildup sequence (section 7.1). Ground winds were light (fig. 7.2-1), and the airload contribution to spacecraft loads during thrust buildup was small. The CM/SM interface loads during thrust buildup are shown in table 7.2-I(b).

Amplitudes of spacecraft lateral accelerations after release were slightly less than during thrust buildup (fig. 7.1-2). The CM/SM interface bending moment after release was less than before lift-off, and its effect on the tension ties was relieved somewhat by the large

compressive axial force occurring at the same time [table 7.2-I(b)]. The maximum bending moments, both before and after launch release, were less than design values. Although in both cases the axial force at the time of maximum bending moment differed considerably from the design value, the combined effect of bending moment and axial force was not critical when compared to design limit load capabilities (fig. 7.2-2).

S-IB mid-boost: Large interface loads during boost generally occur in the region of flight where the product of dynamic pressure and angle of attack is a maximum (max. $q\alpha$).

The winds aloft during the AS-202 boost were very light but exhibited large wind shears in the region of maximum dynamic pressure (fig. 7.2-3). The light winds resulted in a vehicle angle of attack of only 1.0 degree at maximum $q\alpha$. The wind shears and resulting engine gimbal deflections, however, caused significant vehicle bending oscillations (section 7.1). Thus the maximum $q\alpha$ lateral loads for this mission were due primarily to vehicle structural dynamics rather than aerodynamic loading. The CM/SM, SM/SLA, and SLA/IU interface loads during the maximum $q\alpha$ region of flight were derived by the following two procedures:

(a) Predicted loads from a flight simulation using the T-0 winds.

(b) Calculated loads using measured angles of attack and gimbal angles in an MSC elastic body loads program.

Values obtained by each of these methods are compared with the maximum $q\alpha$ design loads in table 7.2-I(c). The CM/SM interface load values are also compared with limit design load capabilities in figure 7.2-2. The predicted and calculated max. $q\alpha$ interface loads include the effects of the internal vent pressure (fig. 7.2-4). The positive vent pressure relieves the compressive interface axial loads due to inertia and aerodynamic drag.

S-IB end of boost: The maximum axial accelerations and maximum compressive interface loads are experienced near the end of S-IB boost, immediately prior to inboard engines cutoff. The end of boost axial acceleration for this mission was nominal, and the calculated compressive loads at all interfaces were less than the design loads [table 7.2-I(d)]. The CM accelerometer data indicated that lateral loads at end of S-IB boost were small.

S-IB/S-IVB staging: The peak-to-peak amplitudes of axial and lateral spacecraft vibrations were very small during this period, indicating that staging was very smooth with no significant dynamic loading.

Spacecraft accelerations during the S-IVB burn and SPS operation were nominal, and no detailed interface loads analyses were made. Maximum accelerations experienced during reentry were less than predicted (fig. 5.1-3) and only 12 percent of the design limit accelerations.

Internal loads.- Internal loads were determined from strain-gage instrumentation mounted on various structural components within the CM, SM, and SLA. (See ref. 14 for actual strain-gage locations and ranges.)

Command module internal loads: There were a total of 28 strain gages located on the CM primary structure. Of this total 16 were attached to the stainless steel substructure of the aft heat shield, and the remaining 12 were located on three of the main longerons in the CM inner structure. All the strain measurements were commutated at a rate of 10 samples per second, and telemetered to earth starting at a time just prior to reentry of the spacecraft into the earth's atmosphere. The main longerons in the conical portion of the CM are designed by loads that occur during boost, or an abort during boost, but the strains in these members were not recorded during this phase of the mission. Following reentry, the strains recorded from the longerons were uniformly low (400 to 800 μin./in. compared to a maximum range setting of ±8000 μin./in.), and the strain magnitude remained approximately constant during the whole entry period up to and including water impact. The same remarks concerning the constant low magnitude of strain apply to the measurements from the gages on the aft heat shield which were ranged for ±5000 μin./in. There was absolutely no variation in the magnitude of recorded strain from the aft heat shield during the buildup of atmospheric deceleration from 0g to 240g or at water impact. The only conclusion, therefore, that can be drawn from the CM strain gage measurements is that the recorded data are not valid, and the reason for it not being valid is not known. Based on a postflight visual inspection, it is known that no structural damage was sustained during the AS-203 mission.

Service module internal loads: There were 23 strain gages located within the SM structure, of which only one was inoperative prior to the launch. Unfortunately this gage was located on one of the radial beam trusses which prevented a strain gage calculation of the station 1010 interface axial force and bending moment. Too many assumptions would have to be made in the calculation concerning the loading distribution for the result to be accurate.

The other strain gages on the radial beam trusses were set to zero prior to the launch in accordance with the checkout procedures. Data from these gages were used to determine changes in loading on the members during the mission events.

Strain data from these gages indicated that structural loads were light during the mission as was expected from the nominal flight. Table 7.2-II shows the loads that were introduced into the CM/SM tension ties during pretension of the bolts, lift-off, max. $q\alpha$, S-IB end boost, and S-IVB end boost. The maximum load shown was only 38 percent of the limit design load.

SLA internal loads: All SLA strain gages were balanced to zero before stacking the various spacecraft components, with the exception of those on the stabilizing cable turnbuckles. These were pretensioned after the stacking operation.

There were 24 strain gages mounted on the SLA skins and stabilizing structure to measure the launch loads. One gage was inoperative prior to lift-off and three more dropped to a zero gage reading at lift-off (see section 7.15).

Strains from the remaining gages on the SLA skins were converted to stresses, corrected for temperature effects, and are presented in table 7.2-III for various events during the boost phase of the mission. This table also gives the stabilizing ring stiffener stresses and cable loads.

All stresses and loads were below the design limit values, indicating that there were no structural failures during the mission. A video tape of the SLA panel deployment during the CSM/S-IVB separation shows that two panels were displaced from the normal 45 degree deployment position by impingement from the SPS engine plume. At this time, loads on the panels exceeded the strength of the retention subsystem, allowing the panels to hinge back toward the side of the vehicle. This was the predicted response to a proximity burn of the SPS engine. The proximity burn would normally occur during an SPS abort mode.

Conclusions.- All structural loads data confirmed that no structural failures occurred during the mission, with the exception of the SLA panel retention cables. All structural components performed as expected from the trajectory flown in the mission, and were well within the structural capability of the vehicle.

Although lift-off structural loads were well below design, it is significant to note that the lateral loads resulted primarily from the unsymmetric thrust buildup. The lift-off structural environment, other than thrust buildups, was not severe for this mission. The effect of unsymmetric thrust buildup on spacecraft structural loads was not

included in the lift-off design criteria but was noted on Mission AS-201 (ref. 9). As a result, the lift-off ground wind go-no go procedure for Mission AS-202 and subsequent missions was revised to include this effect.

TABLE 7.2-I.- EVENTS AND CONDITIONS SIGNIFICANT TO STRUCTURAL ANALYSIS

(a) Event times

Condition	Elapsed time, sec
Saturn-IB engine ignition	-3.1
Lift-off	0.9
Mach 1	64.0
Maximum $q\alpha$	76.0
Maximum axial acceleration	138.6
S-IB/S-IVB separation	144.2

(b) Launch release, maximum bending moment conditions at CM/SM interface

Condition	Before release	After release	Design
Bending moment, in-lb	0.85×10^6	0.7×10^6	2.4×10^6
Axial force at time of maximum bending moment, in-lb	-2 700	-16 100	-6 500

TABLE 7.2-I.- EVENTS AND CONDITIONS SIGNIFICANT TO STRUCTURAL ANALYSIS - Concluded

(c) Interface loading conditions during maximum $q\alpha$

Interface	Condition	Predicted	Calculated	Design[a]
	Flight time, sec . .	73.0	76.0	70.0
	Mach number	1.32	1.45	1.34
	Dynamic pressure, psf	603	[b]654	735
	Angle of attack, deg	1.07	[b]0.95	6.7
CM/SM	Bending moment, in-lb	0.42×10^6	0.24×10^6	2.05×10^6
	Axial force, lb . . .	-63 000	-67 000	-86 500
SM/SLA	Bending moment, in-lb	2.12×10^6	1.95×10^6	7.39×10^6
	Axial force, lb . . .	-123 000	-140 000	-181 500
SLA/IU	Bending moment, in-lb	2.61×10^6	2.68×10^6	23.6×10^6
	Axial force, lb . . .	-130 000	-140 000	-253 500

[a]Block I, Saturn V design loads.

[b]Based on Q-ball measurements.

(d) Interface axial loads at S-IB end of boost

Interface	Condition	Calculated	Design[a]
	Axial acceleration, g	4.2	4.9
CM/SM	Axial force, lb	-86 000	-94 100
SM/SLA	Axial force, lb	-223 000	-332 700
SLA/IU	Axial force, lb	-239 000	-456 700

[a]Block I, Saturn V design loads.

TABLE 7.2-II.- CM/SM TENSION TIE LOADS FOR MISSION AS-202

Gage location	Pre-tension load, lb	Lift-off load, lb	Max qα load, lb	S-IB end boost load, lb	S-IVB end boost load, lb
Tension bolt, beam 2	10 000	9 000	6 000	4 000	11 000
Tension bolt, beam 4	10 000	10 000	7 600	6 400	11 000
Tension bolt, beam 6	10 000	10 000	7 300	7 500	11 000

TABLE 7.2-III.- SLA SKIN AND STABILIZING MEMBER STRESSES AND LOADS FOR MISSION AS-202

Gage location	Lift-off stress, psi	Max. qα stress, psi	S-IB end boost stress, psi	S-IVB end boost stress, psi
Outer shell, circumferential, X_A775, 34°	378	-336	3 620	2 640
Inner shell, longitudinal, X_A775, 34°	-277	-5 230	-1 650	-635
Inner shell, circumferential, X_A775, 34°	1 282	797	10 870	7 360
Outer shell, longitudinal, X_A781, 124°	9 250	4 780	616	9 050
Outer shell, circumferential, X_A781, 124°	-4 200	-3 250	-4 800	-1 085
Inner shell, longitudinal, X_A781, 124°	-2 860	-7 920	-243	-6 300
Inner shell, circumferential, X_A781, 124°	959	1 830	13 100	277
Outer shell, longitudinal, X_A775, 214°	-970	-4 460	-9 280	-740
Outer shell, circumferential, X_A775, 214°	5 400	3 790	3 080	8 840
Inner shell, longitudinal, X_A775, 214°	-8 980	-12 750	-7 390	-1 630
Inner shell, circumferential, X_A775, 214°	-820	-4 200	6 840	-115
Ring stiff, X_A584.7, Y_A115, Z_A0	883	147	94	694
Ring stiff, X_A584.7, Y_A115, Z_A0	1 542	976	1 030	-315
Ring stiff, X_A584.7, Y_A0, Z_A115	1 680	830	3 360	-262
Ring stiff, X_A584.7, Y_A0, Z_A115	588	1 530	4 740	2 690

Gage location	Lift-off load, lb	Max. qα load, lb	S-IB end boost load, lb	S-IVB end boost load, lb
Ring cable, X_A584.7, turnbuckle	770	393	521	970
Ring cable, X_A584.7, turnbuckle	1 133	1 039	1 316	1 354
Ring cable, X_A584.7, turnbuckle	902	907	1 065	1 220
Ring cable, X_A584.7, turnbuckle	489	544	927	567

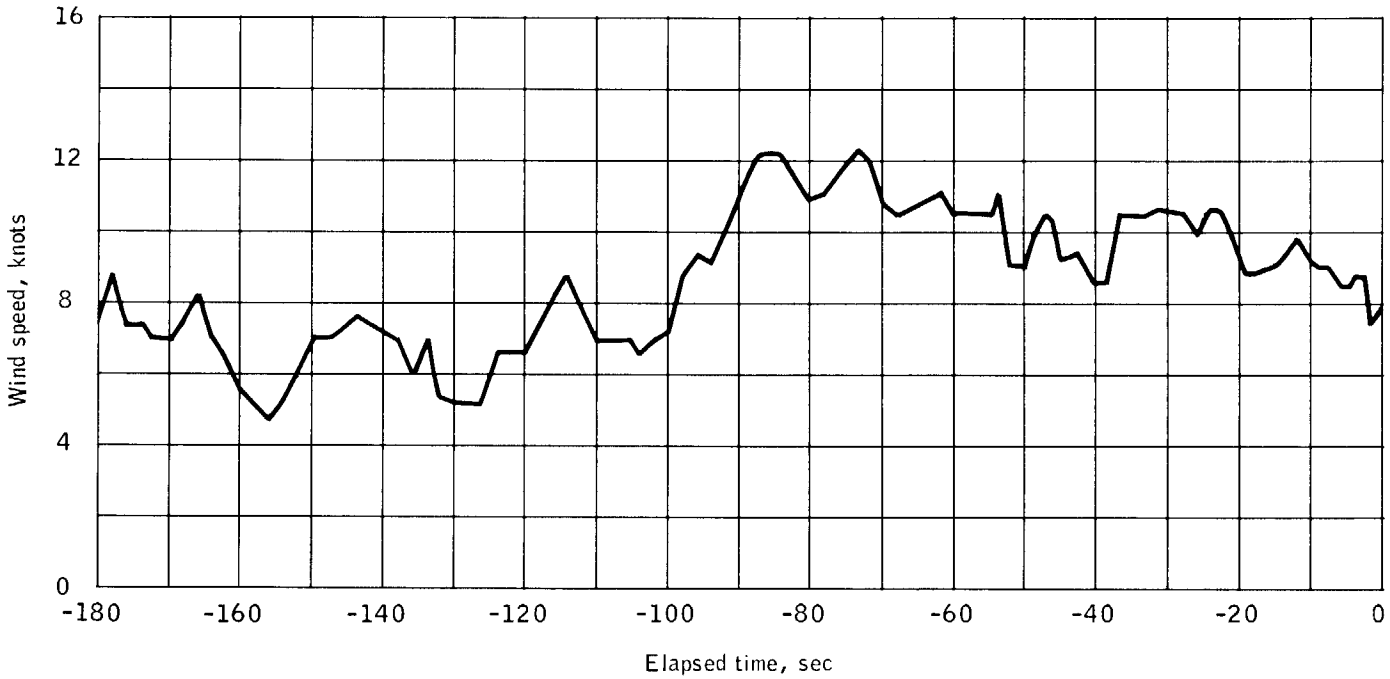

Figure 7.2-1.- Wind speed at 60-foot level of Complex 34 during launch of Mission AS-202.

NASA-S-66-10017

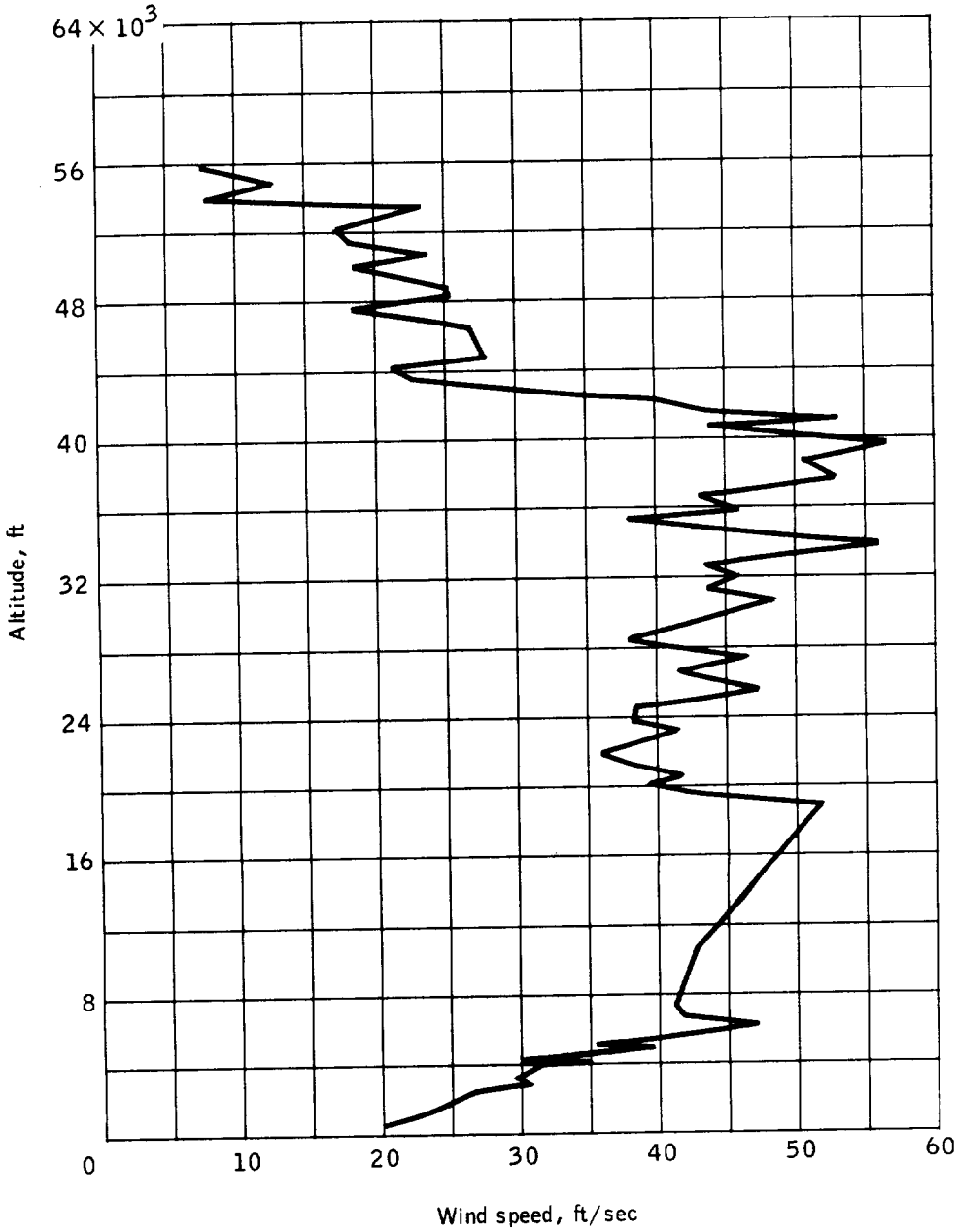

(a) Launch wind magnitude.

Figure 7.2-2.- Launch winds, Mission AS-202.

NASA-S-66-10018

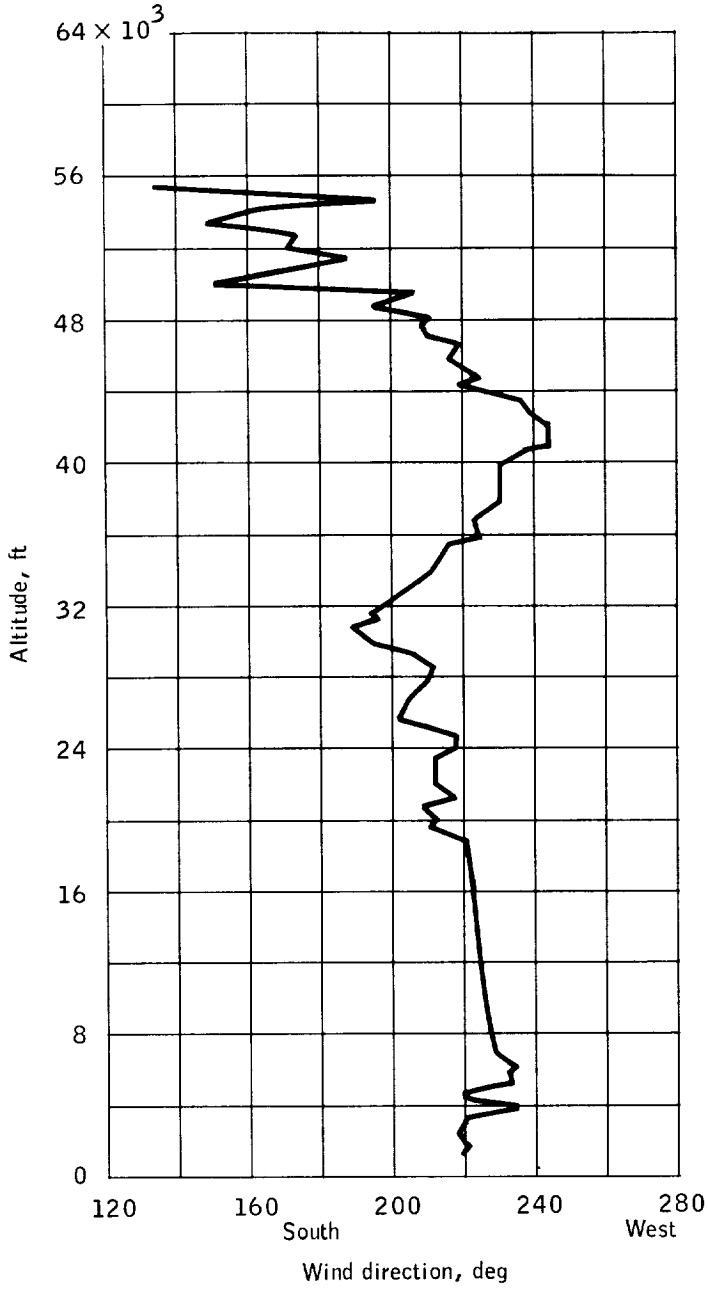

(b) Launch wind direction.

Figure 7.2-2.- Concluded.

NASA-S-66-10019

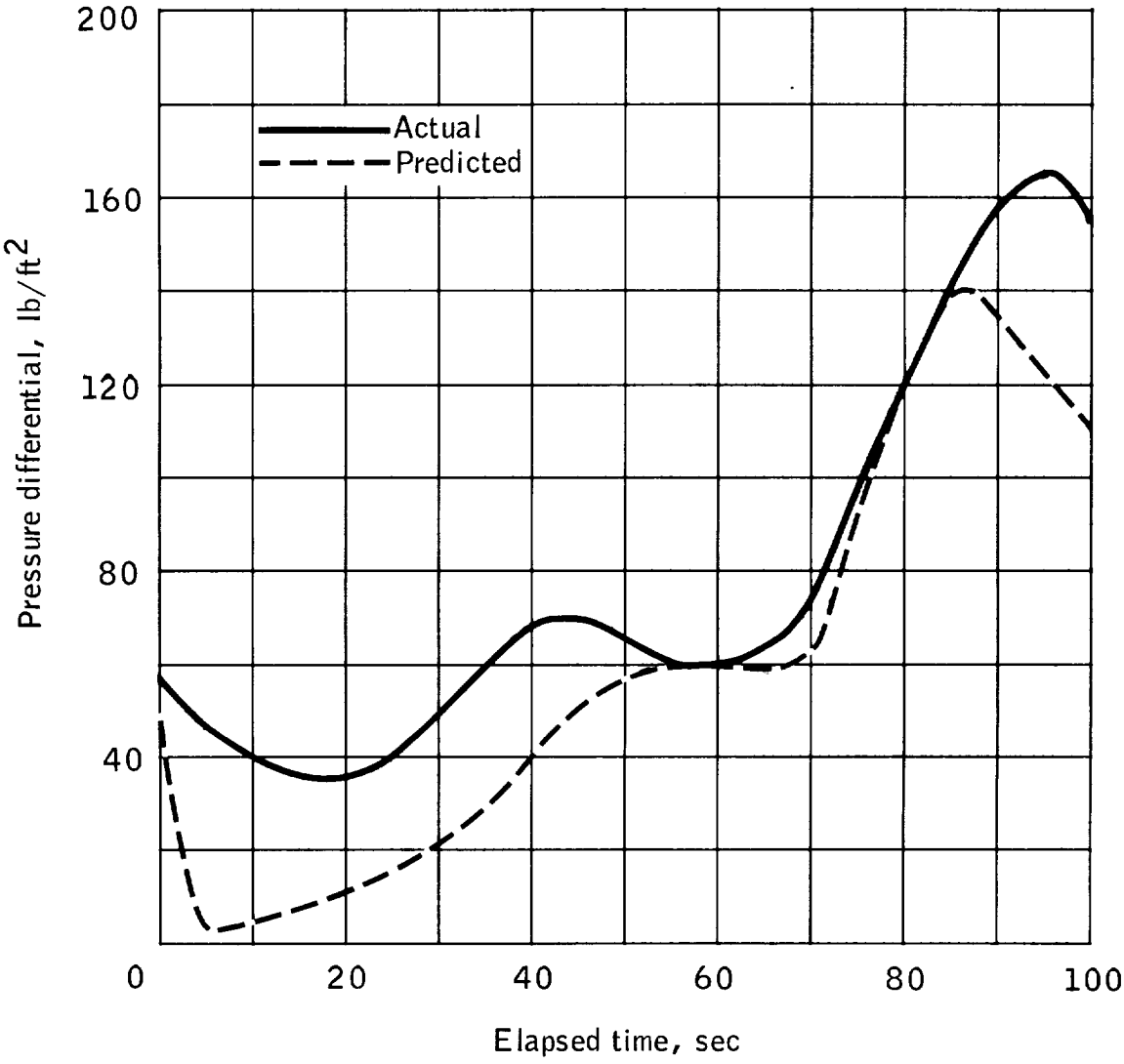

Figure 7.2-3.- Time history of SC-011 SM vent pressure relative to ambient.

NASA-S-66-10020

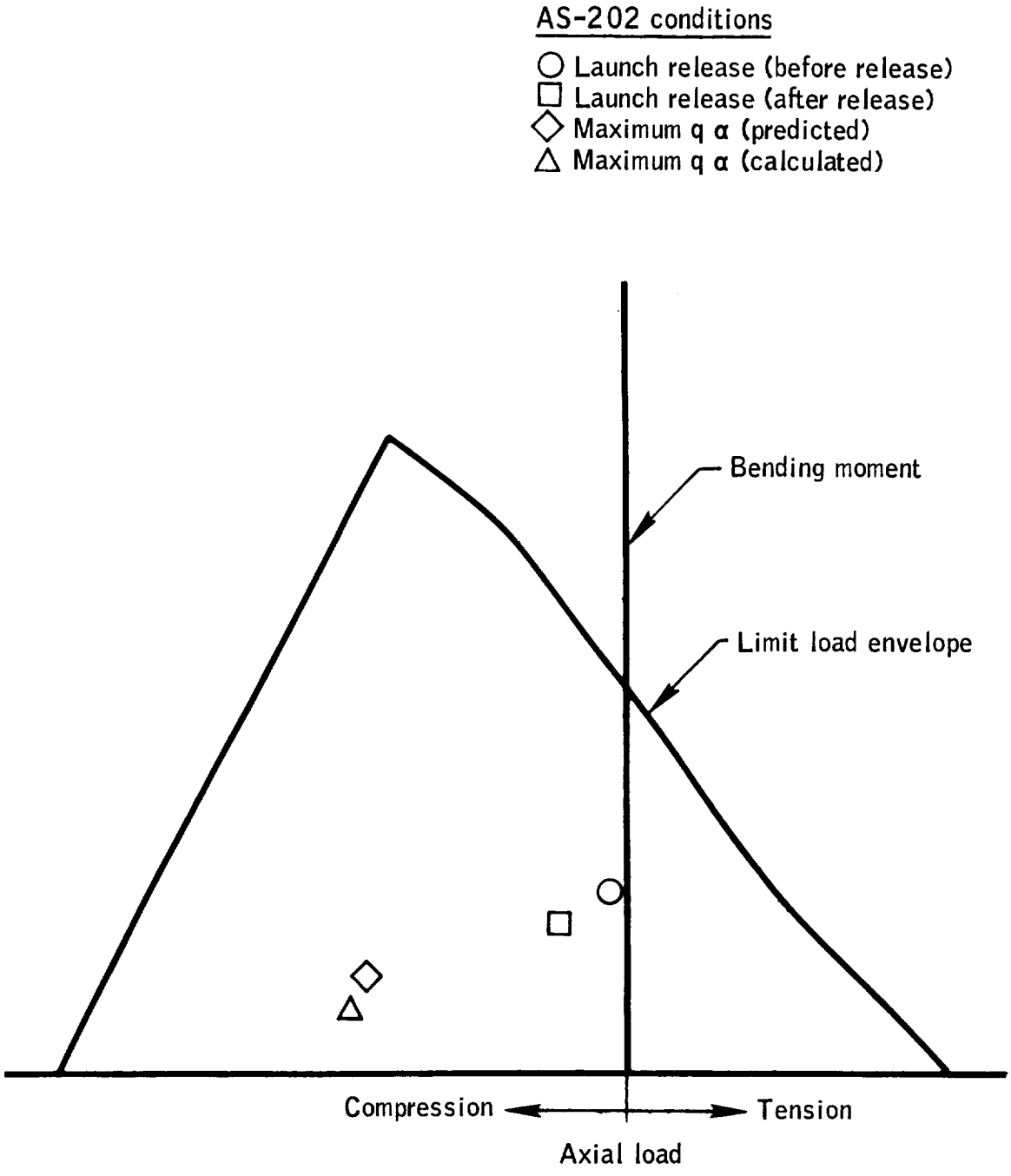

Figure 7.2-4.- Comparison of lift-off and maximum q α CM/SM interface loads with Block I limit design load capabilities, Mission AS-202.

7.3 Aerothermodynamics

Theoretical calculations of heat transfer rate at the maximum heating location on the aft heat shield for its flight trajectory indicated an initial peak rate of 80 Btu/ft^2/sec followed by a decrease to 19 Btu/ft^2/sec and a subsequent rise to a second peak of 44 Btu/ft^2/sec. This calculation was based on a trajectory corresponding to a lift-to-drag ration (L/D) of 0.28 or an angle of attack of 161.5 degrees (see section 5.0). Comparison of this heating rate history with the preflight prediction in figure 7.3-1 indicated that the total heat load experienced by the spacecraft of 20 680 Btu/ft^2 was above that required to achieve the mission objectives.

Pressure measurements.- Of the 35 pressure transducers on the CM, 11 were located on the aft heat shield and 24 on the crew compartment heat shield. Output from the transducers on the crew compartment heat shield indicated that the entry environment pressure on the conical surface was too low to be measured accurately by the transducer subsystem. The accuracy anticipated for the overall subsystem in the low range was not realized.

Representative histories of the pressures measured on the aft heat shield are shown in figure 7.3-2. The lines represent a fairing of the actual raw data which were corrected only for the zero-shift of each instrument that existed prior to reentry. The data were smooth and continuous throughout the reentry.

To correlate the aft heat shield flight data with results obtained from numerical calculations of the flow field, distributions of local measured pressure divided by the highest measured pressure (approximately the stagnation pressure) were obtained and are shown in figure 7.3-3. The numerical calculations with which the data were compared were obtained from an "exact" inverse numerical solution of the flow field for an angle of attack of 158 degrees and a point in the preflight trajectory corresponding to the first peak in the convective heating. The flight data shown for comparison were obtained for Mach numbers greater than 10 and pressures greater than 50 percent of the full-scale deflection value of the transducers. The data are in satisfactory agreement over the pitch plane. In the yaw plane, measurements obtained are somewhat lower than the calculated values. It should be noted that the discrepancy is symmetric about the vehicle centerline, which eliminates spacecraft yaw as a cause. No similar discrepancies were noted during the flight of spacecraft 009. The fact

that spacecraft 011 may have flown at an angle of attack somewhat less than 158 degrees was not sufficient to account for the disagreement between the theoretical predictions and the data.

Pressure measurements may be used to assist in determining the degree to which the spacecraft actually followed a simulated trajectory based on a lift-to-drag ratio of 0.28 (see sections 5.0 and 6.0). Figure 7.3-4 is a comparison of the calculated pressure behind a normal shock for the postulated trajectory with the pressure measured by transducer CA1146P, located near the peak pressure point on the spacecraft. The two curves agree very well until a time of 4875 seconds (through the first heat pulse). Subsequent deviations in the curves indicate that the actual and simulated trajectories may not be in agreement after this time.

Calorimeters.- Two types of calorimeters were installed around the CM to measure heating rates experienced by the spacecraft during atmospheric entry. One was a high range sensor (above 50 Btu/ft^2/sec) which consisted of several graphite wafers stacked to allow removal of single wafers by aerodynamic forces when the surrounding heat shield material had receded, and the other was an asymptotic calorimeter tailored in design to measure low rates at discrete locations on the conical section.

Wafer calorimeter: Numerous malfunctions were observed in the temperature measurements obtained with the high range wafer calorimeters. Details of the possible thermocouple shorting or premature switching of each wafer recording are discussed in section 7.15. No meaningful data are available at present for analysis.

Asymptotic calorimeter: Of the 21 asymptotic calorimeters installed on the conical section, 19 produced useable data. Shown in figure 7.3-5 are histories of the measured heating rates and those calculated for the entry trajectory based on wind-tunnel data for 161.5-degrees angle of attack and the laminar stagnation-point theory of reference 15. The turbulent calculations are based on the theory of reference 16. Some of the measured data exhibit erratic behavior during portions of the entry time. Generally, though, the data appear to be of good quality.

Examination of the measurements shown in figure 7.3-5 reveals a curious history for most of the locations. Higher heating was experienced during the second heat pulse, which occurred at velocities between 20 000 and 4000 ft/sec, than during the high velocity (27 200 to 21 000 ft/sec) period of the first heat pulse. This

behavior suggests the flow was separated during the first pulse and attached during the second pulse. In support of this idea, three histories [fig. 7.3-5(f), (r), and (s)], which are possibly in a separated region throughout entry due to their location on the toroid, behaved in the expected manner.

The large discrepancy between the predictions and the measurements can be attributed, in part, to the inability to predict the level of heating in separated flow. Reference 17, for example, found that heating in a separated region could be as much as 30 to 50 percent less than in an attached region. Thus, the high theoretical predictions during the first pulse is not surprising. On the other hand, the underprediction on the windward ray during the second pulse cannot be explained if the vehicle angle of attack is assumed to be precisely known.

The effect of possible atmospheric variations was explored and shown to be small. The Reynolds numbers throughout most of the entry are so low as to rule out transition to turbulent flow.

A sketch of the CM is shown in figure 7.3-6 to indicate the peak heating rates recorded at each sensor location.

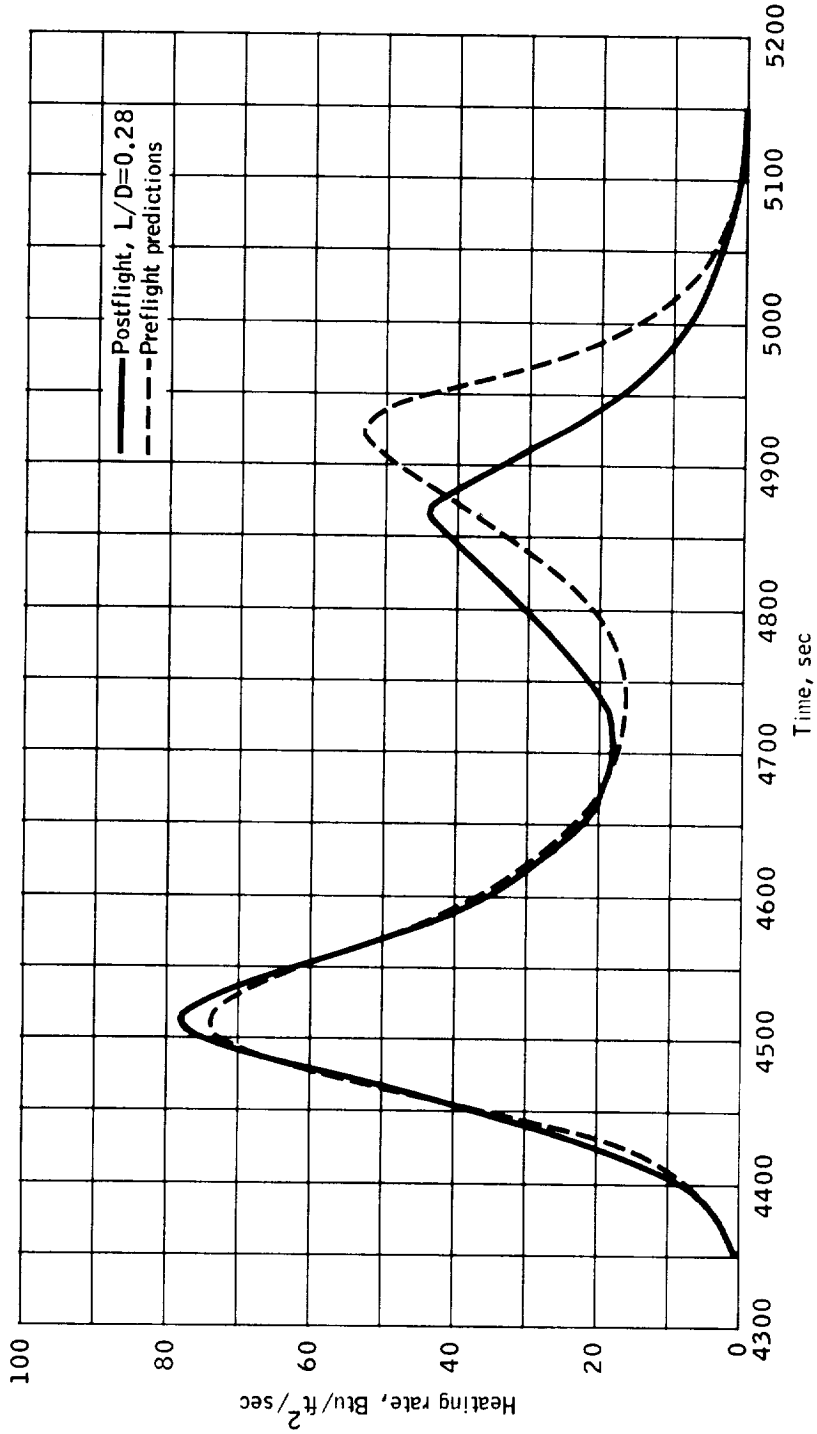

NASA-S-66-10021

Figure 7.3-1.- Comparison of preflight heating rate history with postflight based on a 0.28 L/D trajectory, Mission AS-202.

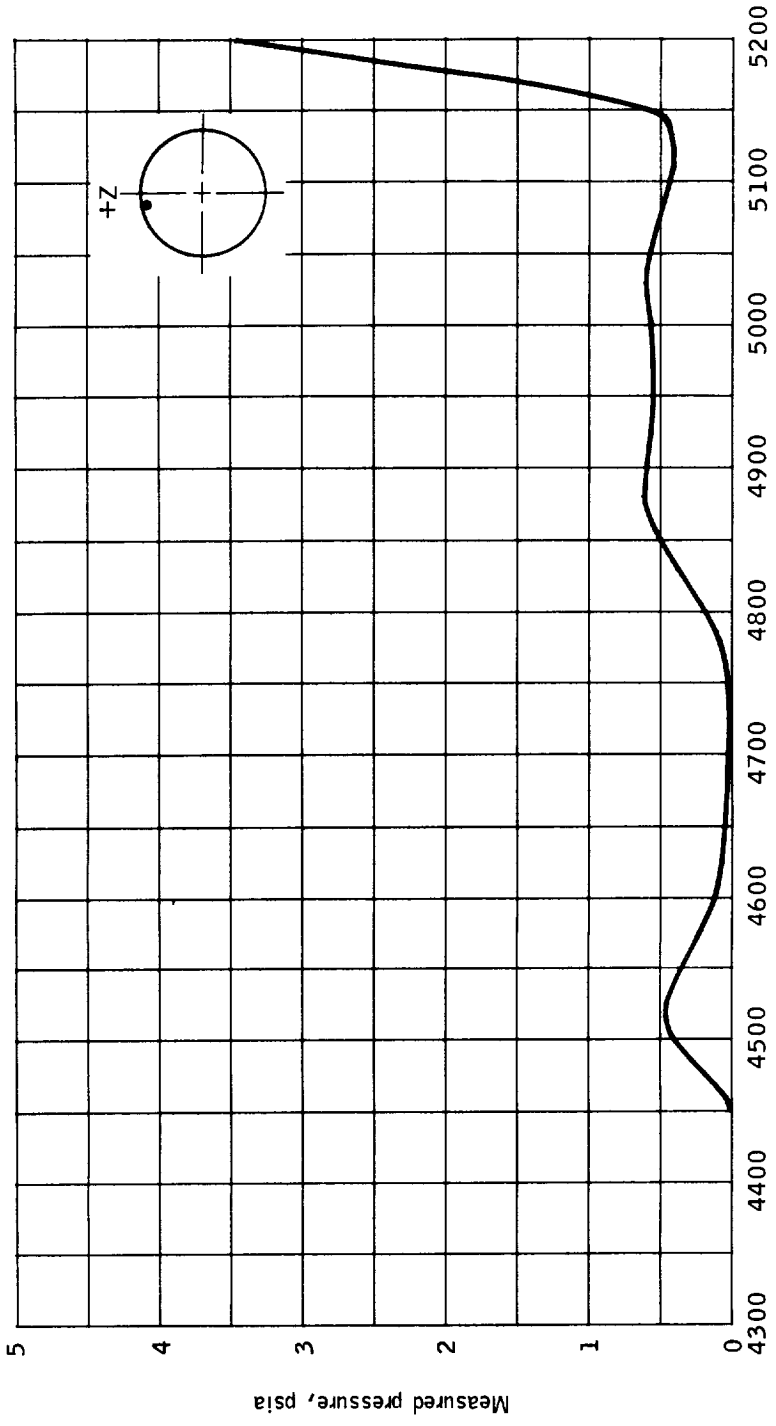

NASA-S-66-10022

(a) CA1141P, Y0, Z75, S/R 1.0.

Figure 7.3-2.- Histories of measured pressures on the blunt face of the CM, Mission AS-202.

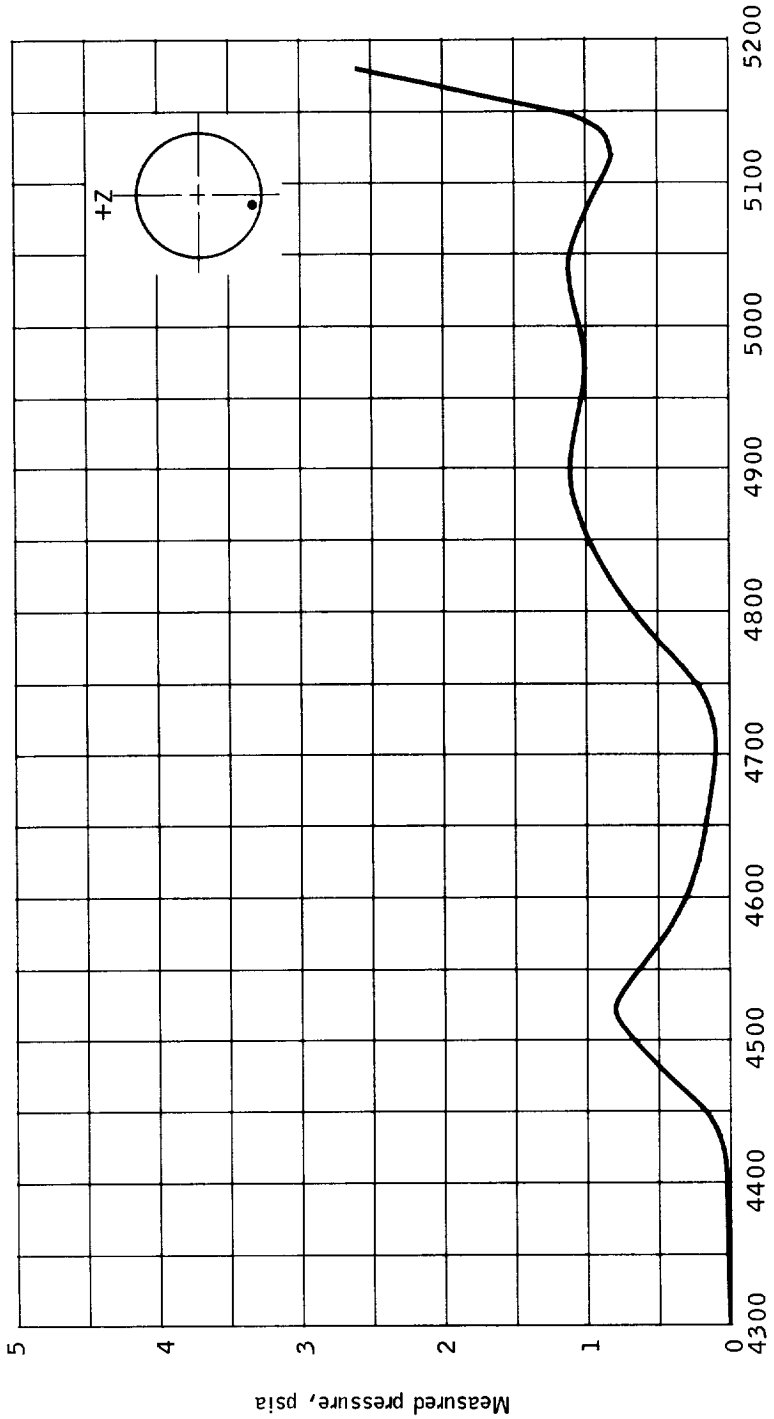

(b) CA1142P, Y0, Z71, S/R .947.

Figure 7.3-2.- Continued.

NASA-S-66-10023

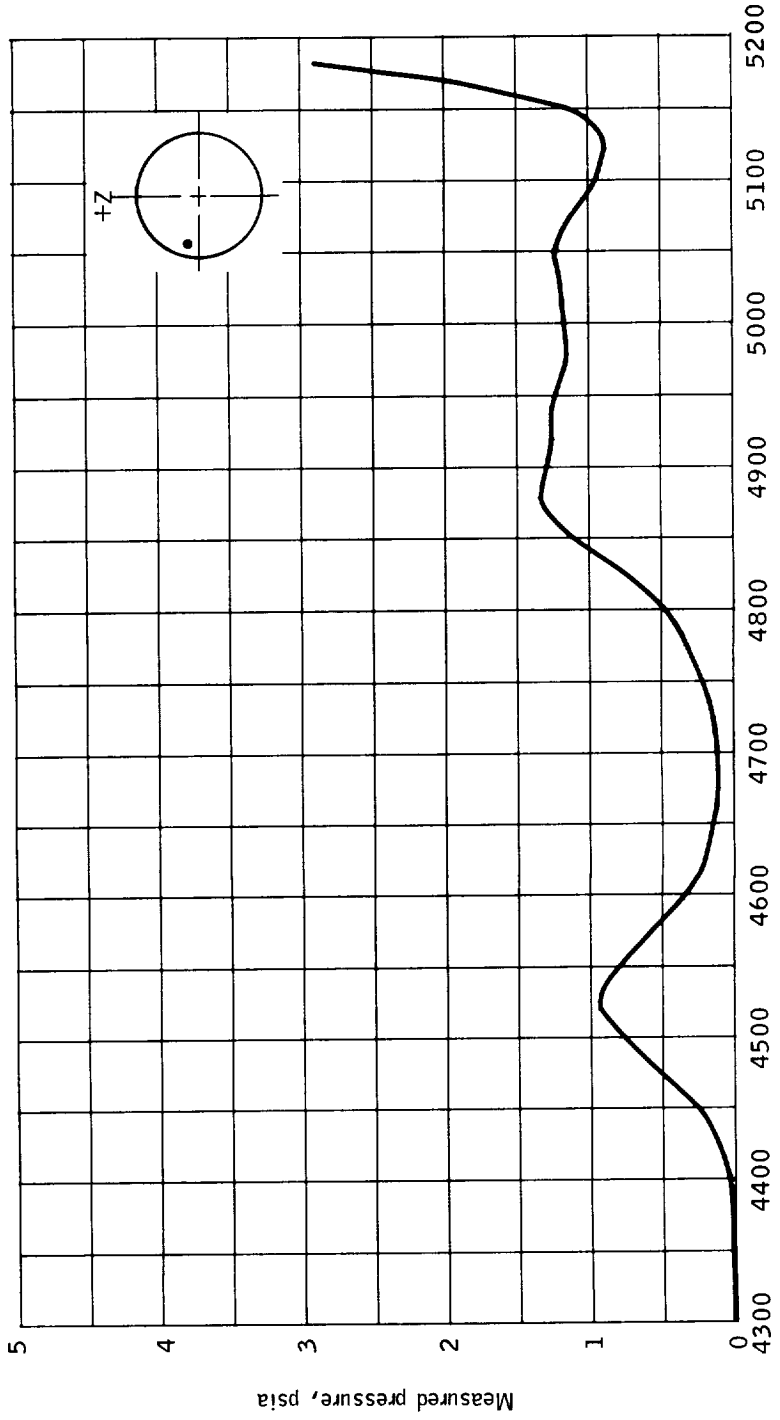

NASA-S-66-10024

(c) CA1145P, Y71, Z0, S/R .947.

Figure 7.3-2.- Continued.

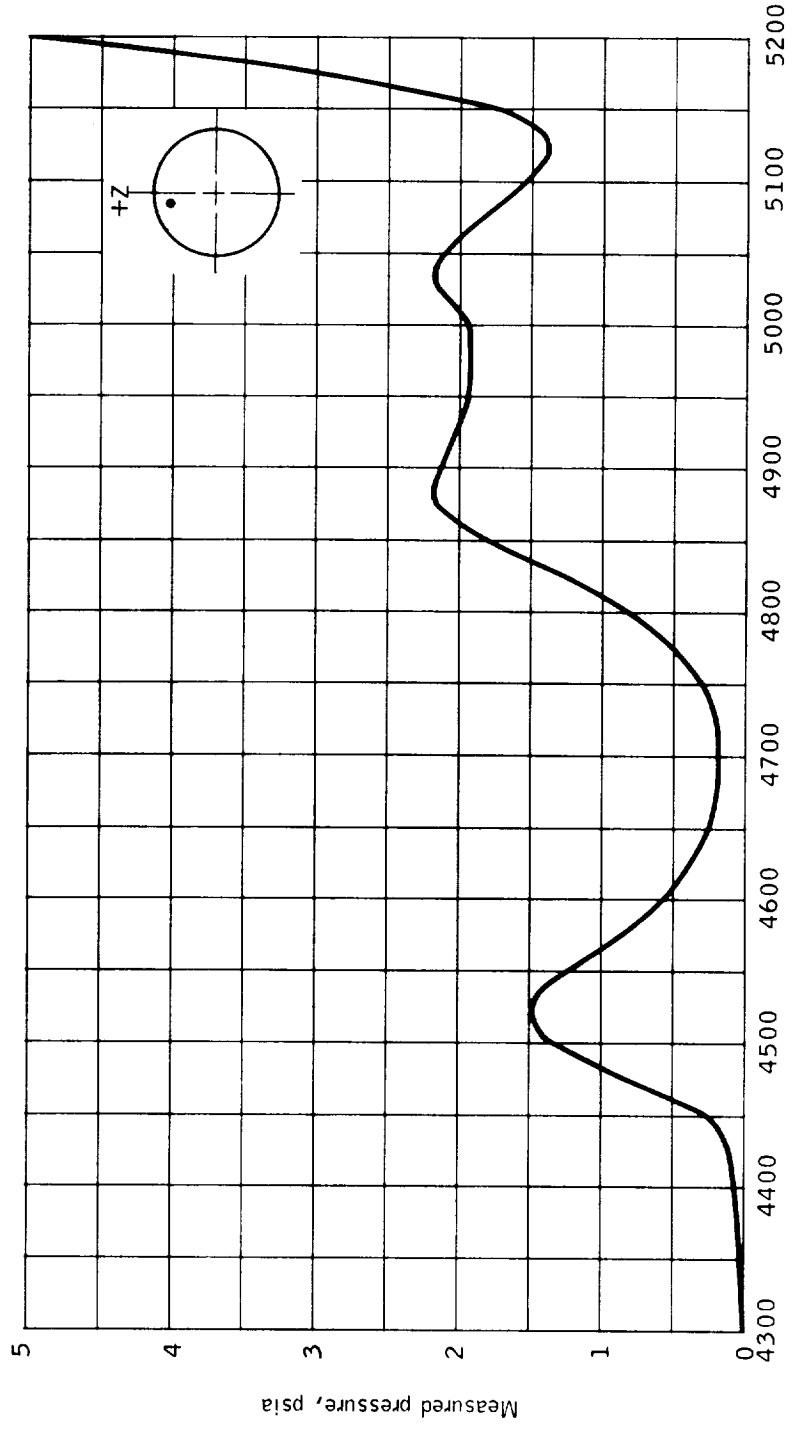

(d) CA1146P, Y0, Z61, S/R .81.

Figure 7.3-2.- Continued.

NASA-S-66-10025

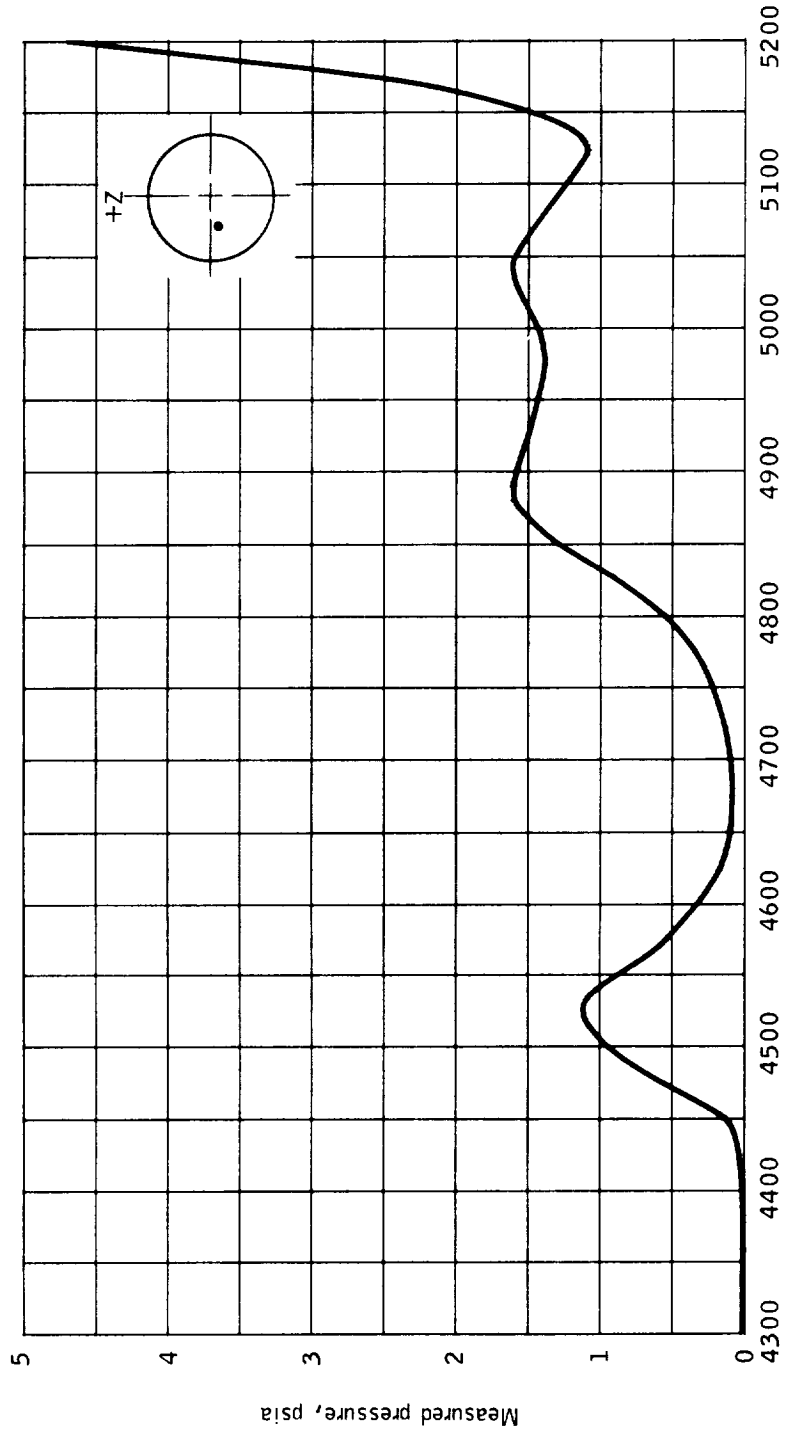

NASA-S-66-10026

(e) CA1150P, Y39, Z0, S/R .51.

Figure 7.3-2.- Continued.

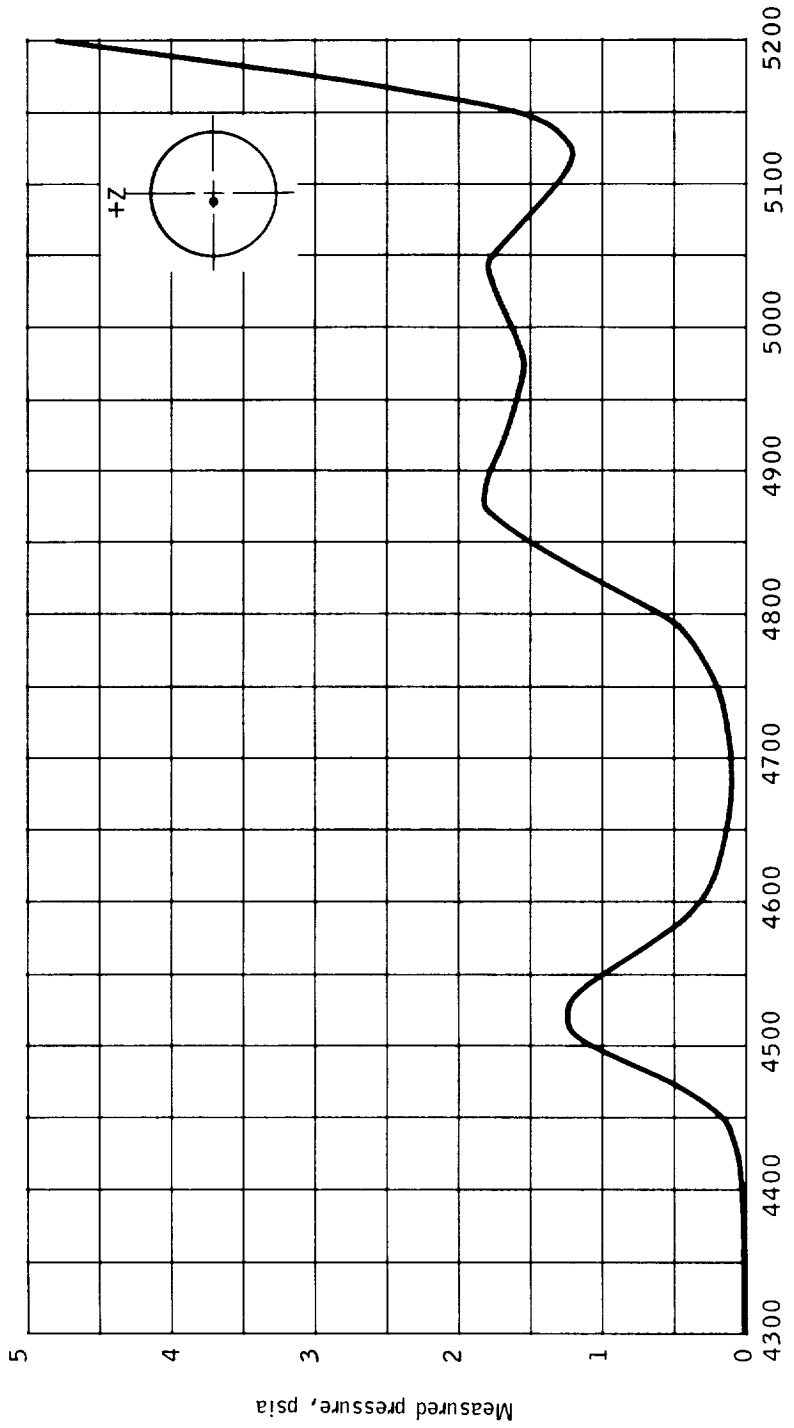

(f) CA1152P, Y0, Z0, S/R 0.

Figure 7.3-2.- Concluded.

NASA-S-66-10027

NASA-S-66-10028

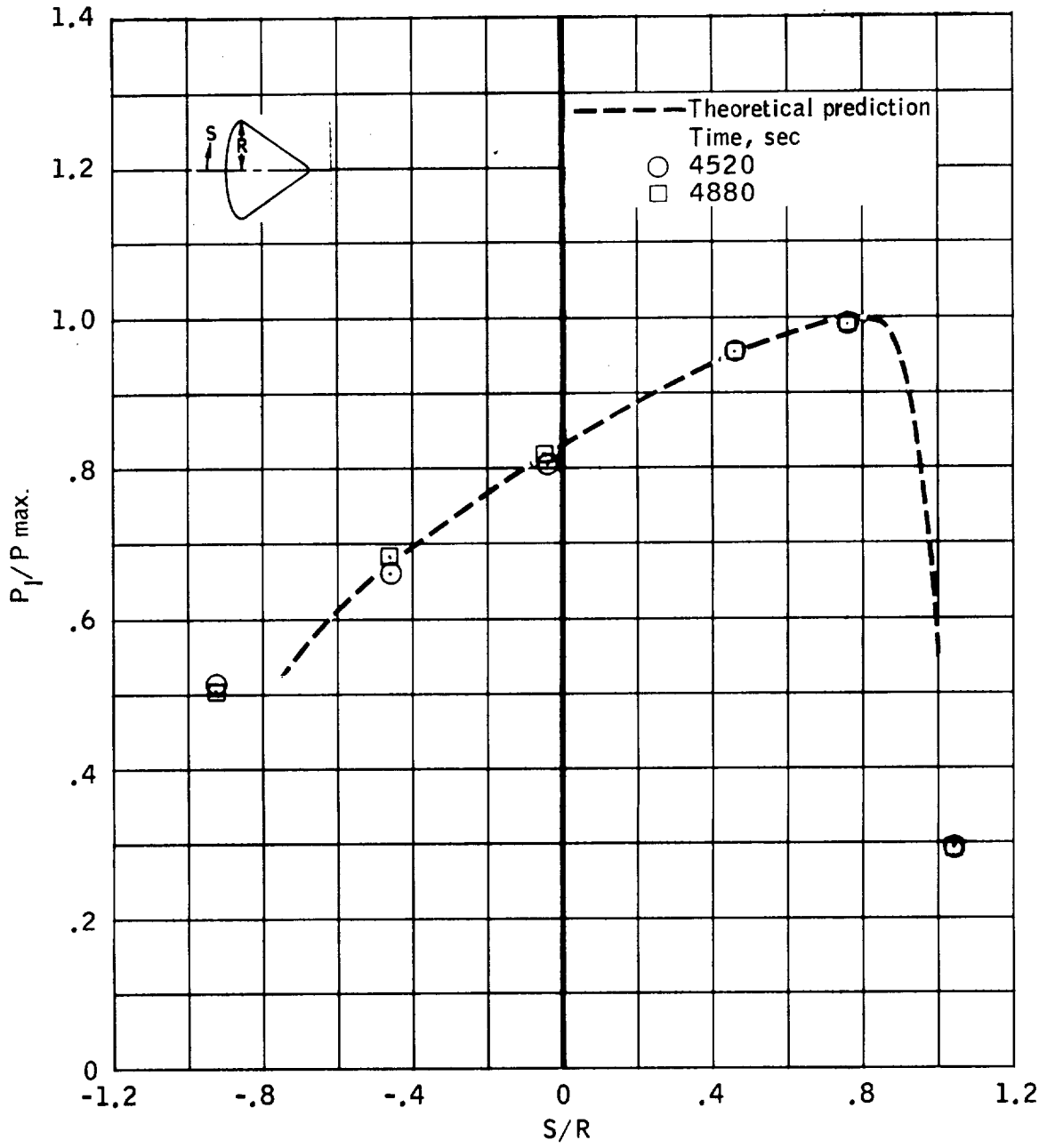

(a) Pitch plane.

Figure 7.3-3.- Comparison of measured and calculated pressure distribution, Mission AS-202.

NASA-S-66-10029

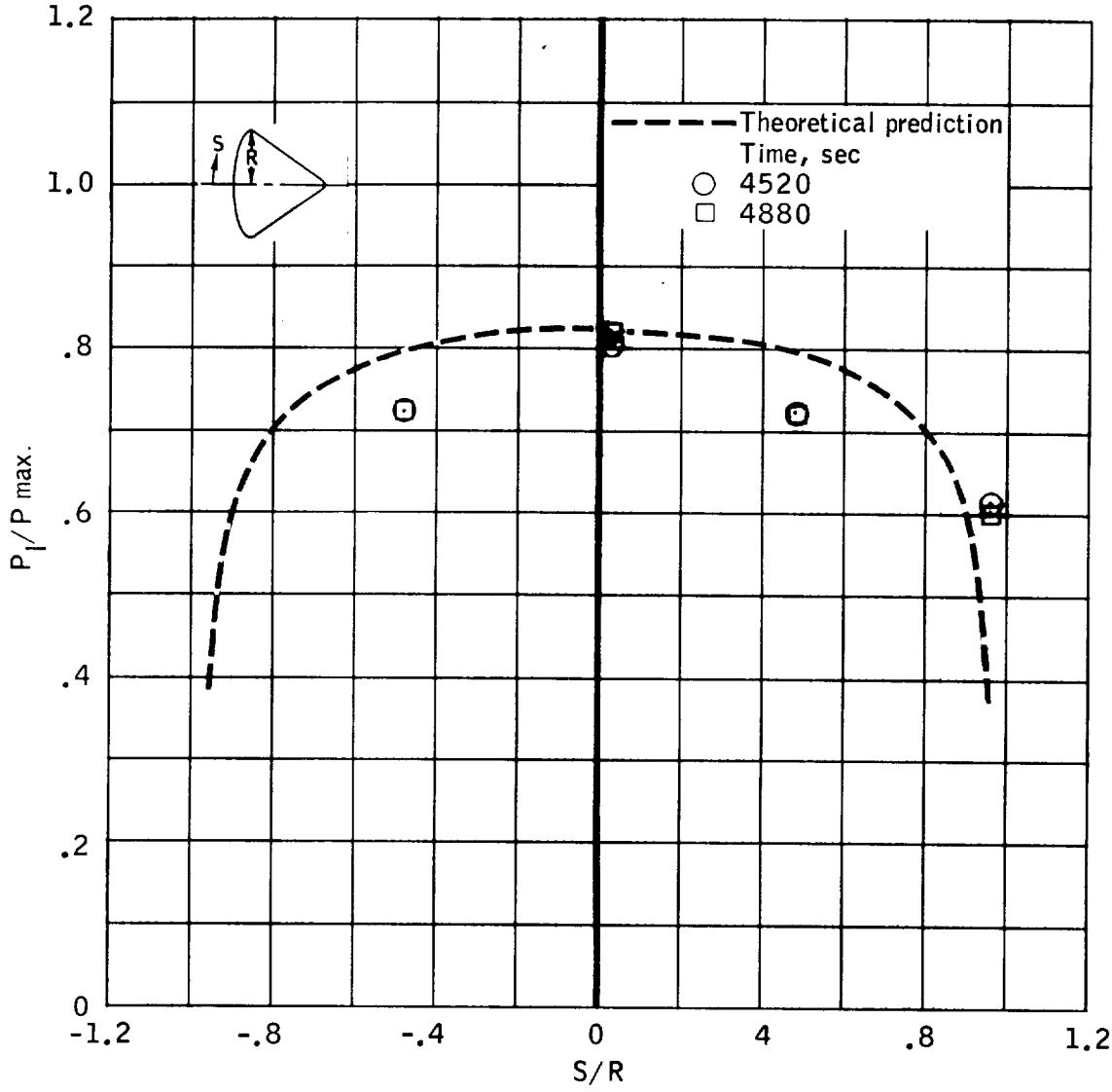

(b) Yaw plane.

Figure 7.3-3.- Concluded.

NASA-S-66-10030

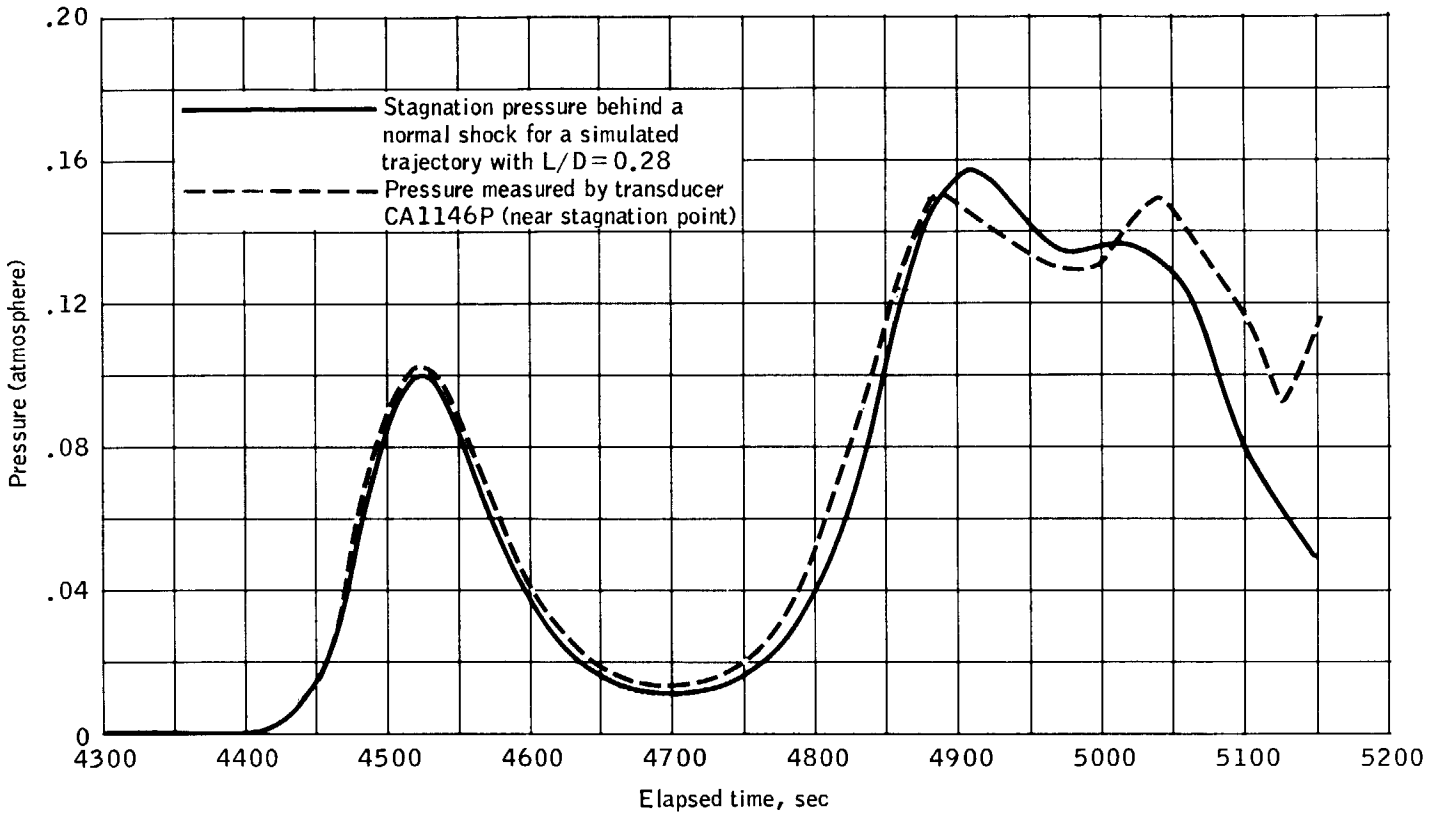

Figure 7.3-4.- Comparison of maximum measured pressure with calculated stagnation pressure, Mission AS-202.

NASA-S-66-10031

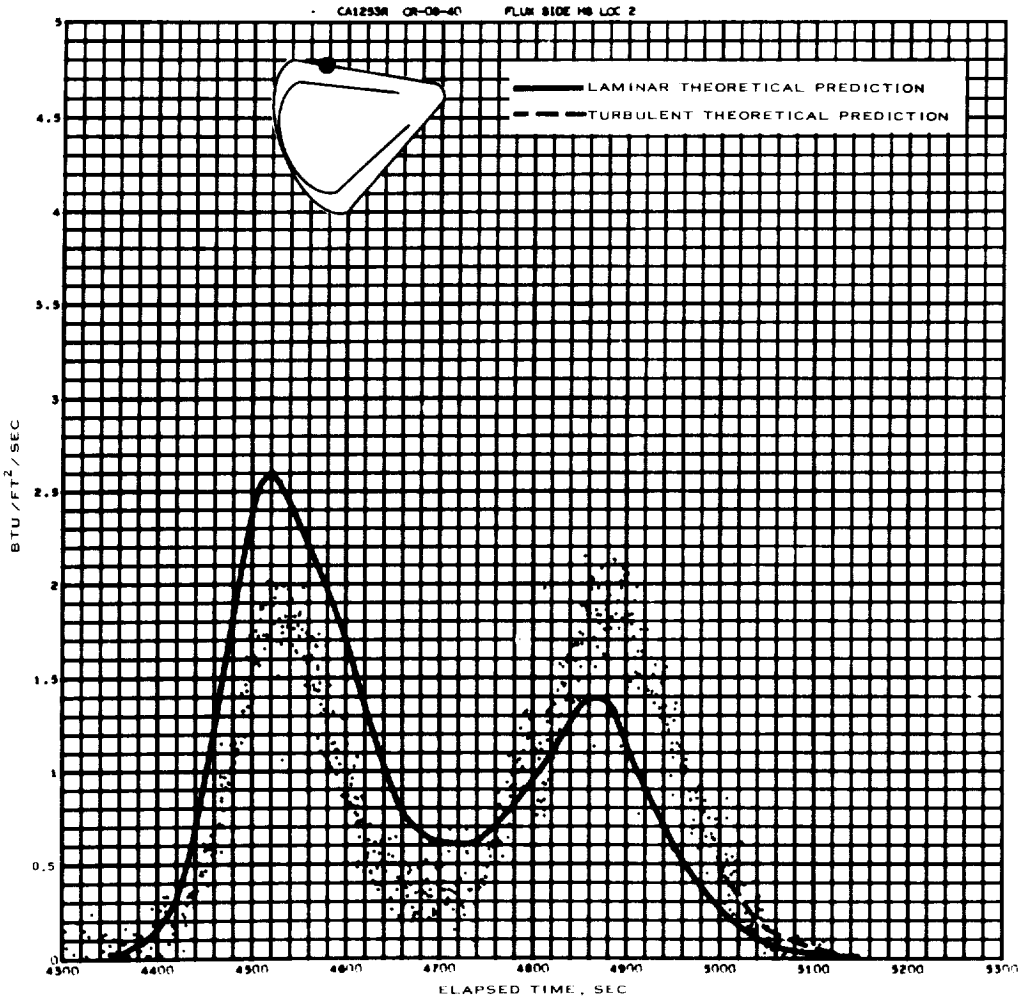

(a) CA1253R.

Figure 7.3-5.- Heating rates as a function of time.

NASA-S-66-10032

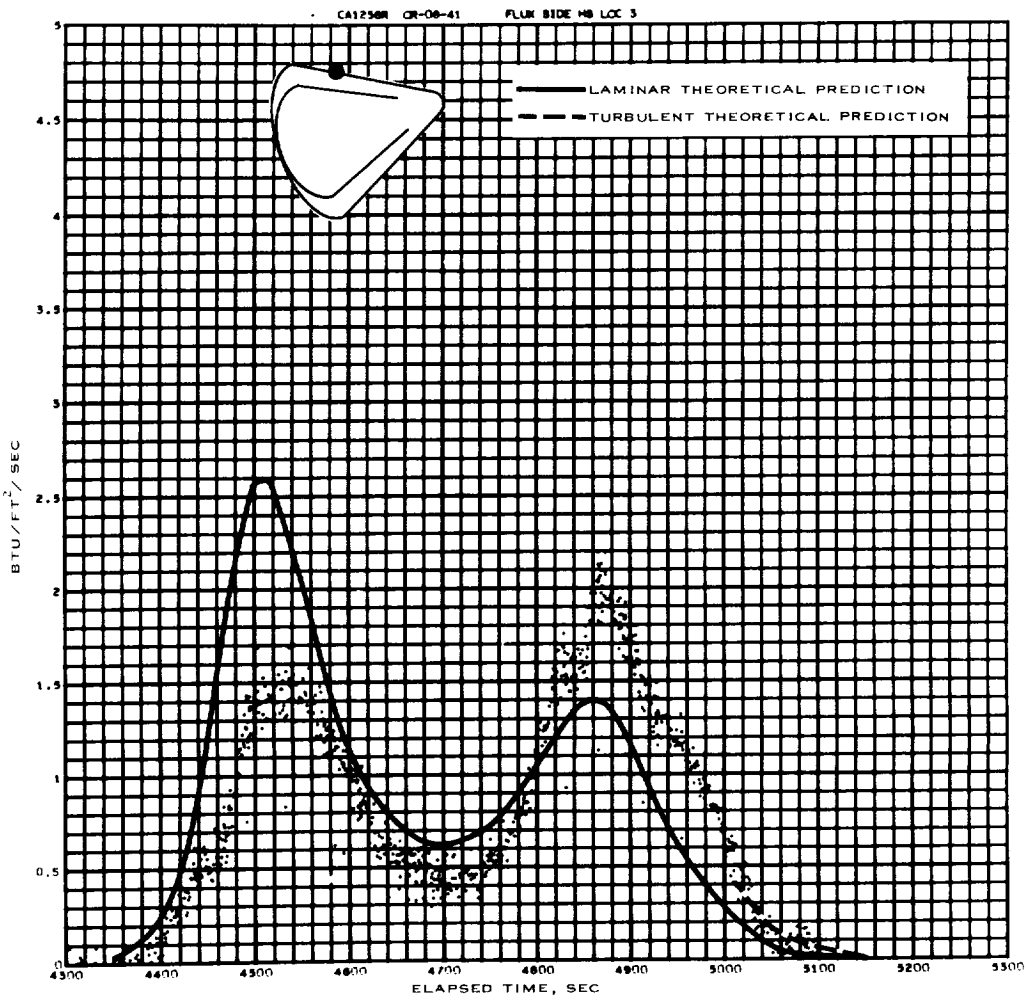

(b) CA1256R.

Figure 7.3-5.- Continued.

NASA-S-66-10033

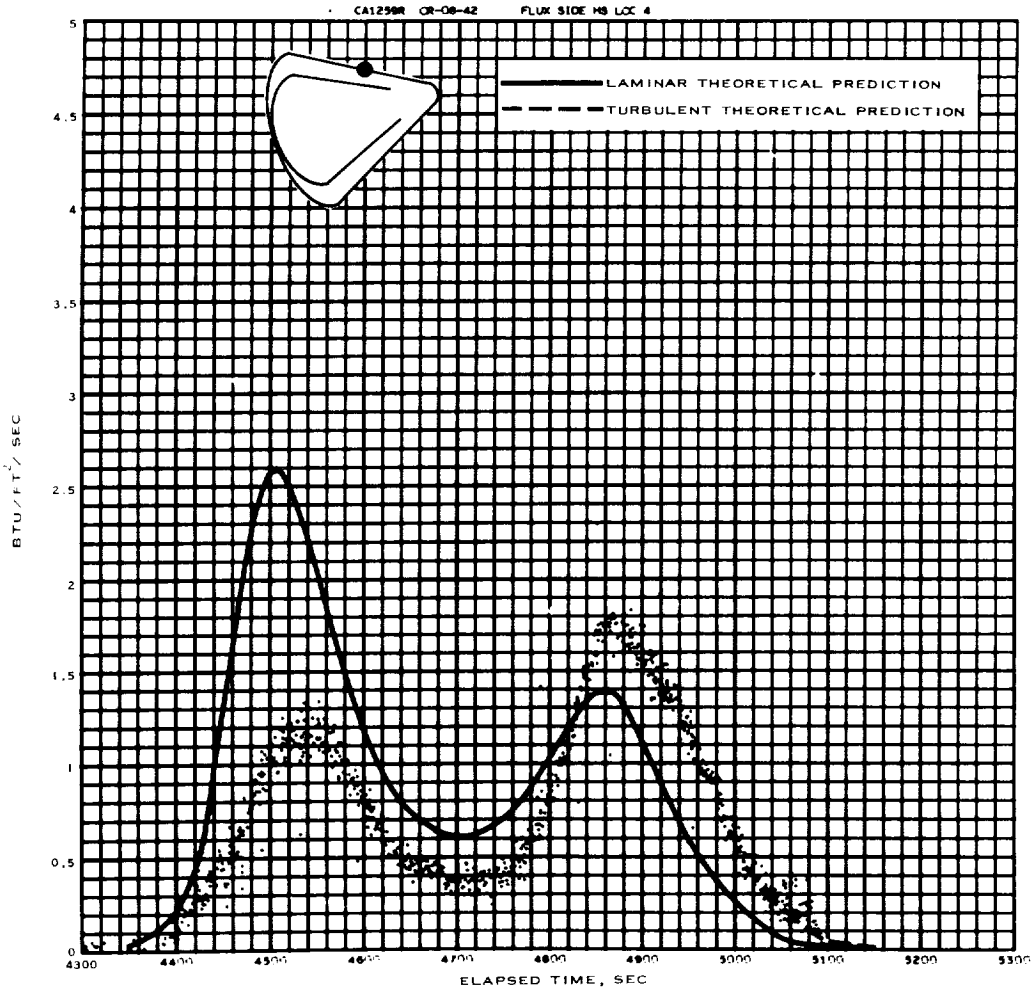

(c) CA1259R.

Figure 7.3-5.- Continued.

NASA-S-66-10034

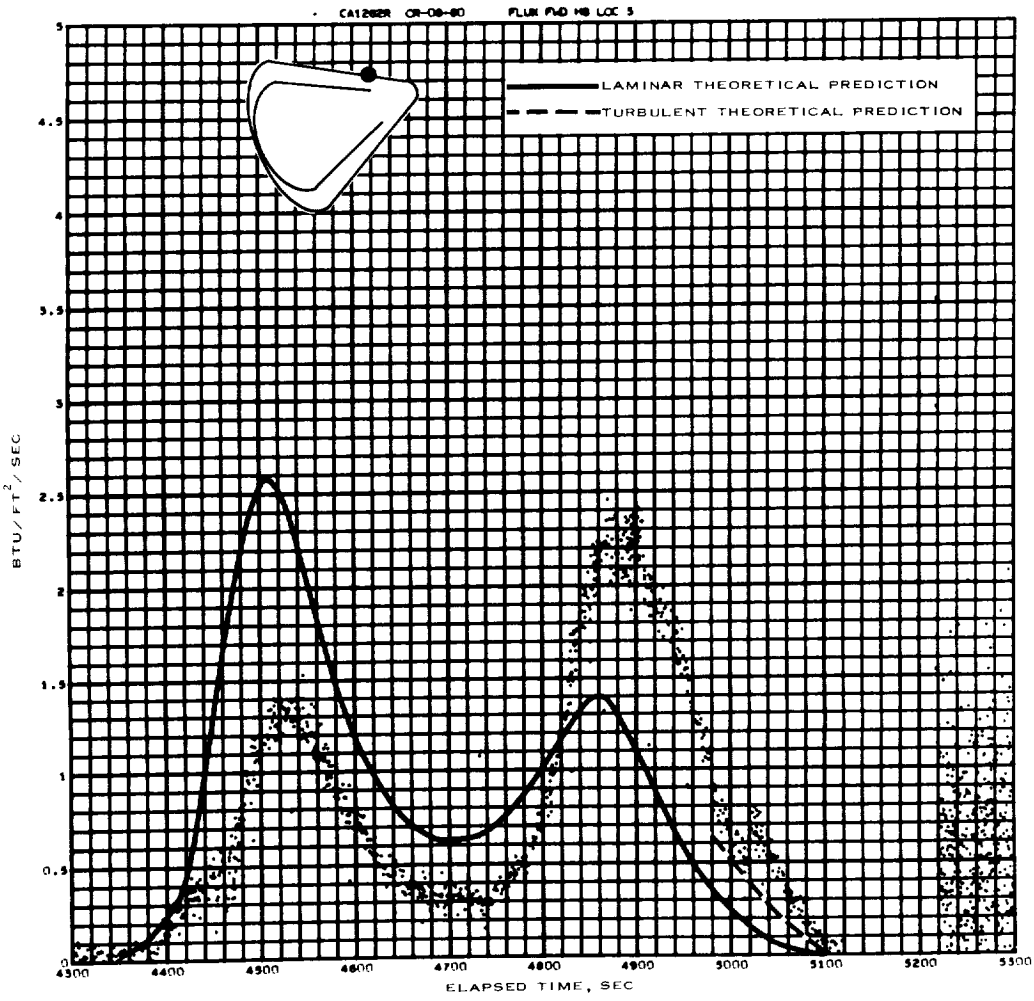

(d) CA1262R.

Figure 7.3-5.- Continued.

NASA-S-66-10035

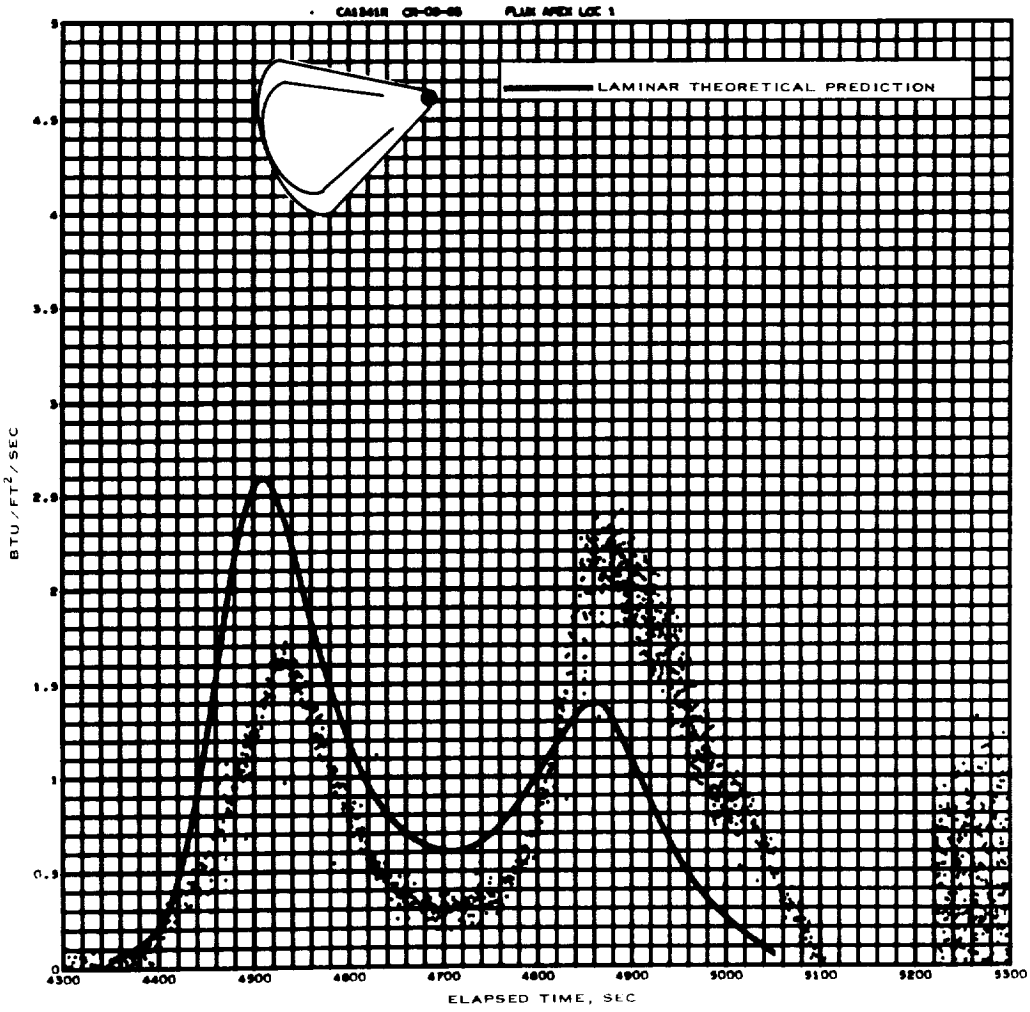

(e) CA1341R.

Figure 7.3-5.- Continued.

NASA-S-66-10036

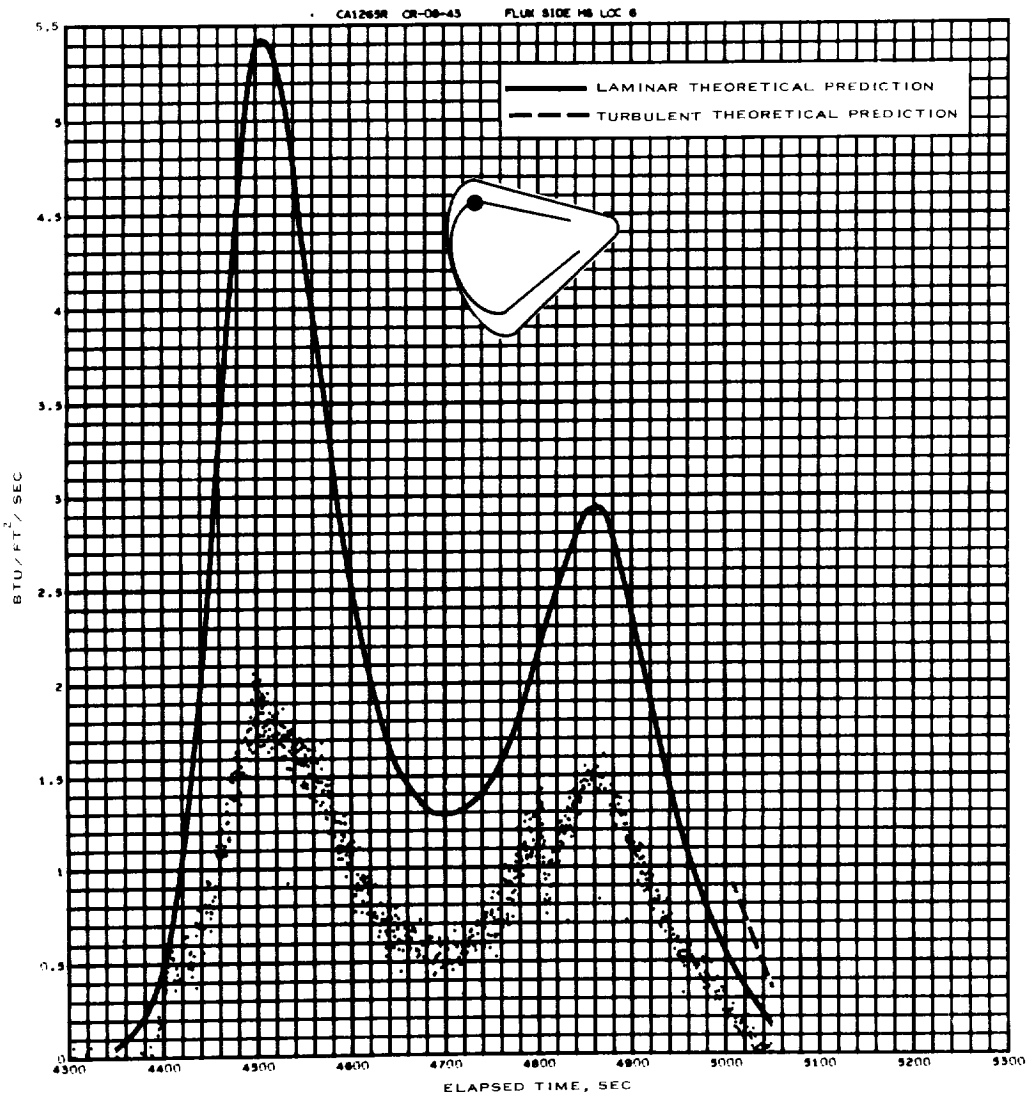

(f) CA1265R.

Figure 7.3-5.- Continued.

NASA-S-66-10037

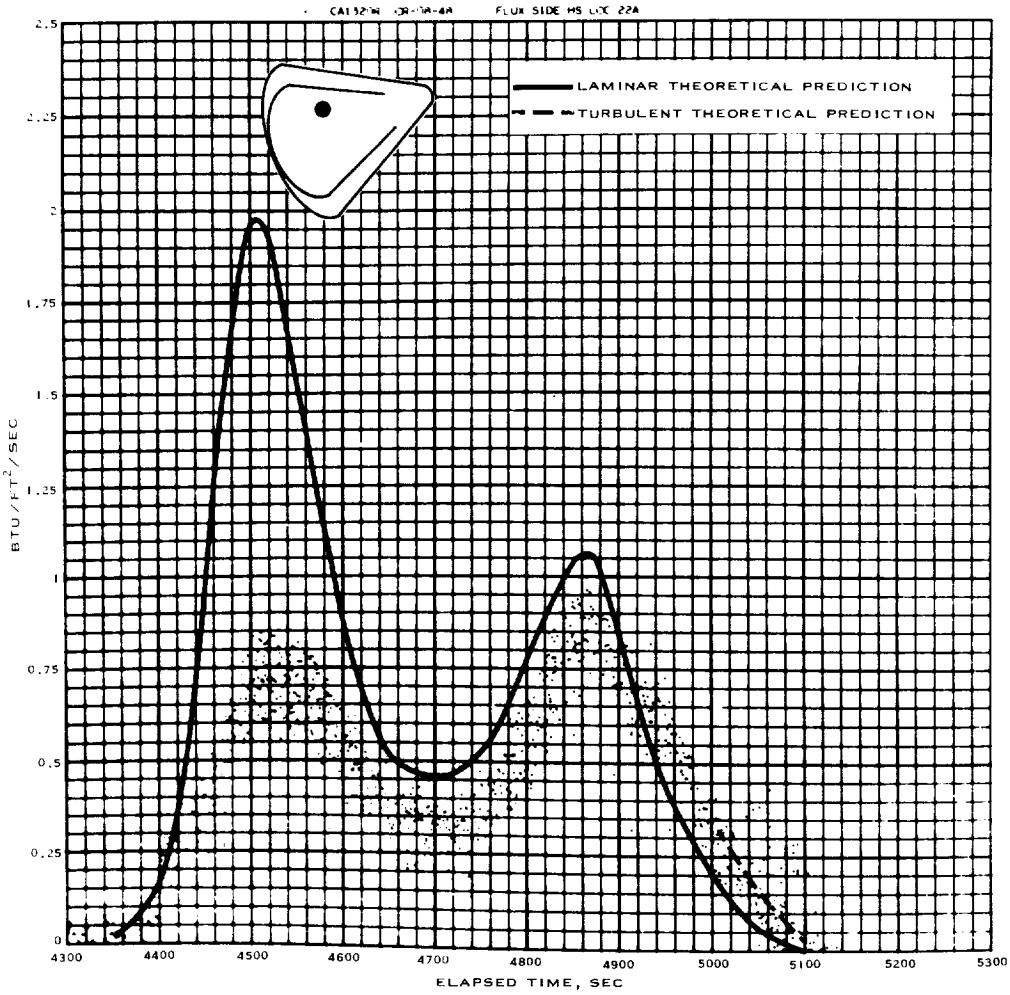

(g) CA1320R.

Figure 7.3-5.- Continued.

NASA-S-66-10038

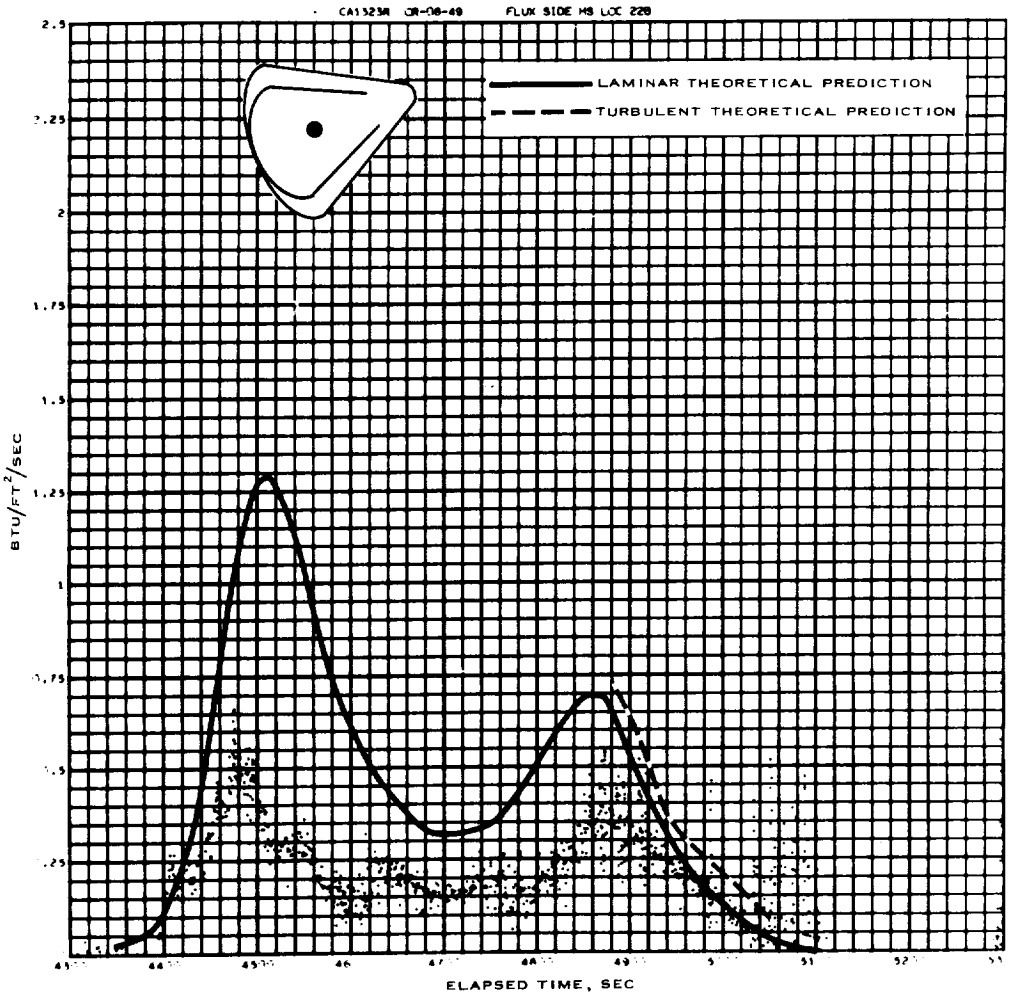

(h) CA1323R.

Figure 7.3-5.- Continued.

NASA-S-66-10039

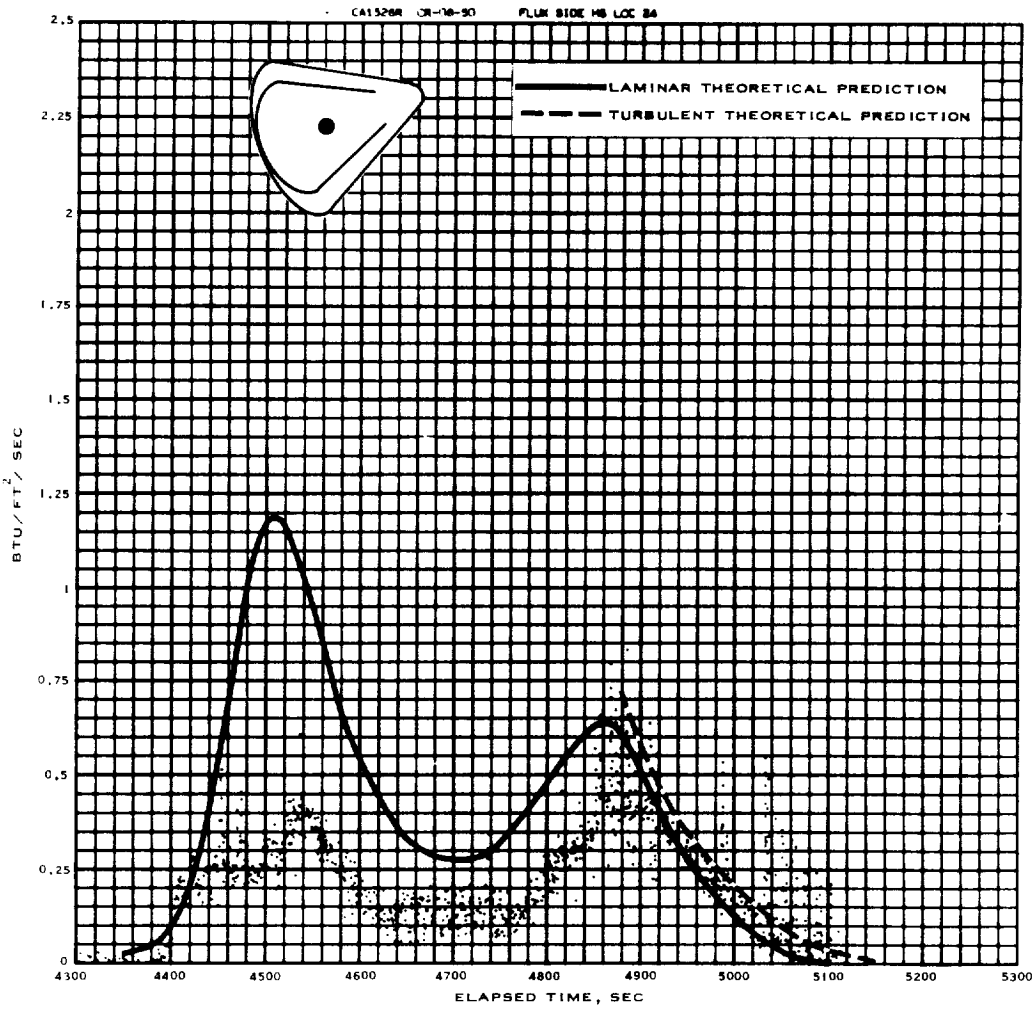

(i) CA1326R.

Figure 7.3-5.- Continued.

NASA-S-66-10040

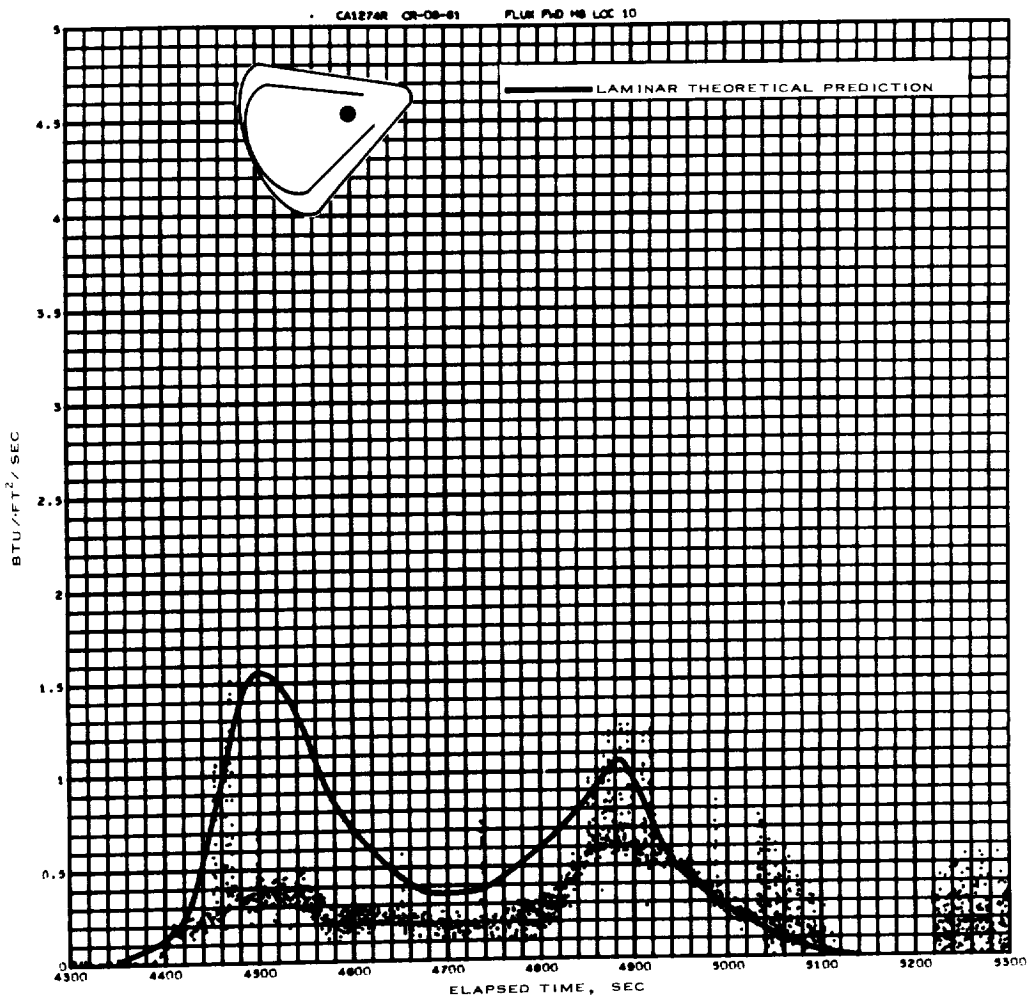

(j) CA1274R.

Figure 7.3-5.- Continued.

NASA-S-66-10041

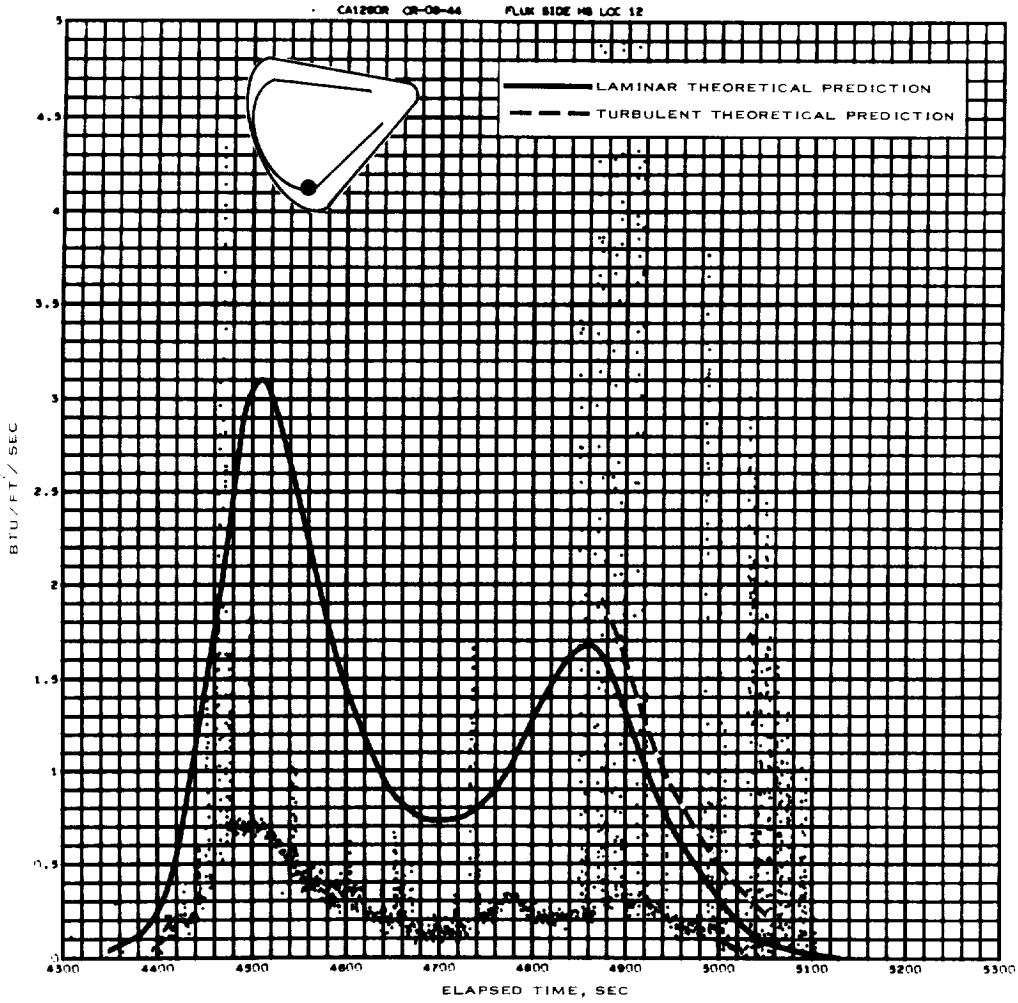

(k) CA1280R.

Figure 7.3-5.- Continued.

NASA-S-66-10042

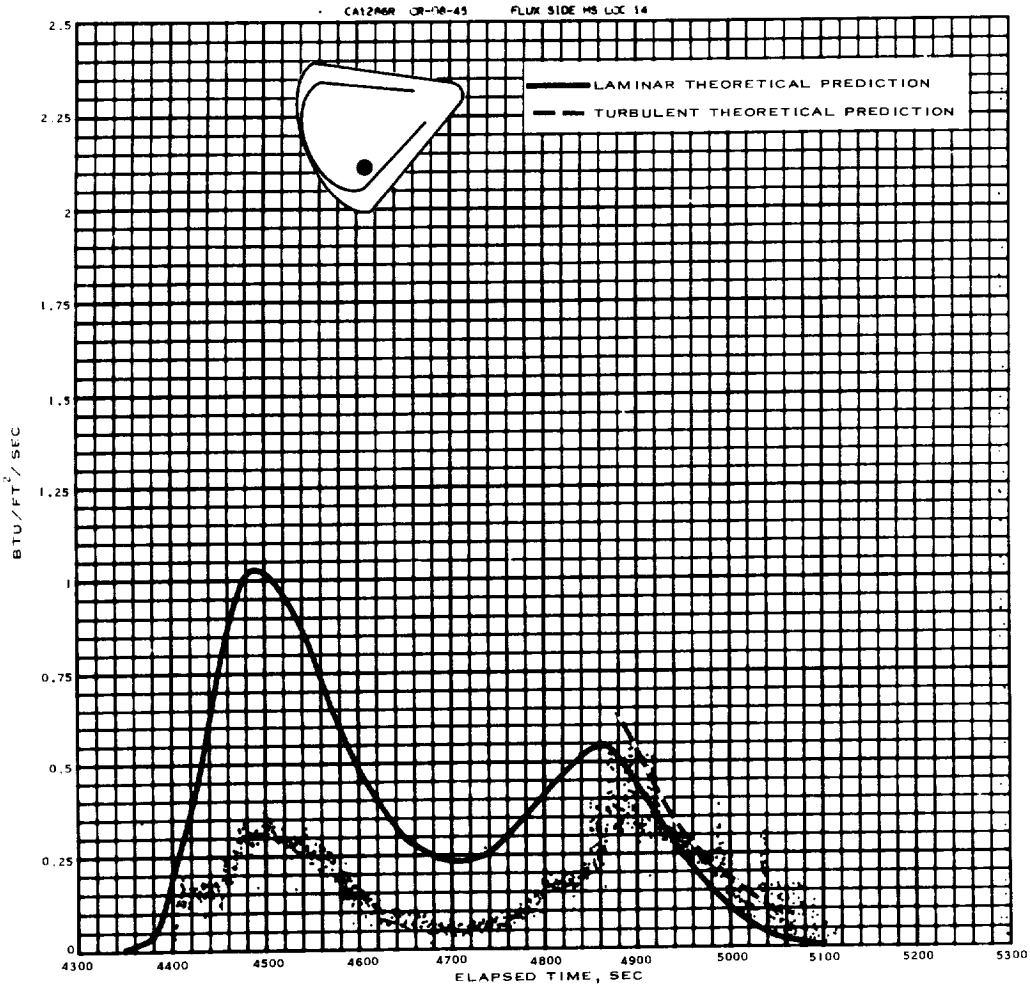

(l) CA1286R.

Figure 7.3-5.- Continued.

NASA-S-66-10043

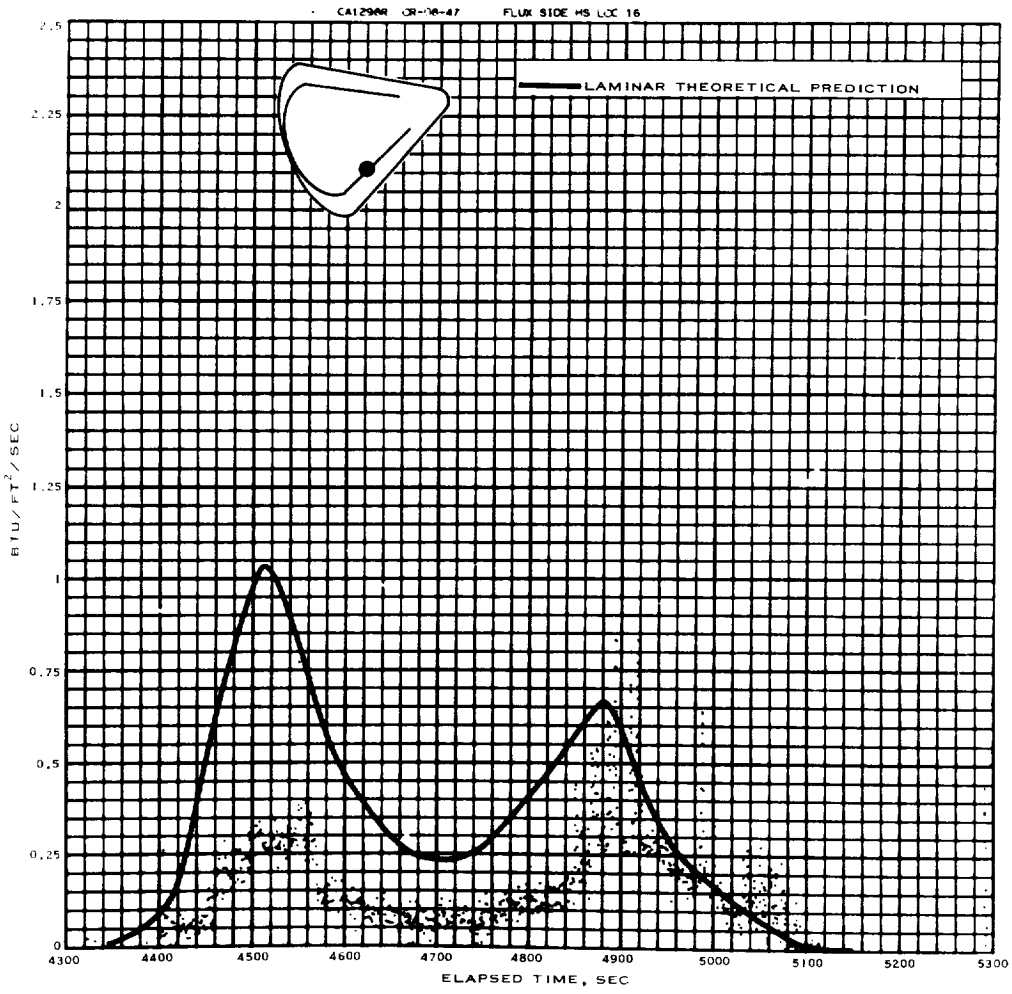

(m) CA1298R.

Figure 7.3-5.- Continued.

NASA-S-66-10044

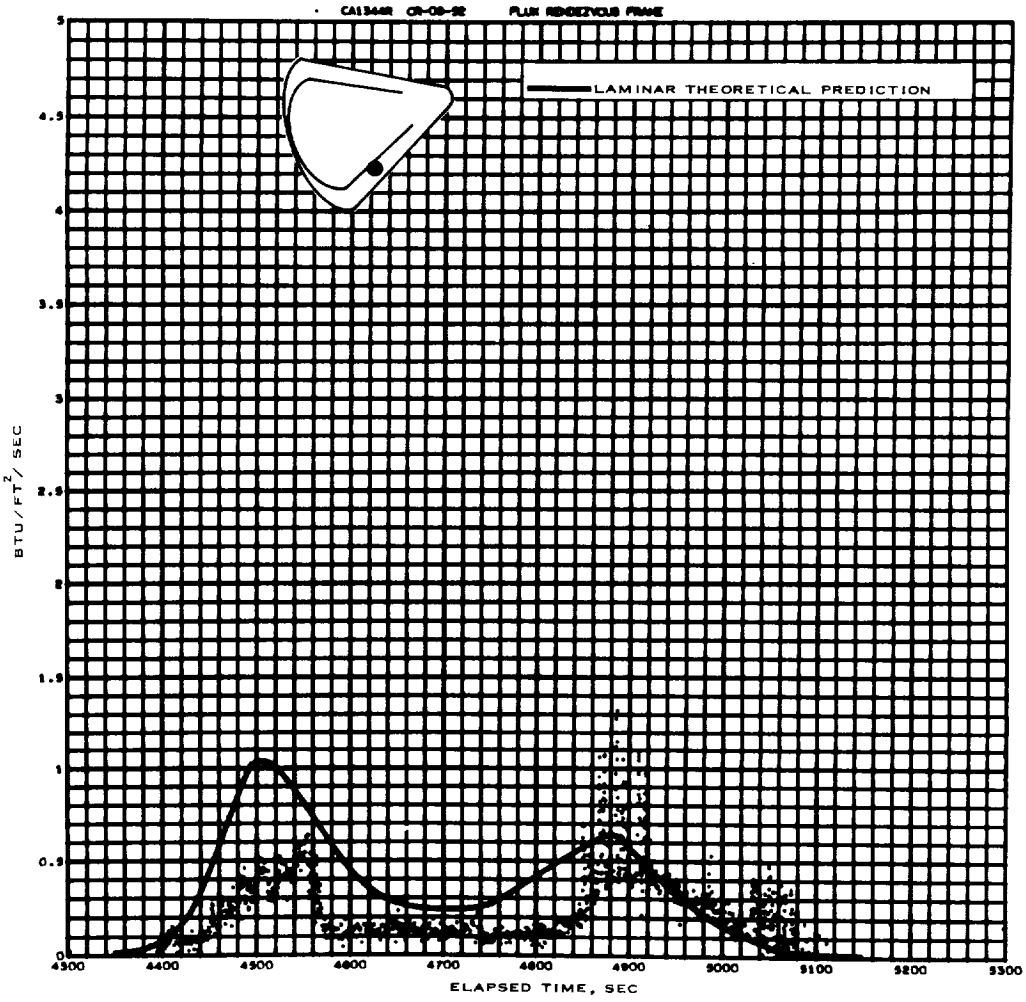

(n) CA1344R.

Figure 7.3-5.- Continued.

NASA-S-66-10045

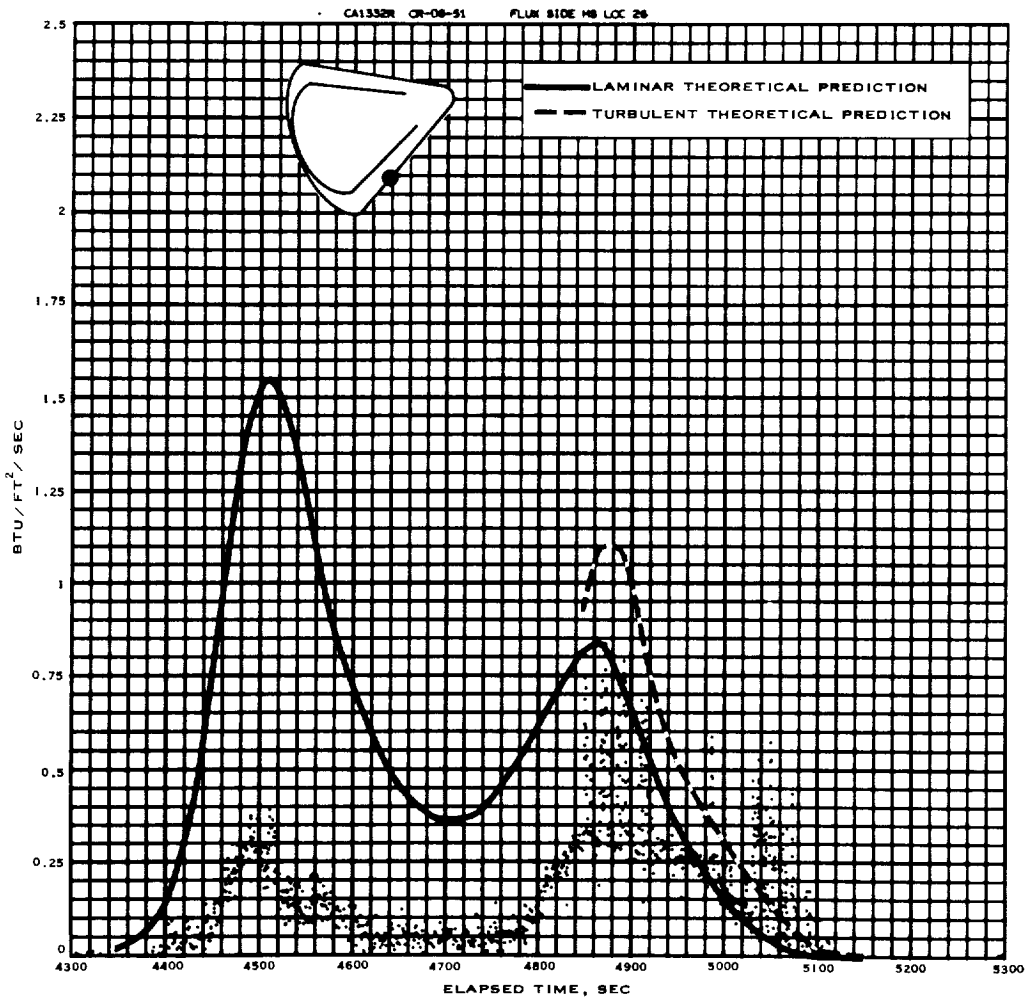

(o) CA1332R.

Figure 7.3-5.- Continued.

NASA-S-66-10046

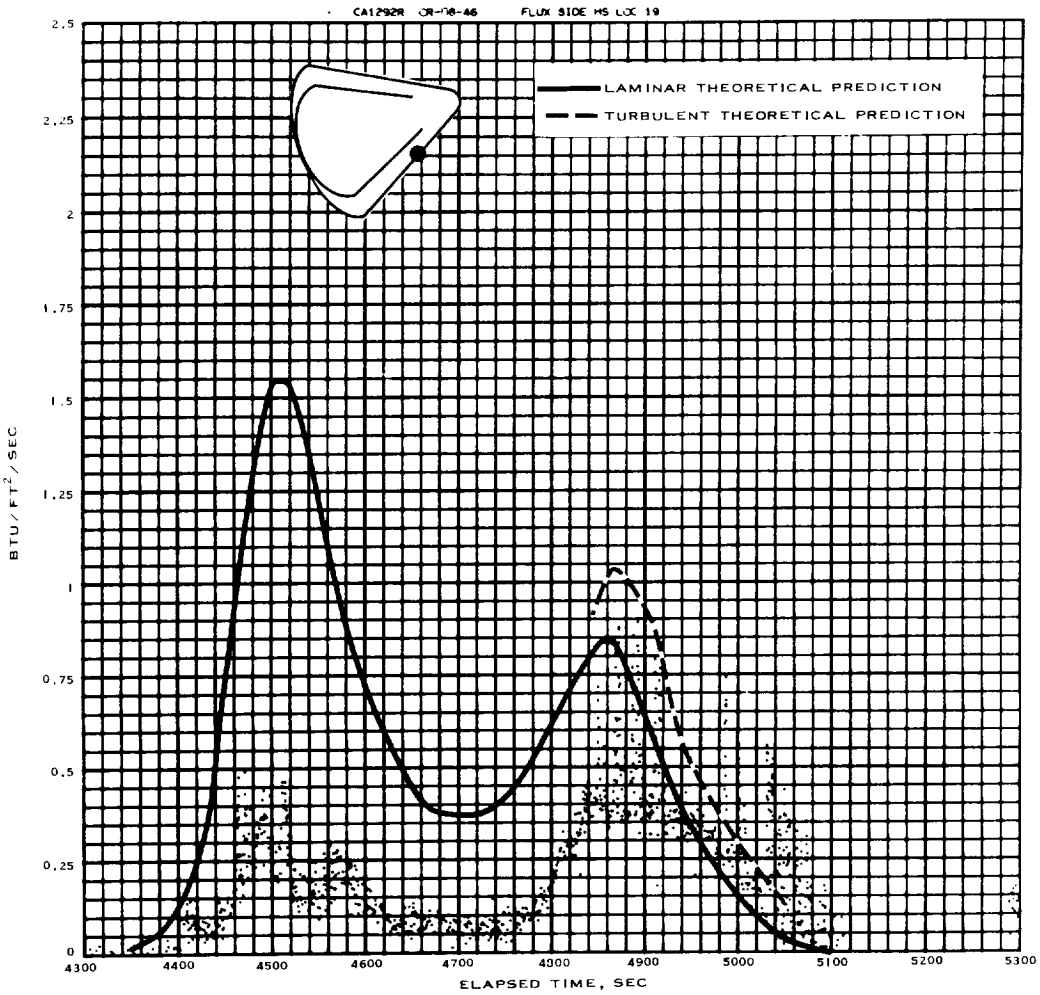

(p) CA1292R.

Figure 7.3-5.- Continued.

NASA-S-66-10047

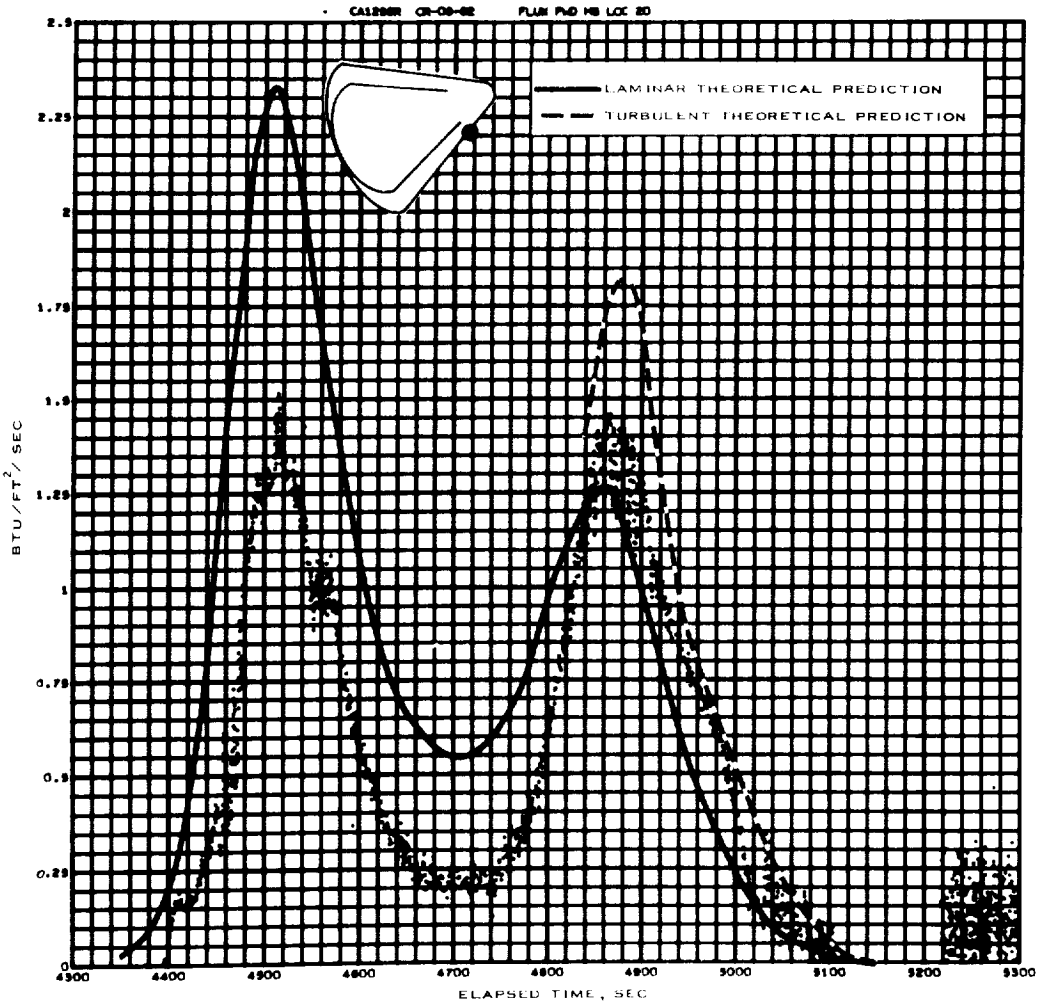

(q) CA1295R.

Figure 7.3-5.- Continued.

NASA-S-66-10048

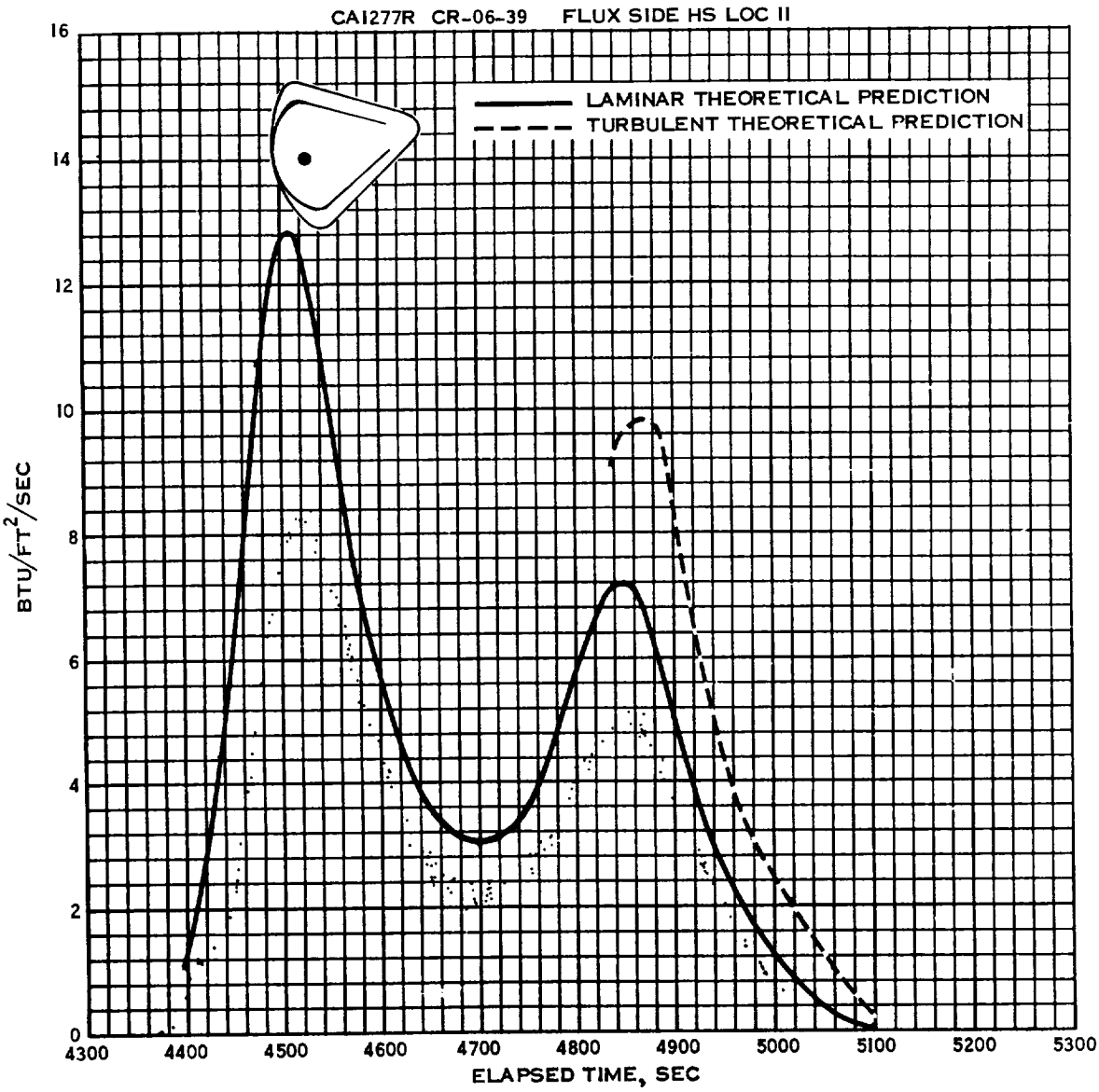

(r) CA1277R.

Figure 7.3-5.- Continued.

NASA-S-66-10049

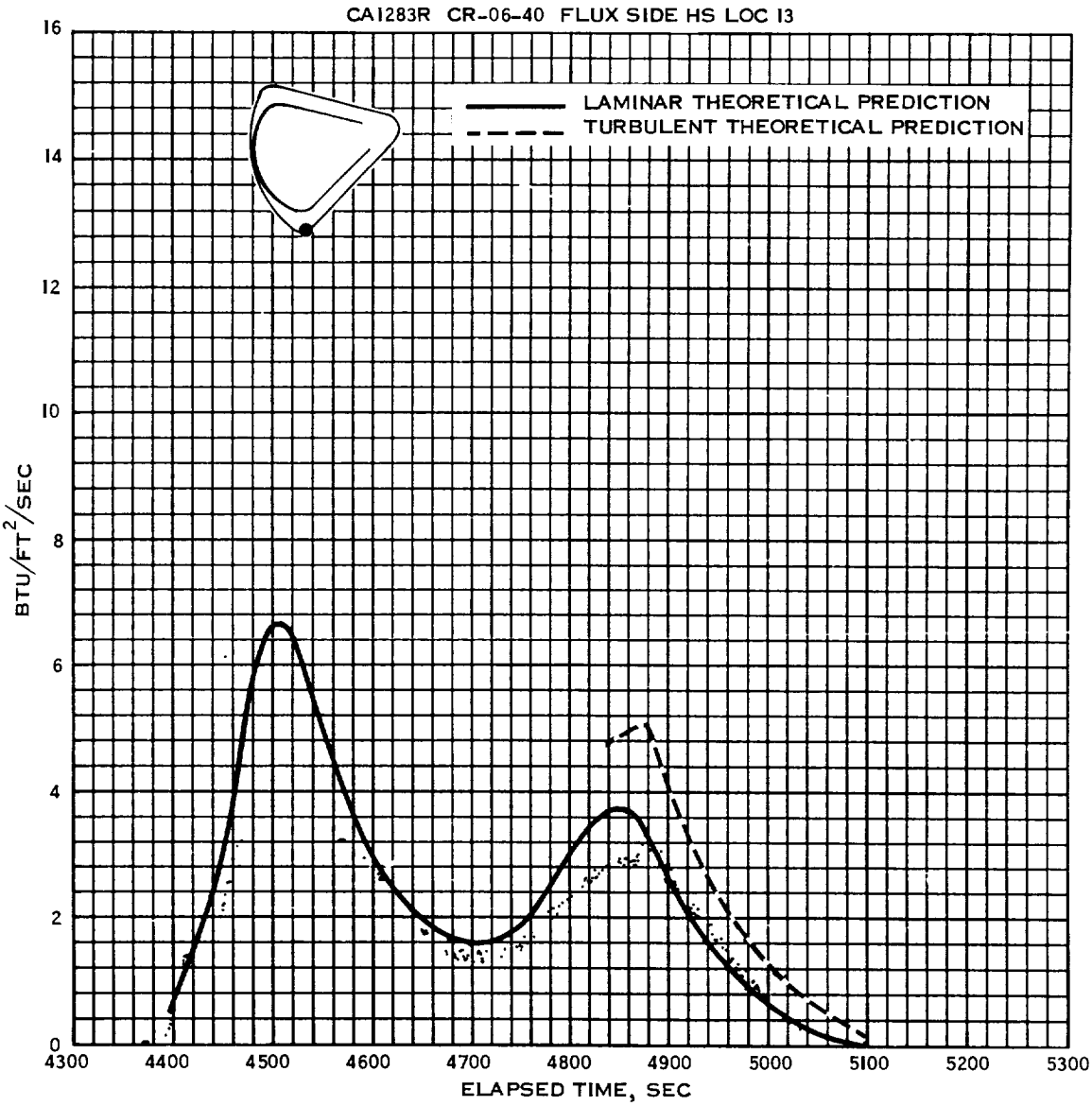

(s) CA1283R.

Figure 7.3-5.- Concluded.

NASA-S-66-10050

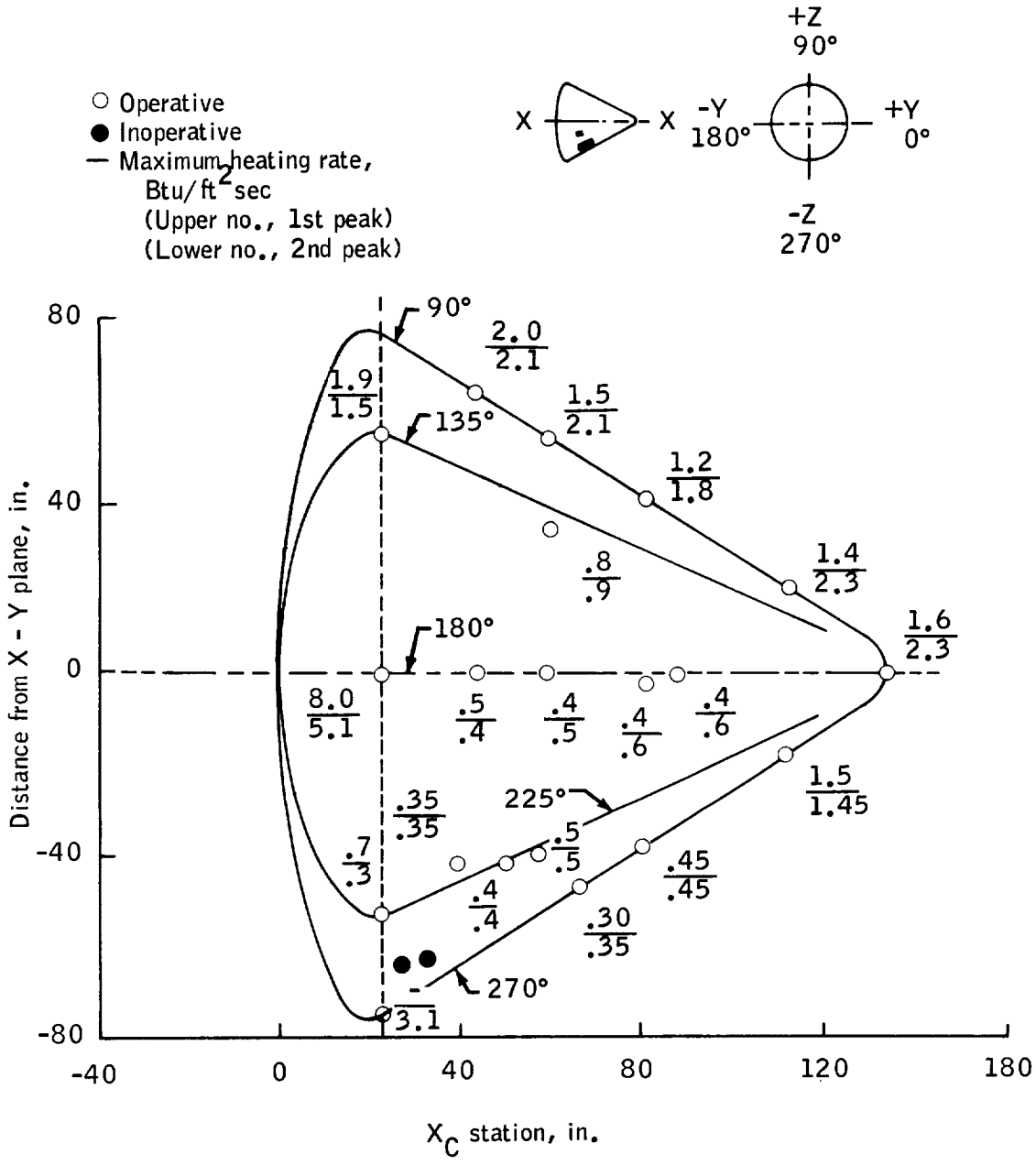

Figure 7.3-6.- Instrumentation locations on the conical surface of the CM, showing actual maximum heating rates, Mission AS-202.

7.4 Thermo Structures

7.4.1 Heat transfer.- The thermal environment of the Mission AS-202 ascent trajectory has been evaluated for the SM and the SLA. The heating parameters were higher than those predicted for the nominal Mission AS-202 trajectory.

The thermal environment was measured by temperature sensors located on the SM and the SLA. This instrumentation measured the inner and outer skin temperatures and several internal structure temperatures during ascent. In the following evaluation of temperatures, the discussion is limited to a representative number of typical temperature locations for the time period from lift-off to about T+300 seconds, which is the portion of the trajectory significant for ascent heating.

Service module temperatures: Figure 7.4.1-1 shows the distribution of peak temperatures measured on the SM outer skin during ascent.

The maximum SM launch temperature of 210° F was measured in front of SM RCS quad A, on the outer skin without cork protection, at longitudinal station X_S350 inches and 253 degrees from the +Y-axis, at T+130 seconds.

The low temperatures of 110° to 130° F, measured by sensors SA7904T, SA7906T, SA7907T, and SA7917T were also located close to quad A but were under the protective cork insulation. The cork insulation on the SM surface around each RCS quad provided protection against aerodynamic heating during ascent, and against plume impingement during RCS engine firing.

No smooth-body conclusions for longitudinal or circumferential variations in maximum temperatures are applicable since each of the sensors located on the same logitudinal or meridional line was also subjected to different interference heating from the effects of protuberances. The effects of the protuberances are large compared with any smooth-body variations due to angle of attach, etc.

Postflight temperature predictions were performed for sensor SA7916T on the SM inner surface at the location (X_S350 inches and 253 degrees) of the highest outside temperature measured. Using the actual ascent trajectory and pressure ratio data obtained from wind tunnel tests, the maximum and minimum predicted temperature response is compared with the measured temperature time history in figure 7.4.1-2. The maximum response was based on SM radiation interchange with the sun and the earth. The minimum response was based on radiation exchange with space only. The RCS motors were not fired during this time period.

The maximum and minimum predicted temperature histories should bracket the expected response. It can be seen from figure 7.4.1-2 that the predicted temperature response band is higher than the measured temperature response. Sensor SA7916T was located approximately 3 inches from the cork-protected area around quad A. The relatively cool skin under the cork provided a heat-sink which allowed a two-dimensional conduction effect which could result in a faster cool-down of the sensor than that which was predicted using a one-dimensional analysis. The internal temperatures on the SM aft bulkhead, SA7913T and SA7914T, did not exceed 100° F.

SLA temperatures: Figure 7.4.1-3 shows the distribution of peak temperatures measured on the SLA outer skin during ascent. The maximum temperature of 475° F was measured by sensor AA7937T (X_A775 inches and 304 degrees) at T+125 seconds. Figure 7.4.1-4 compares the predicted temperature response with the measured temperature time histories for sensors AS7937T and AA7938T (outer and inner skin thermocouples located at X_A775 inches and 304 degrees) and sensors AA7931T and AA7932T (outer and inner skin thermocouples located at X_A775 inches and 124 degrees). Satisfactory agreement is shown in figure 7.4.1-4 for both inner skin and for one outer skin (AA7931T) measurement. The outer skin at sensor AA7937T would not reach 475° F without driving the inner skin well above the observed 150° F level, indicating that AA7937T was not measuring SLA outer skin temperature, but that the high temperature response measured by sensor AA7937T during ascent was indicative of an operating thermocouple attached to a much lower heat capacity structure than the SLA honeycomb skin. The probable cause of the 475° F temperature level was the thermocouple coming off the surface of the SLA (also see section 7.15.1).

Disregarding the measurements from sensor AA7937T, the maximum SLA temperature of 260° F was measured by sensor AA7931T. The low peak temperatures measured by sensors AA7930T, AA7933T, and AA7939T were due to the fact that the sensors were located under the insulation material covering the SLA ordnance system forward circumferential separation splice and longitudinal separation splices. All outer skin temperature measurements aft of X_A610 inches show maximum temperatures below 110° F. These low temperatures were the result of the protection afforded by the cork insulation on the surface of the SLA in this area. Temperatures on the inner surface of the SLA skin, sensors AA7932T, AA7936T, and AA7938T, did not exceed 155° F.

Figures 7.4.1-5 and 7.4.1-6 show measured time histories for SLA sensors AA7931T (outer) and AA7932T (inner), respectively. Temperature predictions were prepared, utilizing the actual spacecraft 011 ascent trajectory and pressure ratio data obtained from wind tunnel tests. A maximum and a minimum predicted response are shown on each of the figures. The maximum response is based on SM radiation interchange with the sun and the earth. The minimum response is based on radiation exchange with space only.

A discontinuity is seen in the measured data at approximately T+145 seconds for sensor AA7931T (fig. 7.4.1-5). A similar jump in temperature was observed at T+145 seconds for all of the outer skin thermocouples (SM and SLA) which were not located under cork or in the vicinity of the vertical splices. This jump in temperature was caused by rocket plume convection and radiation heating from the forward firing retrorockets used to separate the S-IB stage. Launch vehicle data indicated that the increase in temperature due to retrorocket plume impingement was 17° F at the forward end of the S-IVB stage, as compared with 12° F predicted before the flight.

Concluding remarks: The SM and SLA temperatures measured on spacecraft 011 were within their respective design values maximum temperatures of 475° and 490° F, and thereby support the results of Mission AS-201 in thermally qualifying these structures for future operated Saturn I missions.

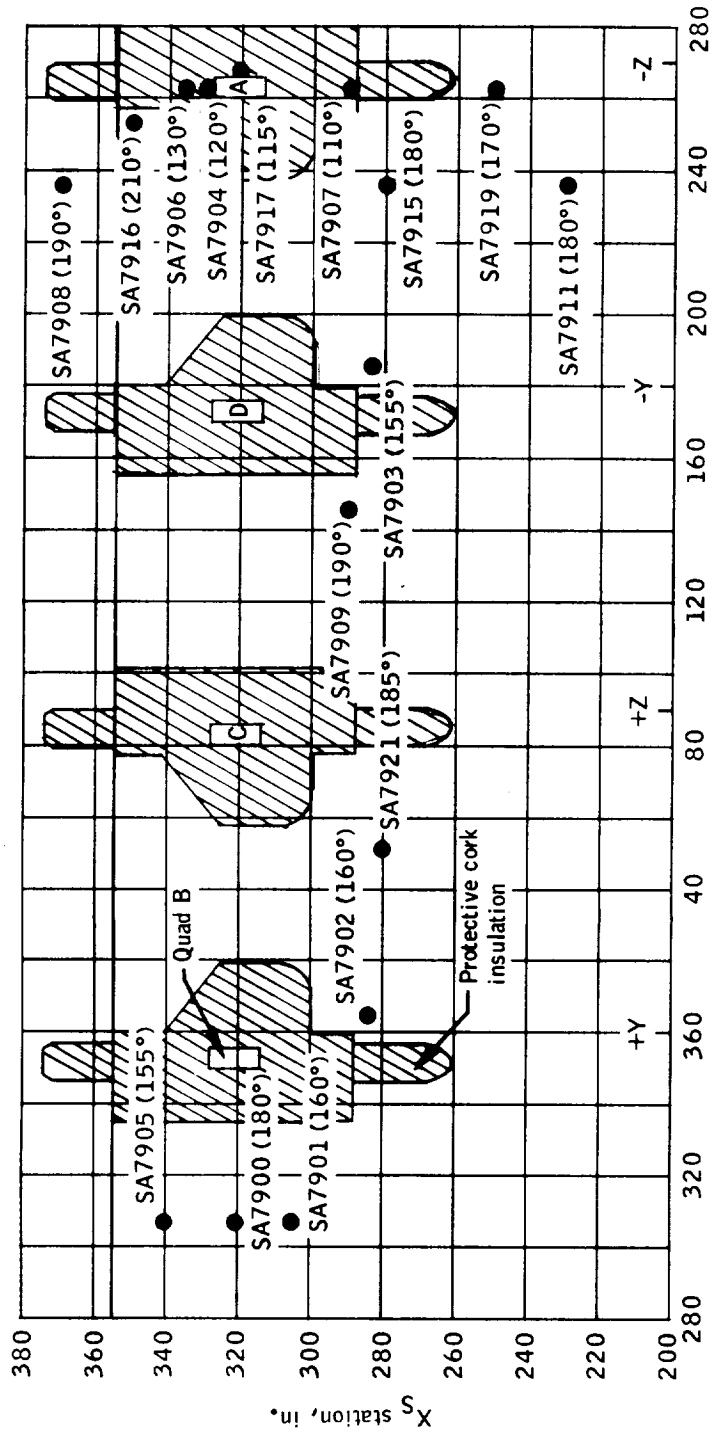

Figure 7.4.1-1.- Peak temperatures measured on SM outer surface during launch phase, Mission AS-202.

NASA-S-66-10051

NASA-S-66-10052

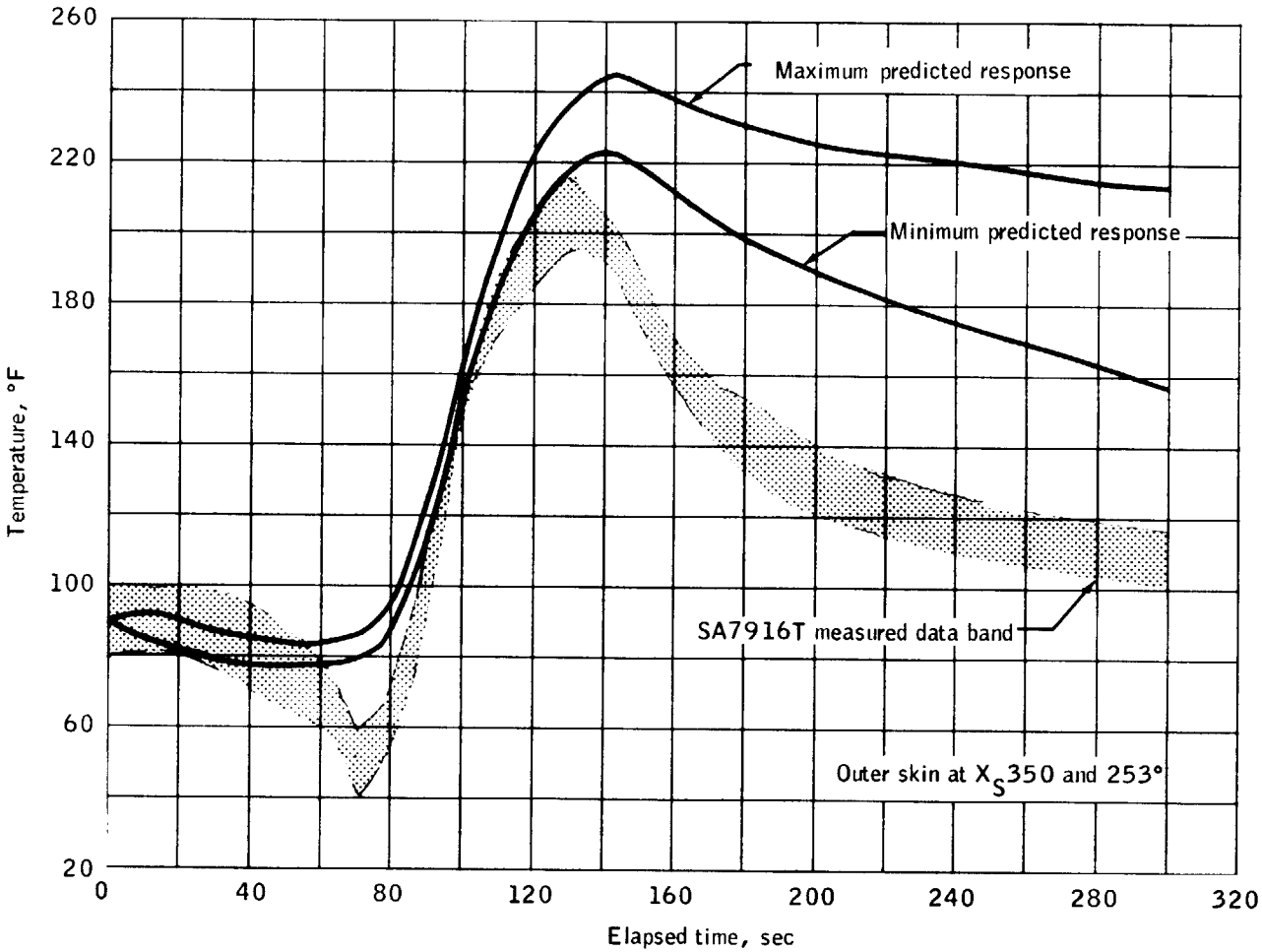

Figure 7.4.1-2.- Temperature time history for service module sensor SA7916T, Mission AS-202.

NASA-S-66-10053

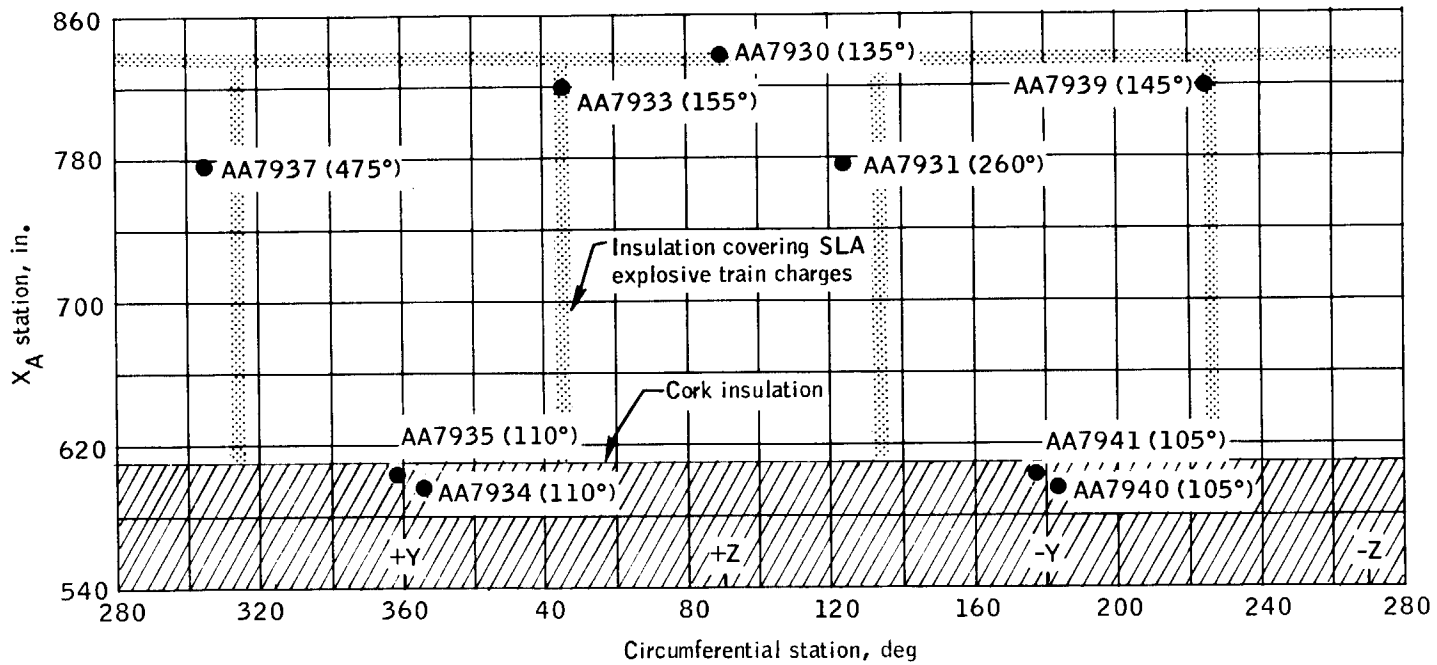

Figure 7.4.1-3.- Peak temperatures measured on spacecraft - LM adapter outer surface during the launch phase, Mission AS-202.

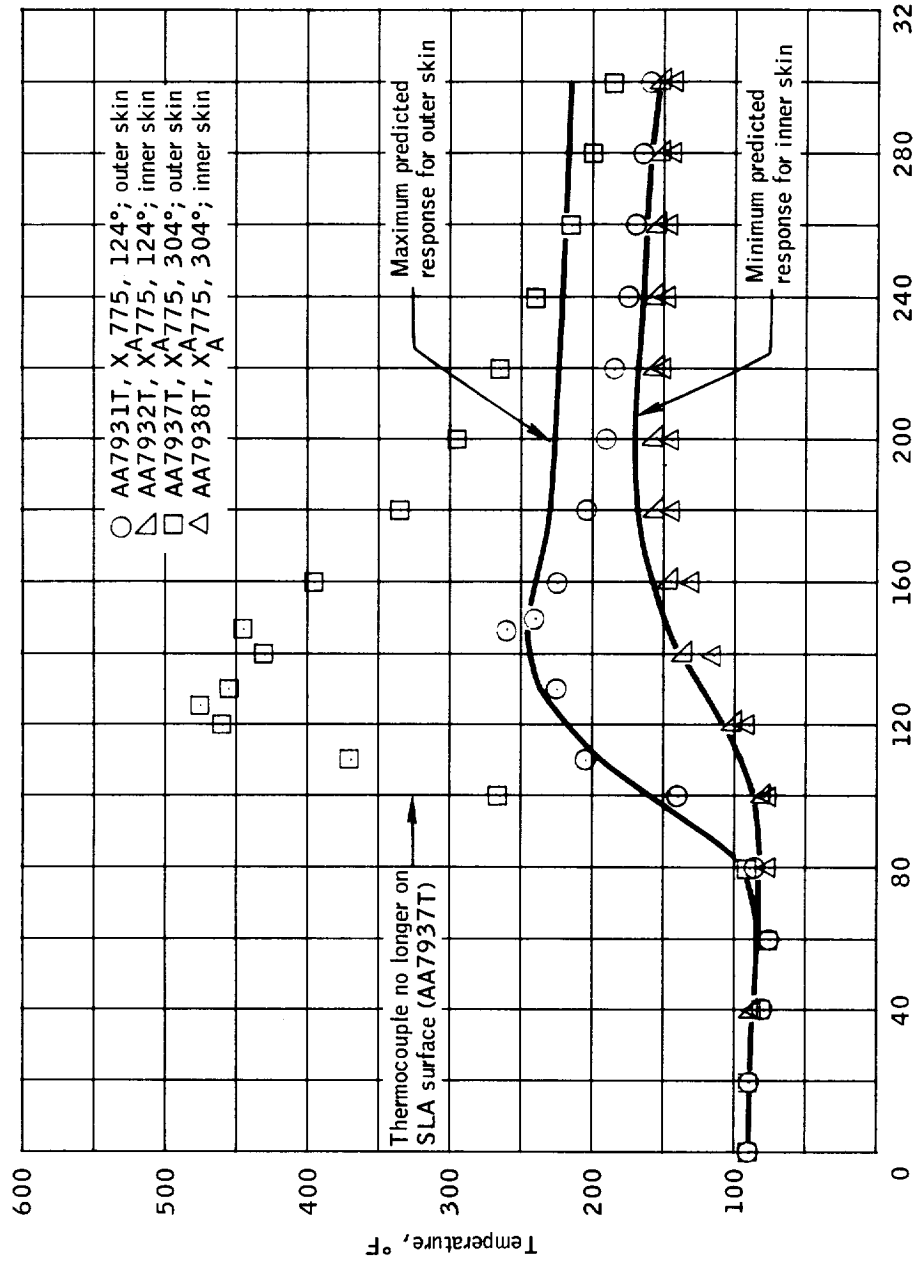

NASA-S-66-10054

Figure 7.4.1-4.- Temperature time histories for spacecraft - LM adapter sensors AA7931T, AA7932T, and AA7938T, Mission AS-202.

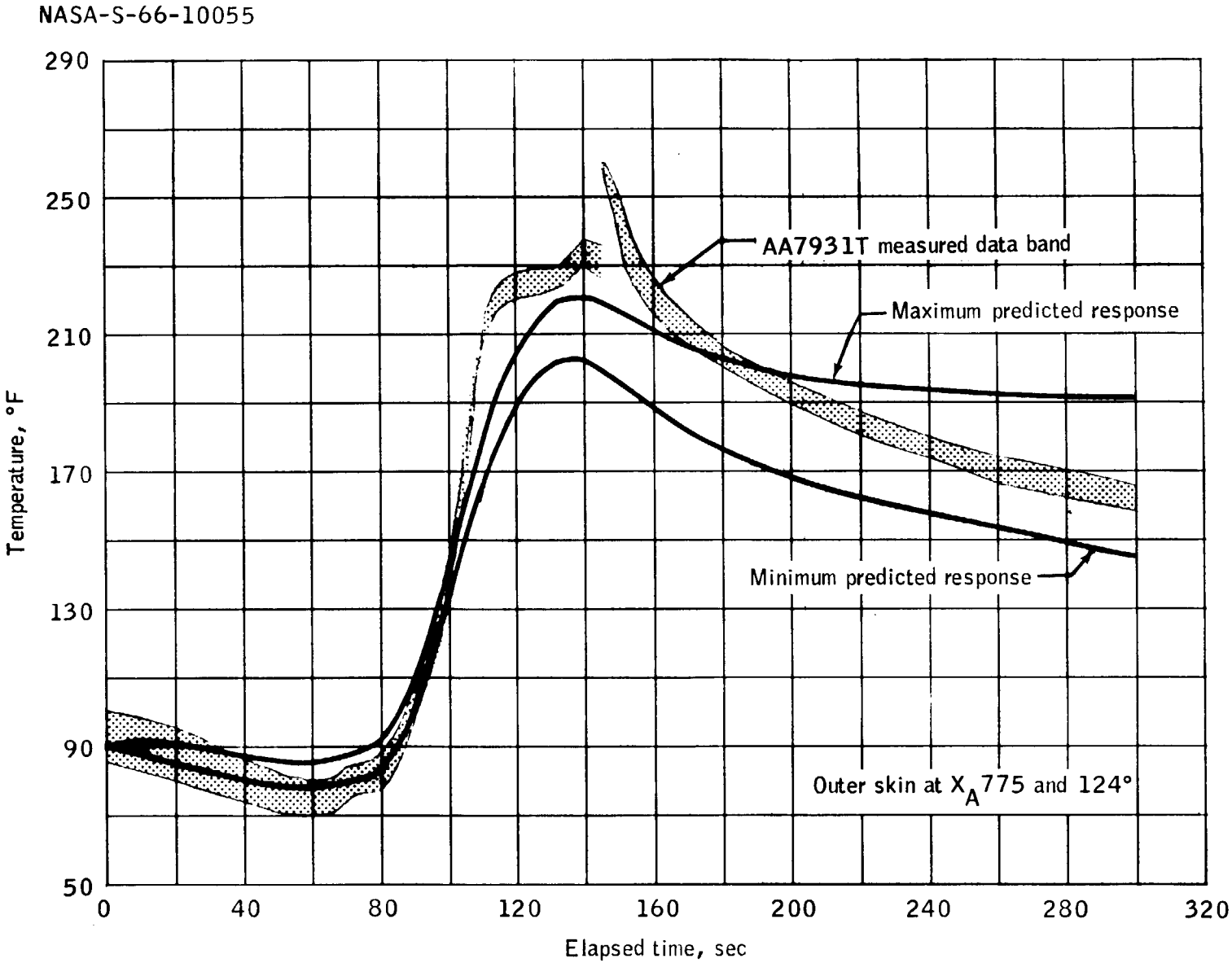

Figure 7.4.1-5.- Temperature time history for spacecraft - LM adapter sensor AA7931T, Mission AS-202.

NASA-S-66-10056

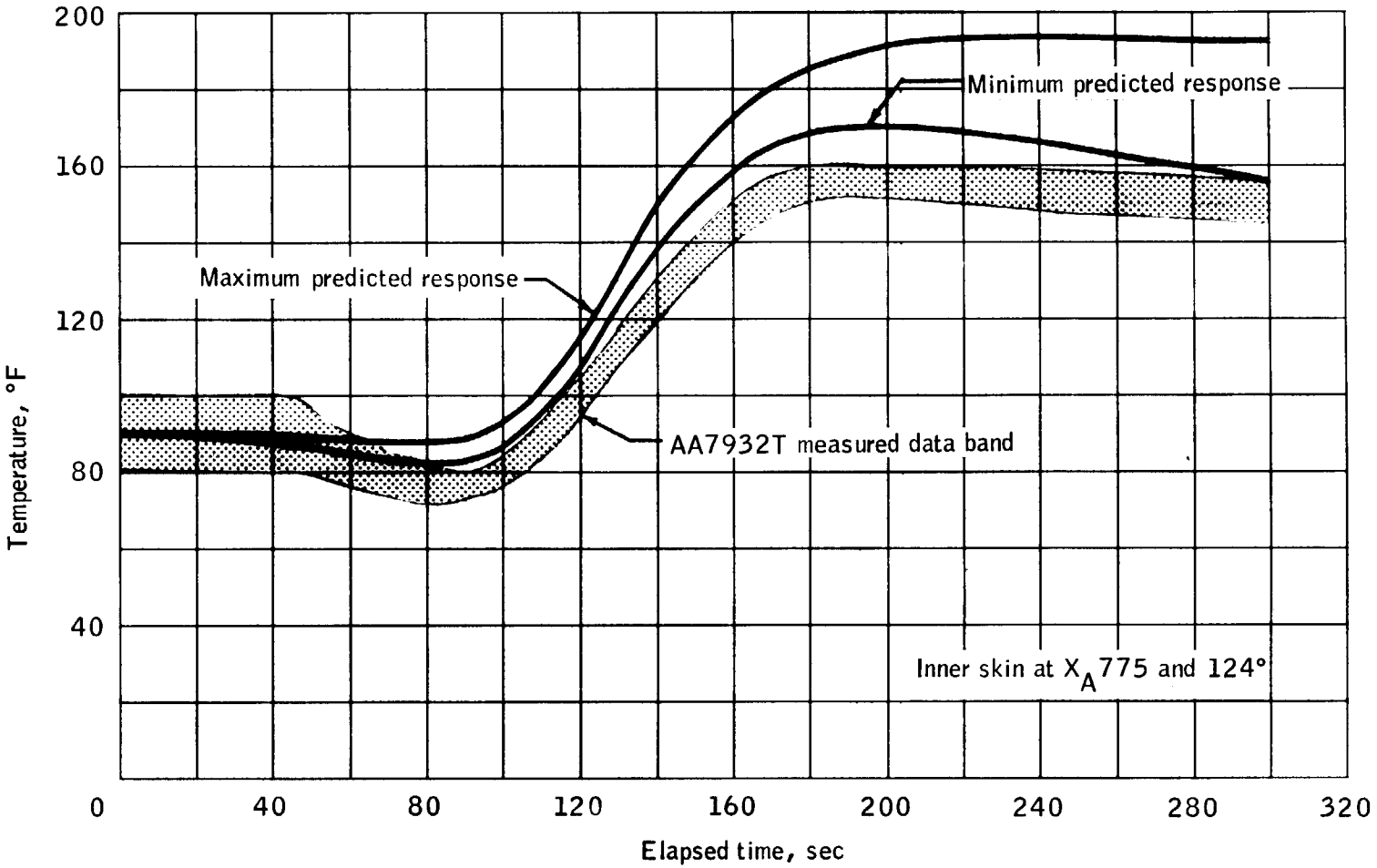

Figure 7.4.1-6.- Temperature time history for spacecraft - LM adapter sensor AA7932T, Mission AS-202.

7.4.2 Heat protection.-

Description: The thermal protection subsystem for Mission AS-202 (SC 011) was similar to that used on Mission AS-201 (ref. 9) with the following exceptions:

(a) Increased ablator thicknesses on the leeward side of the crew compartment.

(b) Increased ablator thicknesses around the aft heat shield shear-compression and compression pads.

(c) Increased ablator thicknesses on the aft heat shield, upstream of the umbilical.

(d) Heat protection for the astrosextant and telescope instead of moveable doors.

Figures 7.4.2-1 and 7.4.2-2 indicate the locations of the temperature measurements.

Performance:

(a) Aft heat shield. The aft heat shield ablator was charred over its entire surface as expected (fig. 7.4.2-3). As expected, the char penetration was deeper than on spacecraft 009. Very little surface erosion was evidenced. There was no evidence of severe erosion on the heat shield around the umbilical, shear-compression and compression pads, although some evidence of erosion was evident between the honeycomb segments and around some ablator repairs.

Examination of cores taken from representative eroded areas showed similar char patterns as cores obtained from other areas of the ablator. It appears that the erosion occurred sometime after entry, possibly by the water at impact. If the erosion occurred during entry there would be more erosion of the cavity sides and edges and deeper penetration of the char underneath. On spacecraft 012 and subsequent heat shields, the spacing between honeycomb segments has been made smaller by improved manufacturing processes and the ablator repair techniques have also been improved.

The three tension tie rods were melted nearly flush with the shear compression pad surfaces. The TRV around the tension ties performed satisfactorily. The pad surfaces were built into the general surface contour of the ablator and the design performed well.

The temperatures measured in the aft heat shield are shown in figure 7.4.2-4. By extrapolating the temperature curves for the temperature in depth, figure 7.4.2-5 shows a reasonable correlation of the 1050° F isotherm compared to the char sensor data.

Table 7.4.2-I gives a comparison of measured char depths from the heat shield cores with the 1000° F isotherm from the extrapolated temperature data and a comparison of the 600° F isotherm with the core discoloration penetration. The first two locations show good correlation using six thermocouples that responded in depth. The disagreement of the data at location Z (34.5) cannot be explained at this time. However, the char depth measurement appears consistent with other core data from intermediate locations where no temperature sensors were located. The remaining locations only had three thermocouples in depth that responded, making it difficult to extrapolate accurately to the depth of the char interface.

(b) Crew compartment heat shield. The crew compartment heat shield showed little or no evidence of ablation and, in some areas, little evidence of aerodynamic heating (fig. 7.4.2-6).

Some ablation did occur near the roll engines by the propellant depletion burn as expected. However, the ablator erosion was not as severe as on spacecraft 009 (Mission AS-201). The windward scimitar (+2) burned off as expected with no effect on the main ablator. The umbilical wires that extended approximately 1 inch in front of the umbilical after being severed were still protruding, giving evidence of lesser heating than on spacecraft 009. A temperature measurement several inches inside the umbilical wires showed a peak value of 460° F. There was no temperature increase in the air vent duct during entry.

Figure 7.4.2-7 shows that the astrosextant thermal protection area received little or no heating. The top of the frame near the parachute on the windward meridian was smudged and gave some indication of impinged heating. Thermosensitive paint on the structure in the parachute bay indicated a temperature of more than 250° F but less than 500° F.

Because of the low heating environment for the astrosextant passive thermal protection subsystem during entry, postflight tests were conducted to temperatures and loads anticipated for an entry with an L/D of 0.4. The results indicated that no failure could be expected for Block I flight with an L/D up to 0.4.

The heat shield performed well during the mission and, since the entry heating load exceeded those predicted for nominal manned earth orbital entries, the Block I heat shield is now considered qualified for high heat load (nondecay) type entries from low earth orbits.

TABLE 7.4.2-I.- COMPARISON OF MEASURED CORE DATA AND EXTRAPOLATED THERMOCOUPLE DATA

Location		Char depth, measured, in.	1000° F isotherm, extrapolated, in.	Discoloration depth, measured, in.	600° F isotherm, extrapolated, in.
Z	Y				
70.25	0	0.68	0.73	1.08	1.07
64.0	0	0.66	0.63	1.00	0.95
34.5	0	0.61	0.47	0.94	0.68
0	1.5	0.59	0.50	0.91	0.80
-67.5	0	0.46	0.52	0.80	0.75
0	+38	0.58	0.40	0.84	0.57
0	+69.5	0.75	0.63	0.96	0.87

NASA-S-66-10205

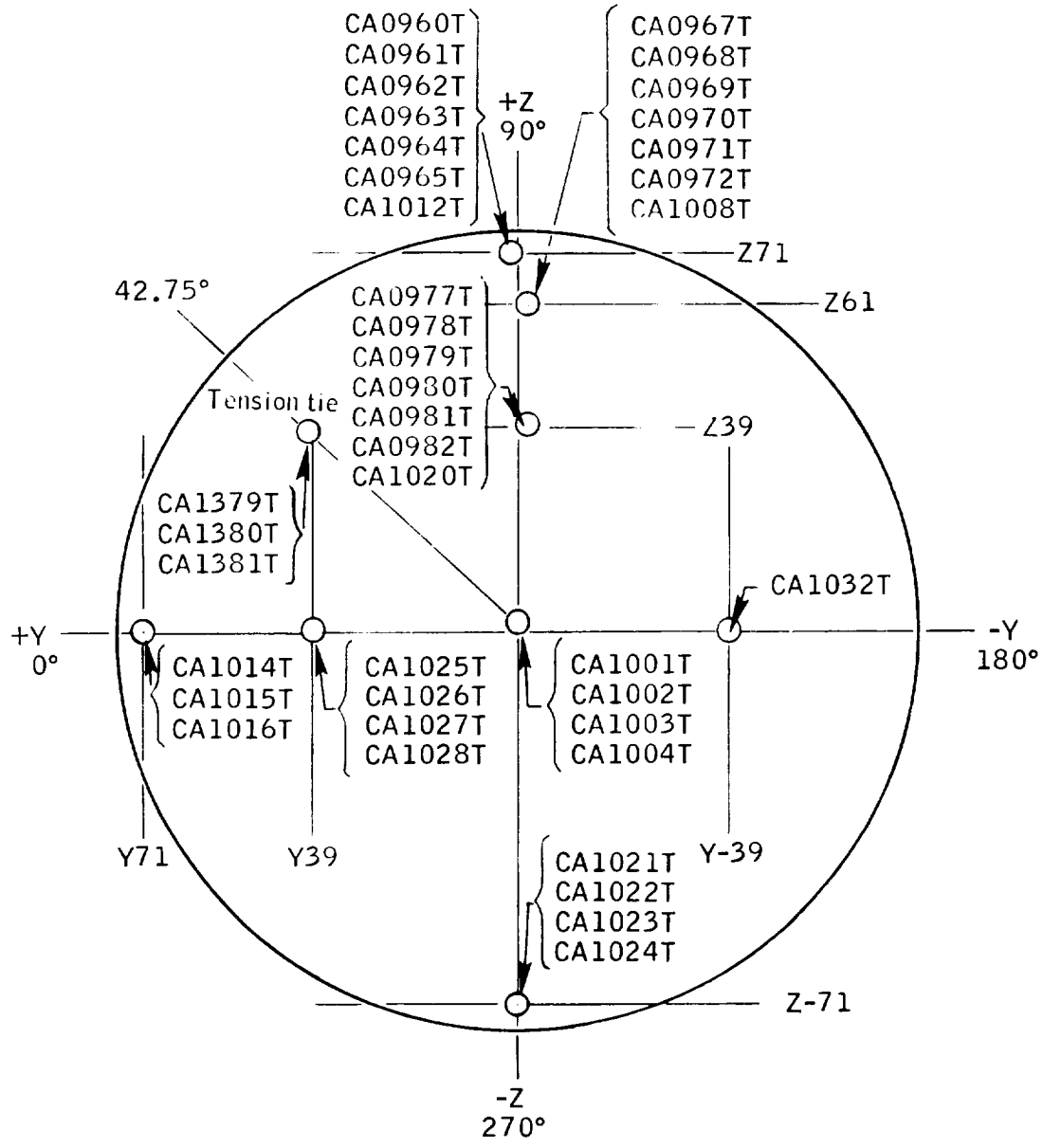

Figure 7.4.2-1.- Aft heat shield ablator temperature measurement locations, Mission AS-202.

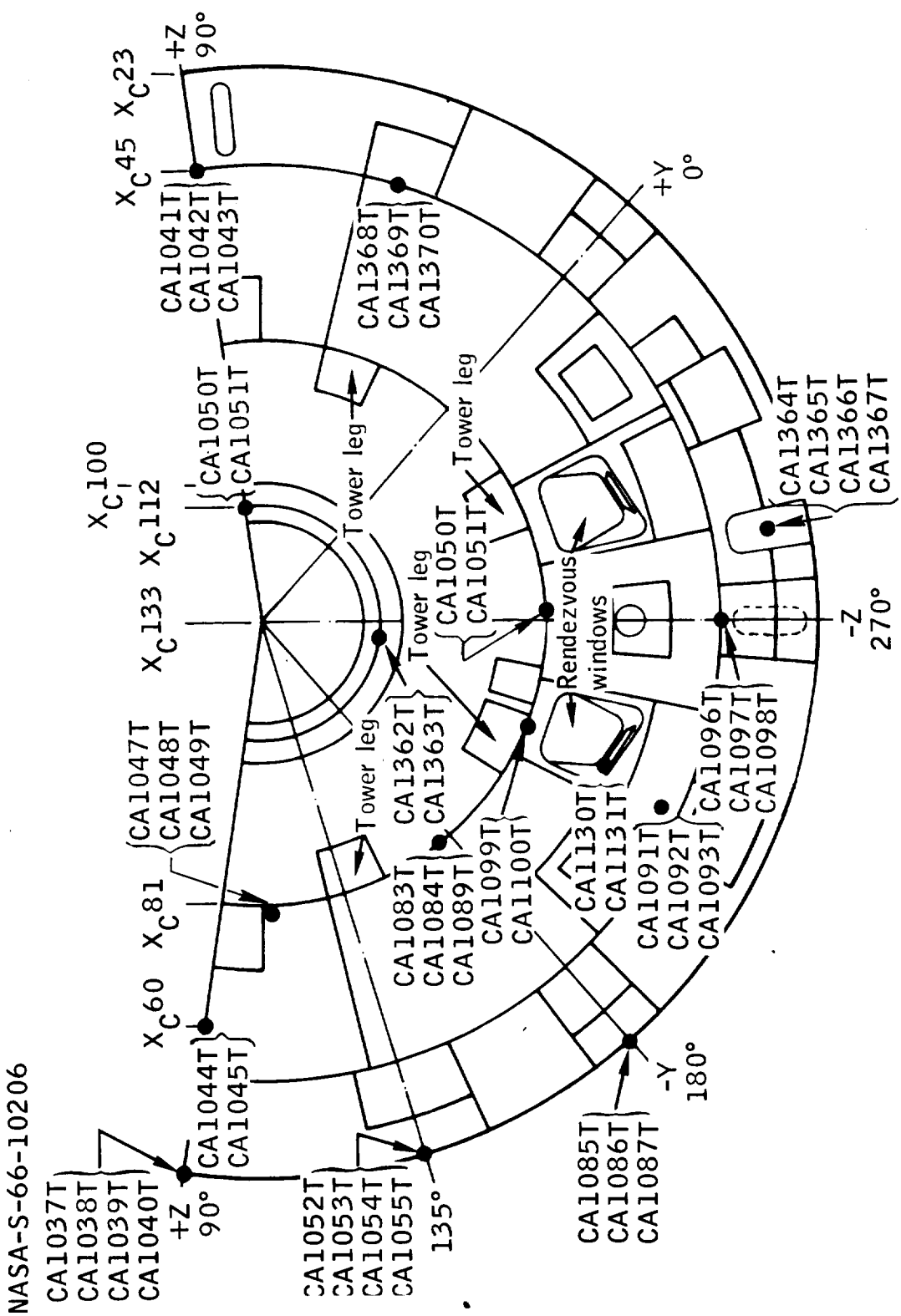

Figure 7.4.2-2.- Temperature measurement locations on CM forward and crew compartment heat shields, Mission AS-202.

NASA-S-66-10207

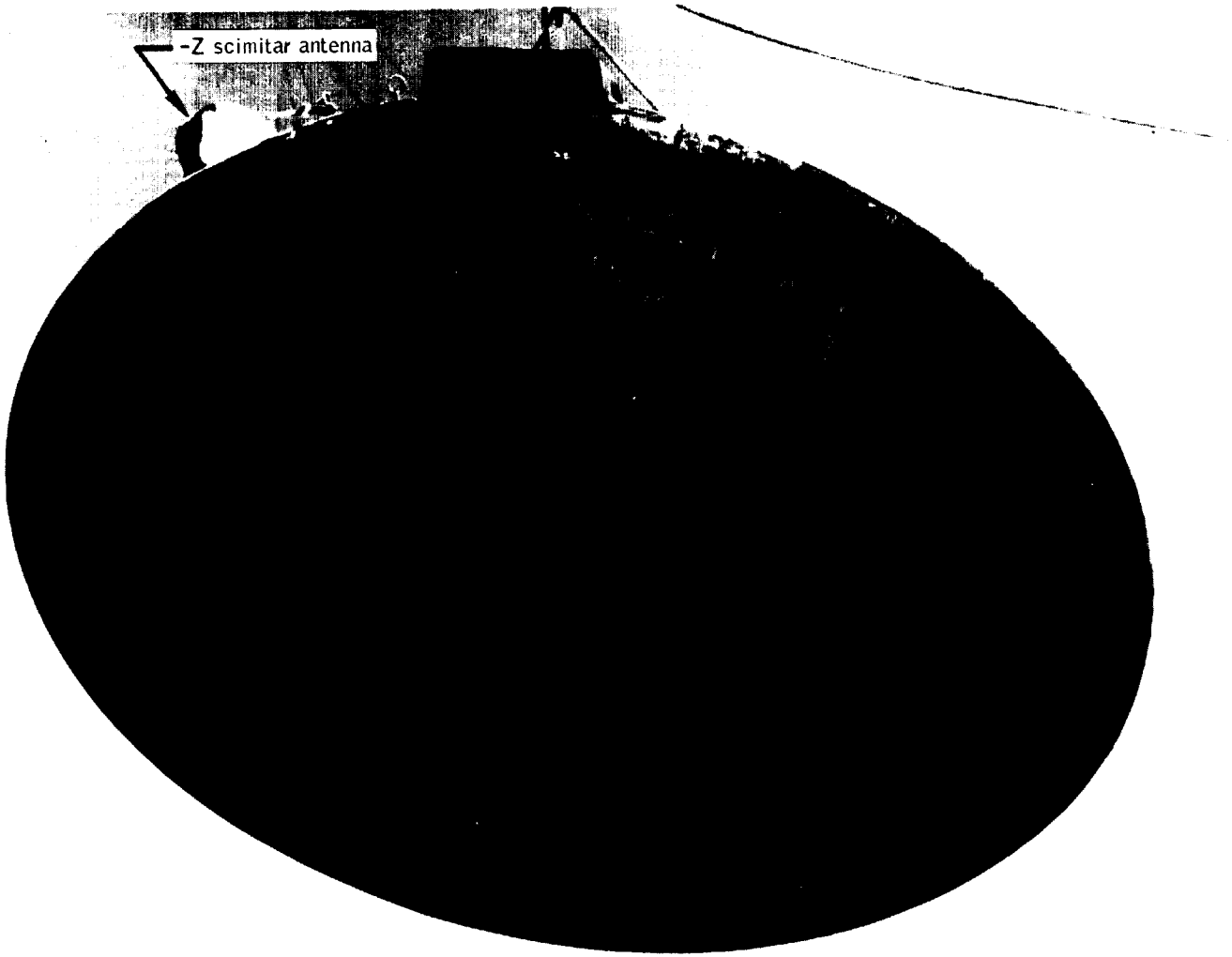

Figure 7.4.2-3.- Char condition of aft heat shield, Mission AS-202.

NASA-S-66-10208

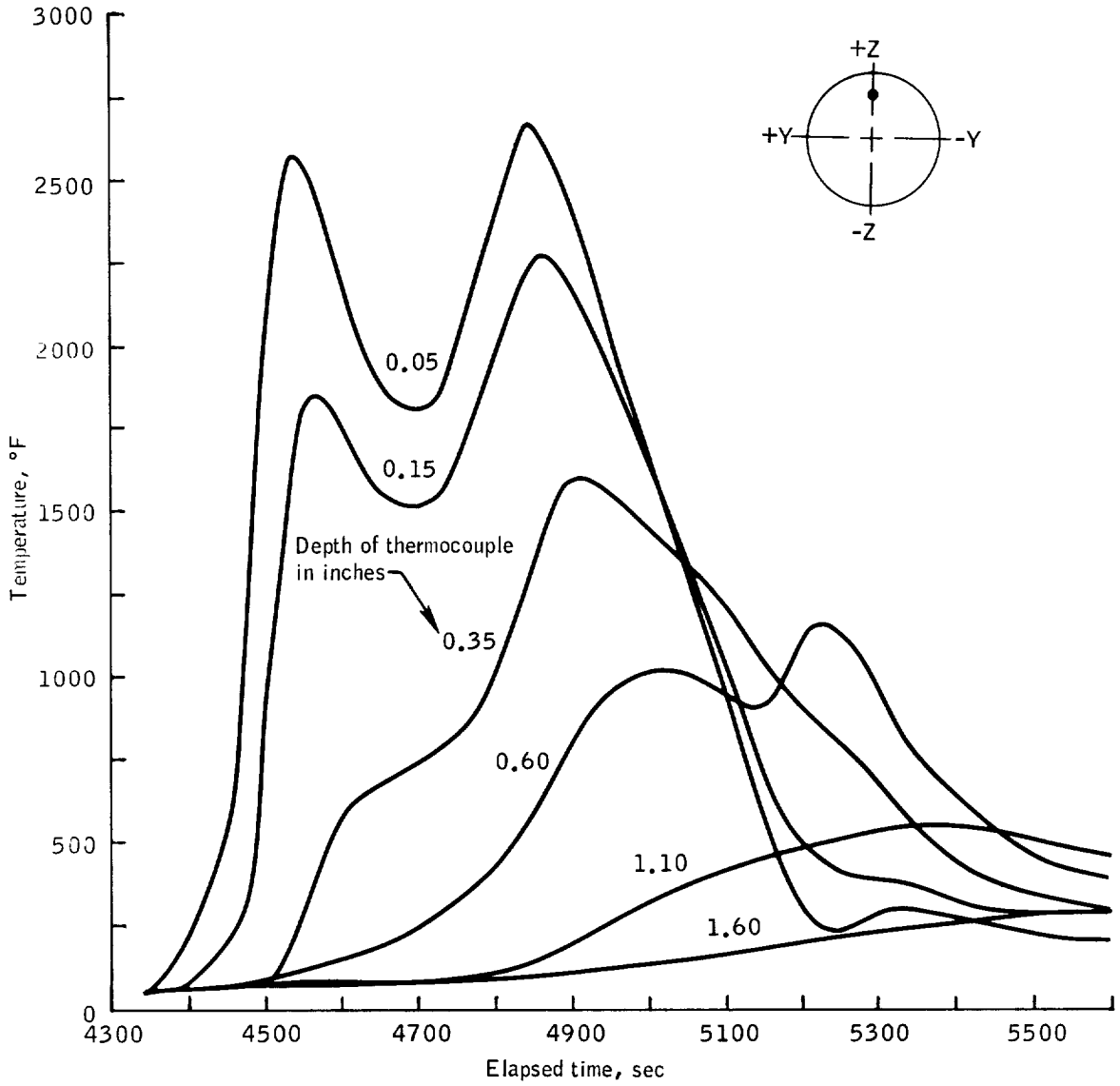

(a) Station Z71, Y0.

Figure 7.4.2-4.- Aft heat shield temperature measurements at depths indicated, Mission AS-202.

NASA-S-66-10209

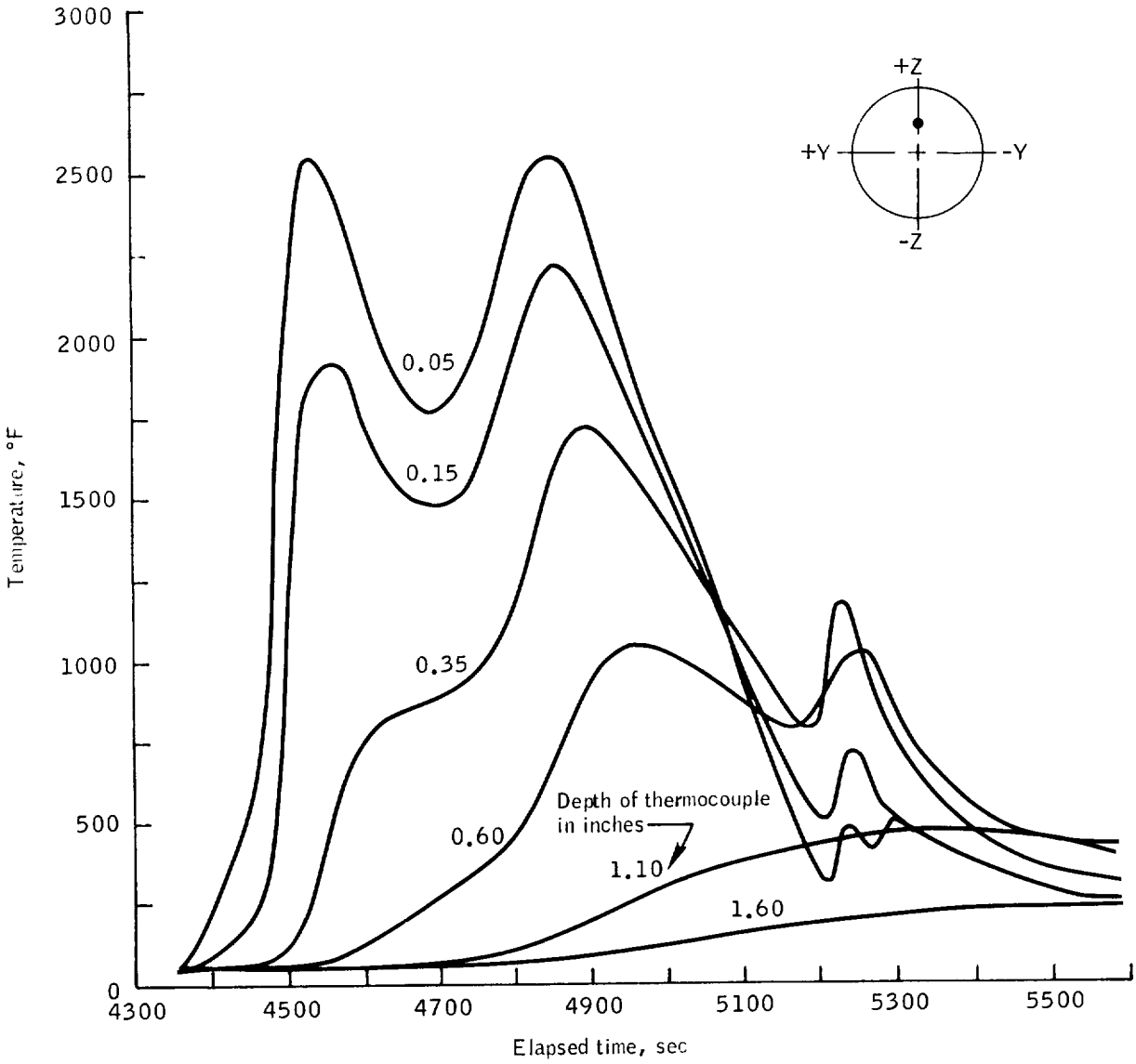

(b) Station Z61, Y0.

Figure 7.4.2-4.- Continued.

NASA-S-66-10210

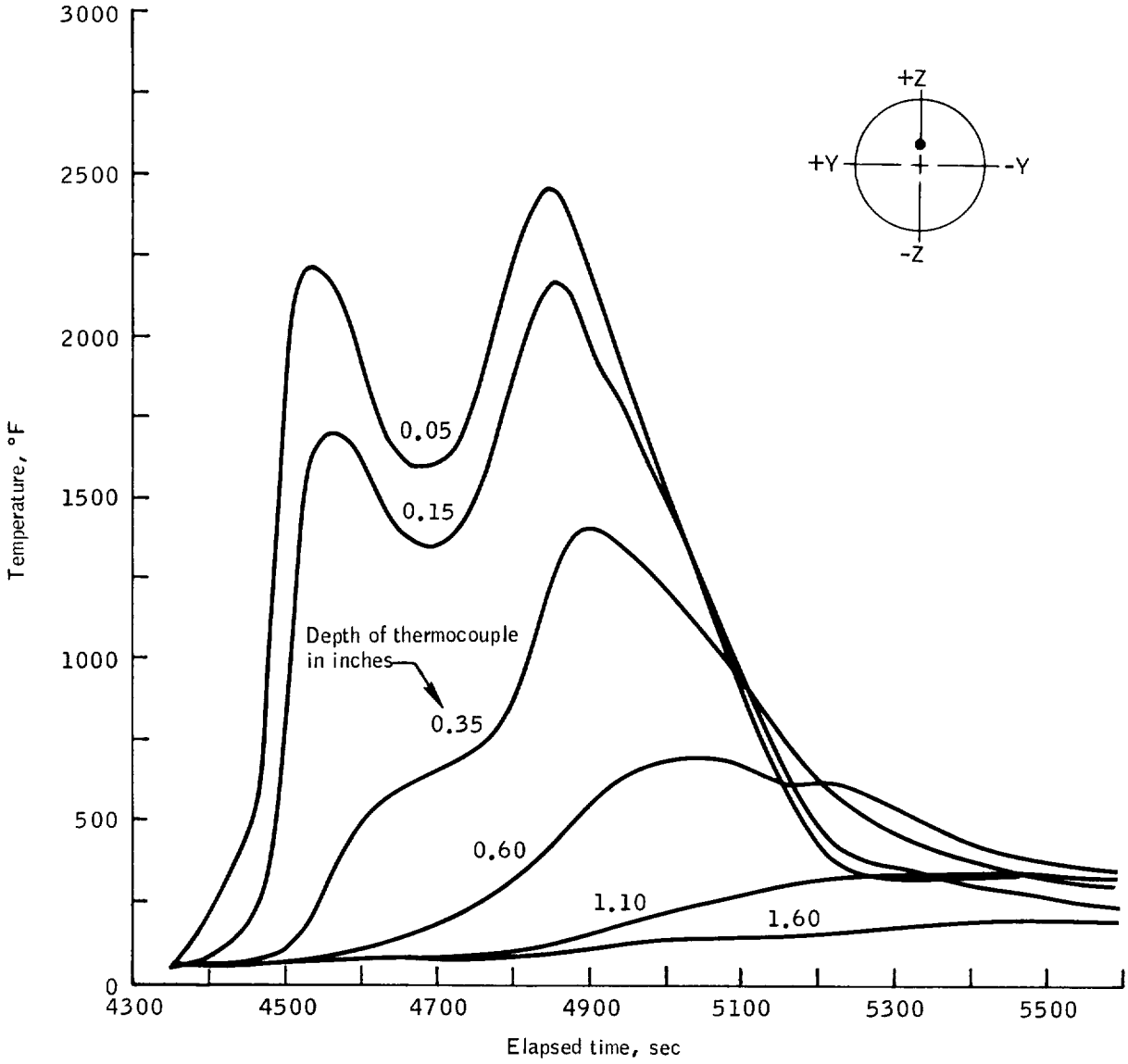

(c) Station Z38, Y0.

Figure 7.4.2-4.- Continued.

NASA-S-66-10211

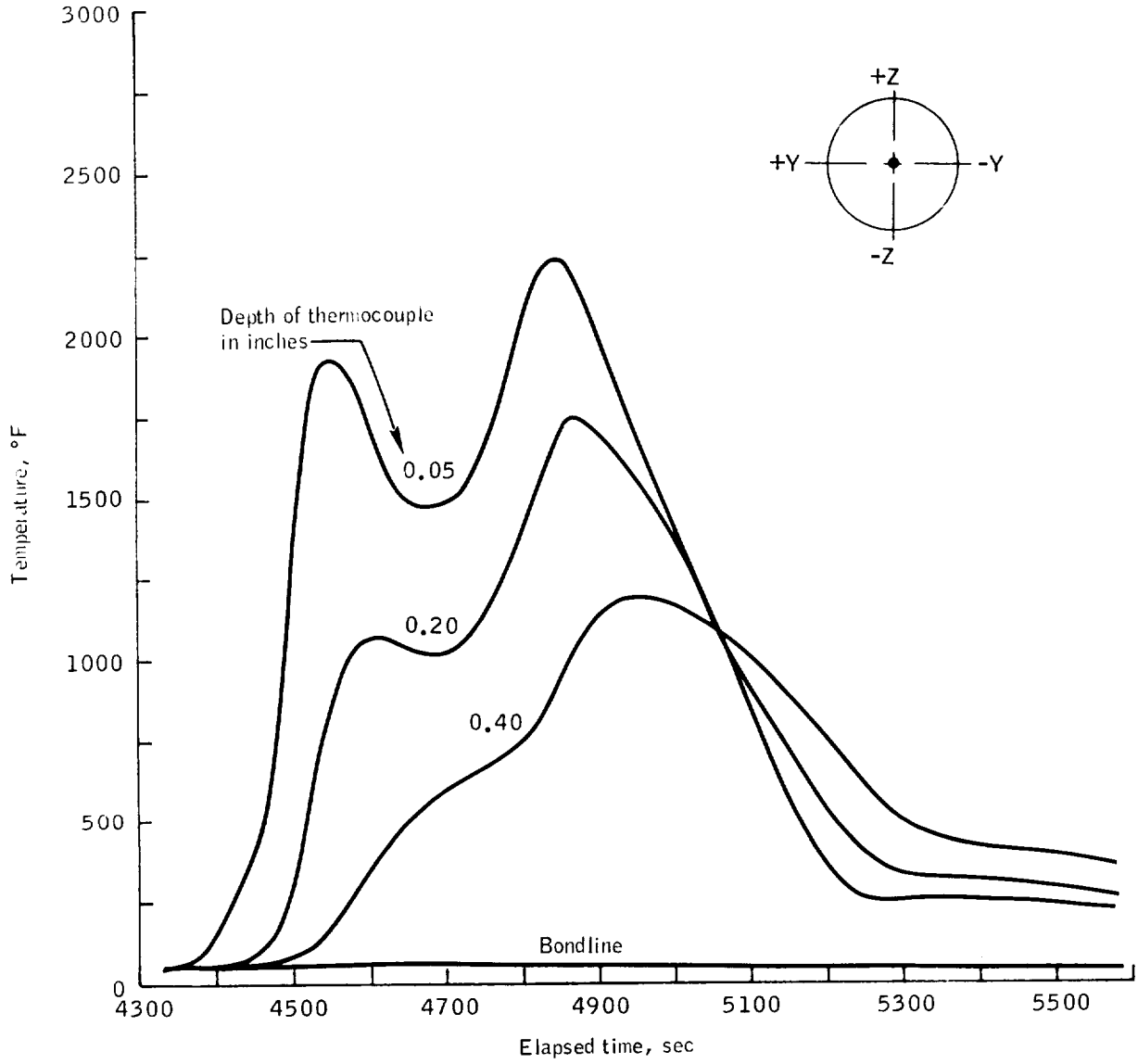

(d) Station Z0, Y0.

Figure 7.4.2-4.- Continued.

NASA-S-66-10212

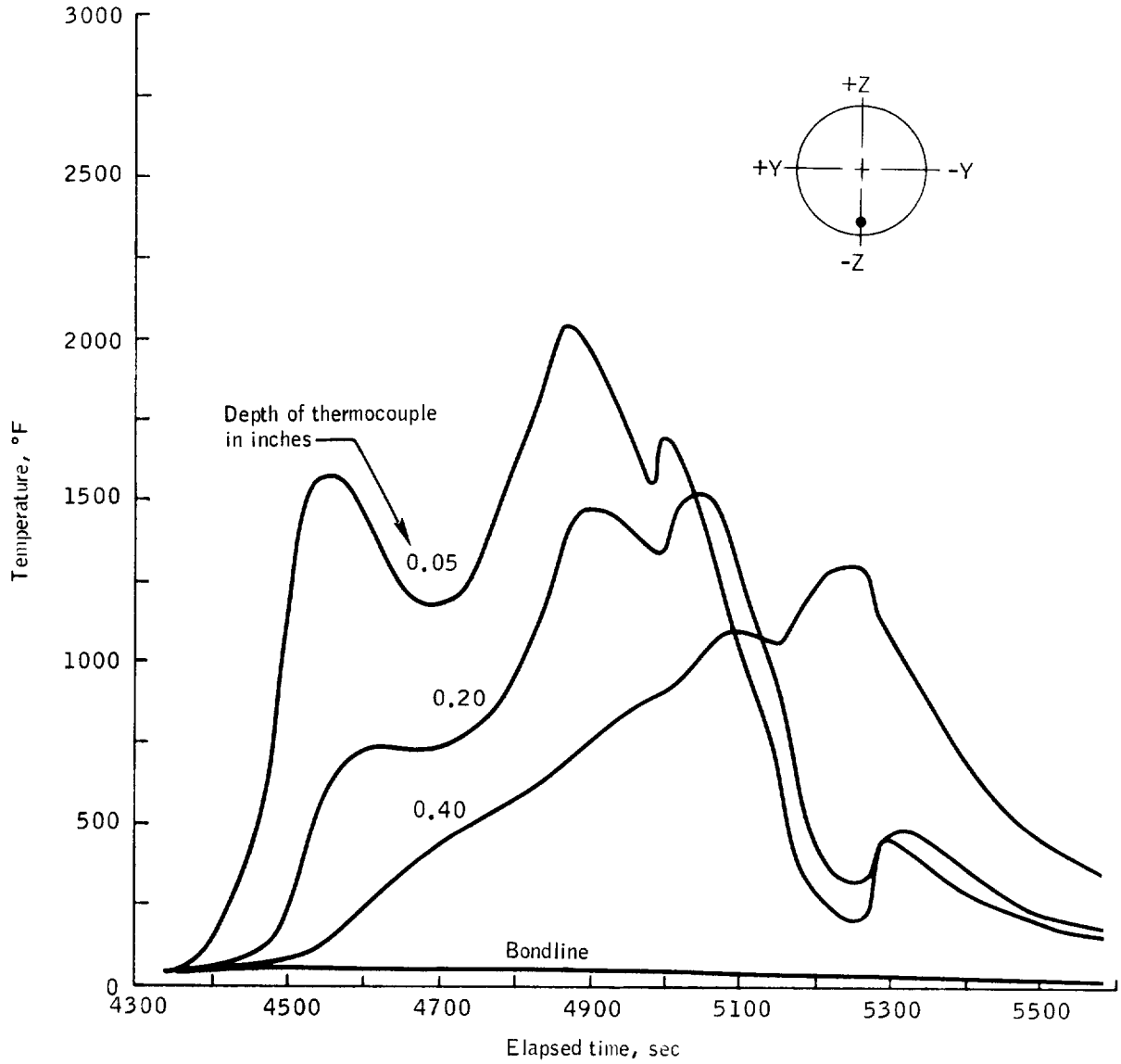

(e) Station Z-71, Y0.

Figure 7.4.2-4.- Continued.

NASA-S-66-10213

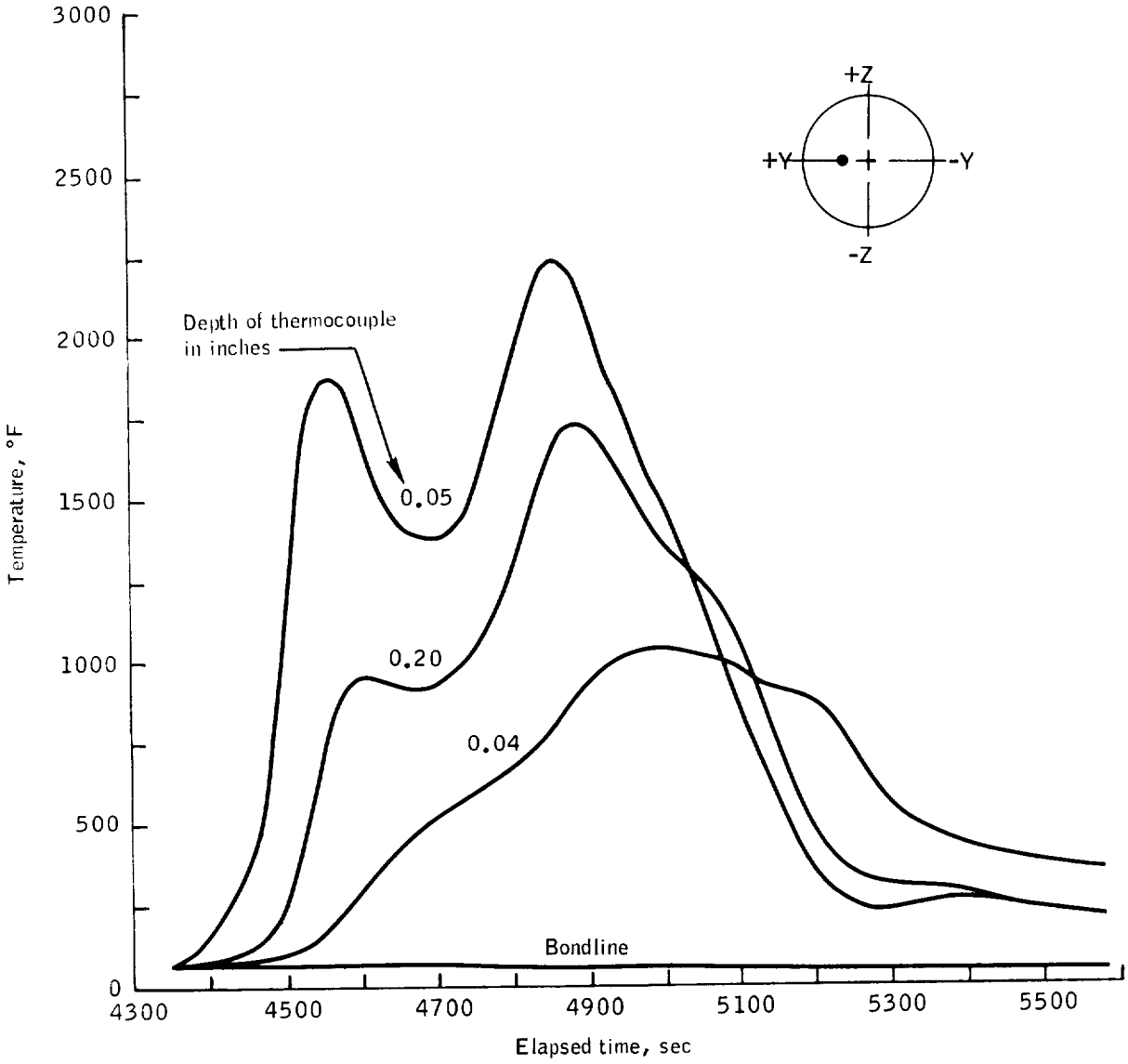

(f) Station Z0, Y33.

Figure 7.4.2-4.- Continued.

NASA-S-66-10214

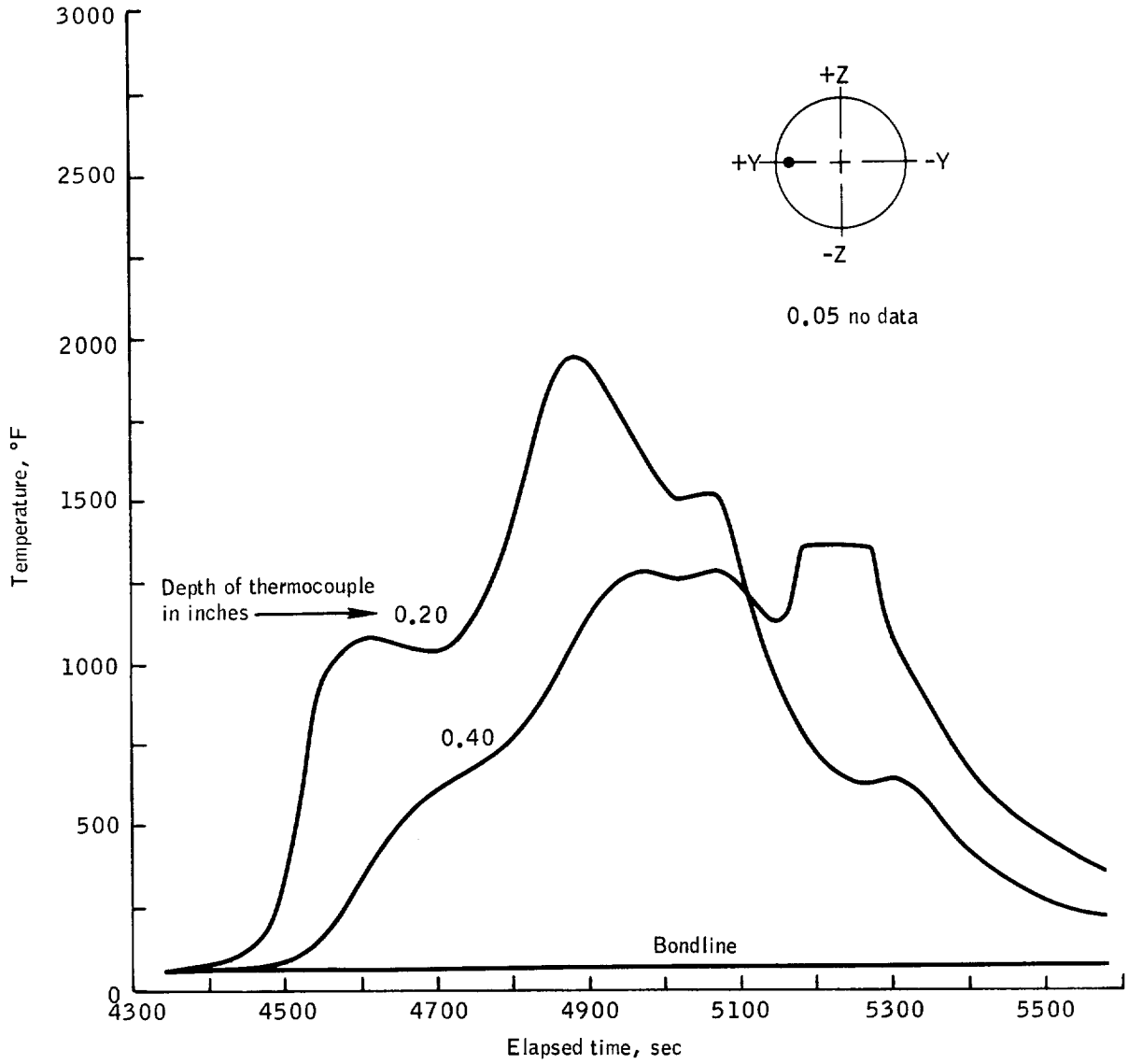

(g) Station Z0, Y72.

Figure 7.4.2-4.- Concluded.

NASA-S-66-10215

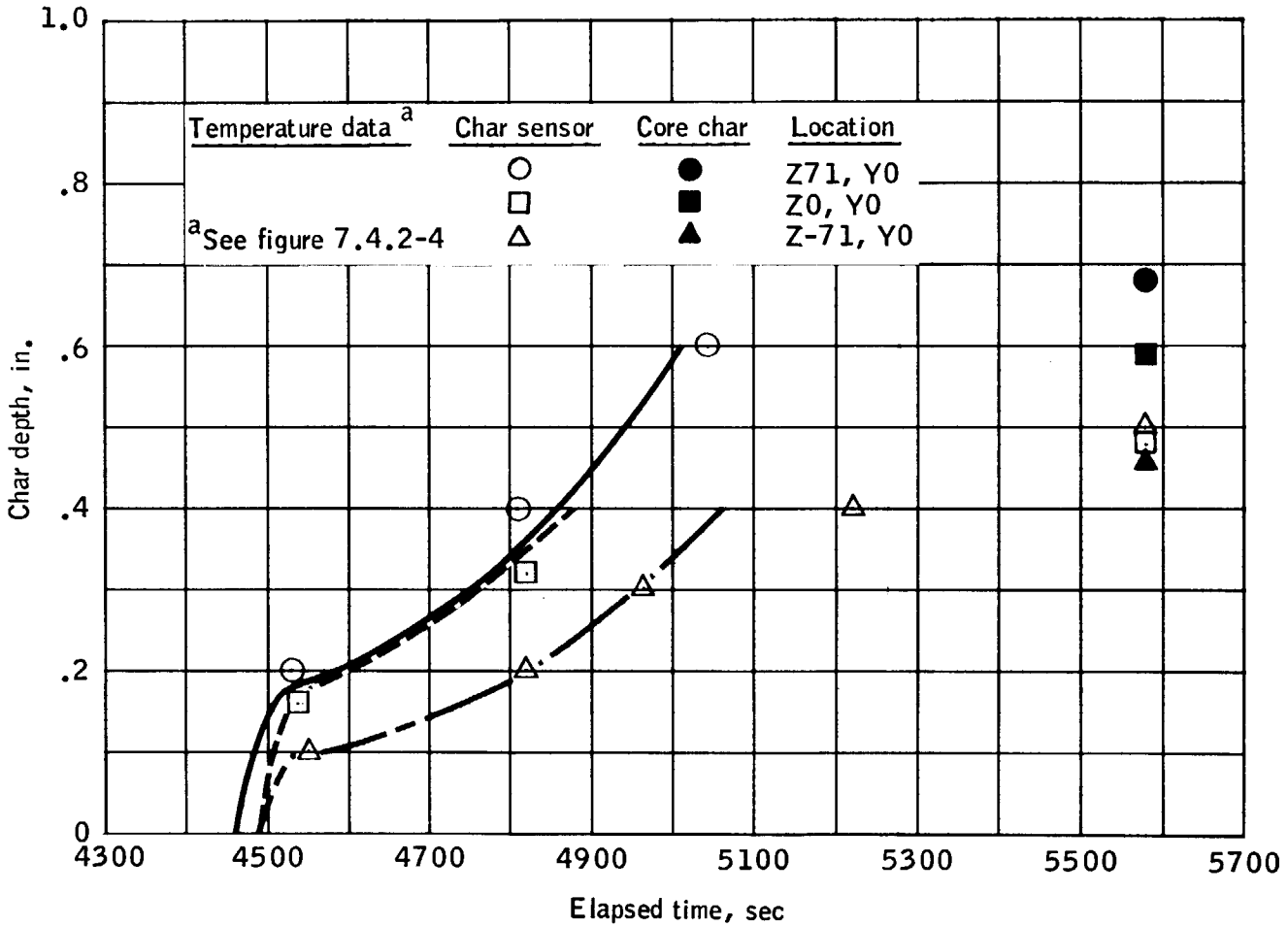

Figure 7.4.2-5.- Aft heat shield 1050 °F isotherm comparison with char sensor and core char, Mission AS-202.

NASA-S-66-10216

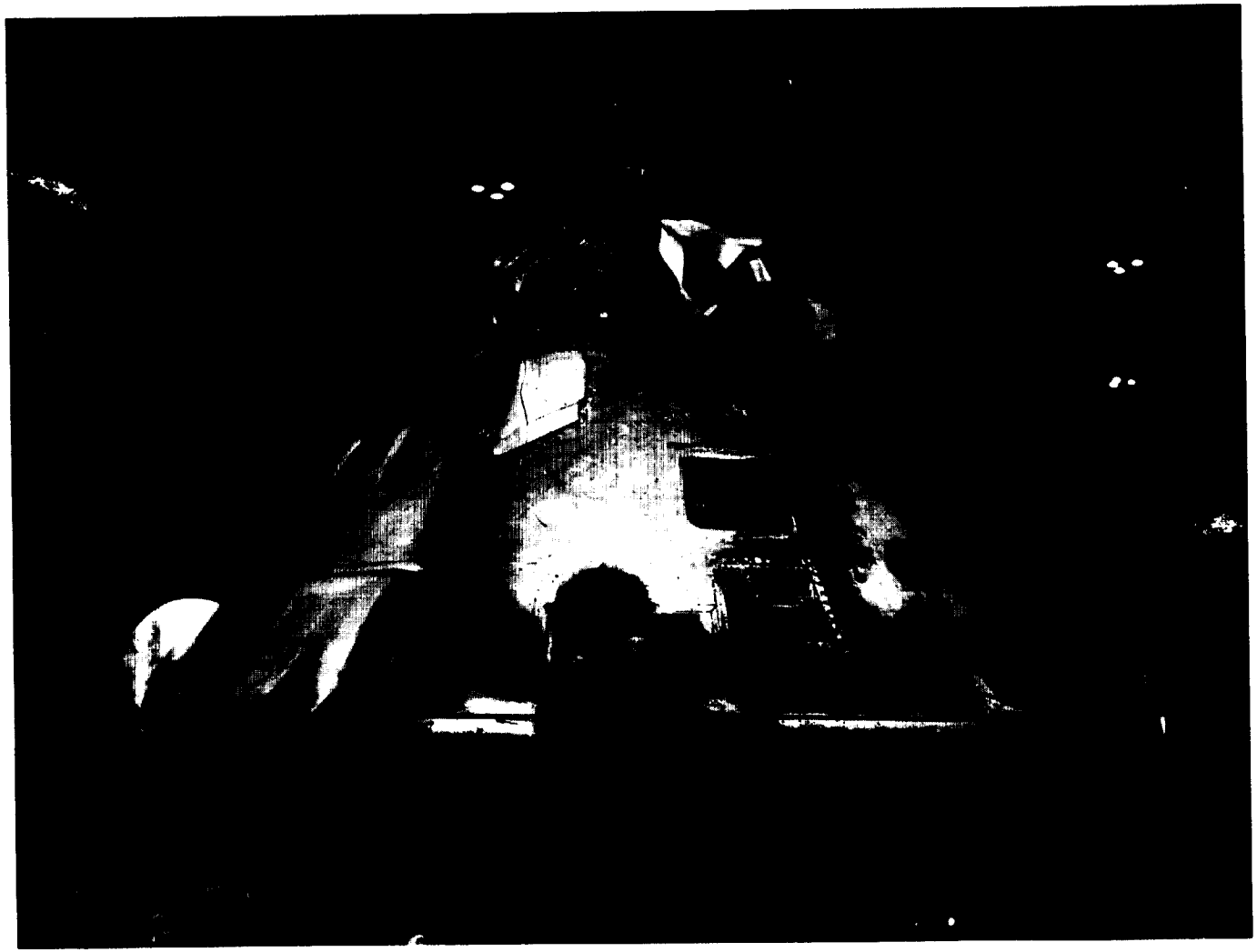

(a) -Z-axis to +Y-axis.

Figure 7.4.2-6.- Char condition of crew compartment heat shield, Mission AS-202.

NASA-S-66-10217

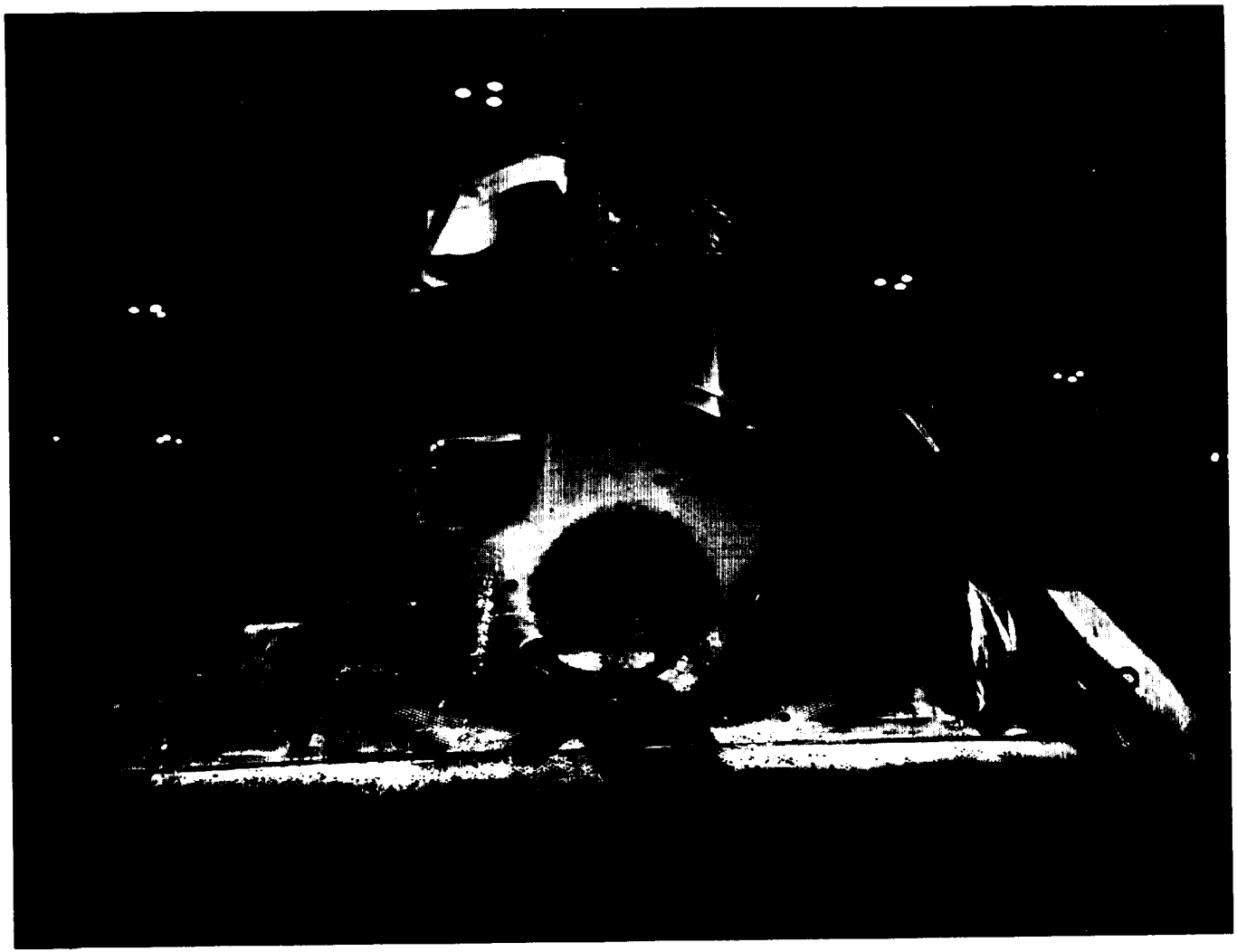

(b) -Y-axis to -Z-axis.

Figure 7.4.2-6.- Continued.

NASA-S-66-10218

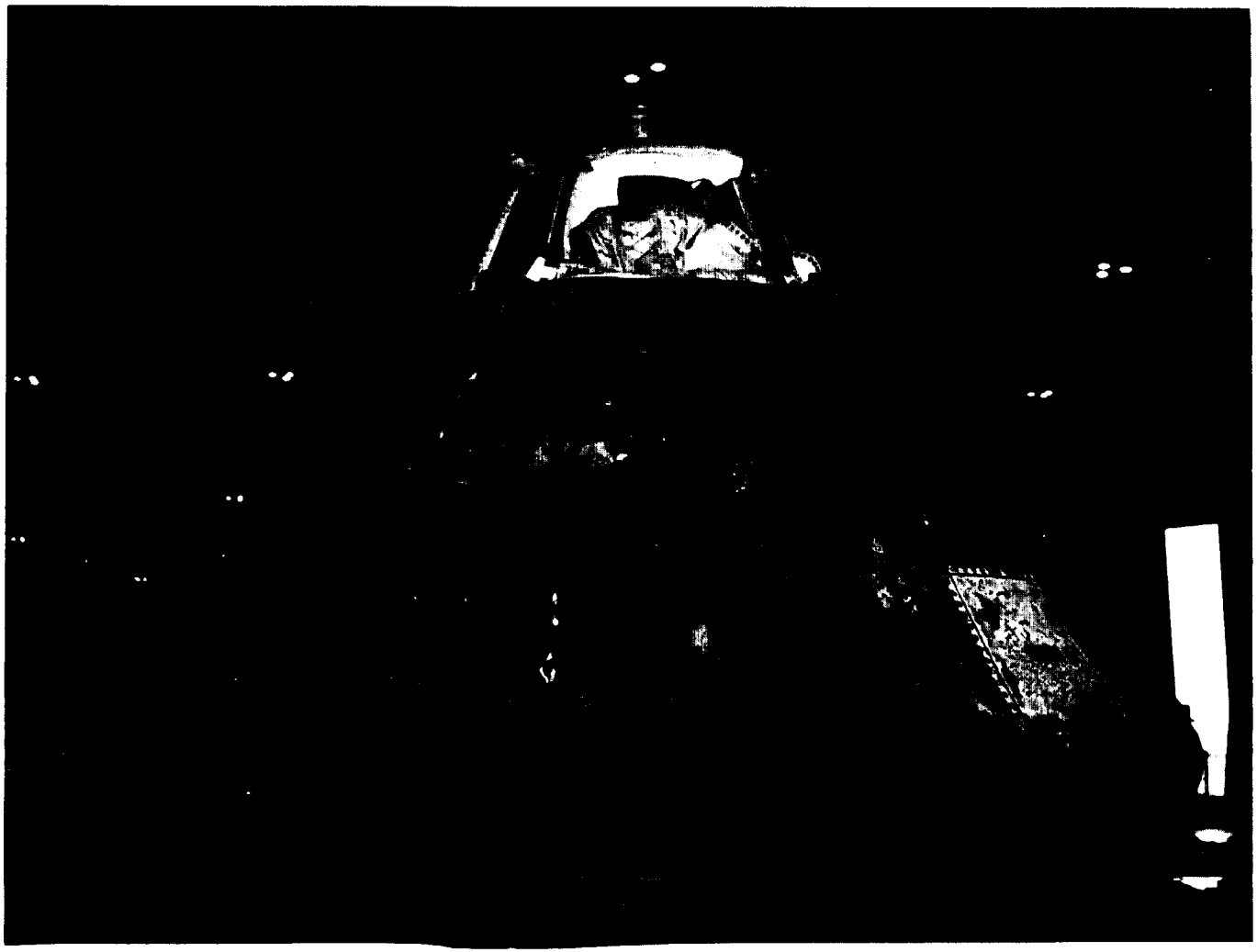

(c) +Z-axis.

Figure 7.4.2-6.- Concluded.

NASA-S-66-10219

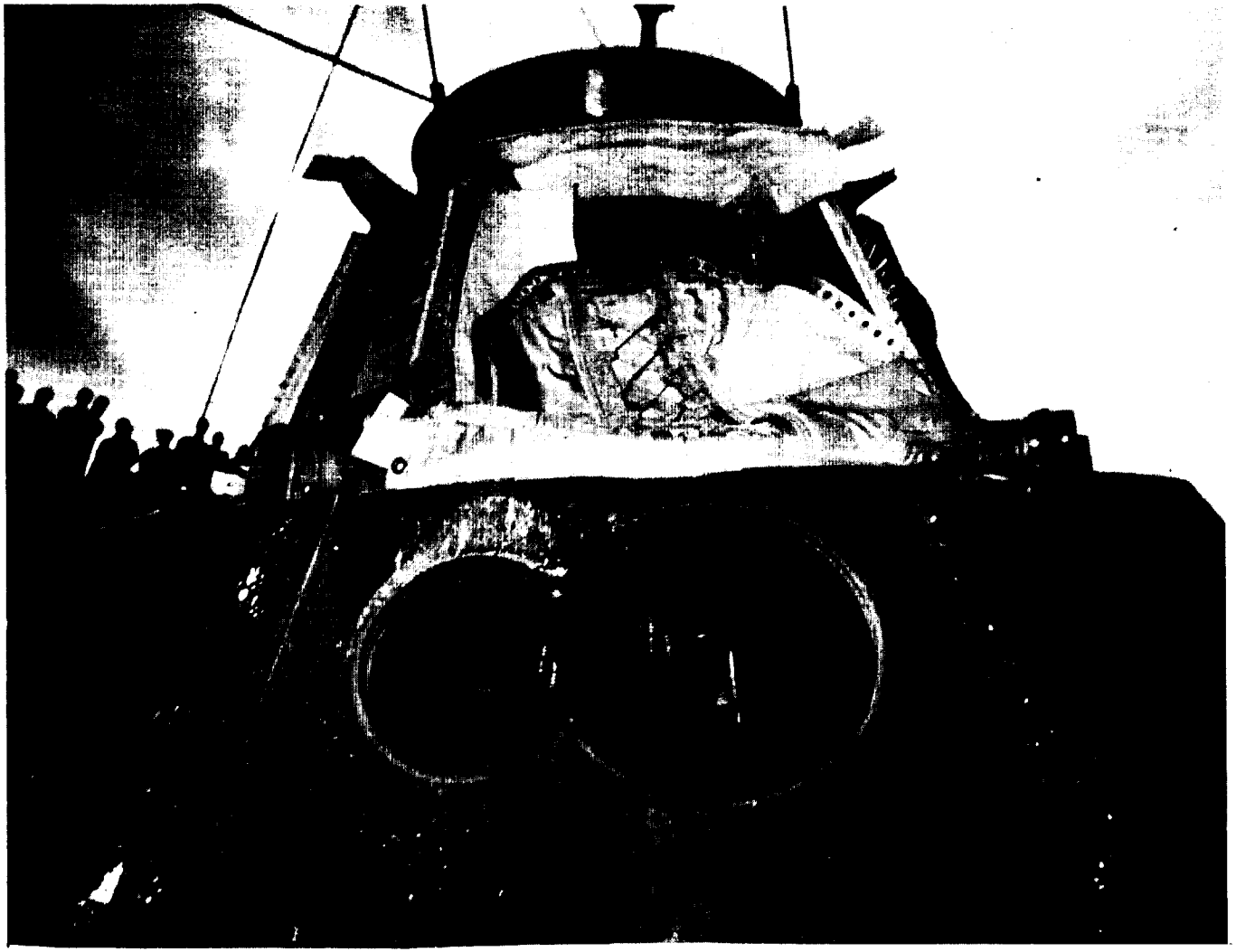

Figure 7.4.2-7.- Char condition of astrosextant passive thermal protection (+Z-axis), Mission AS-202.

7.5 Mechanical Subsystems

Summary.- Components of the mechanical subsystems flown on Mission AS-202 included the canard subsystem, the uprighting subsystem, the deployment mechanisms for the recovery aids, and the latching mechanisms for the side ablative, side pressure, forward pressure, and boost protective cover hatches. All components performed satisfactorily, although the canard and uprighting subsystems were not required to operate because of the nominal nature of this mission.

Subsystems description and performance.- The following paragraphs describe the configuration of each of the components required to operate and its performance.

Recovery aids deployment mechanisms: The deployment mechanisms for the postlanding recovery aids consisted of those used to deploy the VHF and HF antennas, the flashing light, and the sea dye marker/swimmer umbilical. These mechanisms operated properly.

The recovery antennas and flashing light were located in the forward compartment and their deployment mechanisms were identical. Each was activated by a pyrotechnic cutter (section 7.10) actuated by means of a lanyard attached to the parachute riser. When the main parachutes were deployed, the lanyard pull caused the activation of the 8-second time-delay cutter device, which released the spring-operated deployment mechanisms.

Postflight inspection of the antennas and flashing light confirmed that all had erected as planned, and examination of the mechanisms revealed no indication of damage during the flight or at landing. Signals were received from all antennas on spacecraft 011 after deployment. The flashing light was observed to be operating satisfactorily during recovery operations (section 9.3). The flash rate was timed at different periods during recovery operations, beginning at 9 hours after touchdown and ending when the light was turned off at 14 hours after touchdown. The rate was constant at 20 flashes per minute. (It is required to flash 8 to 24 times a minute.) Inspection of the light installation revealed that the bulb was improperly installed, that is, the small compression spring which holds the bulb/connector in place was not inserted in its housing (fig. 7.5-1); consequently, the bulb was loose in its retainer. Inspection of the flashing light assembly on spacecraft 012 indicated that it is properly installed for Mission AS-204.

The sea dye marker/swimmer umbilical deployment mechanism consisted of a rectangular canister which was spring-loaded on a deployment platform located in the -Z bay of the CM upper deck. This

canister contained the dye can which was packed with fluorescein dye. (The dye is dispersed through two small orifices in the can and is required to last 12 hours after deployment while producing a slick of at least 20 000 square feet.)

The deployment mechanism latch was triggered by a lanyard that was pulled when the HF antenna was erected after landing. The canister was deployed overboard by redundant springs but remained attached to the CM by a cable which included the swimmer telephone umbilical. The search aircraft which visually located the spacecraft reported spotting the dye slick at a range of approximately 2 miles. The slick size was subjectively reported as "small" although the observer did comment that the sun reflection hampered his view (section 9.3). The dye restraint cable was used as a tether for a life raft by the first swimmer alongside the spacecraft. This could severely restrict the continuing dispersion of the dye which would influence the subsequent observations which would be made.

Inspection of the swimmer telephone umbilical after recovery revealed that the telephone wire insulation was chafed by the upper deck ablator edge (fig. 7.5-2). It is suspected that the chafing was caused by the use of the cable as described above. It was known prior to the flight that the insulation might be damaged, but preventative action was waived for this unmanned mission. An additional protective sleeve is being included in the cable assembly for spacecraft 012 to provide some abrasion protection.

Side ablative hatch-latching mechanism: The side ablative hatch is located on the -Z side of the outer structure of the CM conical surface. The hatch latches must retain the hatch in place to maintain the integrity of the structure and heat shield ablator. A detailed description is presented in section 5.5 of reference 8. The hardware was of a Block I design and was similar to that used on Missions A-004 and AS-201 with the exception that the emergency release bar was not installed.

The side ablative hatch-latching mechanism performed satisfactorily on this flight. The mechanism retained the hatch in place during flight and was operated satisfactorily after landing. Preflight hatch closure was accomplished without the use of torque wrenches, and so data on preflight torque required to latch the mechanism are not available. Postlanding torque required to unlatch the mechanism was 275 in-lb. The design torque limit was 260 in-lb to either latch or unlatch the mechanism. Previous bench tests of the mechanism have indicated that torques up to 500 in-lb cause no permanent or harmful structural deformation.

Side pressure hatch-latching mechanism: The side pressure hatch is located on the -Z side of the CM and relies on the inside cabin pressure for the "hard" seal against the CM inner structure. The hatch is held in place by machined-edge members on three sides and a latch/release mechanism on the remaining side. A detailed description is presented in section 5.5 of reference 8. The hardware was a Block I design and was similar to that used on Mission A-004 except that the high strength pinion gear, as discussed in the following paragraph, was included. The side pressure hatch-latching mechanism performed satisfactorily for this mission in that the hatch remained latched during flight and released satisfactorily during recovery.

The pinion gear on the hatch-latching mechanism was redesigned and made stronger so that higher torques could be used when operated. This new design was incorporated on spacecraft 011 and on subsequent spacecraft.

Hatch closure was accomplished without the use of torque wrenches thus preflight torque required to latch the mechanism was not recorded. A torque of 200 in-lb was required to unlatch at recovery. The design torque limit of the mechanism was 600 in-lb. The hatch was reinstalled and then removed a second time; both operations required less than 250 in-lb of torque (section 9.3).

Forward pressure hatch-latching mechanism: The forward pressure hatch was located at the top of the tunnel on the upper deck of the CM. The hatch-latching mechanism locked the hatch in position to maintain the structural and pressure-seal integrity of the pressure vessel throughout the mission. The hatch provided a pressure seal seated by means of a breech lock configuration. A bolt-type locking mechanism retained the hatch against rotation and disengagement during the flight.

Boost protective cover hatch-latching mechanism: The BPC hatch-latching mechanism hardware flown on Mission AS-202 was a Block I design, except that it did not include the astronaut push plunger which allows unlatching of the hatch from within the spacecraft while the ablative hatch is still installed on the vehicle. The latching mechanism apparently retained the hatch properly during launch.

NASA-S-66-10057

Figure 7.5-1.- Flashing light installation, Mission AS-202.

NASA-S-66-10058

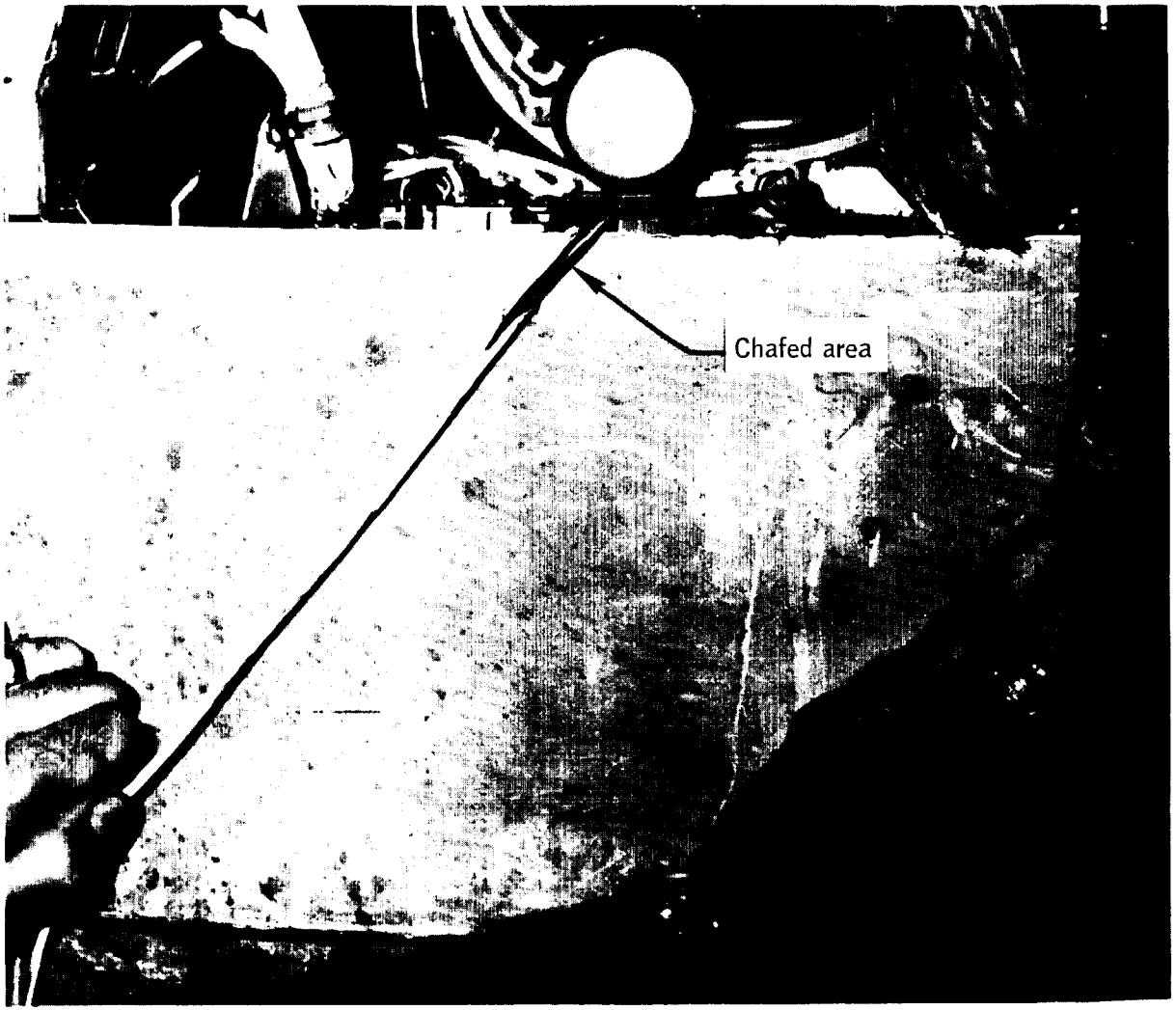

Figure 7.5-2.- Swimmer telephone/sea umbilical, Mission AS-202.

7.6 Earth Landing and Impact Attenuation Subsystem

Earth landing subsystem.-

Description: This was the first flight test of a complete Block I type ELS. The differences from the ELS on Mission AS-201 are shown in table 7.6-I. The Block I ELS, stowed on spacecraft 011 before flight, is shown in figure 7.6.1.

For Apollo Mission AS-202, operation of the ELS was controlled by the earth landing sequence controller (ELSC) baroswitch and logic functions. The functions of the ELSC are sequenced through two redundant earth landing sequence controllers with crossover provided for all events except main parachute harness disconnect.

Performance: As planned for the Mission AS-202 normal entry recovery mode, closure of the high-altitude baroswitches (at T+5217.8 seconds and 10.97 in. Hg) initiated logic power to the master events sequence controller (MESC) for forward heat shield jettison, and to ELSC systems A and B, starting the ELSC 2-second timer. Forward heat shield jettison occurred at T+5218.3 seconds, and drogue mortar fire was initiated after time out of the ELSC 2-second time delay at T+5219.9 seconds.

Drogue disconnect and pilot mortar fire were initiated simultaneously by closure of the low altitude baroswitches at T+5268.2 seconds and 20.14 in. Hg. Landing occurred at T+5582.2 seconds.

Analysis of the onboard motion picture film from camera 4, mounted in the top of the upper airlock hatch, confirmed that the forward heat shield not recontact the CM after jettison. Deployment and inflation of the forward heat shield parachute were normal.

ELS event times were obtained from the data storage equipment (DSE) onboard tape recorder bilevel data. No visual or radar references were available to evaluate ELS performance prior to landing.

A qualitative judgment can be made of the CM/ELS dynamic performance by analyzing the amount of contact between components of the ELS and the CM upper deck structure. No evidence of contact of the drogue parachute steel cable risers with the airlock upper lip (fig. 7.6-2) indicates that the CM was in a favorable aft heat-shield-forward attitude at drogue parachute deployment. Minimal contact of the main parachute harness legs with the drogue mortar cans (fig. 7.6-2) and other ELS components with any upper deck structure indicates a favorable aft heat-shield-forward attitude at main parachute deployment. The main parachutes were disconnected at touchdown

and sank before the recovery forces arrived. The average rate of descent of the CM from 8000 feet to sea level was approximately 27.5 ft/sec. Altitude versus time from ELS sequencer start to impact is plotted in figure 7.6-3. This chart is generated from data received from the onboard barometric static pressure transducer (corrected to actual day).

The discoloration observed on the white Nomex main parachute retention flaps was normal and was from the blast of the forward heat shield thrusters. The discoloration was not so noticeable on the olive drab Nylon retention flaps used on previous missions.

Impact attenuation subsystem.-

Description: The impact system consists of four crushable aluminum honeycomb ribs mounted in the CM toroidal section ±60 degrees from the +Z-axis and eight impact struts attached to the crew couch or instrumentation platform. The X-X and Z-Z struts stroking loads are developed by a frictional device and by crushing of aluminum honeycomb. These struts can stroke in either tension or compression. The Y-Y strut loads are developed by the crushing of aluminum honeycomb alone, and operate only in compression (refs. 8 and 9).

The impact system on Mission AS-202 was the most representative of a manned configuration to date. The Z-Z and Y-Y struts in spacecraft 011 retained the unmanned, stepped, load stroke curve used in Mission AS-201. Manned-type Z-Z and Y-Y struts will not have a stepped load value. The X-X struts were a manned configuration with lockout devices which prevented strut stroking under high reentry accelerations and vibrations. As planned for Mission AS-202, unlocking could occur on impact only if the landing loads were slightly higher than those required for normal, unlocked strut operation (approximately 24g and 1/8-inch stroke for X-X lockout breakout as compared to 18g to 20g for normal operation after lockout breakout). Manned type X-X struts were required for the 985-pound platform weight on spacecraft 011. A manned couch would weigh a maximum of approximately 918 pounds.

The operation and attenuation capacity of the struts is indicated by the load-stroke curves (fig. 7.6-4) as follows; the X-X strut lockout devices supply an additive honeycomb core load to the main strut core and friction load for approximately 1/8 inch of stroke. After breakout, the X-X and Z-Z (which has no lockout) strut operation is similar. The initial stroking load is developed by core crushing and friction. As long as a sufficient load is present, the stroking in the applicable direction continues. If the vehicle were overturned, putting the load on the struts in the opposite direction, the return

load would be provided only by the friction device until honeycomb was encountered at the initial position of the strut piston. If the vehicle were to overturn again so that the load would be in the original direction, the friction device would again supply the load until the remaining core material was encountered, at which time the load would return to the initial stroking load. This cycle can continue until all core is crushed. As previously stated, the Y-Y struts operate only in compression and have no friction devices.

Performance.- System performance was satisfactory. The X-X struts for Mission AS-202 had been static tested preflight to verify a normal 20g reentry capability. Postflight measurements indicated that no strut stroking had occurred. The lockout devices remained in a locked condition throughout the mission and did not break out on impact. Strut stroking is expected to occur in less than 10 percent of all Apollo water landings.

TABLE 7.6-I.- DIFFERENCES BETWEEN EARTH LANDING SUBSYSTEMS

OF MISSION AS-201 AND MISSION AS-202

Item	Mission AS-201	Mission AS-202
Drogue reefing line cutter lanyard knot	Two half-hitches	Chinese finger
Pilot parachute mortar lid	Retained	Expended
Pilot parachute deployment bag	Nylon	Dacron felt sleeve over nylon bag
Main parachute riser loop end boot	None	Dacron felt boot
Main parachute retention flaps	Nylon	High temperature nylon (Nomex) flaps with dacron felt liner

NASA-S-66-10059

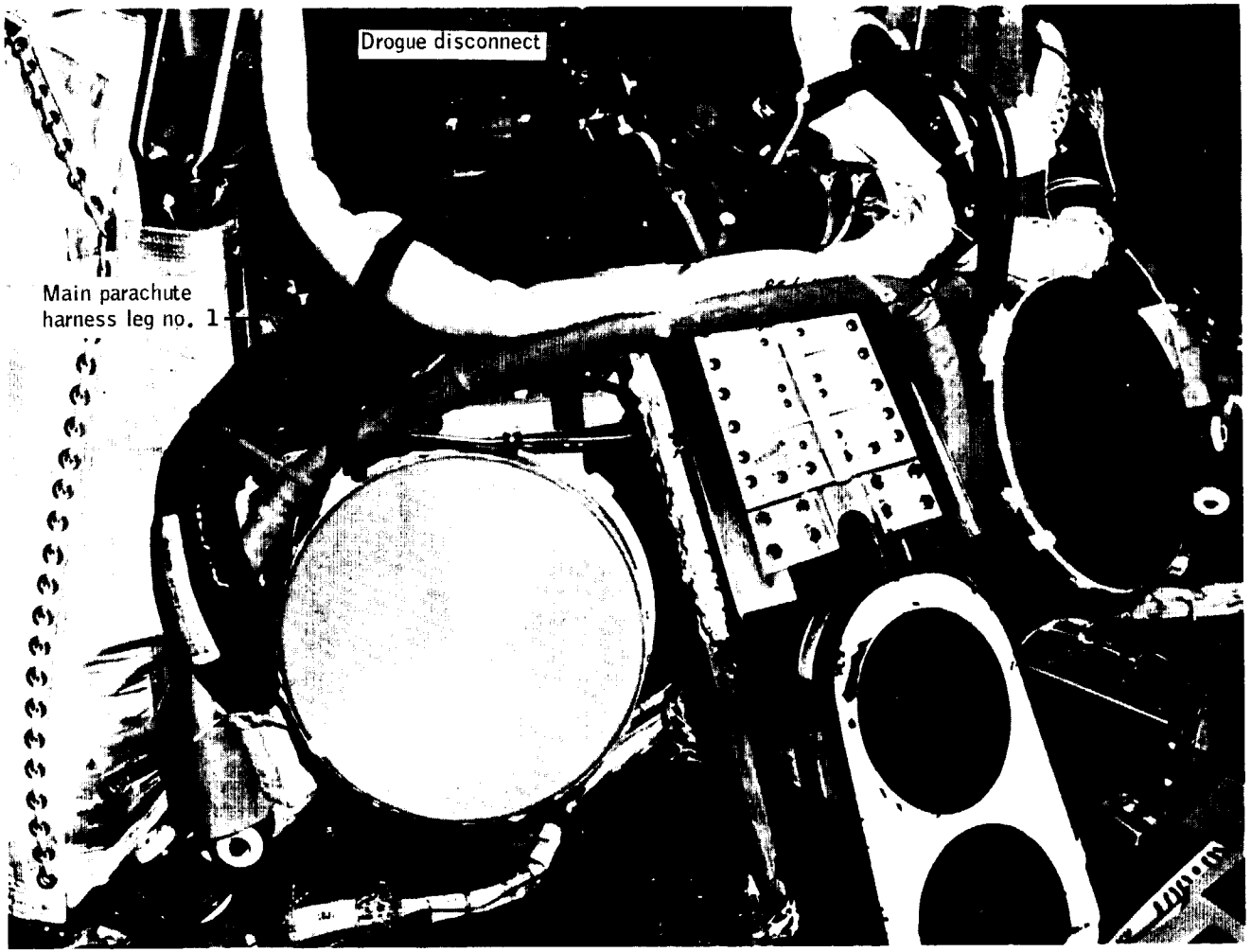

(a) Drogue mortar no. 1.

Figure 7.6-1.- Block I ELS, Mission AS-202.

NASA-S-66-10060

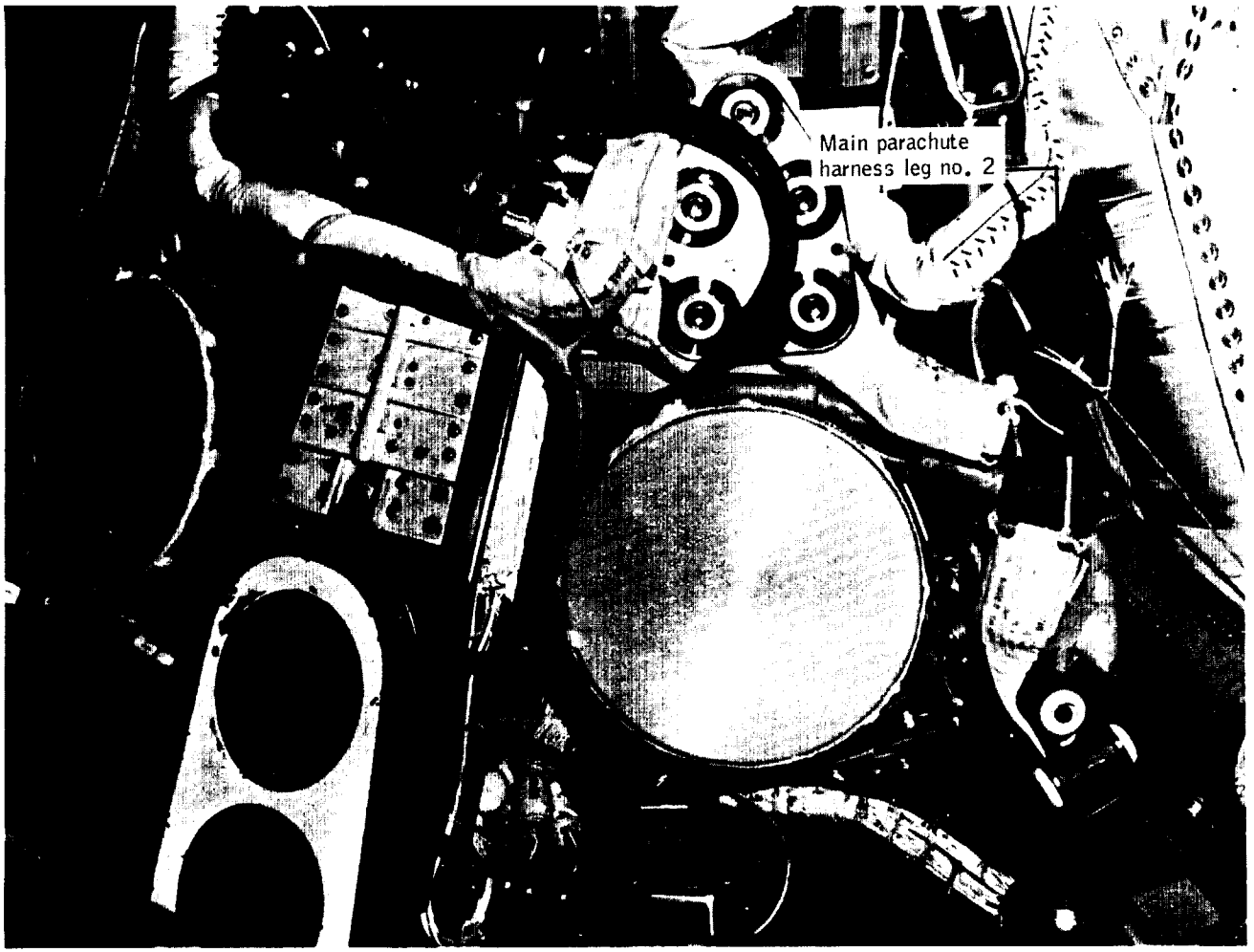

(b) Drogue mortar no. 2.

Figure 7.6-1.- Continued.

NASA-S-66-10061

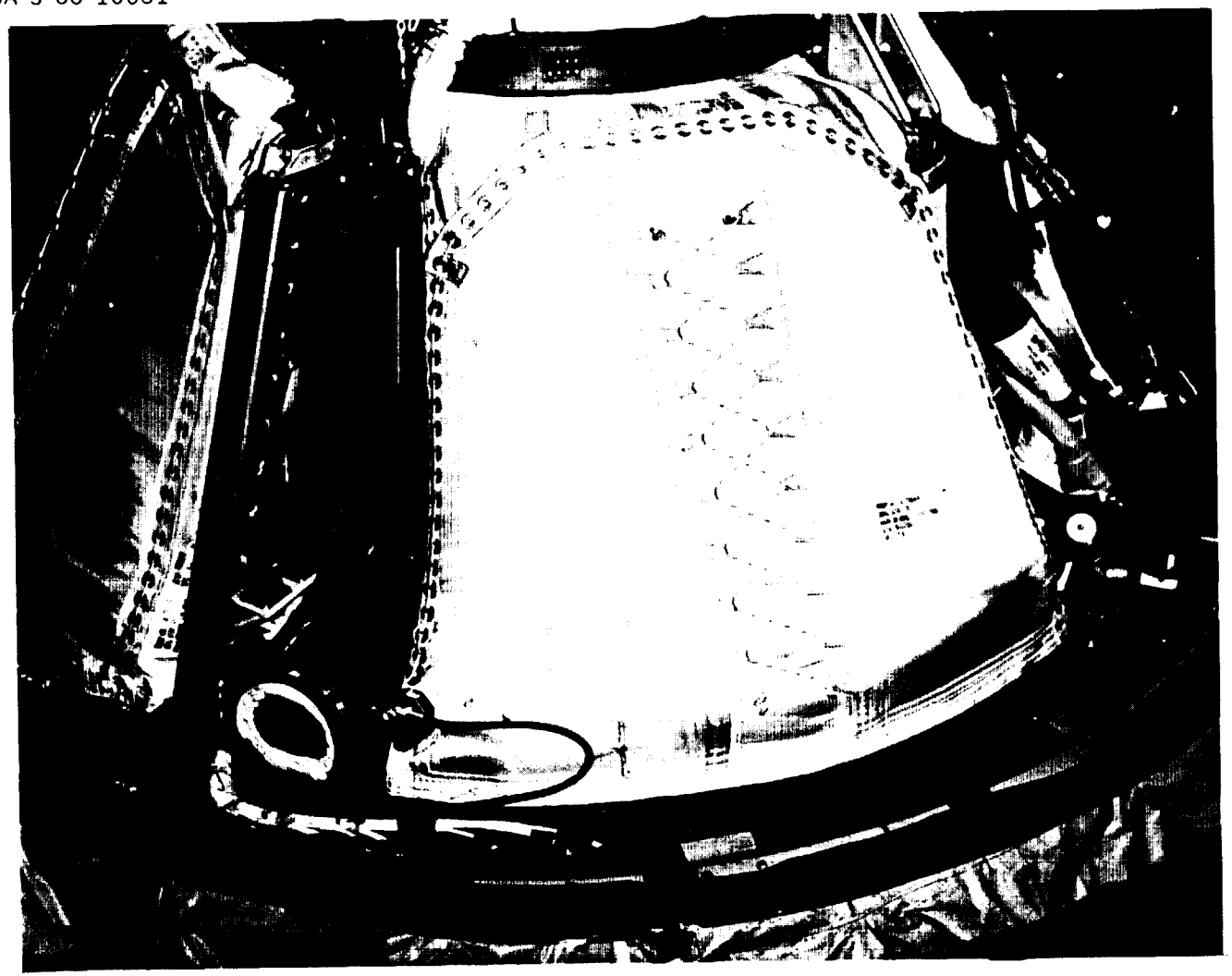

(c) -Y main parachute.

Figure 7.6-1.- Continued.

NASA-S-66-10062

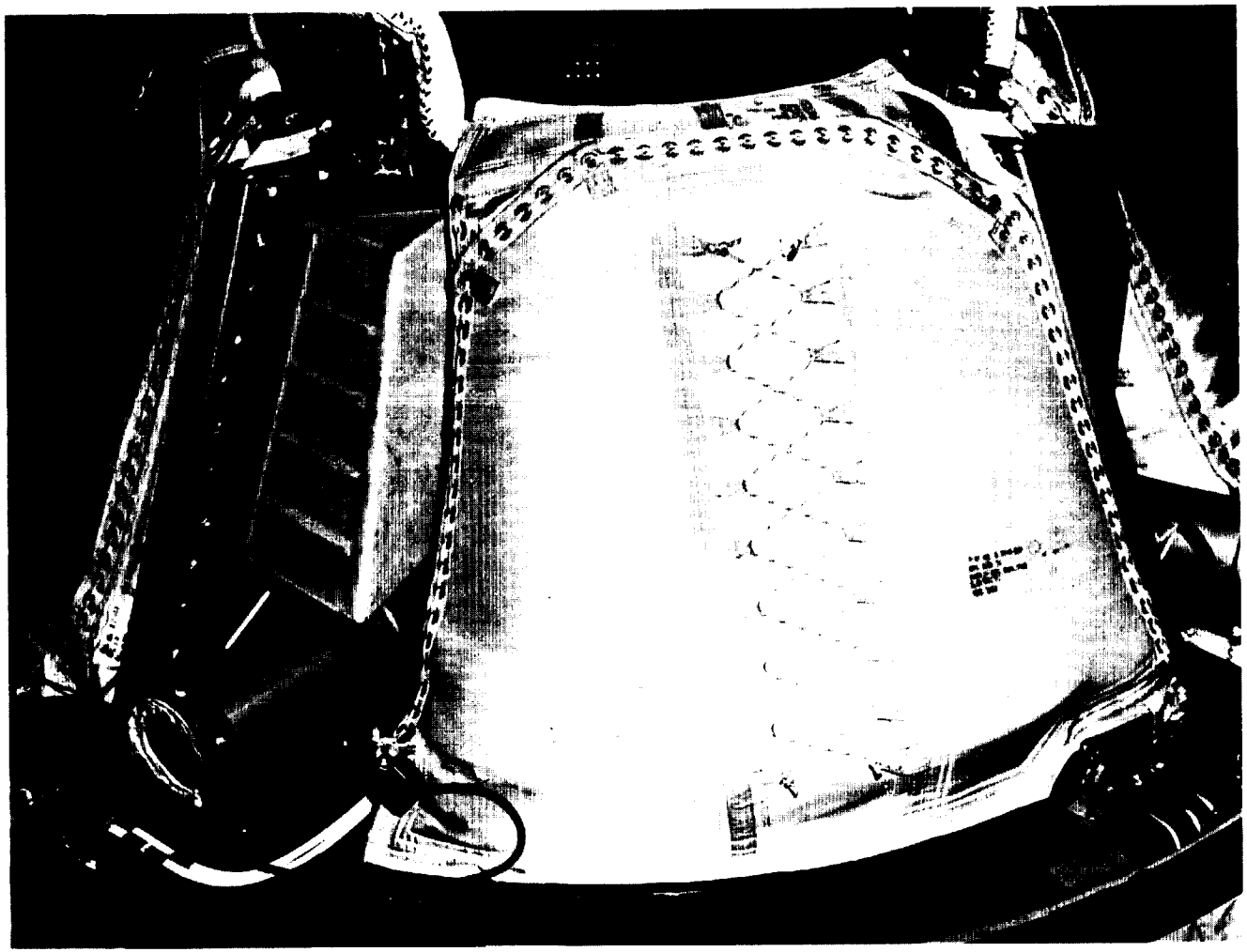

(d) +Z main parachute.

Figure 7.6-1.- Continued.

NASA-S-66-10063

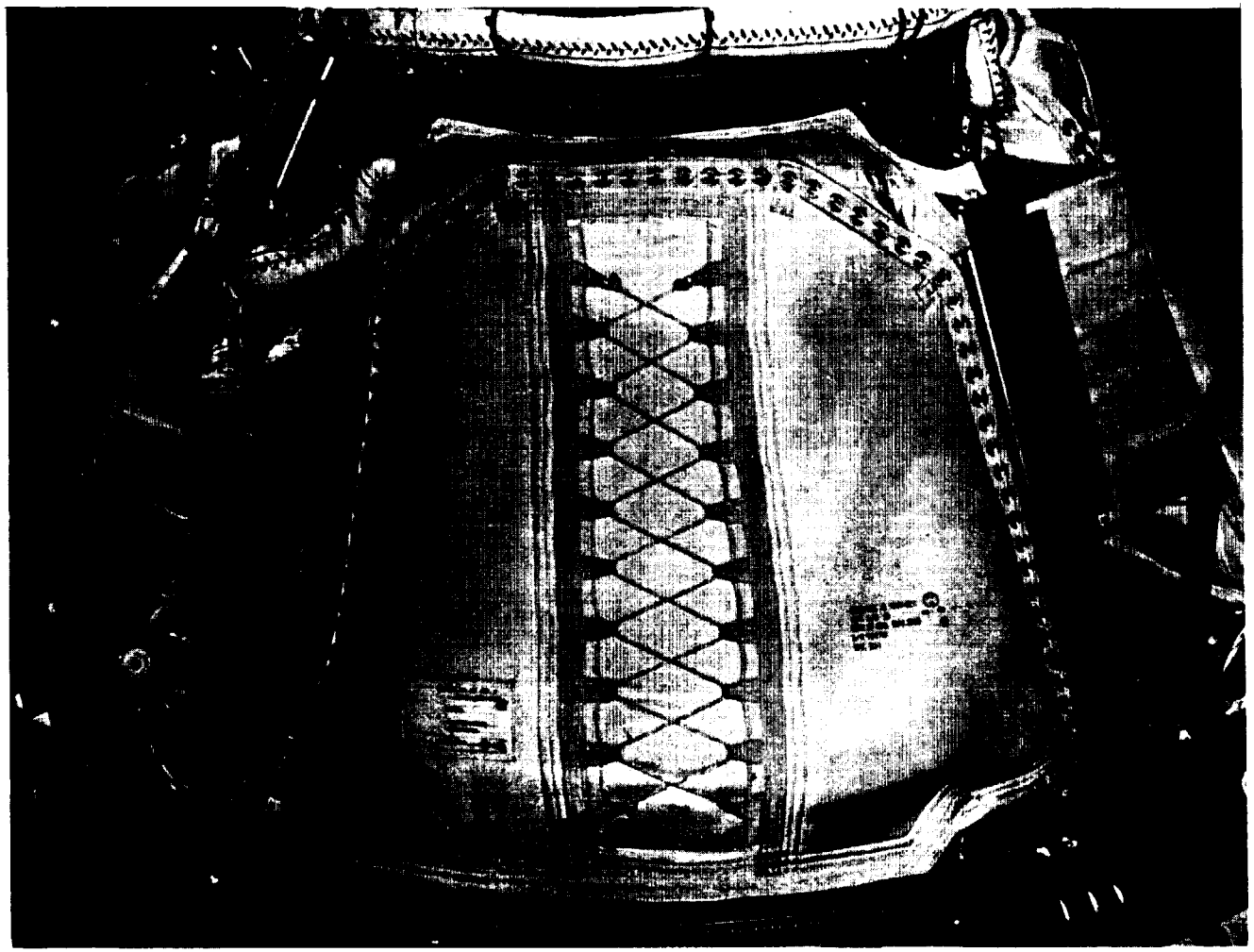

(e) +Y main parachute.

Figure 7.6-1.- Concluded.

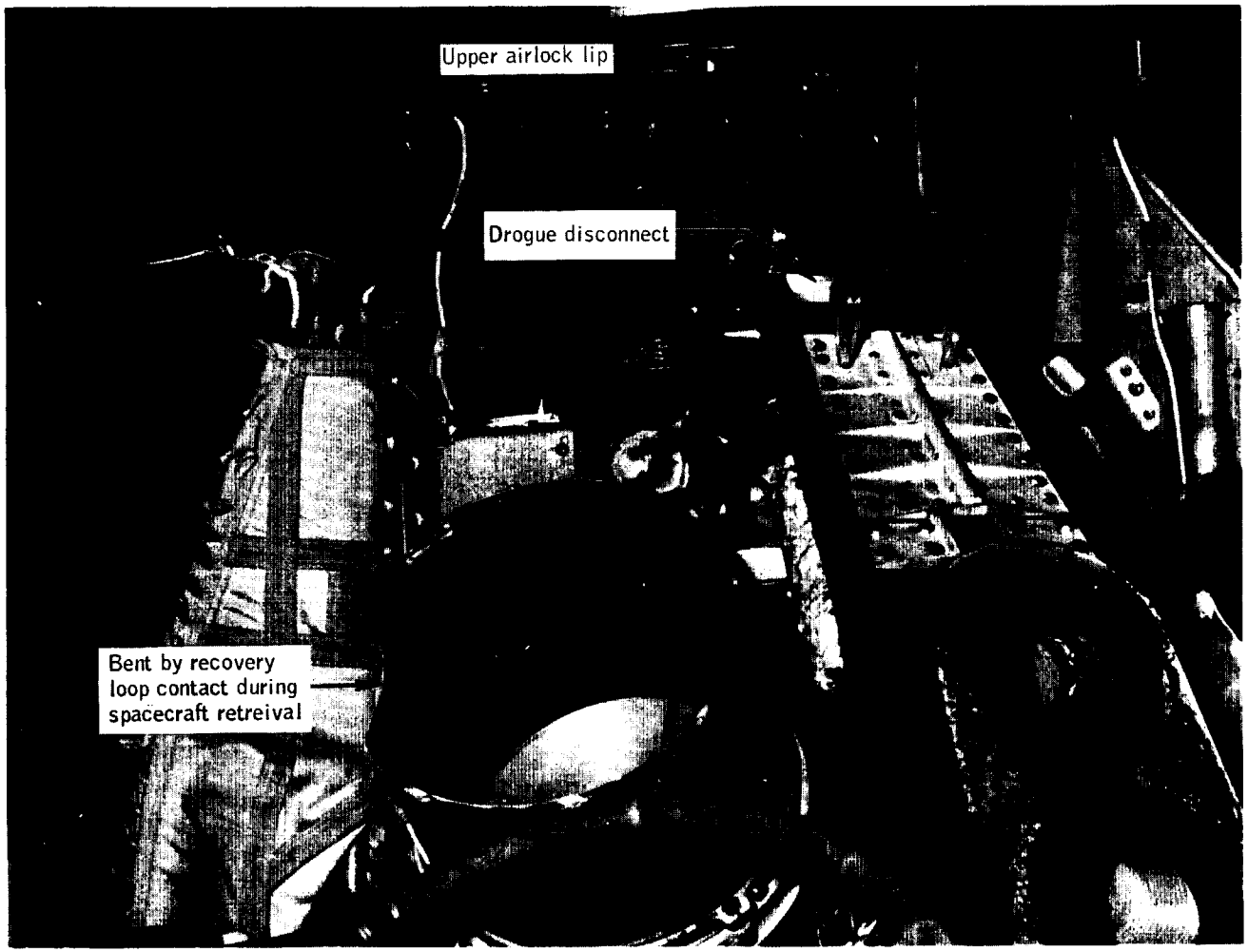

(a) Drogue mortar can no. 1.

Figure 7.6-2.- Post recovery ELS upper deck, Mission AS-202.

NASA-S-66-10065

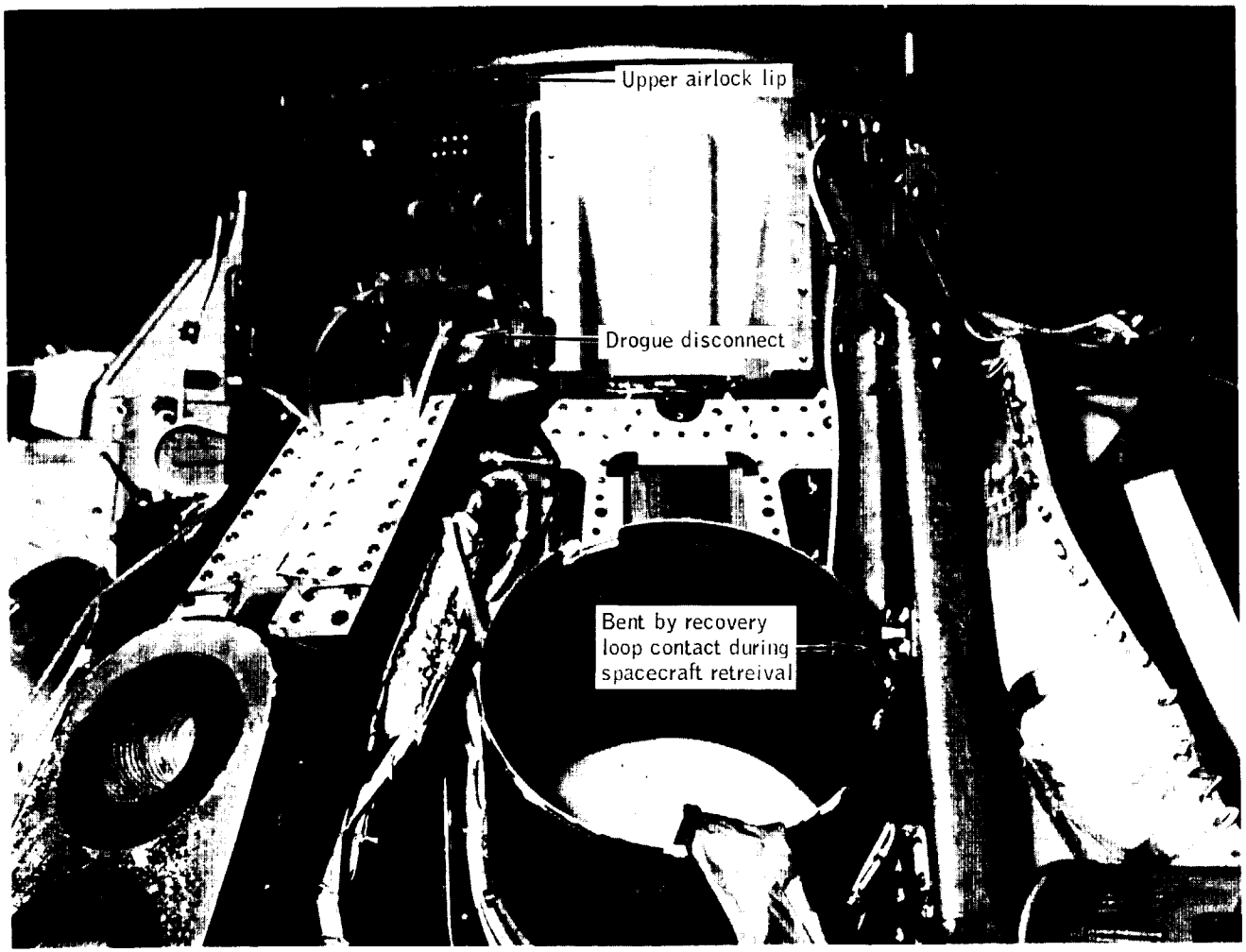

(b) Drogue mortar can no. 2.

Figure 7.6-2.- Concluded.

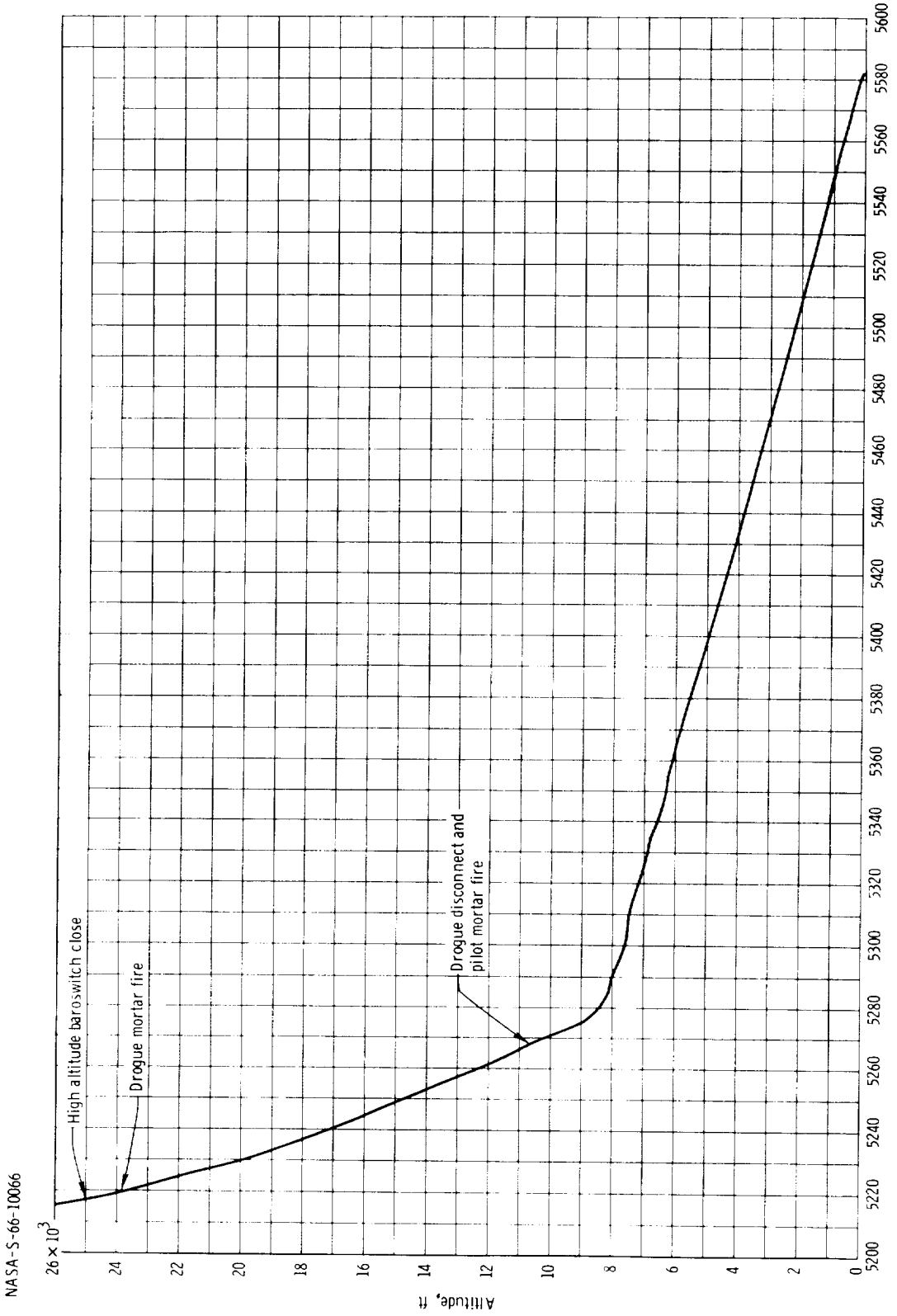

Figure 7.6-3. - Altitude time history of ELS, Mission AS-202.

NASA-S-66-10067

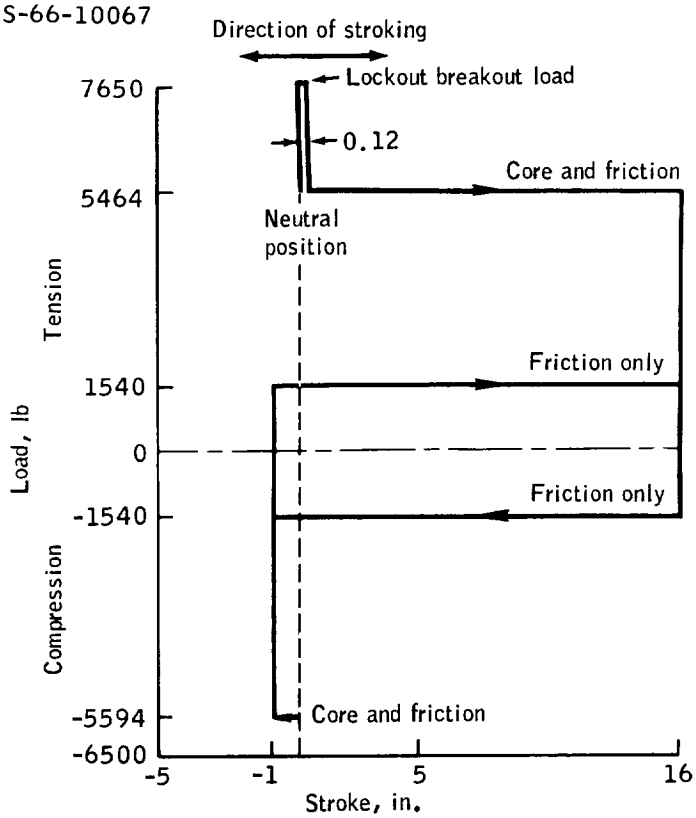

(a) X-X- foot strut.

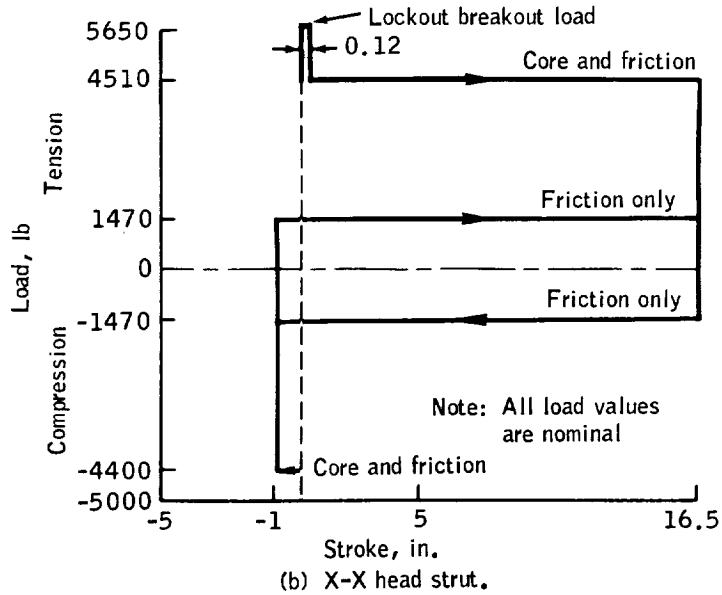

(b) X-X head strut.

Figure 7.6-4.- Impact attenuation strut design load - stroke curves for unmanned mission, Mission AS-202.

NASA-S-66-10068

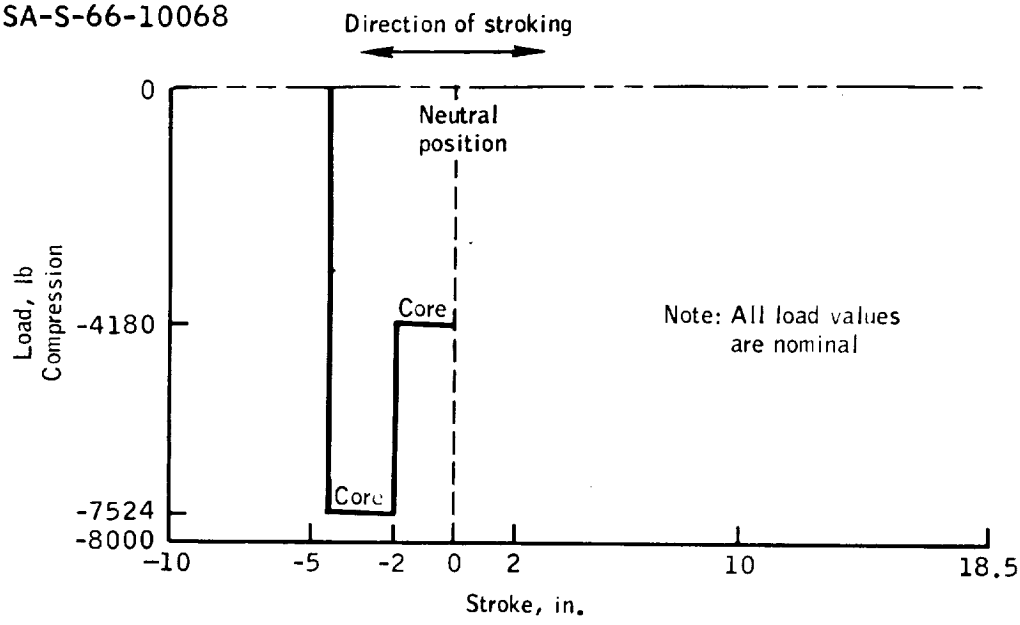

(c) Y-Y strut.

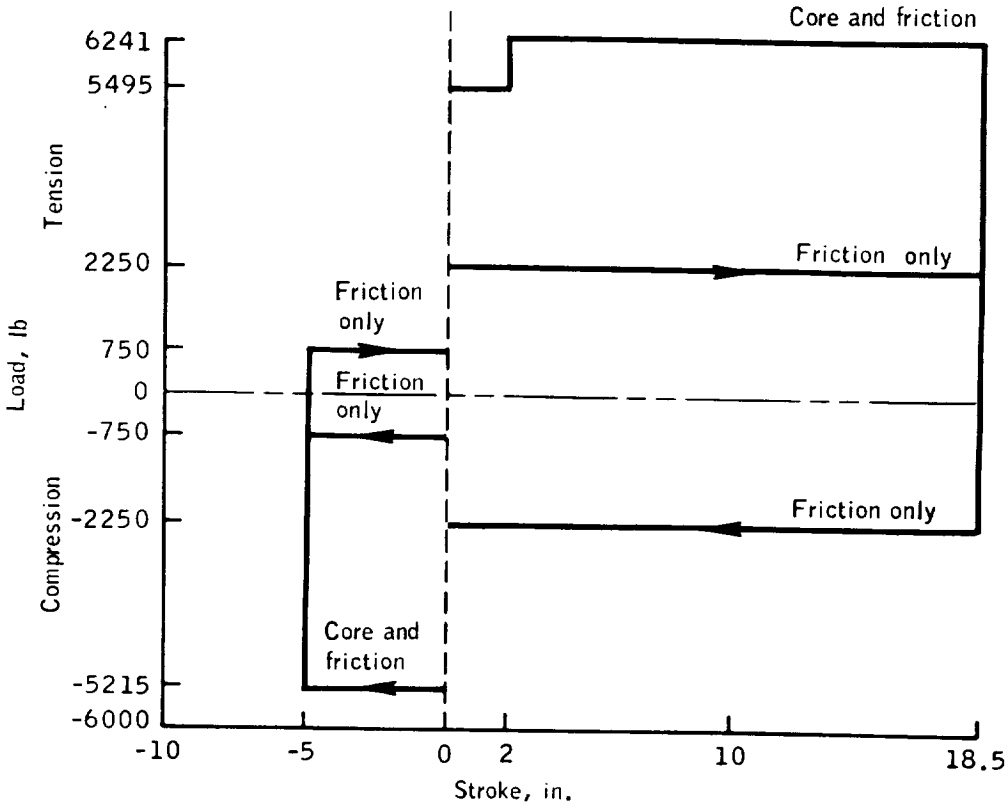

(d) Z-Z strut.

Figure 7.6-4.- Concluded.

7.7 Service Propulsion Subsystem

Summary.- Mission AS-202 was the second flight test of the service propulsion subsystem (SPS). Primary test objectives were to verify SPS standpipe fix by a minimum burn of 198 seconds for the SPS and to demonstrate multiple SPS restarts (at least three burns of a minimum 3-second duration at 10-second intervals). Secondary test objectives were to determine long duration (approximately 200 seconds) SPS performance, including shutdown transient characteristics, and to obtain data on SPS engine burn stability.

Analysis of the data confirms that the SPS related test objectives were satisfied. All four SPS burns were normal, as shown in table 5.1-II. The engine performance was nominal during the ignition, during shutdown transients, and during steady state operation; the flight data verified that no SPS anomalies occurred.

During the first burn (216-seconds duration), the standpipe fix to the retention can in the oxidizer sump tank was verified, in that helium ingestion did not occur when the propellant level dropped to the top of the retention can. During Mission AS-201 flight, severe helium ingestion occurred at this propellant level height, and subsequent investigations indicated that severe damage had been done to the retention can and standpipe during Mission AS-201 vehicle checkout. Figure 7.7-1 shows the retention can design and the redesign obtained by adding a "double wall" for increased strength, as compared to spacecraft 009.

The last 31 seconds of the first burn and the 89 seconds of the second burn were completed with the top of the retention can exposed to the pressurant ullage gas. Only normal propellant flow rates and helium consumption were observed during Mission AS-202 flight indicating that no helium leakage occurred through the retention can.

The double-walled standpipe fix substantially increased the structural integrity, based on design analysis and test data.

No combustion instability was recorded by the engine vibration monitors (see section 7.1).

Description.- The Block I type SPS configuration was described in reference 9, and is indicated in the schematic layout of the SPS subsystem in figure 7.7-2. The differences in Mission AS-202 SPS configuration from the configuration for Mission AS-201 flight were as follows:

(a) The propellant loading was 50 percent of capacity (sump tanks were filled to the top of the transfer line standpipe).

(b) The gaseous nitrogen (GN_2) tanks were initially loaded at 2690 psia.

(c) The retention can standpipe was modified by welding aluminum gussets to the three standpipe-stillwell brackets for additional strength. A stainless steel tube was installed inside the original aluminum standpipe internal to the retention cans of the fuel and oxidizer sump tanks. The aft end was welded to the standpipe elbow and the forward end was flanged external to the zero g can.

(d) The propellant utilization valve was installed, but it was intentionally disabled.

(e) The flight combustion stability monitor (FCSM) unit was installed, but it was intentionally left inoperative since the interface network required for the CM was not installed due to impact of schedule delay for installation. The measurements of one of the FCSM unit's accelerometers were recorded on the onboard flight recorder.

(f) The helium relief valves were relocated downstream of the heat exchanger, as shown in figure 7.7-2.

All SPS components were certified for this short duration mission. Several prelaunch hardware discrepancies existed (table 7.7-I); however, no mission degradation occurred as a result of these discrepancies.

The results of the analyses of the propellant and gas materials loaded are presented in table 7.7-II. The critical life of the SPS components is shown in table 7.7-III.

Propellant loading was accomplished 5 days prior to launch in 12 hours of elapsed time. During the propellant servicing procedures, after the fuel and oxidizer sump tanks were fully loaded to the top of the standpipe, ullage pressures decayed due to leaking ground support equipment (GSE) relief valves. This condition caused 22 pounds of fuel to overflow into the transfer line and the fuel storage tank, as the ullage pressure decayed from 88 psig to 0 psig. This allowed the liquid level to rise above the top of the standpipe. The oxidizer sump tank ullage pressure decayed from 85 psig to 63 psig; however, no oxidizer was reported to have overflowed into the transfer line. The propellant loading procedure for Mission AS-202 was based on a volumetric loading to fall to the top of the sump tank standpipes. Future requirements as presently known will not permit the initial propellant level to be in the vicinity of the top of the standpipe. Thus, no propellant can be transferred back into the storage even if a GSE equipment failure occurs on future spacecraft. The fuel trapped in

the transfer line can permit a 10- to 20-psi pressure drop in the effective ullage pressure, and allow a lower tank feed pressure than is normally expected. Similar problems were experienced on Mission AS-201.

The fuel inlet pressure measured indicated a 1-psi rise instead of a 3.7-psi rise during S-IVB flight. S-IVB shutdown did not show a pressure drop (10.6 psia was expected). This indicated that the fuel transfer line was filled with propellant; however, there were no adverse effects. The oxidizer inlet pressure data did not indicate that the transfer line was filled with oxidizer.

During the pressurant gas servicing, it was discovered that the airborne half GN_2 fill coupling (TP8) on the bank A engine bipropellant valve was damaged during system checkout and leaked excessively with the dust cap removed. To facilitate filling, a Schroeder valve was brazed to the dust cap. However, an undetected leak persisted at the approximate rate of 35 psi/hr. Bubble-fluid leak checks of the system from the GN_2 bottle to the three-way solenoid valves did not locate the leak. All possible leak areas could not be checked due to packaging. The bottle was repressurized at T-2 days to 2690 psig and leaked to 1650 psig at the time of launch.

All other measurements of the system showed normal conditions, including pneumatic and solenoid valve positions.

Performance.- Table 7.7-IV shows that the SPS first burn ignition was 10 seconds early; consequently, the remainder of the SPS sequences were also 10 seconds early. This was due to the above-normal launch vehicle performance which resulted in early launch vehicle/spacecraft separation.

Two modes of shutdown were provided in spacecraft 011: (a) guidance and navigation (G & N) cutoff when the desired delta velocity change had been obtained, and (b) a backup ground command based on minimum propellant interface pressure or chamber pressure, whichever occurred first. All four burns were terminated by G & N cutoff, and close agreement was obtained between the desired and actual delta velocities (table 7.7-IV).

Steady state SPS operation: The four SPS burns were normal, and the performance was about as expected with chamber, inlet, and tank pressures being nominal. Tables 7.7-V and 7.7-VI show the SPS flight measurements for each of the burns and coast periods. The performance of the SPS was analyzed by using an engine mathematical model program, best estimate propulsion parameters (BEPP), which utilized the SPS flight measurements. The engine model program used the flight measured parameters and, by iteration methods, was capable of resolving

measurement bias accurately and of isolating discrepant inputs. This accuracy was achieved due to the continuing refinement of the program in analyzing past data accumulated on the SPS.

Chamber pressure: The chamber pressure analyzed for the four SPS burns was 99 to 104 psia, which was nominal. The chamber pressure time histories indicated no anomalies, and the engine performed satisfactorily. Figures 7.7-3 and 7.7-4 show the recorded chamber pressure for the four burns and also the analyzed chamber pressure. Figure 7.7-3 indicates that chamber pressure showed a 7-psi "hump" for 20 seconds during the first part of the burn, after which chamber pressure increased from 101 to 104 psia during the rest of the burn. Utilizing the vehicle acceleration data, the engine model program proved the flight chamber pressure was 99 to 100 psia, showing that the recorded chamber pressure measurement was biased by +3 psi and that the "hump" was not real. The chamber pressure for the last three burns did not show the "hump," although engine model analysis showed a bias of 3 psi. (See discussion on chamber pressure transducer.) The measured chamber pressure was not used to analyze engine performance since it was biased.

System feed pressures: The tank pressures and engine inlet pressures during the four burns were nominal. The oxidizer tank pressures were 173 psia, and the fuel tank pressures were 172 psia, constant for the four firings. The oxidizer inlet pressure was 156 psia, and the fuel inlet pressure was 152 psia, constant for the four burns (table 7.7-VI). The BEPP program showed, by using the measured inlet feed pressures to derive tank pressures and chamber pressure, that the best vehicle acceleration match was obtained with measured flight accelerations. The differences in the analyzed tank pressures and chamber pressure obtained from the program compared to the measured values obtained during flight are the biases discussed in this report. The contribution of the feed system biases to flow rates is illustrated as the flow rate deviations from nominal values, and the flow rate biases represent the differences between analyzed and flight measured values obtained from the BEPP program.

The engine model program verified that the measured system tank pressures were biased by 2 psia with respect to the interface pressures, and that the interface pressures were more accurate in determining SPS performance.

Flight data analysis obtained from the BEPP program has shown that the quality of instrumentation accuracy is not acceptable for a more detailed analysis. The pressure transducers measuring tank pressures and chamber pressure had small (2 to 8 psi) biases and/or drift. The temperature measurements for the propellant feed system showed biases of 4° to 10° F.

Propellant gaging system: Propellant gaging system data showed that the primary gaging system and the auxiliary gaging system functioned normally. The BEPP program analysis indicated the maximum deviation for the oxidizer flow rate was 0.6 lb/sec above nominal, and for the fuel flow rate was 0.65 lb/sec below nominal (table 7.7-VI).

Both the primary and auxiliary propellant gaging systems had appreciable biases which lowered the readings of the indicated masses of both the fuel and oxidizer.

The propellant mass biases for both systems primarily came from two sources: (a) improper relationships between the propellant loaded onboard and the propellant tank level used as a reference electrical signal input to the gaging system, and (b) a difference in level between the propellant in the tank proper and the propellant in the stillwell.

There was no propellant calibration to equate the propellant loaded onboard and the propellant tank level referenced by the gaging system. The source of bias for the difference between the liquid levels in the tanks and the inside of the gaging system stillwells was that the standpipe was, in essence, a manometer effect and balanced the pressure at the bottom of the stillwell with a fluid head. Under nonflow conditions, this fluid head would equal the level of propellant in the tank. However, when the propellant was flowing, the fluid head in the stillwell was reduced by the dynamic head of the propellant flowing by the bottom of the standpipe. Also, this effect was recently observed in spacecraft 001 testing at White Sands Test Facility and is shown in table 7.7-VII. It is believed that this phenomenon is characteristic of the Block I system design of the propellant utilization and gaging system (PUGS) and will be observed during the flights. Action has been taken to more accurately determine the magnitude of this effect for Block I manned mission real-time support. The Block II retention reservoir is being designed to correct for this effect.

During the real-time support period of Mission AS-202 the propellant flow rates were calculated after correcting the quantity display readings for these biases. The calculated flow rates were in good agreement (1-percent accuracy) with flow rates obtained from the BEPP program.

(a) Primary gaging subsystem. The primary gaging subsystem indicated, after correcting the propellant quantities for the biases, that the propellant flow rates from the primary gaging subsystem during the SPS first and second burns were 0.2 lb/sec of oxidizer above nominal and 0.45 lb/sec of fuel below nominal.

(b) Auxiliary gaging subsystem. The indicated propellant level showed a sudden decrease of 1000 pounds of oxidizer at SPS first burn ignition plus 56 seconds, and 220 pounds of fuel at ignition plus 13 seconds. This was due to the above manometer effect, causing a greater propellant level drop in the stillwell than in the standpipe. These were point sensor resets caused by the large biasing effects of the dynamic head. The oxidizer point sensor (number 1) did not reset because it was uncovered during the initial 4.5 seconds of firing, during which time the sensors were locked out. Thus, the oxidizer value was not reset to account for the bias effect until sensor number 2 uncovered at 56 seconds.

The auxiliary gaging subsystem indicated that after correcting for the effects of the biases during the SPS first burn, the auxiliary subsystem fuel trace agreed with the primary subsystem fuel trace to within 50 pounds, and the auxiliary subsystem oxidizer trace agreed with the primary subsystem trace to within 230 pounds. This caused the deviation of measured flow rate of 1.4 lb/sec of oxidizer above nominal and 1.2 lb/sec of fuel below nominal for the first burn. The auxiliary gaging subsystem indicated the SPS second burn showed flow rates of 0.2 lb/sec of oxidizer above nominal and 0.72 lb/sec of fuel below nominal.

The engine performance noted by specific impulse $\left(I_{sp}\right)$ was 3.3 sec above the nominal $\left(I_{sp}\right)$ for the first and second burns, as shown in table 7.7-VI.

During the coast periods between the SPS burns, all parameters were nominal as predicted (table 7.7-VI).

Helium tank pressure, divided by absolute helium tank temperature (fig. 7.7-5), maintained a steady decline throughout the first and second burns, indicating a constant helium consumption.

Combustion stability: An accelerometer (SP1031D) mounted on the injector in the radial direction indicated a steady state vibration of $\pm$15g to $\pm$25g throughout the burns. The start transient spikes were in the range of 87g to 137g (see section 7.1) peak to peak for 3- to 10-millisecond durations for the four burns. The frequency was 2000 to 2200 cps (fig. 7.1-28). These engine vibration levels were within the specification range of 180g peak to peak for 60 milliseconds at frequencies between 600 and 5000 cps.

Shutdown transient characteristics: The service subsystem shutdown characteristics were determined by measuring the total impulse from the analyzed thrust time history for the first and second burns. The

measured total impulse during shutdown was 11 630 lb-sec for the first burn and 11 400 lb-sec for the second burn. The shutbown transient total impulse obtained from the spacecraft 011 engine acceptance test averaged 8535 lb-sec. These values are within the engine specification range of 8000 to 13 000 lb sec for total impulse.

Absence of quiescent current on the gimbal actuator clutches: Prior to 609.49 seconds, there was no current to the gimbal actuator clutches. Using this mode of operation, there was no restraint to movement of the nozzle extension during the boost phase. Current was applied specifically to retard this movement during Mission AS-201.

Figure 7.7-6 shows the extension positions of both the pitch (CH0034) and yaw (CH1034) actuators during the AS-202 boost. The following conclusions are indicated in figure 7.7-6:

(a) The nozzle extension moved slightly during boost due to expansion of the gimbal actuator case. This was normal and predictable.

(b) The greatest movement occurred during S-IVB separation when the gimbal motors were positioning the nozzle (see section 7.11.3, orbital phase). This movement was normal.

(c) The nozzle extension did not tend to swing in oscillatory motion but, rather, to align itself along the vehicle center line of thrust.

In summary, no requirement appears to exist for restraining movement of the SPS nozzle extension.

Gaging subsystem checkout: The gaging subsystem could not be checked out (table 7.7-I), and this induced an error in setting the amount of propellant to be gaged into the gaging subsystem (see previous discussion). Corrective action is being taken to fix the GSE C14-352 unit to obtain an accurate gaging subsystem checkout. This unit will also permit propellant calibration of the gaging subsystem when the propellant is loaded for future vehicles.

Instrumentation: During the SPS first firing, the chamber pressure measurement showed a "hump" of 7 psi and bias over the actual chamber pressure (fig. 7.7-3).

The chamber pressure transducer is made by micro subsystems and is required to be accurate to 5 percent of full scale (150 psia) and is temperature-compensated to 200° F. The transducer is used in a thermo-environment of 5000° F, and the high heat fluxes are expected to cause a zero shift and a degradation of the instrument linear response.

During the first two burns the instrument showed a bias of 3 psi (3 percent) which is acceptable, considering that the transducer was used in an environment for which it was not designed.

TABLE 7.7-I.- CRITICAL SPS PROBLEMS DURING KSC CHECKOUT OF SPACECRAFT

Problem	When and where discovered	Possible effect on SPS performance	Disposition
Absence of aluminae coating on nozzle extension flange.	During the conduction of Specification MA 0210-0026, SPS nozzle extension installation and leak check at KSC, excessive leakage was discovered at the periphery of the nozzle flange.	Allow excessive side thrust forces and possible nozzle separation during flight.	Investigation showed the aluminae coating applied to the columbium flange for oxidization prevention was very rough and irregular, causing an improper seal to be made. While smoothing these surface irregularities with 200 to 400 grit silicon carbide paper, a negligible amount of coating was removed from columbium inside the sealing surface. This portion would be exposed to the hot gases during engine firings. After reinstallation of the nozzle extension and a series of torque sequences, the majority of the leakage was removed. Both the leakage and absence of aluminae coating on the flange is acceptable to NASA MSC and KSC. The leakage is of such small magnitude that normal heating and expansion of the seal during SC-011 SPS firings will completely eliminate these leaks. It is also felt that the absence of aluminae coating will not degradate the flange during the SC-011 flight duration, even with a small amount of leakage present.
Loss of gimbal bearing lubricant.	Found during the inspection of spacecraft upon its arrival at KSC from Downey.	Potential bearing freeze during flight which would not allow engine to gimbal.	Sufficient vacuum testing completed at AGC to demonstrate, for SC-011 mission duty cycle, that the gimbal bearing would not freeze if loss of lubricant occurred.
Test Port 17 leaking slightly; Test Port 18 leaking excessively.	An unknown foreign material was observed on poppet seals during system checkout OCP-K-4082 performed August 15 to 17.	Loss of pressurant gas, permitting possible low ullage pressures.	When the normal dust caps were installed and locked wired, the test ports did not indicate leakage. Leakage protection was not redundant at these test ports.
Nozzle extension thermocouples 50, 51, 52, and 53 grounding strap broken.	Vehicle checkout during May 20 to 28, 1966, at LC[a] 34.	No effect. Afraid of damage to hardware, as vehicle was already stacked and work area made readily inaccessible.	Fly without the instrumentation; have not experienced any nozzle problems in 2 years and none is expected.
Engine primary GN_2 bottle leaking excessively.	During GN_2 servicing at LC 34 on August 21, 1966, an undiscovered leak existed up to and into the launch.	Loss of gas would inhibit the "A" valve bank actuation.	Could not determine the source of leakage; therefore, there was the potential failure of the system. The leakage rate was considered not to be detrimental to the success of the mission.
Absence of quiescent current to the gimbal actuator clutches.	During simulated runs at MSC on August 22, the requirement for quiescent current was discovered to have been deleted.	Vigorous motion at the engine nozzle would strain propellant lines and cause possible failure. The clutches would have held the nozzle in a null position.	Analytical results indicated that a swing of 5 degrees from null would be required before severe strain could be established. Boost flight phase should not give this severe swing condition.
PUGS checkout unit (C14-352) not usable.	During integrated system test OCP-K-0005 at LC 34 on July 8 to 23.	Cannot verify and set accurately the amount of gageable propellant loaded onboard or check the gaging system.	Previous gaging system checkout was satisfactory. The C14-352 had design problems, and faulty checkout was believed to be source of trouble. Did not perform checkout of the PUGS.
Propellant valve contamination and actuation timing traces.	During SC-012 checkout, aluminum oxide was found in the bipropellant valve. The bipropellant valve (Valve SN 114) for SC-011 vehicle has not been checked for water (aluminum oxide) in the actuator bores.	Improper engine start and shutdown transients due to slow valve timings or no actuation at all.	The timing traces showed that valve no. 2 as 15 to 50 msec slow and valve no. 4 was 15 msec slow in actuation; however, the acutation time did not increase as the valve was actuated. A valve-timing trace can be obtained at the launch complex prior to launch, and the valve timing can be compared to the valve timing history. It was noted that a SPS penumatic bipropellant valve has never failed to operate, and the actuation timing traces indicated the valve should operate satisfactorily.

[a]Launch complex.

TABLE 7.7-II.- RESULTS OF CLEANLINESS ANALYSES OF PROPELLANTS AND PRESSURANT FOR MISSION AS-202

	Constituents											
	N_2O_4, percent	N_2H_4, percent	UDMH, percent	He, percent	H_2O, percent	Chlorides, percent	NO, percent	H_2, ppm	N_2, ppm	O_2/Ar, ppm	H_2O, ppm	Hydrocarbon, ppm
Oxidizer (N_2O_4)												
Purge loop (Pad 34)	99				0.1	0.01	0.51					
Spacecraft bleed unit												
Fuel												
Purge loop (Pad 34)		50.4	46.9		2.7							
Spacecraft bleed unit		50.8	47.8		1.34							
Helium												
SPS-FDS				NA[a]				NA	NA	NA	NA	NA

[a]Not available.

	Particle count (500 ml sample from purge loop, Pad 34)						
	25 to 50μ	50 to 100μ	100 to 175μ	175 to 350μ	over 350μ	100 to 180μ	over 180μ
Oxidizer (N_2O_4)	9	2	0	1	1		
Fuel	150	25				5	2

TABLE 7.7-III.- CRITICAL LIFE COMPONENTS, MISSION AS-202

Part number	Serial number	Nomenclature	Maximum allowable preflight operation	Expended time
ME901-0484-0002	001890000029	Engine, SPS, lifetime, sec	90	42.6
AGC1118931	001890000114	Ball valve, fuel, cycles		
		Wet	250	--
		Dry	50	21
		Ball valve, oxidizer, cycles		
		Wet	250	--
		Dry	50	21
ME901-0615-0016	001890000032	Gimbal actuator motor, pitch, sec		
		Pitch motor no. 1	18 000	15 618
		Pitch motor no. 2	18 000	15 618
ME901-0615-0016	001890000027	Gimbal actuator motor, yaw, sec		
		Yaw motor no. 1	18 000	14 599.4
		Yaw motor no. 2	18 000	14 599.4
VI7-343002-61	100384300014	Propellant tank, cycles	1 350	7
VI7-343002-61	100384300013	Propellant tank, cycles	1 350	7
VI7-342002-61	100384200012	Propellant tank, cycles	1 350	7
VI7-342002-61	100384200011	Propellant tank, cycles	1 350	7
VI7-347102	00407ACX0015	Helium tank, cycles	1 350	4
VI7-347102	00407ACX0016	Helium tank, cycles	1 350	4

TABLE 7.7-IV.- SERVICE PROPULSION SUBSYSTEM PERFORMANCE, MISSION AS-202

Event	Elapsed time, sec		Change in velocity due to SPS thrust, ft/sec	
	Planned	Actual	Planned	Actual
First burn				
Beginning direct ullage	610.8	597.0		
SPS thrust on	623.3	609.7		
SPS thrust off	841.1	825.6	4036.8	4033.4
Second burn				
Beginning +X translation	3941.6	3926.1		
SPS thrust on	3971.6	3956.1		
SPS thrust off	4061.2	4044.5	2292.8	2291.4
Third burn				
Beginning +X translation	4062.2	4045.5		
SPS thrust on	4071.2	4054.5		
SPS thrust off	4074.2	4057.5	89.0	91.5
Fourth burn				
Beginning +X translation	4075.2	4058.5		
SPS thrust on	4084.2	4067.5		
SPS thrust off	4087.2	4070.5	89.8	92.5

TABLE 7.7-V.- PREIGNITION SERVICE PROPULSION SUBSYSTEM MEASUREMENTS, MISSION AS-202

[At T+600 seconds]

Measurement no.	Measurement (a)	Value
SP0001P	Helium tank pressure, psia	3900
SP0002T	Helium tank temperature, °F	82.0
SP0003P	Oxidizer tank pressure, psia	171.5
SP0005T	Oxidizer line temperature, °F	72.3
SP0006P	Fuel tank pressure, psia	174.5
SP0008T	Fuel line temperature, °F	71.1
SP0009P	Oxidizer interface pressure, psia	172.0
SP0010P	Fuel interface pressure, psia	173.0
SP0020T	Thrust chamber outer skin temperature, °F . . .	70
SP0040T	Fuel at interface temperature, °F	81.1
SP0041T	Oxidizer at interface temperature, °F	81.5
SP0050T	Nozzle outer skin temperature, °F	lost
SP0060T	Injector manifold temperature, °F	54.1
SP0600P	GN_2 tank (primary) pressure, psia	1608
SP0601P	GN_2 tank (secondary) pressure, psia	2435
SP0661P	Thrust chamber pressure, psia	1

[a]All propellant valves were closed.

TABLE 7.7-VI.- SPS ENGINE PERFORMANCE SUMMARY, MISSION AS-202

Measurement number	Measurement	Measured values								
		First burn, 216 sec	Coast, 3130 sec	Second burn, 88 sec	Coast, 10 sec	Third burn, 3 sec	Coast, 10 sec	Fourth burn, 3 sec	Coast	Predicted value
SP0003P	Oxidizer tank pressure, psia	173	178	172.5	174	172.5	174	172.0	174	175
SP0005T	Oxidizer temperature in feed line, °F	63.5	68	63.5	63.5	63.5	63.5	63.5	63.5	67
SP0008T	Fuel tank pressure, psia	174	176	172	176	172	176	173	174	175
SP0008T	Fuel temperature in feed line, °F	69	72	69	69	69	69	69	69	67
SP0009P	Oxidizer inlet pressure, psia	156	179	157.5	176	156.5	176	155.5	175	156
SP0010P	Fuel inlet pressure, psia	152	175.5	151.5	176.5	154.5	175.5	150.5	175.5	159
SP0661P	Chamber pressure, psia	[c]102	0	106.5	0	106.5	0	106.5	0	102
SP0001P	Helium tank pressure, psia		2587		2075		2075		2065	
	Oxidizer flow rate compared to nominal[a], ± lb/sec	+0.6		+0.2		NA[b]		NA		
	Fuel flow rate compared to nominal, ± lb/sec	-0.55		+0.45		NA		NA		
	Thrust compared to nominal, ± lb	+402		+611		NA		NA		
	Specific impulse compared to nominal, ± sec	+3.8		+3.3		NA		NA		
	Mixture ratio	1.99		1.88		NA		NA		

[a]Nominal is in reference to engine class values.

[b]Not available due to short burn duration.

[c]These measured values are biased as they indicate 3 psi greater than was obtained for analyzed chamber pressure.

TABLE 7.7-VII.- PROPELLANT QUANTITY DISPLAY

[From spacecraft 001 tests at White Sands Test Facility]

Sensor level number	Actual, lb	Readout, lb	Bias of manometer effect, lb
Propellant, oxidizer			
1	11 760	11 040	720
2	10 240	9 700	540
3	7 840	7 320	520
4	3 820	3 340	480
5	2 490	2 620	360
6	2 230	1 920	310
7	1 060	720	340
Propellant, fuel			
1	5 970	5 710	260
2	5 190	5 010	180
3	3 960	3 760	200
4	1 900	1 710	190
5	1 470	1 300	170
6	1 110	950	160
7	490	330	160

NASA-S-66-10069

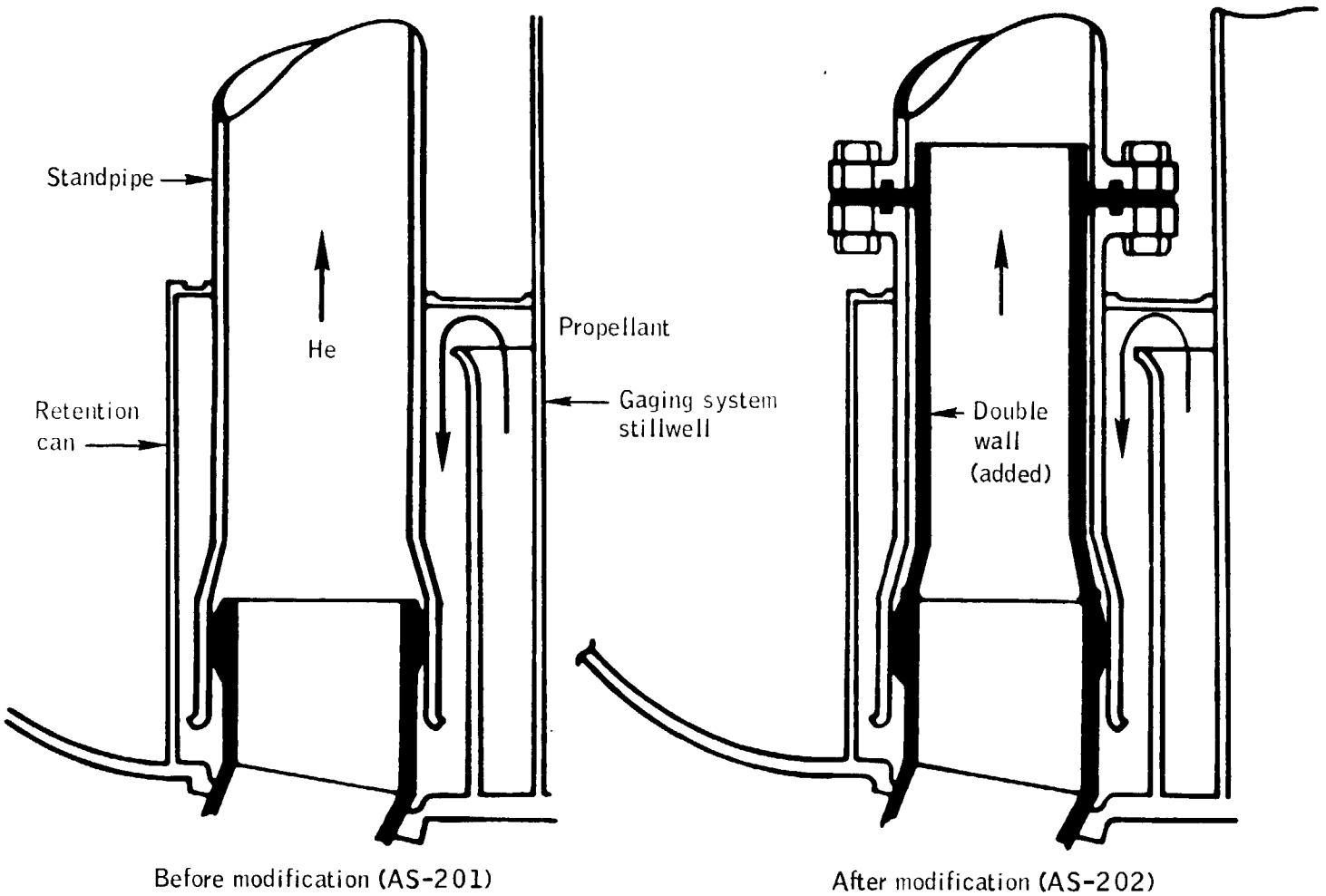

Figure 7.7-1.- Modifications to SPS retention can standpipe after Mission AS-201.

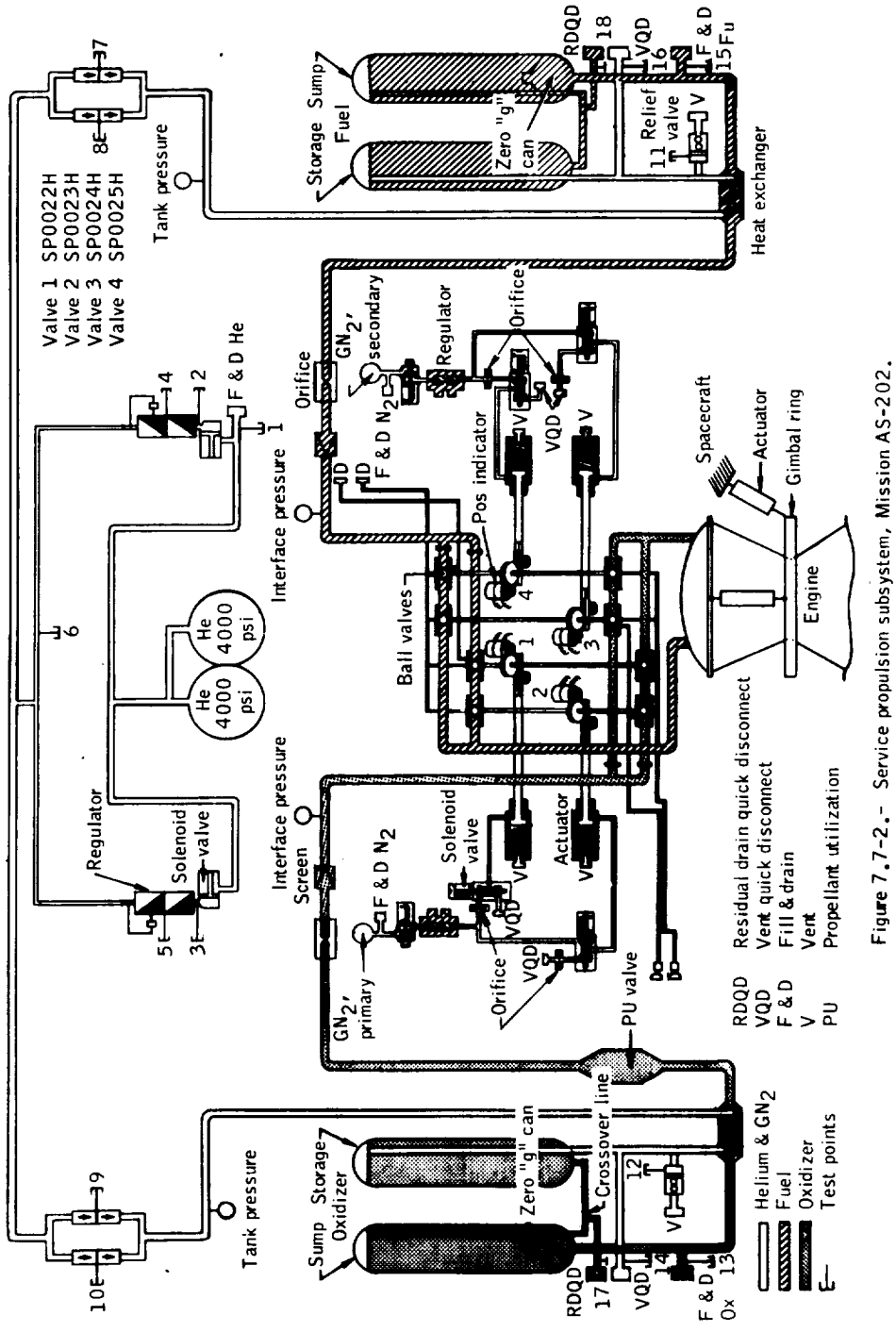

Figure 7.7-2.- Service propulsion subsystem, Mission AS-202.

NASA-S-66-10070

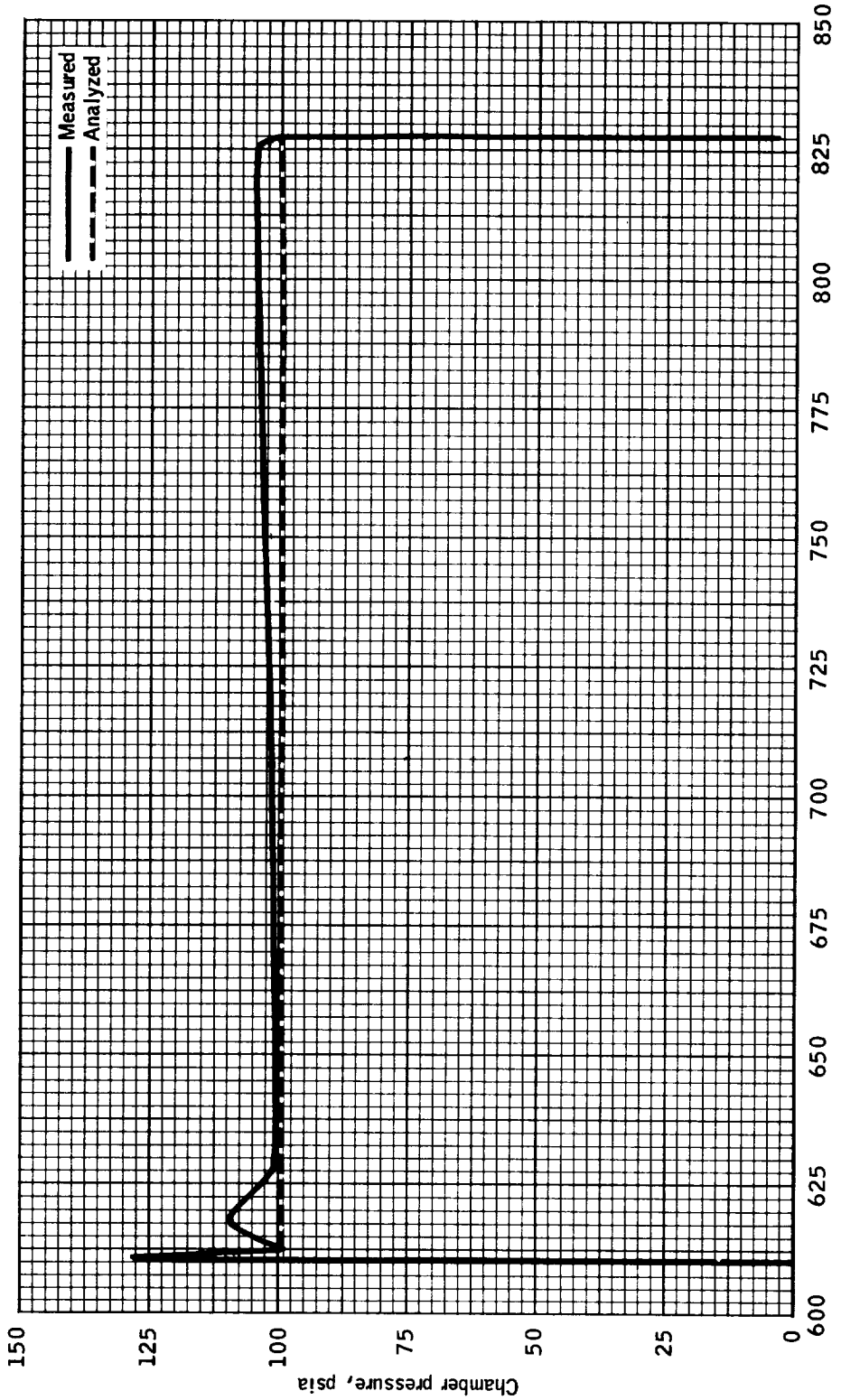

NASA-S-66-10071

Figure 7.7-3.- Time history of chamber pressure during first SPS burn, Mission AS-202.

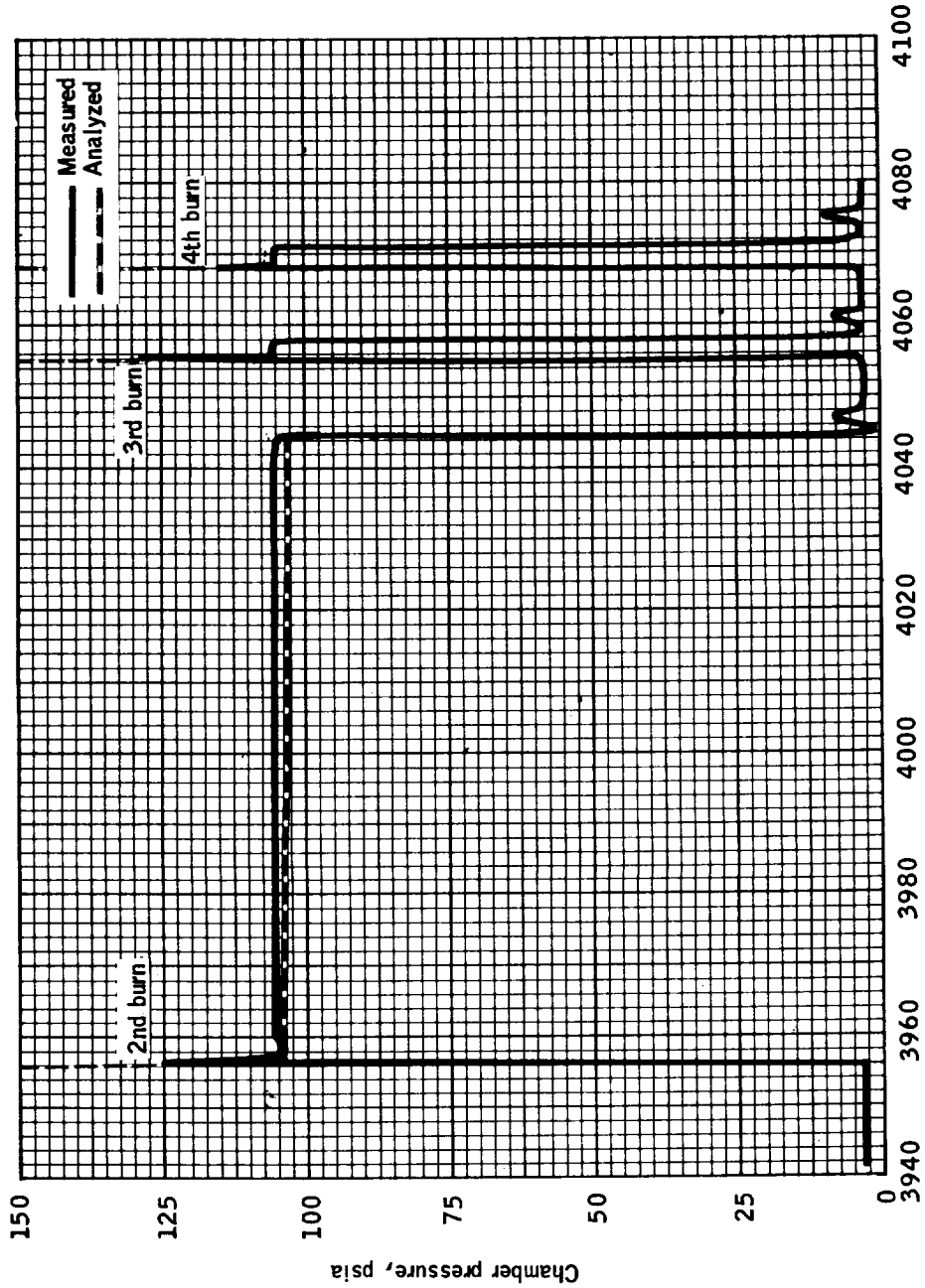

NASA-S-66-10072

Figure 7.7-4.- Chamber pressure time history for 2nd, 3rd, and 4th SPS burn, Mission AS-202.

NASA-S-66-10073

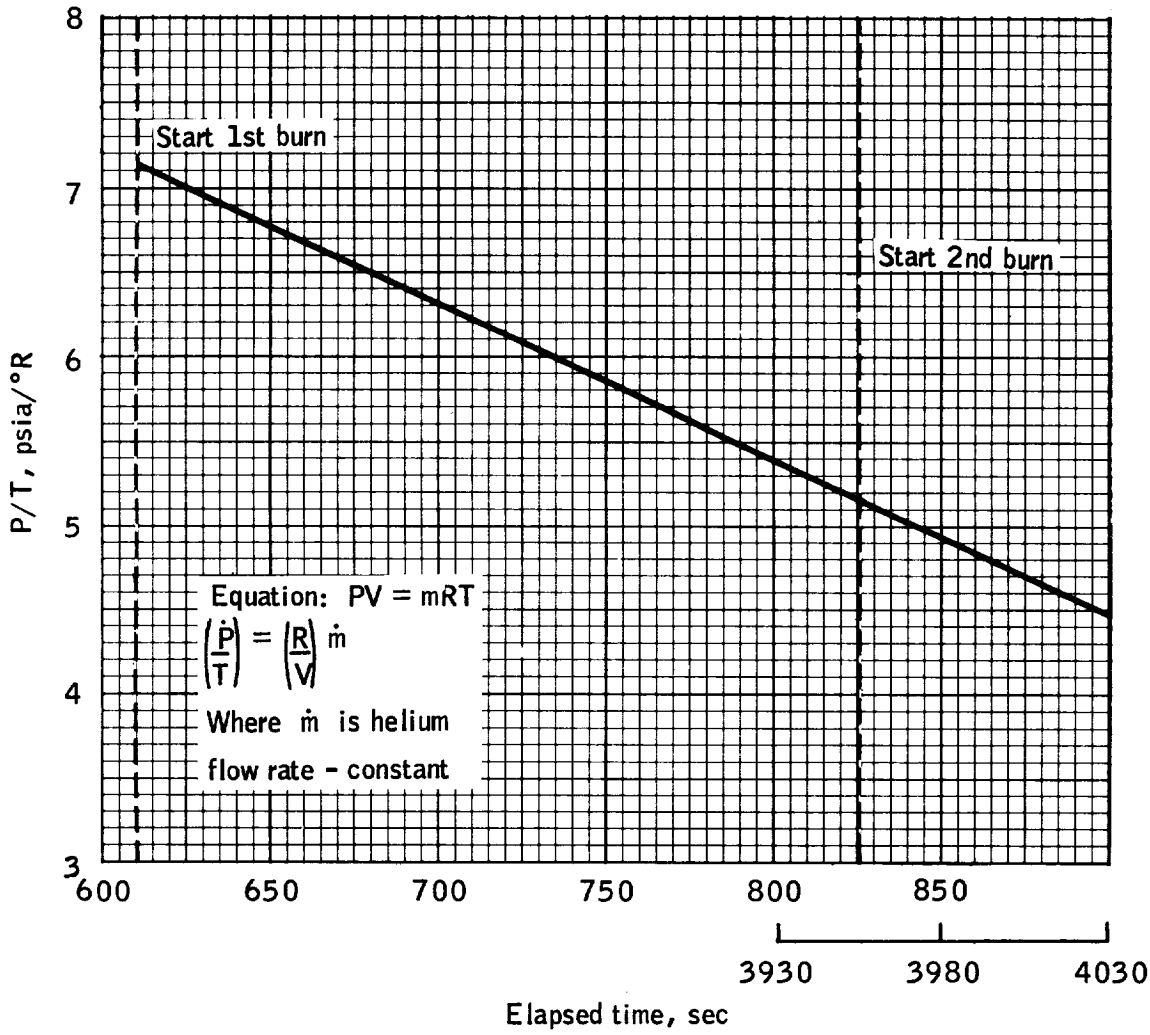

Figure 7.7-5.- Time history of helium consumption during 1st and 2nd SPS burn, Mission AS-202

NASA-S-66-10074

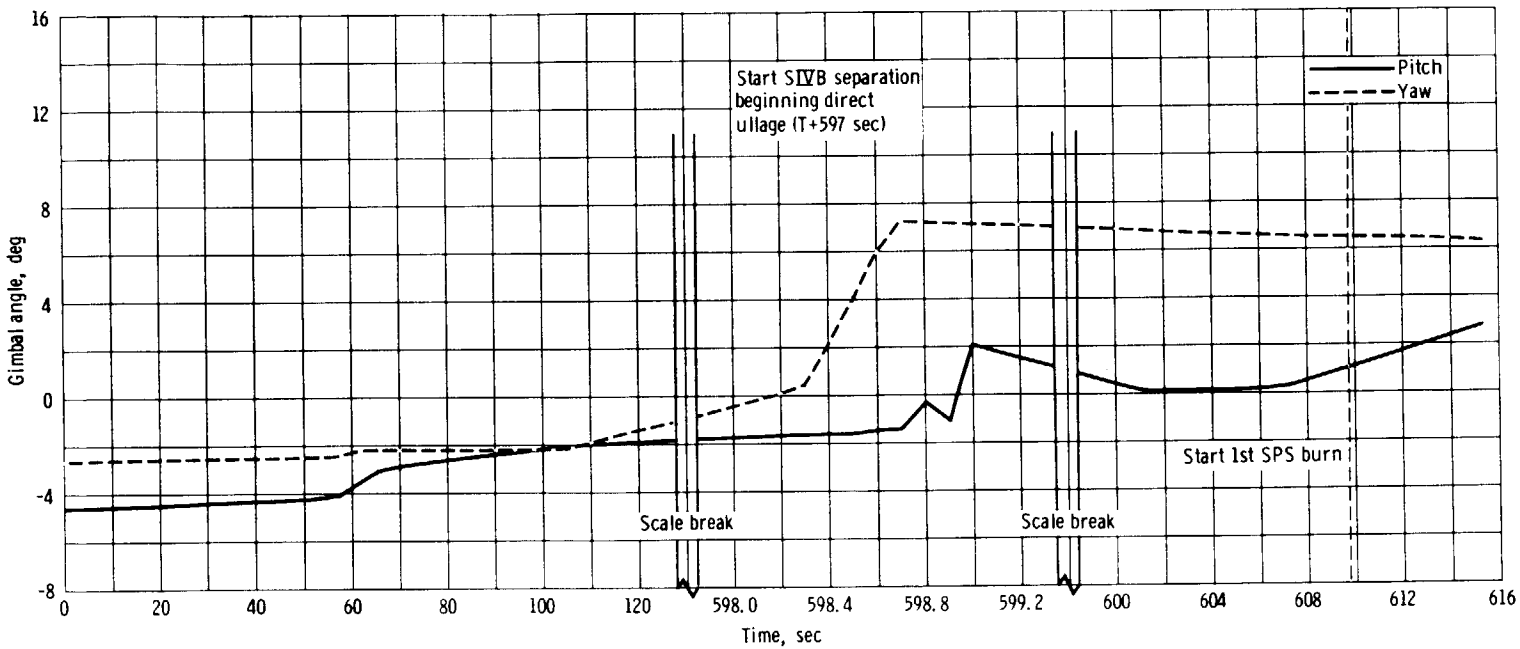

Figure 7.7-6. - Time history of nozzle swing during boost, Mission AS-202.

7.8 Launch-Escape Subsystem

Description.- The launch escape subsystem for Mission AS-202 was a Block I type configuration; however, provisions for abort initiation by ground radio command and initiation of tower jettison by a launch vehicle instrument unit signal or a ground radio command were added for this unmanned mission. The Block I type LES has been flight tested successfully on previous Apollo missions. The LES consisted of a nose cone with Q-ball, canard assembly, ballast enclosure, pitch-control motor, tower-jettison motor, launch-escape motor, and the launch-escape-tower structure. The boost protective cover was attached to the LES tower legs.

Performance.- Analysis of tracking camera film indicated that performance was satisfactory and that the tower-jettison motor fired as programmed (approximately 20 seconds after S-IVB ignition), removing the LES and boost protective cover from the CM as planned.

7.9 Reaction Control Subsystem

Performance summary of the CSM reaction control subsystem (RCS).- The CM and SM RCS inflight performance was entirely nominal throughout the mission. All maneuvers using RCS thrusters were completed as planned, and the attitude rates attained were as predicted. The sequence of CM and SM RCS events is given in table 7.9-I.

Service Module RCS.-

Description: The service module RCS configuration on spacecraft 011 was identical to that on spacecraft 009 (ref. 9) with the following exceptions:

(a) The SM RCS engine for spacecraft 011 was of the spacecraft 012 configuration, that is, it produced 100 pounds of thrust rather than 95 pounds of thrust, and had a fuel valve thermal standoff to increase thermal resistance between the valve and injector.

(b) The propellant isolation valves were of a new design with improved performance and propellant compatibility.

(c) The helium isolation valve was of the spacecraft 012 configuration, that is, an improved poppet design.

All SM RCS components on spacecraft 011 were certified for the mission and no components were known to be malfunctioning or failed prior to lift-off. However, a quad C relief valve burst diaphragm was ruptured as the result of a pressure surge during activation. This item is further discussed in the paragraphs which follow.

Servicing: The SM RCS propellant and helium pressurant servicing was accomplished during the period of T-6 to T-5 days. System activation was accomplished at T-4 hours 35 minutes. System servicing and activation data are presented in table 7.9-II. The RCS propellant analysis is given in table 7.9-III.

Anomalies: The only anomaly encountered during the SM RCS prelaunch countdown or mission occurred during activation of quad C on the pad approximately 4-1/2 hours prior to launch. When the helium isolation valve on quad C was opened to pressurize the propellant tanks, the pressure downstream of the regulators surged to 320 psia during the activation transient and ruptured the relief valve burst diaphragm. The pressure subsequently stabilized at 220 psia following activation, indicating that the overpressure ruptured the burst diaphragm and vented overboard through the relief valve. At the first SM RCS burn, the pressure downstream of the regulator dropped to nominal regulated pressure indicating that the regulator was functioning properly.

During system activation, with a pressure pad of less than regulated pressure downstream of the regulator, the regulator poppet is initially in the full open position and cannot start to close until regulated pressure is attained. Since the total system ullage volume is only about 340 cubic inches, regulator response is very critical.

Resolution of anomaly and impact: This anomaly will be avoided on future missions by precluding the necessity for the poppet to travel from full open to full closed in this extremely short time period. This will be accomplished by completing the following helium servicing procedure:

During helium servicing, helium will be supplied to the fill port with the helium isolation valves in the open position. This will allow the volume downstream of the regulator to attain regulated lockup pressure causing the regulator poppets to travel to the closed position. Servicing of helium to the source tank will continue to 4150 psia. A system decay check will be performed after equilibrium has been attained by closing the helium isolation valves and monitoring system decay.

Since no hardware change is involved, no schedule impact will occur.

Another possible anomaly was evidenced when the master caution and warning light came on approximately 3 seconds into the flight. Examination of the RCS quad regulated helium manifold pressures revealed that during the first 110 seconds of the mission, the regulated helium pressure transducer output on quad D indicated a considerable amount of data scatter, some points going below 155 psia. The first time this occurred was approximately T+3 seconds. Since other instrumentation (propellant manifold pressures) showed the regulated pressure to be proper, it could only be assumed that the transducer was malfunctioning. Recognizing that a helium manifold pressure signal below 155 psia would activate the caution and warning light, this data scatter should have, and apparently did, activate the warning light.

Since the output from the quad D regulated helium pressure transducer was completely nominal after T+110 seconds and remained so throughout the flight, the malfunction would have had to been intermittent and probably associated with high vibration at launch. A history of problems has been associated with the splice between transducers and the spacecraft wiring. High resistances and poor contact in general were found in several instrumentation splices during spacecraft 011 checkout at KSC. These splices were remade at KSC and verified to be satisfactory. Nevertheless, it could have been possible for the vibration during launch to cause momentary bad connections which would show up as voltage (hence, pressure) decrease spikes. To preclude the

problems on spacecraft 012, the splicing procedures were reviewed for inadequacies, better quality control was initiated, and each splice was potted and bonded to the quad D panel to prevent flexing which could cause failures.

SM RCS performance: Performance of the SM RCS throughout the mission was nominal in every respect. All mission objectives were met and the system performance was verified as satisfactory for the AS-204 mission. Spacecraft accelerations produced by the RCS were nominal for both attitude hold and maneuvering. All measured pressures and temperatures were also nominal, showing no unusual or unexpected results except for the quad C regulated pressure during the boost phase as discussed in the anomalies.

During the AS-202 mission, the SM RCS performed four +X translation maneuvers, one direct ullage translation, four pitch maneuvers, and maintained attitude control in pitch, yaw, and roll. The sequence of events is shown in table 7.9-I. Spacecraft accelerations in pitch, yaw, and roll during various phases of the mission are shown in table 7.9-IV. In general, the correlation with the predicted accelerations is quite good, considering uncertainties and inaccuracies in the evaluation technique, the center-of-gravity locations, and the spacecraft moment of inertias. The velocity changes and average accelerations produced during the four translation maneuvers are shown in table 7.9-V. The delta velocities (ΔV) were taken from the G & N pulse integrating pendulous accelerometers (PIPA) data. These integrating accelerometers are intended primarily for the larger delta velocities associated with the SPS burns and are relatively inaccurate for the low level RCS delta velocities. Also the short duration of the burns and data quality (data dropout) added considerable inaccuracy. Even with these handicaps, the accelerations and velocities produced were quite close to the theoretical values.

SM RCS propellant consumption for the mission and for discrete maneuvers or periods of the mission were calculated using two techniques and compared to the planned propellant budget. Using the helium source, regulated pressures, estimated helium tank and propellant tank temperatures (which were not measured on spacecraft 011), a PVT calculation was used to establish the propellant usage. The second technique involved summing the engine "on-times" or firing times and establishing an average propellant flow rate for a discrete period from the realized duty cycles and theoretical flow rate data. Table 7.9-VI shows the average flow rates and total propellant used per quad for the various maneuvers and phases of the mission. Figure 7.9-1 shows the overall SM RCS propellant budget as computed by summation of engine firing times and PVT, and compares these to the preflight planning budget. The budget, as determined by summation of engine firings, was most accurate with an estimated inaccuracy of ± 1 to 2 percent. The

inaccuracy is primarily due to variations of the propellant flow rate with pulse widths. Maximum deviation of the PVT budget from this is 75 pounds. Overall inaccuracy for the PVT is estimated to be ±10 percent (75 pounds deviation out of 800 pounds total for the system). Maximum overshoot for the PVT technique due to transient conditions was 10 pounds and lasted for approximately 20 seconds. During the early portions of the mission, when little propellant had been used, the correlation between PVT and engine burn times was very good. Near the end of the mission significant deviations appeared. This was due to the fact that no temperature measurements, hence corrections, were made. Significant improvement is expected when temperature measurements are made, as is demonstrated by the PVT calculations made with temperature measurements for the CM RCS (see CM performance evaluation). Considerable deviation exists between the actual propellant budget (from engine firings) and the flight plan budget because of assumptions, estimations, and simplifications made in the flight plan budget.

Figures 7.9-2 through 7.9-5 show a more detailed breakdown of propellant consumption for four typical maneuvers. Again, the curve from summation of burn times was quite accurate (±1 to 2 percent of full load inaccuracy). The average deviation of the PVT curve during the first maneuver was approximately 3 pounds over the 5 pounds actually used. Table 7.9-VII shows the helium source pressure drops associated with these maneuvers.

Figures 7.9-6 and 7.9-7 show the distribution of pulses for a +X translation maneuver and a pitch maneuver, respectively. These figures show the number of pulses fired for various pulse widths based on a 5-millisecond sample interval. As shown for most attitude maneuvers, most pulses are in the 50-millisecond range, while for the translation maneuvers there is a distribution between 50-millisecond pulses and 700-millisecond pulses as well as the steady state burns (greater than 1 to 2 seconds).

Command Module RCS.-

Description: The command module RCS configuration on spacecraft 011 was identical to that on spacecraft 009 (ref. 9) with the following exceptions:

(a) The propellant isolation valves were of a new design with improved performance and propellant compatibility.

(b) The CM RCS engine for spacecraft 011 was of the spacecraft 012 configuration with epoxy-coated throat and liner and improved valve design.

(c) The oxidizer and fuel tanks on Mission AS-202 were of the spacecraft 012 configuration which uses net-size bladders in both tanks and 9-mil ends on the oxidizer tank bladders. Both tanks also had liquid side vents.

All CM RCS components on spacecraft 011 were certified for the mission and no components were known to be malfunctioning or failed prior to lift-off.

Servicing: The CM RCS propellant and helium pressurant servicing was accomplished during the period of T-6 to T-5 days. Servicing data are presented in table 7.9-VIII. The propellant analysis is given in table 7.9-III.

Anomalies: One anomaly was identified during the CM RCS prelaunch countdown or mission. The anomaly identified concerned the CM A system oxidizer and the B system fuel relief valve burst diaphragms that were found ruptured during postflight inspection. An examination of the data at the time of CM RCS activation indicated a pressure surge occurred similar to that described in this report for the SM RCS quad C. In the case of the CM, the ullage volumes are even smaller than in the SM. Because of this, restrictive orifices have been placed in the helium supply lines to limit the maximum helium flow rate. It has been determined that the orifice size currently being used is marginal. The Block II orifice was therefore reduced to a smaller size.

CM performance evaluation: Performance of the CM RCS from activations, just prior to CM/SM separation, until system purge was entirely nominal. All mission objectives were met and performance was verified as satisfactory for the AS-204 mission. CM accelerations in pitch, yaw, and roll were nominal throughout reentry as were the spacecraft attitudes. All measured system pressures and temperatures were also nominal, showing no unusual or unexpected results.

During the reentry portion of the mission, the CM RCS performed a pitch maneuver and several roll maneuvers, as well as provided attitude hold control. Spacecraft accelerations, produced with dual system control, are shown in table 7.9-IV. Again, correlation between the theoretical accelerations was quite good considering the accuracy of the evaluation data and techniques.

CM RCS propellant consumption for the mission was again calculated using PVT techniques and accumulated engine firing times. For the PVT calculation, helium source and regulated pressure and helium source gas temperature were used as inputs. Table 7.9-VI gives the calculated average engine propellant flow rate and total propellant used for both systems of the CM RCS. Figure 7.9-8 shows the total propellant used

(budget) during the reentry phase of the mission, comparing PVT with "on-time" calculations and the predicted budget. The amount of propellant required for the various maneuvers (pitch and roll) can be read from this figure. As in the case of the SM RCS, the propellant depletion derived from the engine burn times was the most accurate (approximately 1 to 2 percent). The maximum deviation of the PVT curve from the summation curve was 2.5 pounds. Overall inaccuracy for the PVT calculations was estimated to be ± 3 to 6 percent of full load. Maximum overshoot for the PVT technique was 4 pounds and lasted for approximately 50 seconds. In general, PVT correlation was very good. The initial PVT readings at 4260 to 4400 seconds were useless, probably due to pneumatic and thermal transients associated with the CM RCS activation and initial firings. Once stabilization was reached (approximately 2 minutes after separation), the data were acceptable. Due to the PVT technique, the data must be calibrated to the initial load and a fixed bias must be established to adjust the PVT data to the 0 usage point (prior to any firing). For the A system this was +2.8 pounds; for the B system, +4.04 pounds. Again the flight plan budget deviates significantly from the actual usage (derived from firing times) due to assumptions, estimations and simplifications made in the flight plan budget. The propellant depletion burn was accomplished successfully, burning off approximately 177.3 pounds of propellant. The helium purge was also successfully accomplished. Figure 7.9-9 shows the helium source pressure depletion corresponding to the propellant consumption curves. Figure 7.9-10 shows the distribution of pulses for the CM RCS. As shown, most pulses were in the 50- to 80-millisecond range.

TABLE 7.9-I.- RCS EVENT TIMELINE, MISSION AS-202

Event	Time, sec	
	On	Off
Direct ullage	597.0	600.0
+X translation	600.0	610.7
First SPS burn[a]	609.7	825.6
Pitch to local vertical	837.1	886.7
+X translation	3926.1	3957.1
Second SPS burn[a]	3956.1	4044.5
+X translation	4045.5	4055.5
Third SPS burn[a]	4054.5	4057.5
+X translation	4058.5	4068.5
Fourth SPS burn[a]	4067.5	4070.5
Pitch to separation attitude	4188.2	4213.0
Transfer to CM control	4263.9	N/A
Pitch maneuver to reentry attitude	4272.2	4279.7
Roll maneuver to lift vector up	4450	4475
Last CM RCS control pulse	5216.10	5216.14
Propellant depletion burn	5287.8	5340.1
Helium purge	5539.0	5590.0

[a]During SPS burns the RCS pitch and yaw channels were inhibited 1 second after the initiation of SPS burn. RCS attitude control was maintained at all other times during the mission.

TABLE 7.9-II.- SM RCS SERVICING AND ACTIVATION DATA, MISSION AS-202

(a) SM RCS servicing

Parameter	Quad			
	A	B	C	D
Nominal oxidizer load, lb	139.6	139.6	139.6	139.6
Oxidizer loaded, lb	136.0	137.2	137.2	136.0
Nominal fuel load, lb	70.4	70.4	70.4	70.4
Fuel loaded, lb	69.5	69.5	69.7	69.4
Nominal helium source pressurization, psia at 70° F	4150	4150	4150	4150
Actual helium source pressurization, psia	4260	4340	4350	4330
Helium tank temperature at servicing, °F	88	92	94	91
Helium manifold pad pressure, psia	160	158	159	157

(b) SM RCS activation

Parameter	Quad			
	A	B	C	D
Helium source pressure prior to activation, psia	4047	4151	4184	4200
Helium source pressure after activation, psia	3970	4045	3994	4095
Helium manifold pressure prior to activation, psia	140	143	101	115
Helium manifold pressure after activation, psia	199	197	222	201

TABLE 7.9-III.- RCS PROPELLANT ANALYSIS, MISSION AS-202

Propellant	Requirement		Serviced	
	SM	CM	SM	CM
Fuel (A-50 for SM, MMH for CM), percent	N_2H_4, 50	MMH	51.0	MMH
	UDMH, 50		47.5	
Purity, percent	98 min.	98 min.	98.5	98.9
Water equivalent, percent	2 max.	2 max.	1.5	1.1
Density, g/mL	--	0.872 ± 0.002 max.	--	0.872
Transmittancy, percent	--	90 min.	--	91.50
Filterable solids, mg/liter	1.0 max.	1.0 max.	1.9	0.026
Oxidizer (N_2O_4)	N_2O_4	N_2O_4	N_2O_4	N_2O_4
Purity, percent	99.5 min.	99.5 min.	99.0	99.53
Water equivalent, percent	0.1 max.	0.1 max.	0.1	0.096
Chloride, as nitrosylchloride, percent	0.08 max.	0.08 max.	0.01	0.030
Filterable solids, mg/liter	1.0 max.	1.0 max.	0.8	0.1
Nitrogen oxide, percent	0.85 max.	0.85 max.	0.48	0.43

TABLE 7.9-IV.- CSM RCS MANEUVER ACCELERATIONS, MISSION AS-202

Configuration	Maneuver	Actual acceleration,[a] deg/sec^2	Predicted acceleration, deg/sec^2
Prior to first SPS burn	Pitch to first SPS burn attitude	1.25	1.28
	Yaw control	--	1.25
	Roll control	7.16	6.99
After first SPS burn	Pitch to local vertical	1.61	1.42
	Yaw control	1.5	1.42
	Roll control	11.8	9.63
After fourth SPS burn	Pitch to SM jettison attitude	1.96	1.95
	Yaw control	--	2.0
	Roll control	12.7	11.95
CM control after SM jettison (dual system control)	Pitch to reentry attitude	+10.5/-7.3	+10.25/-7.17
	Yaw control	+10.1/-11.2	+11.29/-11.37
	Roll control	+8.1/-7.8	+8.17/-8.22

[a]Actual accelerations were determined from the rate of change of the spacecraft body rates. Due to the evaluation technique and the short burn pulses (burn duration), these numbers have an estimated inaccuracy of ±0.3 to ±0.8 deg/sec^2.

TABLE 7.9-V.- SM RCS +X TRANSLATION ΔV AND AVERAGE ACCELERATIONS, MISSION AS-202

Maneuver and time	Actual			Theoretical		
	ΔV,[a] ft/sec	Average acceleration,[a] ft/sec^2	ΔT, sec	ΔV, ft/sec	Average acceleration, ft/sec^2	ΔT, sec
First translation (3 sec direct ullage plus 11 sec +X translation) (597 to 610.7 sec)	3.6 ± 0.5	0.26 ± 0.05	13.7	3.9	0.278	14
Second translation (30 sec +X translation) (3926.2 to 3957.1 sec)	11.6 ± 0.8	0.37 ± 0.05	30.9	12.5	0.417	30
Third translation (10 sec +X translation) (4045.6 to 4055.5 sec)	5.2 ± 0.5	0.52 ± 0.05	10	4.81	0.481	10
Fourth translation (10 sec +X translation) (4058.5 to 4068.5 sec)	5.2 ± 0.5	0.52 ± 0.05	10	4.86	0.486	10

[a]Inaccuracies in actual data are due primarily to poor quality of accelerometer data and the resolution of this data at the low ΔV levels of the RCS translations.

TABLE 7.9-VI.- CSM RCS AVERAGE PROPELLANT FLOW RATES, MISSION AS-202

Maneuver	Quad	Average propellant flow rate, lb/sec	Total propellant used, lb
During first +X translation (10.7-sec period)	A	0.359	3.8
	B	0.359	3.9
	C	0.369	4.0
	D	0.371	4.0
During first SPS firing (roll control, 215-sec period)	A	0.408	2.3
	B	0.408	2.3
	C	0.408	2.3
	D	0.408	2.3
During 4 deg/sec pitch to local vertical attitude (49.6-sec period)	A	0.386	3.6
	B	0.409	1.3
	C	0.383	3.5
	D	0.408	1.3
During second +X translation (30.9-sec period)	A	0.359	10.1
	B	0.358	10.1
	C	0.359	10.1
	D	0.371	10.5
During fourth +X translation (10-sec period)	A	0.364	3.6
	B	0.359	3.6
	C	0.359	3.6
	D	0.363	3.3
During attitude hold after the fourth SPS firing (116-sec period)	A	0.410	0.86
	B	0.414	0.78
	C	0.410	0.86
	D	0.414	0.78
During 4 deg/sec pitch maneuver to reentry attitude (25-sec period)	A	0.387	2.0
	B	0.414	0.7
	C	0.387	2.0
	D	0.414	0.7
During local vertical attitude hold maneuver (3038-sec period)	A	0.417	48.4
	B	0.420	49.0
	C	0.417	48.0
	D	0.420	48.9
CM RCS average during reentry	A[a]	0.346	32
	B[a]	0.346	32

[a]System.

TABLE 7.9-VII.- SM RCS SOURCE PRESSURE DROPS DURING MANEUVERING, MISSION AS-202

Helium pressurization tank	Time, G.e.t., sec		Event	Source pressure,[a] ΔP, psia
	On	Off		
Quad A	600	610	First +X translation	80
Quad B	600	610	First +X translation	70
Quad C	600	610	First +X translation	[b]50
Quad D	600	610	First +X translation	70
Quad A	838	880	Pitch to local vertical	75
Quad B	826	830	Pitch to local vertical	40
Quad C	838	880	Pitch to local vertical	75
Quad D	826	830	Pitch to local vertical	40
Quad A	3928	3950	Second +X translation	220
Quad B	3928	3955	Second +X translation	250
Quad C	3928	3955	Second +X translation	250
Quad D	3928	3955	Second +X translation	250
Quad A	4050	4070	Third and fourth +X translation	150
Quad B	4046	4067	Third and fourth +X translation	150
Quad C	4046	4067	Third and fourth +X translation	150
Quad D	4046	4067	Third and fourth +X translation	170

[a]Relative accuracy (tank to tank) is approximately 1 bit count, or 20 psi.

[b]Quad C was overpressurized on the pad, hence the initial source pressure drop was somewhat less than quad A.

TABLE 7.9-VIII.- CM RCS SERVICING AND ACTIVATION DATA,

MISSION AS-202

(a) CM RCS servicing

Parameter	System	
	A	B
Nominal oxidizer load, lb	90.1	90.3
Oxidizer loaded, lb	88.75	88.8
Nominal fuel load, lb	45.3	45.3
Fuel loaded, lb	45.0	45.0
Nominal helium source pressure, psia at 70° F	4150	4150
Actual helium source pressure at servicing, psia	4430	4380
Helium tank temperature at servicing, °F	100	96
Helium pressure fuel tank, psia	45	45
Helium pressure oxidizer tank, psia	45	45

(b) CM RCS activation

Parameter	System	
	A, psia	B, psia
Helium source prior to activation	4309	4239
Helium source after activation	3804	3732
Helium pressure fuel tank prior to activation	46.6	44.2
Helium pressure fuel tank after activation	290.6	290.2
Helium pressure oxidizer tank prior to activation	52	54
Helium pressure oxidizer tank after activation	292.1	288.7

NASA-S-66-10075

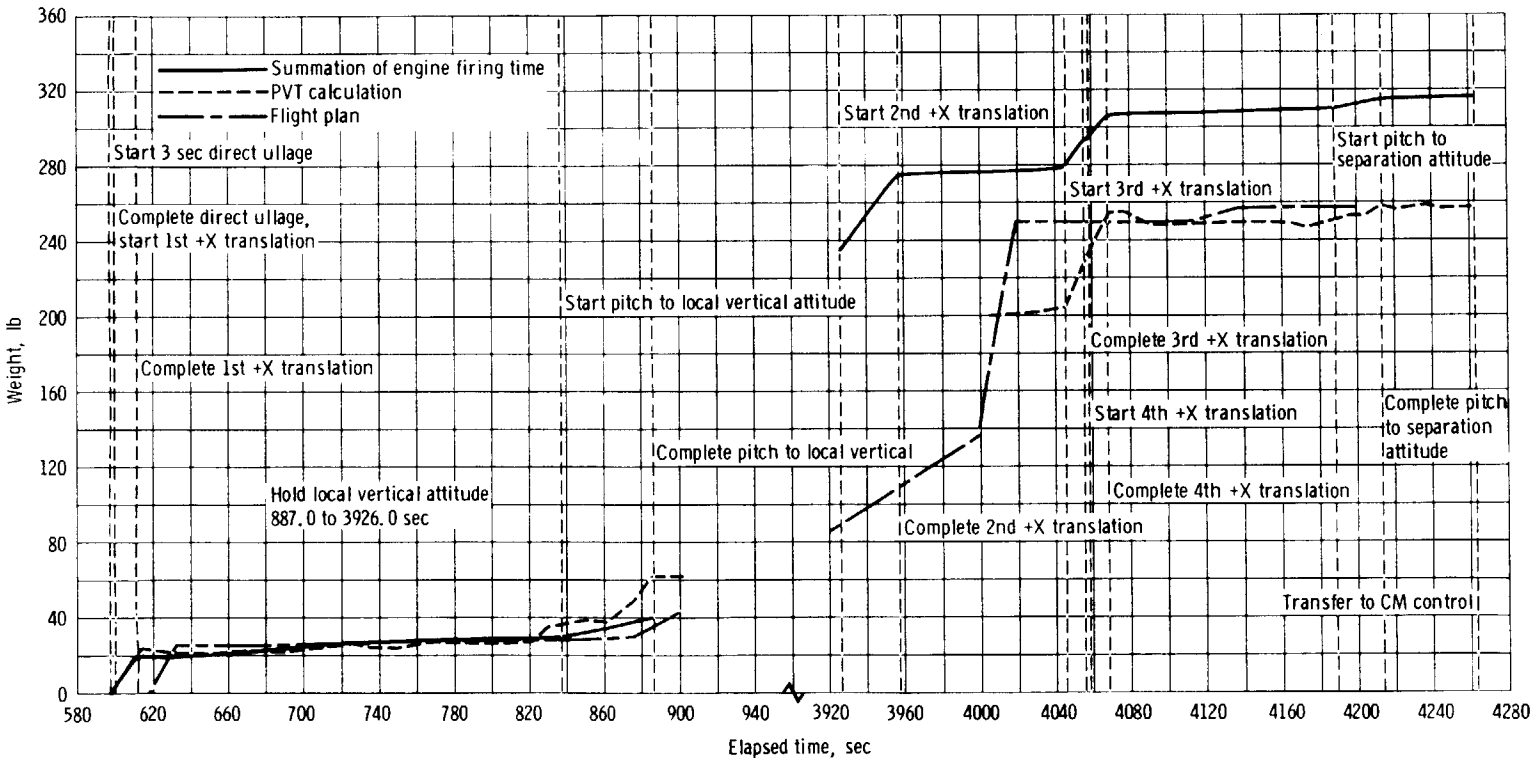

Figure 7.9-1. - SM RCS propellant consumption, Mission AS-202.

NASA-S-66-10076

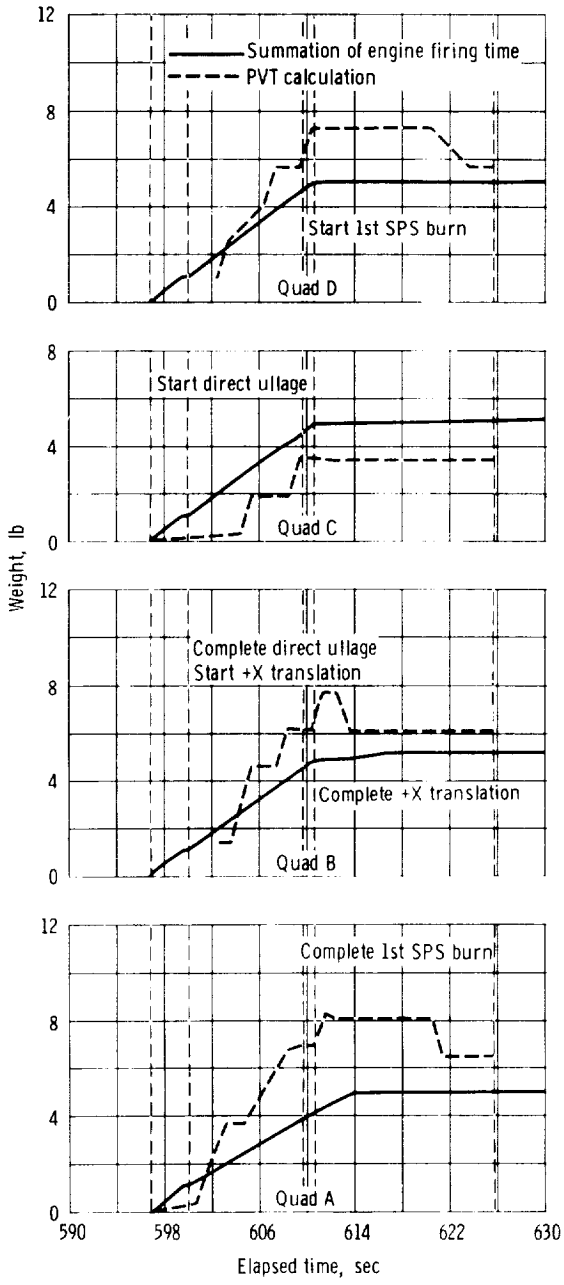

Figure 7.9-2.- SM RCS propellant consumption during first +X translation, Mission AS-202.

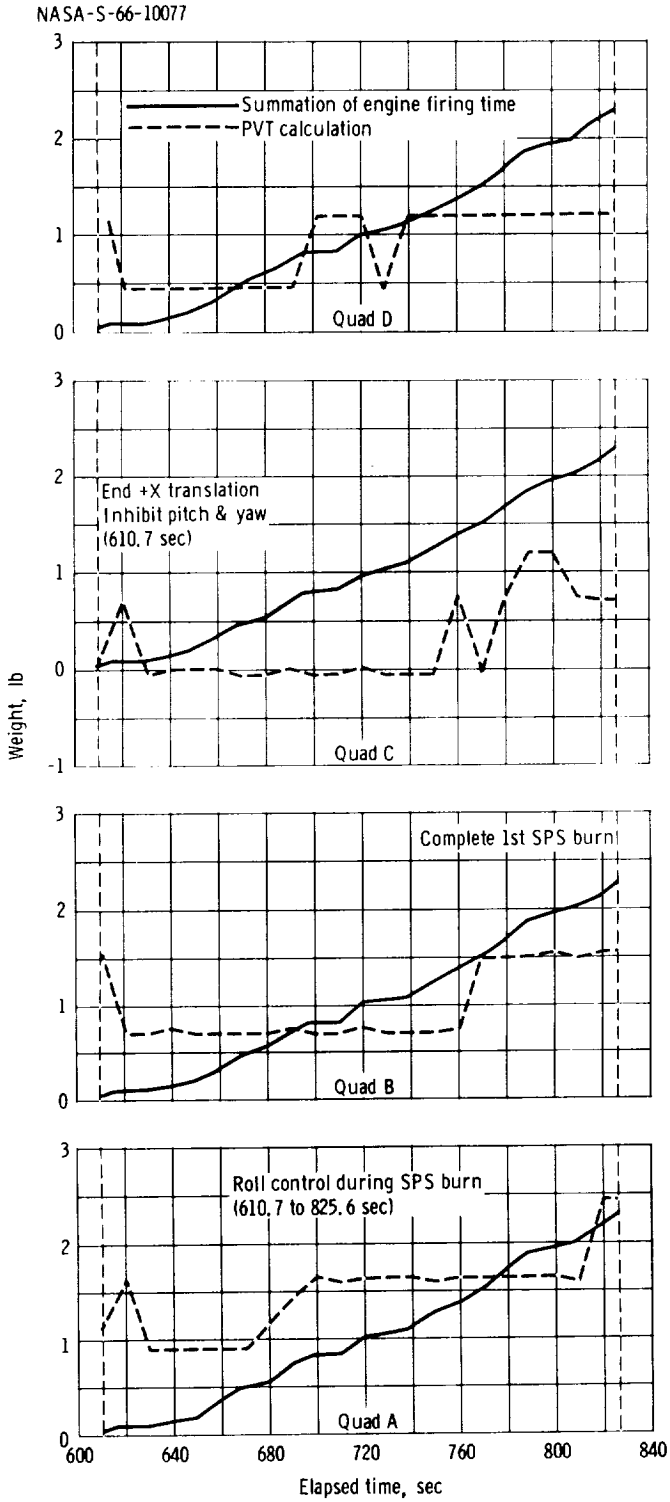

Figure 7.9-3.- SM RCS propellant consumption during first SPS burn, Mission AS-202.

NASA-S-66-10078

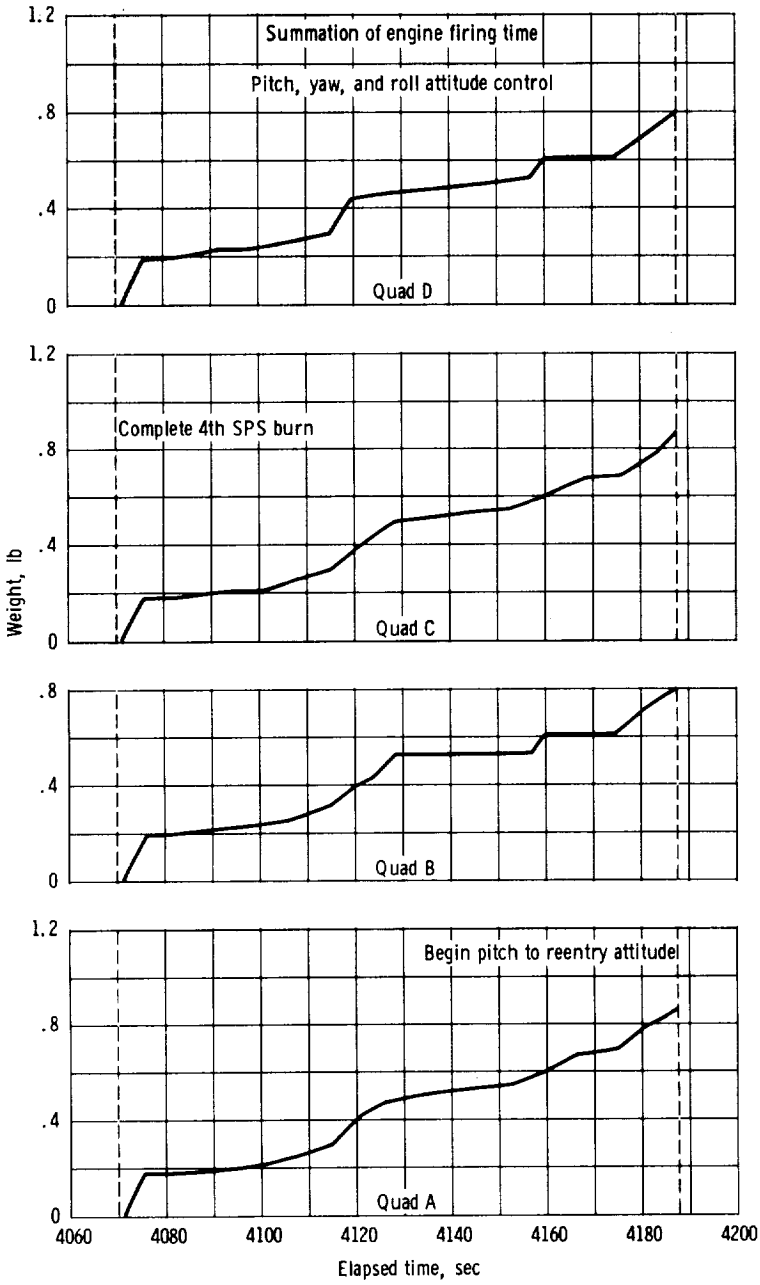

Figure 7.9-4.- SM RCS propellant consumption during attitude hold control, Mission AS-202.

NASA-S-66-10079

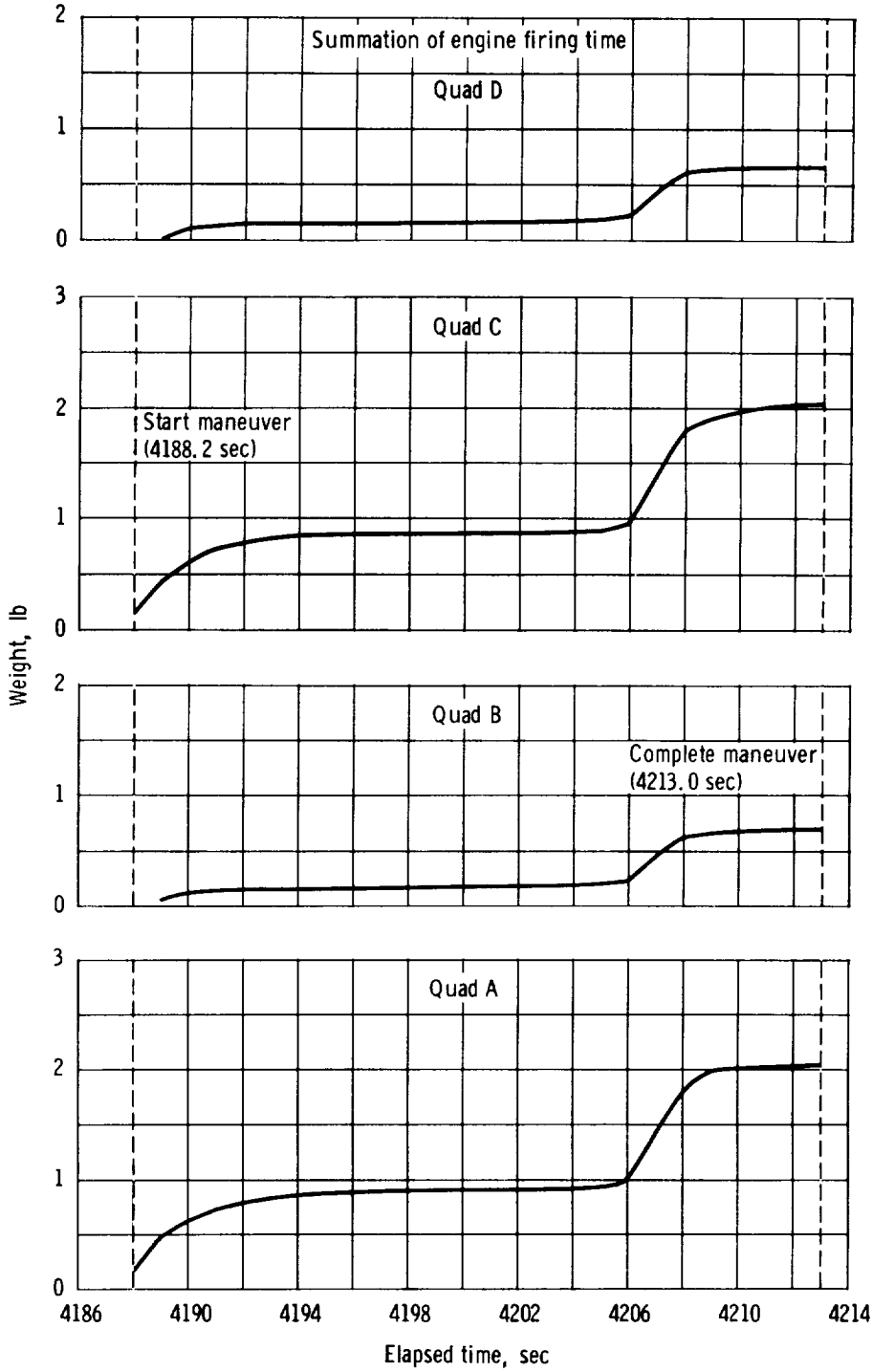

Figure 7.9-5.- SM RCS propellant consumption during pitch maneuver to separation attitude, Mission AS-202.

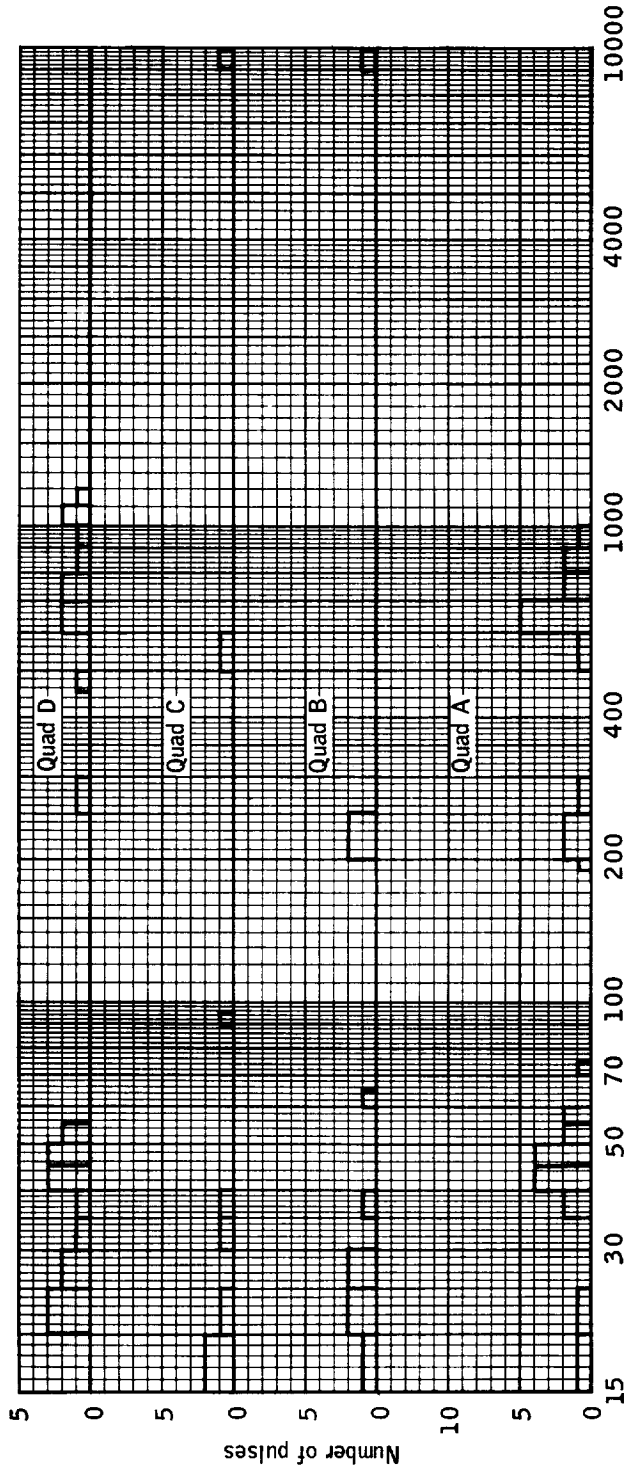

NASA-S-66-10080

Figure 7.9-6.- SM RCS +X translation pulse distribution prior to 4th SPS burn, Mission AS-202.

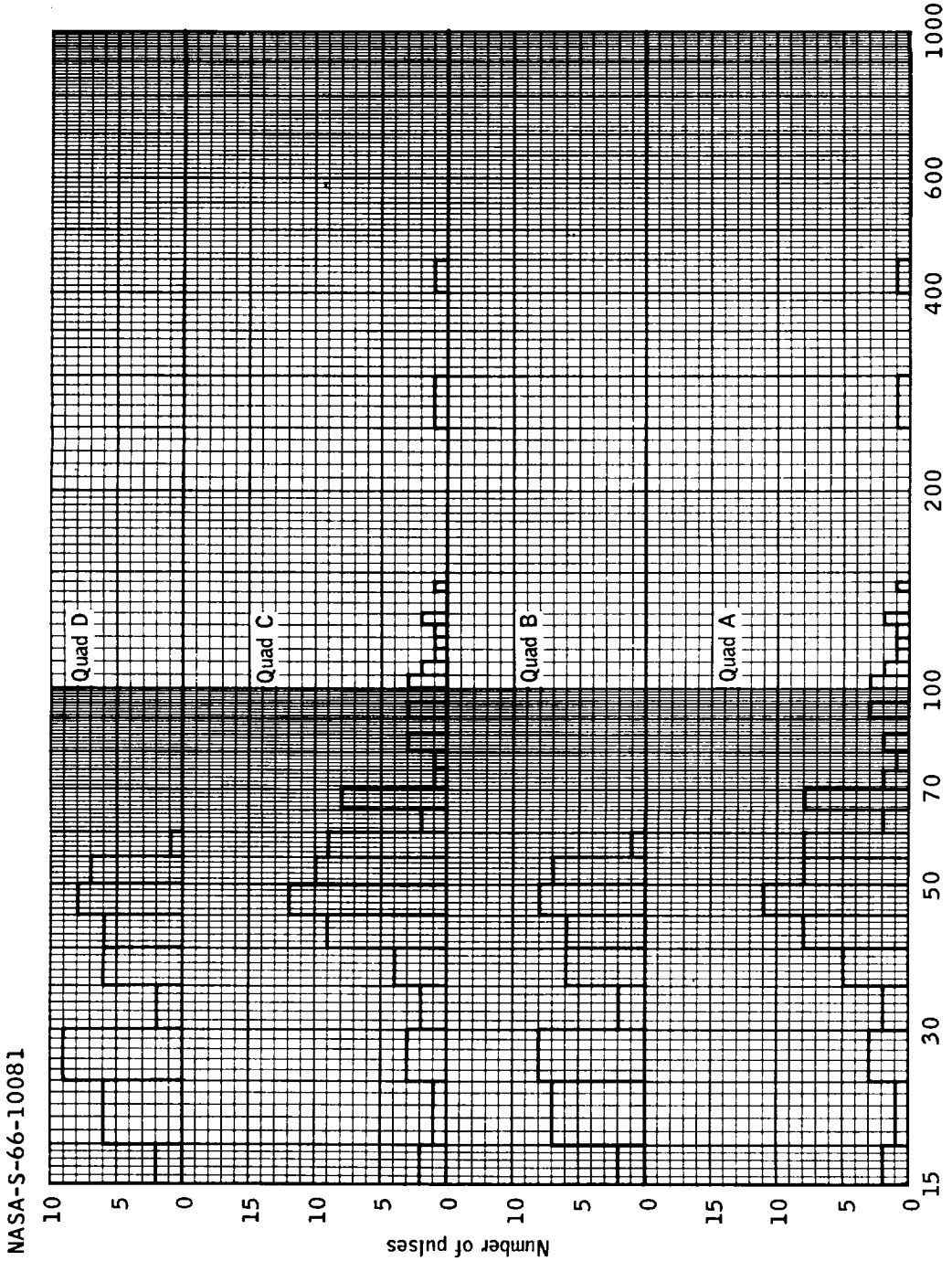

Figure 7.9-7.- SM RCS pulse distribution during pitch maneuver to separation attitude, Mission AS-202.

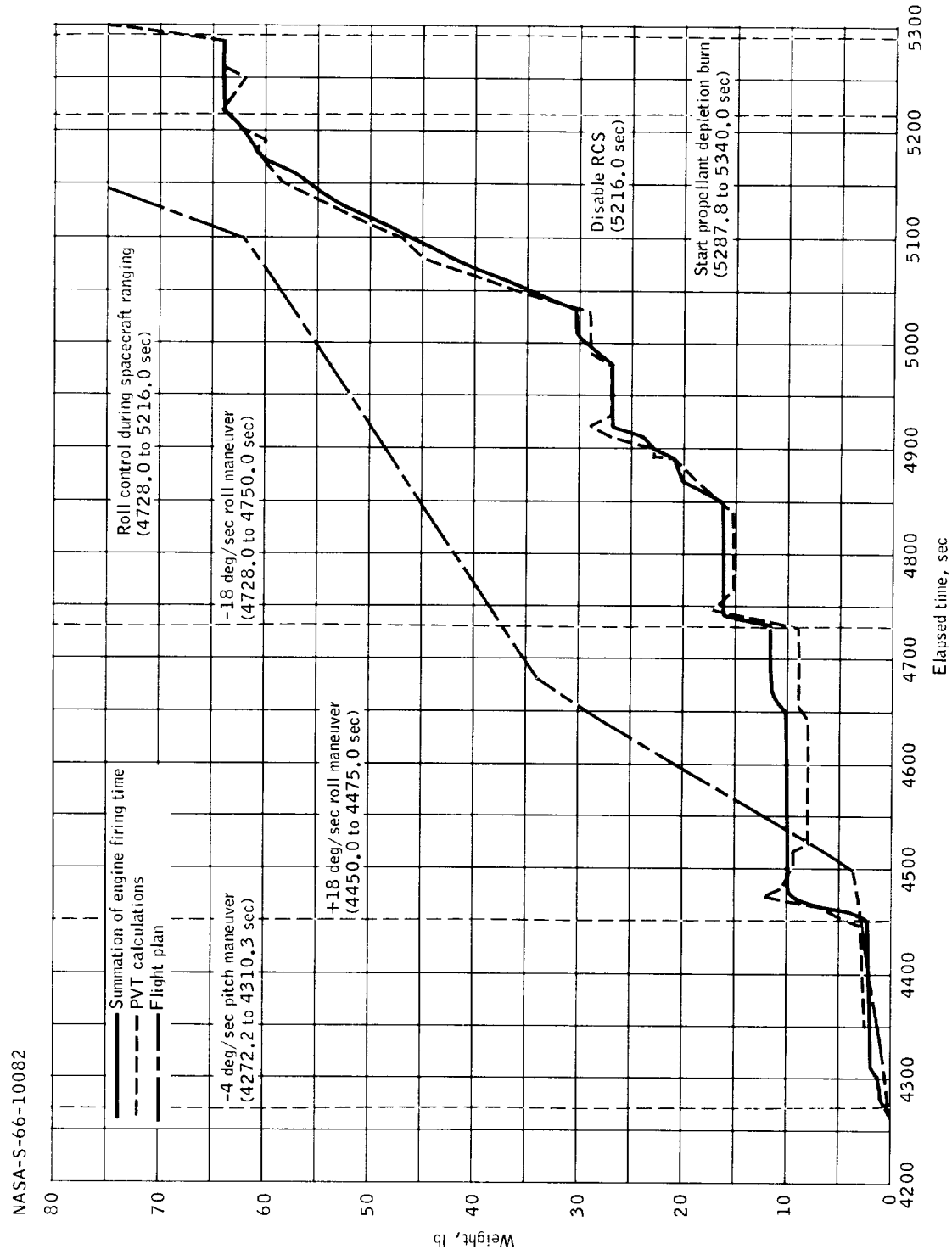

Figure 7.9-8.- CM RCS propellant consumption, Mission AS-202.

NASA-S-66-10083

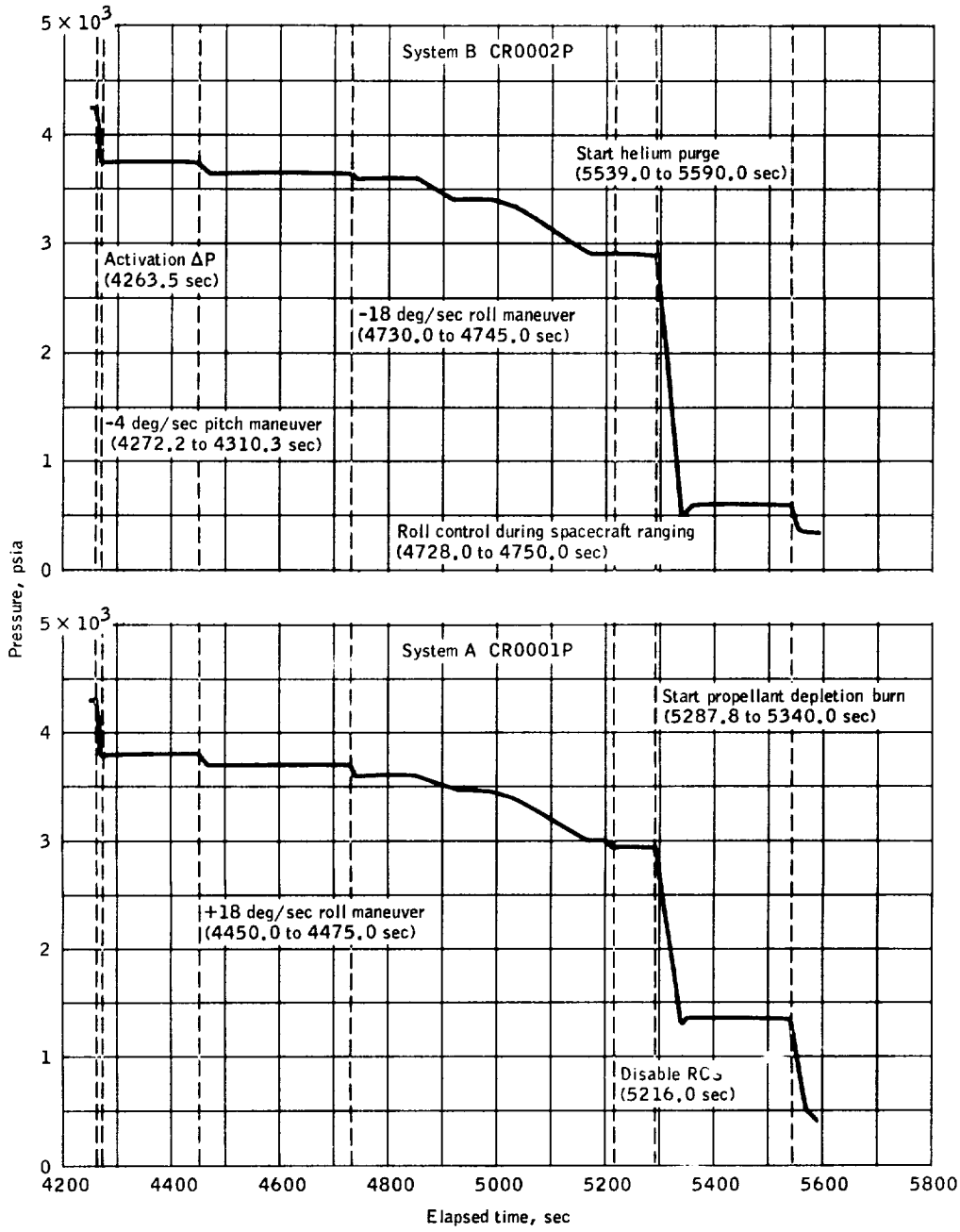

Figure 7.9-9.- CM RCS helium source pressure, Mission AS-202.

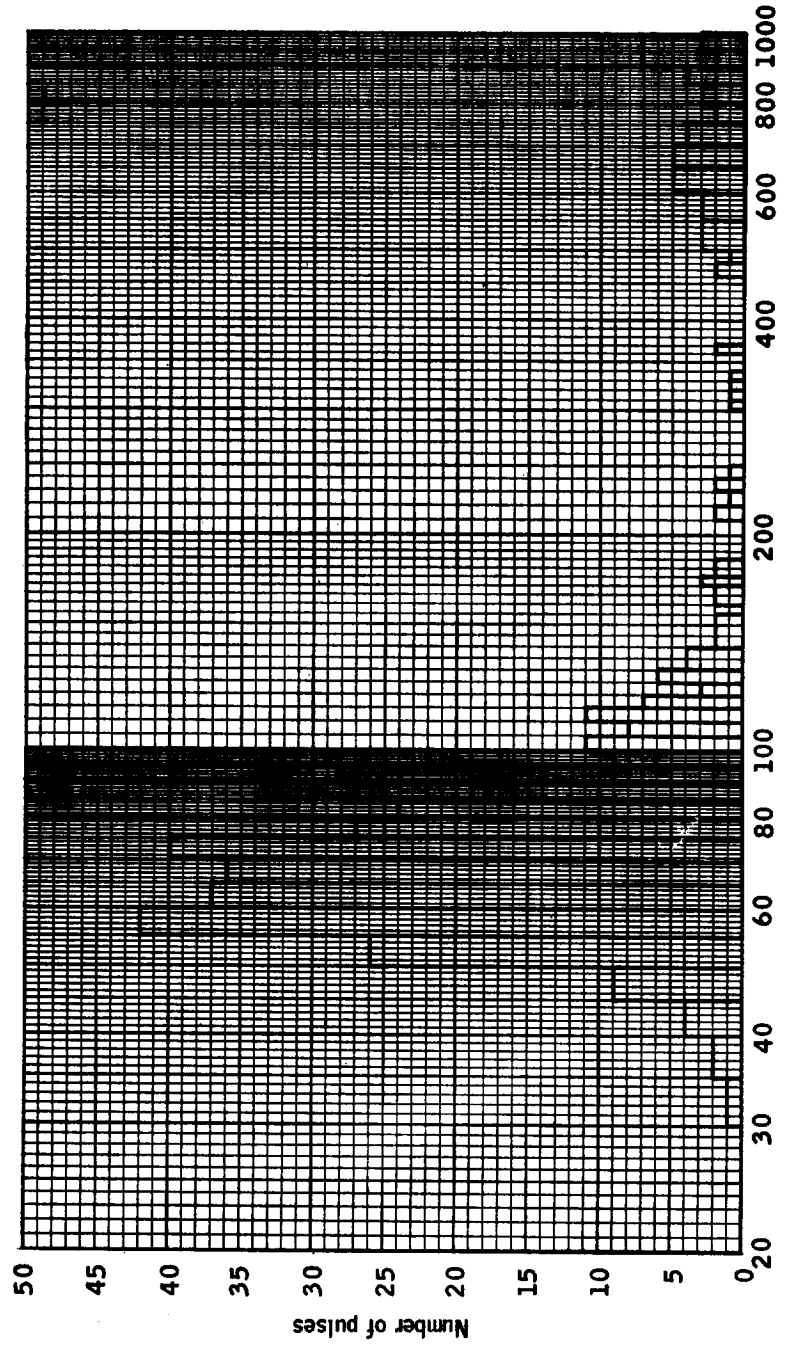

NASA-S-66-10084

Figure 7.9-10.- CM RCS pulse distribution, all thrusters, A and B systems, Mission AS-202.

7.10 Pyrotechnic Devices

Description.- The pyrotechnic devices used on Mission AS-202 were of the same type as those used on Mission AS-201 except that the launch escape system (LES) tower to command module (CM) separation system used a frangible nut, ME114-0013-0001, for separation in place of the single mode bolt.

The function of the LES tower to CM separation system is to separate the LES tower from the CM. Frangible nuts were installed at the four tower-attach points as shown in figure 7.10-1. Each nut contained two Apollo standard detonators, either of which is capable of separating each nut into two pieces through the plane of separation (fig. 7.10-2).

Performance.- All pyrotechnic devices functioned as prescribed on Mission AS-202. However, two nitrogen purge valve cartridges were fired in the valve at KSC prior to launch. The cartridge electrical connectors were intentionally left disconnected during the flight.

Two CM oxidizer dump valves, each of which contained a pressure cartridge, were not required to function during Mission AS-202 and were recovered as live ordnance.

Prior to launch it was discovered that one of the four frangible nuts on the tower to CM separation system was cracked. Upon removal from the spacecraft, the nut fractured and broke into two fragments and revealed that the washer was also fractured.

Examination of the fragments showed deposits of salt and visual indications that the nut and washer had been in contact with salt water for a considerable period of time. The fracture faces were corroded, indicating that the nut and washer had failed some time prior to discovery of the failure. The probable origin of failure, as located by visual examination of the fracture faces, was on the thread face at the middle of one of the nut torquing grooves. Secondary cracking was observed 180 degrees from the probable origin of failure.

Metallographic examination and microspecimens taken at the critical locations showed that the plating on the failed nut was missing from several areas of the thread faces and that the plating was cracked or broken in several places on the thread root. There was evidence of pitting at the thread root and in some areas on the thread face.

A new nut was sectioned to compare with the failed nut and similar pitting conditions were observed, indicating that these nuts may be pitted as received. Subsequent immersion in salt condensate would result in immediate attack on the steel beneath the plating. Procedures now require immediate closing of the leg access door after nut installation so as to protect the nut from exposure to salt spray.

NASA-S-66-10085

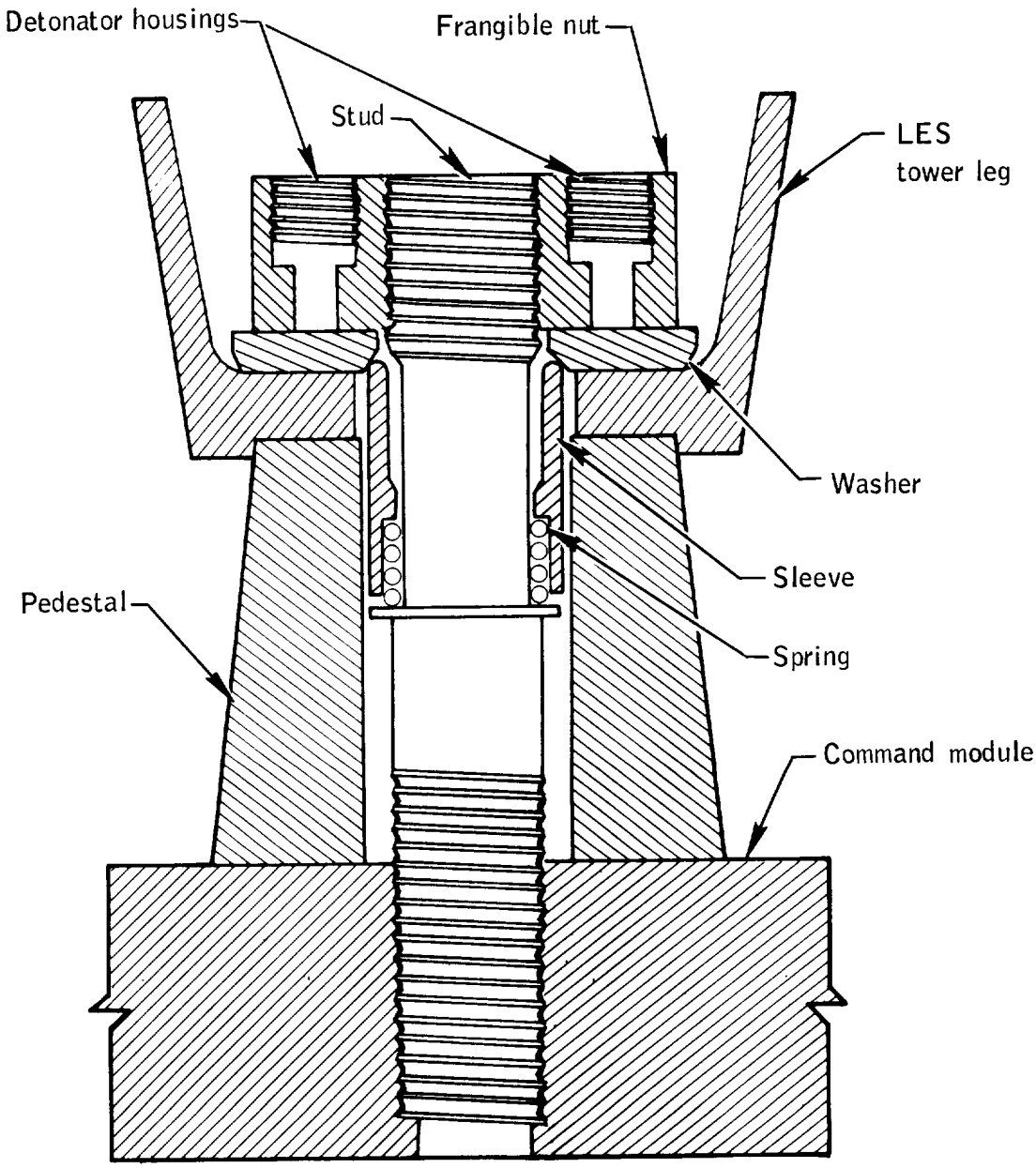

Figure 7.10-1.- Frangible nut installed, Mission AS-202.

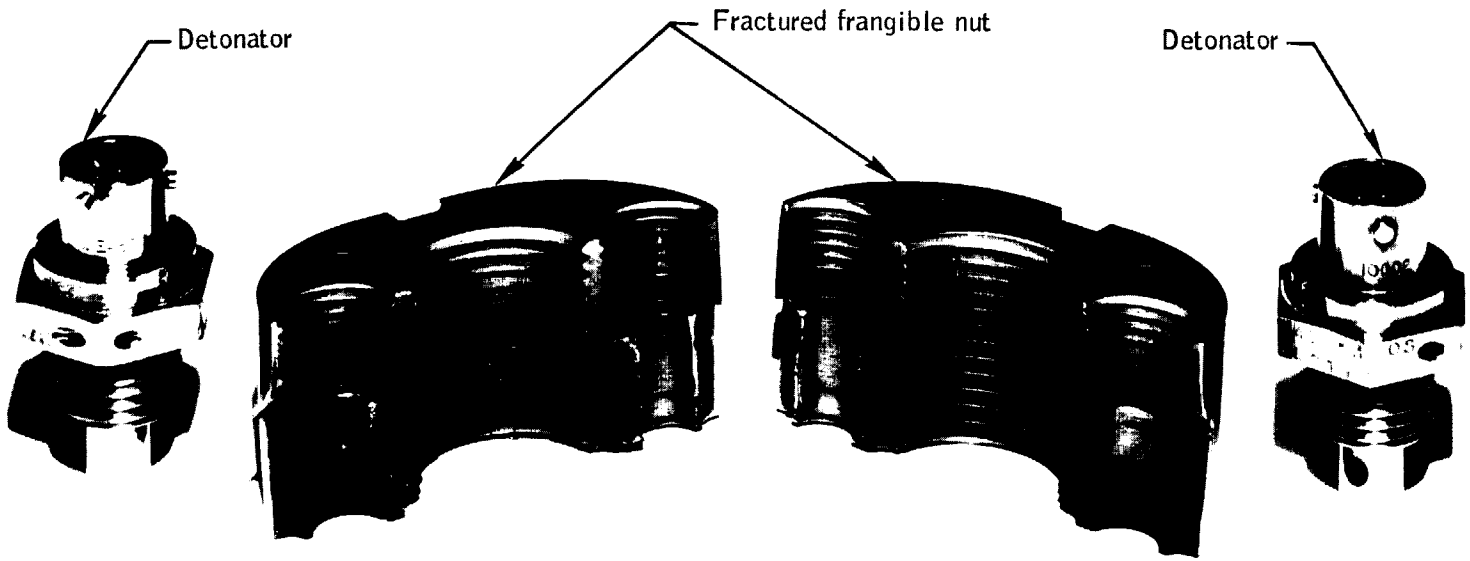

Figure 7.10-2.- LES tower separation frangible nut of type used on spacecraft 011, Mission AS-202.

7.11 Guidance and Control

Summary.- The guidance and navigation (G & N) and stabilization and control (SCS) subsystems fulfilled or demonstrated the capability for fulfillment of all mission objectives. Boost monitoring performance was excellent, with attitude information from both subsystems indicating close agreement with that from the launch vehicle. Guidance and thrust vector control during the SPS burns were close to nominal as was attitude control throughout the mission. The bank angle history during reentry indicates that the system was properly attempting to correct for the undershoot condition. All major functions of the G & N subsystem were exercised except those associated with the sextant and scanning telescope. All interfaces between the G & N and SCS subsystems were exercised except those necessary for minimum impulse control and for G & N synchronization to spacecraft attitude. Operation was proper throughout. Sequencing as performed by the G & N system and the mission control programmer was nominal.

Guidance and navigation subsystem.-

Description: The subsystem is further divided into three major subsystems: inertial, optical, and computer. These subsystems or combintations of subsystems are used to perform the following functions:

(a) Maintain an inertial reference, which is used as a basis for measurements and computations.

(b) Calculate the position and velocity of the spacecraft.

(c) Generate attitude error signals and thrust commands necessary to maintain the required spacecraft trajectory.

The spacecraft 011 G & N equipment, Block I, series 50, consisted of a navigation base, inertial measurement unit (IMU), optical unit assembly (OUA), power and servo assembly (PSA), Apollo guidance computer (AGC), and the display and control (D & C) panel. The computer display and keyboard (DSKY), coupling display units (CDU), and associated displays and controls were mounted on the D & C panel. Figure 7.11-1 is a block diagram of the subsystem.

The inertial subsystem (ISS) consists of the IMU, three coupling display units, portions of the PSA, and portions of the lower D & C panel. The ISS is used for spacecraft guidance and control, and performs three major functions:

(a) Measures spacecraft attitude with respect to inertial frame

(b) Assists in generating steering commands

(c) Measures spacecraft velocity changes

To accomplish these functions, the IMU provides an inertial reference consisting of a stable member gimballed for three degrees of freedom and stabilized by three inertial rate integrating gyros (IRIG) and associated servos. Prior to launch, the stable member is aligned in azimuth by means of a gyrocompassing routine and to the local vertical by PIPA which sense gravity reaction force. Resolvers, mounted on the gimbal axes, act as angular sensing devices and measure the attitude of the spacecraft with respect to the stable member. These angular measurements (gimbal angles) are compared with the desired spacecraft attitude as calculated by the AGC and displayed on the coupling data units. Any difference between the gimbal angles and the CDU angles causes an attitude error signal to be generated and sent to the stabilization and control subsystem, which drives the spacecraft RCS during coast phases and the thrust vector control subsystem during SPS thrust phases to control spacecraft attitude. Acceleration of the spacecraft is sensed by the three pulse integrating pendulous accelerometers mounted orthogonally on the stable member. The resultant signals from the accelerometer loops are supplied to the AGC, which then calculates the present velocity. The ISS modes of operation were controlled by the AGC on this mission.

The optical subsystem (OSS) consists of the OUA, two coupling data units, and portions of the PSA and D & C panel. The OSS, which will be used on manned missions to determine the position of the spacecraft and orientation of the IMU in space, contains a sextant and scanning telescope. On this mission the OSS was used for prelaunch IMU alignment verification only. Because of mechanical problems, created during installation of the astrosextant door modification, the motor drive signals to the scanning telescope were disabled. These signals were not required for ground tests or flight.

The computer subsystem, consisting of the AGC and portions of the D & C panel, was used to perform data handling and computations. The AGC is a general purpose digital computer employing a core rope memory, parallel operation, and a built-in, self-check capability. Programs are stored in the AGC until selected for use. Flight program selection for this mission was performed automatically with some backup capability available through the digital command subsystem. The computer subsystem performs five major functions:

(a) Calculates steering signals and SPS engine discretes necessary to keep the spacecraft on the required trajectory.

(b) Positions the stable member in the IMU to a coordinate system defined by precise optical measurements (not used inflight on this mission).

(c) Positions the optical unit to celestial objects (not used inflight on this mission).

(d) Conducts limited malfunction isolation by monitoring the level and rate of subsystem signals.

(e) Supplies pertinent spacecraft condition information to the D & C panel.

Performance:

(a) Ascent phase: The G & N subsystem was powered up at T-22.3 hours and platform alignment including gyro compassing began at T-12 hours. The guidance reference release signal was inhibited on this mission to avoid the possibility of misalignment caused by a hold in the countdown after the receipt of this signal at a normal 5 seconds before lift-off. As a result, the platform did not go inertial until T+1.33 seconds when the lift-off signal was received from the launch vehicle, or 0.6 second after first motion.

During the S-IB operation, the G & N subsystem monitored actual vehicle attitude and computed desired attitude based on a pitch polynominal designed to describe the nominal pitch profile. A comparison of the Y-axis CDU angles, which displayed the polynominal calculation, the IMU pitch gimbal angles, and the launch vehicle (ST-124 inertial platform) gimbal angles indicated agreement within 1 degree during this period, demonstrating nominal performance.

At T+171 seconds the AGC mode changed to "tumble monitor" and the IMU mode to "fine align," causing the computer to examine the vehicle attitude for excessive body rates. These rates did not exceed 1.5 deg/sec during this period, and therefore the abort flag (triggered at rates above 5 deg/sec) was not set, indicating proper subsystem operation up to the separation sequence.

The spacecraft/S-IVB separation sequence began at T+597 seconds upon receipt of the separation discrete from the S-IVB instrument unit. At this time the G & N subsystem began preparations for separation by commanding SPS gimbal motor power "on," +X translation, and SCS G & N attitude control mode.

An analysis of the subsystem has been performed by comparing the position and velocity sensed during the ascent phase with like quantities

from the launch vehicle system and from GLOTRAC ground radar tracking data. Velocity differences between the G & N and the other two subsystems are shown in figures 7.11-2 and 7.11-3. Figure 7.11-3 also contains velocity differences compensated for errors in the calculation of gravitational acceleration and velocity differences which would accrue from a selected set of error sources. Although the GLOTRAC data became unreliable after 418 seconds, the trends shown are similar to the comparisons with the launch vehicle subsystem and indicate G & N errors at S-IVB cutoff of -4.69, +13.99, and -0.16 m/sec in the X-, Y-, and Z-axes, respectively. The initial difference in the X-axis comparison was caused by the 0.6-second late receipt of the guidance reference release signal and should not be considered a system error.

The predominant uncorrelated errors which combine to produce an error propagation history for a given ascent trajectory can be determined from the velocity differences. Those errors which are correlated can only be determined in a "most likely" sense through judicious use of a priori data such as preflight test history, etc. The vertical (X-axis) velocity error can be accounted for within 0.2 m/sec by an X-axis accelerometer misalignment about the Y stable-member axis of 83 arc seconds. The value of this term measured in factory acceptance testing was 117 arc seconds. The major cause of out-of-plane (Y-axis) error was a misalignment in gyrocompassing of approximately 1.6 milliradians, an error of the order of those noted in preflight tests and well within the specification value of 5 milliradians. The remainder of the error noted in this axis is attributed to a 74-arc-second misalignment of the Z-axis gyro and a 9-arc-second misalignment of the Y-axis accelerometer both about the X stable-member axis. Both of these values were measured in factory testing. The negligible error recorded in the Z- (downrange) axis reflects excellent performance and a correct choice of accelerometer bias and scale factor values.

Figure 7.11-4 contains preflight histories of the major inertial component (gyro and accelerometer) error coefficients along with the values chosen for compensation during the mission. That the compensation values were accurate is evident since none of these error sources has been identified as a major contributing factor in the error analysis.

Table 7.11-I contains a comparison of insertion conditions as recorded by the various onboard and ground systems. Table 7.11-II shows the contribution to the turn velocity error at insertion directly attributable to IMU performance. The remainder is navigation error resulting from errors in the calculation of acceleration due to gravity caused by position errors.

(b) Suborbital flight phase: The primary functions of the G & N subsystem during this phase were control of spacecraft attitude and orbit shaping. Performance was satisfactory throughout.

Figure 7.11-5 contains a time history of commanded and actual spacecraft attitude during the maneuver to the first SPS burn attitude and continuing through the burn. The divergence of the values during the thrust period was caused by center of gravity (c.g.) shift as propellant was consumed and agrees with the SPS gimbal positions, indicating accurate "tracking" of the c.g. by the guidance and control subsystem.

Figure 7.11-6 contains a time history of commanded and actual spacecraft attitude during the maneuver to local vertical. The initial pitch maneuver computed was 124 degrees and was performed properly at 4 deg/sec. Because of the 38 seconds required to complete the initial maneuver, an additional attitude change of approximately 2.6 degrees was required. The computations were made, assuming an instantaneous attitude change, and are therefore correct only at the time of initiation of the command. The local vertical changed at orbital rates during the maneuver, and since a new computation was not made until the end of the maneuver, a converging iterative operation was required. Figure 7.11-7 compares the spacecraft pitch angle during the local vertical phase with preflight predictions and with values computed from trajectory data based on ground radar tracking. Very close agreement was noted throughout, indicating nominal performance.

The pitch response during the maneuver to CSM separation attitude is shown in figure 7.11-8. The rate achieved (4.06 deg/sec) agreed within 0.1 deg/sec of that commanded, although approximately 4 seconds were required to reach steady-state conditions at each end of the maneuver. The resulting lag was approximately 8 degrees. The maneuver to entry attitude after CSM separation is shown in figure 7.11-9. The lag noted between the subsystems was approximately the same as that seen during CSM maneuvers.

During the two major orbit changes using the SPS subsystem, guidance commands were generated by the AGC based on erasable memory constants loaded prelaunch. The guidance scheme used is described in reference 18.

Figure 7.11-10(a) shows the time history of velocity-to-be-gained (Vg) for the first SPS burn. Figure 7.11-10(b) shows the thrust termination period on expanded scale. The computation of Vg was terminated approximately 4 seconds prior to SPS cutoff. The velocities

during termination and tailoff were derived by summing accelerometer output pulses to evaluate the prelaunch estimate of the tailoff velocity increment. The velocity error accrued in each axis was less than 1 m/sec.

The eccentricity (e) and semilatus rectum (p) of the orbit achieved, derived from the computer state vector, was compared to the same parameters loaded in the computer. The eccentricity agreed well with the desired value but the semilatus rectum was approximately 1 km larger than desired. These data are summarized in table 7.11-III. The sensitivities of the orbital parameters to variations in velocity indicate the errors in the orbital parameters could be accounted for by velocity errors of 0.01 and 0.72 m/sec in the X- and Z-axis, respectively. The observed velocity errors were -0.01 and 0.80 m/sec in these axes. Orbital parameters from external tracking data are included in table 7.11-III for information. The deviations from actual orbital parameters appear commensurate with the navigation error accrued by the G & N during boost.

Figure 7.11-11(a) shows the velocity-to-be-gained time history for the second SPS thrust period. In contrast to the first burn, where the Vg computation was terminated approximately 4 seconds prior to Vg reaching zero, the termination occurred approximately 10 seconds prior to attaining the second orbital velocity assuming constant thrust level. The time was increased to account for the velocity acquired during the third and fourth SPS burn periods of 3 seconds each and during the two 10-second +X translations. The post SPS 2 cutoff velocity changes are shown in figure 7.11-11(b). The Vgy error was less than 1 m/sec, Vgz was approximately 3.9 m/sec low, and the Vgx was approximately 6.4 m/sec low. The resultant orbital parameters as derived from the AGC state vector are summarized in table 7.11-IV. Although the differences between actual and desired orbital parameters were relatively large, the error can be accounted for by considering two sources: velocity error due to erroneous estimation of the velocity increment from tailoff, +X translation, and the two short burns; and change in the effectiveness of the velocity increment because of the relatively long time (30 seconds) between computation of the velocity required and attaining that velocity. The velocity errors caused by thrust variations from the prelaunch estimates were -6.4 and 3.9 m/sec in the X- and Z-axes, respectively. The velocity errors computed from orbital parameter sensitivities were -5.8 and 3.1 m/sec in these axes. Approximately 0.5 m/sec per axis of sensed velocity error was compensated by the change in effectiveness of velocity increments which was due to nonimpulsive thrusting.

Navigation computations were discontinued 12 seconds after SPS 1 cutoff and resumed 30 seconds prior to SPS 2 ignition. During the

intervening period, uncompensated accelerometer outputs were accumulated and this total was telemetered at the resumption of navigation. This value represents the PIPA bias plus any acceleration sensed during those attitude maneuvers which took place during the coast phase. Table 7.11-V compares the computed bias from flight data and the preflight calibrations. The error in the computed bias may be explained in part by body accelerations caused by the attitude maneuvers during the intervening period. An additional bias check was made during the period of free flight between SPS 4 shutdown and the manuever to entry attitude. The biases indicated during this period are also included in table 7.11-V.

(c) Reentry phase: The reentry phase began when the spacecraft reached an altitude of 400 000 feet and terminated at drogue parachute deployment (23 500 feet). During this time, the spacecraft trajectory was controlled by closed loop inertial guidance logic as described in reference 19. The reentry consisted of five distinct phases as shown in the time history of altitude contained in figure 7.11-12. During the first phase, the CM was held in a lift-vector-down attitude until a total acceleration of 2.21 m/sec^2 was sensed by the G & N subsystem. The second phase consisted of roll attitude hold with lift-vector up until an altitude rate of -206 m/sec was sensed. The third phase (up control) controlled the CM through an analytically computed reference trajectory designed to provide an atmospheric skip, such that during second entry, the spacecraft would follow a nominal half-lift trajectory with a 60-degree bank angle. The fourth phase (Kepler) was a skip phase which began at a total acceleration of 1.78 m/sec^2 and ended when the total acceleration reached 2.02 m/sec^2. In the fifth and final phase (second entry), CM control was based on linear perturbations about a stored reference trajectory. Computer mode switching and logic changes were proper throughout, and have been corroborated by correlating the commanded bank angle history with the acceleration and velocity sensed by the subsystem.

Time histories of commanded bank angle, derived from the actual CDU angles, and lateral range from the AGC downlink are shown in figure 7.11-13. Correlation of these two parameters with actual and predicted range-to-go, shown in the same figure, indicated that the AGC sensed the uprange error and was attempting to correct for it. The bank angle commands are computed from the difference between actual range-to-go and predicted range-to-go, the available range based on the half-lift reference trajectory. After 0.2g was sensed, the AGC-commanded lift vector remained within 15 degrees of full lift except for a short period prior to and during the Kepler phase. Since the aerodynamic forces acting on the spacecraft are low during the Kepler phase, the 45 degrees

commanded can be considered insignificant in degrading the ranging capabilities of the spacecraft. Fifteen degrees are allocated to lateral control by the guidance equations.

Figure 7.11-14 contains a comparison of the touchdown point computed onboard with that reported by the recovery forces. The difference was 16 nautical miles. The suspected causes of the miss distance of 205 nautical miles are a combination of lower than nominal trim lift-to-drag (L/D) ratio (see section 6.0), and a steeper than nominal reentry inertial flight-path angle γ_i. The following plots are presented to illustrate the relationship of the possible causes. In figure 7.11-15, miss distance is plotted as a function of γ_i for a range of lift-to-drag ratios. The range corresponding to the actual miss distance is also indicated. Figure 7.11-16 illustrates the relationship of γ_i to L/D for a miss distance of 205 nautical miles.

(d) Inflight environment: The PIPA and IRIG temperatures remained within nominal limits throughout the flight, and IMU heater and blower currents were normal. A rise of approximately 8° occurred in both the PSA and AGC temperatures. This rise is attributed to the rise in water-glycol temperature but did not exceed equipment limits. System voltages remained well within specification ranges throughout.

Stabilization and control subsystem.-

Description: The stabilization and control subsystem, a J model Block I configuration, was the same as that flown on Mission AS-201; however, two major components of the subsystem were utilized for the first time. These were the flight director attitude indicator (FDAI) and the auxiliary electronic control assembly (AUX ECA). The SCS was modified to allow switching functions normally provided by a pilot to be initiated by the MCP. A block diagram is contained in figure 7.11-17.

The FDAI provides a visual display of the spacecraft attitude, attitude errors, and body rates. For this mission it was modified to delete SCS total attitude signals. The AUX ECA contains the electronics and servo mechanisms required to generate Euler angles from body-mounted attitude gyro (BMAG) signals. The Euler angles are then transformed into torquing signals which keep the SCS body-mounted attitude gyros aligned to an inertial reference. This allows the SCS to provide a backup attitude reference and increases the spacecraft reliability for mission success.

The remaining portions of the SCS were identical to the components flown on Mission AS-201 and include:

(a) Attitude gyro and accelerometer package

(b) Rate gyro package

(c) Pitch, yaw, roll, and display electronic control assemblies

(d) Attitude set/gimbal position indicator

(e) Velocity change indicator

Performance: The body-mounted attitude gyro's were uncaged from a backup rate configuration and caged through the attitude gyro coupling unit (AGCU) at T-8 minutes. Earth rate torqued the AGCU/BMAG backup reference to initial conditions of pitch = -33.2 degrees, yaw = -3.5 degrees, and roll = -176.7 degrees. At lift-off, this compares to IMU gimbal angles of pitch = -32.552 degrees, yaw = -2.047 degrees, and roll = -175.273 degrees. The differences between the AGCU/BMAG angles (Euler) and the IMU gimbal angles for the ascent phase are shown in figure 7.11-18. The data verify the capability of the SCS to maintain a backup attitude reference in the boost environment.

Small oscillations of approximately ± 0.5 deg/sec were indicated by the spacecraft rate gyros at S-IB ignition. These oscillations damped to negligible values in all axes within 4 seconds and remained small during most of the ascent phase. Vehicle rate peaks occurred at each significant event in the boost phase, but in each case were quickly damped back to nominal. Maximum rates occurring at selected boost phase events are contained in table 7.11-VI.

(a) Orbital phase. The CSM/S-IVB separation sequence was started at T+597 seconds. At T+597.1 seconds, the attitude control mode and SPS gimbal motor power "on" commands were sent to the MCP by the G & N subsystem. The SCS pitch and yaw thrust vector control channels were changed to a delta V configuration by the SPS engine hold function from the MCP. The remainder of the SCS electronics was maintained in the monitor mode for 2.3 seconds. The SPS gimbal motor start sequence was initiated by the MCP 1 second after receipt of the G & N command. Prior to flight the gimbal position thumbwheels on the attitude set indicator were set to 2.5 degrees in pitch and 7.3 degrees in yaw. These values correspond to the first gimbal trim settings in the MCP. The data show that the gimbals stabilized at 2.4 degrees in pitch and 7.4 degrees in yaw. Physical separation of the CSM and S-IVB was indicated at T+598.6 seconds. The separation rate transients shown in figure 7.11-19 are a result of both SPS gimbal motion and physical

separation, since the gimbals were being positioned at that time. Separation was nominal with no excessive torques applied to the CSM. A rate peak of 1.13 deg/sec was sensed in the yaw axis, but this was quickly damped within the rate deadband when the SM RCS was activated.

Separation was effected by a direct translation which was initiated by the MCP at T+597 seconds for a period of 3 seconds. At T+600 seconds the RCS was enabled, and +X translation through the automatic RCS coils was initiated. Translation was periodically interrupted by pitch and yaw rotational thruster firings as attitude control was maintained during the ullage maneuver. This verified that the jet select logic was correct, and that rotational commands had priority over translational commands.

The SCS received the command from the G & N to begin the maneuver to the first SPS burn attitude at T+603.6 seconds. SPS engine ignition was commanded at 609.7 seconds. Attitude control and +X translation continued until the pitch and yaw attitude channels were disabled at 610.6 seconds. Body rate transients produced by SPS ignition are shown in figure 7.11-19.

The first SPS gimbal position values set into the MCP prior to launch were 2.55 degrees in pitch and 7.31 degrees in yaw. The flight values were 2.5 degrees in pitch and 7.4 degrees in yaw. Three seconds after SPS engine ignition, the gimbal position was 2.8 degrees in pitch and 7.2 degrees in yaw, indicating a small miscalculation of the initial c.g. position. Rate and attitude control throughout the burn were nominal, with SPS gimbal motion indicating satisfactory tracking of the c.g. The RCS activity in roll shows limit cycle periods varying in length between 0.5 and 13.8 seconds. It was also noted that the roll control torque produced by four RCS engines gave a slight rate overshoot which required operation of the opposing thrusters to reduce the rate below the rate deadband (0.2 deg/sec). As the vehicle mass decreased during the burn, the rate overshoots became more prominent. The maximum transients which were present immediately after the SPS "off" command were 0.17 deg/sec in pitch and 0.38 deg/sec in yaw. The rates are developed due to SPS tailoff effects during the normal 1-second period after the engine "off" command before RCS control is restored in pitch and yaw. When the pitch and yaw RCS was enabled, the vehicle rotated until the X-body axis was aligned to the thrust vector direction at cutoff.

The G & N commanded the maneuver to local vertical at T+837 seconds. During the local vertical phase, pitch and yaw limit cycle periods were approximately 12 and 20 seconds, respectively. In the roll axis, it was again evident that four jet controls provided excess rate when correcting an attitude error. Examples of typical limit

cycles in pitch, yaw, and roll are shown in figure 7.11-20. During this phase, an unusual series of roll rate indications were noted in that several small body rate reversals and changes in slope occurred with no corresponding RCS activity seen in the data. Examples of this roll rate activity are shown in figure 7.11-20. The most probable cause for these indications was fuel slosh in the SPS tanks created by attitude control thruster operation. Further evidence in support of this theory is the long tailoff of the rate gyro signal in response to thruster firings. It should be noted that this condition did not adversely affect the ability of the SCS to maintain attitude control during the flight.

The maneuver to the second burn attitude was started approximately 45 seconds after completion of the local vertical phase. Telemetry coverage of the spacecraft was not available for the end of the local vertical mode or during the maneuver to second burn position. After the maneuver, the spacecraft was maintained at an inertially fixed attitude for approximately 1000 seconds. At the conclusion of this CSM coast phase, the G & N subsystem commanded delta V mode "on" and the SPS gimbals were positioned to the second set of values from the MCP. The initial gimbal positions for this thrusting period are shown in table 7.11-VII. The deviations between the settings and the final gimbal positions from the first burn represent errors in the estimate of c.g. location. A constant attitude was maintained from the end of the second burn until the end of the fourth burn. Figure 7.11-21 shows position feedbacks, differential clutch currents, body rates, and pitch and yaw RCS activity for this period. Performance was nominal throughout.

FDAI align was commanded at T+1117.8 seconds. This event aligned the Euler reference to preflight settings on the attitude set indicators. These settings were based on preflight predictions of the IMU gimbal angles. A tabulation of initial errors at lift-off, accumulated errors in flight, and alignment accuracy is shown in table 7.11-VIII. The 2-degree error noted in pitch was of the order of the switching transients observed during preflight testing at the end of the alignment procedure.

The maneuver to CSM separation attitude was commanded at T+4187.6 seconds and was completed at T+4213 seconds. This maneuver is shown in figure 7.11-22. Damping and attitude control during the maneuver was nominal in the pitch and yaw axes; however, the roll RCS solenoid driver and roll rate gyro outputs indicated a spacecraft disturbance in the roll axis. Fuel slosh and acceleration torques from the pitch axis appear to have coupled into the roll axis, creating a disturbance torque in the negative roll direction. Each time the positive roll thrusters fired in response to the error signal the rate

deadband was exceeded, causing negative thruster operation. This second thruster firing tended to cancel the corrective action of the positive thrust, resulting in an essentially zero net effect. The disturbance torque then forced the spacecraft out of the deadband and the cycle repeated. As the pitch motion decreased at the end of the maneuver, the coupling disturbances disappeared and the roll axis motion damped to a normal limit cycle.

(b) Reentry phase. The CSM separation sequence started at T+4263.7 seconds when the SCS mode was changed to G & N entry. Separation transients were nominal with maximum rates of 0.8 deg/sec and 1.5 deg/sec in the pitch and yaw axes, respectively. Roll rates remained below 0.2 deg/sec. Postflight data indicated that all entry deadbands, limiters, and gains were nominal, and that gain changes were effected at 0.05g as required.

The maneuver to entry attitude was initiated at T+4271 seconds, and is shown in figure 7.11-23. The body rate response during this and all succeeding CM maneuvers correlated properly with the thruster firing indications. This substatiated the conclusion that the rate deviations noted during CSM operations were caused by fuel slosh.

The SCS accelerometer sensed 0.05g at T+4426.9 seconds and the SCS switched to a rate damping mode in pitch and yaw axes, and roll rate was coupled into the yaw rate channel. Pitch and yaw rate deadbands were increased to $\pm$2 deg/sec, roll attitude deadband to $\pm$4.2 degrees and roll rate deadband to $\pm$18 deg/sec.

The SCS was commanded by the G & N to roll the CM 179 degrees at T+4450 seconds in order to orient the lift vector up. During the remainder of the entry phase the lift vector was controlled as required for ranging by G & N guidance commands.

The vehicle pitch and yaw attitude is determined by vehicle aerodynamic trim during this post 0.05g entry phase, and vehicle rates remained within the rate deadbands for long periods. This resulted in long vehicle limit cycles at relatively low rates in pitch and yaw, with roll control required primarily when commanding lift vector reorientation.

All SCS control functions were nominal during this phase. SCS channel disable of all RCS thrust commands occurred at T+5217 seconds which is equivalent to approximately 25 000-ft altitude. Vehicle attitudes, rates, and RCS thrust commands for the entry phase are shown in figure 7.11-24.

Mission control programmer subsystem.-

Description: The MCP consisted of three separate packages; the spacecraft command controller (SCC), the ground command controller (GCC), and the attitude and deceleration sensors (ADS). The MCP contained the logic networks, time delays, and switching capability required to initiate the events normally provided by the pilot through manual switches. Ground backup of some onboard switching functions was available through the GCC. Also included in the MCP were an 0.05g sensor, an impact switch and an attitude indicator. The 0.05g sensor was a backup to the G & N and SCS subsystems. This impact switch coupled to the proper logic circuits with the earth landing sequence controller (ELSC) and MCP attitude indicator initiated the recovery instrumentation at splashdown. A spacecraft stable I or stable II position after impact was sensed by the attitude indicator and the corresponding logic signal issued.

Performance: There was no flight PCM instrumentation for the MCP; however, most events could be verified through proper operation of interfacing subsystem. Operation throughout the flight was nominal. The MCP provided the required commands after receipt of an input within the limits of the time delays and sequence of relay operation. The functions of the MCP for Mission AS-202 are shown in table 7.11-IX.

TABLE 7.11-I.- INSERTION CONDITION COMPARISON AT S-IVB CUTOFF

	Total velocity, m/sec	Flight path angle, deg	Vertical velocity (X-axis), m/sec	Cross-range velocity (Y-axis), m/sec	Down-range velocity (Z-axis), m/sec
Preflight operational trajectory	6799.6	3.99	--	--	--
Spacecraft G & N system	6801.7	3.82	-1510.4	-71.8	6631.5
Launch vehicle guidance system	6800.7	3.85	-1505.5	-86.2	6631.4
Postflight trajectory	6800.1	3.99	-1496.9	-85.3	6634.6

TABLE 7.11-II.- NAVIGATION ERRORS AT S-IVB CUTOFF

	$\dot{X}$, m/sec	$\dot{Y}$, m/sec	$\dot{Z}$, m/sec
IMU	-3.64	+13.14	0
AGC[a]	-1.05	+0.85	0.26
TOTAL	-4.69	+13.99	+0.26

[a]Error in g computation due to position errors.

TABLE 7.11-III.- COMPARISON OF ORBITAL PARAMETERS, FIRST SPS FIRING

Source	p,[a] meters	e[b]
AGC	6 763 880	0.100405
Preflight nominal	6 762 850	0.100353
Preliminary tracking	6 770 297	0.100952

[a]Semilatus rectum.

[b]Eccentricity.

TABLE 7.11-IV.- COMPARISON OF ORBITAL PARAMETERS, SECOND, THIRD, AND FOURTH SPS FIRINGS

Source	p,[a] meters	e[b]
AGC	7 974 210	0.238505
Preflight nominal	7 962 818	0.236855
Preliminary tracking	7 973 562	0.238160

[a]Semilatus rectum.

[b]Eccentricity.

TABLE 7.11-V.- ACCELEROMETER BIAS COMPARISON

[In cm/sec/sec]

Source	Axis		
	X	Y	Z
Computed bias (coast phase)	-0.918	-0.202	+0.239
Computed bias (preentry)	-0.895	-0.225	+0.251
Bias obtained from preflight calibrations	-0.71	-0.14	+0.36

TABLE 7.11-VI.- ASCENT RATE HISTORY

	Pitch, deg/sec	Yaw, deg/sec	Roll, deg/sec
S-IB ignition	-0.37	0.48	0.57
S-IB/S-IVB separation	-0.17	-0.52	-0.30
LES jettison	-1.31	-0.82	-0.25
S-IVB mixture ratio change	0.96	0.08	0.16
CSM/S-IVB separation	0.37	1.13	0.21

TABLE 7.11-VII.- SPS ENGINE GIMBAL SET ERRORS

	Pitch, deg	Yaw, deg
Gimbal position at end of first firing	1.3	3.4
Gimbal position set for second firing	0.54	3.4
Δ gimbal position	0.76	0
Gimbal position at end of second firing	0.25	0.8
Gimbal position set for third firing	-0.56	0.7
Δ gimbal position	0.81	0.1
Gimbal position at end of third firing	0.174	0.8
Gimbal position set for fourth firing	-0.56	0.7
Δ gimbal position	0.73	0.1

TABLE 7.11-VIII.- AGCU ERRORS FROM LIFT-OFF TO FDAI ALIGN

Event	Pitch, deg	Yaw, deg	Roll, deg
Differences between IMU/FDAI - Euler at lift-off	0.67	1.47	1.43
Differences between IMU/FDAI - Euler at FDAI align	6.32	3.32	2.18
Differences between IMU/FDAI - Attitude values at FDAI align	0.95	1.96	0.65
Differences between IMU/FDAI - Euler after alignment	2.08	0.21	0.83

TABLE 7.11-IX.- MISSION CONTROL PROGRAMMER

FUNCTIONS FOR MISSION AS-202

Event
Prelaunch phase
Aux bus on main buses
Auto oxidizer dump enable
G & N monitor mode on
Select minimum deadband
BMAG's to backup rate
Remove BMAG's from backup rate
Aux bat on aux bus
Glycol shutoff valve closed
Back-pressure controller on
Glycol pump 1 to ac bus 1
FQ recorder on
Cine cameras on
Start PAM/FM/FM calibrator
Stop PAM/FM/FM calibrator
Boost phase
Lift-off
Start auto oxidizer timer
Start glycol shutoff valve timer
Auto oxidizer dump enable off
LET jettison phase
Start E/T jettison sequence A and B
FQ recorder off
Wetness control start
Glycol temperature control start
LES motor fire A and B
Launch vehicle separation phase
Separate/abort command on
FQ recorder on

TABLE 7.11-IX.- MISSION CONTROL PROGRAMMER

FUNCTIONS FOR MISSION AS-202 - Continued

Event
Launch vehicle separation phase - Continued
Entry batteries to main buses
SPS engine hold on
Y1 gimbal motor start
Y1 gimbal motor on
P1 gimbal motor start
P1 gimbal motor on
Y2 gimbal motor start
Y2 gimbal motor on
P2 gimbal motor start
P2 gimbal motor on
SPS thrust A and B arm
SPS engine hold off
Arm G & N mode control
Monitor mode off
G & N attitude control mode on
Prepilot valves A and B on
Select first gimbal position set
+X translation on
Separate/abort A and B off
MESC pyro bus A and B safed
MESC logic bus A and B safed
G & N attitude control mode off
Monitor mode on
G & N ΔV mode on
Monitor mode off
+X translation off
Gimbal motors off
Select second gimbal position set
Remove entry batteries from main bus
FQ recorder off
Cine camera off
Prepilot valves A and B off
G & N ΔV mode off

TABLE 7.11-IX.- MISSION CONTROL PROGRAMMER FUNCTIONS

FOR MISSION AS-202 - Continued

Event
Launch vehicle separation phase - Concluded
Monitor mode on
G & N attitude control mode on
Monitor mode off
FDAI align on
FDAI align off
Glycol shutoff valve open
Thrust maneuvers phase
+X translation on
Entry batteries to main bus
FQ recorder on
DSE recorder on
Prepilot valves A and B on
Y1 gimbal motor start
Y1 gimbal motor on
P1 gimbal motor start
P1 gimbal motor on
Y2 gimbal motor start
Y2 gimbal motor on
P2 gimbal motor start
P2 gimbal motor on
G & N attitude control mode off
Monitor mode on
G & N ΔV mode on
Monitor mode off
Gimbal motors off
Select third gimbal position set
Remove entry batteries from main bus
Prepilot valves A and B off
Entry batteries to main bus
Prepilot valves A and B on
Y1 gimbal motor start
Y1 gimbal motor on

TABLE 7.11-IX.- MISSION CONTROL PROGRAMMER

FUNCTIONS FOR MISSION AS-202 - Continued

Event
Thrust maneuvers phase - concluded
P1 gimbal motor start
P1 gimbal motor on
Y2 gimbal motor start
Y2 gimbal motor on
P2 gimbal motor start
P2 gimbal motor on
+X translation off
Gimbal motors off
Remove entry batteries from main bus
Prepilot valves A and B off
G & N ΔV mode off
Monitor mode on
G & N attitude control mode on
Monitor mode off
G & N attitude control mode off
Monitor mode on
CM/SM separation phase
Entry mode on
Monitor mode off
MESC pyro bus A and B arm
MESC logic bus A and B arm
Heat shield instrumentation on
Entry batteries to main bus
Isolate O_2 supply
Close glycol shutoff valve
Arm G & N 0.05g
Arm 0.05g backup
Select maximum deadband
FQ recorder on (backup)
DSE recorder on (backup)
CSM separation command

TABLE 7.11-IX.- MISSION CONTROL PROGRAMMER

FUNCTIONS FOR MISSION AS-202 - Concluded

Event
Entry phase
0.05g command
ELS activate
Cine cameras on
Switch to -Z antenna
Start impact backup timer
Activate RCS fuel dump
C battery to F and PL bus
Arm impact switch
VHF recovery beacon on
VHF survival beacon on
RCS purge
Landing
Main parachute disconnect
Connect aux bat to F and PL bus
Connect entry bat to F and PL bus
Remove aux bat from aux bus
Remove entry bat from main bus
MESC logic A and B off
Flashing light on
CB45 open
VHF/AM receiver off
VHF/AM transmitter off
Cine cameras off
Flotation pumps off
Deploy HF recovery antenna
HF transceiver on
MESC pyros safed

NASA-S-66-10087

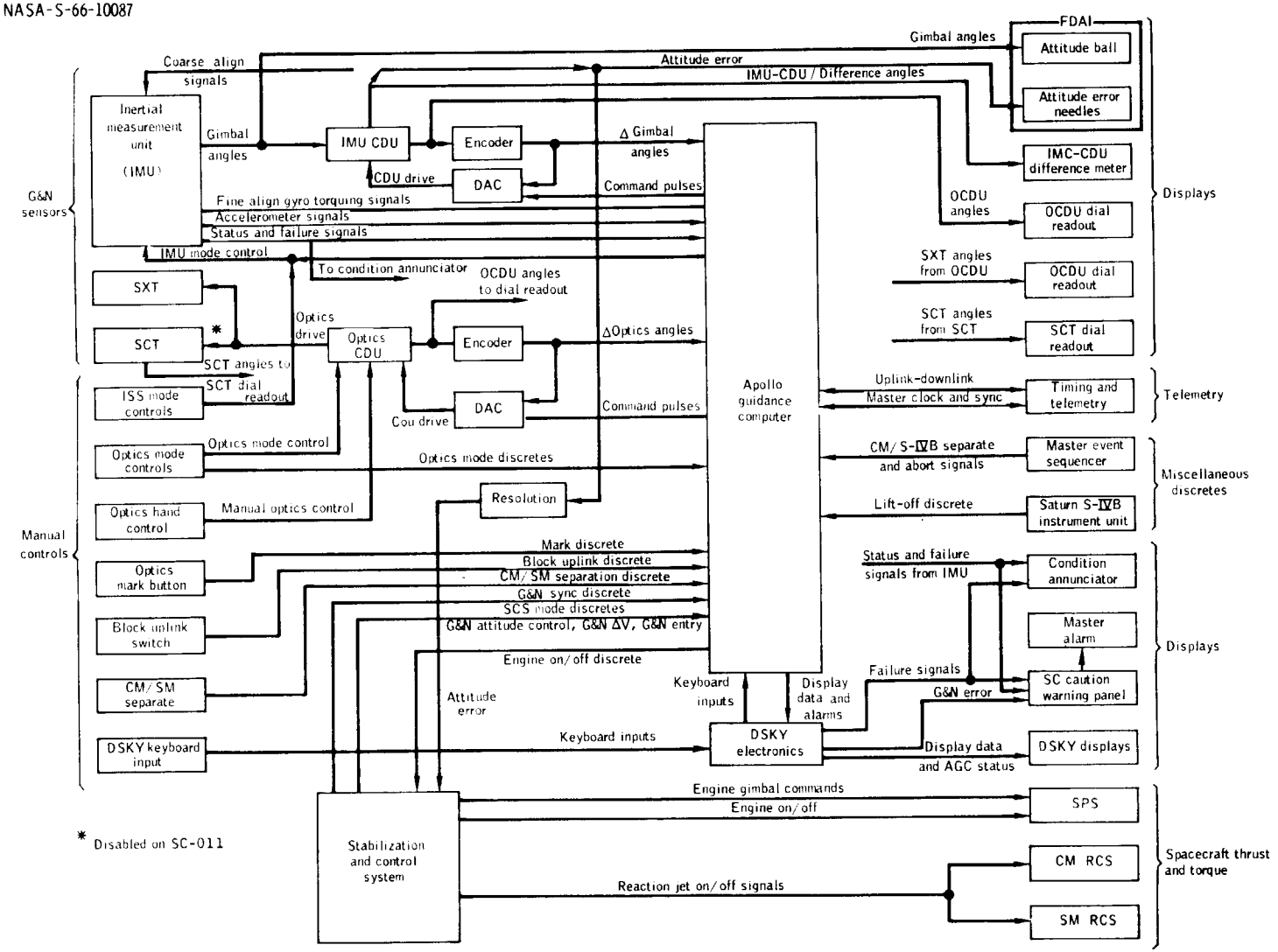

Figure 7.11-1. - G & N system block diagram, Mission AS-202.

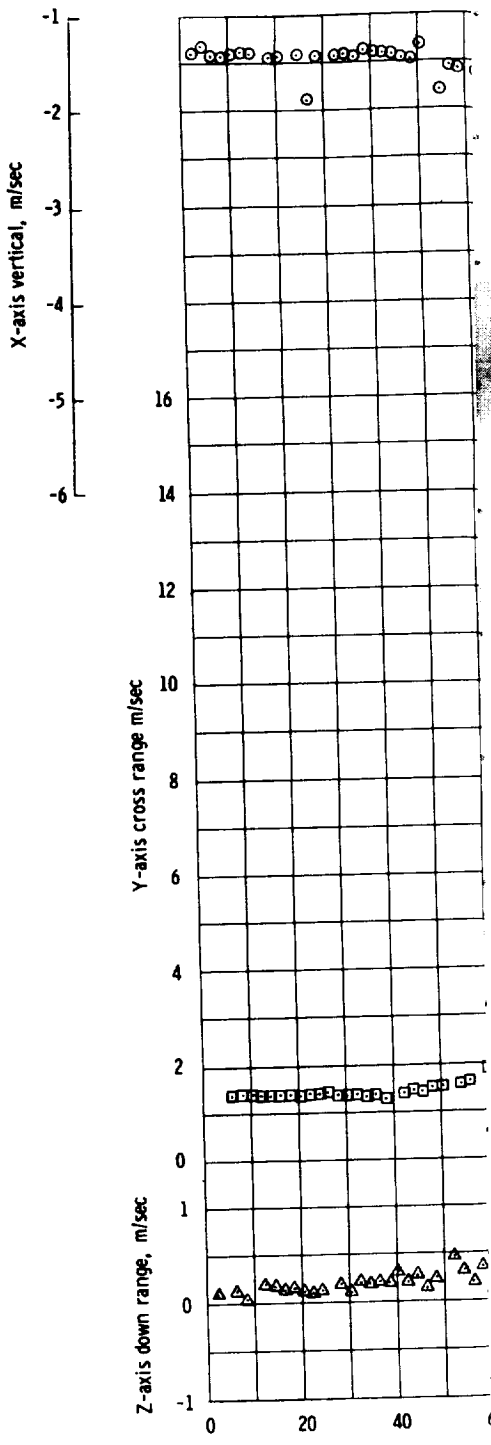

FOLDOUT FRAME 1

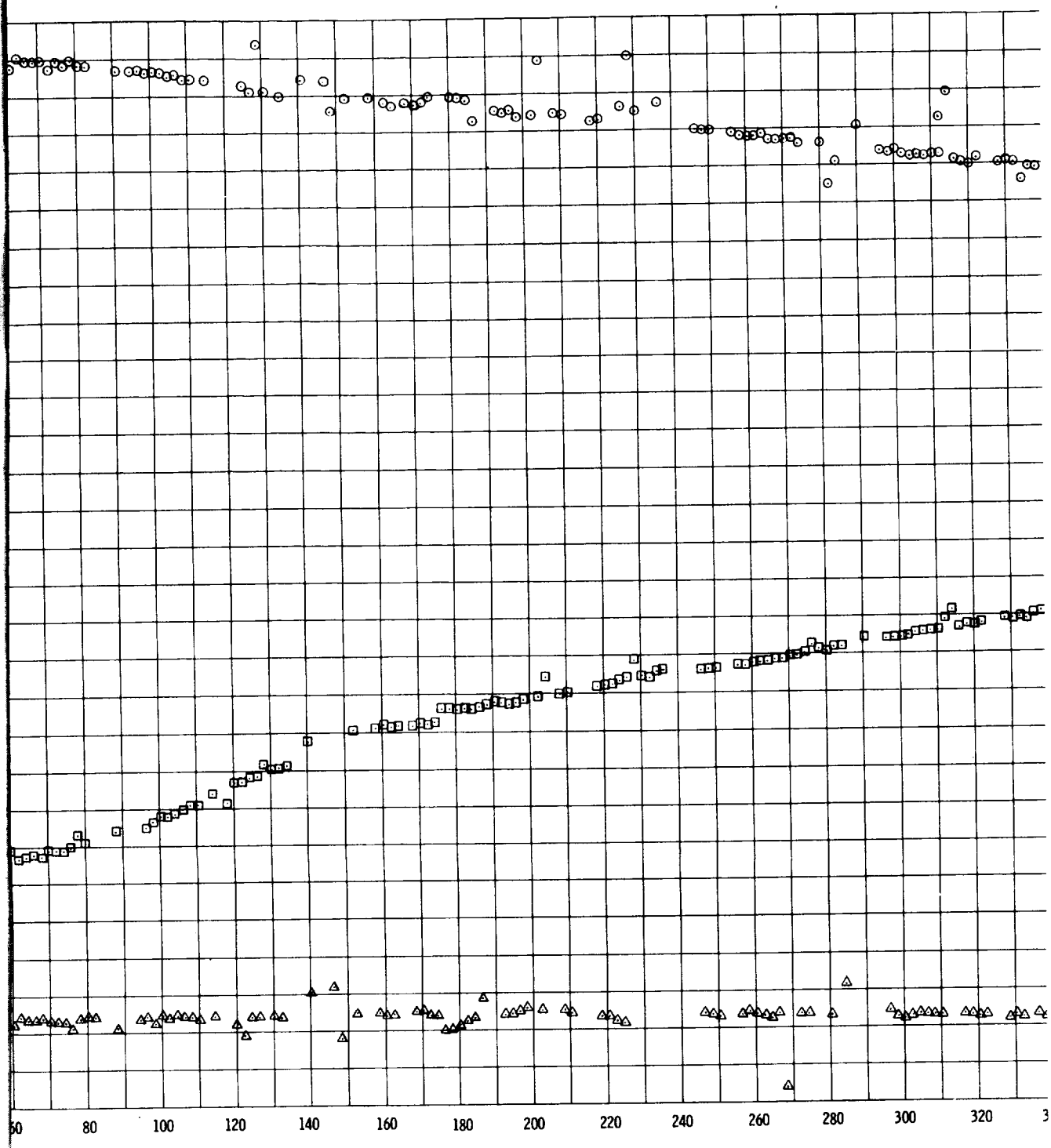

FOLDOUT FRAME 2

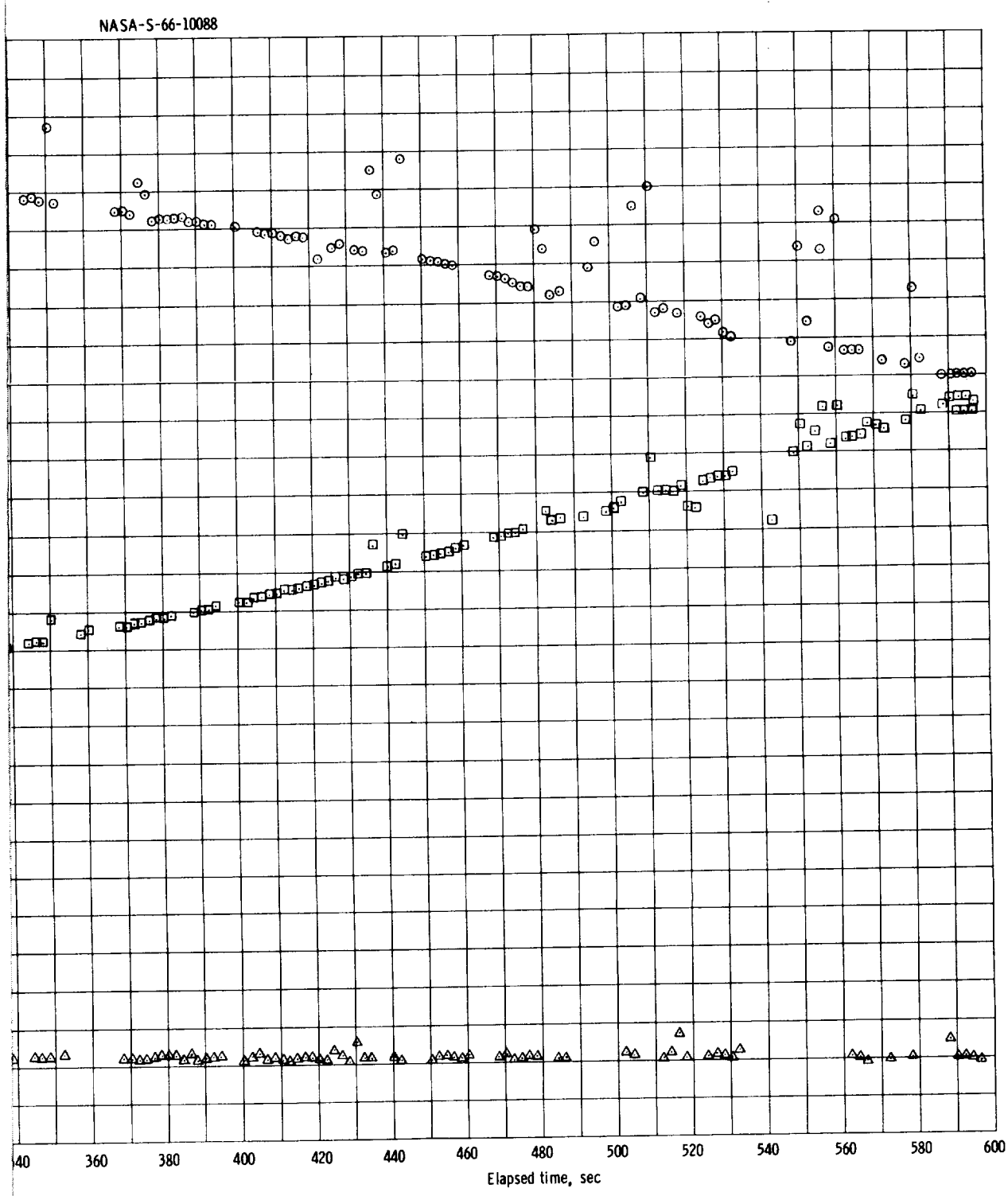

Figure 7.11-2.- Ascent velocity comparison, G & N minus S-IVB/IU, Mission AS-202.

FOLDOUT FRAME 3

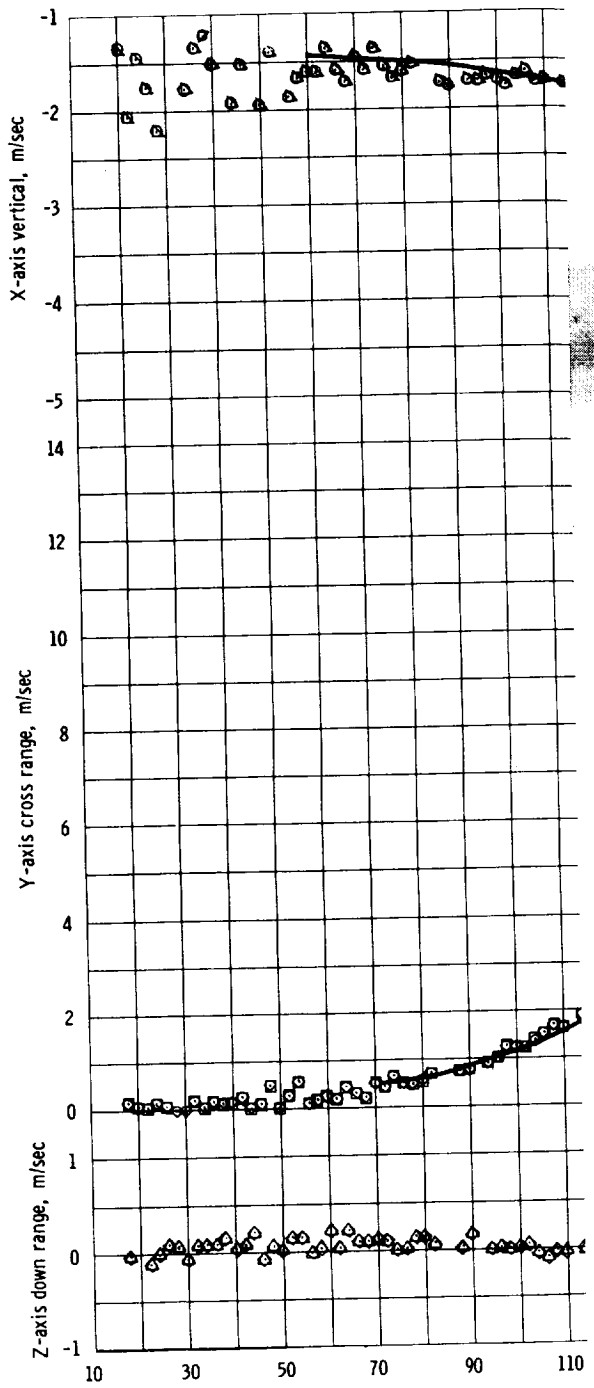

FOLDOUT FRAME /

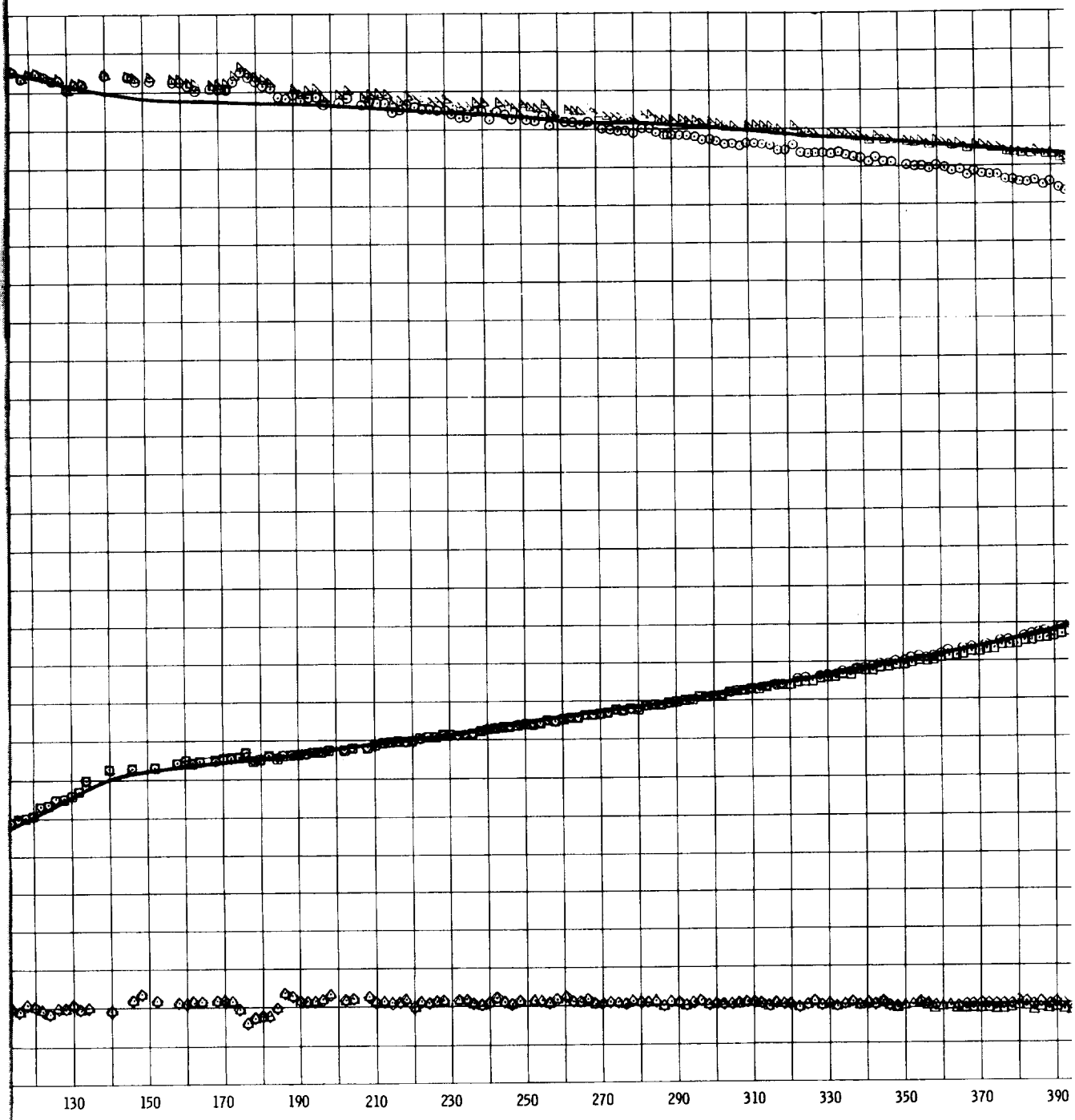

FOLDOUT FRAME 2

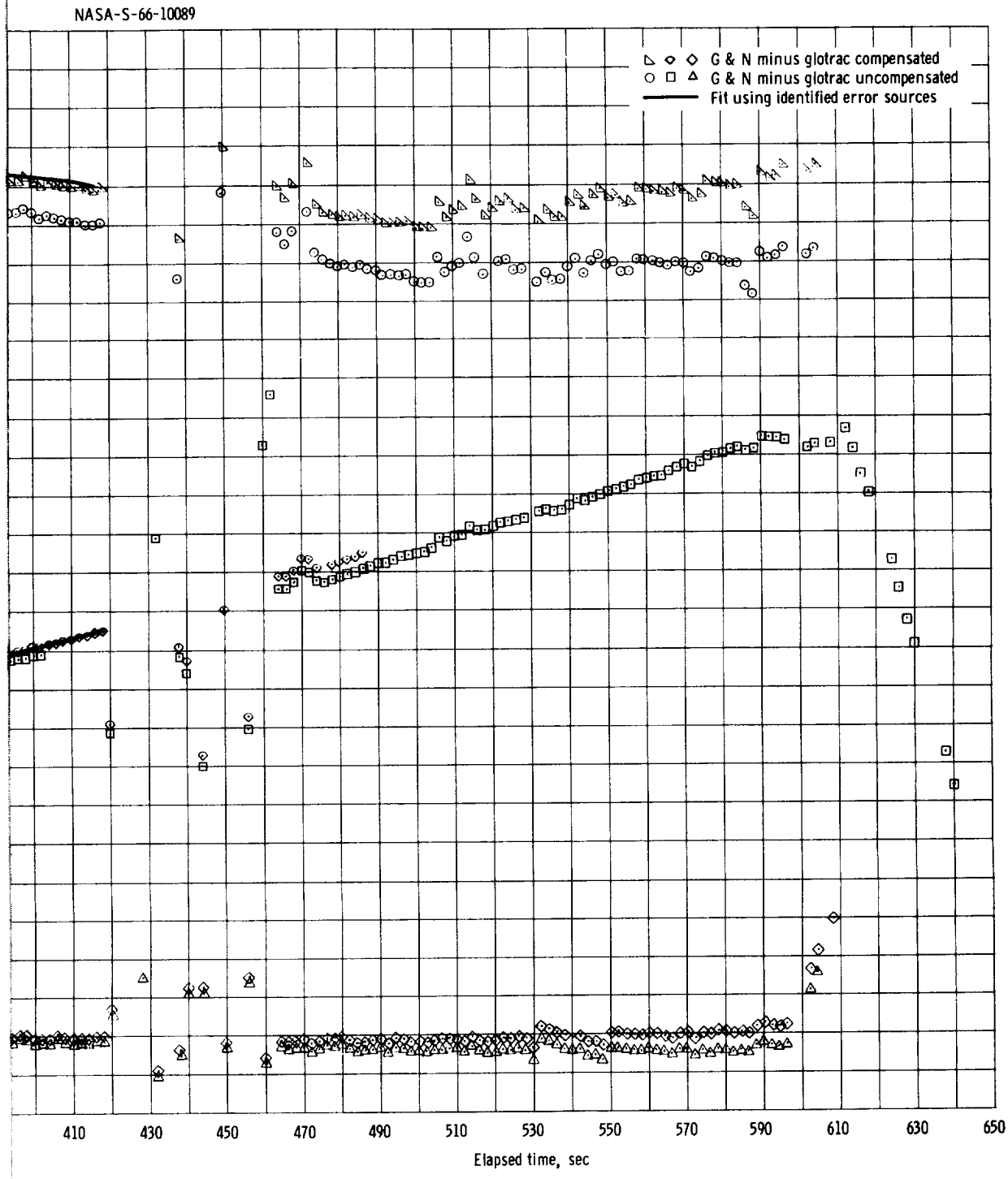

Figure 7.11-3.- Ascent velocity differences, G & N minus glotrac, Mission AS-202.

FOLDOUT FRAME 3

NASA-S-66-10090

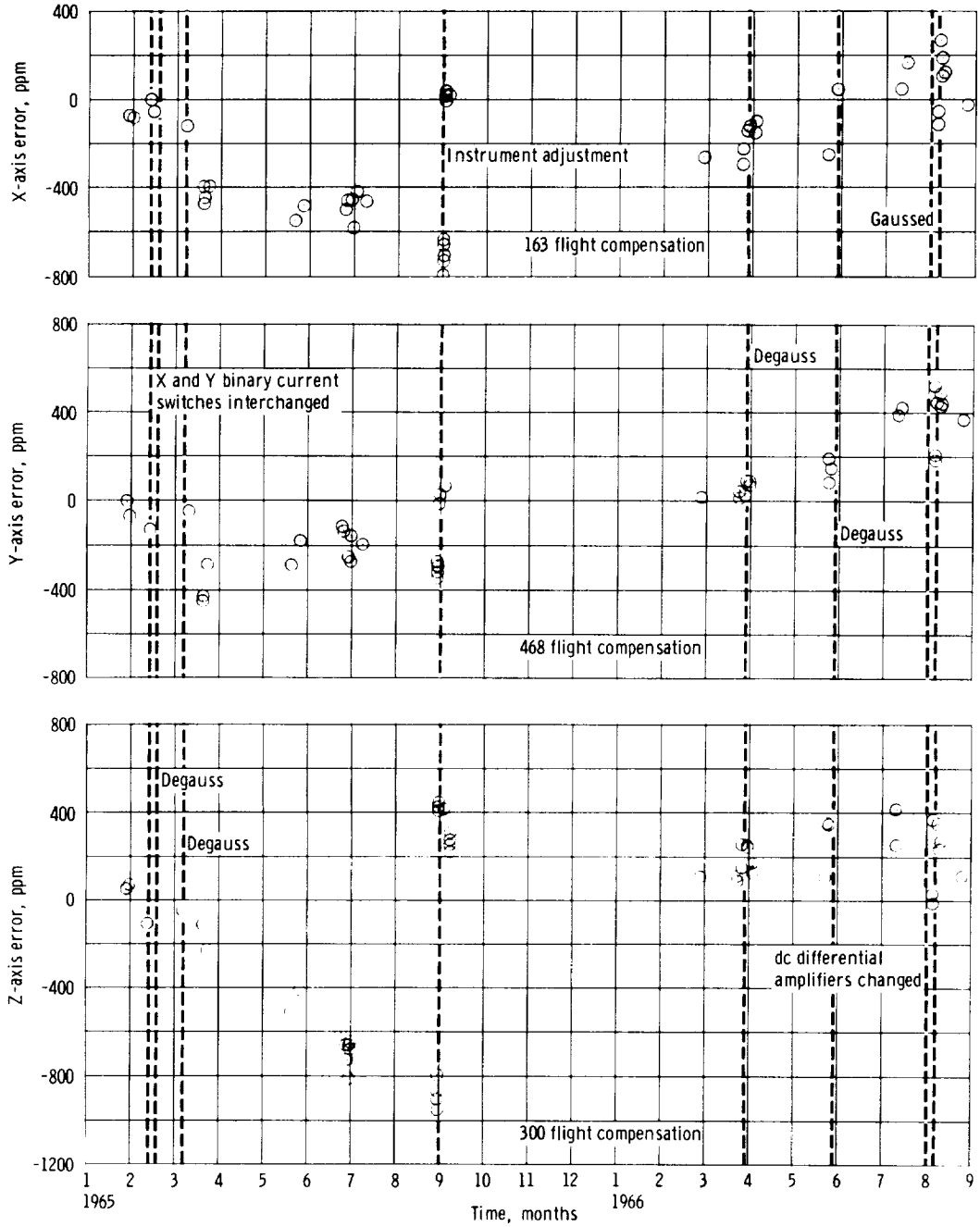

(a) Accelerometer scale factor errors.

Figure 7.11-4. - Preflight test histories of guidance and navigation subsystem inertial instrument coefficient errors for SC-011, Mission AS-202.

NASA-S-66-10091

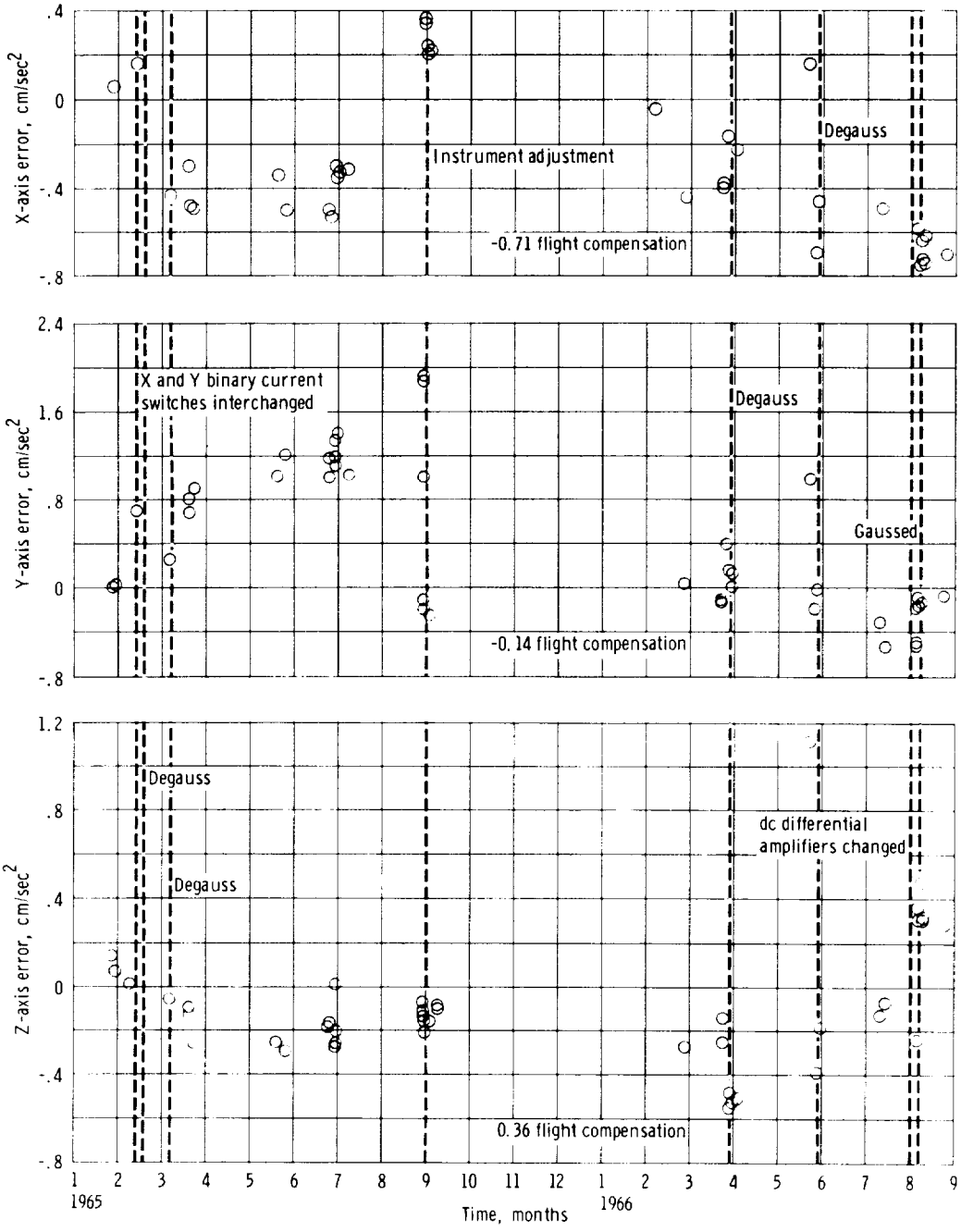

(b) Accelerometer bias errors.

Figure 7.11-4. - Continued.

NASA-S-66-10092

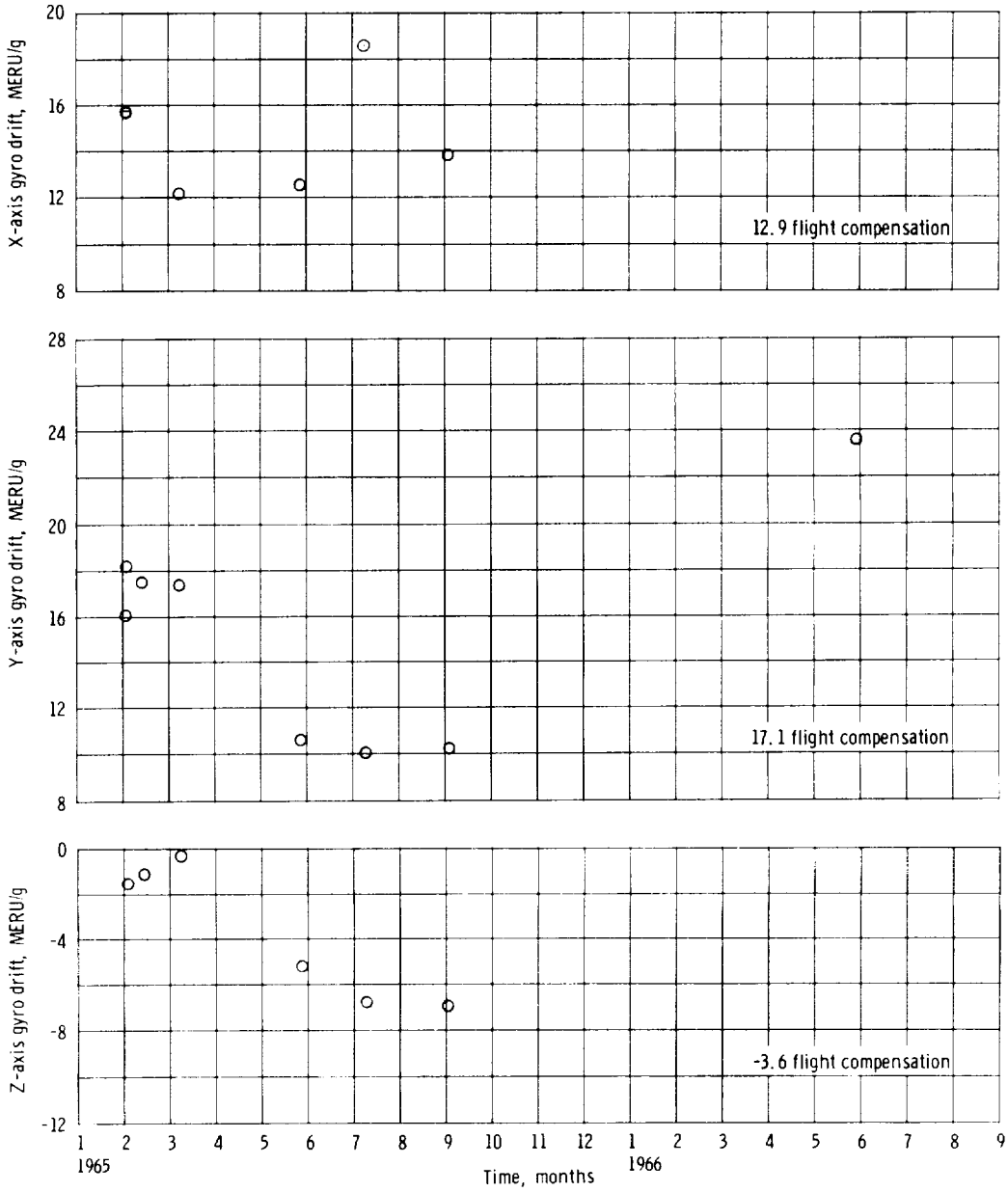

(c) X-, Y-, and Z-axis gyro drift errors along acceleration drift input axis (ADIA).

Figure 7.11-4. - Continued.

NASA-S-66-10093

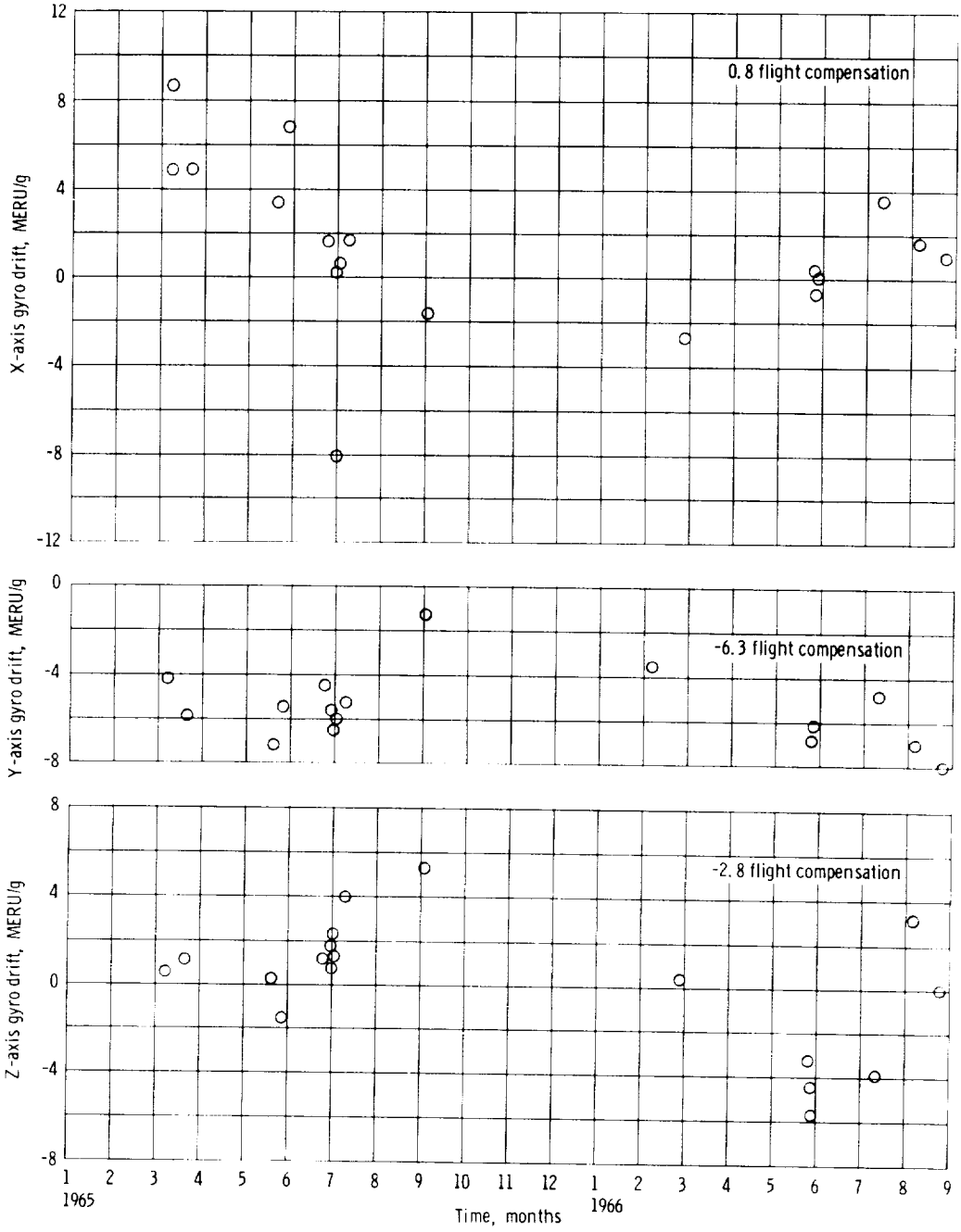

(d) Gyro drift errors acceleration along spin reference axis (ADSRA).

Figure 7.11-4. - Continued.

NASA-S-66-10094

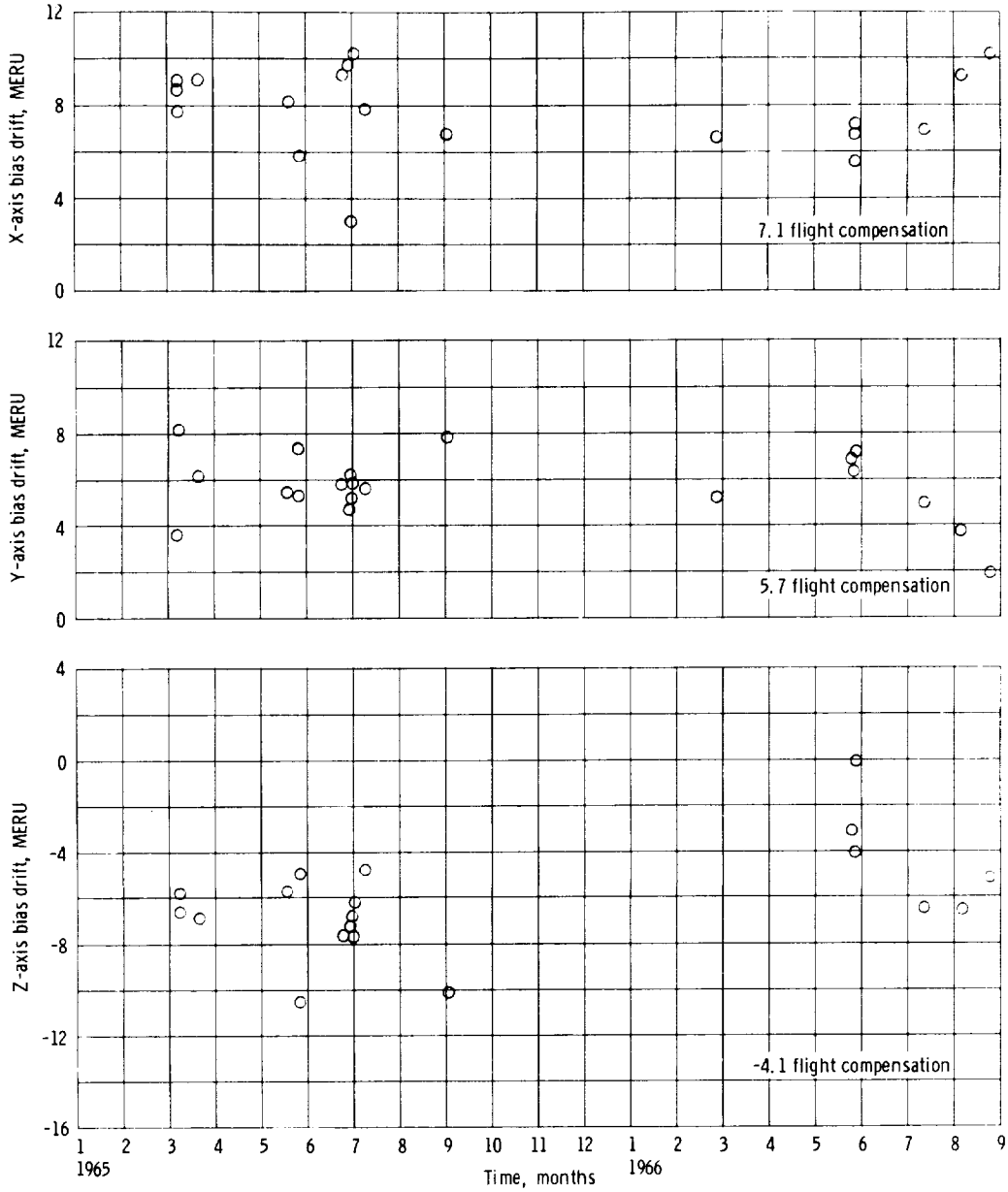

(e) Gyro null bias drift errors (NBD).

Figure 7.11-4.- Concluded.

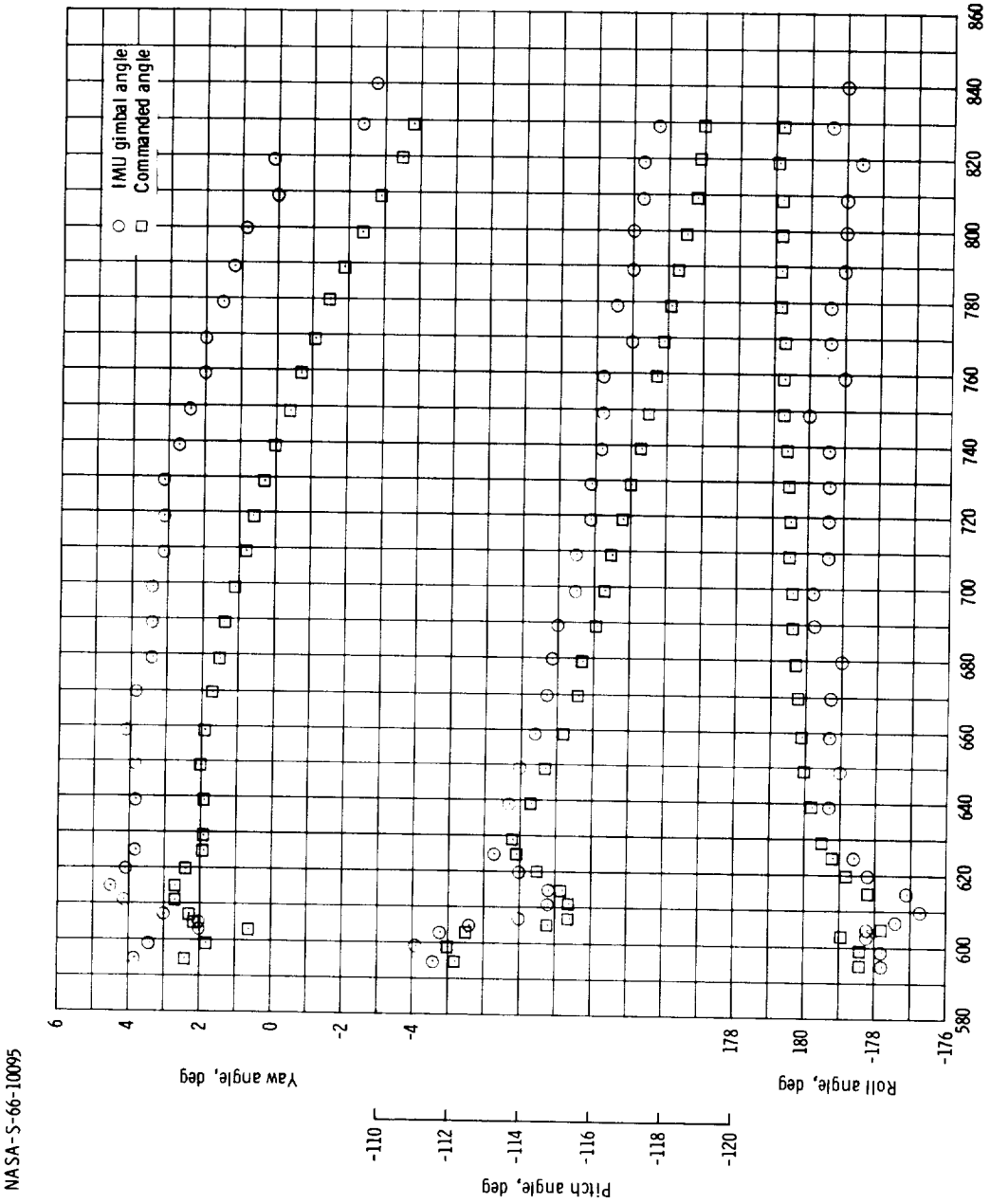

NASA-S-66-10095

Figure 7.11-5.- Maneuver to 1st SPS attitude during burn, commanded and actual angles, Mission AS-202.

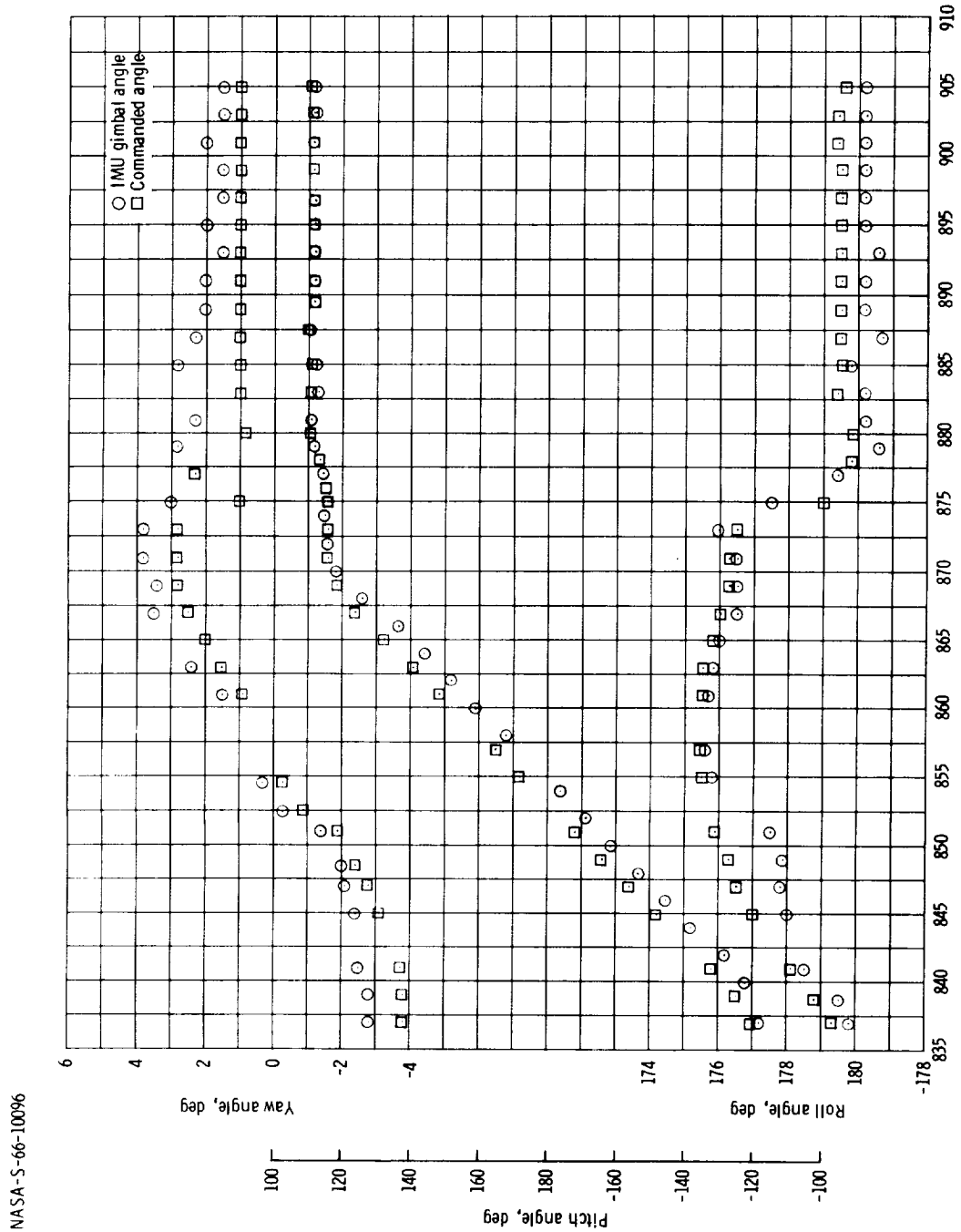

Figure 7.11-6. - Maneuver to local vertical, commanded and actual angles, Mission AS-202.

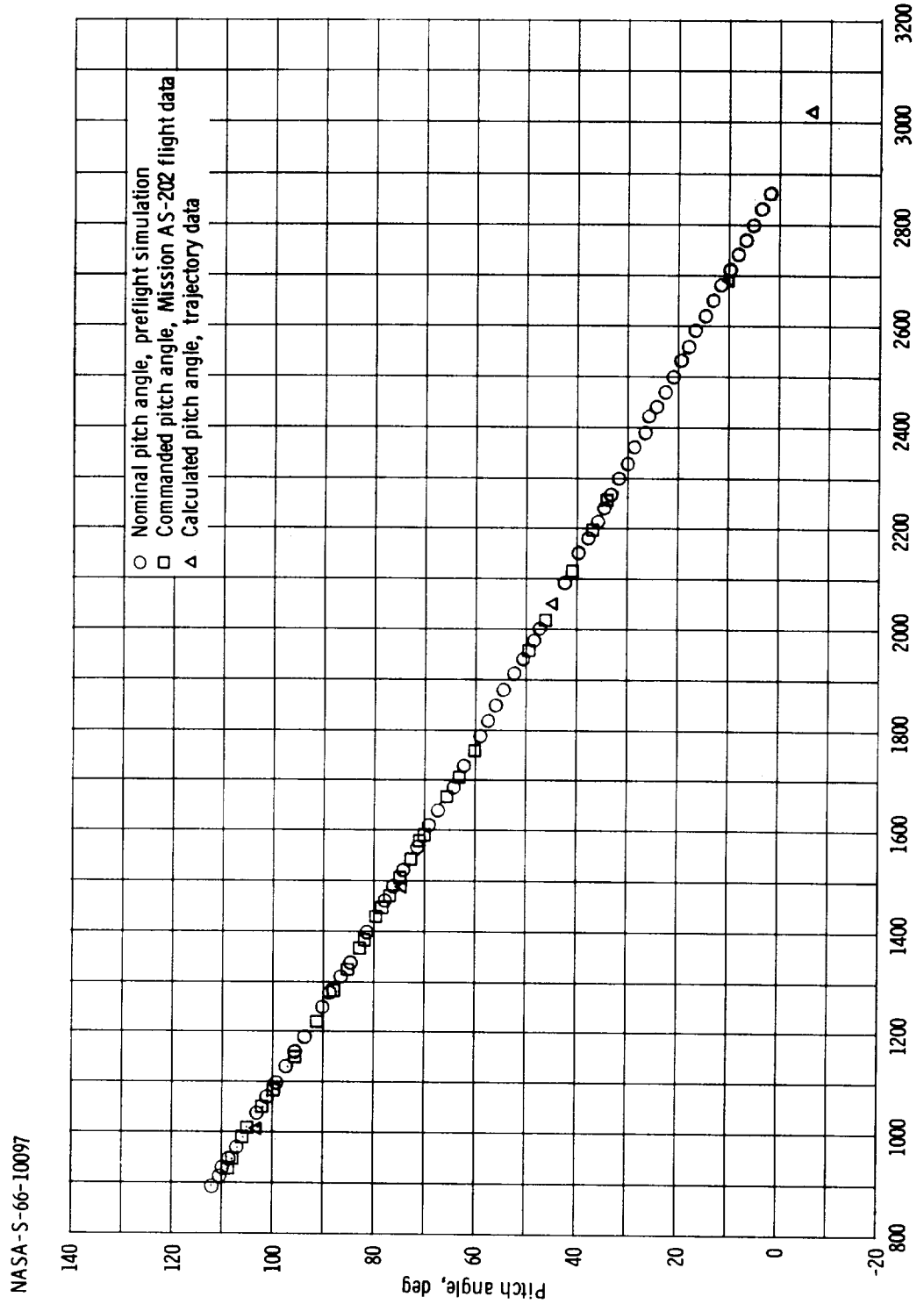

NASA-S-66-10097

Figure 7.11-7.- Spacecraft pitch attitude during local vertical phase, Mission AS-202.

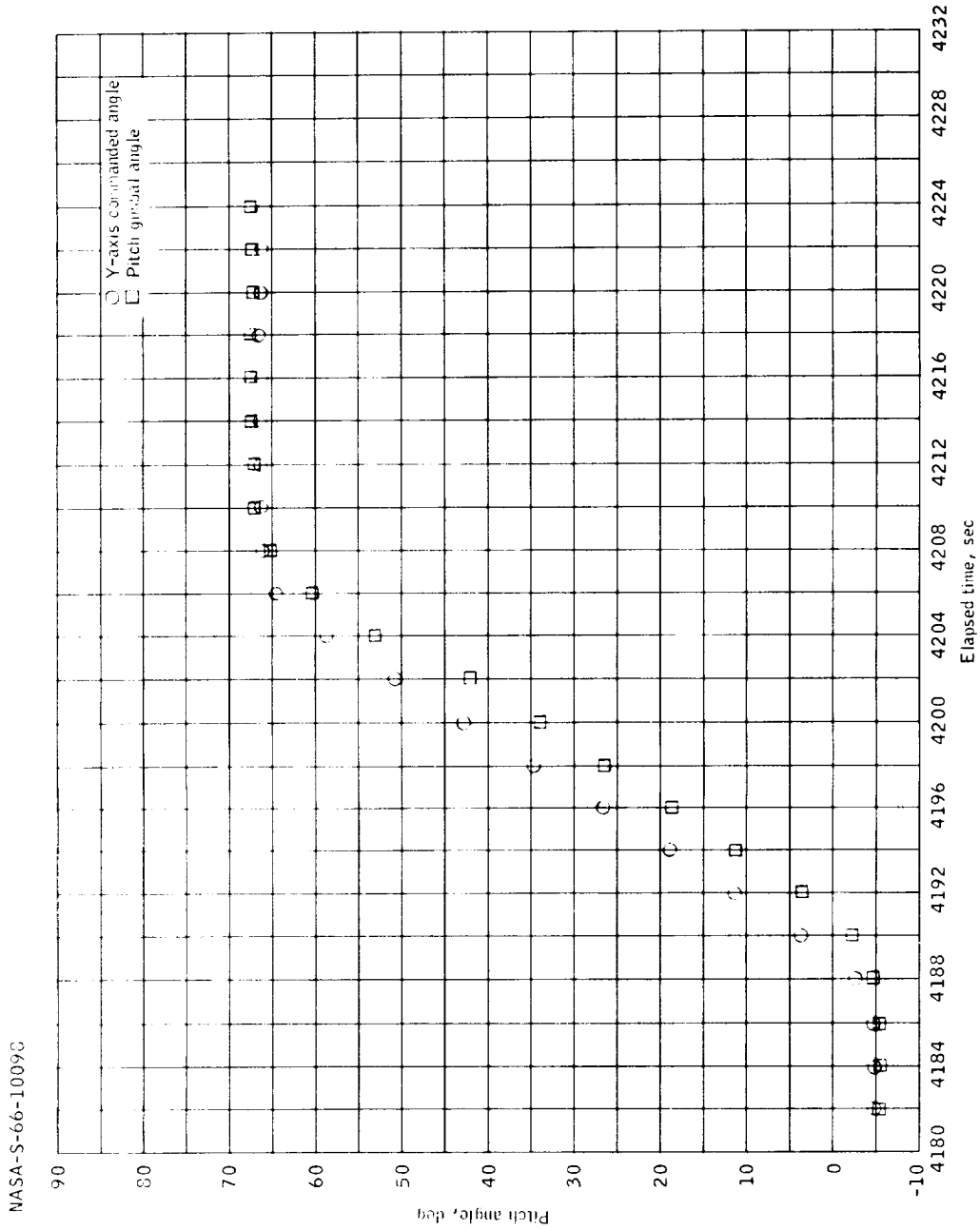

Figure 7.11-8.- Maneuver to CM/SM separation attitude, commanded and actual pitch attitude, Mission AS-202.

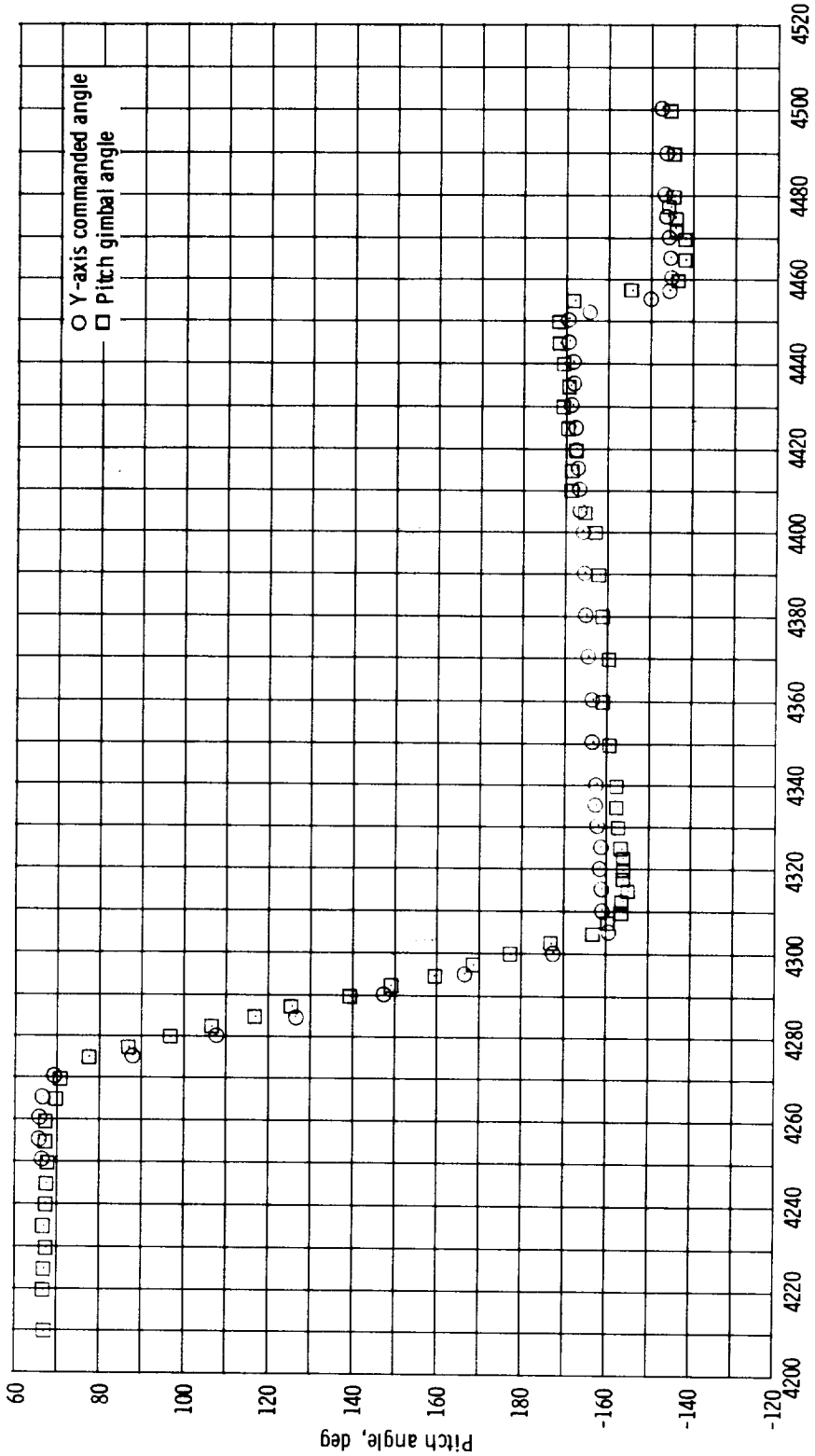

NASA-S-66-10099

Figure 7.11-9. - Pitch maneuver to entry attitude, commanded and actual angles, Mission AS-202.

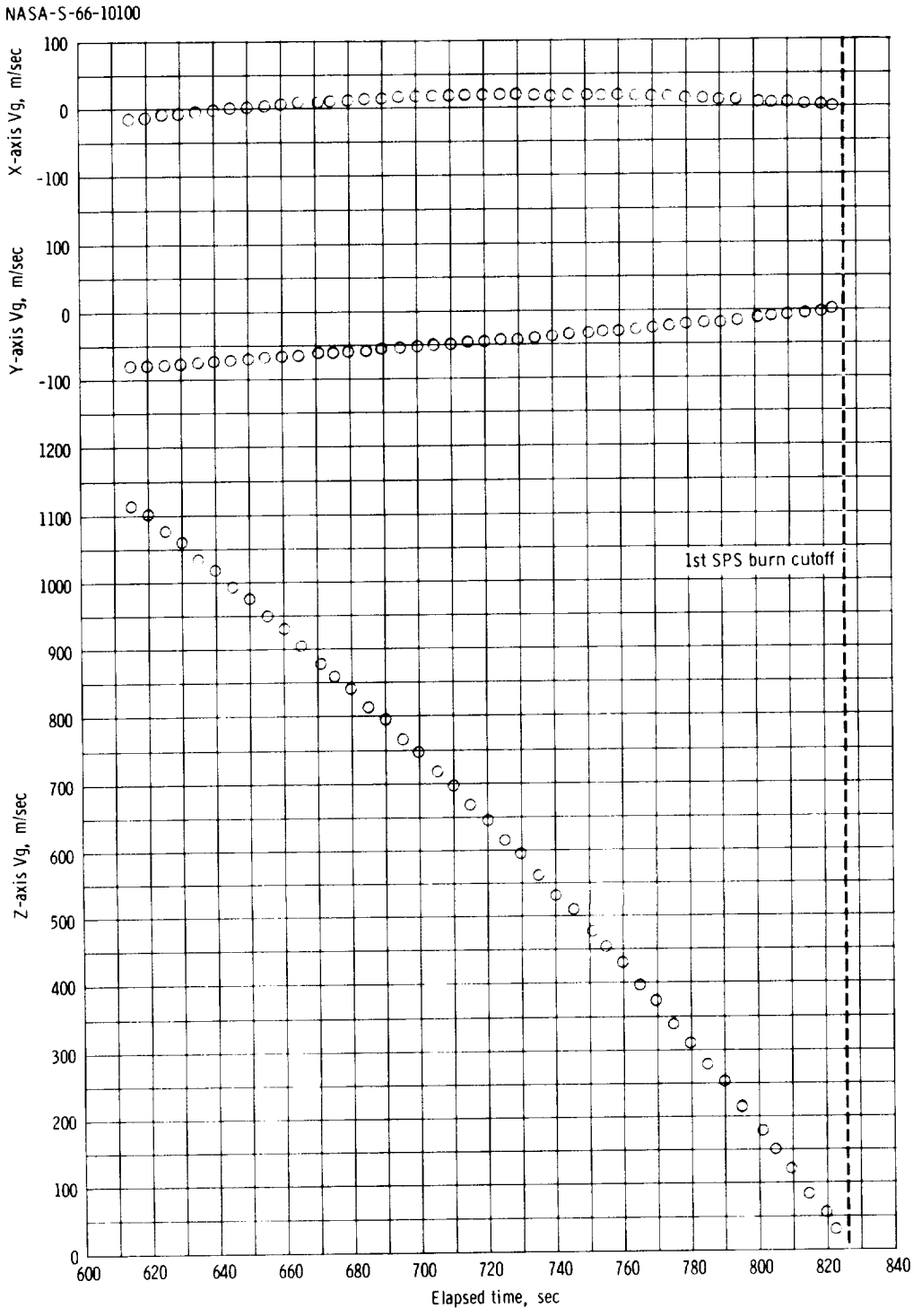

(a) Pre-cutoff.

Figure 7.11-10. - Velocity to be gained (Vg), first SPS burn, Mission AS-202.

NASA-S-66-10101

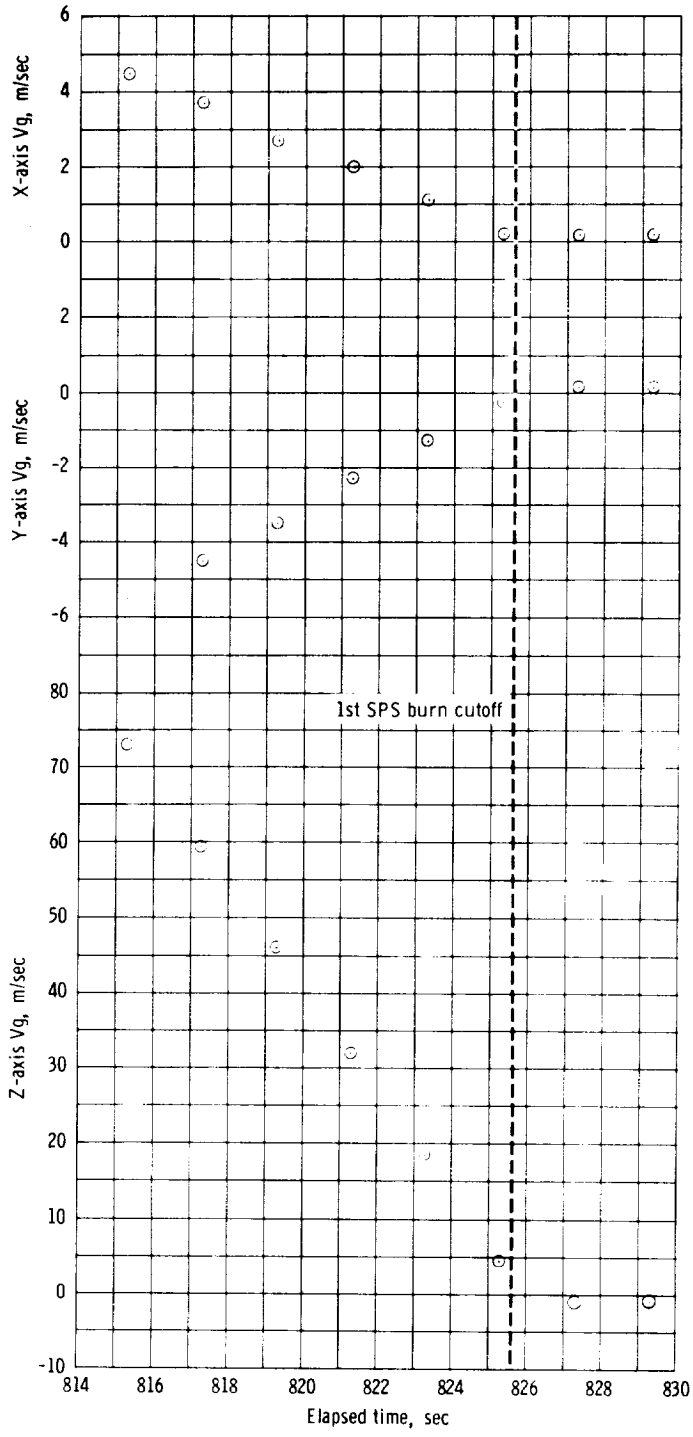

(b) Post-cutoff.

Figure 7.11-10. - Concluded.

NASA-S-66-10102

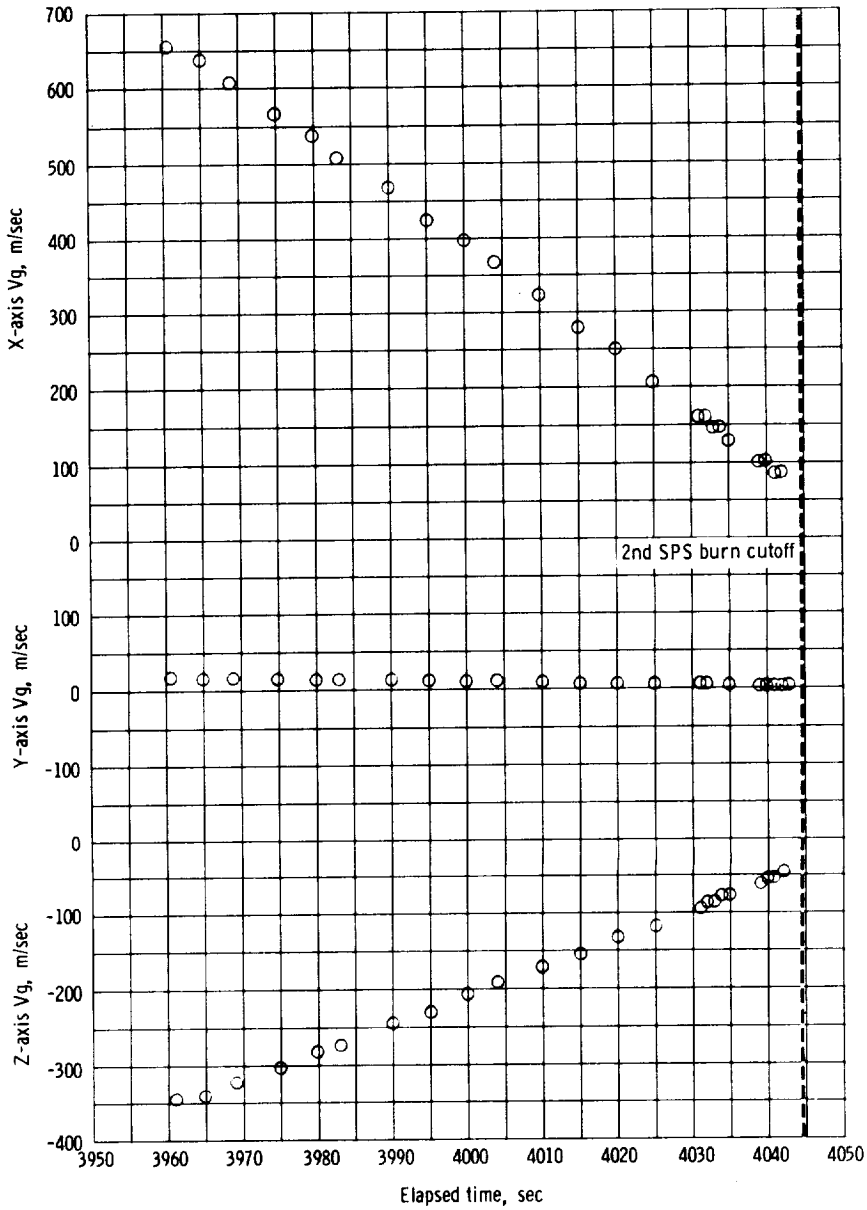

(a) Pre-cutoff of 2nd SPS burn.

Figure 7.11-11.- Velocity to be gained (Vg), 2nd, 3rd, and 4th burns, Mission AS-202.

NASA-S-66-10103

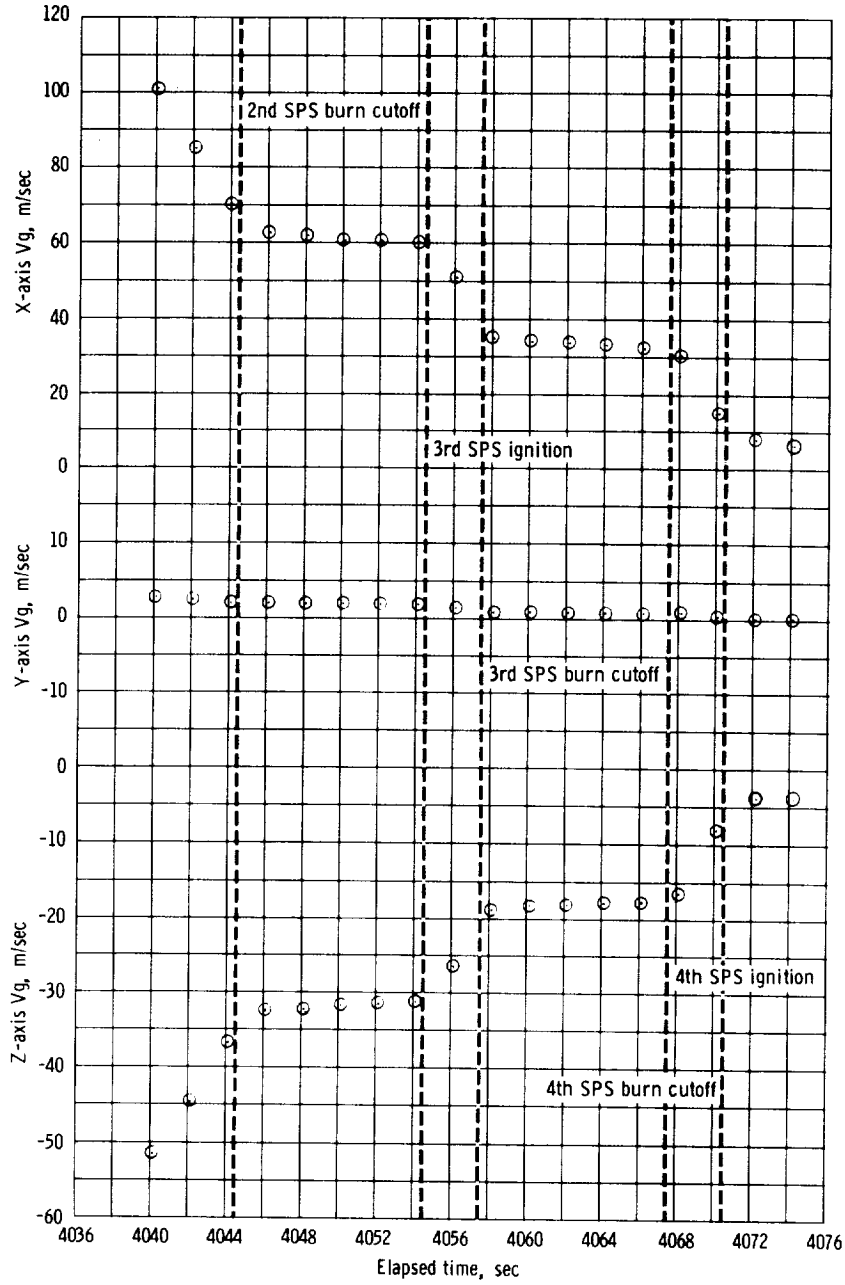

(b) Post-cutoff of 2nd SPS burn.

Figure 7.11-11. - Concluded

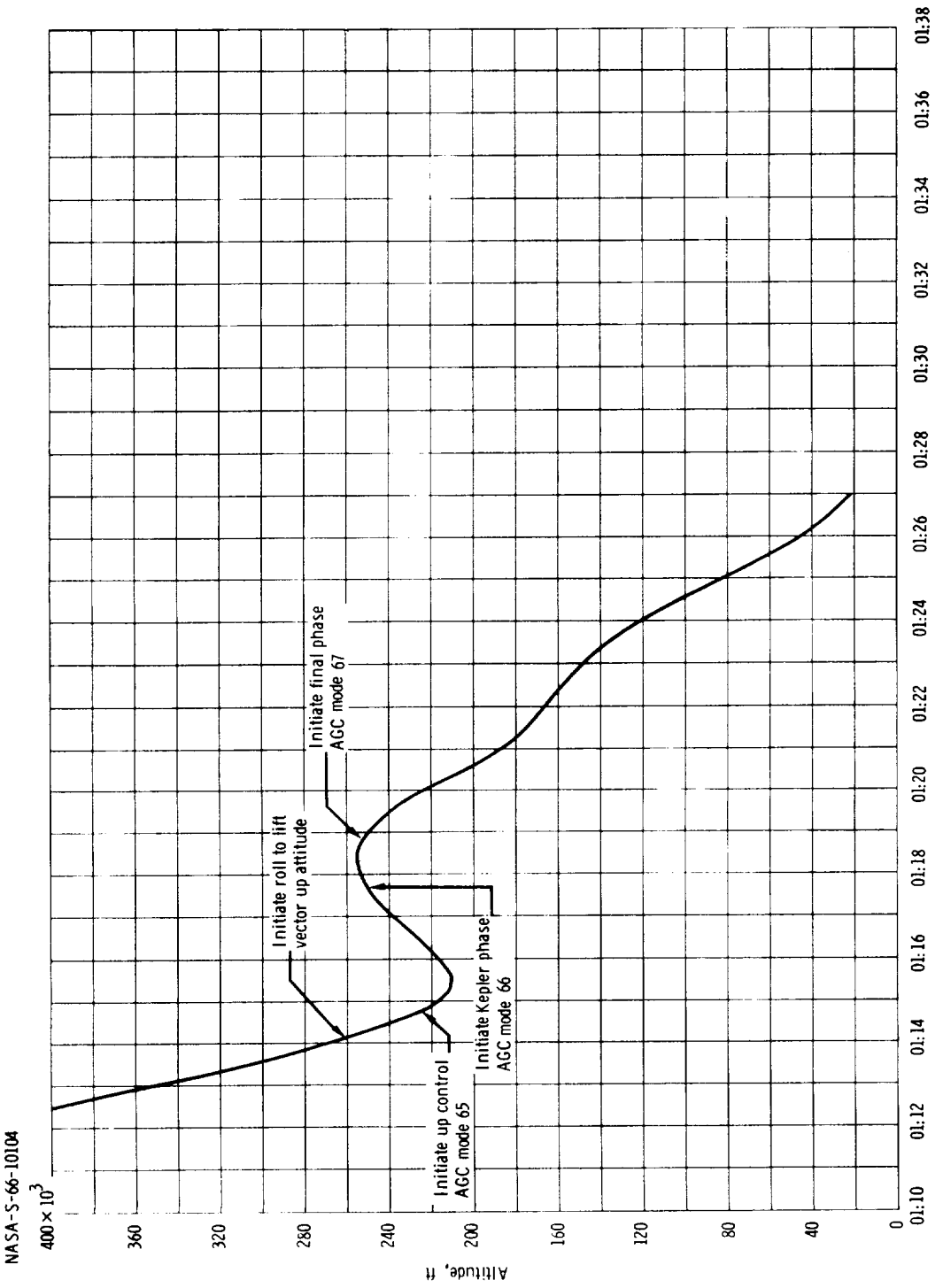

Figure 7.11-12. - Time history of altitude reentry phase, Mission AS-202.

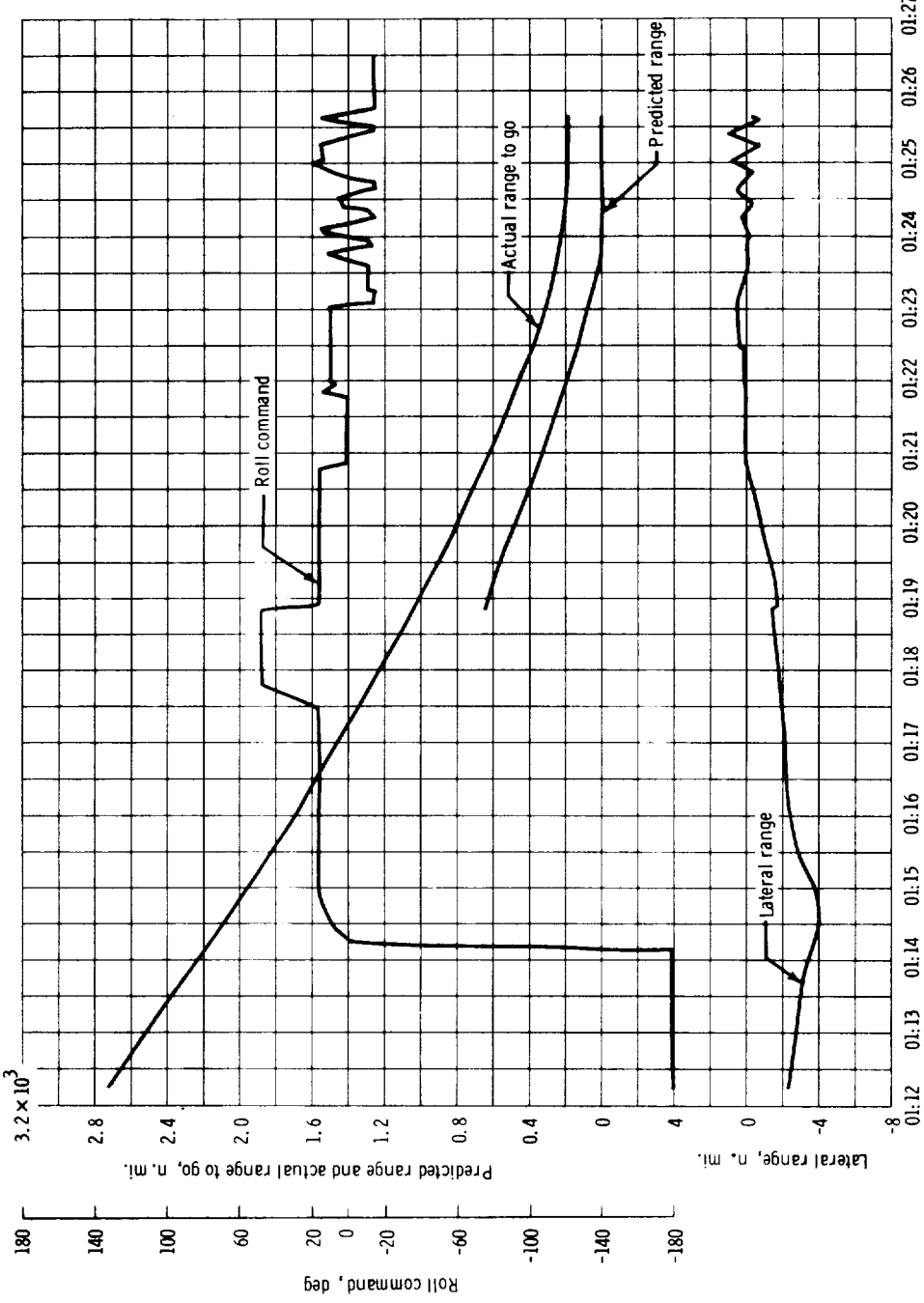

Figure 7.11-13. - Actual and predicted range to go, lateral range and roll command plotted against time, Mission AS-202 reentry phase.

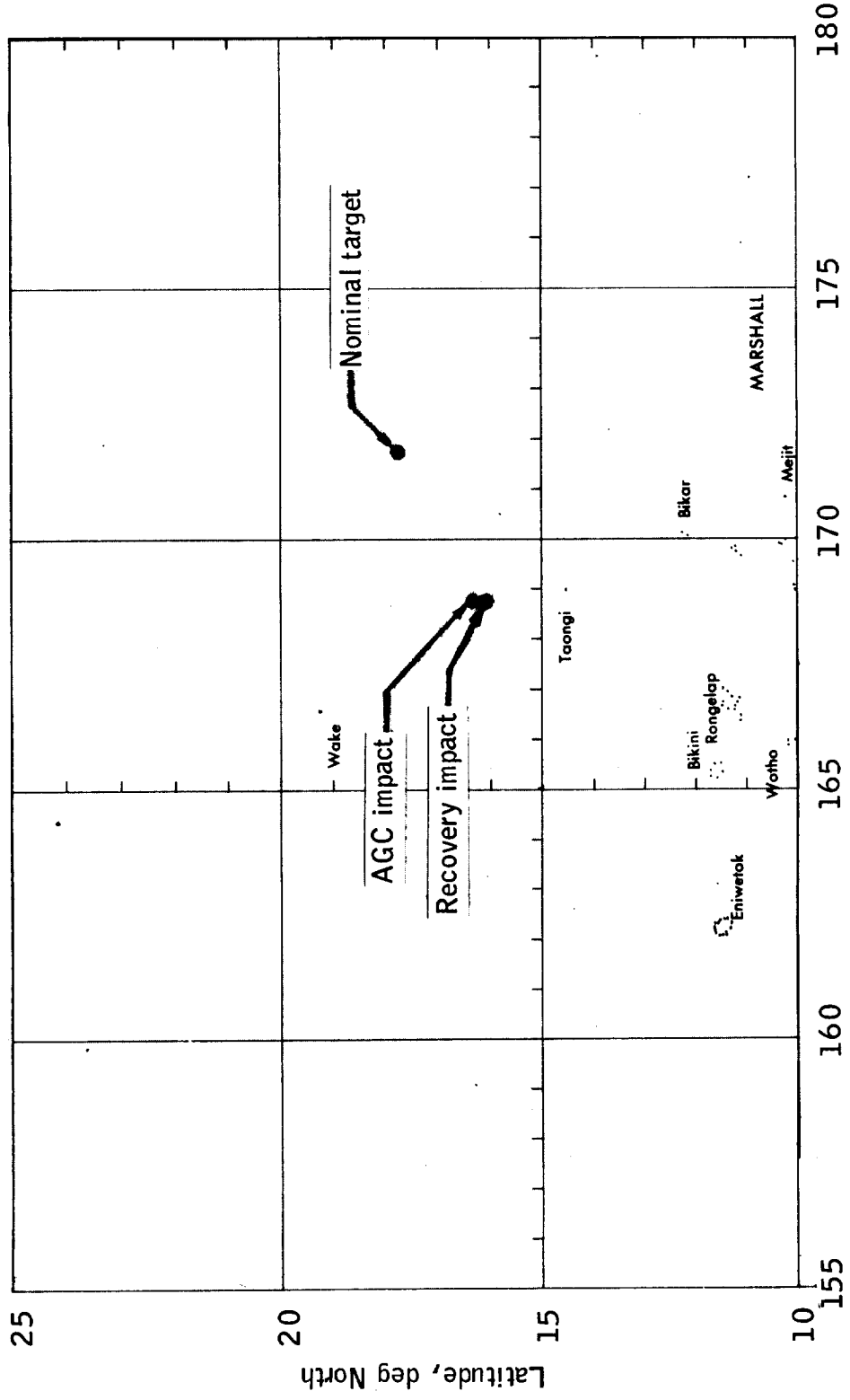

Figure 7.11-14.- Impact and target locations for Mission AS-202.

NASA-S-66-10107

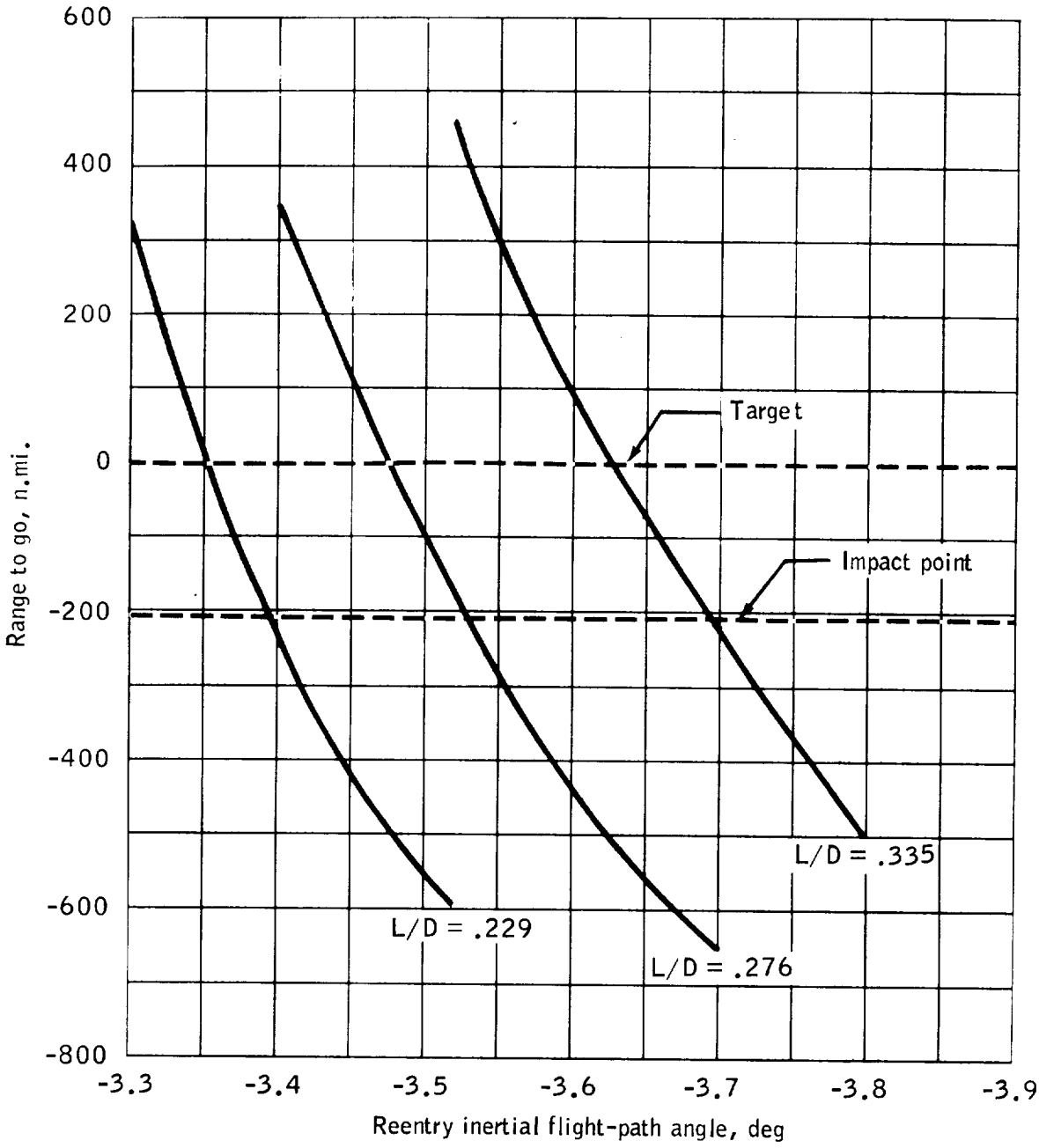

Figure 7.11-15.- Reentry miss distance plotted against reentry inertial flight-path angle, Mission AS-202.

NASA-S-66-10108

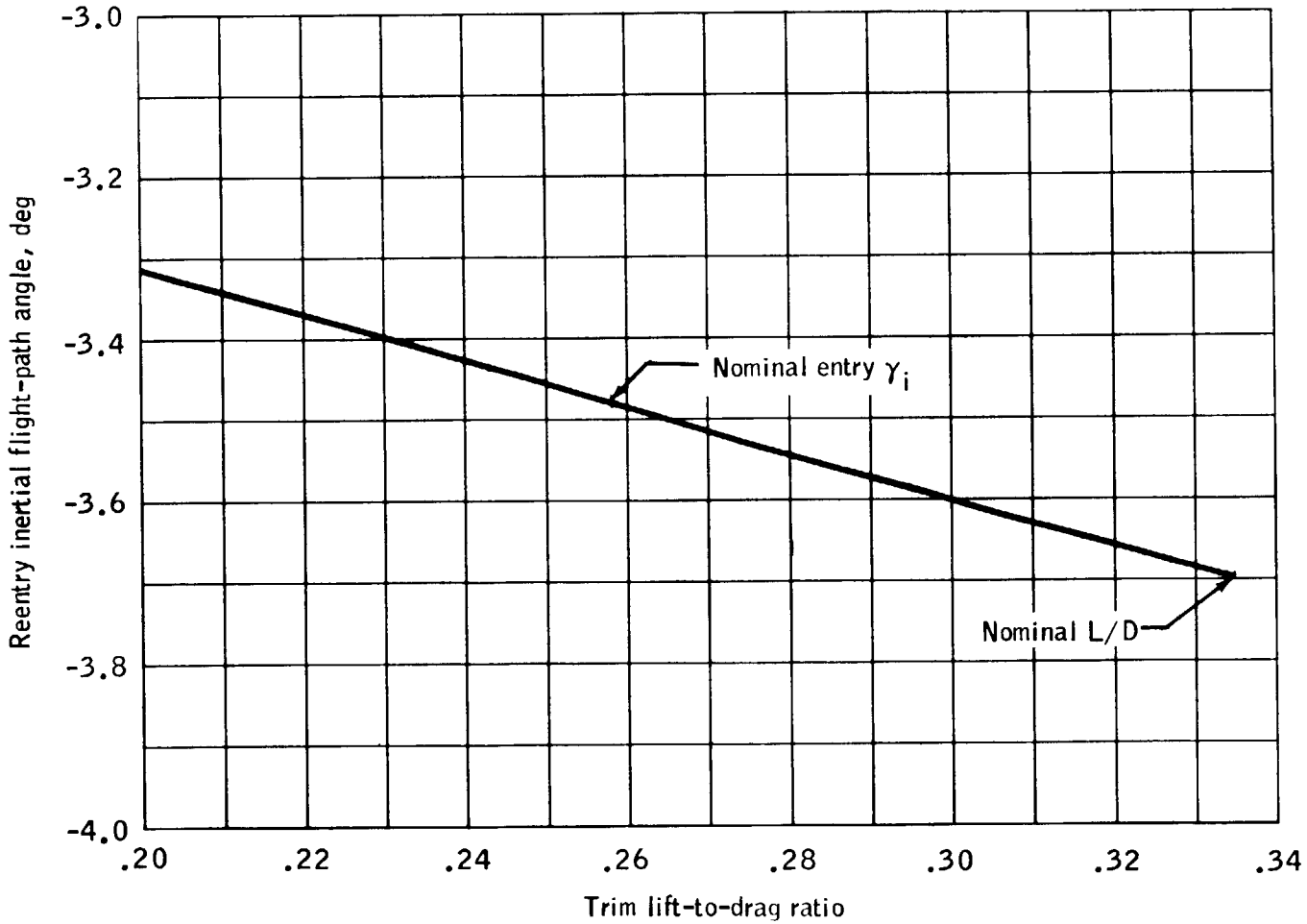

Figure 7.11-16.- Reentry inertial flight-path angle plotted against lift-to-drag ratio for constant 205 nautical miles miss distance, Mission AS-202.

NASA-S-66-10109

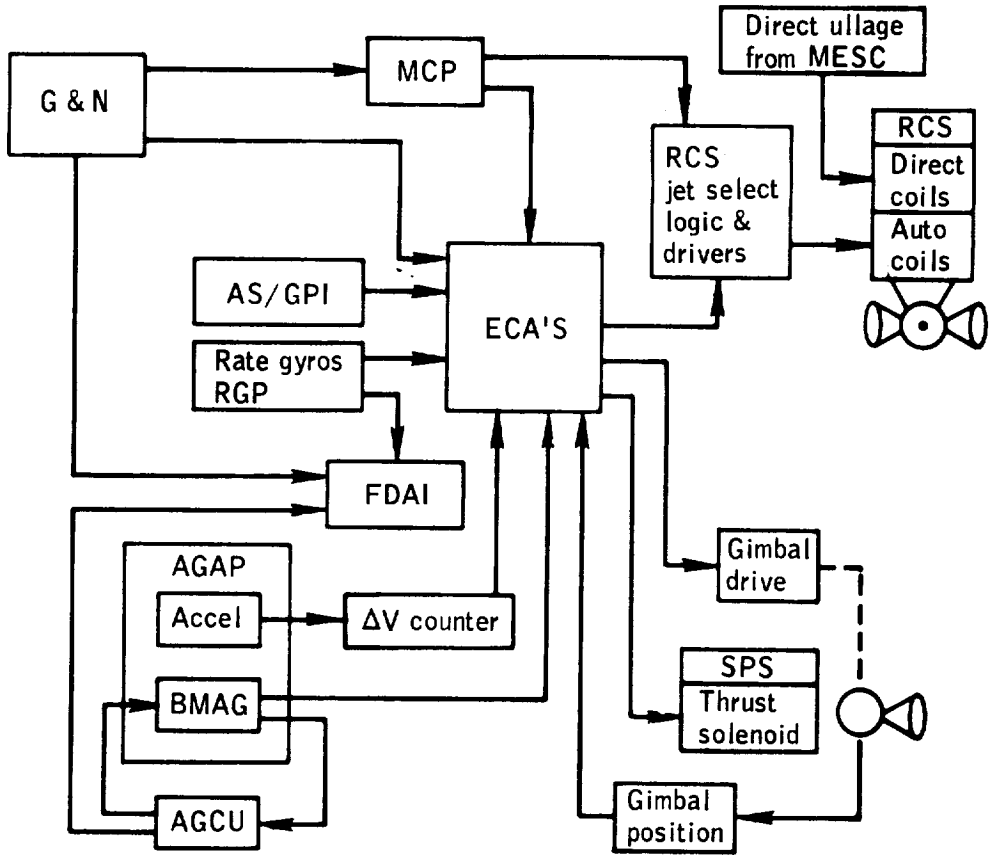

AGAP	Attitude Gyro Accelerometer Package
AGCU	Attitude Gyro Coupling Unit
AS/GPI	Attitude Set and Gimbal Position Indicator
BMAG	Body Mounted Attitude Gyro
ECA	Electronic Control Assembly
FDAI	Flight Director Attitude Indicator
G & N	Guidance and Navigation
MCP	Mission Control Programmer
MESC	Mission Events Sequential Controller
RCS	Reaction Control System
RGP	Rate Gyro Package
SPS	Service Propulsion Subsystem

Figure 7.11-17.- Stabilization and control system, Mission AS-202.

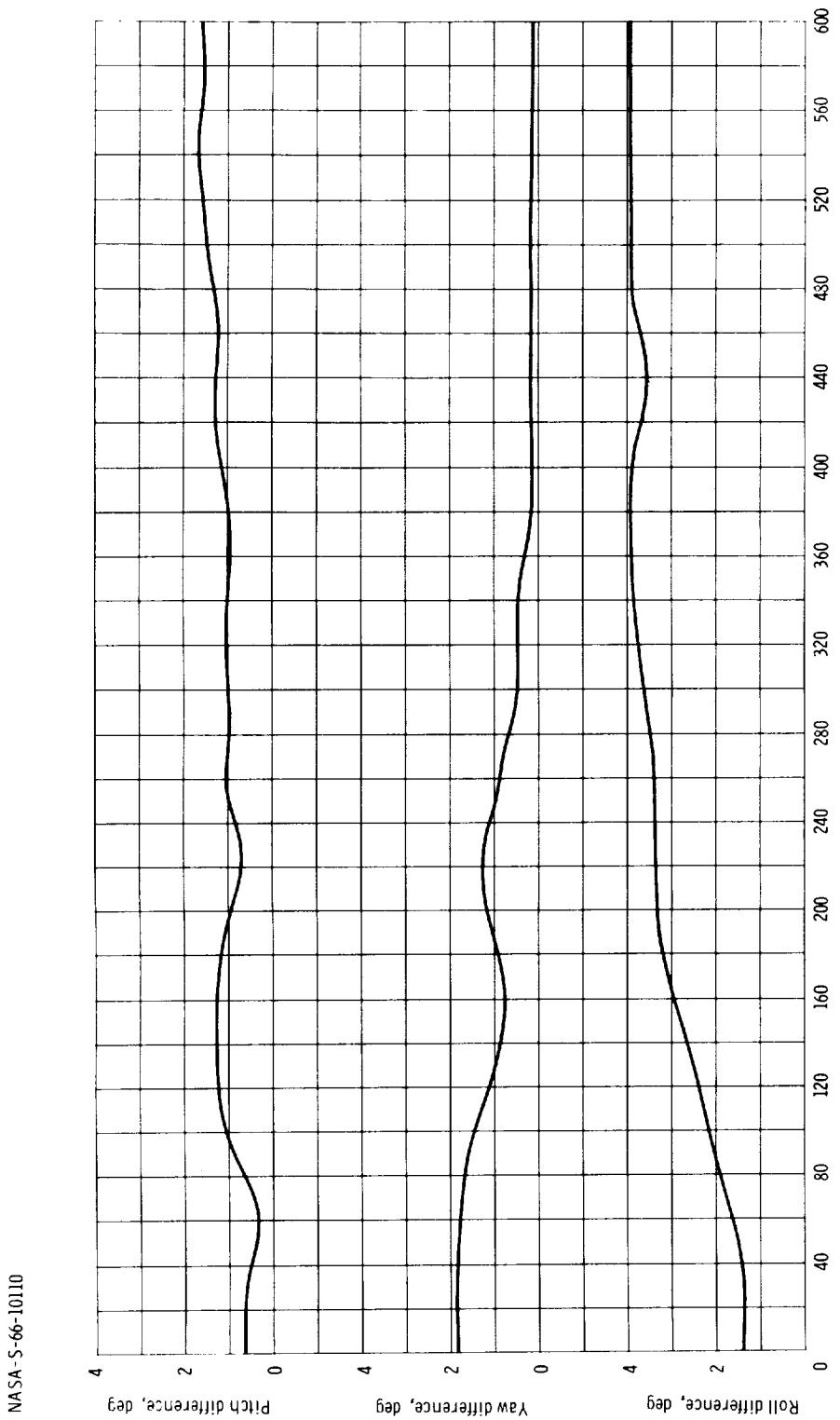

Figure 7.11-18.- Comparison of G & N IMU gimbal angles and SCS attitude gyro coupling unit Euler angles during ascent phase, (IMU minus Euler), Mission AS-202.

NASA-S-66-10111

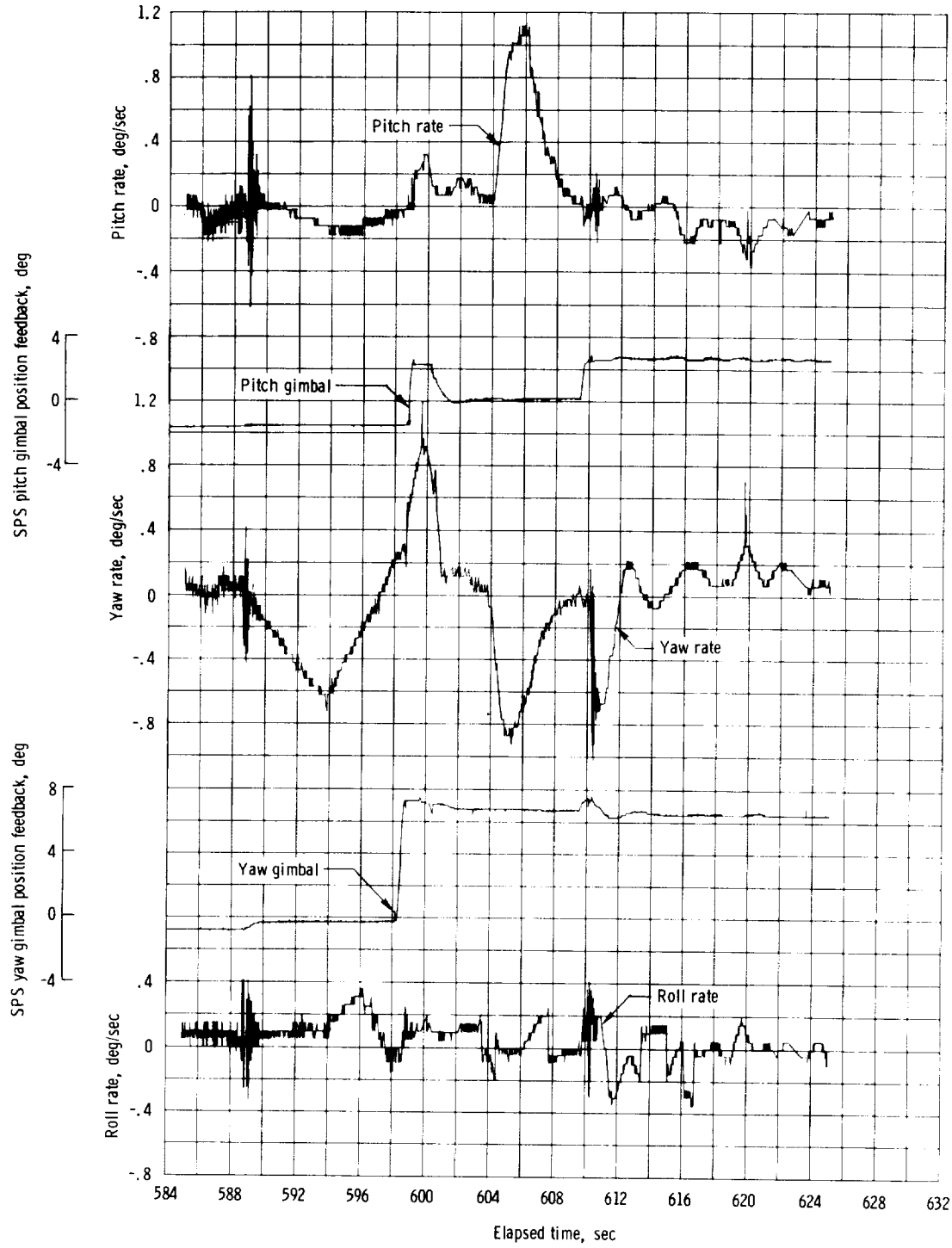

Figure 7.11-19.- Separation of SC/LV and beginning of first burn, SC body rates, and SPS gimbal position feedback, Mission AS-202.

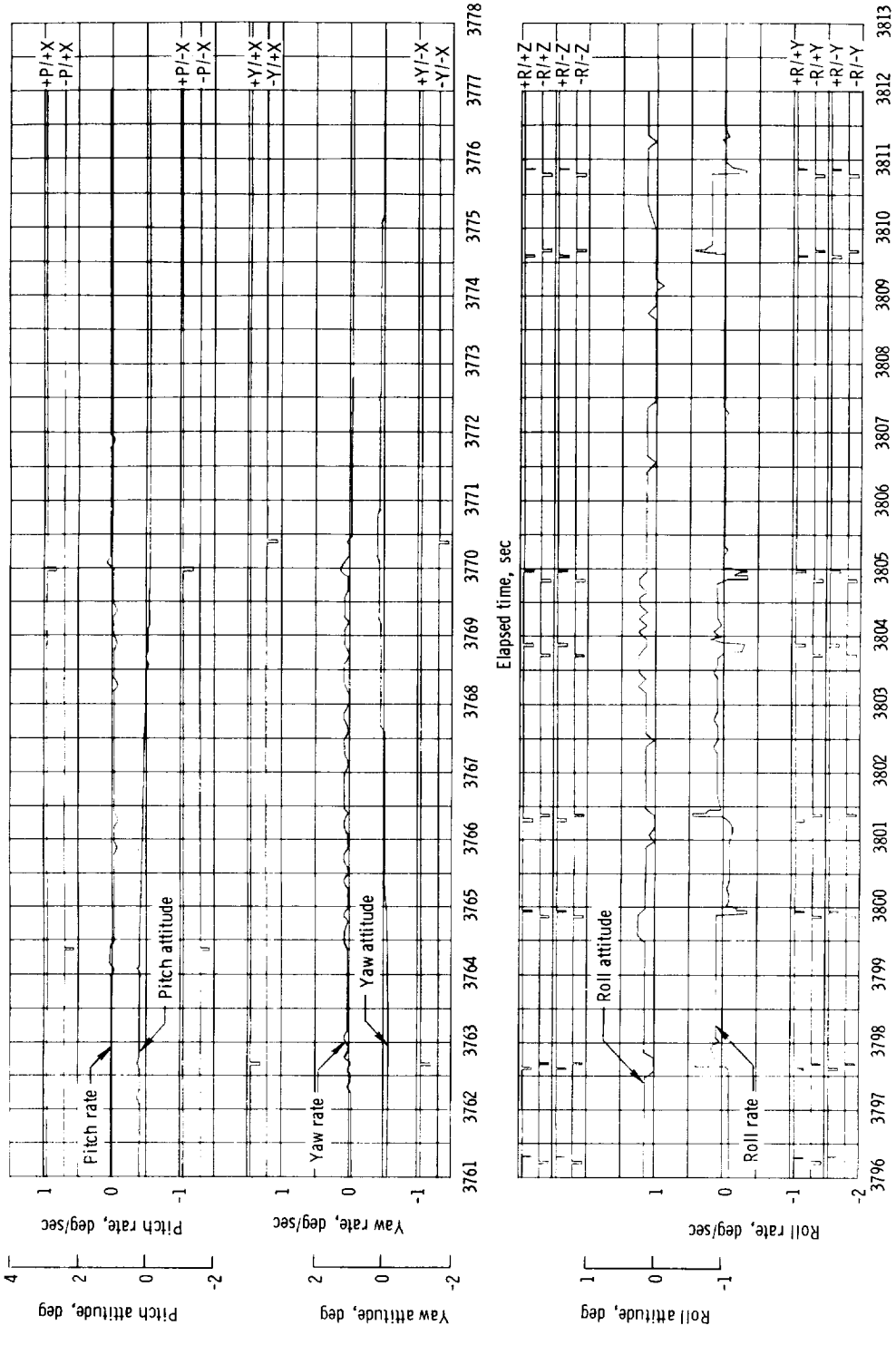

Figure 7.11-20. - Typical limit cycle, Mission AS-202.

NASA-S-66-10113

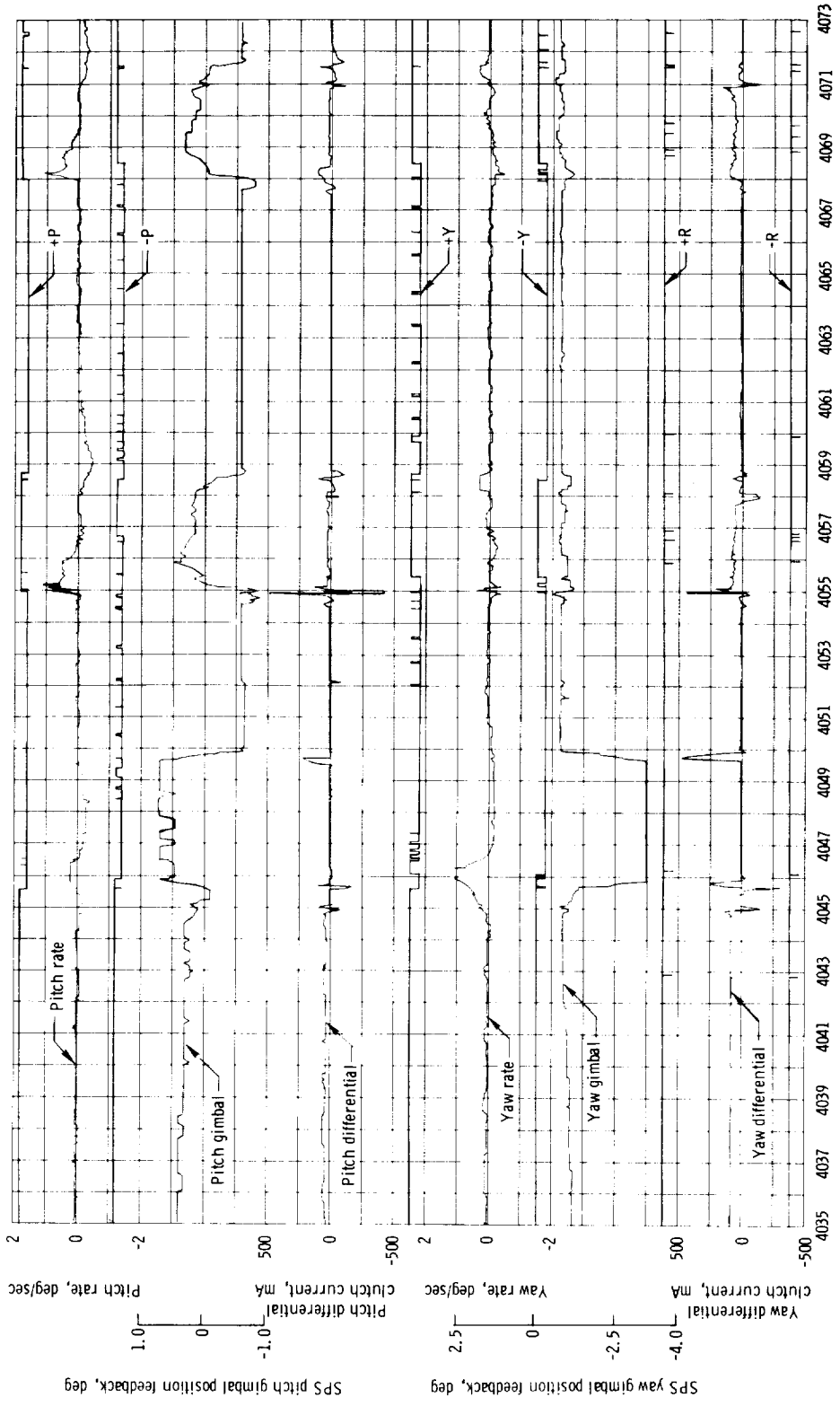

Figure 7.11-21.- Thrust vector control operation, 2nd, 3rd, and 4th burns, Mission AS-202.

NASA-S-66-10114

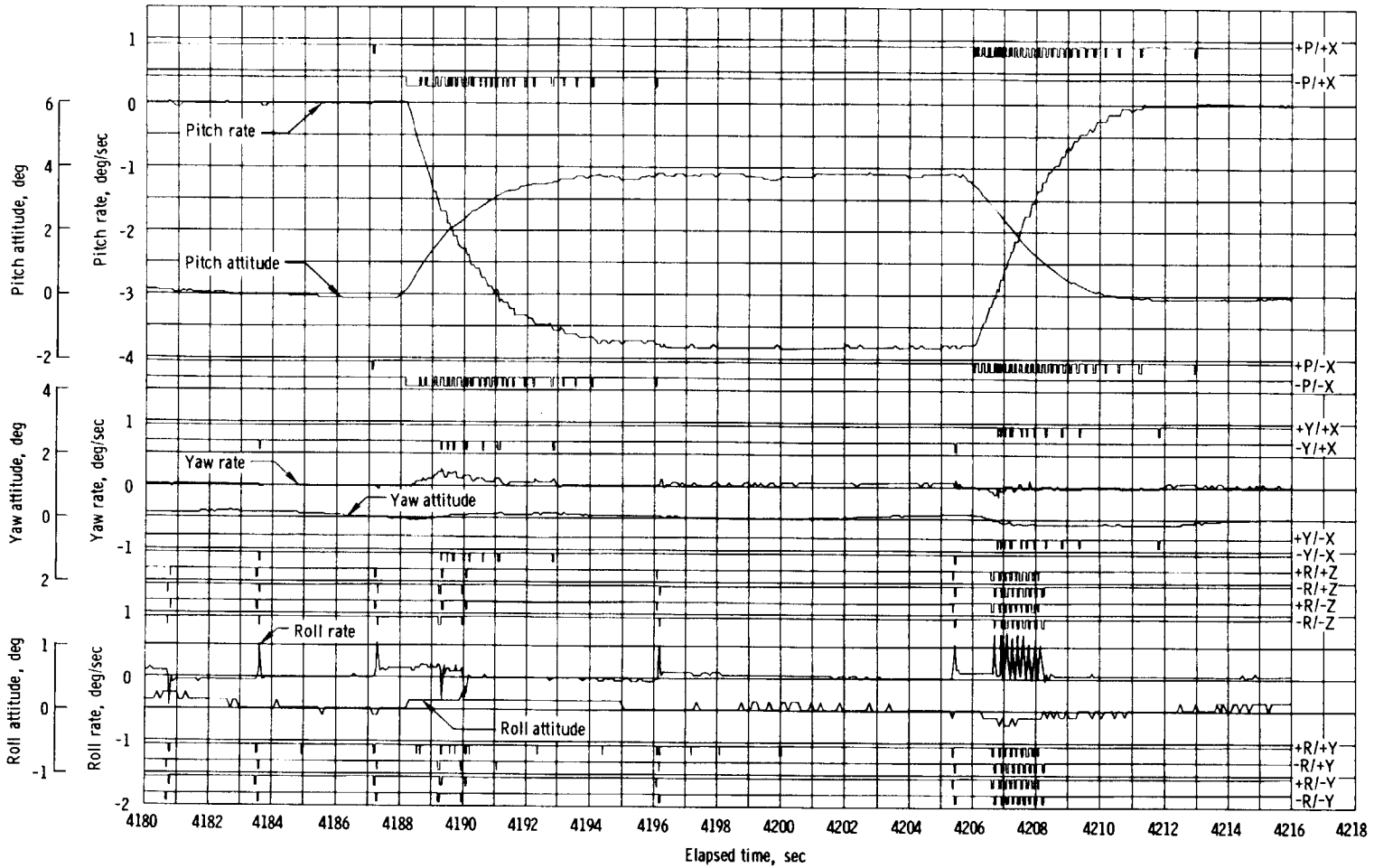

Figure 7.11-22.- Separation attitude maneuver of the command service module, Mission AS-202.

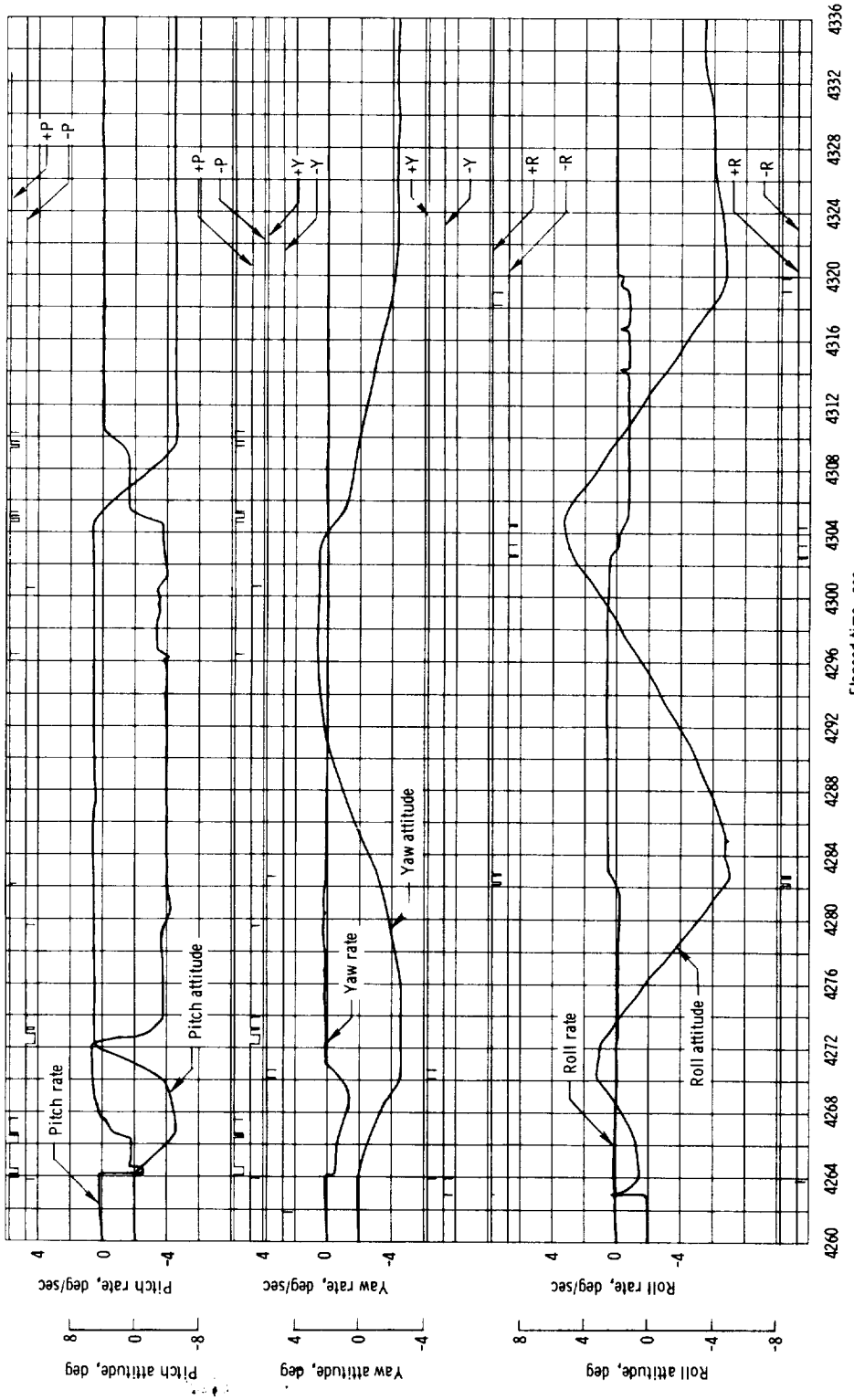

Figure 7.11-23.- Command module entry attitude maneuver, Mission AS-202.

NASA-S-66-10116

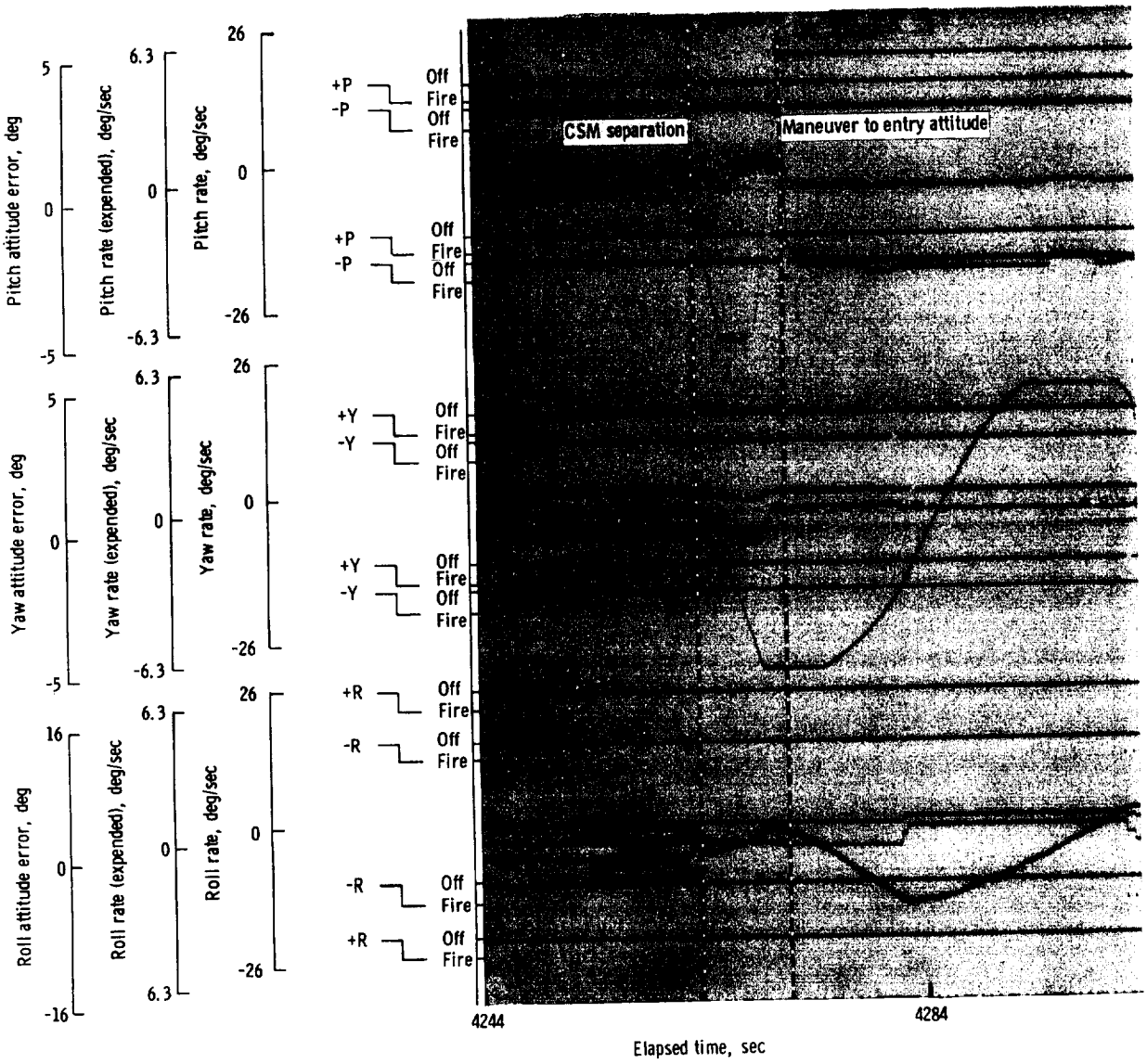

(a) 4244 to 4484 seconds.

Figure 7.11-24. - Reentry time history, Mission AS-202.

FOLDOUT FRAME 1

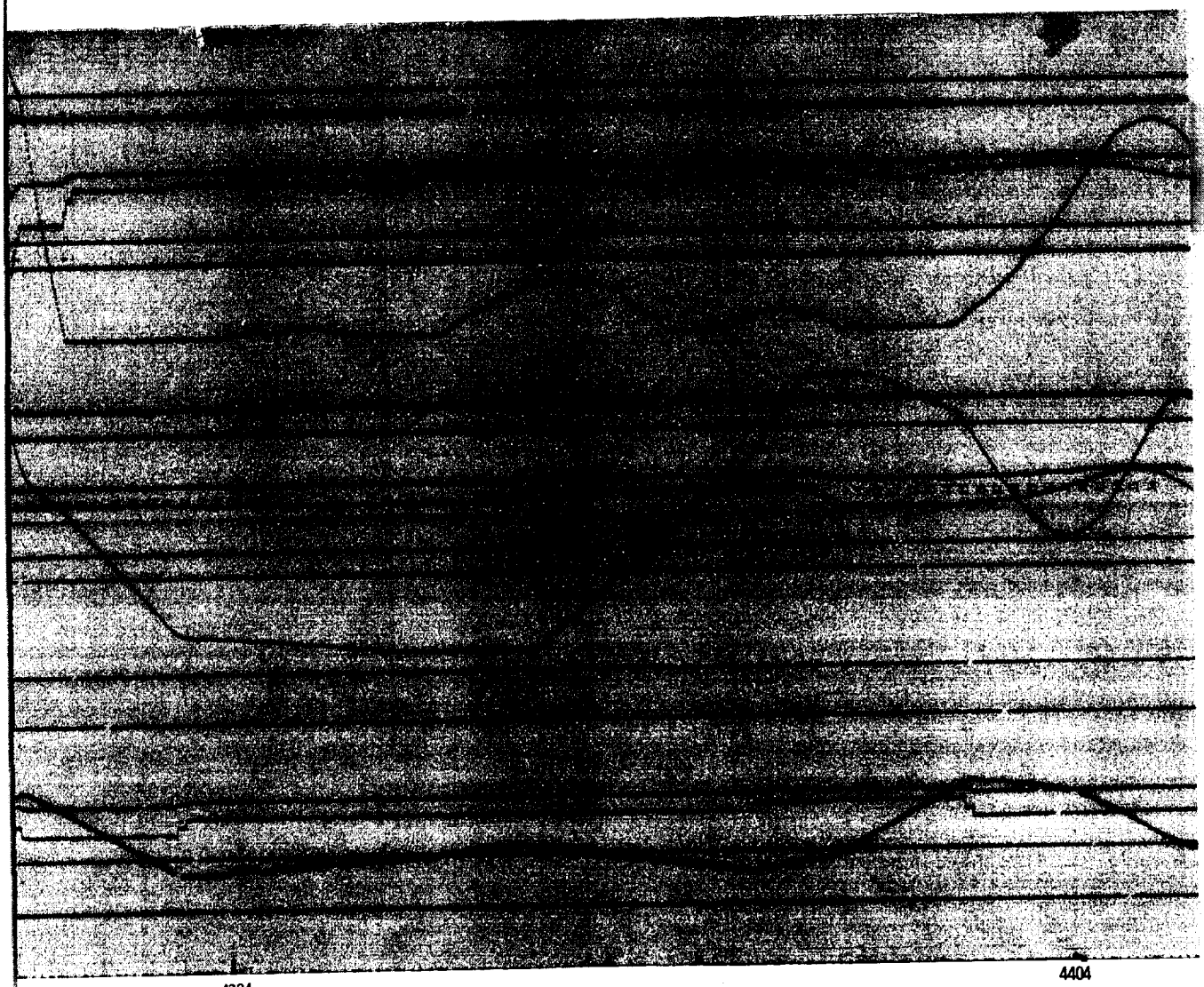

FOLDOUT FRAME 2

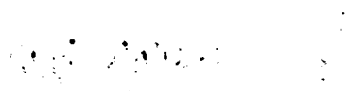

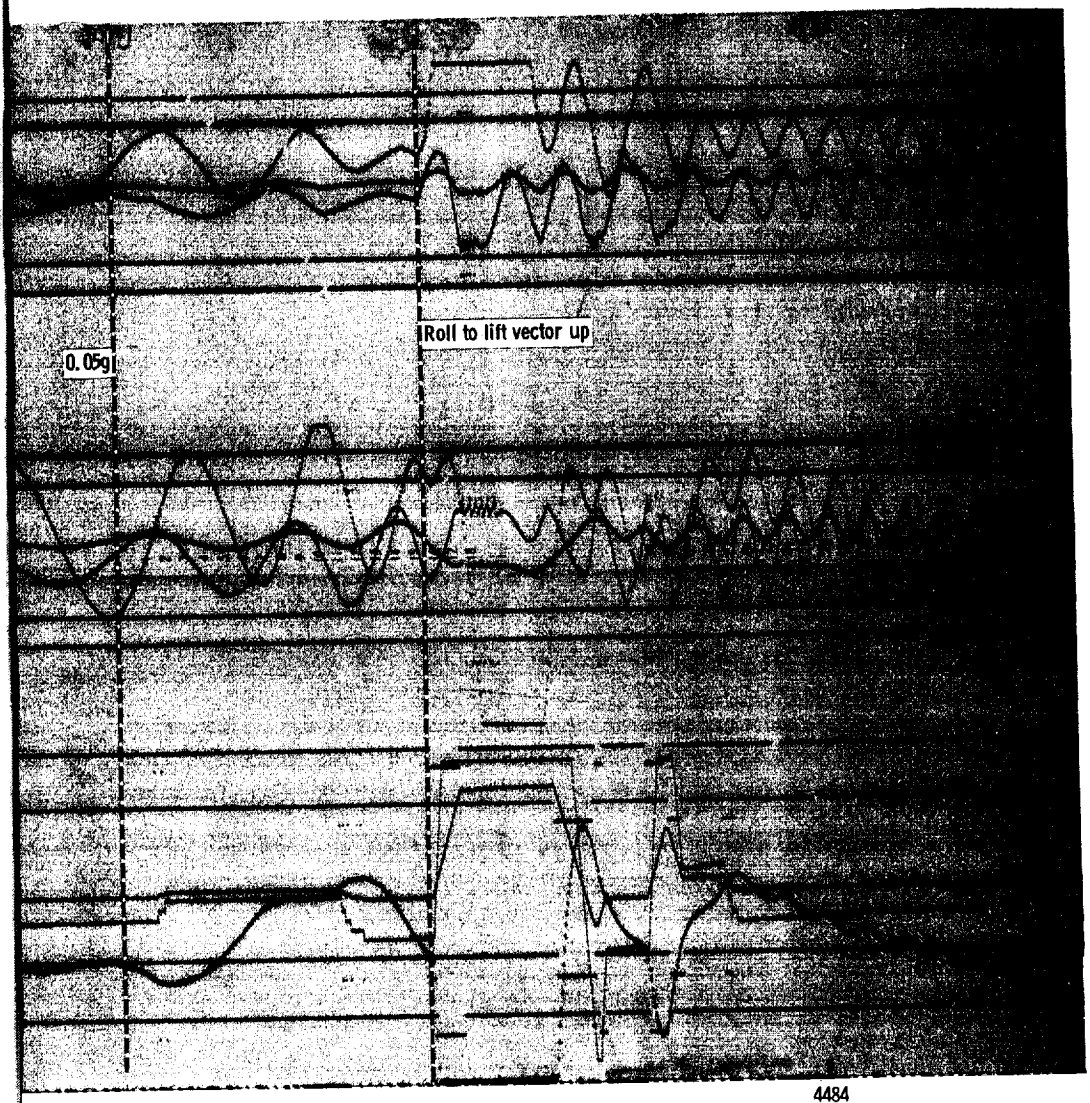

4484

FOLDOUT FRAME 3

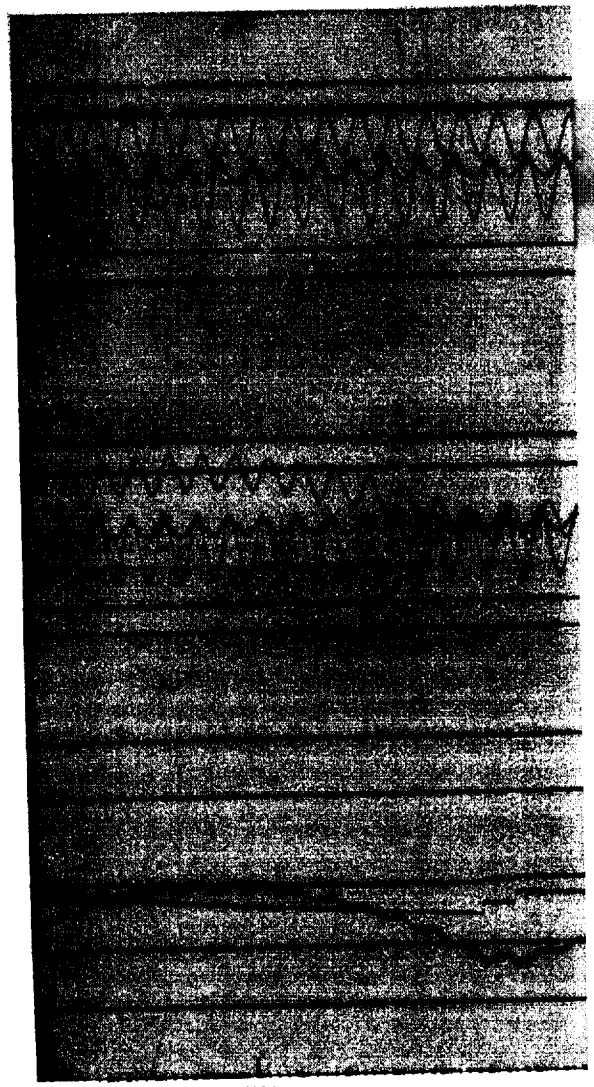

4524

FOLDOUT FRAME 1

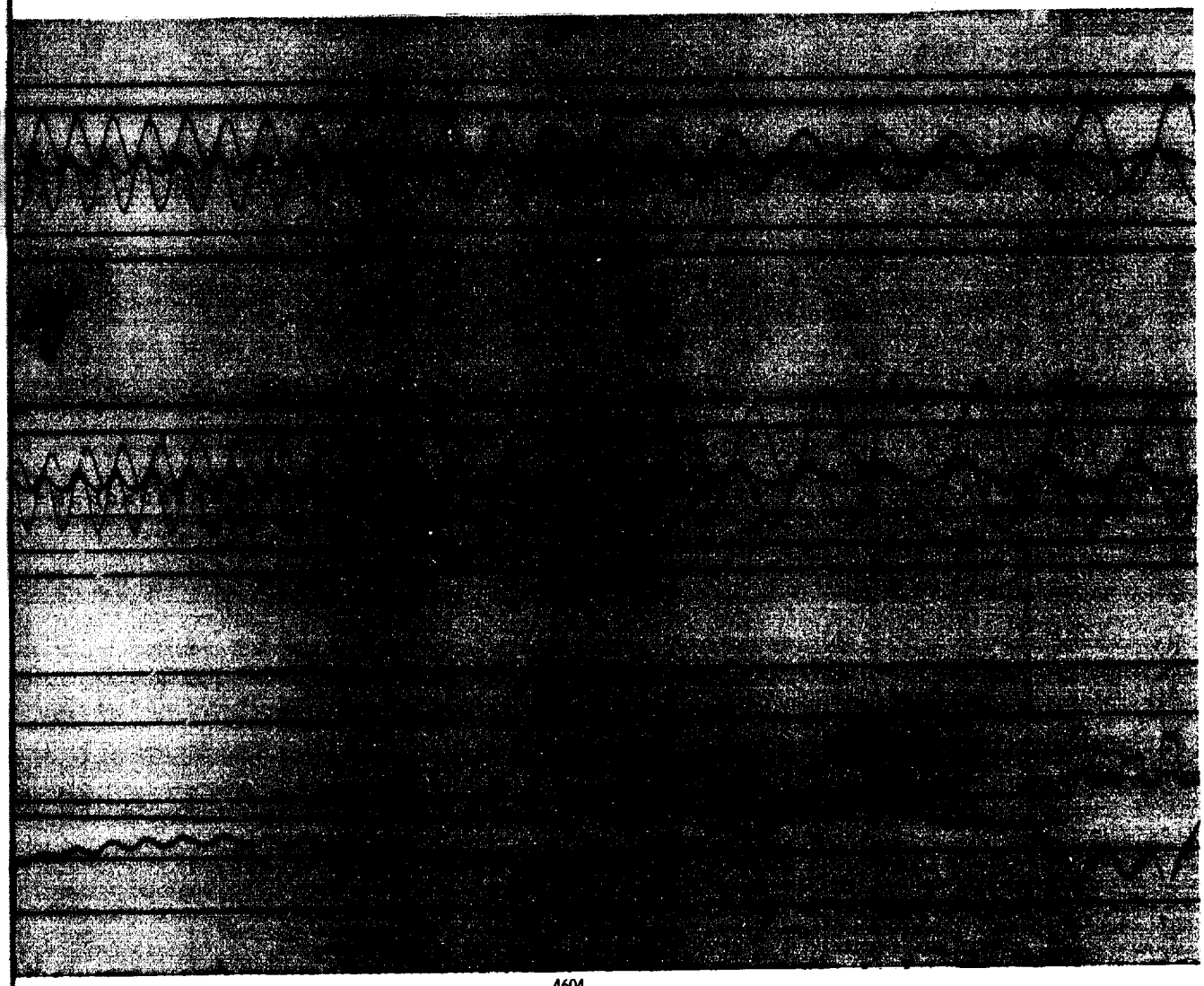

4604

FOLDOUT FRAME 2

NASA-S-66-10117

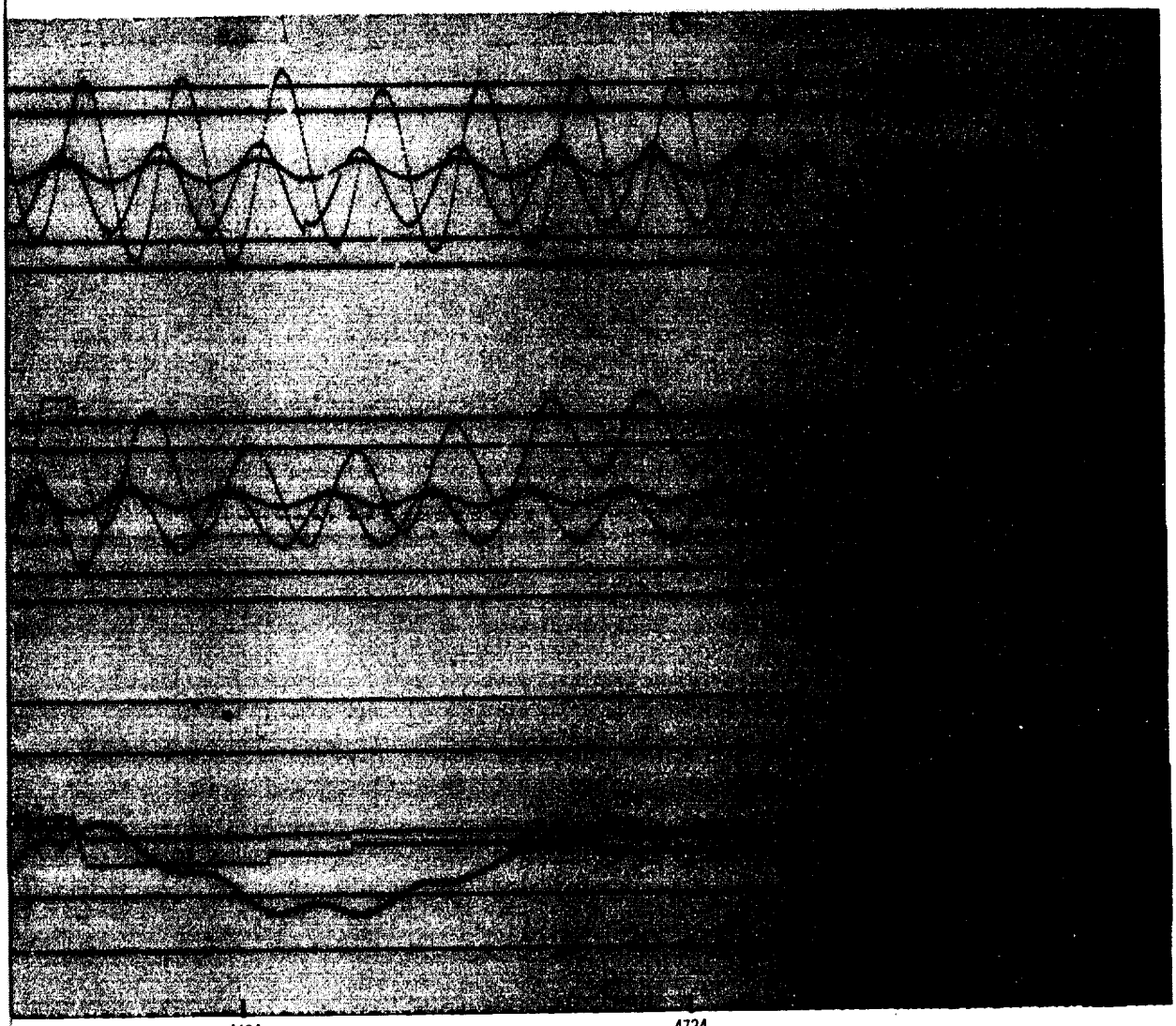

4684 4724

Elapsed time, sec

(b) 4484 to 4724 seconds.

Figure 7.11-24. - Continued.

FOLDOUT FRAME 3

NASA-S-66-10118

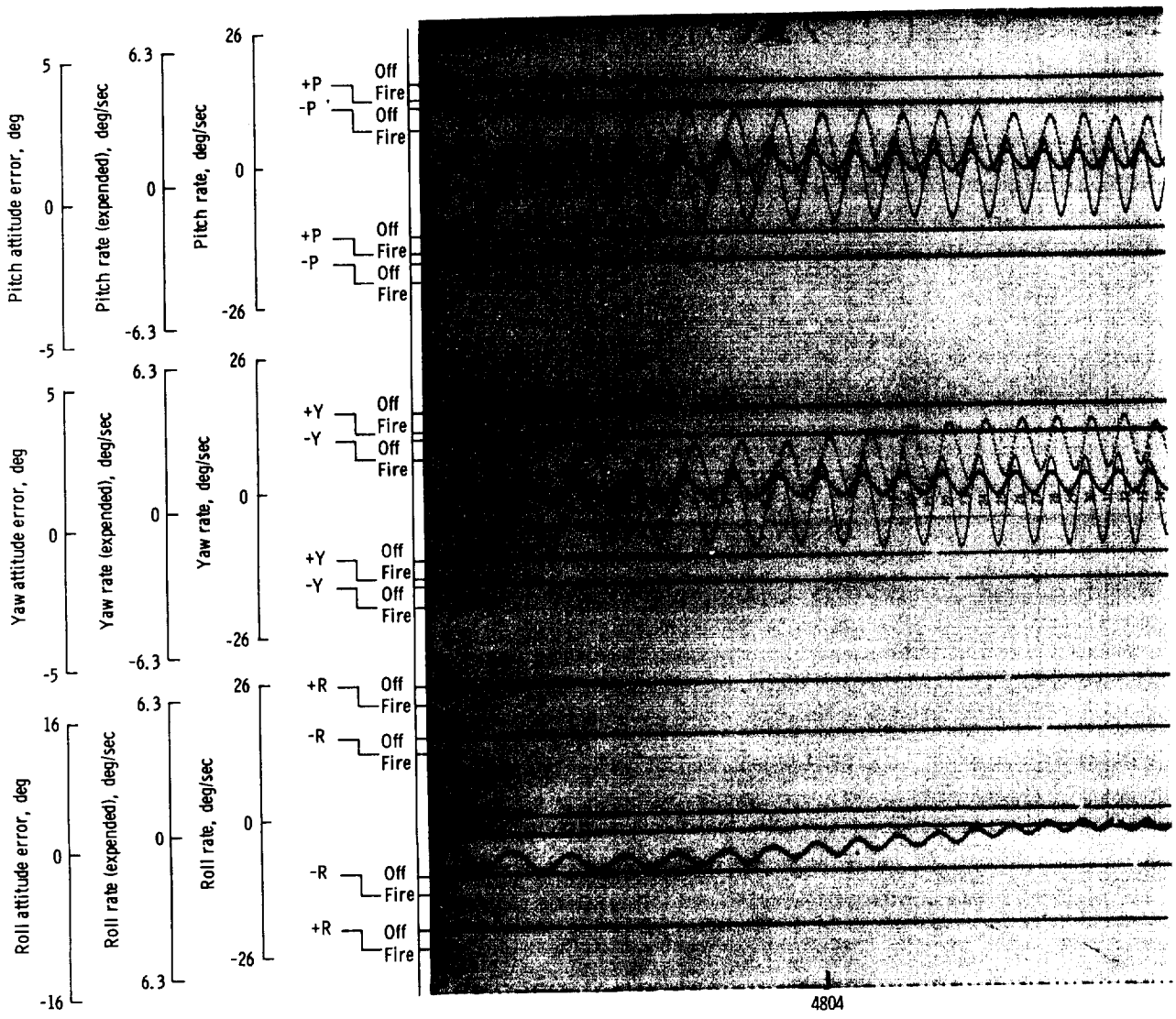

(c) 4724 to 5004 seconds.

Figure 7.11-24.- Continued.

FOLDOUT FRAME 1

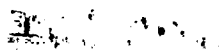

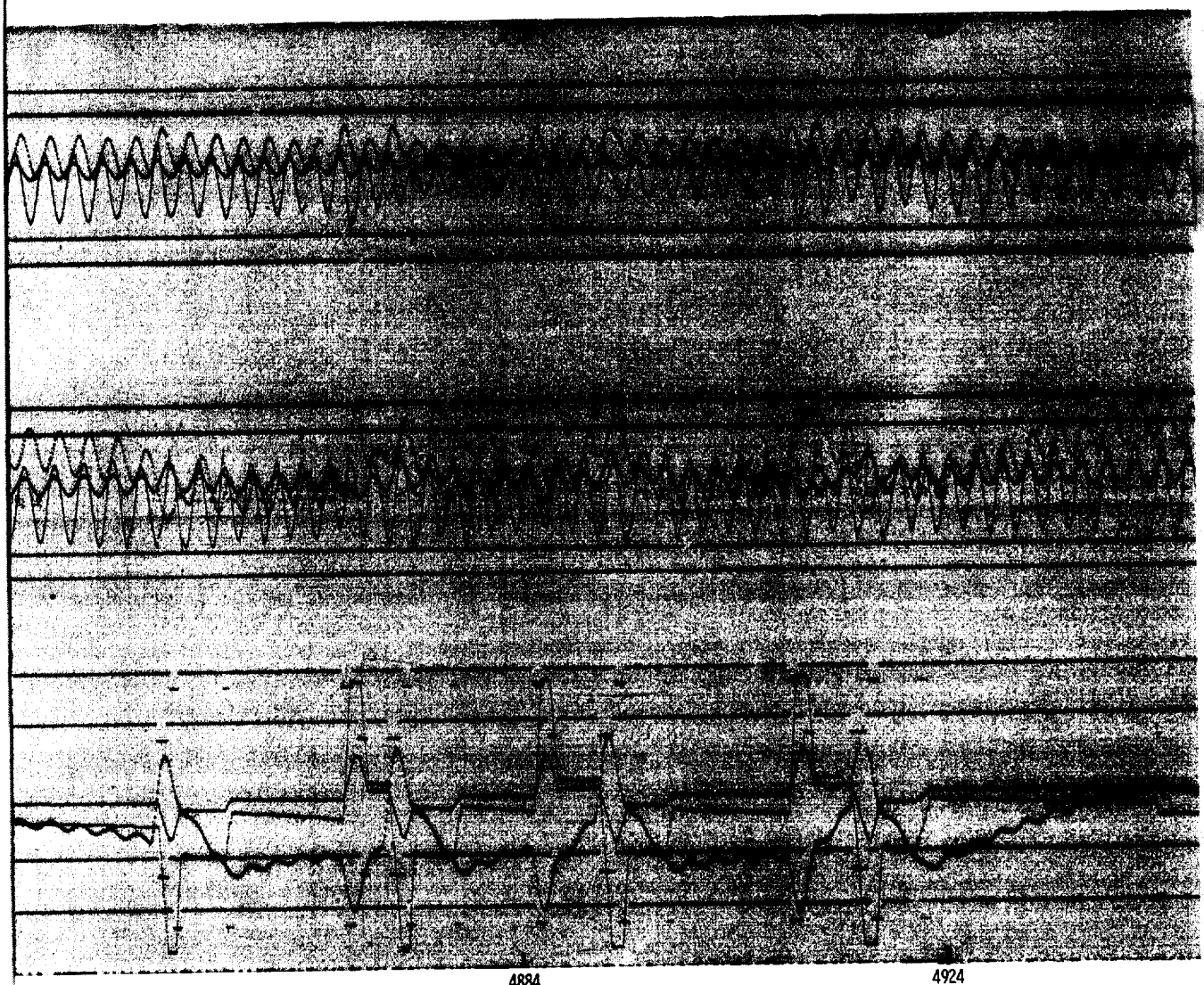

FOLDOUT FRAME 2

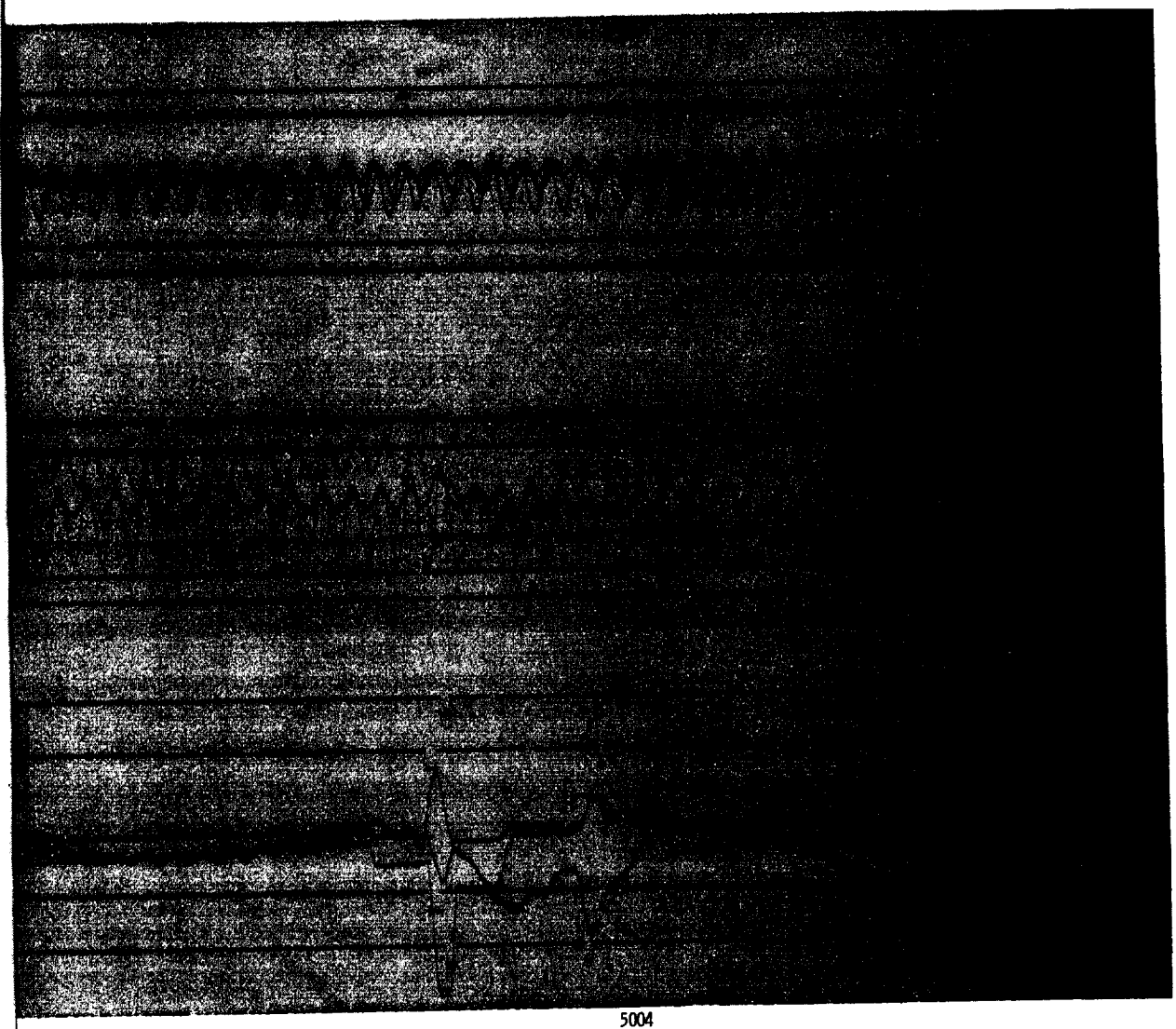

5004

FOLDOUT FRAME 3

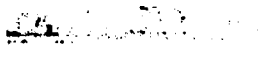

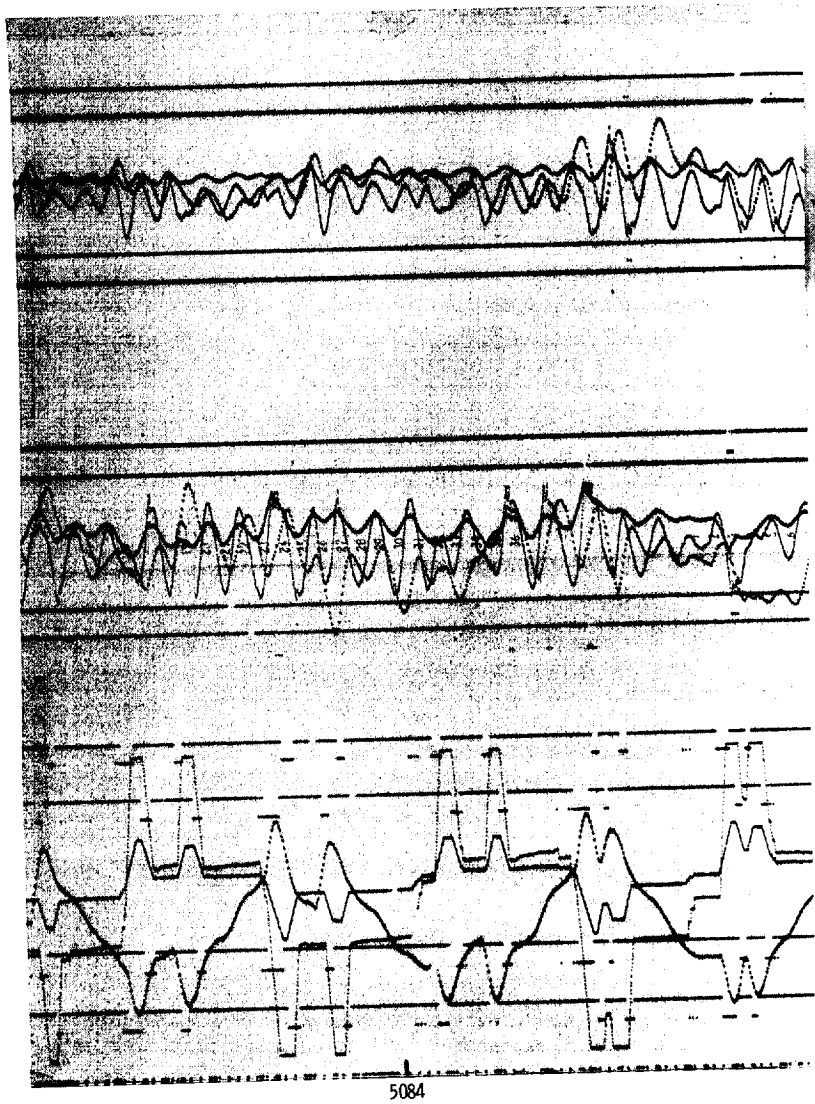

5084

FOLDOUT FRAME 1

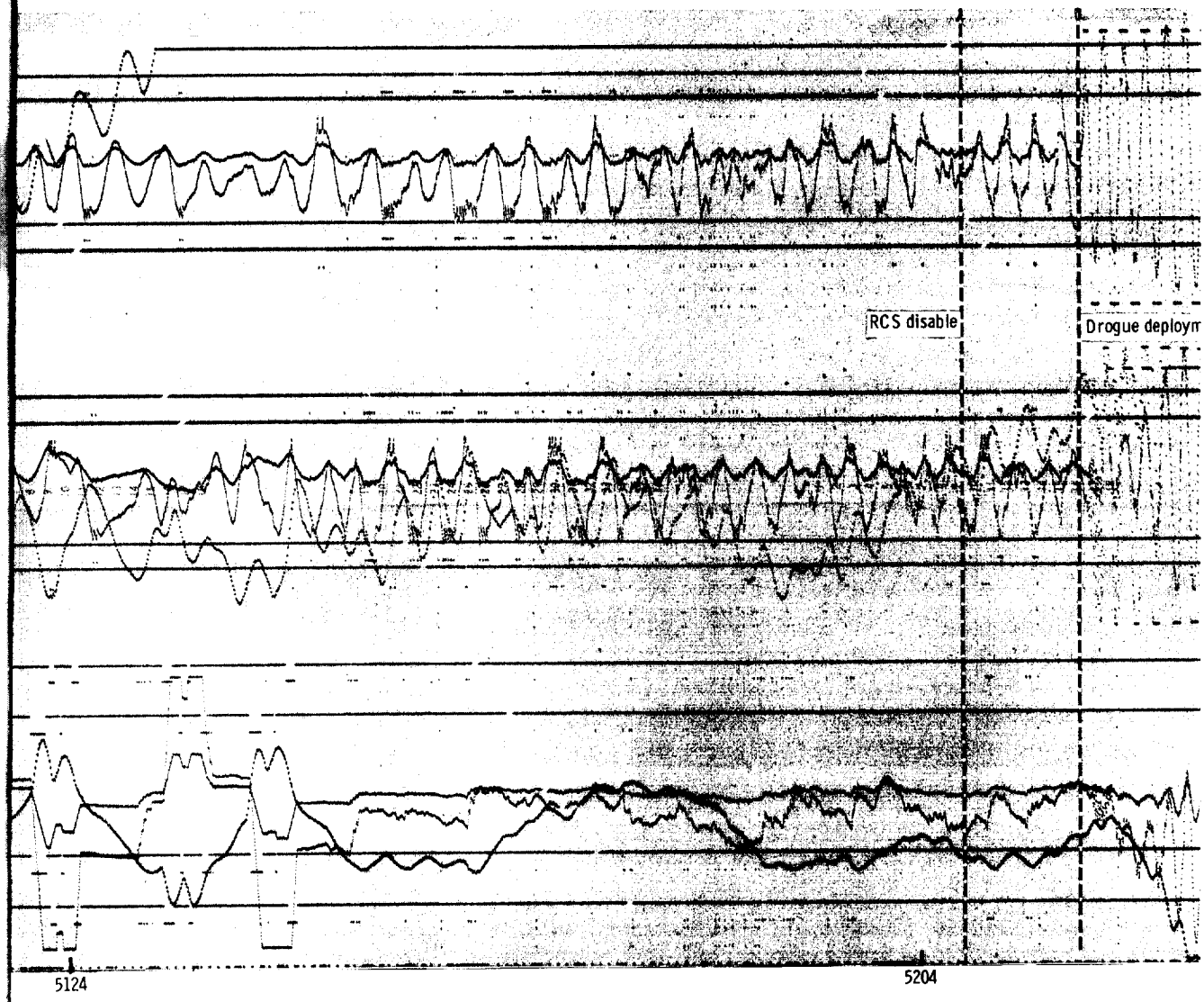

FOLDOUT FRAME 2

NASA-S-66-10119

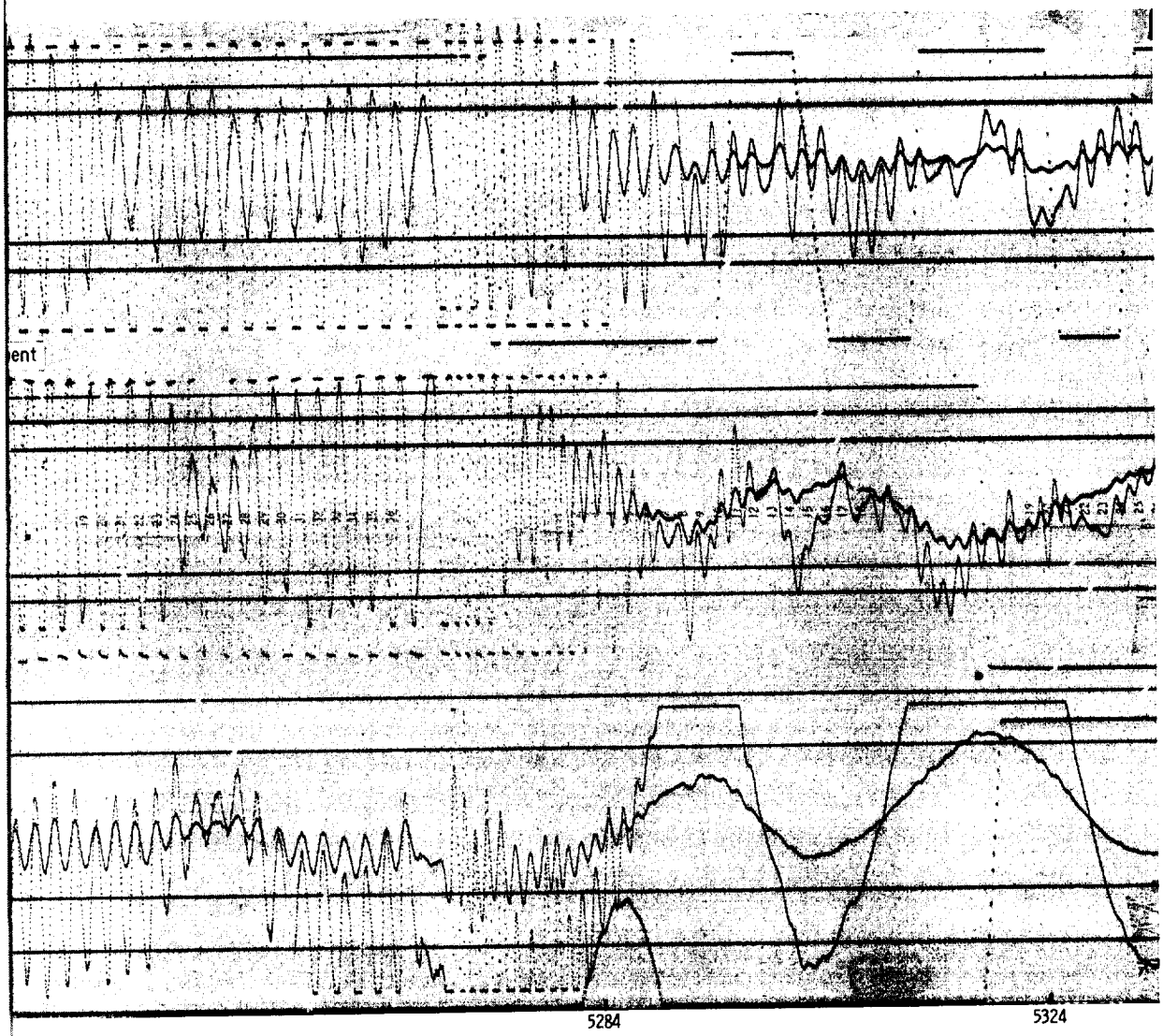

Elapsed time, sec

(d) 5004 to 5324 seconds.

Figure 7.11-24. - Concluded.

FOLDOUT FRAME 3

7.12 Electrical Power Subsystem

Description.- The electrical power subsystem (EPS) supplied, controlled, and distributed all electrical power in the spacecraft from lift-off through recovery. Three major differences existed between the EPS aboard spacecraft 011 and the Block I configuration:

(a) Three auxiliary batteries were installed in the (CM) to augment the fuel cells because of the additional instrumentation and MCP loads.

(b) The MCP performed part of the power switching that will be performed by the flight crew on manned missions.

(c) Only two fuel cell power plants were operative.

Main dc power was supplied by two fuel cell power plants augmented by three auxiliary batteries. Power was distributed through two redundant dc buses, A and B. Pyrotechnic devices were powered by two pyro batteries in the CM, and two additional batteries in the SM powered the SM jettison controller after CM/SM separation. Three-phase, 400 cps, ac power was provided by three inverters, powered from the dc buses, and distributed through two ac buses.

Prior to launch, the three auxiliary batteries were placed on the CM main dc buses A and B along with the two fuel cell power plants which fed these buses through the SM main buses A and B. During each of the SPS firings the entry batteries were also connected to the CM main dc buses A and B to insure an adequate voltage level during the application of the high gimbal motor starting load requirement. Just prior to CM/SM separation, the entry batteries were connected to the CM main buses. Approximately 20 seconds after main parachute deployment, entry battery C was connected to the postlanding bus; at impact, the three auxiliary batteries and entry batteries A and B were connected to the postlanding bus. Eleven seconds after impact, the three auxiliary and entry batteries were removed from the main buses to prevent unnecessary drain and to allow maximum recovery time.

The cryogenic storage subsystem provided gases to the spacecraft subsystems, hydrogen to the EPS, and oxygen to the ECS and EPS. The fluids were stored in four Dewar vessels located at sector I of the SM, two for oxygen and two for hydrogen (fig. 7.12-1). Pressure in the subsystem was maintained by heaters and uniform density was maintained by circulating fans. Oxygen was delivered at 900 $\pm$ 35 psia and hydrogen at 245 $\pm$ 15 psia.

The prime power units were bacon-type, chemical fuel cell power plants, each rated to produce up to 1.42 kW at 29 ± 2 volts dc, located in sector IV of the SM. Only two power plants were operating at launch. The third one, power plant number 2, had been rendered inoperative during checkout as a result of a checkout equipment wiring error. One fuel cell power plant is shown in figure 7.12-2 and a flow diagram is shown in figure 7.12-3. A fuel cell power plant consists of a power conversion section, a reactant control subsystem, a waste heat and water removal subsystem, and instrumentation. The conversion section is housed in a titanium pressurized tank which is positioned on three shock mounts in the support cone. The tank is insulated with glass matting and aluminum foil. The accessory section rests on top of the power section and support cone, and consists of a nitrogen pressurization subsystem, three regulators, motor drive pumps, a secondary (glycol) loop, components of the primary (hydrogen) regenerative loop, and the necessary plumbing. The 31 cells, approximately 1 volt each, are stacked in series inside the pressure jacket and held together by torsion tie rods. Oxygen and hydrogen are distributed through individual lines, feeding from the intake manifolds, to each of the 31 cells. Regulators reduce the gas supply pressure to the required operating pressure of 53 psia for nitrogen, 64 psia for oxygen, and 61.5 psia for hydrogen.

Performance.- The electrical power distribution subsystem operation was nominal throughout the flight. All test objectives were met. All power switching occurred as planned and programmed. Main buses A and B were maintained essentially constant except during the periods of highest current transients during SPS motor gimbaling. Figure 7.12-4 shows the main bus A dc voltage level between T+240 seconds and T+500 seconds which is representative of the entire flight except for peak power periods. Figure 7.12-5 shows dc main bus A volts during the period of T+597 seconds to T+601 seconds, and figure 7.12-6 shows total spacecraft current during the same time period. It is noted that high current peaks caused less than 1-volt variation from the nominal 29 volts. This is representative of the subsystem stability during peak power periods. The ac voltage exhibited similar stability throughout the flight. Figure 7.12-7 shows the voltage level of bus 1, phase A and B, which is typical of all ac voltages throughout the flight.

Current distribution between the fuel cells and batteries followed the expected ratios. The percentage of total load furnished by the fuel cells varied from approximately 60 percent during nominal periods to approximately 45 percent during peak load periods.

It was noted that entry battery A maintained a consistently higher case temperature than the other two entry batteries. This appeared

normal in view of the fact that battery A was located next to Inverter 1 whose operating temperature was approximately 130° F.

The cryogenic subsystem performance was satisfactory throughout the flight. Data show that pressures, temperatures, quantity, and flow rates were maintained nominal. Reactant flows compared with fuel cell current changes showed the expected response in rates and time.

Fuel cell power plant electrical performance was normal; however, EPS related test objectives were only partially met since condenser exit temperatures of power plants 1 and 3 were out of regulation during the later portion of the flight. Figure 7.12-8 shows related parameters during this period. It is noted that the condenser exit temperature of power plant 3 leveled off at 199° F for the last 60 seconds of flight. Power plant no. 1 shows a similar loss of temperature control though it leveled off at 173.5° F. This anomaly did not adversely affect the subsystem's primary objective to supply the spacecraft with electrical power. All bus voltages were within prescribed limits, and load sharing between the fuel cells and batteries was satisfactory. The high condenser exit temperature was evidence that the cooling capacity of the secondary cooling loop was effectively reduced. Failure to maintain thermal control of the fuel cells on space flights with a duration similar to spacecraft 012 would adversely affect the fuel cell power-producing capability and shorten its life.

A considerable amount of heat was generated by the electro-chemical reaction in the fuel cell module. The heat not used for regenerative purposes, or waste heat, was radiated into space by the secondary, or coolant loop. The components of this loop consisted of an accumulator, the coolant regenerator and sensor controlled bypass valve, the coolant pump, the condenser (common to the hydrogen loop), the oxygen and hydrogen preheaters, and the space radiators. An analysis of the data showed that variation beyond the nominal operating range (155° to 165° F) occurred for power plant no. 1 for the last 9 minutes of flight and for power plant no. 3 the last 50 minutes of flight.

The high condenser exit temperature indicated a reduced cooling capacity of the secondary loop which could have resulted from one of the following: (a) reduced glycol flow resulting from a plugged, or partially plugged, coolant pump filter, (b) an imcomplete coolant loop fill, or (c) reduced effectiveness of the condenser caused by zero g environment. The first two conditions have been evidenced in test programs. Condition (a) occurred at the subcontractor's facitity during water glycol inhibitor tests. By-products (contaminants), formed in the coolant (not the type used in the spacecraft) during special tests

plugged the filters, resulting in a high condenser exit temperature. A flow check of pump filters from spacecraft 001 and spacecraft 008 did not reveal plugging. They did, however, operate in a 1g environment and reduced vibration during these tests. Condition (b) occurred at White Sand Test Facility (WSTF) and at MSC, and resulted in both high and low condenser exit temperatures. Air was noted in the lines during a bleeding process. It has been shown in tests at MSC that bleeding the coolant lines does not remove all entrapped air in the system and that a pressure-volume (PV) technique is an effective method for checking for the presence of gas in the water glycol loop. In reference to condition (c), there is no data on the performance of heat exchangers similar to the condenser in a zero g environment. However, Lewis Research Center has conducted tests on an Apollo type condenser and was unable to find any gravity related changes in performance during 1g multiaxis testing. ECS flight experience likewise shows no solely gravity related performance change in condensing heat exchangers.

Differences between the modified Block II pump configuration to be used on spacecraft 012 and the Block I configuration used on spacecraft 011 are indicated in table 7.12-I. Bench tests accomplished by the subcontractor show that the Block I pump used on spacecraft 011 is more susceptible to cavitation caused by entrapped gas than the Block II pump used on spacecraft 012 or subsequent spacecraft. In addition, N_2 slug tests on the spacecraft 012 type pump show the minimum volume of gas required to cause cavitation in a one g environment in random orientation at 53 psia and 120° F was determined to be 10 cubic centimeters.

Test data from the reservicing of the coolant loop on spacecraft 008 at MSC, with vacuum fill and a PV fill check technique, are being used to determine criteria for a good fill. Since the zero g environment aggravates this problem, the final allowable gas volume criteria to be established will be less than determined in ground test. Spacecraft 012 is to be reserviced using a vacuum fill, deaerated water glycol, and a PV fill check to the criteria to be established.

TABLE 7.12-I.- COMPARISON OF WATER GLYCOL COOLANT PUMPS

FOR MISSIONS AS-202 AND AS-204

	Spacecraft 011	Spacecraft 012
Type of pump	Vane	Gear[a]
Pump rotor clearance, in., min.	0.0005	0.0020
Pump filter active area, sq in.	0.73	6.60
Rating:		
Nominal, μ	40	75
Absolute, μ	60	100

[a]Block II pump retrofitted to Block I flow characteristics.

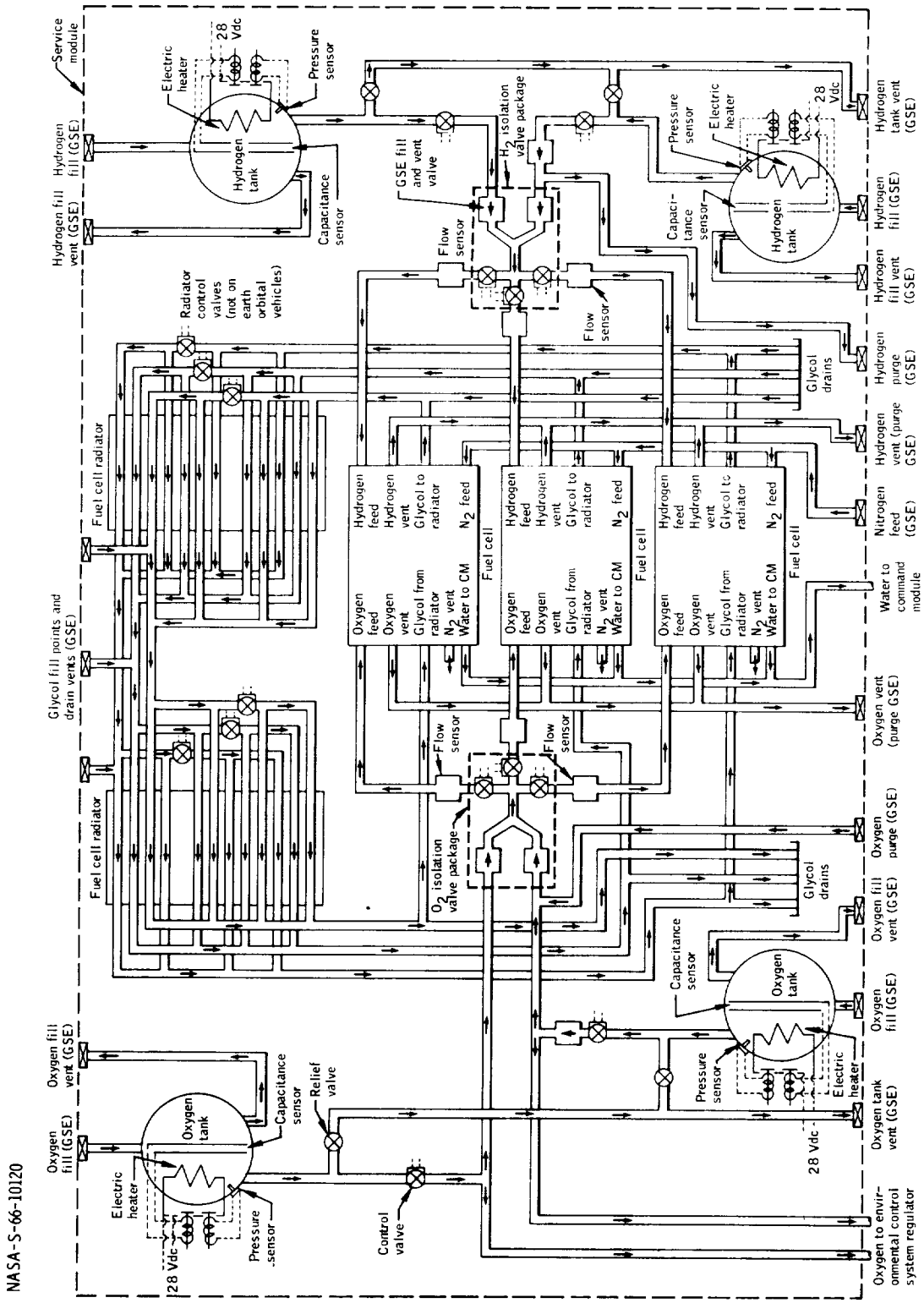

Figure 7.12-1. - CSM cryogenic storage schematic, Mission AS-202.

NASA-S-66-10121

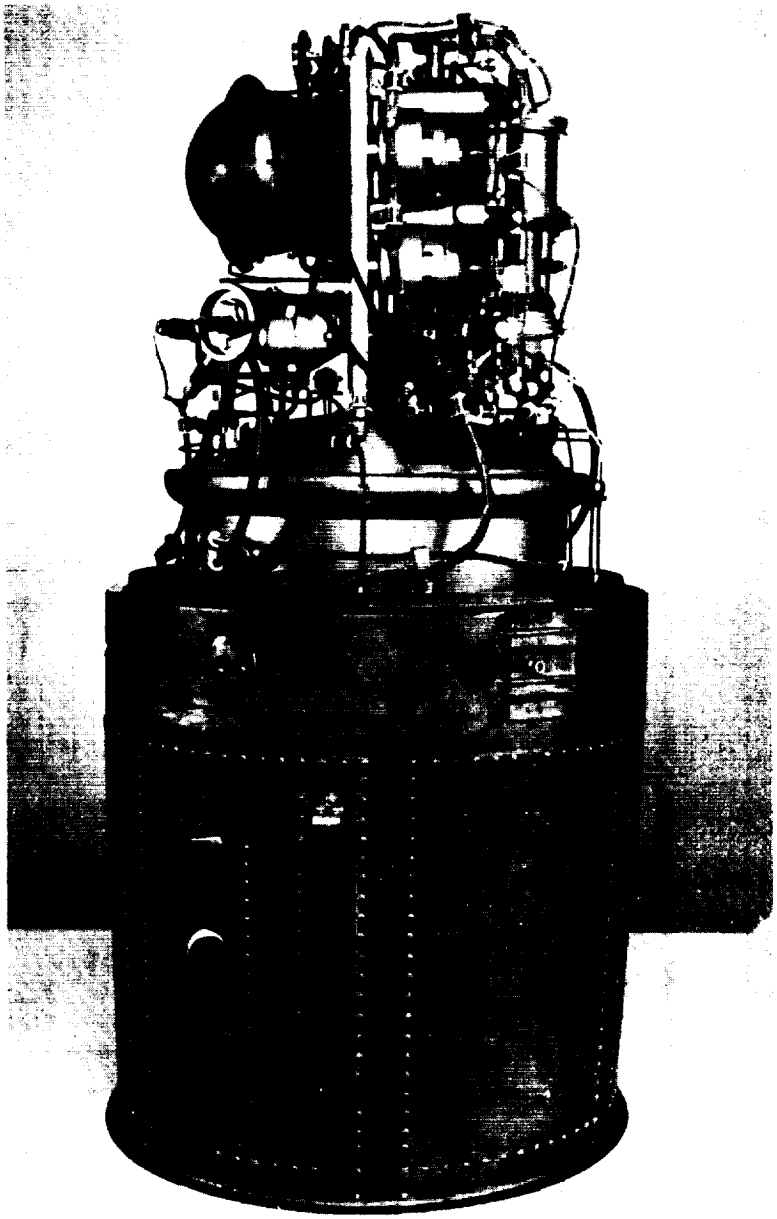

Figure 7.12-2.- Fuel cell power plant, Mission AS-202.

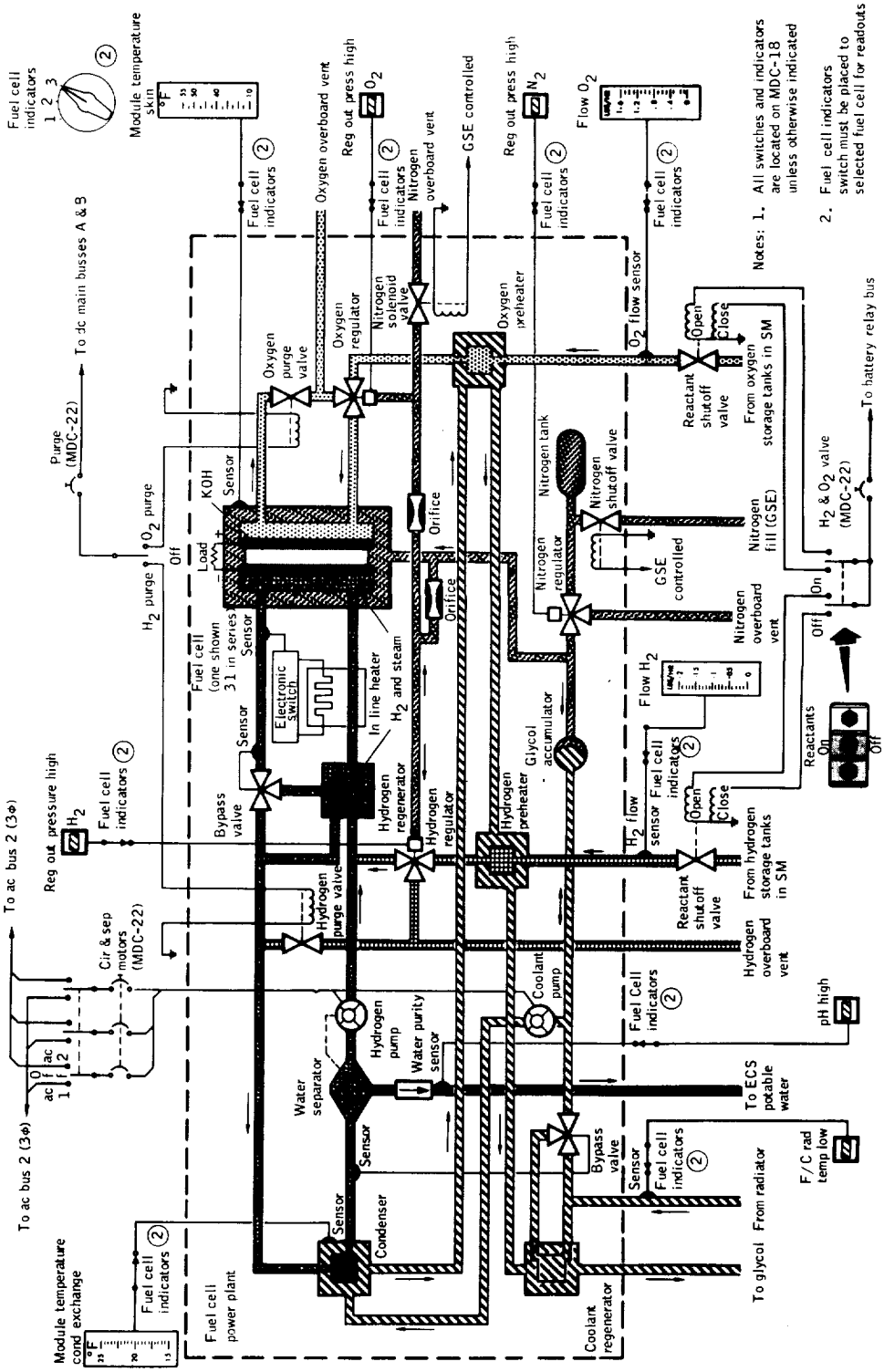

Figure 7.12-3. - Fuel cell power plant flow diagram, Mission AS-202.

NASA-S-66-10122

Figure 7.12-4.- Main bus A dc voltage from T+240 to T+500 seconds, Mission AS-202.

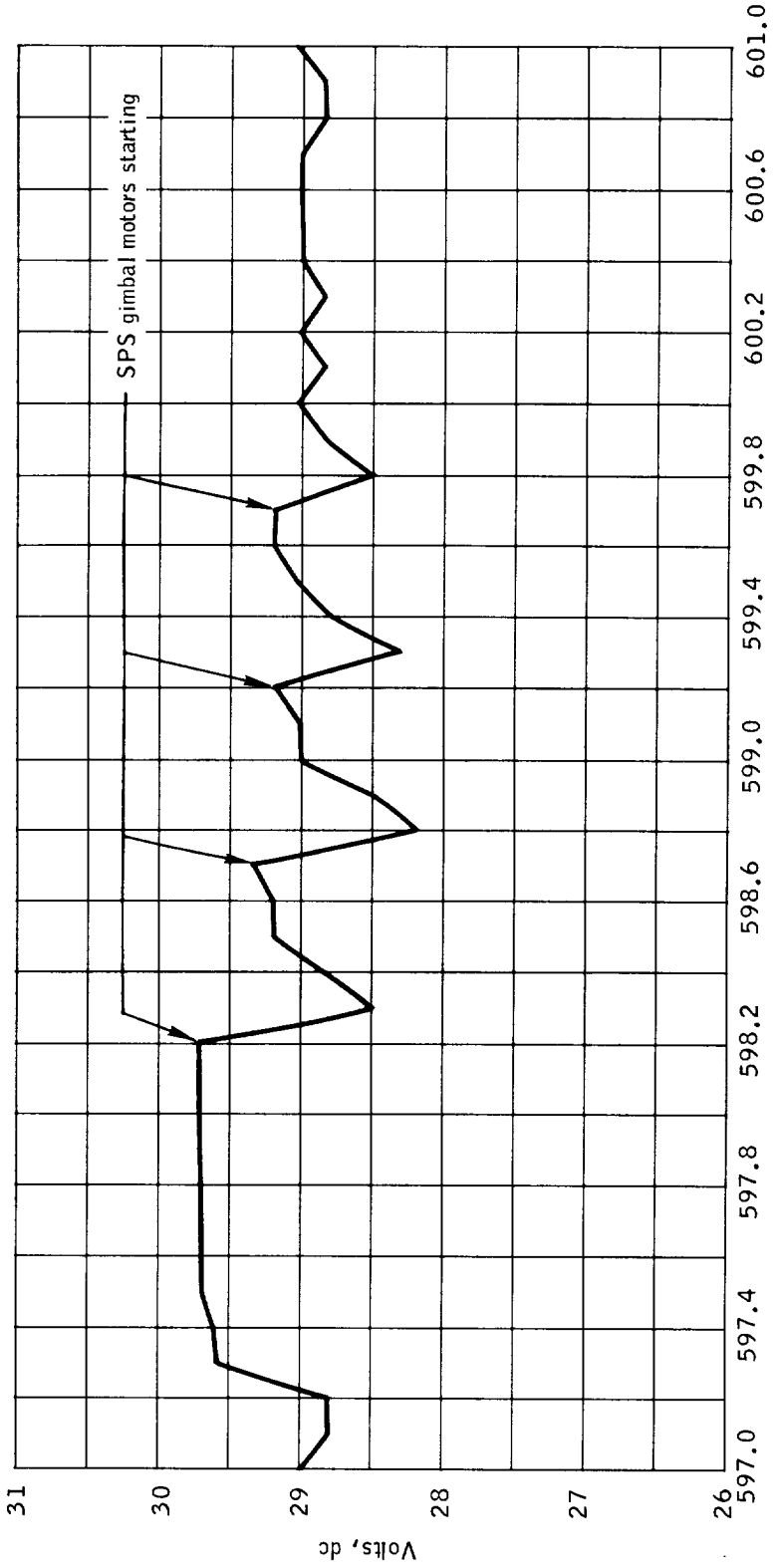

NASA-S-66-10124

Figure 7.12-5.- Main bus A dc voltage from T+597 to T+601 seconds, Mission AS-202.

NASA-S-66-10125

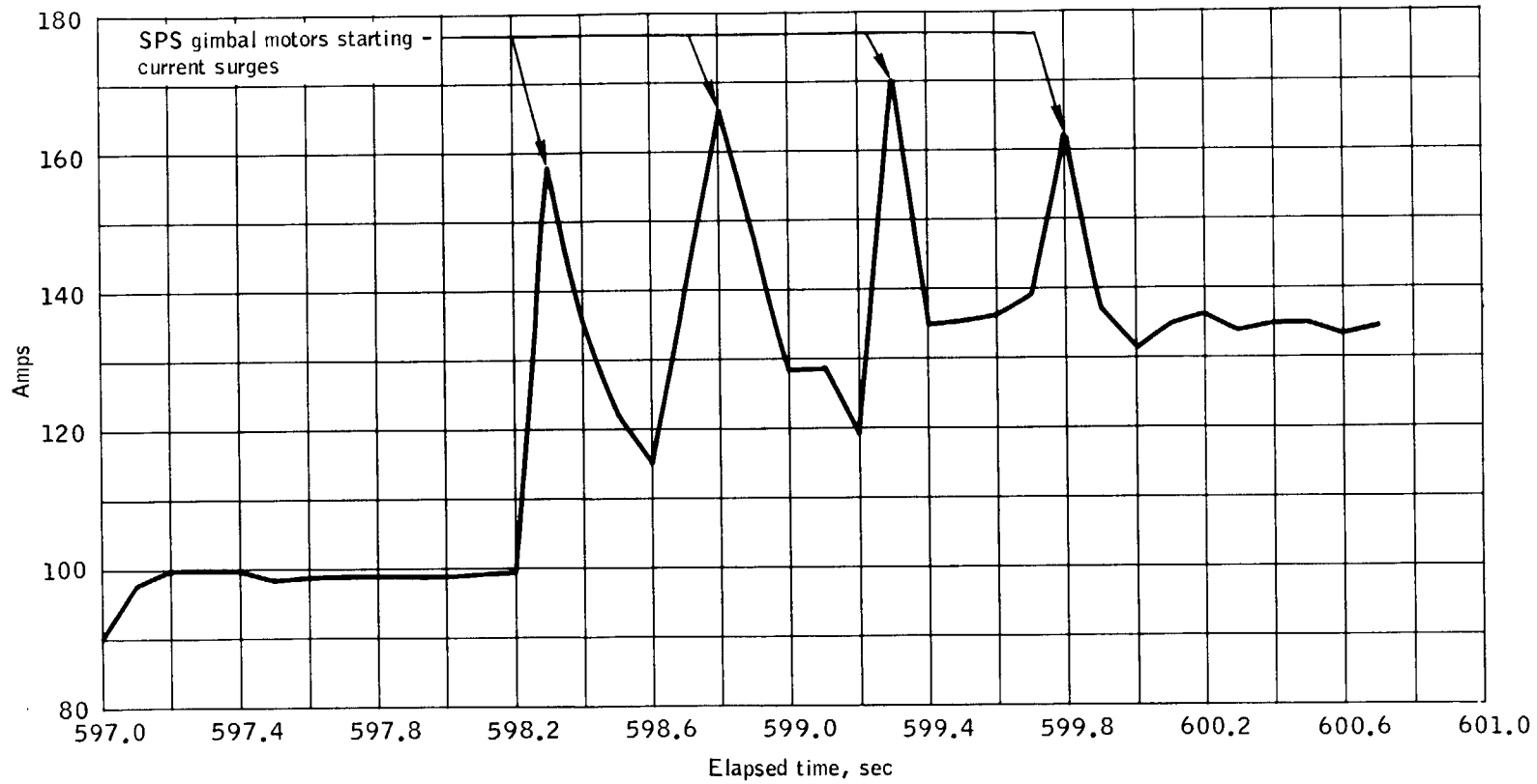

Figure 7.12-6.- Total spacecraft dc current during the period from T+597 to T+601 seconds, Mission AS-202.

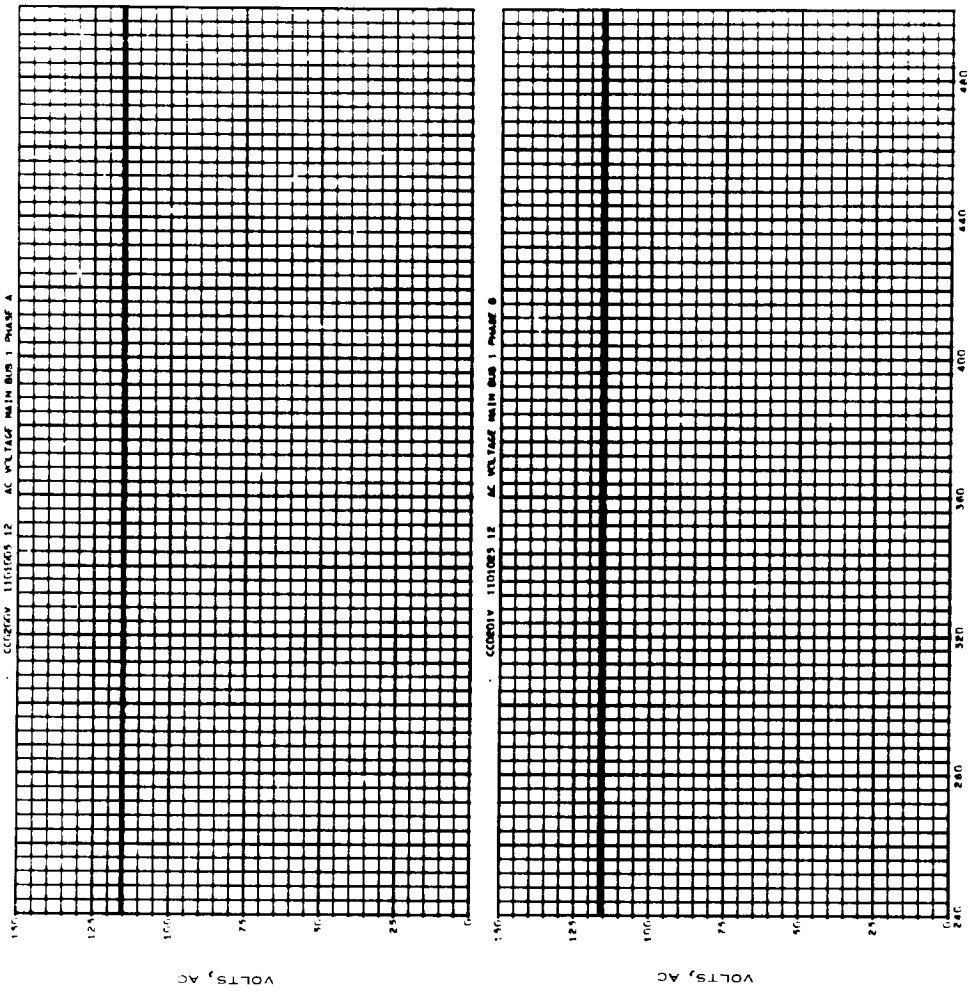

NASA-S-66-10126

Figure 7.12-7.- Main bus 1 ac voltages, phase A and B from T+240 to T+500 seconds, Mission AS-202.

NASA-S-66-10127

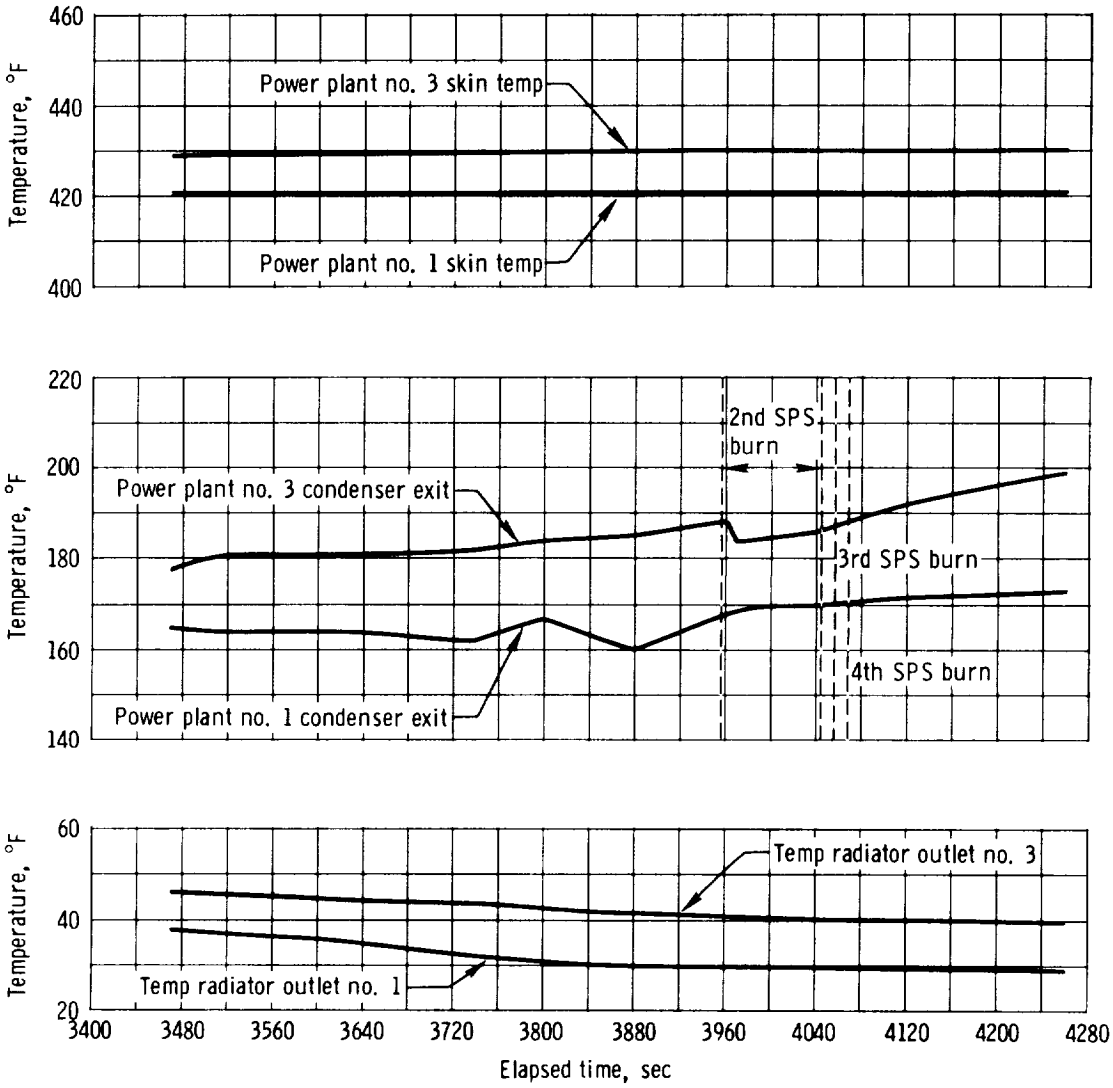

Figure 7.12-8. - Fuel cell power plant parameters, T+3460 seconds to CSM separation, Mission AS-202.

7.13 Sequential Subsystem

Description.- The sequential events control subsystem (SECS) aboard spacecraft 011 consisted of a master events sequence controller (MESC), service module jettison controller (SMJC), earth landing sequence controller (ELSC), reaction control subsystem controller (RCSC), and pyro continuity verification box (PCVB). SM batteries powered the SMJC while all other controllers received power from batteries in the CM. The Block I PCVB was the only controller not previously flight tested on spacecraft 009 (Mission AS-201).

The MCP automated the SECS controls normally operated manually by the flight crew.

The MESC controlled the logic power, pyrotechnic power, and timing functions required to initiate and terminate events associated with ascent and separation. Transfer of the RCS electrical control from the SM to the CM during CM/SM separation and control of the CM RCS fuel and oxidizer depletion burn and purge was provided by the RCSC. The SMJC programmed the SM maneuvers required to minimize the probability of recontact of the two modules after separation. Events associated with drogue parachute deployment and release and pilot parachute deployment were controlled by the ELSC and PCVB; main parachute disconnect was initiated by the impact switch in the MCP. Figure 7.13-1 shows the SECS together with major related spacecraft items.

Performance.- The SECS functioned satisfactorily throughout the flight, and the related test objectives were met. See table 2.0-I for a list of significant flight events with planned and actual times. Entry and pyro batteries maintained logic and pyro bus voltages nominal throughout the flight. Telemetry indication of main parachute disconnect at impact, CE0321X and CE0322X, was not obtained though parachute disconnect did occur. This was caused by the fact that logic bus power was commanded off by the MCP, as programmed, approximately 35 to 40 milliseconds after parachute disconnect occurred. Since the signal sampling rate was once each 100 milliseconds, the indication of the event was lost.

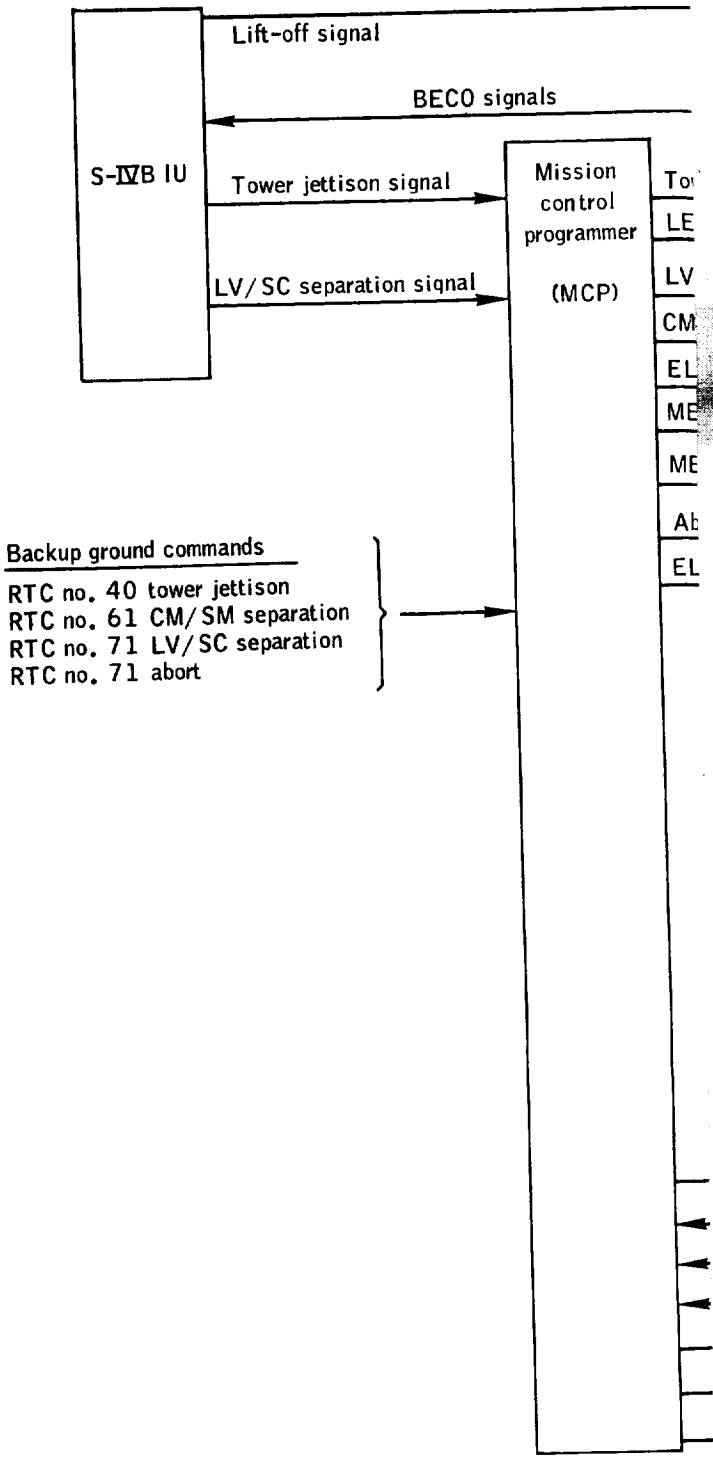

FOLDOUT FRAME

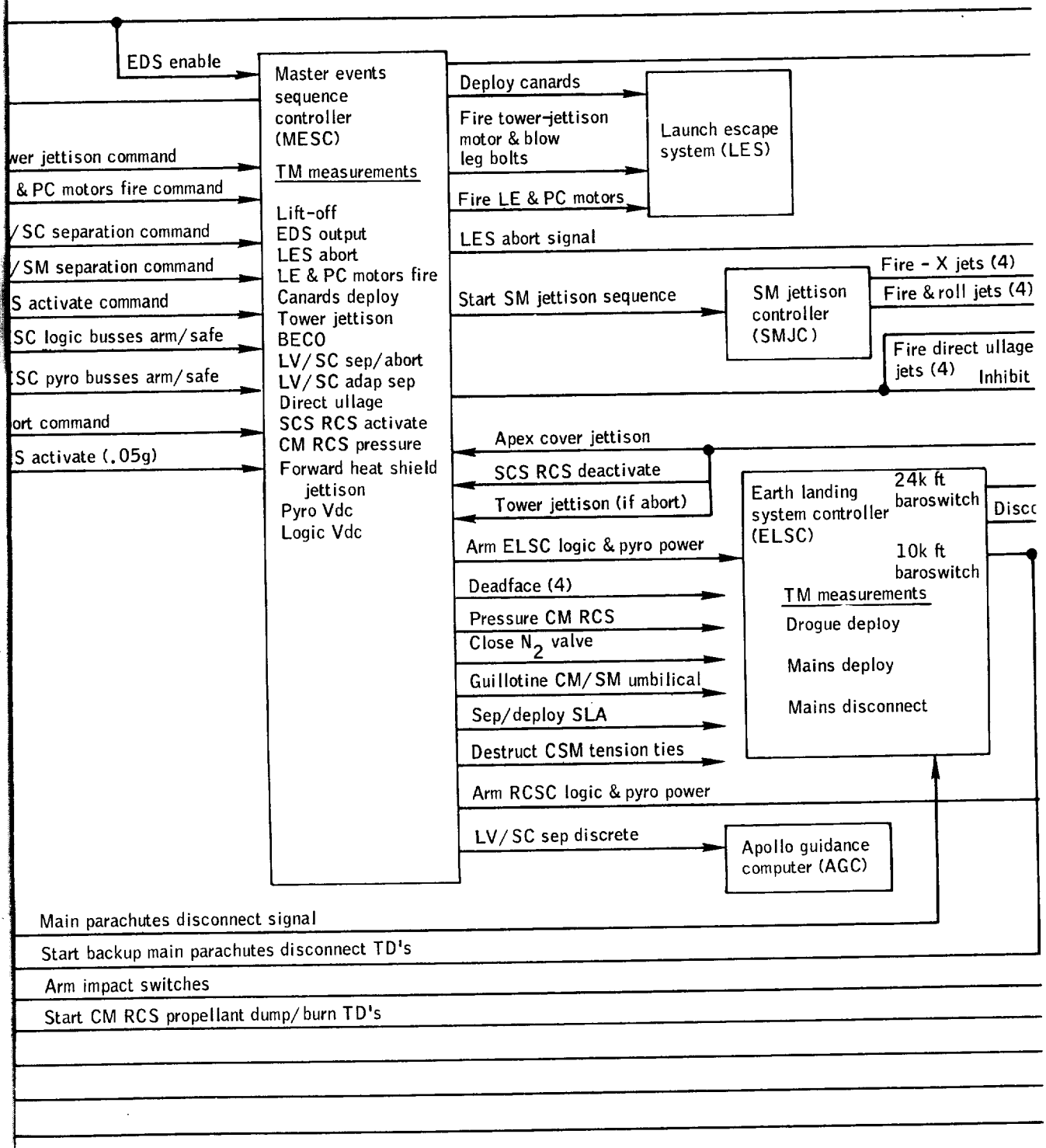

FOLDOUT FRAME 2

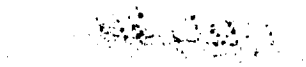

NASA-S-66-10128

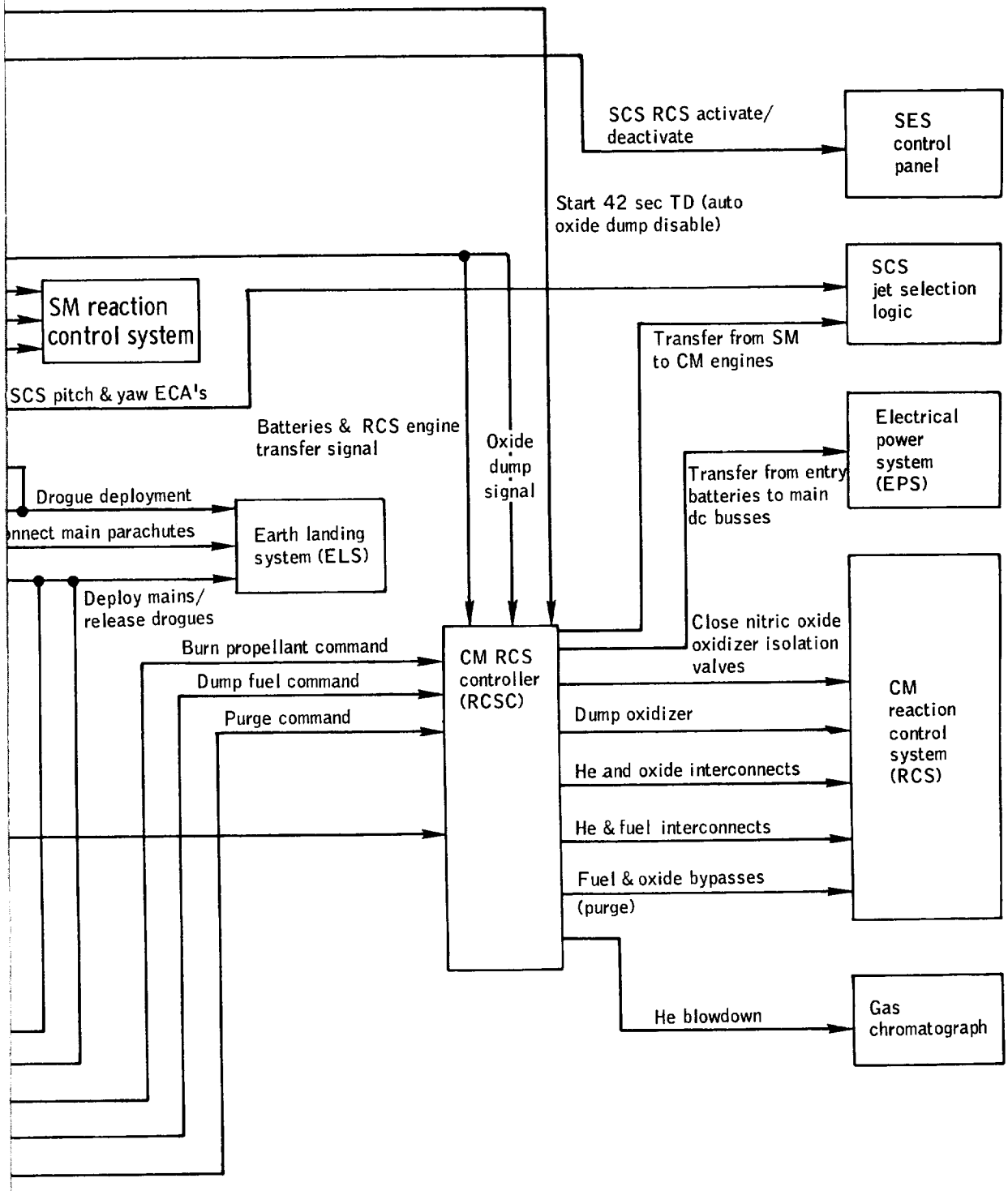

Figure 7.13-1.- Sequential events control system (SECS) functional block diagram, Mission AS-202.

FOLDOUT FRAME 3

7.14 Emergency Detection Subsystem

Summary.- A primary objective of Mission AS-202 was to evaluate the performance of the emergency detection subsystem in the closed-loop mode (with automatic abort capability enabled). The subsystem performed nominally, with the exception of the Q ball, which failed at 93 seconds flight time (see ref. 19).

Description.- The EDS is designed to receive indications of emergency during the launch phase from the launch vehicle, from spacecraft systems, and from the Q-ball mounted at the apex of the launch-escape tower.

From lift-off until tower jettison, the subsystem had the capability of automatically initiating abort in the event of: (a) excessive vehicle angular rates, (b) loss of thrust on two first stage engines, or (c) interruption of the electrical interface between the command module and the instrument unit. Automatic response to (a) and (b) was deactivated by the launch vehicle prior to normal first stage cutoff.

Crew displays of EDS parameters were omitted in Mission AS-201. In Mission AS-202 they were fully operational and were photographed by a cine camera for evaluation. The displays are as follows:

Flight director's attitude indicator: Spacecraft-measured vehicle attitude, angular rates, and attitude errors in pitch, yaw, and roll. Attitude errors are available during first stage flight only, and are referenced to the nominal launch vehicle trajectory.

Q-ball differential pressure meter: A measure of the aerodynamic side load, or dynamic pressure angle-of-attack product, measured by the Q-ball and presented nondirectionally as a percentage of abort limit (0 to 150 percent).

Launch vehicle engine status lights: These lights are on when the individual engines fall below normal thrust.

Launch vehicle overrate light: This light is on when rate gyros and associated circuitry in the launch vehicle instrument unit indicate rates in excess of preset limits.

Launch vehicle guidance light: This light is on when the launch vehicle attitude reference system produces an unreasonable output.

As in Mission AS-201, provisions for tower jettison and nonautomatic abort, which normally would be pilot functions, were included in the MCP.

During checkout of spacecraft 011 at KSC, damage was discovered in the automatic abort and launch-vehicle cutoff wiring at the heat shield penetrations adjacent to the CM/SM tension ties. To eliminate the possibility of further damage, these circuits were rerouted in spacecraft 011 and subsequent vehicles to the main CM/SM umbilical.

Performance.- The EDS was evaluated in the open-loop mode in Mission AS-201. An anomaly in the output of the launch vehicle angular rate gyros in that flight required addition of noise filters, which were successfully flight tested in Mission AS-203. Mission AS-202 was the first flight of the subsystem in the closed-loop mode.

No automatic abort signals were generated during the mission. No conditions approaching automatic or manual abort levels were encountered at any time. The automatic abort circuit was properly enabled by action of launch vehicle and spacecraft logic at lift-off, and deactivated by the launch vehicle sequencer prior to staging.

Indications of the angle-of-attack display were normal for the very low wind conditions experienced during this flight until 93 seconds. From this time until source power was removed from the Q-ball at 139 seconds, the Q-ball output to the CM display was erratic. Transients in the pilot's panel display meter occurred at 93, 111, 122, and 128 seconds. These transients have been correlated with launch-vehicle data and are consistent with the Q-ball failure analysis reported in reference 19.

The transients endured less than 0.2 second each, and would not have been interpreted as an abort cue by the crew. After 93 seconds, however, the output of the Q-ball could not have been used. It is required as an abort indication from 50 to 100 seconds time of flight. The failure is reported by Marshall Space Flight Center to be random in nature and in timing.

7.15 Instrumentation Subsystem

Spacecraft 011 included instrumentation in both the operational and flight qualification categories. Some of the instrumentation was actually an integral part of an operating spacecraft subsystem (such as some G & N, SPS, and ECS measurements), and is discussed in the evaluation of the associated subsystem. The remainder of the instrumentation is discussed in this section of the report. Because of certain differences in development and application concepts, analysis personnel are separated into those evaluating the contractor furnished instrumentation and government furnished instrumentation. The following evaluation has been divided into two subsections accordingly. A block diagram of the instrumentation subsystem is shown in figure 7.15-1.

Instrumentation - contractor furnished.-

Description: Instrumentation used on spacecraft 011 was essentially the same as that used on spacecraft 009. The differences between the two systems existed due to the upgrading of a few devices on spacecraft 011. These were:

(a) Improved insulation for the high temperature thermocouples system used in the ablative heat shield.

(b) The 10-volt power supplies were redesigned to compensate for qualification failures.

(c) The data storage equipment (DSE) contained improved clutches, flanged pulleys, and improved belts.

(d) Minor modifications were made to the central timing equipment (CTE) to reduce its noise susceptibility.

Performance: The DSE and flight qualification recorder (FQR) yielded data on all channels and were turned on and off as programmed. A comparison of range time and mission elapsed time accumulated by the CTE showed that the CTE operated properly throughout the flight. The signal conditioning equipment (SCE) operation was proper on all channels. The SCE 5-volt reference varied from 5 volts to a low of 3.2 volts between T+4511 and T+4583 seconds and T+4787 and T+5091 seconds. The data system was not affected by this voltage drop. This voltage was used to supply the CM/SM separation monitor. It was not deadfaced, and the wires were exposed to the reentry environment. The wires were fused to 3 amperes instead of 1/4 ampere due to an engineering error. It was concluded that the wires were exposed to reentry plasma causing shorting with a resulting drop in voltage.

The spacecraft 011 flight instrumentation measurement system consisted of 673 measurements at lift-off, 19 of which failed to operate properly during flight. The 19 which failed to furnish satisfactory data throughout the flight are listed in the following paragraphs.

(a) CF0010Q, potable water tank quantity. Erratic data were received during the power and maneuvering phases of the flight. The calibration characteristics of the transducer made accurate readings difficult to obtain (see section 7.17 and fig. 7.17-4). The water quantity transducers which have been redesigned for spacecraft 012 and subsequent vehicles display more satisfactory calibration characteristics.

(b) SP0661P, engine chamber pressure. The chamber pressure showed a 7-psi hump for the first 20 seconds of the first burn, after which it was normal. Vehicle acceleration data and feed pressures indicate that the chamber pressure hump was not real. This hump has appeared during tests of spacecraft 001 at White Sands Missile Range (WSMR), and to a lesser extent during the flight of spacecraft 009. This was due to the thermal environment imposed on the transducer and was expected, thus no corrective action is planned.

(c) AA7937T, SLA outer skin surface temperature. This measurement was unexpectedly high during this flight, reading a maximum of 470° F (during max. q) against an expected 250° F. As indicated by the differential of inside and outside skin temperatures and the tracking characteristics of the SLA skin temperatures for the rest of the flight, it appears that the high temperature was the result of the thermocouple coming off the surface. This measurement is not on spacecraft 012.

(d) AA8132S, SLA outer shell longitudinal strain, position 4; AA8134S, SLA inner shell longitudinal strain, position 4; and AA8135S, SLA inner shell circumferential strain, position 4. These three measurements dropped to zero strain at lift-off. These measurements, plus AA8133S, which was inoperative prior to lift-off, are all served by one signal conditioner. Qualification data indicate that the sensors and signal conditioners successfully passed all tests, including vibration of 16.5g rms. This signal conditioner utilized snap-in type input and output connectors, which were not safety-wired. It is concluded that the failure occurred due to a connector disconnect, caused by either vibration or a combination of improper installation and vibration. These measurements are not on spacecraft 012.

(e) CS0100X, CM/SM physical separation monitor. The physical separation monitor did not function during CM/SM separation. Some

difficulty has been noted with this transducer on spacecraft 011 on two different occasions at KSC, the last time on the day before launch. This is a yoyo-type device with a tape reel which allows the determination of separation distance versus time. On both occasions it was noted that the tape had been partially pulled out. Once the tape has been pulled out, proper restowing is required to assure that it will operate satisfactorily. This tape is made of fiber glass and is 1/4 inch wide and 0.005 inch thick. On the day before launch this tape was also noted as being frayed. It is concluded that either the tape was not properly stowed, so that the device could not operate, or that the tape broke at the instant of separation because of the fraying. Spacecraft 012 has redundant transducers for this function, and has a total of six of this type of sensing device. All six will be inspected before launch to assure proper functioning during the mission.

(f) Aft heat shield high range calorimeters. Some of the data from the high range heat flux measuring systems are difficult to interpret at this time. Interpretation consists of calculating heating rates based on temperatures of graphite wafers stacked seven deep and embedded in the ablative heat shield. These calculations involve accounting for heat storage, radial and axial heat losses, and reradiation from the surface. Two problems appear to preclude interpretation; one is whether the calorimeter behaved as expected, and the other is whether the measuring system performed as required.

The expected behavior of the calorimeter was that each graphite wafer would be removed by the forces of reentry as the surface of the ablator receded. Since only one instrumentation channel was assigned to each stack of wafers, an automatic switching device was provided to connect the thermocouple of the exposed wafer to the data channel, sequentially. There is evidence that the wafers were not removed as expected, and there is evidence that the switching device operated prematurely. Failure of the wafers to be removed may be explainable by the fact that entry conditions for spacecraft 011 did not provide sufficient shear forces or heating rates for timely removal. Premature switching is considered to be the result of noise susceptibility of the sensing circuitry, and the switches of spacecraft 017 will carry additional capacitors and ground wires to prevent the difficulty on Mission AS-501. No action is being taken against the wafer removal problem, because the reentry profile of spacecraft 017 is expected to provide sufficient shear and heating rates to insure proper action of the wafers. However, further effort on the interpretation process is scheduled to be completed before Mission AS-501.

(g) SR5830P, Service module quad D, helium tank pressure. This measurement revealed intermittent spikes to less than 155 psia at

T+3 seconds, which caused the master caution and warning light to illuminate. The probable cause of this anomaly is a defective 32-gage wire splice. This assumption is based on the fact that both the transducers and signal conditioner successfully completed qualification including vibration testing to 16.5g rms. Data after T+100 seconds indicated that the measurement was operating properly (see section 7.9).

In addition, data from the following two event measurements were not recorded.

(h) CE0321X, main parachute disconnect A monitor; and CE0322X, main parachute disconnect B monitor. These measurements indicating main parachute disconnect were not recorded on the DSE. Disconnect did occur as proved by recovery forces. The spacecraft 011 design was such that pyro firing for parachute disconnect should have occurred approximately 10 msec after impact, with logic buses being disconnected approximately 40 msec later.

Data indicates that this sequence of events did occur properly. The data sampling rate for the disconnect monitors, however, is only once each 100 msec. It seems improbable that the change would have been sampled before logic power was removed. This condition will not affect spacecraft 012, since on manned flights an indication will be received of the manual disconnect event and logic power-down will occur manually later.

The following measurements were waived or inoperative prior to flight:

CA0967T	CA1670R	SP0052T	AA8133S	SC2088T	SC2323X
CA1013T	CA1143P	SP0053T	SC2114C	SC2140R	SC2324X
CA1207R	CA1162P	CR4553T	SC2061P	SC2143R	SC2325X
CA1225R	CA1163P	SA4002S	SC2067P	SC2144R	CA0409S
CA1405S	CA7649P	SA4006S	SC2070P	SC2161X	CA0411S
CA1046T	SP0050T	AA8120S	SC2082T	SC2121X	CA0403S
CA1132T	SP0051T	AA8124S	SC2085T	SC2126X	CH1103X

Instrumentation - government furnished.- Some of the flight qualification instrumentation on spacecraft 011 was government furnished. This instrumentation included three 90 X 10 commutators, a CM PAM/FM/FM telemetry package, an SM PAM/FM/FM telemetry package, a time code generator, and a five-point calibrator, all of which were similar to those used on Mission AS-201 (SC-009). The flight cameras were similar to those on spacecraft 002 and BP-22. This equipment is discussed separately because of certain differences in development and application concepts.

Description: The CM PAM/FM/FM telemetry package (fig. 7.15-2) interfaced with the communications subsystem and processed 60 measurements from the structural subsystem, the communication and instrumentation subsystem, the service propulsion subsystem, and the reaction control subsystem. The package consisted of the following standard IRIG components: a 90 X 10 high-level commutator, a five-point calibrator, a nine-channel modulation package, and a 5-watt, 247.3-Mc, FM transmitter. The components were mounted internal to a spacecraft electronic package (SEP) which was installed in the lower equipment bay of the CM. A redundant commutator differentiated pulse duration modulation (DPDM) output was also recorded on the DSE, track no. 12.

The SM PAM/FM/FM telemetry package (fig. 7.15-3) interfaced with the communications subsystem and processed 93 measurements from the structural subsystem. The package consisted of the following standard IRIG components: a 90 X 10 low-level commutator, a five-point calibrator, a 15-channel modulation package, and a 5-watt, 257.3-Mc, FM transmitter. The components were mounted on a plate attached to the bottom side of the shelf between beams 3 and 4 in the SM. This package was added to the original flight qualification subsystem on both spacecraft 009 and spacecraft 011 as a modification kit for collecting SM and SLA structural integrity data.

The three CM 90 X 10 commutators (fig. 7.15-2), two low-level mechanical and one high-level electronic type, were utilized to process 190 heat-shield measurements from the structural subsystem. Each commutator data channel was sampled 10 times per second. The DPDM output of these commutators was recorded on the DSE. The commutators were mounted in the aft equipment bay.

The time code generator and five-point calibrator, installed internal to the FQR, were utilized to provide a timing reference on the FQR and DSE flight tapes and to provide preflight calibration to the FQR wideband FM record amplifier modules. The time code generator provided an output coded to one-tenth of a second and recycled each hour. See reference 20 for performance characteristics of both components.

The flight camera system consisted of four cameras, two control boxes, two batteries, one timing pulse generator, and one barometric switch. Three of the cameras were mounted in the crew compartment (fig. 7.15-4) with one battery, one control box, and the timing pulse generator, and interfaced with the MCP for on/off signals. Cameras 1 and 2 photographed the main display console, left and center sections (fig. 7.18.1-1), to provide data for the analysis of the controls and displays subsystem performance (see section 7.18.1 and refs. 21 and 22). Camera 3, looking through a right-angle prism,

photographed the right-hand rendezvous window to provide data confirming that the horizon may be detected during entry and indication of minimum window fogging (section 7.18-2 and ref. 23). Camera 4 was provided to photograph forward heat shield (FHS) jettison to verify positive separation without recontact between the CM and FHS (section 7.6.1 and ref. 24). The camera, equipped with a Fairchild 10-mm lens and right-angle prism, a battery, a control box, and 30 000-foot barometric switch, was attached to a mounting plate and covered with a protective aluminum dome (fig. 7.15-5). This assembly was mounted on the egress tunnel. The aluminum dome assured that the parachute risers would neither be cut by nor become entangled with the camera equipment.

Performance: All GFE instrumentation components and packages performed satisfactorily.

The performance of the CM PAM/FM/FM telemetry package was nominal throughout the flight. A total of 60 PAM commutated measurements was transmitted over the telemetry link. The PAM commutated data were telemetered, received, and decommutated satisfactorily. The DPDM output of this commutator recorded on the DSE was also recovered satisfactorily.

The reentry RF blackout period of T+4416 to T+5008 seconds prevented reception of the CM PAM/FM/FM data, but since the commutator DPDM output from this package was redundantly recorded on the DSE which operated from T+3940 to T+5590 seconds, no data were lost.

The SM PAM/FM/FM telemetry package transmitted 10 continuous and 83 PAM commutated measurements. The SM telemetry package performed satisfactorily until transmission was terminated at CM/SM separation. The calibrator of the telemetry package operated properly to provide preflight calibration.

The performance of the three CM commutators processing heat-shield data was satisfactory. The SCE commutator reference output was degraded after T+4488.8 seconds by the CM/SM separation measurement anomaly (see section 7.15.1). The two high-level commutators data were reduced from T+4488.7 to T+5591 seconds by programming the data reduction equipment to use the reference level at T+4488.7 seconds as a synthetic reference.

The time code generator and five-point calibrator in the FQR performed satisfactorily prior to and during the flight. The five-point calibrator provided preflight calibration of the FQR wideband subcarrier oscillators. The time code generator read 20 minutes 41.2 seconds ($\pm$0.05 sec) at range zero and continued to

provide timing on the FQR, cycling through one hour to zero, until FQR shutdown at 48 minutes 31.2 seconds.

The four flight cameras performed satisfactorily during Mission AS-202. Cameras 1, 2, and 3 operated from T-121.1 to T+837.4 seconds and T+4422.5 to T+5595.1 seconds (splashdown plus 11 seconds). Camera 4 was activated by a 30 000-foot barometric switch at approximately 11.3 seconds prior to forward heat shield jettison and ran for 98.7 seconds, providing film which indicated satisfactory forward heat shield separation without recontact and also deployment of drogue and main parachute and disreefing of the main parachutes. The satisfactory performance of camera 4 also indicated nominal operation for the battery which had been activated and mounted in an inaccessible location under the forward heat shield for 7 weeks prior to launch.

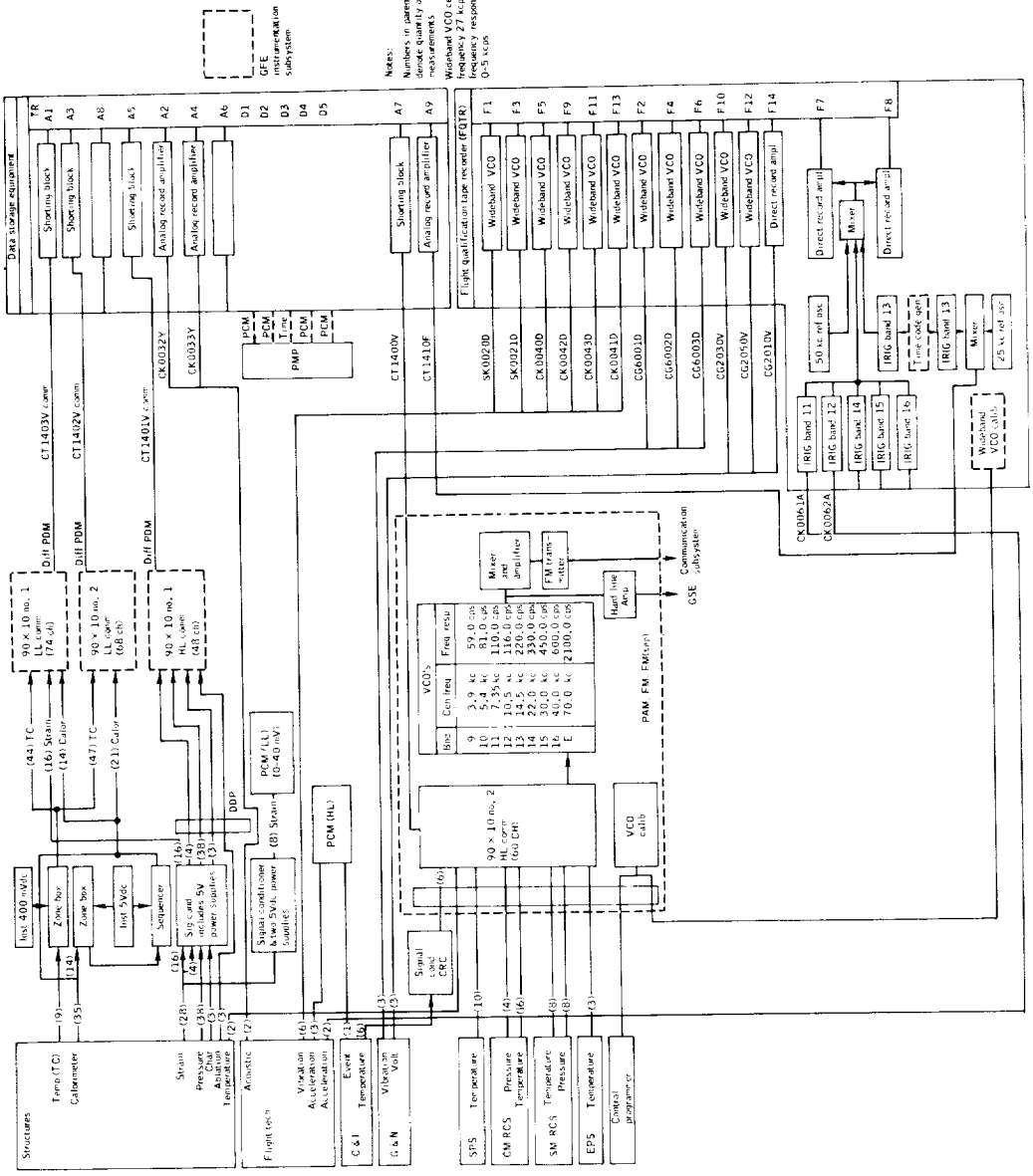

Figure 7.15-1.- Flight qualification instrumentation system, Mission AS-202.

NASA-S-66-10130

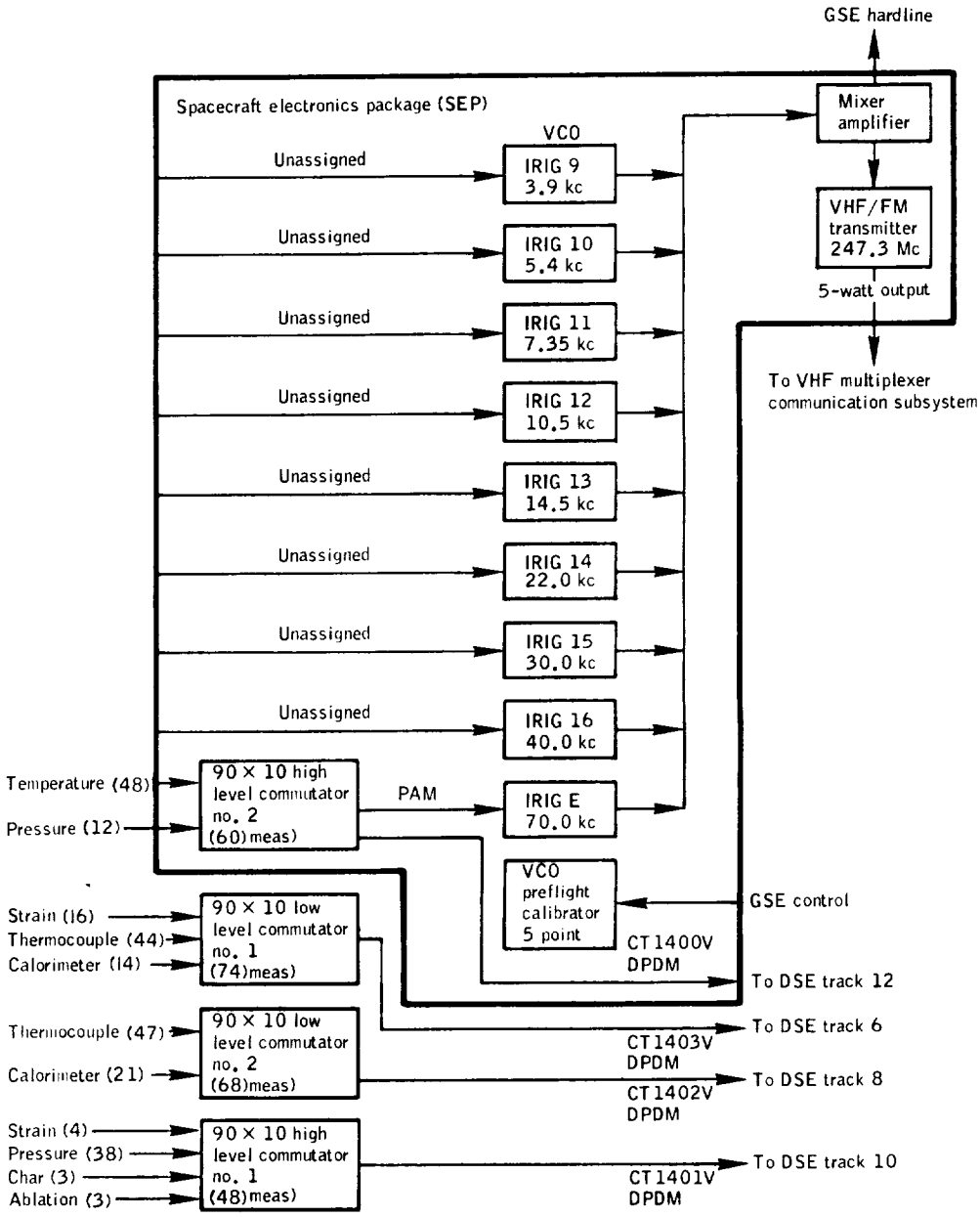

Figure 7.15-2.- GFE instrumentation CM PAM/FM/FM telemetry package and 90 × 10 commutators, Mission AS-202.

NASA-S-66-10131

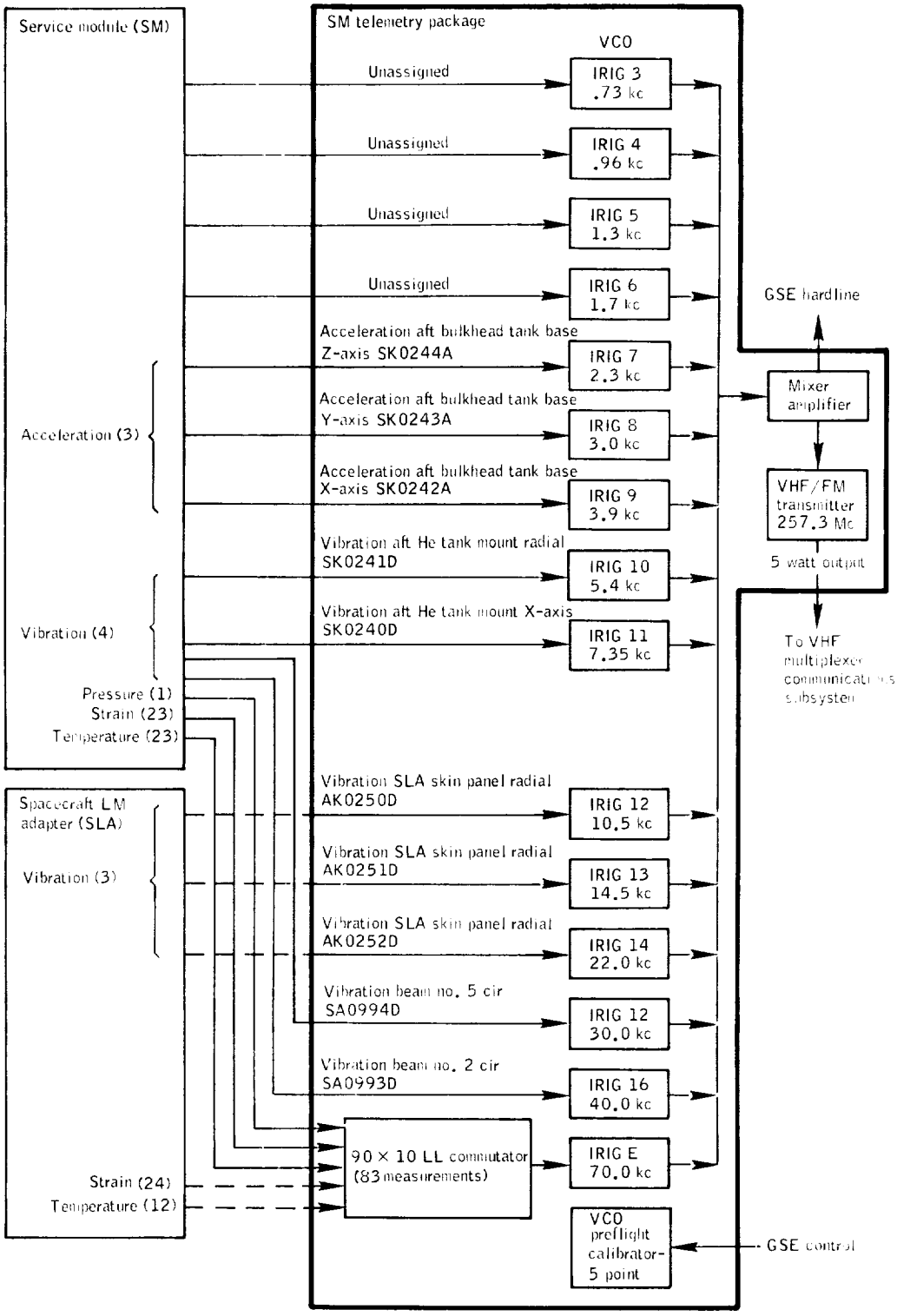

Figure 7.15-3. - GFE instrumentation SM PAM/FM/FM telemetry package, Mission AS-202.

NASA-S-66-10132

Areas A and B make up the field of view of camera no. 1
Areas C and D make up the field of view of camera no. 2
Area E field of view of camera no. 3 out the right-hand rendezvous window
Lamp no. 1 illuminates Area-A
Lamp no. 2 illuminates Area-B
Lamp no. 3 illuminates Area-C
Lamp no. 4 illuminates Area-D

Note: Reference figure 7.18.1-1 for definition of areas A-B and C-D

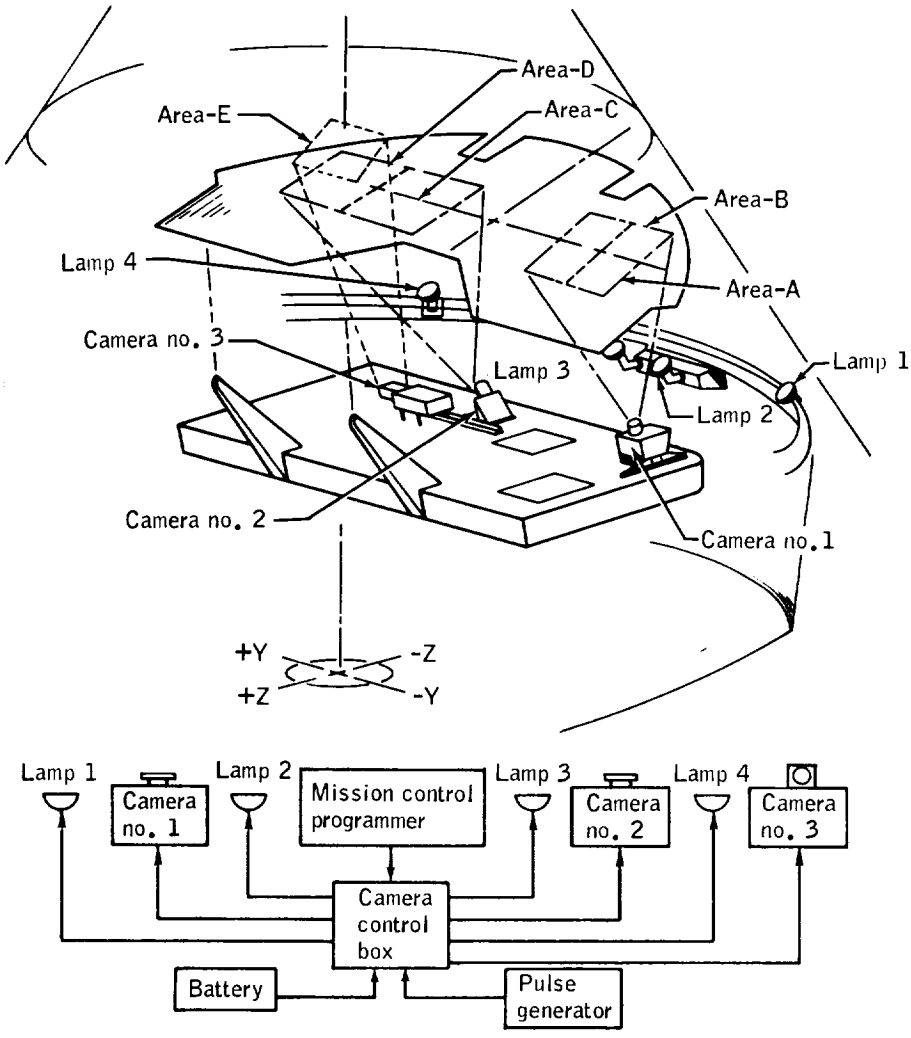

Figure 7.15-4.- Crew compartment cine camera system, Mission AS-202.

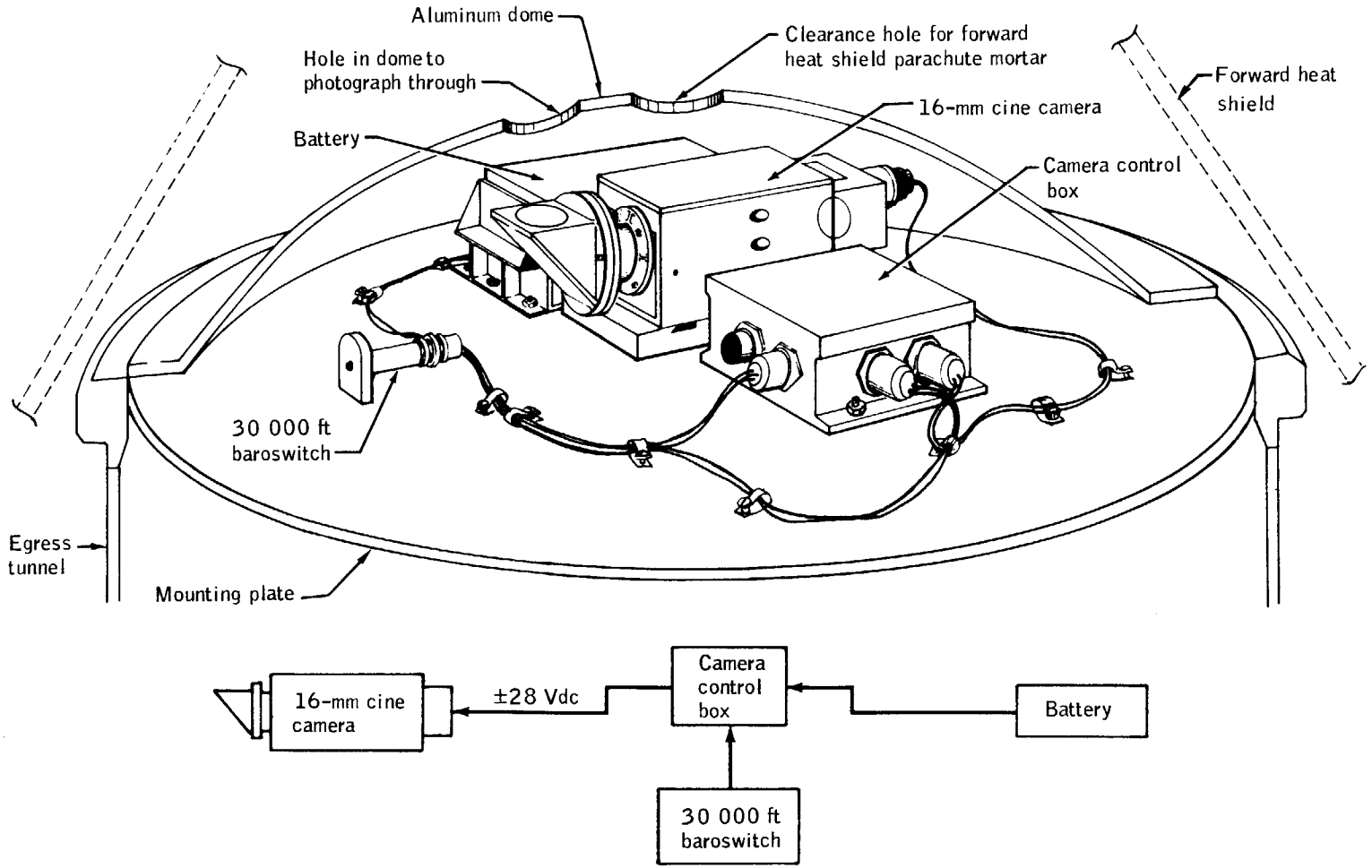

Figure 7.15-5.- Forward heat shield jettison cine camera system, Mission AS-202.

7.16 Communications Subsystem

The spacecraft 011 communications subsystem provided for the operational and data communications links between the spacecraft and the ground network, and included the onboard equipment required for high frequency (HF), very high frequency (VHF), ultra high frequency (UHF), and unified S-band (USB) transmission and for C-band tracking (see fig. 7.16-1). The subsystem differed from the spacecraft 009 subsystem (ref. 9) in that (a) the two omniscimitar antennas could receive and transmit both S-band and VHF, (b) the digital up-data link (UDL) equipment with UHF and S-band receiver capability was added, and (c) the unified S-band equipment (USBE) was added.

Analysis of the data indicated that the spacecraft communications subsystem performed satisfactorily throughout the mission. However, problems associated with the subsystem included: (a) the CM/SM separation command attempts from the USNS COASTAL SENTRY QUEBEC (CSQ), (b) the lower than predicted signal levels on USB reported at the Merritt Island launch area (MILA) and Bermuda (BDA) S-band stations, and (c) the delayed recognition of two-way lock at the Carnarvon (CRO) S-band station.

HF, VHF, and UHF communications.-

Description: The HF and VHF communications provided during this mission were essentially the same as those during Mission AS-201 (ref. 9): HF transceiver and VHF recovery and survival beacons provided direction-finding information to the recovery forces, the pulse code modulation (PCM) and VHF/FM transmitter provided spacecraft measurements to the ground network, and the VHF/FM signals were transmitted to the ground network. Differences from spacecraft 009 are as follows:

(a) The (UDL) was added for this flight. It had the capability to update the AGC and to perform real-time commands. The UDL had the capability to receive via UHF (450 MHz) or S-band. Only the UHF receiver was used on this flight.

(b) The inflight omniscimitar antennas were different in that they transmitted and received both S-band and VHF; whereas, the spacecraft 009 antennas could only transmit or receive VHF. This dual capability was provided for by a notch antenna in the scimitar blade for S-band. Only the -Z antenna was used on this flight for S-band, but the VHF was capable of being switched from one to the other. VHF antenna switching from +Z to -Z was satisfactorily performed at T+207 seconds by ground command.

Performance: Analysis of the mission indicates that no spacecraft hardware changes are necessary for future Block I missions.

The audio center performance was normal in that it provdied simulated woice (400 Hz) to be transmitted via VHF/AM and S-band. This 400-Hz signal was properly received at all properly equipped ground stations, except as noted in the S-band performance section.

The VHF/AM transmitter-receiver performed normally during all mission phases. A 400-Hz signal was transmitted for postflight evaluation. No uplink VHF/AM signals were transmitted.

All properly equipped ground stations tracked the spacecraft via the C-band transponder. Transponder performance was normal in every respect. PCM data were received and recorded at all stations. No measurement anomalies are attributed to the PCM equipment. The VHF/FM transmitter properly transmitted the PCM telemetry. All ground stations received PCM data with only minor dropouts. All spacecraft VHF carriers were received at the ground receiving stations, indicating proper multiplexer operation. No uplink VHF was transmitted.

At main parachute deployment, the VHF/recovery beacon and VHF/survival beacon began operation as planned. Recovery aircraft received the signals and proceeded to home in on the spacecraft. After touchdown, the HF transmission from the HF transceiver and HF antenna was received, and a fix on the spacecraft location was made, using these HF signals. The VHF portion of the scimitar antennas was successfully used for the transmission of all VHF/RF carriers and provided for reception of the UHF uplink command at T-207 seconds. This command switched the transmission/reception from the +Z antenna, which was used prior to 207 seconds, to the -Z antenna, which was used for the duration of the mission.

Only the -Z antenna was used for S-band transmission and reception. Performance was less than nominal in that circuit margins were not as predicted. Predictions were based on patterns taken on a one-third scale mockup without the launch escape tower (LET), boost protection cover (BPC), or the launch vehicle. These configuration differences could explain the difference in patterns experienced.

The UDL responded properly to the real time command at T+207 seconds to switch VHF transmission/UHF reception from the +Z antenna to the -Z antenna. A validity signal was generated and received on the ground, and the antenna switching was accomplished.

The CSQ initiated a CM/SM separation command to the spacecraft, but did not receive a validity signal response from the spacecraft UDL, indicating that the command had been received. The command was sent eight times (four times at T+4302 seconds and four times at T+4316 seconds), each time with negative results.

CSQ has verified by playback of the command recording that the bit structure of the transmitted commands was correct. Spacecraft-received RF signal strength at the time of the real time commands was well within the limits for proper operations.

During postflight testing at Downey, the spacecraft successfully received and responded to the proper command signal. Transmission of the command signal from a copy of the CSQ tape during postflight tests at Downey was not accepted by the spacecraft. Figure 7.16-2 compares the signal from the CSQ with the signal sent from the Mission Control Center at Cape Kennedy (MCC-K), indicating that the CSQ signal had considerable phase and amplitude distortion.

The CSQ composite signal indicated that there was approximately 50 microseconds of delay distortion between the 1- and 2-kc components (2 kc leading). In addition to this distortion, the amplitude of the 2-kc component was about 20 percent lower than the 1-kc component, and the frequency of both the 1-kc and 2-kc components was off by more than 3 percent.

Information from GSFC indicates that MSFN procedures include testing and setting phase relationship between the 1- and 2-kc updata signal component to a tolerance of at least an order magnitude better than the CSQ signal received from the recording. GSFC is investigating the cause for the 50-microsecond delay in the CSQ recording.

Unified S-band communications.- This section includes the analysis of spacecraft and MSFN communications compatibility.

Summary: Operation of the USBE during Mission AS-202 was required to verify USB communications operations for simulated downvoice (400-Hz tone) and simulated upvoice (1-kHz tone) modes, with secondary objectives to verify the turnaround ranging mode and downlink PCM telemetry (51.2 kilo bits/sec) mode.

The Mission AS-202 operational modes planned for the mission and the transmission modes actually employed at each site during transmission are indicated in table 7.16-I. There was no requirement for the USB communications to provide prime operational functions on this mission. Data received during the mission have shown that both the downvoice and upvoice links were functioning satisfactorily during periods of adequate signal levels. However, there were periods at all sites during which two-way voice communication would have been impossible due to either low signal levels or lack of two-way RF lock. Detailed evaluation of the channel quality is still under investigation. It should be pointed out that the upvoice channel verification is only valid to the output of the spacecraft USBE receiver and does not include the upvoice

discriminator and audio center equipment. Verification of the operation of this equipment was not possible due to lack of spacecraft instrumentation.

PCM telemetry data were received on the S-band link at all sites, and present evaluation indicates satisfactory performance of this channel during the period of adequate signal levels. Again, there were periods where valid telemetry was not received. For example, valid USB telemetry was lost at MILA after T+260 seconds where VHF/FM telemetry was received at MILA until T+420 seconds. The average bit error rates for S-band telemetry taken over 1-minute sampling intervals ranged from 3×10^{-3} to 1×10^{-5}. The pseudorandom noise (PRN) ranging subsystem was utilized at all sites and valid data were obtained from MILA and BDA. The CRO ranging data could not be reduced from the tapes supplied, and low speed data printouts indicated that the data which were obtained on site were not valid. Basic design compatibility between the spacecraft and ground USB subsystem was verified for those modes tested in the flight.

Generally, subsystem performance appeared nominal with the exceptions of weak signal levels during the launch and powered flight phases, and acquisition problems encountered at CRO and BDA (handover acquisition).

During the launch and powered flight phases, adverse look angles from the MILA site and effects of low-elevation angles at BDA are believed to be the primary cause for weak signal levels during these times.

Description:

(a) Spacecraft USB: Figure 7.16-1 shows a simplified spacecraft communication subsystem. The block diagram presents the spacecraft VHF and USB communication subsystems. The VHF (the primary communication subsystem) subsystem was utilized in USB evaluation of spacecraft-received carrier power, downvoice and PCM telemetry.

The USB spacecraft subsystem is comprised of a premodulation processor, transponder, power amplifier and associated microwave circuitry, and omnidirectional antenna. The premodulation processor accepts voice and PCM telemetry signals from the spacecraft for transmission to the ground. It also recovers the voice and updata signals received from the ground. The CSM transponder is basically a narrowband pulse modulation (PM) receiver, narrowband PM transmitter exciter, and wideband PM receiver for the data channels. The transponder feeds and is fed by a package containing the power amplifier and microwave switching and diplexing circuitry. The microwave circuitry feeds the two spacecraft omniantennas (only the -Z antenna was connected to

the USBE during Mission AS-202) which are manually selectable. The PM receiver has a local oscillator phase-locked to the received carrier, which provides the frequency and phase reference for the PM transmitter exciter and wideband data channel detector.

The simulated downvoice signal was obtained from the 400-Hz power source and coupled through the spacecraft audio center to frequency modulate the downvoice subcarrier (1.25 MHz) in the premodulation processor. The voice subcarrier then phase-modulated the downlink S-band carrier at 0.84 radian. The voice signal was clipped in the premodulation processor (PMP) and the subcarrier frequency deviation was maintained at 7.5 kHz peak. A 400-Hz simulated voice signal was also transmitted over the VHF/AM voice link. The PCM telemetry was simultaneously transmitted over the USB and VHF/FM links.

The USB PCM data were biphase modulated on a 1.024-MHz subcarrier which phase-modulated the S-band carrier frequency at 1.1 radians. The wideband data channel of the USB transponder also served as a turnaround receiver for the pseudorandom range code which was transmitted to the spacecraft as phase modulation on the uplink S-band carrier. The range code was detected in the wideband phase detector of the USBE and phase-modulated on the downlink S-band carrier with approximately the same modulation index used on the uplink, provided that the received signal level in the transponder was sufficiently strong to prevent range code suppression in the spacecraft USBE receiver intermediate frequency (IF) limiter. Spacecraft instrumentation was not available for detection and recording of the simulated upvoice 1-kHz tone. Therefore the only check on upvoice performance was in recovering the turned around uplink subcarrier received at the MSFN sites. The updata link decoder was not connected to the S-band receiver for any portion of the flight, and no data were transmitted on the 70-kHz updata subcarrier during any time of the AS-202 mission.

(b) MSFN USB: Figure 7.16-3 shows a typical USB subsystem 30-foot antenna facility. This block diagram presents only the USB portion of the MSFN facility. The basic USB subsystem consists of a high gain antenna, acquisition antenna, microwave circuitry, a main reference channel receiver, acquisition reference channel receiver, two main angle channel receivers, two acquisition angle channel receivers, a transmitter exciter, data demodulation circuitry, ranging circuitry, premodulation circuitry, acquisition and programming circuitry, and data handling and peripheral equipment.

The acquisition channels, transmitter exciter, and acquisition antenna were used initially to acquire the spacecraft signal. This operation consisted of a search in angle with the acquisition antenna and a search in frequency with the exciter and acquisition reference

channel receiver for the central PM carrier component of the spacecraft signal. The ground receiver local oscillator phase locked to the received carrier, thus activating the angle channels. When the acquisition angle channel errors were sufficiently nulled, the drive for the antenna servos was switched from the acquisition to the main angle channels.

The ranging circuitry contained digital equipment for generating the range code and making range measurements, doppler measuring circuitry, and a range code receiver which was fed by the reference channel 10-megacycle IF output. The ranging circuitry fed the range code to the transmitter phase modulator, where it was effectively summed with other up-going data in the premodulation circuitry.

The data demodulator accepted PM data from the main reference channel receiver and the acquisition reference channel. Since the two reference channel receivers were identical, the acquisition reference channel was available, after completion of acquisition, for the reception of other data. For Mission AS-202, this receiver was to remain on the acquisition antenna; thus, approximately a 20-dB weaker signal would be obtained on this receiver.

Performance:

(a) USB anomalies: No spacecraft USB hardware or software changes were anticipated as a result of USB anomalies. GSFC is implementing some procedural and hardware changes to correct recognized deficiencies noted during this flight.

(1) Low signal strength at MILA and BDA. The S-band uplink and downlink received carrier powers were 8 to 40 dB lower than predicted at MILA and BDA. BDA acquired the downlink prior to T+396 seconds, but dropped lock when the signal level decreased 24 dB in less than 50 seconds. Since BDA did not have downlink lock, the handover at T+420 seconds was unsuccessful. BDA acquired late, and obtained less than 1 minute of ranging data prior to the "key-hole" (antenna angle limits).

The signal level predictions were based on one-third scale models of the CSM without booster. Flight data indicated that the accuracy of these patterns was poor, particularly at look angles from the MILA station. A station at Grand Bahama Island is being installed to improve the coverage during the early powered flight. This station will be available for Block II missions.

Full-scale patterns for the Block I antennas will be determined at MSC. These data will provide more definite information for future

predictions and will allow a selection of the best antenna for the launch phase of missions where antenna switching is possible.

(2) Recognition of two-way lock at CRO. Inability to recognize uplink lock and consequently to accomplish proper two-way lock was partly due to failure of the MSFN USB operator's Apollo guidance computer (AGC) meter to read the transponder AGC voltage. This meter was located on the main tracking receiver.

The AGC meter was driven from the VHF telemetry subsystem, and the analog output voltage was routed via various patch panels to the USB operator's console. Postmission tests run from the digital-to-analog converter to the meter confirmed proper circuit operation. Cause for failure is unknown, and exact patching instructions are not available.

Goddard Space Flight Center postflight investigations indicated that a fault in acquisition circuitry produced uplink frequency transients which caused loss of transponder carrier lock several times during initial acquisition attempts. This fault was present only at the Carnarvon station and it was a major contributor to the late two-way lock at CRO.

(3) Degraded upvoice channel at Bermuda. The simulated upvoice (1000-cycle tone) received at BDA was relatively noisy when compared to the same channel as received at MILA under similar signal strength conditions. The reason for this has not been determined but could be caused by a low modulation index of the signal transmitted from BDA.

(4) Invalid ranging data at CRO. The CRO station ranging data were invalid. Doppler data were good for the last 3 minutes of the pass after valid two-way lock was achieved and the synthesizer loop was locked.

(b) MILA RF subsystem: Two-way RF lock was achieved prior to launch. Manual velocity tracking was employed prior to initiating automatic tracking at approximately T+23 seconds, and automatic tracking was maintained until T+480 seconds at which time the antenna system was switched to program track.

Figure 7.16-8 is a plot of received downlink carrier power at MILA as a function of time into the mission. Also shown in figure 7.16-8 is the expected carrier power based on the reference trajectory for Mission AS-202. The predicted curve included antenna pattern effects based on one-third scale patterns. New predictions based on the actual trajectory and look angles are not yet available. Based on the predictions

presently available, there was a difference of 20 to 30 dB between measured and predicted signal levels at MILA.

During most of the launch phase the predicted look angle θ, (see figs. 7.16-4 and 7.16-5) for the MILA site was less than 10 degrees from the X-axis of the spacecraft. The predicted look angles (θ and ϕ) for the MILA site are shown in figure 7.16-5. The effects on signal levels due to these adverse look angles are felt to be a major cause for the variations between predicted and measured received carrier power at MILA.

An abrupt drop of approximately 7 dB in received carrier power occurred at T+170 seconds. This time corresponds to the time of launch-escape subsystem (LES) jettison. The probable cause for this drop is changes in antenna patterns due to removal of the BPC and possible flame effects from jettison rockets.

Figure 7.16-6 is a plot of received uplink carrier level as a function of time into the mission, and again a predicted carrier level is shown on the same plot. These predictions were obtained by adjusting the predicted downlink carrier level by a factor of 33 dB which takes into account the difference in uplink transmitted power, and carrier suppression due to modulation. This adjustment is only valid after T+300 seconds since uplink carrier power was varied prior to that time at MILA. Also, after T+420 seconds, the uplink was acquired by the BDA station and the adjustment is not valid after that time. From figure 7.16-6 it is seen that the uplink signal levels differ from the predictions by the same relative amounts as seen in the downlink case (20 to 30 dB). This result indicates that a failure of the spacecraft USB power amplifier did not cause the weak signal levels observed during the launch phase of the mission. To further illustrate the point, figure 7.16-7 shows a plot of the measured uplink signal levels and the calculated uplink signal levels between T+300 and T+420 seconds. The calculated uplink signal levels were obtained by adjusting the measured downlink signal levels received at MILA during the times stated above by 33 dB. This figure shows that there is good agreement between the calculated and measured uplink signal levels, which again indicated that both uplink and downlink signal levels were weaker than expected by similar amounts. These factors tend to indicate that the weak signal levels encountered were most likely due to antenna pattern uncertainties in the predictions and not an equipment malfunction. Additional information will be provided in this area in a supplement to this report. Some effects in received carrier level due to flame attenuation were observed at T+90 to T+100 seconds (main engine plume effects), at T+144 to T+146 seconds staging effects (retroburn), and possibly at T+170 seconds LES jettison. The magnitude of the attenuation effects does not appear extremely severe; however, efforts to more accurately define the amount of attenuation actually due to flame effects and comparison of this

attenuation with theoretical predictions are still in progress and will be presented in the supplemental report.

The handover attempt between MILA and BDA was initiated at T+418 seconds; however, handover was not successful since BDA had lost downlink lock, and BDA had to initiate exciter sweep to reacquire two-way RF lock. A more detailed discussion of the handover operations is presented in BDA RF system performance.

Figure 7.16-9 shows the predicted and measured two-way RF doppler at MILA. The figure indicated a relatively constant difference between the measured and predicted curves of about 2kHz. Revised predictions based on actual trajectory will be provided in the supplemental report. The fact that the curves agree quite well indicated that the MILA site had a valid doppler track.

(c) BDA RF subsystem: BDA acquired the downlink signal at approximately T+284 seconds. At this time MILA was still transmitting the uplink carrier to the spacecraft transponder with a full uplink modulation mode. Figure 7.16-10 is a plot of the received downlink carrier level at BDA as a function of time. Also included in figure 7.16-10 is a plot of the expected received carrier level at BDA. As seen from the figure, the measured and expected received carrier levels at BDA from T+282 seconds to T+420 seconds differ from 10 to 40 dB. A point of interest here is the drop in signal levels from T+360 seconds to T+400 seconds, at which time BDA lost downlink lock. This occurred prior to the time that MILA and BDA were to attempt handover operations. During this time (powered flight phases at BDA), the elevation angle does not exceed 4 degrees due to the extreme southerly launch azimuth. Multipath (fading) effects due to these low elevation angles are believed to be a primary cause for the weak signal levels from acquisition of signal (AOS) to T+400 seconds. Figure 7.16-11 is a plot of measured and predicted two-way RF doppler at BDA, including the predicted and measured pseudo two-way RF doppler from T+280 seconds to T+420 seconds. The pseudo two-way RF doppler is in effect the algebraic summation of downlink doppler at BDA due to a closing range rate (plus doppler frequency) and the uplink doppler from MILA due to an opening range rate (negative doppler). As seen from figure 7.16-11 the measured doppler is approximately +38.0 kHz, and the predicted doppler -5.9 kHz at T+300 seconds. During the time from T+280 seconds to T+420 seconds the BDA exciter was offset by approximately -40.8 kHz as per the PCD-4 instructions, thus biased doppler readings would not agree with those predicted which assumed a nominal exciter frequency reference to the MSFN doppler extractor subsystem. To show how this doppler readout could occur, the following calculation is required:

At T+300 seconds, the predicted downlink (one-way) doppler due to MILA uplink lock was -18.8 kHz at the same time the predicted downlink

(one way) doppler for BDA is +12.9 kHz. This gave a predicted pseudo two-way doppler of -5.9 kHz. When the MSFN subsystem was in one-way downlink lock condition as at BDA, the biased doppler obtained was a function of exciter VCO frequency due to the doppler extractor mechanization.

The equation for the biased doppler output is given by:

$$D + 1.0 \text{ MHz} = \left(\frac{240}{221} T_F - F_R\right) + 1.0 \text{ MHz}$$

where D = doppler frequency

F_T = S-band uplink transmitted frequency

F_R = S-band downlink received frequency

Assuming that the BDA transmitted frequency was biased by -40.8 kHz as per PCD-4 instructions, the biased doppler frequency obtained at BDA under one-way lock conditions was calculated below:

$$\text{Biased doppler} = 1.0 \text{ MHz} + \left(\frac{240}{221} \; 2106.365472 - 2287.492332\right)$$

$$= 1.0 \text{ MHz} + (2287.453924 - 2287.492332)$$

$$= 1.0 \text{ MHz} - 38.4 \text{ kHz}$$

$$= 961\,600 \text{ Hz}$$

This indicated a doppler frequency of +38.4 kHz would be obtained at BDA for the conditions indicated. This agreed with the measured doppler at BDA of +38 kHz at T+300 seconds.

The handover operation between MILA and BDA was initiated at T+418 seconds when BDA initiated uplink S-band transmitter power. The spacecraft AGC and spacecraft phase error data indicated that BDA acquired uplink lock immediately; however, since downlink lock was lost prior to initiating handover, BDA could not recognize successful uplink acquistion. Thus, the exciter acquisition sweep was initiated and two-way RF lock was achieved at T+460 seconds. Indications are that handover

may have been successful if BDA had not lost downlink lock prior to the handover attempt. As seen from figure 7.16-10 from T+460 to T+580 seconds, the measured and predicted downlink signal levels track very well with a constant difference of 8 to 10 dB. At approximately T+580 seconds the antenna reached the prelimits, and tracking was inhibited. The reduction in signal level from this time on was expected due to the spacecraft moving out of the main antenna beam width and eventually downlink lock was lost at T+590 seconds. Uplink transmitted power was increased to 10 kW at T+580 seconds. The antenna was manually moved through the keyhole area and two-way lock was achieved occasionally until loss of signal (LOS) at T+780 seconds. (The keyhole problem encountered here is unique to southerly launch azimuths only and will not occur for all flights.)

Figure 7.16-12 shows the measured and predicted uplink received carrier power for BDA. As seen from the figure, uplink lock was achieved at the handover point and maintained until T+480 seconds with a short out of lock condition from T+684 to T+688 seconds. This indicated that the spacecraft was maintained in lock even during the keyhole time at BDA. Again, from T+460 to T+560 seconds, the predicted and measured signal levels agree in trend, and an average difference of approximately 10 dB appears. Also from figure 7.16-10 it appears that a valid two-way lock was established from T+480 seconds to T+590 seconds, and from T+730 to T+780 seconds. This was based on the comparison of measured and predicted two-way RF doppler which agreed quite well in trends; however, some bias error is present.

From the results obtained it appeared that the RF subsystem equipment performed normally, however, additional analysis is required to establish definite causes for signal strength variations causing loss of downlink lock at T+400 seconds.

(d) CRO RF subsystem: A simplified block diagram of the MSFN equipment and operational setup as used for Mission AS-202 is shown in figure 7.16-13. Premission calibrations were begun at AOS -8 hours and were completed at AOS -15 minutes. Uplink sweep and antenna sweep were initiated at a ground elapsed time (g.e.t.) of T+3375 seconds (this corresponds to AOS -85 seconds) and two-way RF lock on tracking receiver I was achieved at a g.e.t. of T+3461 seconds which compares to a predicted AOS of T+3460.24 seconds. Two-way lock is confirmed by observing the plot of exciter sweep and ground receiver static phase error voltages shown in figure 7.16-14 wherein it may be seen that the ground receiver service propulsion engine (SPE) was varying in synchronism with the uplink sweep. The SPE voltage was lagging the exciter sweep voltage by approximately 1 second; however, this phenomenon also occurs when operating the ground station via its test translator, and has been isolated to a grounding problem in the RF acquisition control circuitry

at the CRO station. Downlink signal levels at the time of AOS were 7dB lower than predicted. Automatic tracking was initiated at a g.e.t. of T+3465 seconds.

The operations which occurred during the pass should be reviewed in order that the data presented may be viewed in the correct light. Although two-way lock was achieved at very nearly the predicted time, it was not recognized by the exciter/main receiver operator due to a malfunction in the spacecraft-telemetered AGC voltage meter channel. This voltage was displayed on a meter located on the operator's console and was derived via the VHF telemetry link as shown in figure 7.16-13. The reason for the circuit failure is unknown. The operator, noting the 0 volt reading on the meter, assumed he did not have proper two-way lock and proceeded to attempt several manual acquisitions. As may be observed from a plot of the doppler profile (fig. 7.16-15) and the uplink received carrier power (fig. 7.16-16) two-way lock was actually acquired and lost several times, which was possibly due to a fault in the RF acquisition circuitry that introduced uplink frequency transients which caused the transponder carrier loop to drop lock. This circuit malfunction has been confirmed by GSFC. At a g.e.t. of approximately T+80 seconds, two-way lock was recognized by observing the UHF 0-degree doppler indication displayed on the console oscilloscope.

Figure 7.16-17 is a time history of downlink main beam received carrier level as compared to the predicted levels. With the exception of an interval beginning at T+3770 seconds and ending at T+3840 seconds, general good agreement is shown between the two curves. Antenna patterns are a possible explanation for the low signal levels.

Figure 7.16-18, which depicts main and acquisition received carrier levels, shows that the same phenomeon occurs on the acquisition receiver beginning at T+3760 seconds and in the interval from T+3917 to T+4000 seconds.

Figure 7.16-17 is a time history of spacecraft received carrier levels. Considerable data were lost due to the fact the uplink was not locked during a major portion of the pass. The data points obtained showed general good agreement with predicted values and were on an average within 5 dB of the expected levels.

The doppler profile curve shown in figure 7.16-15 confirms that two-way lock was achieved at AOS and was lost subsequently and regained several times during the interval from 3517 to 3980 seconds. From 3980 seconds to LOS, there is close agreement between predicted and measured curves. The doppler frequency changes during the uplink out of

lock interval may be explained in part by the doppler extractor mechanization and its output response due to ground transmitter voltage controlled oscillator (VCO) frequency variations when in one-way downlink lock.

The equation for the biased doppler output is given by:

$$D = 1.0 \text{ MHz} = \left(\frac{240}{221} F_T - F_R\right) + 1.0 \text{ MHz} \qquad (1)$$

where D = doppler frequency

F_T = S-band uplink transmitted frequency

F_R = S-band downlink received frequency

Under normal two-way lock conditions F_R is approximately related to F_T by:

$$F_R = \frac{240}{221} F_T \left(1 - 2\frac{V}{C}\right) \qquad (2)$$

and substitution of this equation in equation (1) results in:

$$D + 1.0 = 1.0 \pm 2\frac{V}{C} \text{ MHz}$$

which is simply the two-way doppler translated about the 1.0 MHz reference.

It may be seen from equation (1) that the biased doppler frequency is a function of the uplink transmitted frequency, and this relationship is true whether or not the system is in two-way lock because of the method used to extract the doppler frequency. Therefore, any variation of exciter VCO frequency will result in an apparent shift in the received doppler. As an example, assume that at a g.e.t of 3526 seconds, the following conditions existed:

(a) The spacecraft is transmitting at F_{nom} = 2287.5 MHz

(b) One-way downlink lock is attained

(c) The exciter VCO frequency is varied 200 Hz from F_{nom} of 21.941732 MHz

(d) Automatic acquisition aid bias is set to -50 kc

Then the received frequency

$$F_R = 2287.5 + \frac{\text{two-way doppler}}{2} = 2287.546250$$

and the transmitted frequency will be

$$F_T = (21.941011 - 0.0002)96 - 2106.317856 \text{ MHz}$$

Substituting these values in equation (1)

$$D + 1.0 = \frac{240}{221} \times 2106.317856 - 2287.546250 + 1.0$$

$$D = 142.4 \text{ kHz}$$

This is approximately what is shown as the doppler readout at this time, and illustrates how such readings can be obtained when the transmitter frequency is not at nominal frequency F_{nom} and the doppler selector switch is in the two-way position. Further analysis along this line would probably explain most of the doppler frequency readings obtained during the intervals when uplink lock was lost and may point out if false locks occurred.

Spacecraft SPE curves show that the receiver SPE varied in synchronism with the uplink sweep until loss of lock. Large phase errors in terms of S-band frequency deviation occurred from T+3981 to T+4004 seconds with two-way lock established. These variations were in the order of $\pm$140 kHz. At 4004 seconds, these variations ceased, and the SPE measurement took on a more normal rate of change. The time 4004 seconds also coincided with the moment at which the MSFN exciter synthesizer loop came into lock. Prior to this time, the synthesizer loop filter had been in the operate position. It is believed that due to the synthesizer/exciter VCO phase lock loop, which is energized when the filter switch is in operate, the exciter VCO was being frequency-modulated and this modulation was being fed to the SPE telemetry channel, thus causing apparently large amounts of frequency variations. Experimental verification of this phenomenon is planned and results will be published in a supplemental report. It is noted that the percentage

of telemetry channel utilization for this SPE measurement was rather small due to the signal conditioning networks through which the error voltage was processed prior to encoding, and possibly more meaningful data could be obtained with more efficient use of the full-scale telemetry range. Up to 3770 seconds, manual sweep acquisition techniques were being utilized and since this entails audiomonitoring of the received signal, the main tracking telemetry receiver I bandwidth switch was in the 4.5-kHz position. With the switch in this position, no downlink telemetry or voice subcarriers are present at the input to the signal data demodulator subsystem (SDDS), thus no data on these channels were received until the telemetry switch was placed in the 3.3-MHz position at T+3770 seconds.

At a g.e.t. of approximately T+3980 seconds, all switches were put in normal positions and abbreviated tests involving modes 1A (ranging only), IF (upvoice, ranging and updata), and 1G (updata only) were performed. Results of these tests are discussed in the appropriate subsections of this report.

Uplink received signal lock was lost at T+4179 seconds, and downlink received main beam signal lock was lost at T+4175 seconds, which is in reasonable comparison to predicted LOS of T+4160 seconds. Acquisition receiver LOS occurred at T+4165 seconds.

In summary, although several problem areas caused a loss of desired data and make the analysis of available data somewhat complicated, it is believed that from an RF standpoint the subsystem equipment operation was normal with the exception of the RF acquisition circuitry. Investigation is continuing on the as yet unexplained phenomena pointed out in this section.

(e) Downvoice channel: Figure 7.16-19 is a block diagram of the downvoice test configuration typical of the MSFN USB sites for Mission AS-202. The simulated voice signal (400 Hz) tone was received on the S-band reference receiver nos. 1 and 2. Receiver no. 2 derived its input from the acquisition antenna, which was approximately 20 dB weaker than receiver no. 1 signal levels. The voice subcarrier (1.25 MHz) was detected in the PM detector of the telemetry receiver and coupled to the signal data demodulators. The voice demodulator was a modulation tracking phase lock loop, where the 400-Hz tone, which (FM) modulates the 1.25-MHz subcarrier, was detected. The detected 400 Hz from both signal data demodulators was recorded on a voice tape recorder (FR-1100) or equivalent. The PM composite signal from receiver nos. 1 and 2 was also recorded directly on a wideband tape recorder (mincom 22 or equivalent).

The VHF/AM voice signal (400-Hz tone) was detected in the VHF/AM receiver and recorded on the same voice tape recorder as the detected USB simulated voice signal.

(1) Downvoice at MILA. The detected 400 Hz tone at MILA was audible until approximately T+400 seconds. Figure 7.16-20 is a plot of signal-to-noise in a noise bandwidth of 706 Hz as a function of time at MILA. This plot was obtained from the baseband tape recording at MILA of the PM composite signal from receiver no. 1. The absolute values of the signal-to-noise ratios obtained are in general agreement with expected values. However, with the measurement techniques available for processing the flight data the accuracy of absolute signal-to-noise ratios might be expected to vary from predicted values.

(2) Downvoice at BDA. Figure 7.16-21 shows the signal-to-noise ratio of the downvoice 400-Hz tone in a 706-Hz bandwidth as a function of time at BDA. This plot was again, from the baseband tape recording of the PM composite signal from receiver no. 1. Again the measured values agree generally with expected results.

(3) Downvoice at CRO. Figure 7.16-22 is a plot of downvoice signal-to-noise ratio of the 400-Hz tone in a 706-Hz bandwidth as a function of time at CRO. This plot was from the baseband tape recording of the PM composite signal from receiver no. 1. From figure 7.16-22 it is seen that a voice signal was not received at CRO or receiver no. 1 until T+3770 seconds. This time corresponds to the time at which the 3.3 megacycle IF bandwidth was selected based on the event recorded data obtained. Again the measured signal-to-noise ratios agree generally with expected values.

(f) Upvoice channel: The uplink voice channel was tested during the AS-202 mission. However, there was no instrumentation onboard the spacecraft to recover the simulated uplink voice signal (1 kHz tone). Therefore, the only check on upvoice performance was in recovering the turned-around uplink subcarrier received at the MSFN sites. The 30-kHz upvoice subcarrier appeared in the downlink spectrum since it was detected in the spacecraft wideband phase detector and remodulated on the downlink along with the PRN range code, thus the baseband recording of the PM composite signal from the MSFN receivers contains the 30-kHz subcarrier. Figure 7.16-23 is a block diagram of the typical MSFN USB upvoice test configuration for Mission AS-202. As seen from the figure, a 1-kHz tone FM modulated the upvoice 30-kHz subcarrier, which is in turn phase-modulated on the S-band carrier. The transmitted signal was sampled by the verification receiver where the 30-kHz modulation was detected, and the 1-kHz tone was recovered and recorded to verify that transmission was occurring. The downlink S-band signal

was received, and the PM information was detected in the telemetry receivers. The output of the telemetry receiver was essentially a baseband spectrum of all downlink and turned-around uplink modulation. The signal was recorded on a wideband tape recorder on-site.

(g) Upvoice MILA: The reception of the upvoice signal in the downlink spectrum at MILA verified that the transmission link was operable. The quality of the 1-kHz tone obtained indicated that adequate subcarrier power was received at the output of the spacecraft wideband data channel to provide useable voice data from the upvoice discriminator. A more detailed analysis of the uplink voice channel performance including signal-to-noise ratio measurements will be provided in a supplemental report.

(h) Upvoice at BDA and CRO: The uplink voice signal data reduced from the BDA tape indicated degraded performance which could possibly be due to low modulation indexes. Additional data evaluation is presently underway and results will be presented in a supplemental report. The CRO upvoice subcarrier apparently was not modulated with the 1-kHz tone. The verification receiver output and the 30-kHz turned-around upvoice subcarrier both indicated that the tone was not present. At CRO the upvoice subcarrier was received in the downlink spectrum during the times that it was applied to the uplink, as evidenced by a noise-quieting effect in the Block I spacecraft discriminator.

(i) USB and VHF transmission of PCM telemetry: Figure 7.16-24 is a block diagram of the PCM telemetry test configuration typical of the MSFN USB sites for Mission AS-202. The S-band telemetry subcarrier signal was detected in the telemetry receiver and the 1.024-MHz biphase modulated subcarrier was then filtered and demodulated in the signal data demodulators. Both receivers were utilized with receiver no. 2 connected to the acquisition antenna, giving approximately 20-dB weaker signal levels on that receiver. The demodulated PCM bit stream from receiver no. 1 was coupled to the wideband signal conditioner, where the decision circuitry (that is, whether a one or a zero was received) is contained. The output bit stream from the wideband signal conditioner was then recorded on the wideband tape recorder. The VHF FM telemetry was detected and coupled to the narrowband signal conditioner, and the conditioned bit stream recorded on the wideband tape recorder.

The unconditioned VHF/FM and S-band PCM bit streams were also recorded on the wideband tape recorder. In addition, the PM composite signal from both S-band receivers were recorded simultaneously with the above data.

(j) PCM telemetry at MILA: Table 7.16.2-II(a) shows the bit error rates obtained at MILA for the 1-minute time samples indicated.

These bit error rates were based on the synchronization word error rates. As seen from the table, the S-band telemetry was lost completely after T+260 seconds. At that time the received S-band carrier power had fallen below -120 dBm, which was below threshold for the 51.2 kilo bits/sec telemetry channel. Figure 7.16-23 shows the received VHF/FM power at MILA as a function of time. The calibration given for the VHF AGC was not valid for signal levels greaten than -67 dBm, and the times where the AGC indicated signal levels greater than that are indicated on the figure. From figure 7.16-25 and the S-band received carrier power figure 7.16-8, it is seen that the S-band telemetry performance was essentially as good as that of VHF for the time intervals utilized even though the received S-band signal carrier levels were considerably weaker. It should be noted here that the telemetry subcarrier modulation loss was -7.2 dB which means that telemetry signal power for the S-band system and S-band carrier power (which was 7 dB down from the total power) were essentially the same, and figure 7.16-8 could be labeled received telemetry power (S-band) for this particular case.

(k) PCM telemetry at BDA: Table 7.16.2-II(b) shows the bit error rate obtained at BDA for the 1-minute samples indicated. These bit error rates are based on the synchronization word error rates. As seen from the table, the S-band telemetry was out of lock from T+380 to T+470 seconds and was completely lost after T+590 seconds. After T+590 seconds, the received S-band carrier power had fallen below -120 dBm which is below threshold for the 51.2 kilo bits/sec telemetry channel. Received VHF/FM power was not available from BDA; therefore, a comparison between S-band and VHF AGC levels affecting PCM data could be made. The S-band PCM performance was essentially as good as that of VHF for the in-lock portion of the pass.

(l) PCM telemetry at CRO: Table 7.16.2-II(e) shows the bit error rates obtained at CRO for the 1-minute time samples indicated. These bit error rates are based on the synchronization word error rates. As seen from the table, the S-band telemetry bit error rate (BER) for the seven intervals indicated was worse than VHF telemetry BER for two intervals, better for two intervals, and equal to for three intervals. VHF PCM tab printout began at T+3463 seconds; however, for comparison with S-band PCM, the VHF telemetry BER prior to T+3780 seconds is not shown in the table. S-band PCM data were not received until T+3770 seconds on receiver no. 1. This time coincided with the 100-channel event recorder marker of the 3.3-MHz IF BW selection. The 3.3-MHz BW was to be selected prior to AOS, but the event marker indicated this was not the case.

(m) Ranging performance: Figure 7.16-26 is a block diagram of the typical MSFN USB site test configuration for the PRN ranging during Mission AS-202. The pseudorandom range code was transmitted to the

spacecraft where it was turned around and transmitted via PM modulation of the downlink S-band carrier to the MSFN receiver. The range code clock served as a signal for a separate phase-locked receiver where a correlation process occurred with the receiver range code during the code acquisition process. During code acquisition the range data were updated on clock doppler and after acquisition has been accomplished (that is, state P-7 was reached). The range data began updating on UHF doppler, which was essentially one-sixteenth of the two-way RF doppler. The output of the ranging subsystem is strobed every 6 seconds, and the tracking data processor accepted the range data for formatting. The formatted range data, along with other data handled by the tracking data processor (TDP), were coupled from the TDP to a 205A data modem where the bit stream was converted to a modulated sinewave and recorded directly on the wideband tape recorder.

(n) Ranging performance at BDA and CRO: Figure 7.16-27 presents the measured range for the BDA MSFN USB site obtained from the pseudorandom range system during Mission AS-202. Prediction of the range at BDA based on measured trajectory data is not yet available and will be included in a supplemental report. The range data received from CRO were not valid. The exact cause for the bad range data at CRO has not yet been established; however, there are some indications that correlation voltage levels were not set correctly, which can cause erroneous range code acquisitions. This area is still under investigation and will be described in more detail in a supplemental report. The measured range shown in figure 7.16-27 includes correction factors for spacecraft code delay, MSFN-USB system delay, and corrections for range receiver phase error due to doppler and time correlation errors of range number printouts with actual time of range number sampling.

(o) Ranging performance at MILA: Correct ranging acquisition was performed before lift-off, and doppler updating of the range numbers began at lift-off while still in the presence of multipath effects. At lift-off the received signal strength was a nominal -80 dBm at the USBE and -100 dBm at the MSFN receiver. The received ranging mode 1A acquisition threshold for an integration time of 2^6 is approximately -118 dBm or greater. For mode 1F and 2^6 this received signal strength should be greater than -112 dBm. Any range acquisitions performed in mode 1A with signal strengths less than -118 dBm requires an increase in ranging integration time (approximately 3 dB per each integration switch setting).

Continuous valid ranging information was received until 303.5 when an intentional reset of the ranging subsystem was performed. At this time (T+303 sec), the received signal strength was -123 dBm and the tracking and range receivers were in two-way lock with mode 1F

modulation. The ranging system having been reset, a new range acquisition was attemped in mode 1F using clock instead of PRN modulation (T+309 sec) also with less than required signal strengths for mode 1F ranging threshold. The correlation voltage at this time was not low enough to drop clock loop lock. The ranging subsystem went through with an acquisition with clock-only modulation, and when this happens, erroneous ranging information is read out regardless of mode or signal strength. The range number readout at (T+310 sec) with clock modulation was 184 507 nautical miles. Numerous range acquisitions were attempted from T+309 sec to T+394 sec, using PRN modulation some of the time, and also variable integration switch settings at various intervals. Signal strengths during this time interval went from -124 to -133 dBm, which would normally have required an integration time of 2^{13} and approximately 4 minutes to complete. With these conditions prevailing, ranging acquisition and readouts were in error. At T+399 sec, ranging acquisition was concluded.

Figure 7.16-26 presents the measured range for the MILA USB site obtained from the pseudorandom range subsystem during Mission AS-202. Prediction of the actual range based on measured trajectory data is not yet available and will be included in a supplemental report. The measured range shown in figure 7.16-28 includes correction factors for spacecraft code delay, MSFN-USB system delay, and correction for range receivers phase errors due to clock doppler and time correlation errors or range number printouts with actual time of range number sampling.

TABLE 7.16-I.- USB OPERATIONAL AND TRANSMISSION FOR MISSION AS-202

Used by	Mode	Subcarrier frequency	Subcarrier modulating signal	Carrier modulating index, radians
MILA BDA CRD	Downlink Mode B-1	Ranging 1.024 MHz 1.25 MHz	PRN[a] - Lunar code PCM[b] - 51.2 kilo bits/sec Voice - 400 Hz tone (Δf = 7.5 kHz)	0.3 1.10 0.84
MILA CRO	Uplink Mode 1-F	PRN 30 kHz 70 kHz	Lunar code 1 kHz tone (Δf = 7.5 kHz) Updata (subcarrier only)	0.3 0.61 0.61
CRO	Uplink Mode 1-G	30 kHz 70 kHz	1 kHz tone (Δf = 7.5 kHz) Updata (subcarrier only)	0.55 0.55
BDA CRO	Uplink Mode 1-A	Carrier Ranging	-- PRN lunar code	-- 0.3
None	Uplink Mode 1-B	30 kHz	Voice 1 kHz tone (Δf = 7.5 kHz)	0.93
None	Uplink Mode 1-C	70 kHz	Updata (subcarrier only)	0.93
BDA	Uplink Mode 1-D	30 kHz Ranging	Voice 1 kHz tone (Δf = 7.5 kHz) PRN - Lunar code	0.93 0.3

[a] Pseudo-random noise.

[b] Pulse code modulation.

TABLE 7.16-II.- USB/VHF COMPARISON OF PCM TELEMETRY

(a) Merritt Island Launch Area (MILA)

Time, sec	Word error rate, kilo bits/sec	Bit error rate, kilo bits/sec	System
0 to 60	1.03×10^{-2}	4×10^{-4}	S-band
61 to 120	1.6×10^{-2}	6×10^{-4}	
121 to 180	2.2×10^{-2}	8.5×10^{-4}	
181 to 240	8.3×10^{-3}	2.2×10^{-4}	
241 to 260	8.86×10^{-2}	3.4×10^{-3}	
0 to 60	3.3×10^{-3}	1.25×10^{-4}	VHF
61 to 120	6.6×10^{-4}	2.5×10^{-5}	
121 to 180	5.1×10^{-2}	2×10^{-3}	
181 to 240	6.6×10^{-4}	2.5×10^{-5}	
241 to 300	1.3×10^{-3}	5×10^{-5}	
301 to 360	1.3×10^{-3}	5×10^{-5}	
361 to 420	1.66×10^{-2}	6.2×10^{-4}	

TABLE 7.16-II.- USB/VHF COMPARISON OF PCM TELEMETRY - Continued

(b) Bermuda (BDA)

Time, sec	Word error rate, kilo bits/sec	Bit error rate, kilo bit/sec	System
300 to 360	1×10^{-3}	3.9×10^{-5}	S-band
361 to 380	2×10^{-2}	7.5×10^{-4}	
Out of lock			
470 to 530	3.3×10^{-4}	1.2×10^{-5}	
530 to 590	No errors		
250 to 310	6.6×10^{-4}	$2,5 \times 10^{-5}$	VHF
311 to 370	4.3×10^{-3}	1.75×10^{-4}	
371 to 430	1.06×10^{-2}	4×10^{-4}	
431 to 490	3.3×10^{-4}	1.2×10^{-5}	
491 to 550	3.3×10^{-4}	1.2×10^{-5}	
551 to 610	6.6×10^{-4}	2.5×10^{-5}	
611 to 670	3.3×10^{-4}	1.2×10^{-5}	
671 to 730	3.3×10^{-4}	1.2×10^{-5}	
731 to 790	1×10^{-3}	3.9×10^{-5}	

TABLE 7.16-II.- USB/VHF COMPARISON OF PCM TELEMETRY - Concluded

(c) Carnarvon

Time, sec	Word error rate, kilo bits/sec	Bit error rate, kilo bits/sec	System
3780 to 3840	2.6×10^{-2}	1×10^{-3}	S-band
3841 to 3900	No errors		
3901 to 3960	4×10^{-3}	1.5×10^{-4}	
3961 to 4020	1×10^{-3}	3×10^{-3}	
4021 to 4080	3.3×10^{-4}	1.25×10^{-5}	
4081 to 4141	3.3×10^{-4}	1.25×10^{-5}	
4141 to 4170	3.6×10^{-2}	1.3×10^{-3}	
3780 to 3840	2.6×10^{-2}	1×10^{-3}	VHF
3841 to 3900	No errors		
3901 to 3960	4×10^{-3}	1.5×10^{-4}	
3961 to 4020	6.6×10^{-4}	2.5×10^{-5}	
4021 to 4080	1.3×10^{-3}	5×10^{-5}	
4081 to 4140	6.6×10^{-4}	2.5×10^{-5}	
4141 to 4180	2.3×10^{-2}	9×10^{-4}	

NASA-S-66-10134

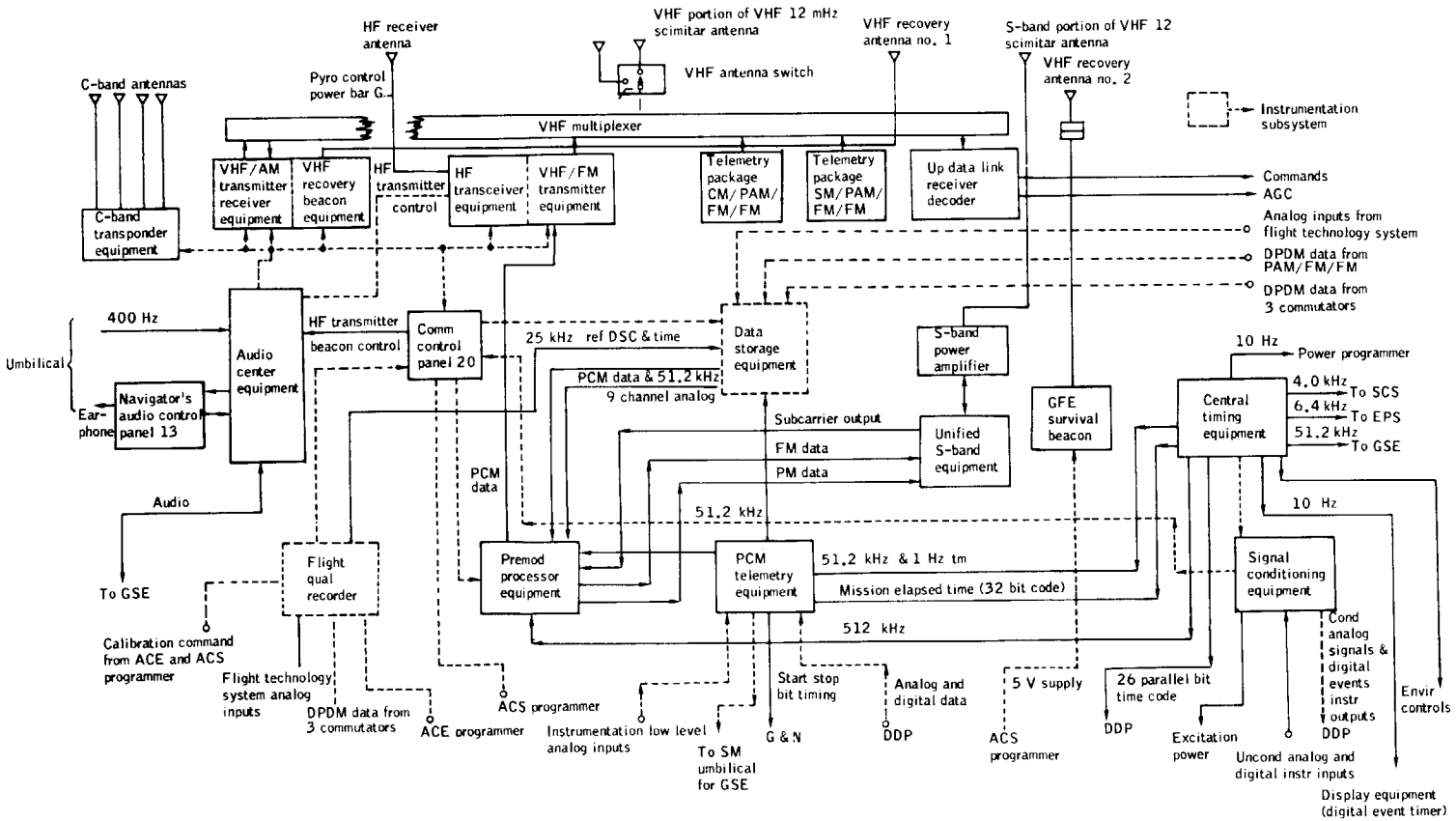

Figure 7.16-1.- Communications subsystem, Mission AS-202.

NASA-S-66-10135

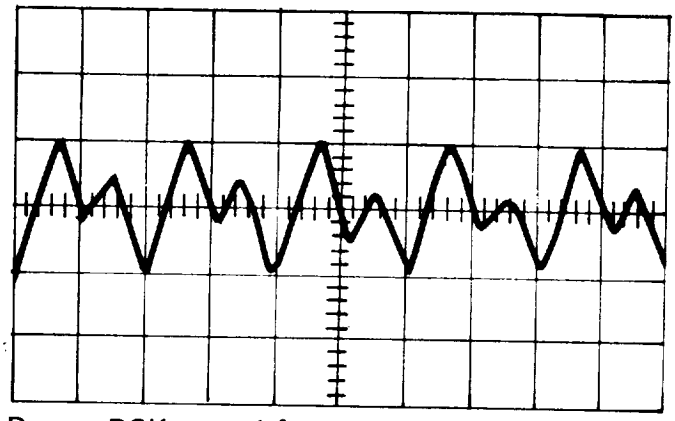

Proper PSK signal from Mission Control Center at Cape Kennedy (MCC-K)

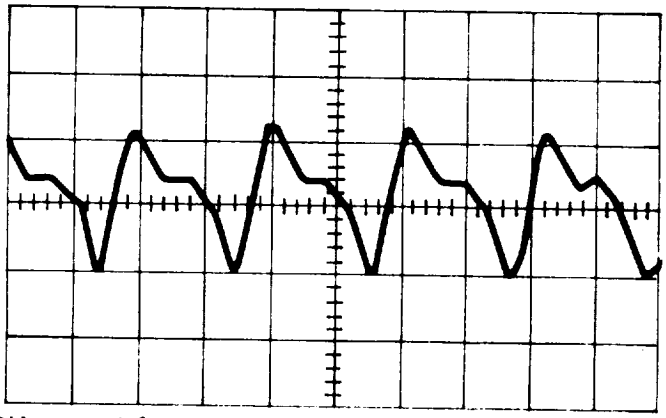

PSK signal from USNS Coastal Sentry Quebec (CSQ)

Figure 7.16-2.- Real time command PSK signal wave form comparison, Mission AS-202.

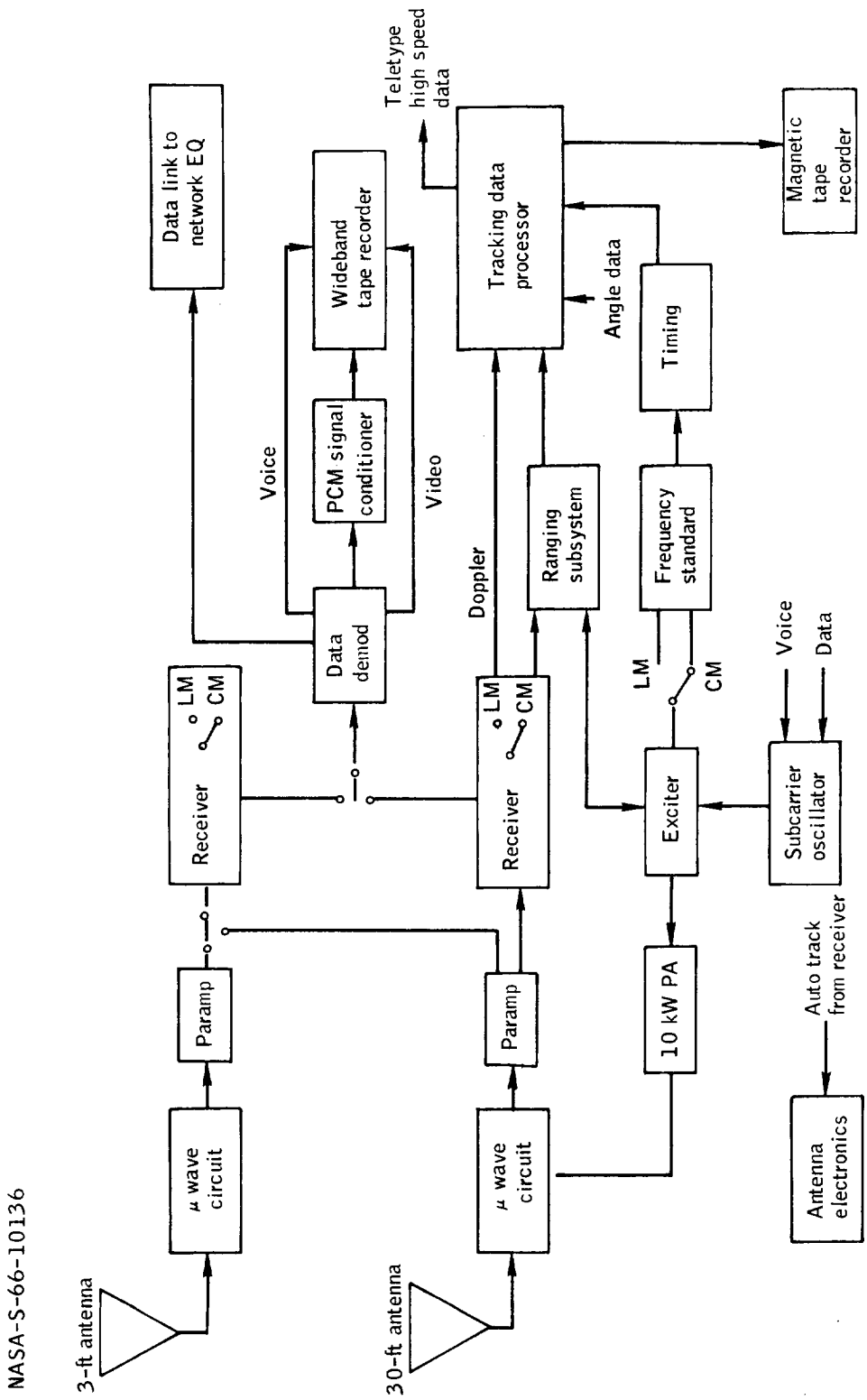

Figure 7.16-3.- Typical USB subsystem 30-foot antenna facility, Mission AS-202.

NASA-S-66-10137

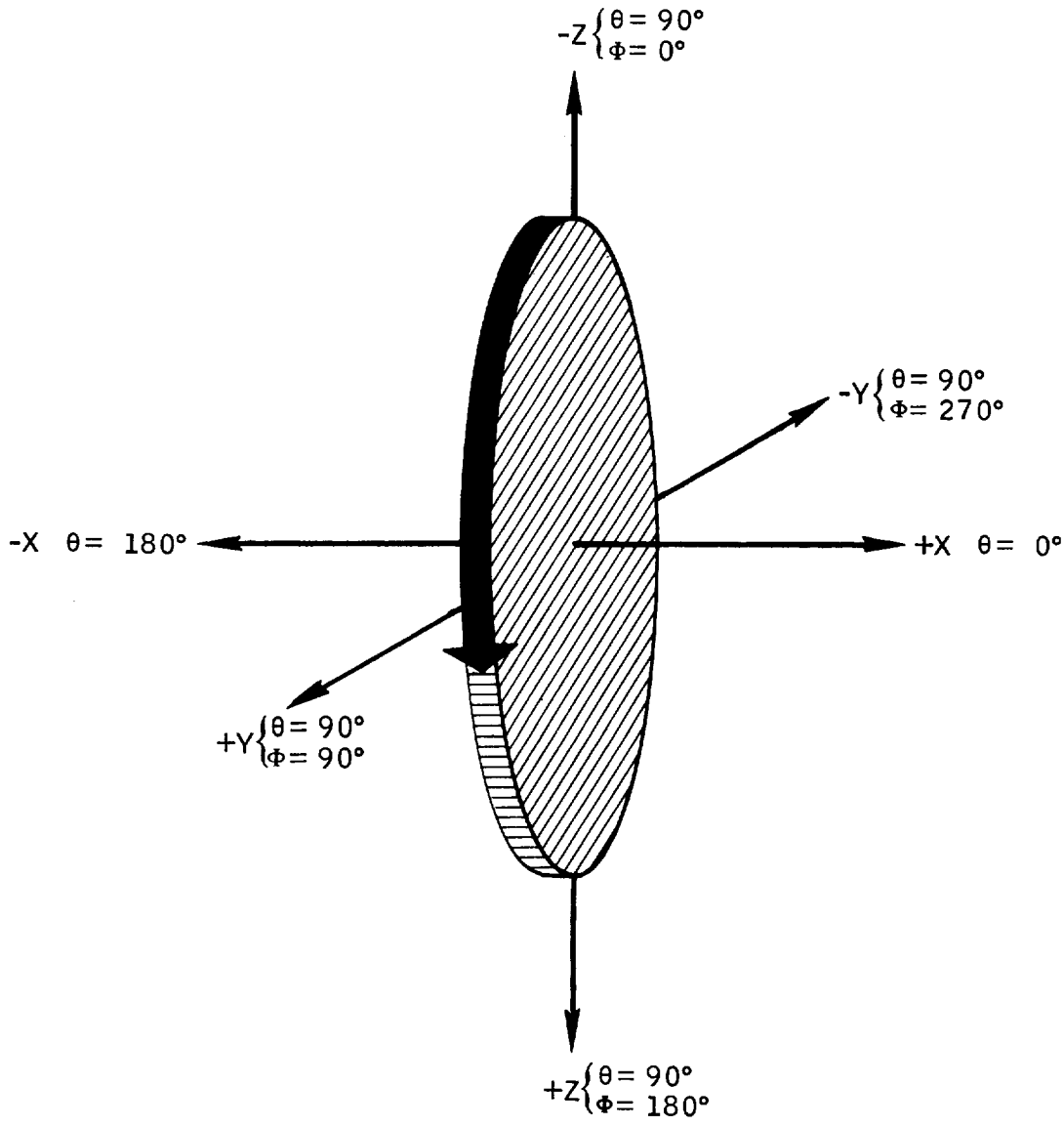

Figure 7.16-4.- Antenna look angles related to spacecraft coordinates, Mission AS-202.

NASA-S-66-10138

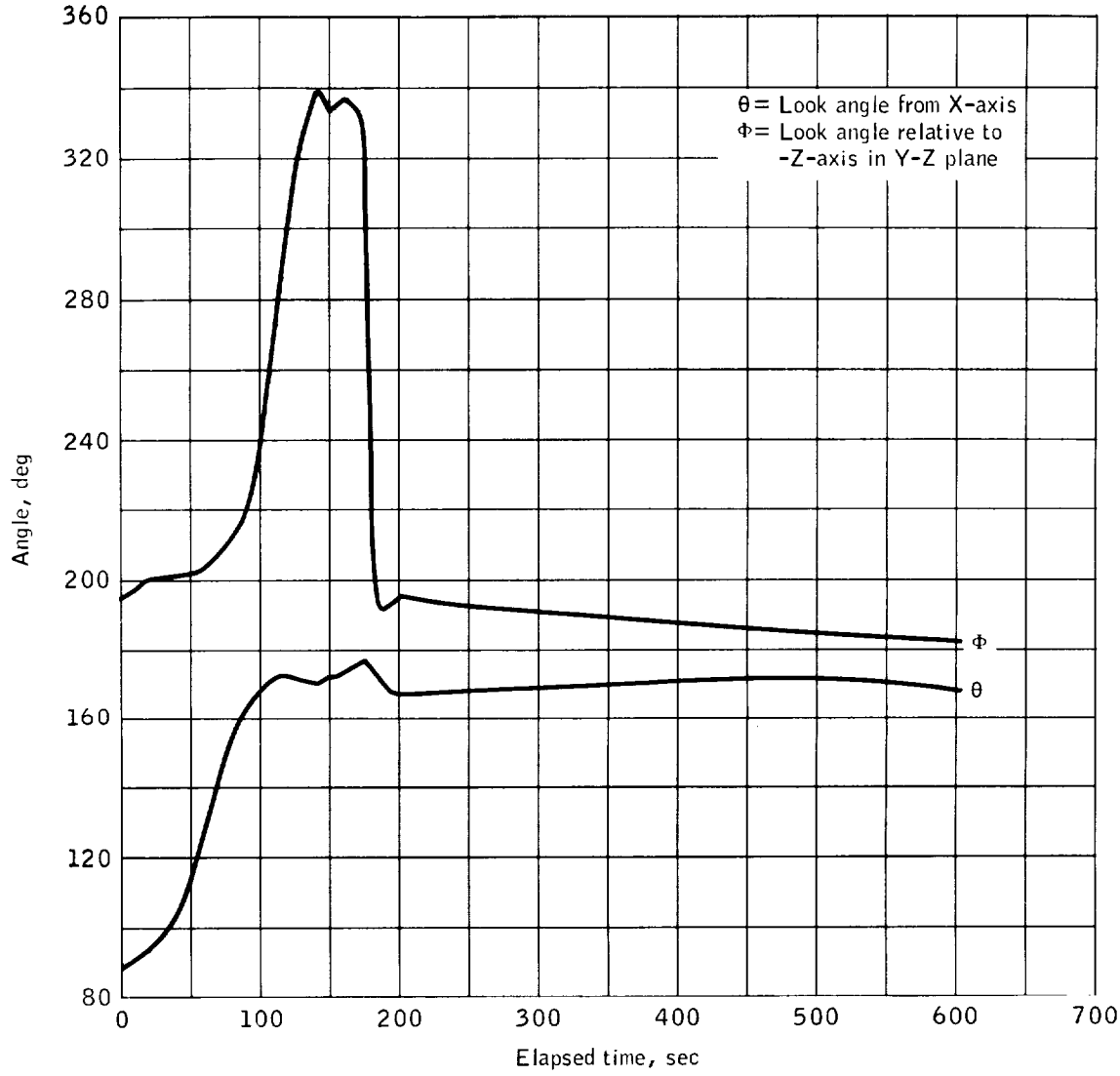

Figure 7.16-5.- Time history of predicted look angles for +Z scimitar antenna from MILA, Mission AS-202.

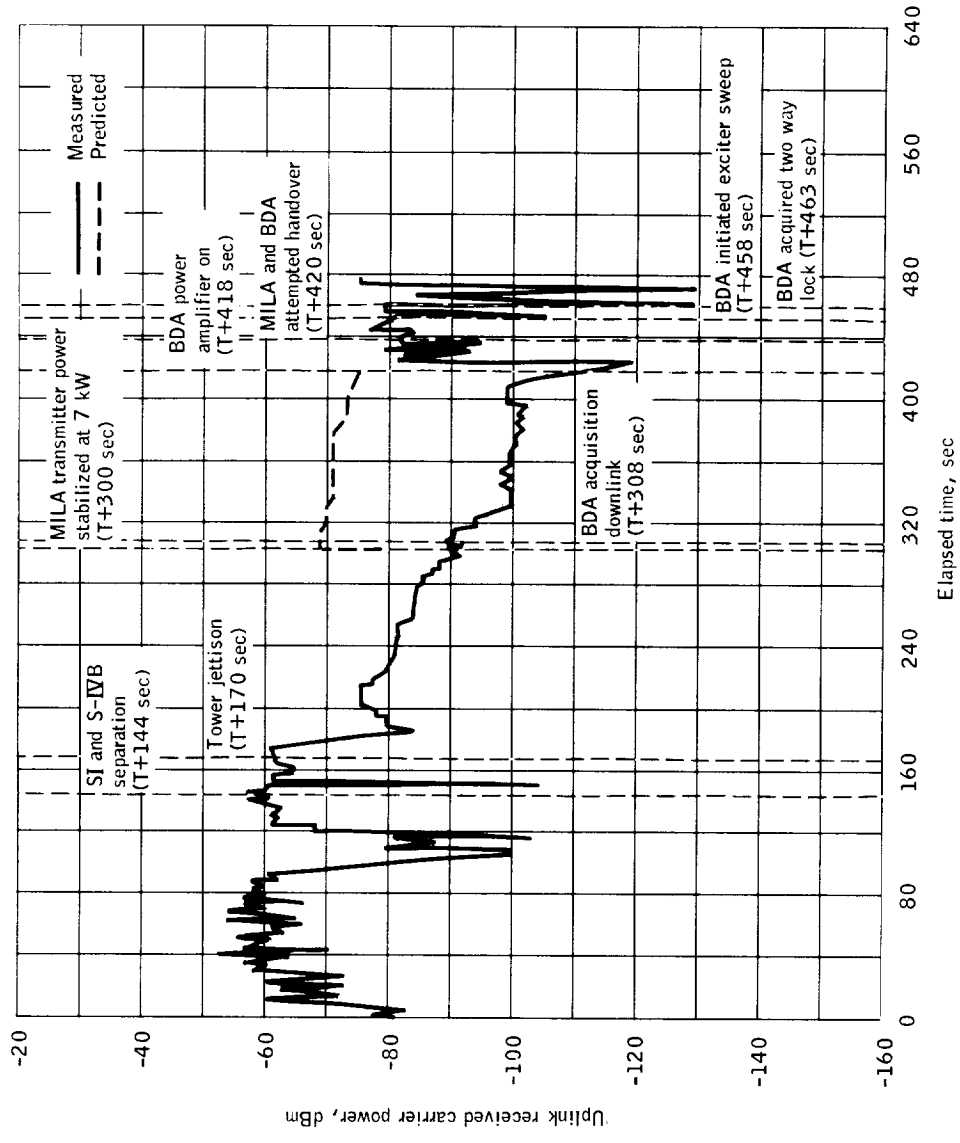

NASA-S-66-10139

Figure 7.16-6.- Uplink SC received carrier power as a function of time into pass - MILA, Mission AS-202.
(Predictions based on 100 percent antenna efficiency, for the 50 percent efficiency subtract 3 dB).

NASA-S-66-10140

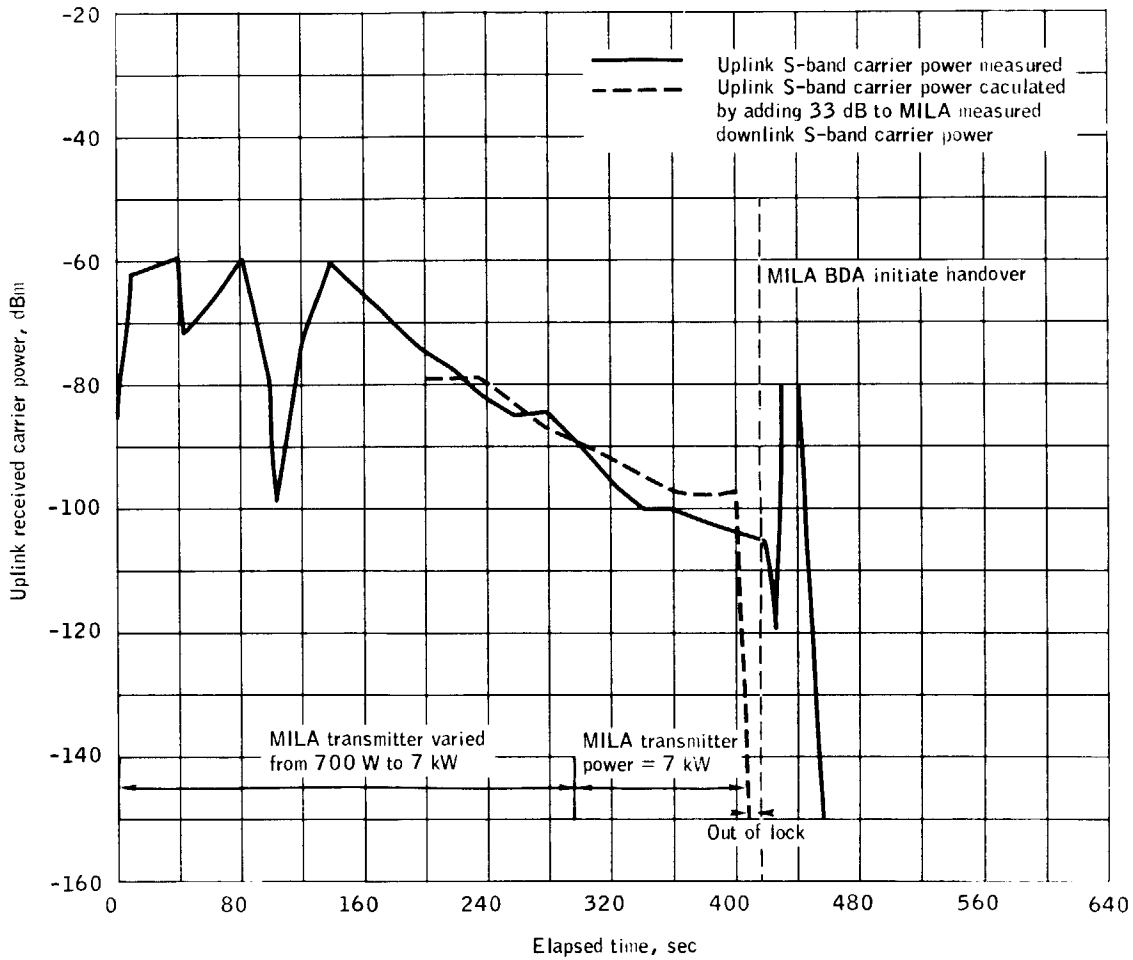

Figure 7.16-7.- Uplink received carrier power as a function of time into pass - MILA, Mission AS-202. (Predictions based on 100 percent antenna efficiency, for the 50 percent efficiency subtract 3 dB).

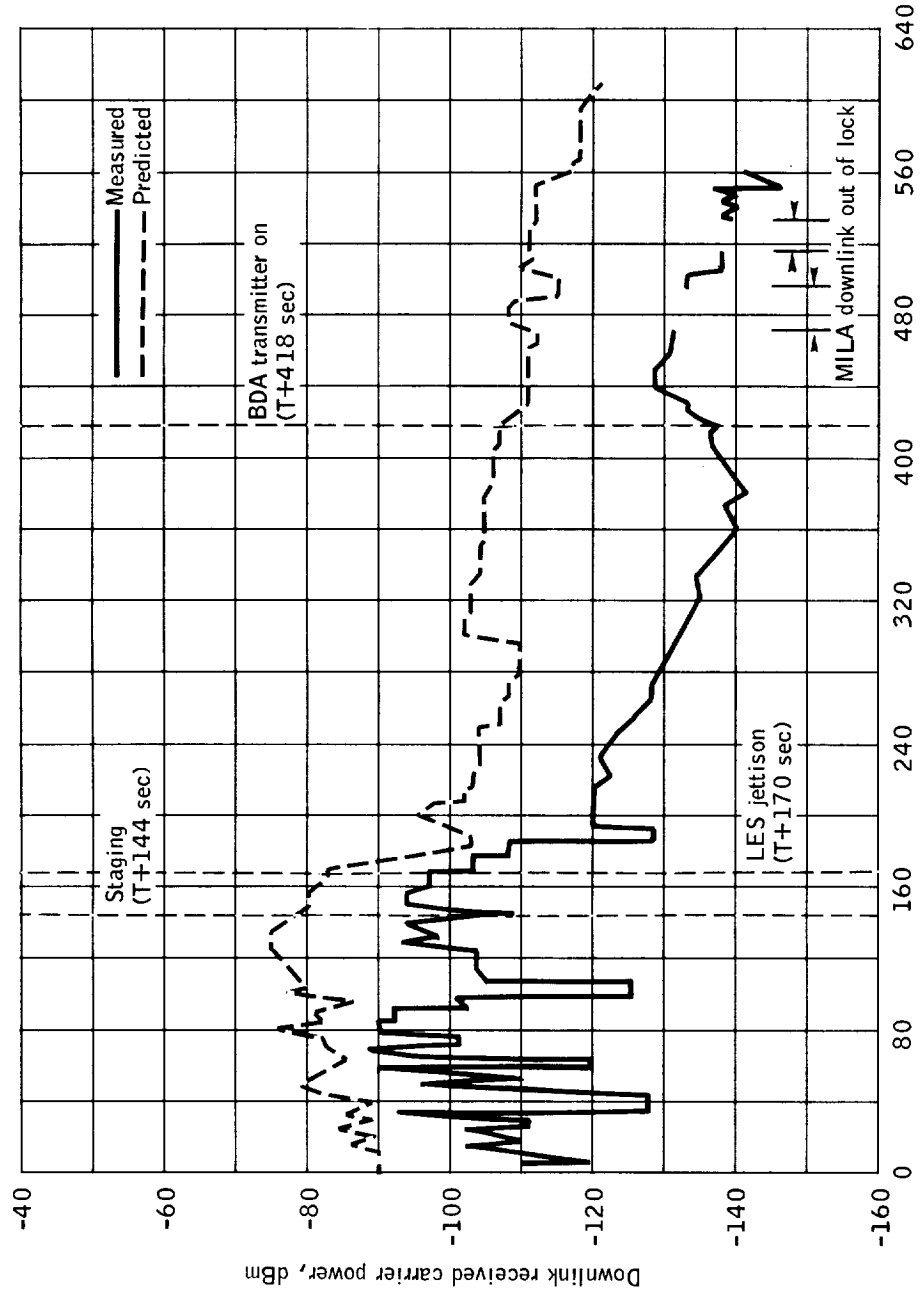

NASA-S-66-10141

Figure 7.16-8.- Downlink received carrier power as a function of time into pass - MILA, Mission AS-202. (Predictions based on 100 percent antenna efficiency, for the 50 percent efficiency subtract 3 dB).

NASA-S-66-10142

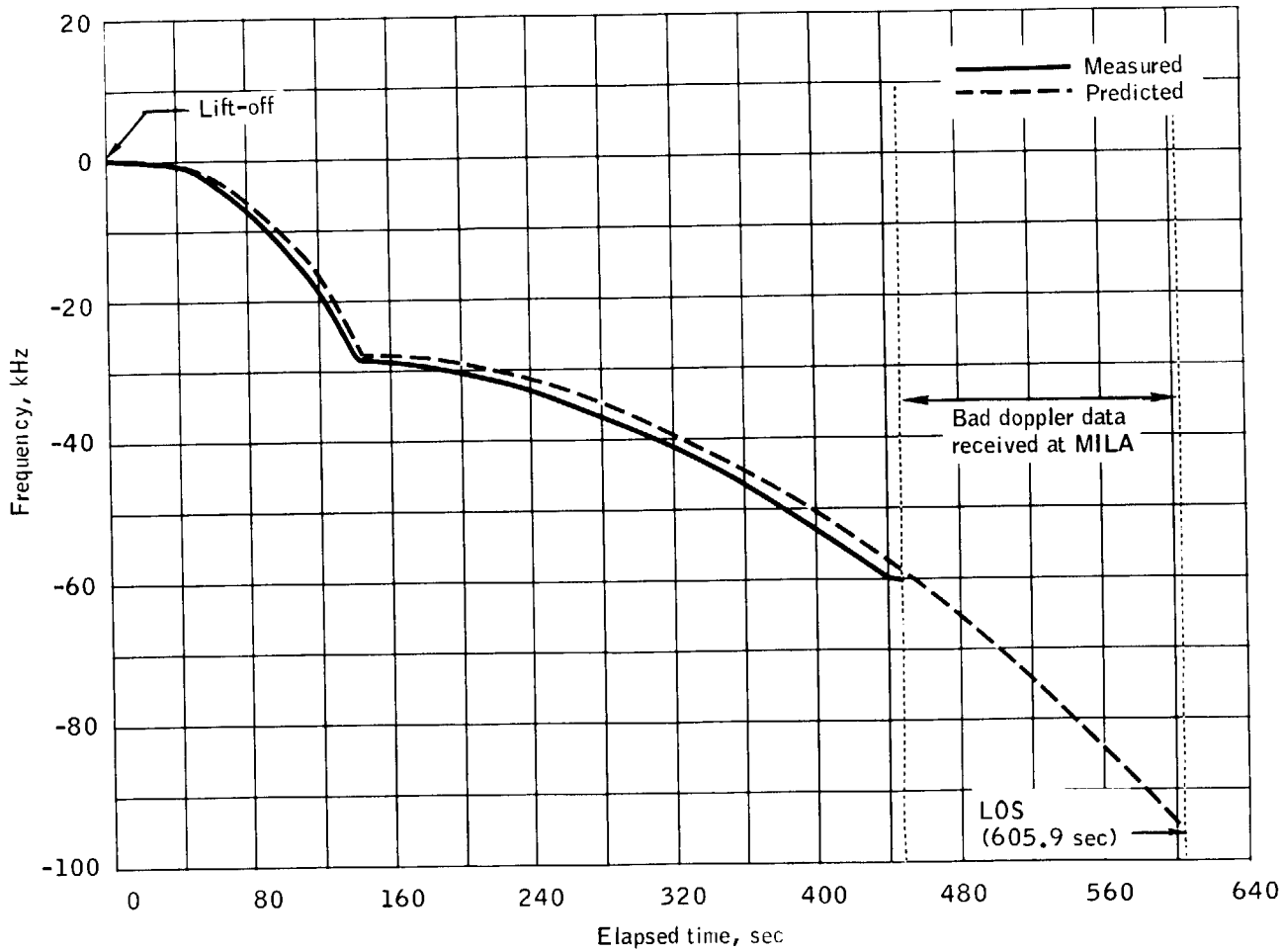

Figure 7.16-9.- Two way RF doppler as a function of time into pass - MILA-USB site, TDP data-track 10, Mission AS-202.

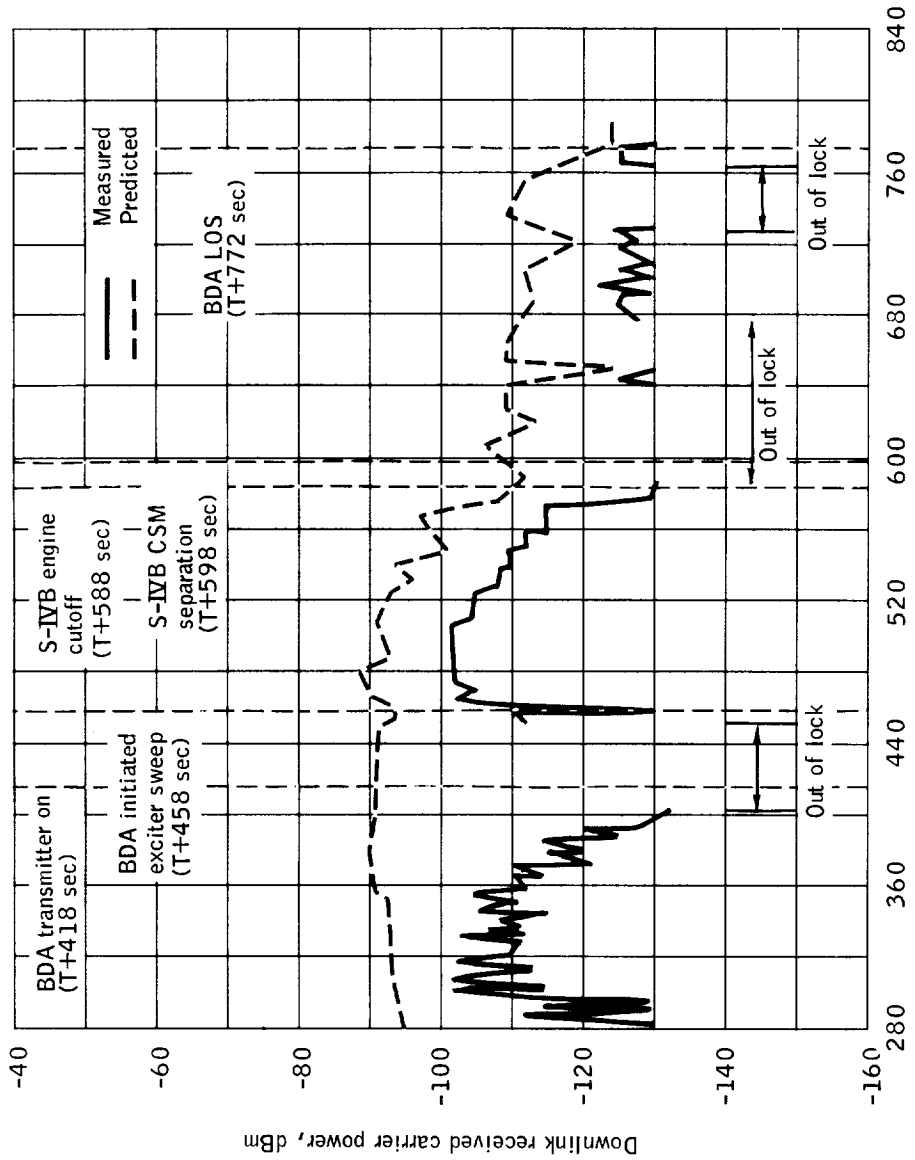

Figure 7.16-10.- Downlink received carrier power as a function of time into pass - BDA, Mission AS-202. (Predictions based on 100 percent antenna efficiency, for the 50 percent efficiency subtract 3 dB).

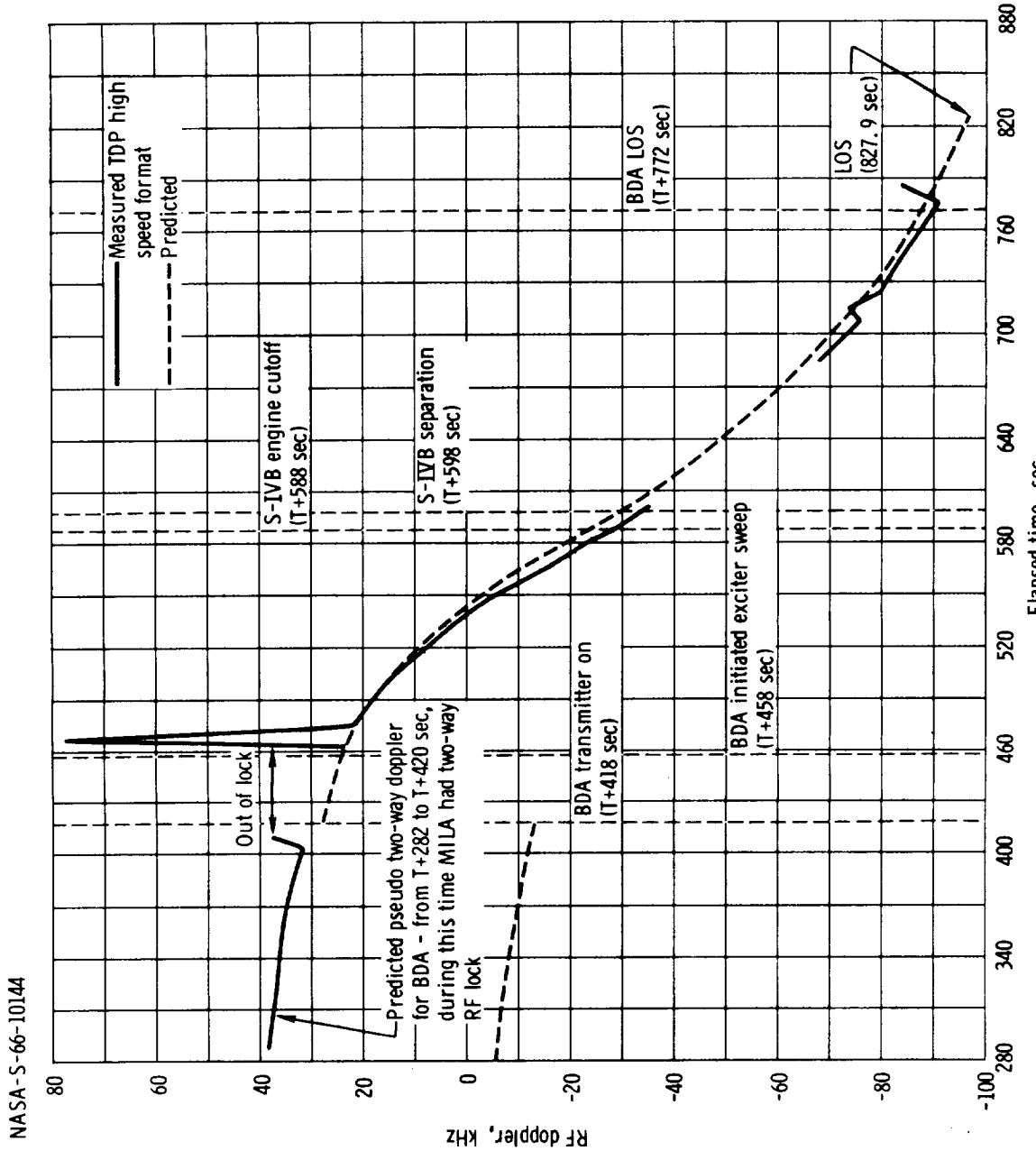

NASA-S-66-10144

Figure 7.16-11. - Two way RF doppler as a function of time into pass - BDA, Mission AS-202.

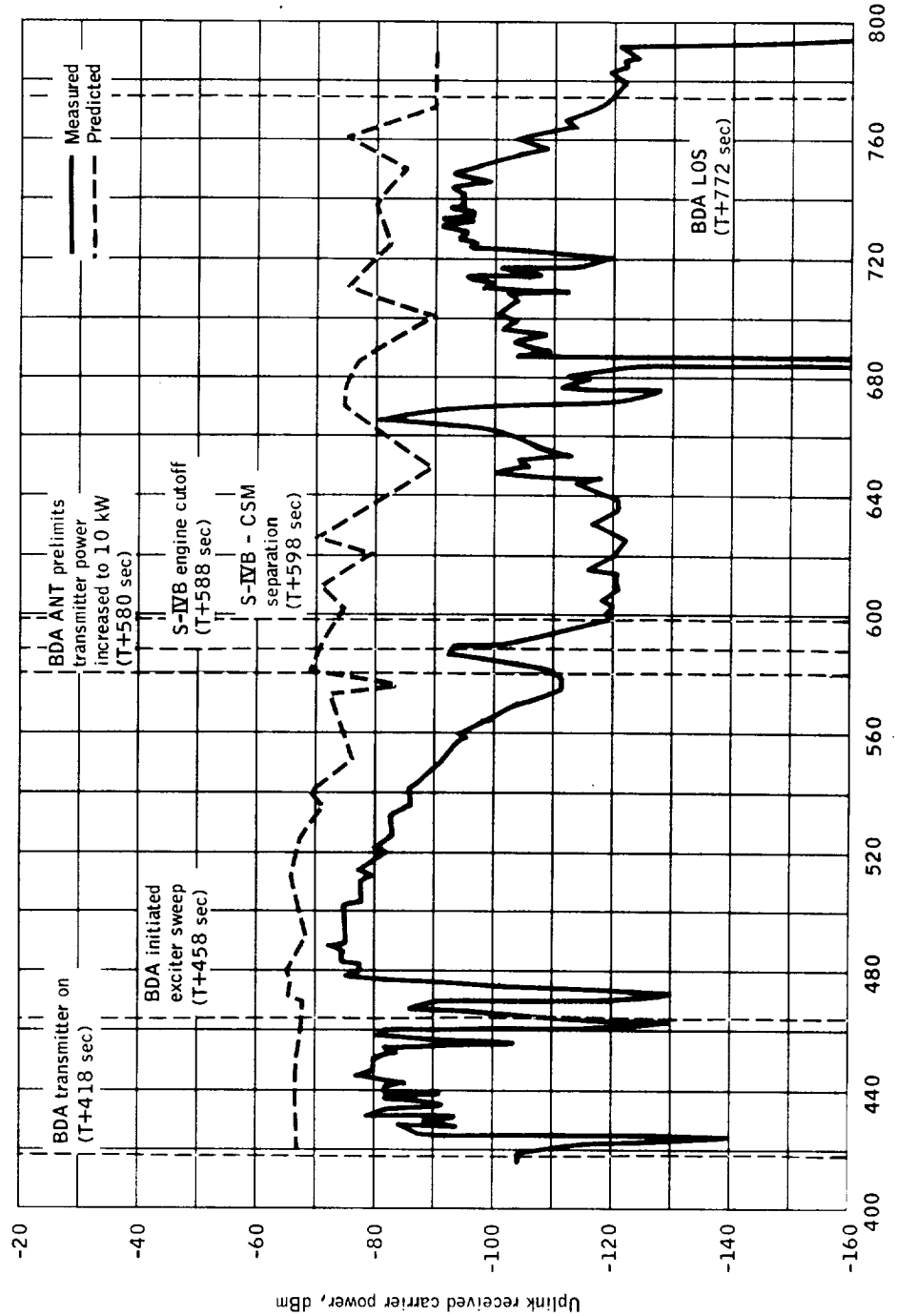

NASA-S-66-10145

Figure 7.16-12.- Uplink received carrier power as a function of time into pass - BDA, Mission AS-202. (Predictions based on 100 percent antenna efficiency, for the 50 percent efficiency subtract 3 dB).

NASA-S-66-10146

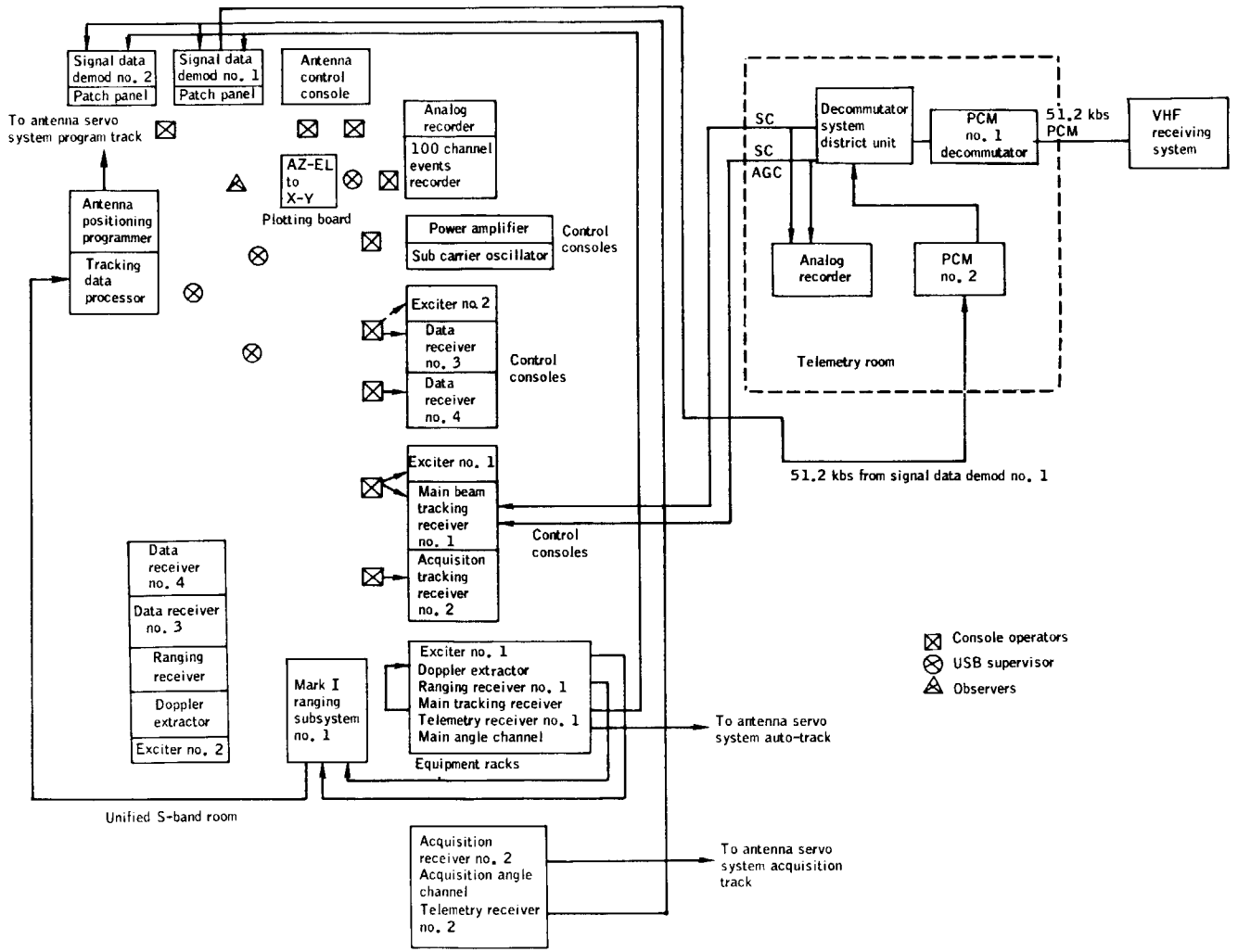

Figure 7.16-13. - CRO equipment and operational configuration, Mission AS-202.

NASA-S-66-10147

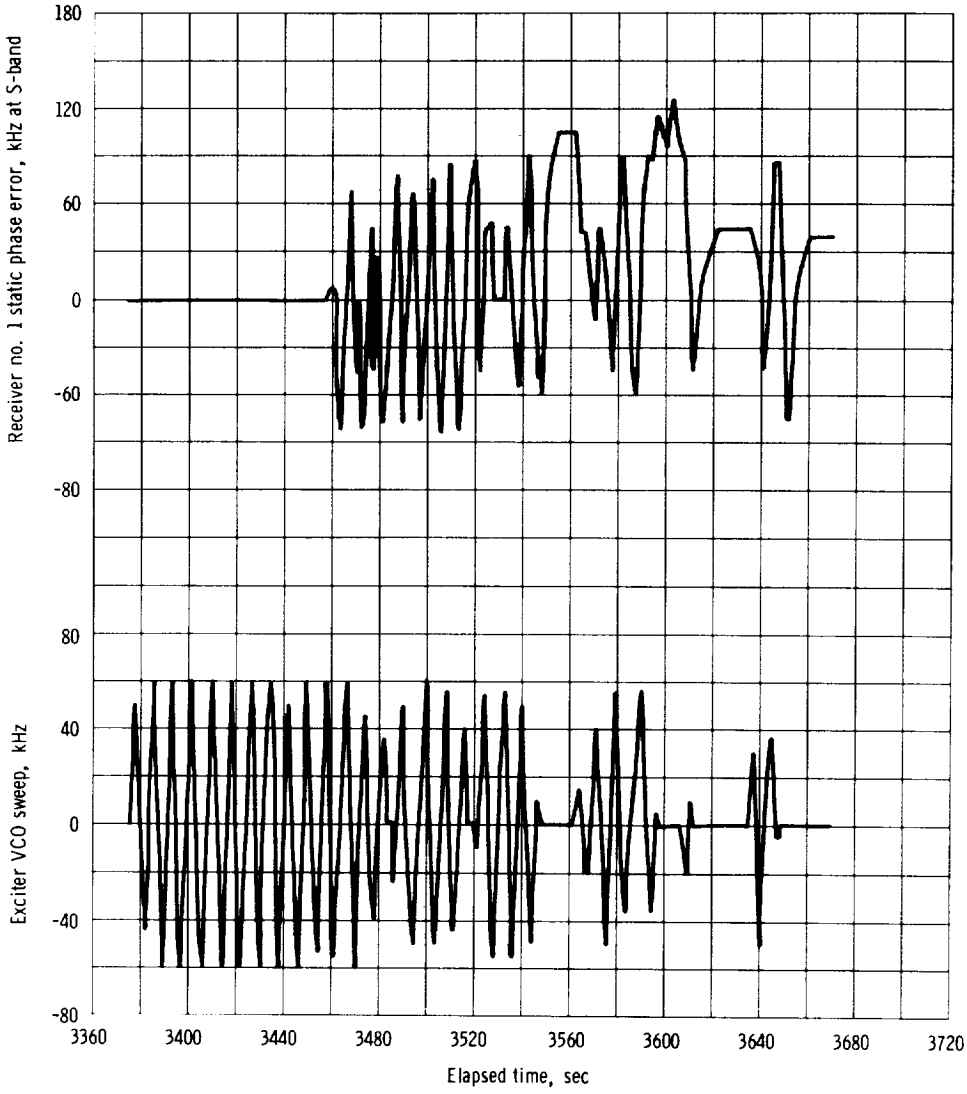

Figure 7.16-14. - Receiver no. 1 static phase error and exciter VCO sweep as a function of time into pass - CRO dynagraph strip chart, Mission AS-202.

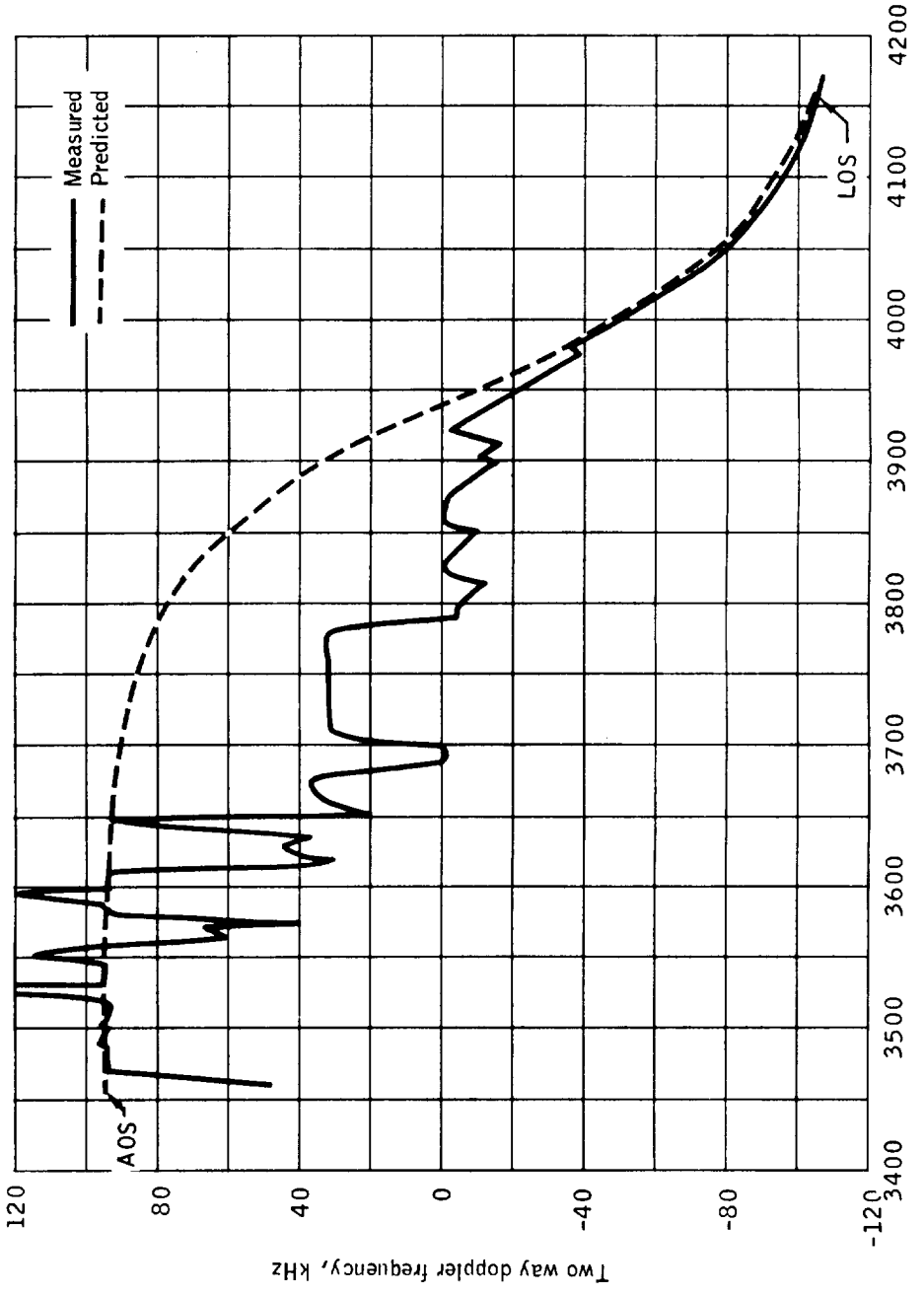

NASA-S-66-10148

Figure 7.16-15.- Two way RF doppler as a function of time into pass - CRO-USB site, Mission AS-202.

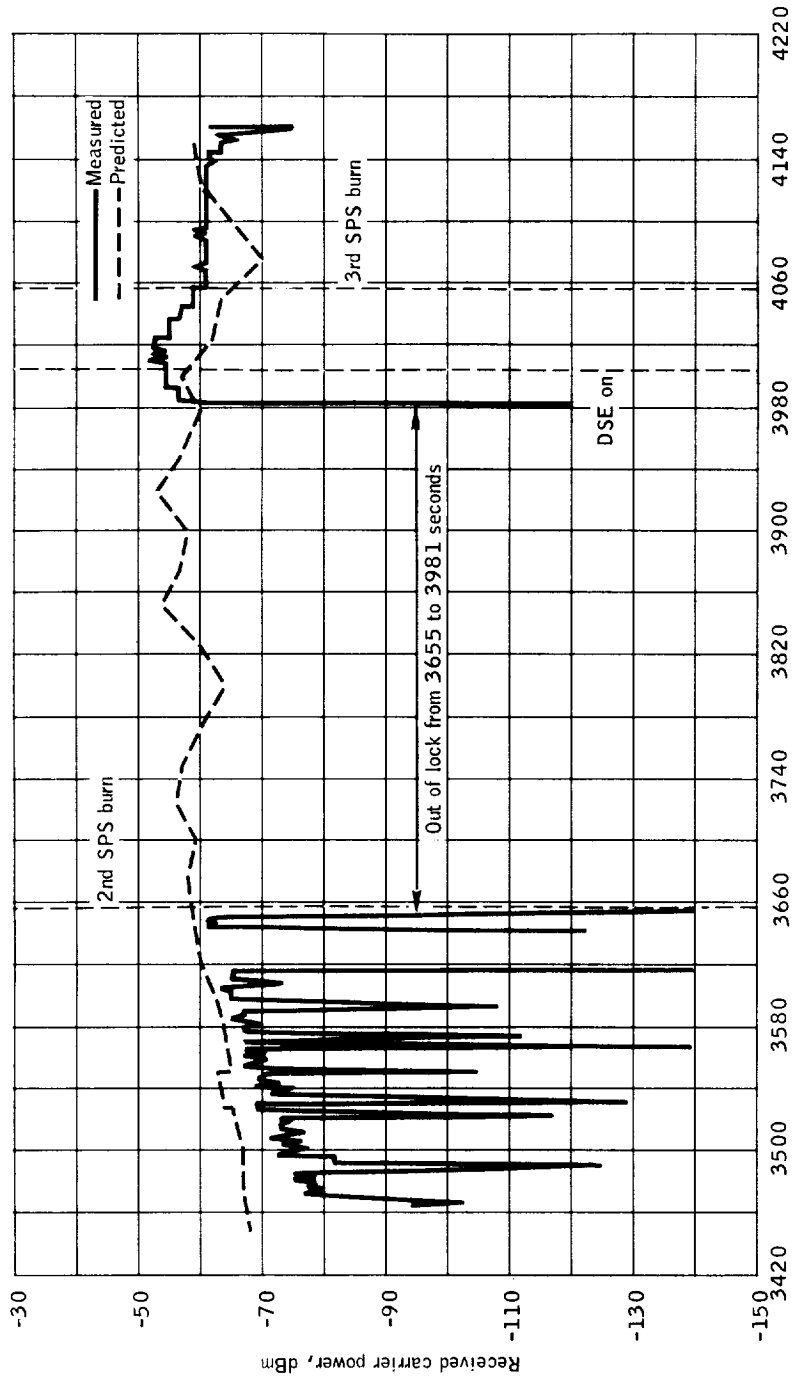

NASA-S-66-10149

Figure 7.16-16.- Spacecraft received carrier power as a function of time in pass - CRO PCM tab group numbers 91 and 92, Mission AS-202. (Predictions based on 100 percent antenna efficiency, for the 50 percent efficiency subtract 3 dB).

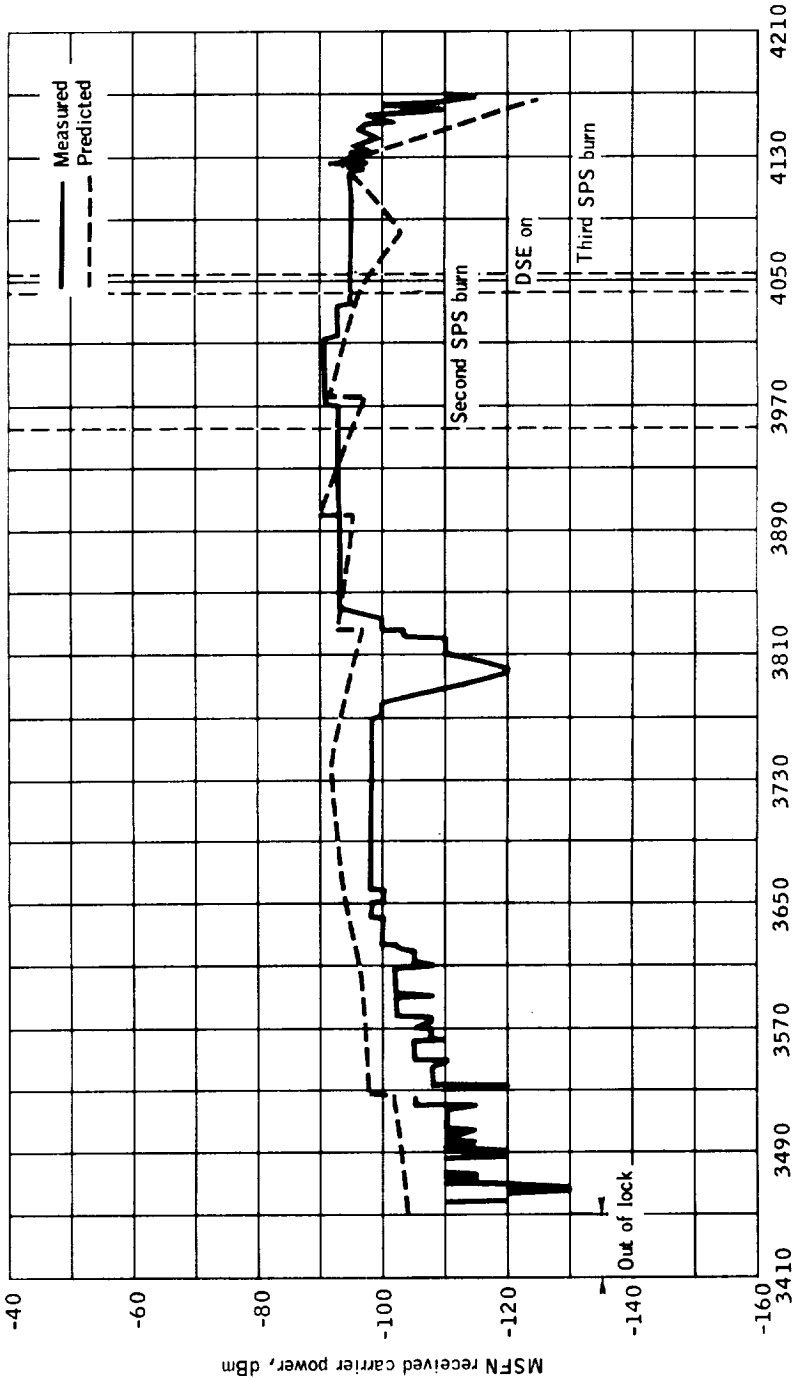

NASA-S-66-10150

Figure 7.16-17.- MSFN received carrier power as a function of time into pass - CRO, Mission AS-202. (Predictions based on 100 percent antenna efficiency, for the 50 percent efficiency subtract 3 dB).

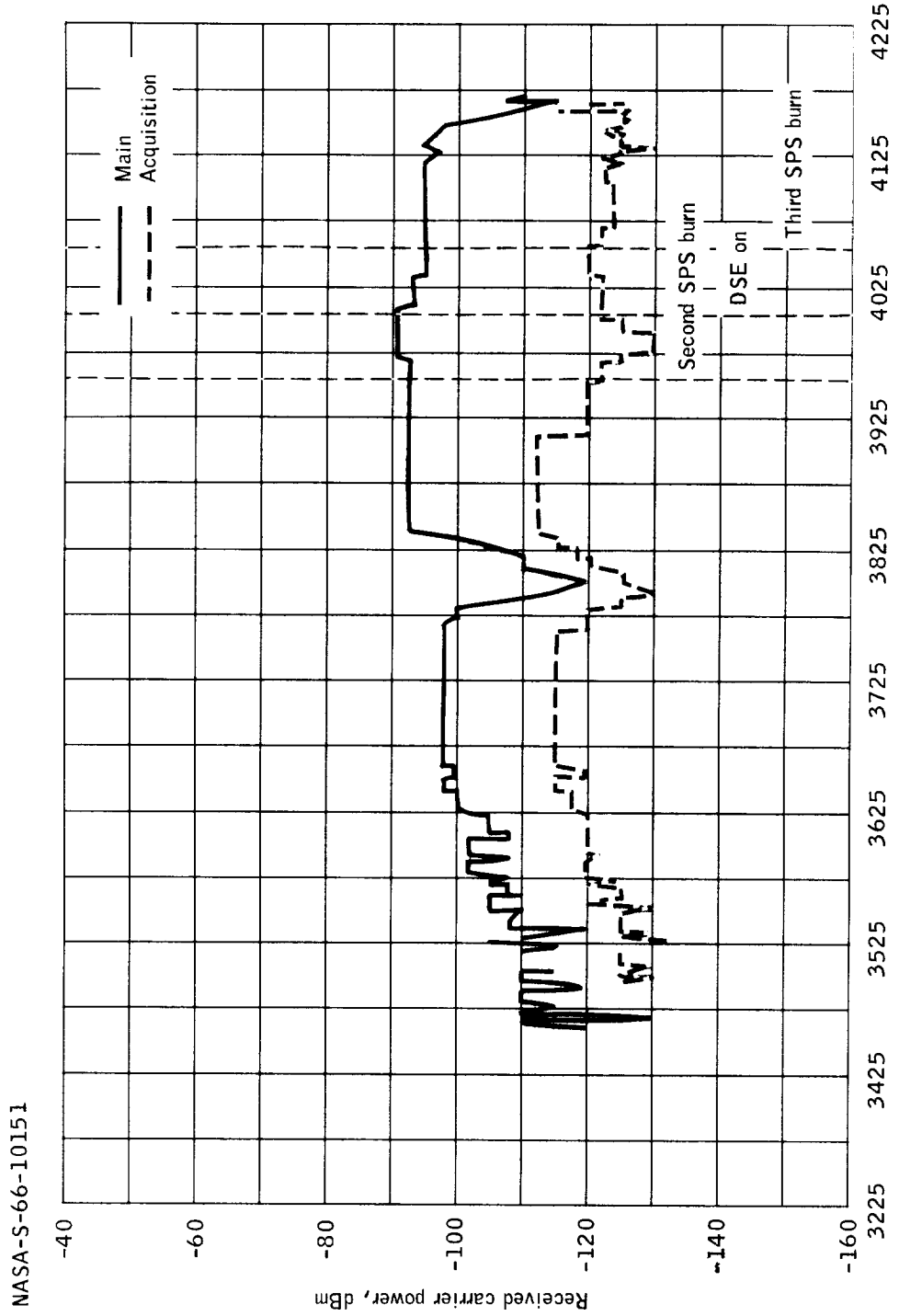

Figure 7.16-18.- MSFN receiver, main and acquisition, received carrier power as a function of time into pass - CRO, Mission AS-202.

NASA-S-66-10152

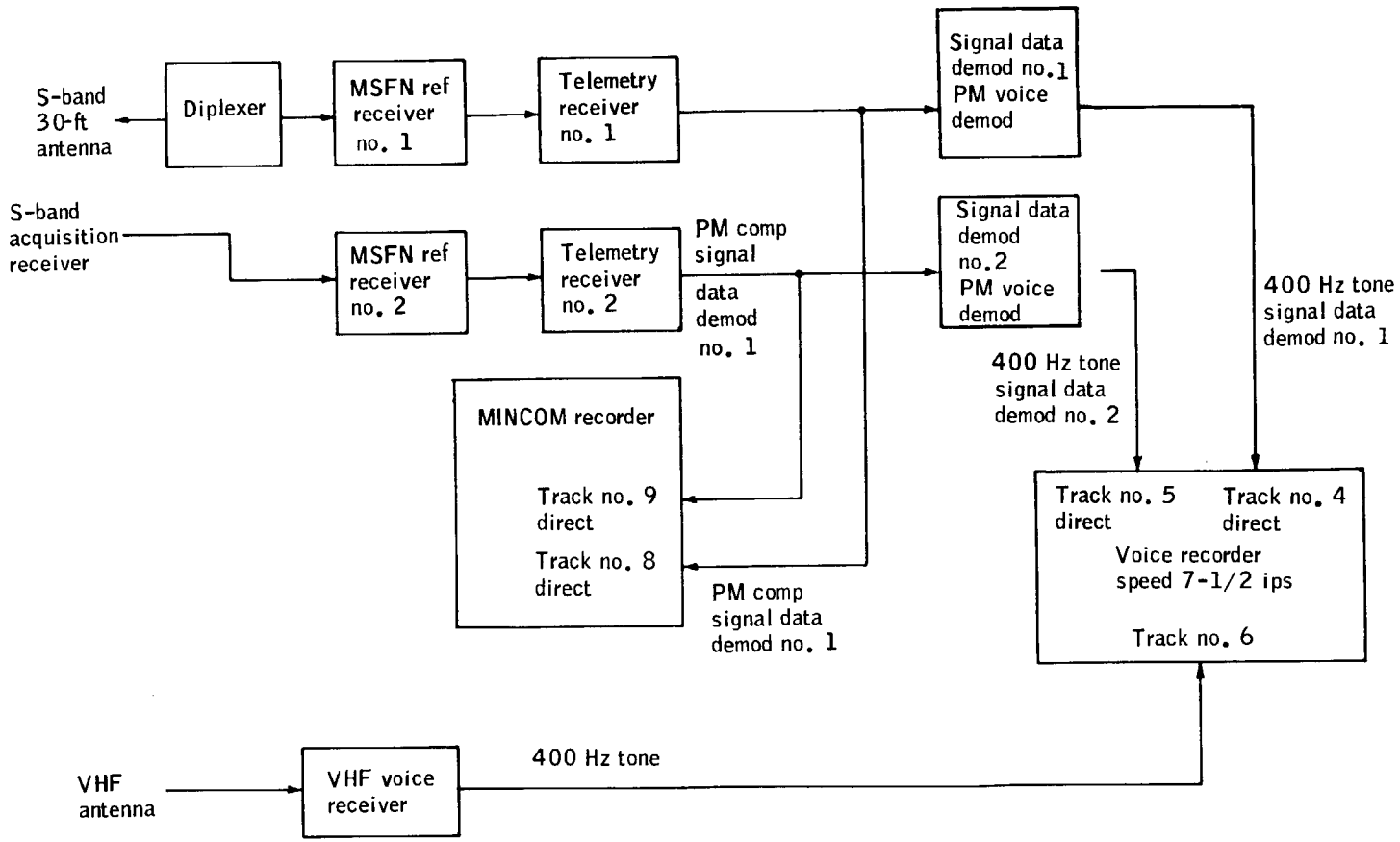

Figure 7.16-19.- Typical MSFN USB downvoice test configuration, Mission AS-202.

NASA-S-66-10153

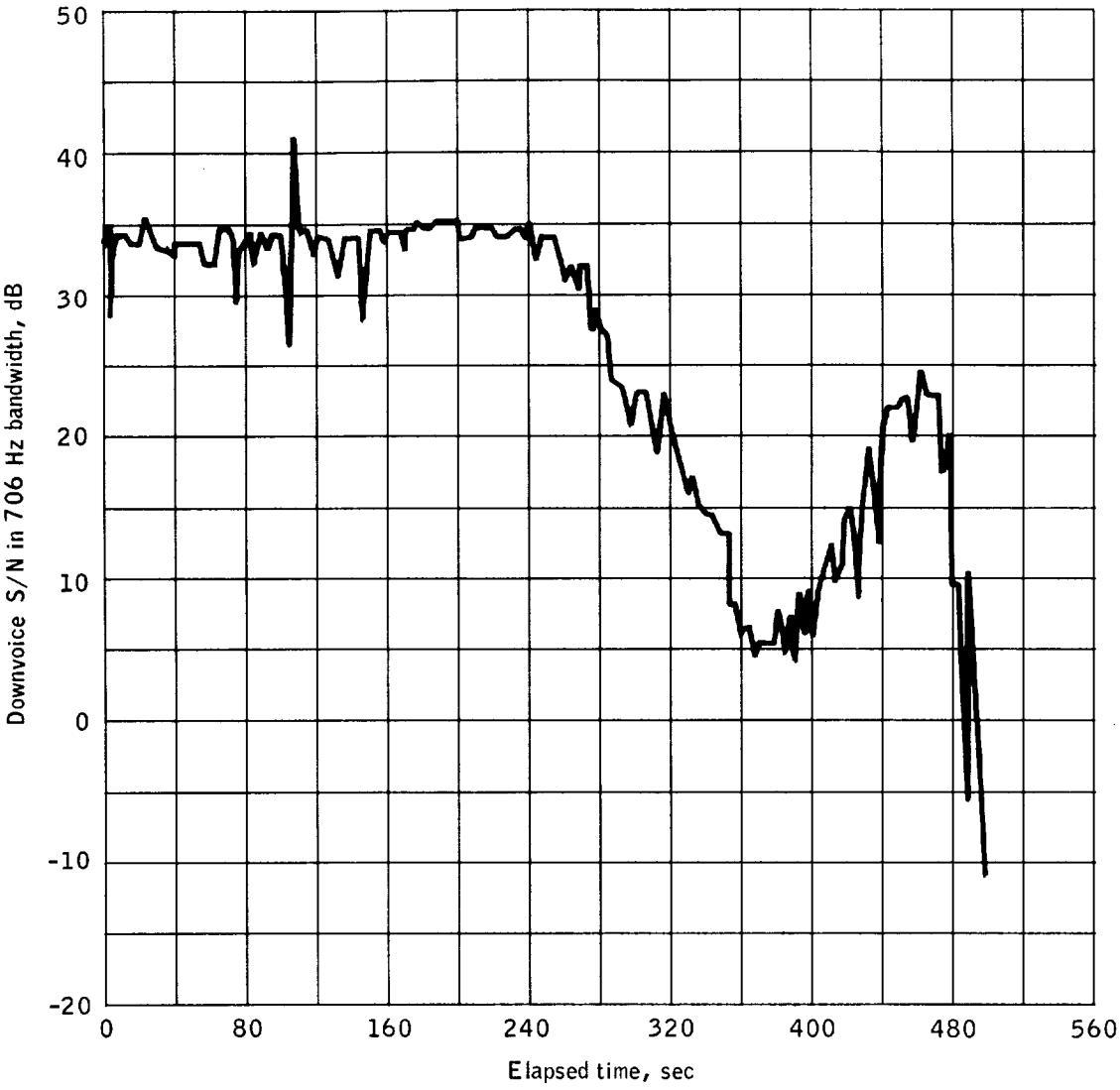

Figure 7.16-20.- Downvoice S/N as a function of time into pass, 400 Hz tone, phase modulated composite signal receiver no. 1 - MILA, Mission AS-202.

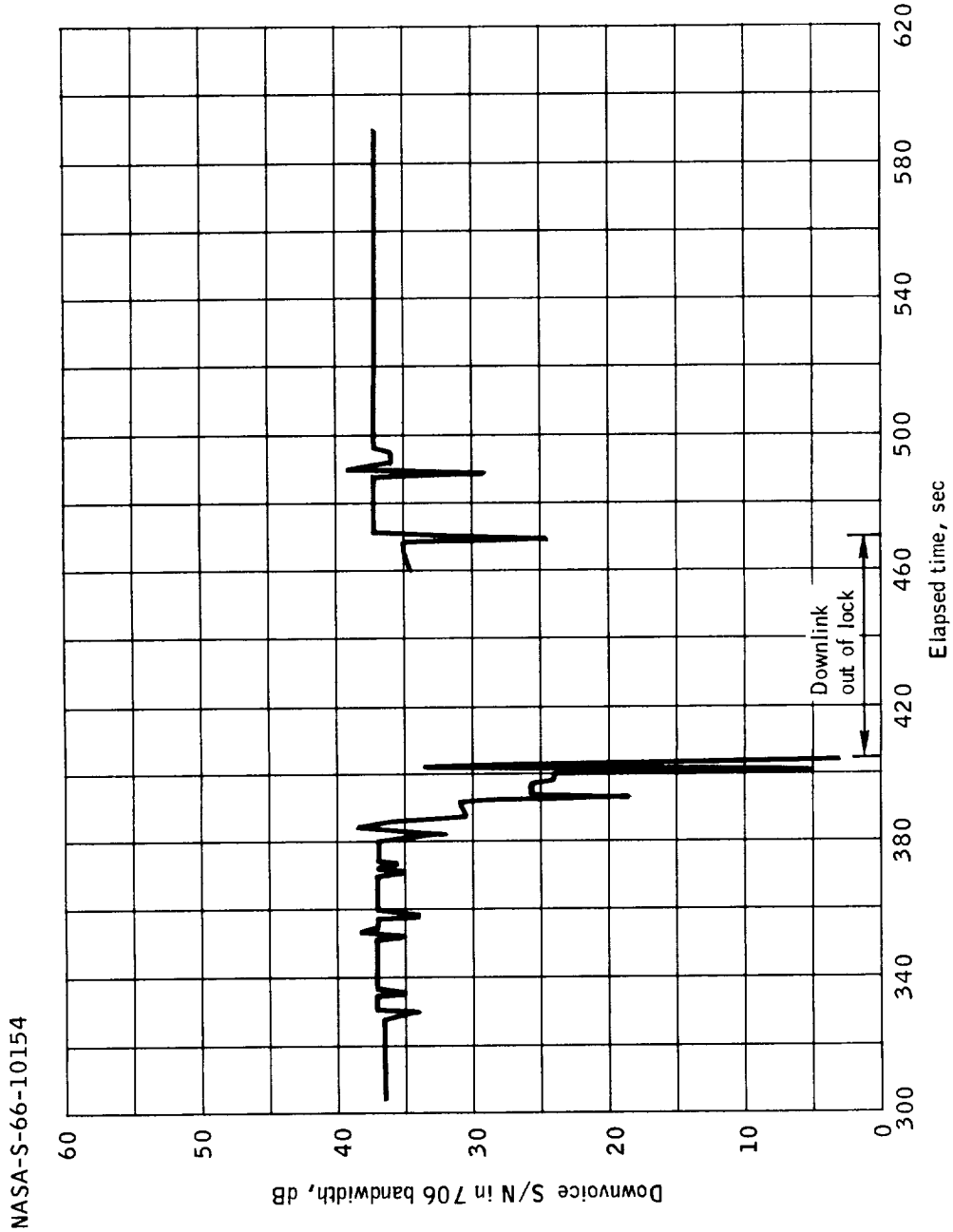

Figure 7.16-21.- Downvoice S/N as a function of time into pass, 400 Hz tone, phase modulated composite signal receiver no. 1 - BDA, Mission AS-202.

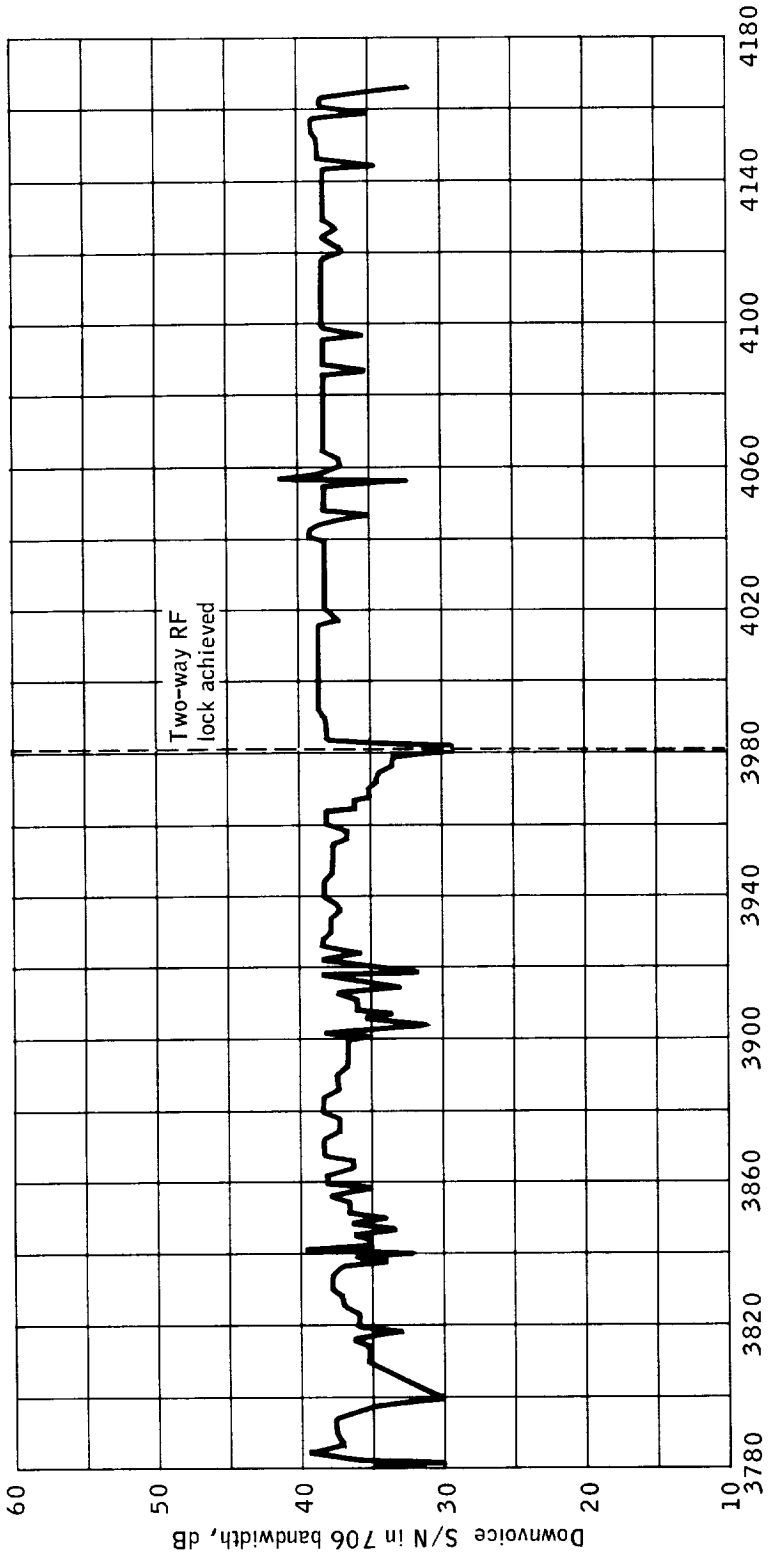

NASA-S-66-10155

Figure 7.16-22.- Downvoice S/N as a function of time into pass, 400 Hz tone, phase modulated composite signal receiver no. 1 - CRO, Mission AS-202.

NASA-S-66-10156

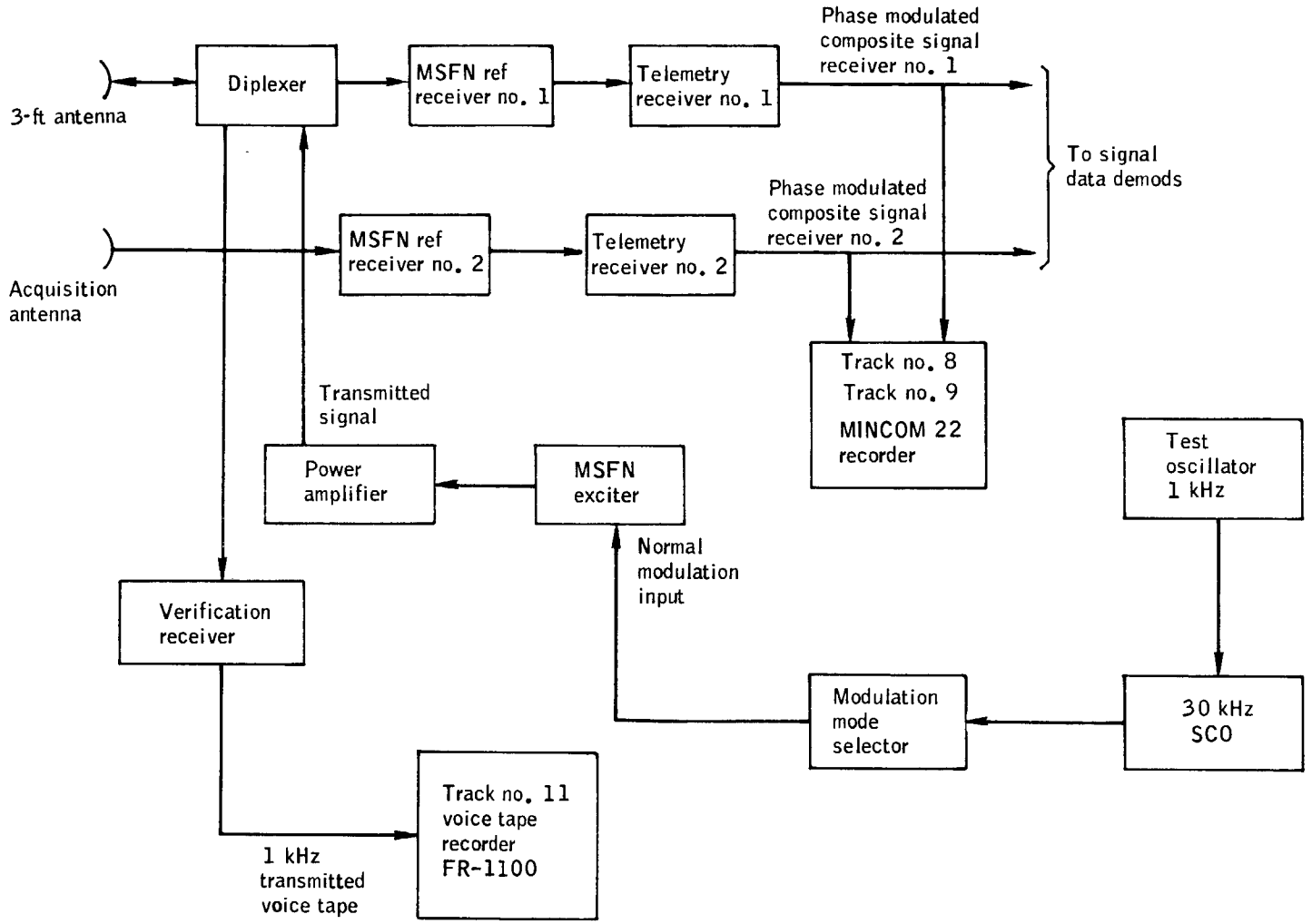

Figure 7.16-23.- Typical MSFN USB up voice test configuration, Mission AS-202.

NASA-S-66-10157

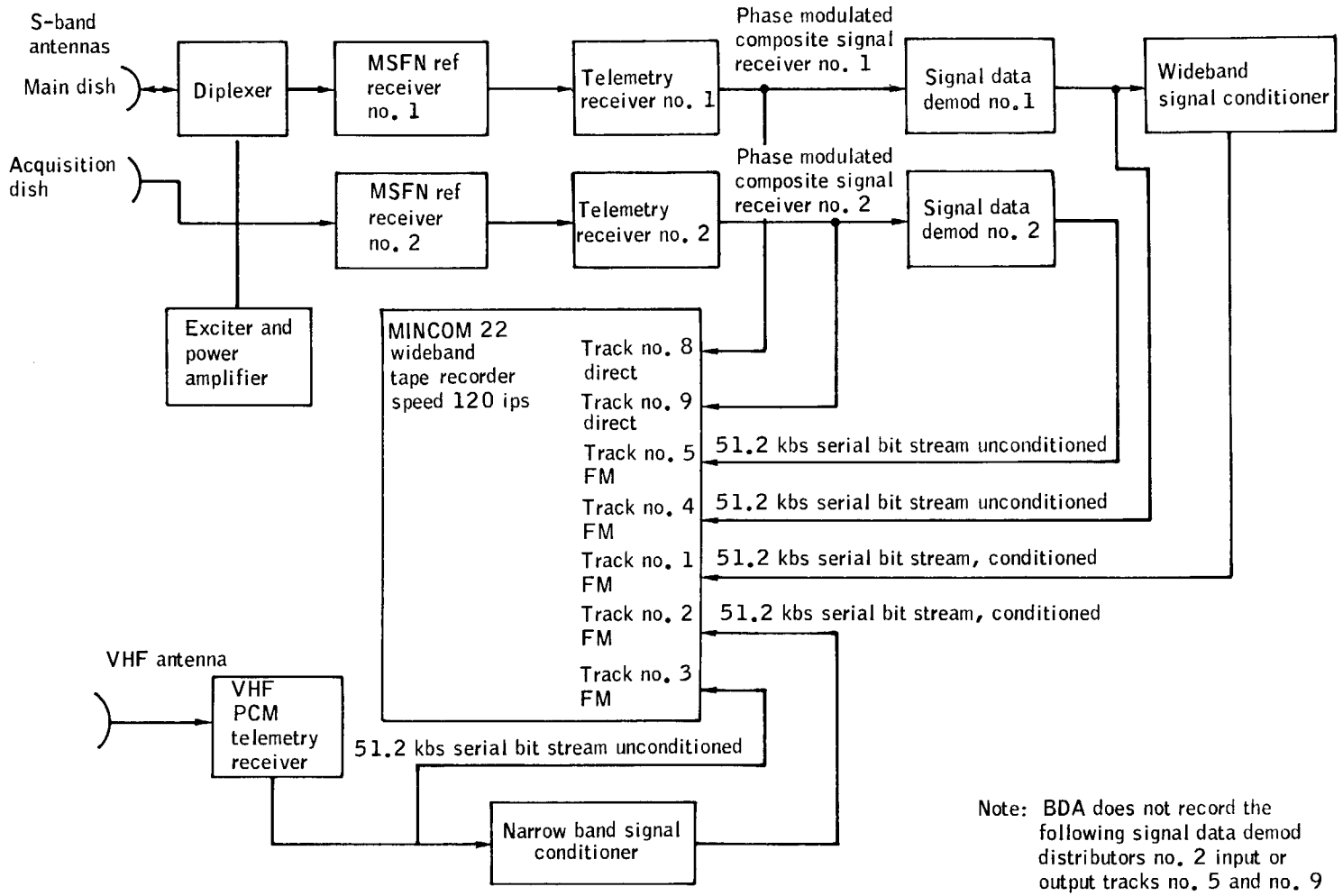

Figure 7.16-24.- Typical MSFN USB PCM telemetry test configuration, Mission AS-202.

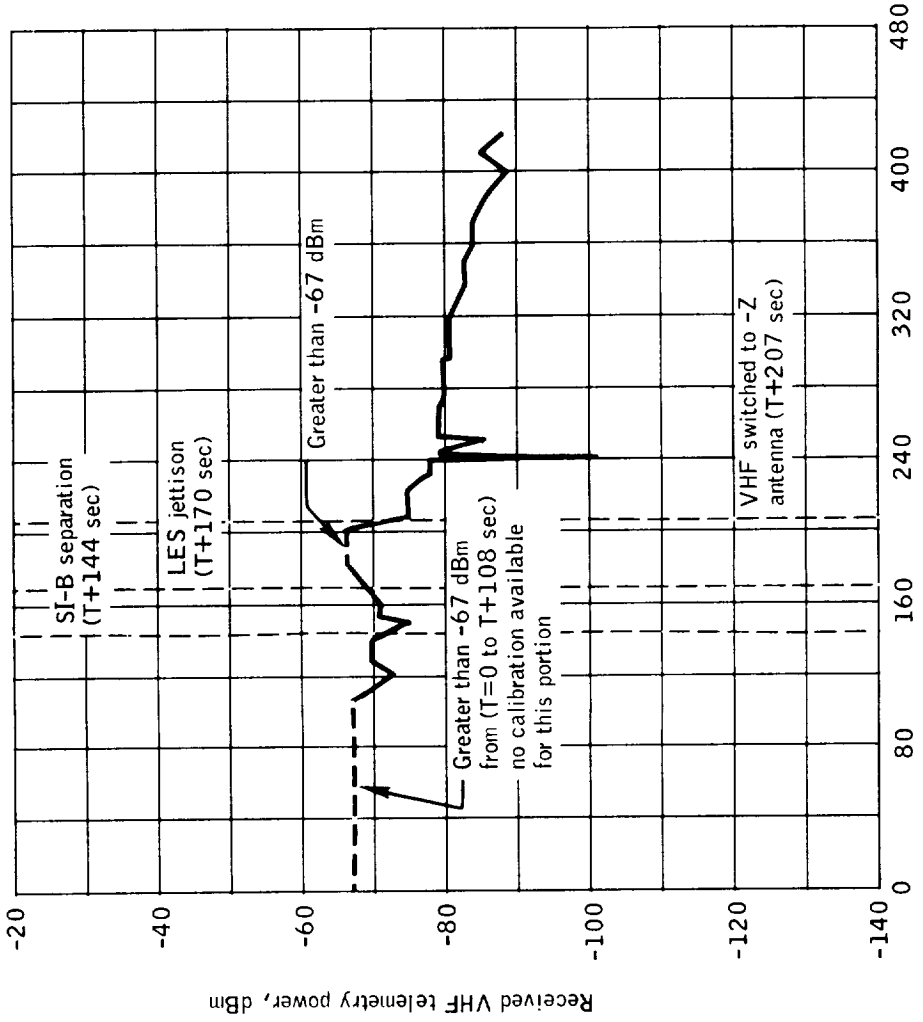

Figure 7.16-25.- Received VHF telemetry power as a function of time into pass - MILA, Mission AS-202.

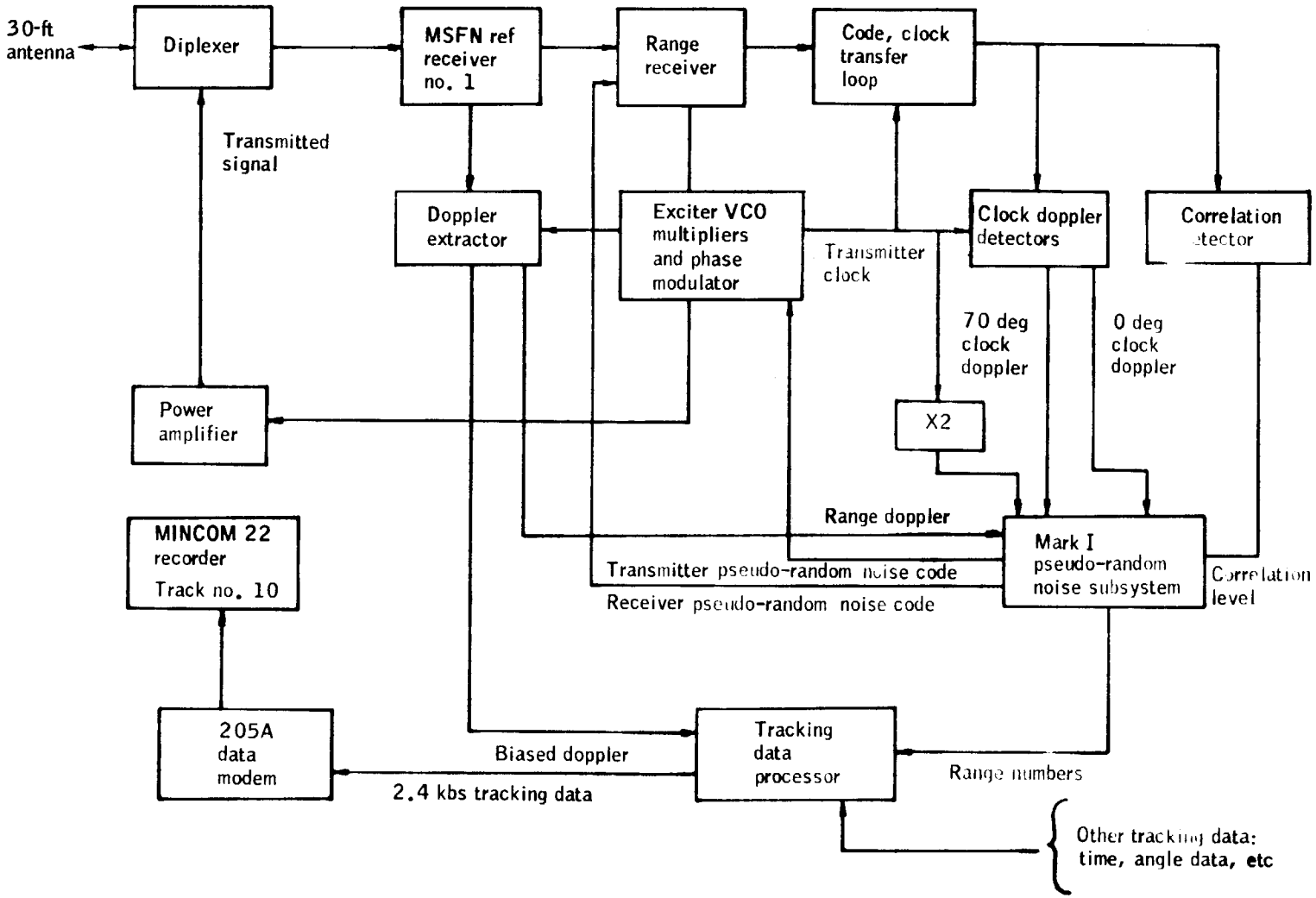

Figure 7.16-26.- Typical MSFN USB pseudo-random noise ranging test configuration, Mission AS-202.

NASA-S-66-10160

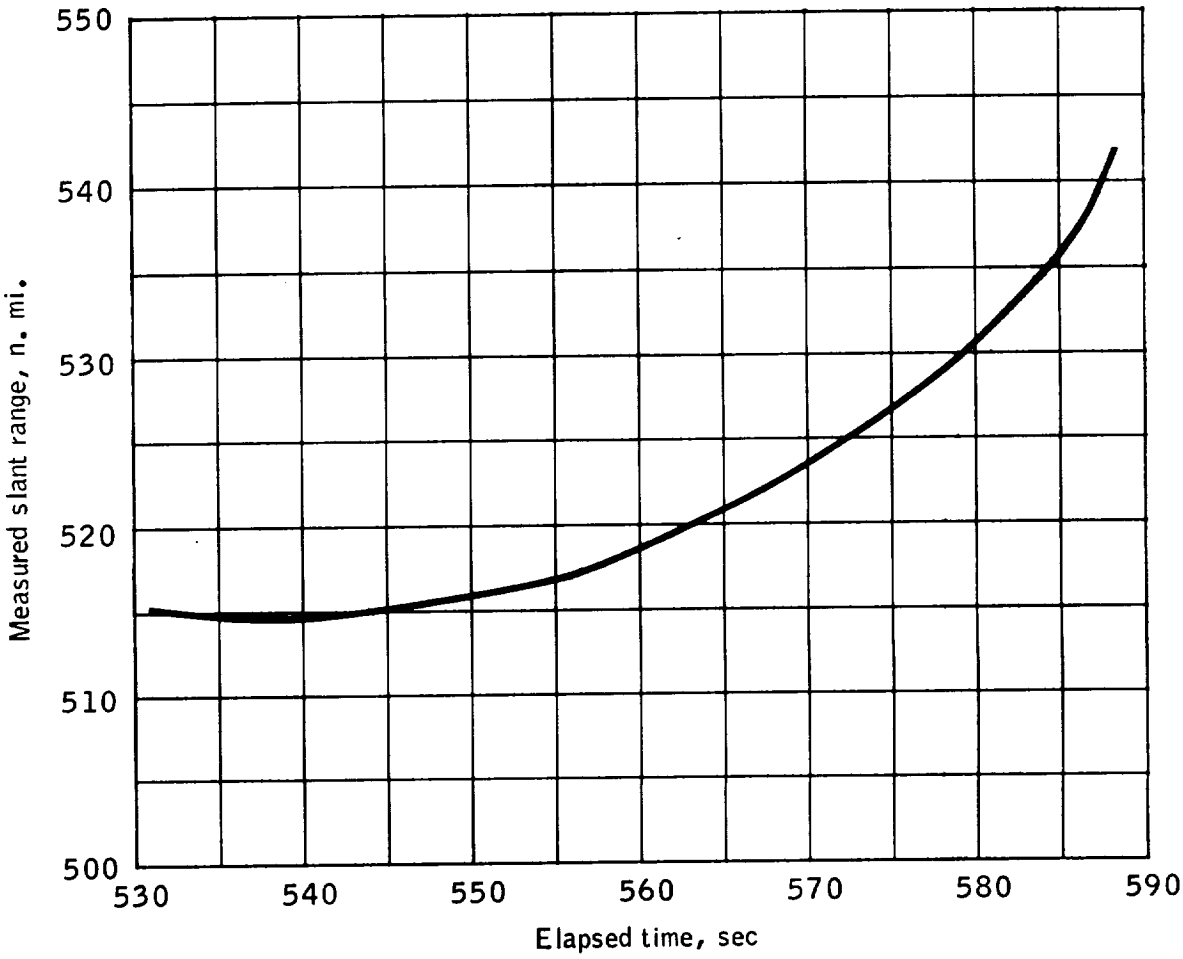

Figure 7.16-27.- Measured slant range as a function of time into pass, tracking data track no. 10 - BDA, Mission AS-202.

NASA-S-66-10161

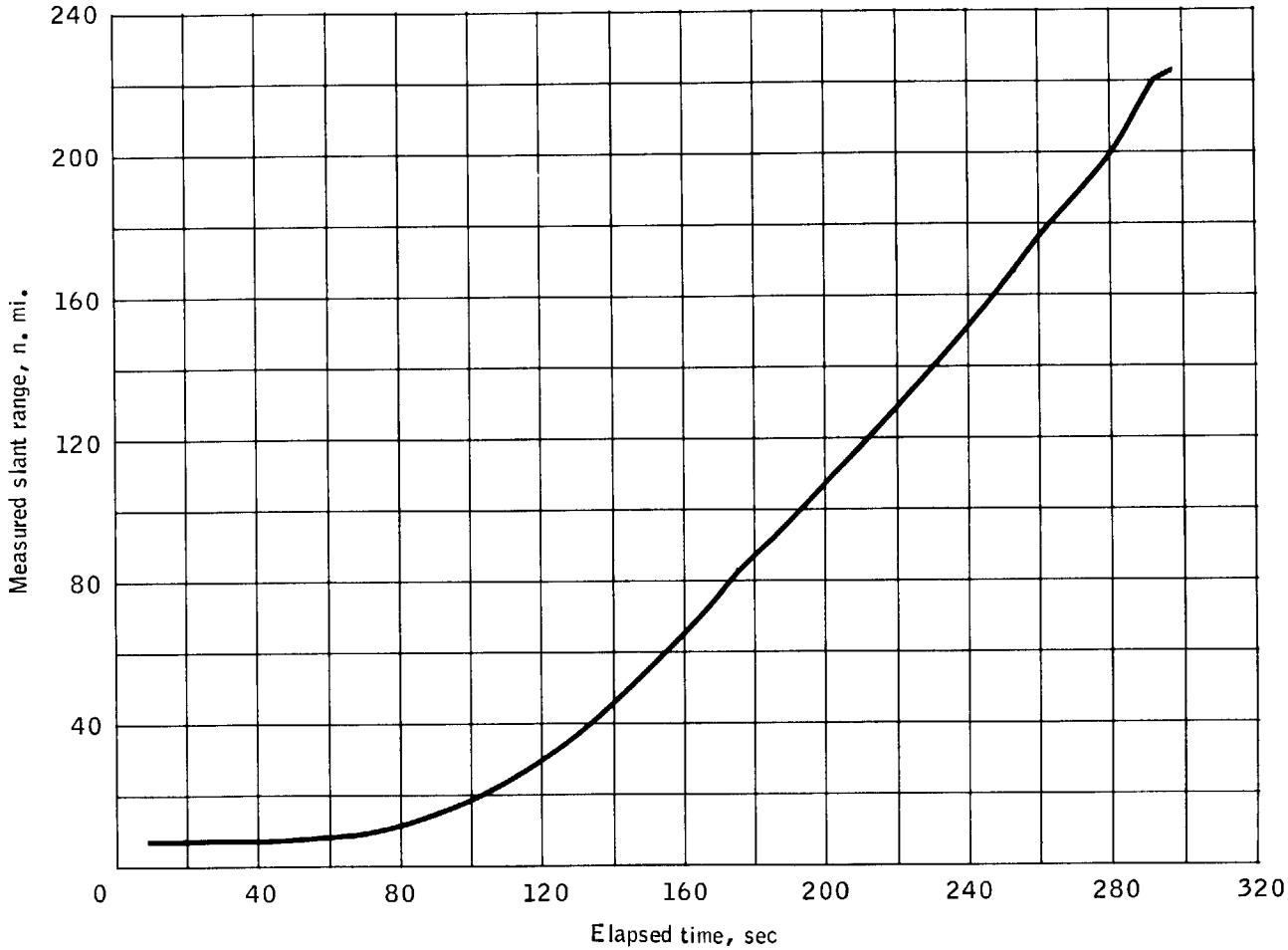

Figure 7.16-28.- Measured slant range as a function of time into pass, tracking data - MILA, Mission AS-202.

7.17 Environmental Control Subsystem

With the exception of the glycol evaporator malfunction which resulted in out-of-tolerances temperatures, the ECS performed within specified limits in partially satisfying the ECS related test objective.

Description.- The ECS regulated the thermal and pressure conditions of the CM cabin and electronic equipment. The spacecraft 011 subsystem was essentially a Block I configuration with the following exceptions:

(a) Equipment installed on spacecraft 011 but not required on manned spacecraft:

(1) Mission control programmer coldplate was installed between the suit and cabin heat exchangers in the thermal control subsystem.

(2) Motorized oxygen supply shut-off valve.

(3) Motorized water-glycol (W/G) inlet-to-radiator shut-off valve.

(b) Equipment omitted from spacecraft 011:

(1) Postlanding ventilation system.

(2) One-pound oxygen tank.

(3) Surge tank isolation and relief valves.

(4) Steam duct tip heater.

(c) Significant design changes for spacecraft 012:

(1) Glycol evaporator and control system redesigned.

(2) Urine dump nozzle separated from the steam duct.

(3) Water tank quantity transducers redesigned.

(4) Steam back-pressure sensor located upstream of the back-pressure valve.

(5) Suit boiler control system and back-pressure valve added.

Performance.-

Launch phase temperature and pressure control: Thermal control of the CM equipment was provided by circulating the heat transport fluid from the thermal coldplates and heat exchangers to the glycol evaporator. The MCP activated the back-pressure valve and closed the motorized W/G valve to the radiators at T-75 seconds. The radiators were isolated during boost to preclude aerodynamic heating effects on the CM thermal control subsystem. Although the glycol evaporator was wetted prelaunch and some evaporation occurred during boost, the MCP fully activated the evaporator at T+169 seconds by energizing the wetness controller. Water boiling provided the only active cooling until T+30 minutes, when a time delay opened the W/G valve to permit W/G flow to the radiators. Radiators then provided the cooling and the evaporator was to supply supplemental cooling requirements. The oxygen for system use and cabin pressure control was supplied from the cryogenic gas storage system in the SM.

Reentry phase temperature and pressure control: At CM/SM separation, the MCP closed the oxygen supply and W/G supply shut-off valves. Water boiling in the glycol evaporator provided cooling during reentry, until ambient pressure rose above 0.25 psia when subsequent cooling was supplied only by the glycol reservoir and system thermal storage capability. The suit evaporator was electrically deactivated for the mission. The suit compressor operated during the mission but the gas flow was directed through the suit bypass valve, since the pressure suits and suit supply and return hoses were not onboard. The waste management subsystem blower was not activated during the mission. The potable water supply assembly hot water heater, which heats the water for astronaut food reconstitution, was activated for the mission.

Pressure control: The gaseous oxygen storage and pressure control subsystem operated normally. The 100-psi oxygen system operated at 112 psig, which was 2 psi above the required 100 $\pm$ 10 psig. This small out-of-tolerance condition was also experienced during the spacecraft 011 vacuum chamber test and has no effect on overall system operation.

The cabin leakage was approximately 0.2 lb/hr and the cabin did not bleed down from the final cabin seal-off pressure of 5.7 psia to the anticipated pressure control point of 5.18 psia. The cabin pressure regulator did not operate, and an analysis from the prelaunch cabin leak test indicates that operation of the cabin regulator would not have occurred until T+4 hours. This situation is normal and is not an anomaly. Although it is possible that the steam duct was blocked when reentry began, either the obstruction was upstream of the cabin pressure relief valve or had been cleared before cabin relief began at an ambient pressure of 6.1 psia. The cabin pressure began building up at a cabin

negative pressure differential of 0.48 psi and maintained a 0.35 to 0.40 negative pressure until landing. These values are within the normal operating range of the cabin pressure relief valve.

Less than 100 cubic centimeters of water were found in the cabin after spacecraft recovery. Chemical analysis showed this water to be sea water which probably entered the spacecraft through the cabin pressure relief valve. This valve has a manually operated sealing feature which can be actuated during manned missions. A slight positive pressure was noticed in the cabin after recovery and is attributed to oxygen system leakage. Oxygen system leakage was within required tolerances, but enough leakage occurred during the 10 hours before hatch opening to raise the cabin pressure 1 or 2 inches of water above ambient.

ECS radiators: An evaluation of radiator performance, based upon an assumed cabin heat loss and radiator inlet temperature, indicates that the radiators performed approximately as expected with an inlet temperature of 89° to 98° F and an outlet temperature of 65° F (fig. 7.17-1). The operation of the radiators prevented excessive temperatures in the coolant loop. No electronic equipment malfunctioned due to the glycol evaporator anomaly.

Determination of radiator thermal coating performance was not possible due to insufficient instrumentation.

Glycol evaporator malfunction: A significant ECS anomaly was the failure of the glycol evaporator to provide cooling from T+14 until T+68 minutes (fig. 7.17-2). At T+169 seconds, the glycol evaporator began to operate, as indicated by the decrease in back-pressure, steam, and glycol evaporator outlet liquid temperatures. The evaporator outlet liquid temperature decreased below the 45° $\pm$ 3° F design control point and the vapor momentarily indicated a freezing temperature of 31° F at T+9 minutes 51 seconds. However, this situation had been observed during the initial startup of the evaporator on Mission AS-201 and other ground tests of the evaporator, including the spacecraft 011 vacuum chamber test at KSC. This deviation has been attributed to a slow response from the wetness sensor to the control system. Usually the system had achieved control limits after 30 minutes of operation. However, on Mission AS-202 at T+14 minutes, the evaporator outlet liquid temperature increased from 40° to 58° F in 40 seconds and exceeded 75° F (full-scale reading) at T+17 minutes. Steam duct pressure increased to full scale, 0.25 psia, during this period of increasing temperature. This data indicates that the steam duct became obstructed downstream of the steam duct pressure sensor, which is downstream of the evaporator back-pressure valve. The obstruction is attributed to an ice formation resulting from an excess amount of water being expelled from the evaporator system in a liquid form. It is noted that marked

reversals of the back-pressure trends occurred at S-IVB cutoff and SPS cutoff. These reversals could indicate that free water was expelled from the evaporator core during these periods of deceleration, and that during acceleration the water was held in the boiler system. Orientation of the evaporator with respect to the X-axis acceleration forces is consistent with this hypothesis (fig. 7.17-3). The source of this water is attributed to one or a combination of three possibilities:

(a) Excessive water remaining in the evaporator after the altitude chamber test. The water valve to the glycol evaporator was open for 12-1/2 minutes during the return to sea level phase of the test, when the chamber pressure was too high for the evaporator to function. Approximately 2 pounds of water was supplied to the evaporator during this time, some of which could have overflowed into the suit evaporator. The water system was subsequently purged with dry nitrogen for 12 hours through the evaporator but for only about 5 minutes through the suit evaporator. No quantitative evaluation of the system dryness was performed.

(b) Excessive water admitted to the evaporator from an improper countdown servicing procedure. The water subsystem was serviced for the mission at T-18 hours by being filled and emptied as a flush. The water was removed and the system was purged with GN_2 from service valves. The evaporator water control valve was then opened and the water system purged with GN_2 through the evaporator, allowing some water to enter the evaporator. (A postflight repeat of this procedure indicated that approximately 0.3 pound of water flowed into the evaporator from this flush.) After GN_2 purging on the launch pad, the evaporator was subsequently serviced with approximately 0.9 pound of water to wet the wicks as recommended by the contractor.

(c) Leaking water control valve. A postflight test of the water system leakage indicates that the two water control valves and two cyclic accumulators leaked an equivalent of 0.017 lb/hr of water or an 0.3-pound total during the countdown operations. The water valves and cyclic accumulators cannot be individually leak-checked in the installed configuration.

The following hardware changes have been made to the spacecraft 012 ECS which will improve performance of the water and evaporator systems:

(a) The boiler performance is controlled by a thermistor imbedded in the evaporator wicks rather than the spacecraft 011 wetness sensor

which is in the steam collection pan at the exit of the evaporator. This change will enable faster response to the control system, since the spacecraft 012 configuration thermistor senses the wetness of the evaporator directly through capillary action, whereas the spacecraft 011 wetness sensor relied upon the steam convection forces to carry free water droplets out of the heat exchanger core to the sensor.

(b) The seal design of the water valve is a ball, rather than a plug-type seal, and the solenoid activating force has been doubled. This change should preclude malfunction of these valves from contamination, since the stronger solenoid forces permit larger flow areas, thus making the activation of the valve less prone to contamination. Prior difficulties with the spacecraft 011 configuration valve resulted from contamination buildup in the annular space between the solenoid core and the valve poppet, due to small clearance dimensions (0.002 inch).

(c) A 1/2-micron nominal, 3-micron absolute filter is installed upstream of each water control valve to control contamination.

(d) A manually operated shutoff valve has been added to the inlet of each water valve. This manual feature is separate from the solenoid valve and does not affect its operation. This valve will prevent inadvertent addition of water to the evaporators during ground operations.

The following procedural changes are being made to preclude excess water in the evaporator system on subsequent vehicles.

(a) The water valve will be manually closed as well as electrically deactivated at all times when the water system is serviced, except during boiling operations in the attitude chamber test.

(b) The evaporator system will be boiled dry at vacuum conditions just prior to termination of the altitude chamber tests.

(c) The evaporator system will be purged with dry gas after each wetting of the evaporator wicks.

(d) The water valves into the evaporators will not be used to flush the system unless the evaporators subsequently are purged and checked for dryness.

The steam duct remained obstructed until T+67 minutes when the steam duct pressure and system temperatures decreased. The control system again began hunting for the control temperature, but the back-pressure again went off-scale at T+82 minutes. The back-pressure

decreased briefly at T+85 minutes, but ambient pressures were increasing due to reentry, and further boiling was precluded. It is noted that the steam duct temperature changed at SPS thrust on, third burn, indicating that the change in acceleration precipitated boiling. A possible explanation is that if the ice had been melting until at T+67 minutes 35 seconds it was a very wet ice, the acceleration may have caused the ice to move and break up. This is substantiated by a gradually increasing steam duct temperature which could indicate some boiling at a high temperature (80° F).

ECS CM/SM umbilical: At the CM/SM separation signal at T+4264 seconds, the glycol pump outlet pressure and glycol accumulator quantity decreased rapidly. The glycol pump outlet pressure returned to the operating pressure, 41 psia, within 15 seconds and the glycol accumulator returned to about 44 percent of the operating quantity within 15 seconds. The MCP separation signal actuated the CM/SM umbilical guillotine and the W/G inlet-to-radiator shutoff valve at the same time. The umbilical guillotine does not seal the severed tube. The W/G inlet-to-radiator shutoff valve takes up to 17 seconds to fully open or close. The W/G flowed from the tube until the valve closed. It is estimated that 0.9 pound of W/G was lost. This is not considered an anomaly. Manned spacecraft have manual valves on the water glycol system and oxygen system lines which will be closed just prior to CM/SM separation.

Potable water tank quantity measurement: The only ECS instrumentation anomalies were the waste and potable water tank quantity transducers. Erratic data was received during the power and maneuvering phases of the flight, particularly from the potable tank transducer. This is attributed to the movement of the water within the tank which is stored around the pressurizing bladder. The transducers are delta pressure instruments which measure the difference in oxygen and water pressure, or actually the bladder stretch. The bladder stretch is not linear with water quantity and the calibration of the instrument is not within the $\pm$10 percent accuracy requirement (fig. 7.17-2).

The instrument output signal was 5 to 0 volts for an 0- to 100-percent water quantity (fig. 7.17-4). The calibration curve was such that a quantity change of 18 to 65 percent as is an 0.2 volt or only 4 percent output signal change. The potable tank was partially filled, resulting in operation on this part of the calibration curve during the mission. The potable quantity indication at launch was 26 percent, as expected. The waste water tank was full at launch and, therefore, not as susceptible to water movement during powered flight.

The water quantity transducers have been redesigned for spacecraft 012. The new configuration is a potentiometer which measures the

change in position of the tank bladder by means of a wire attached from the potentiometer shaft to the bladder. The spring-wound shaft compensates for the nonlinearity of the bladder displacement as the wire is wound around the shaft.

Gas chromatagraph: Although the purpose of the gas chromatograph is to analyze the spacecraft suit and cabin atmosphere (cabin and suit air may be analyzed on alternate 80-minute cycles or the unit may be programmed to sample cabin air or suit air only), the primary purpose for including it on this mission was to qualify the helium pressure vessel and pyrotechnic device.

During prelaunch servicing of this unit, a leak was noted in sample valve A3SV1 (fig. 7.17-5). This valve has two positions shown schematically in figure 7.17-5 as "cross" or "straight." The other sample valve (A3SVZ), also has the same two positions. These two valves are designed to be switched together so that either one is in the "straight" position or both are in the "cross" position. When valves A3SV1 and A3SV2 were in the "straight" position, helium from the storage tank should flow through valve A3SV1, through valve A3SV3, and then through valve A3SV2. On this unit, however, the leak resulted in an additional helium flow directly from valve A3SV1 to valve A3SV2 and then through the metering orifice to space vacuum.

It was decided that the loss in helium pressure due to this excessive flow could not be tolerated but that the unit could be flown in a noncperating mode and still qualify the pressure vessel and pyrotechnic device for the worst case condition.

Postflight disassembly and examination of the helium dump valve disclosed that the valve had operated properly and that the 6000-psig helium pressure had been released, verifying that the required qualification had been accomplished.

Postflight evaluation of the CO_2 sensor has not been completed.

NASA-S-66-10162

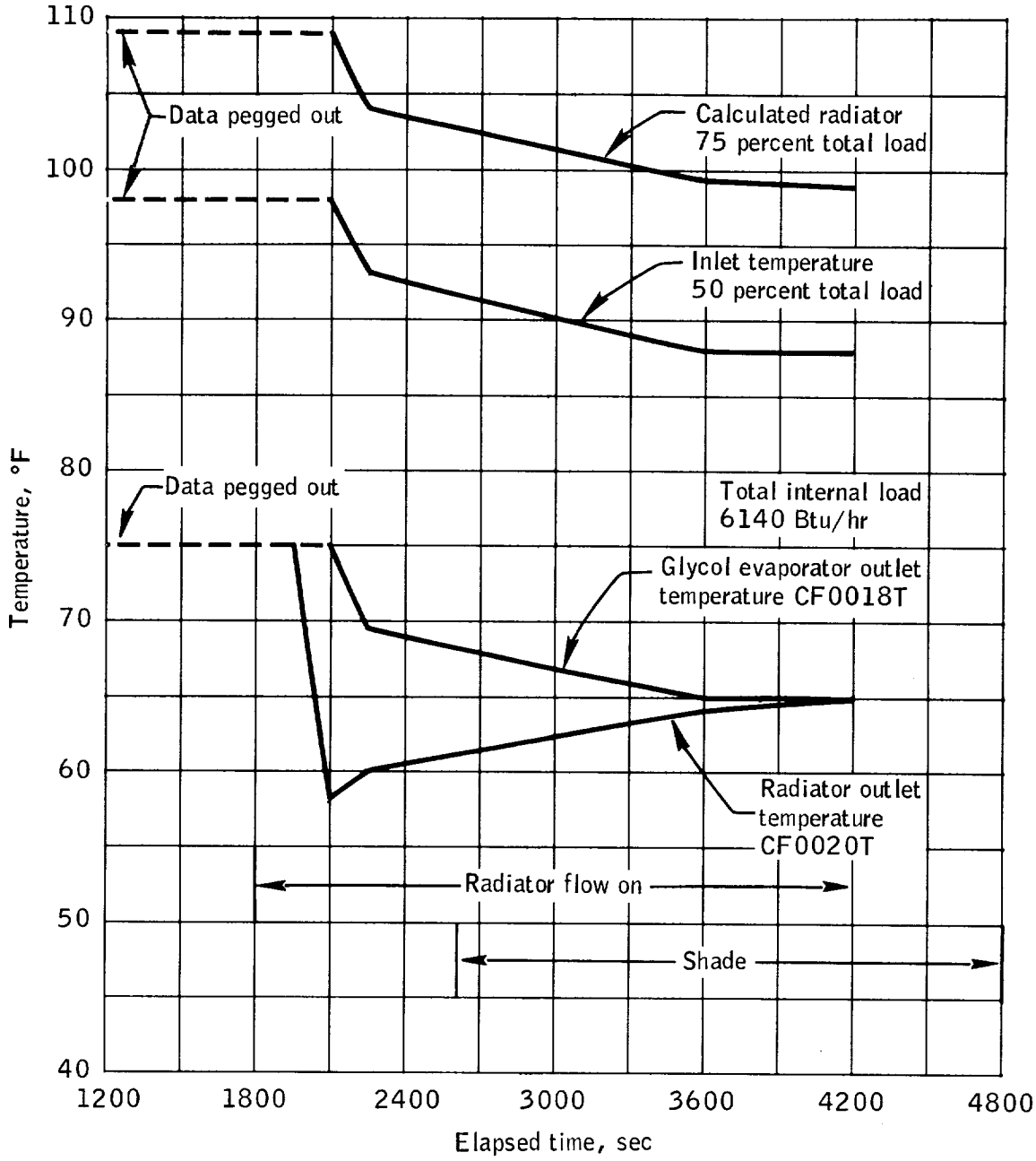

Figure 7.17-1.- Spacecraft 011 ECS radiator performance, Mission AS-202.

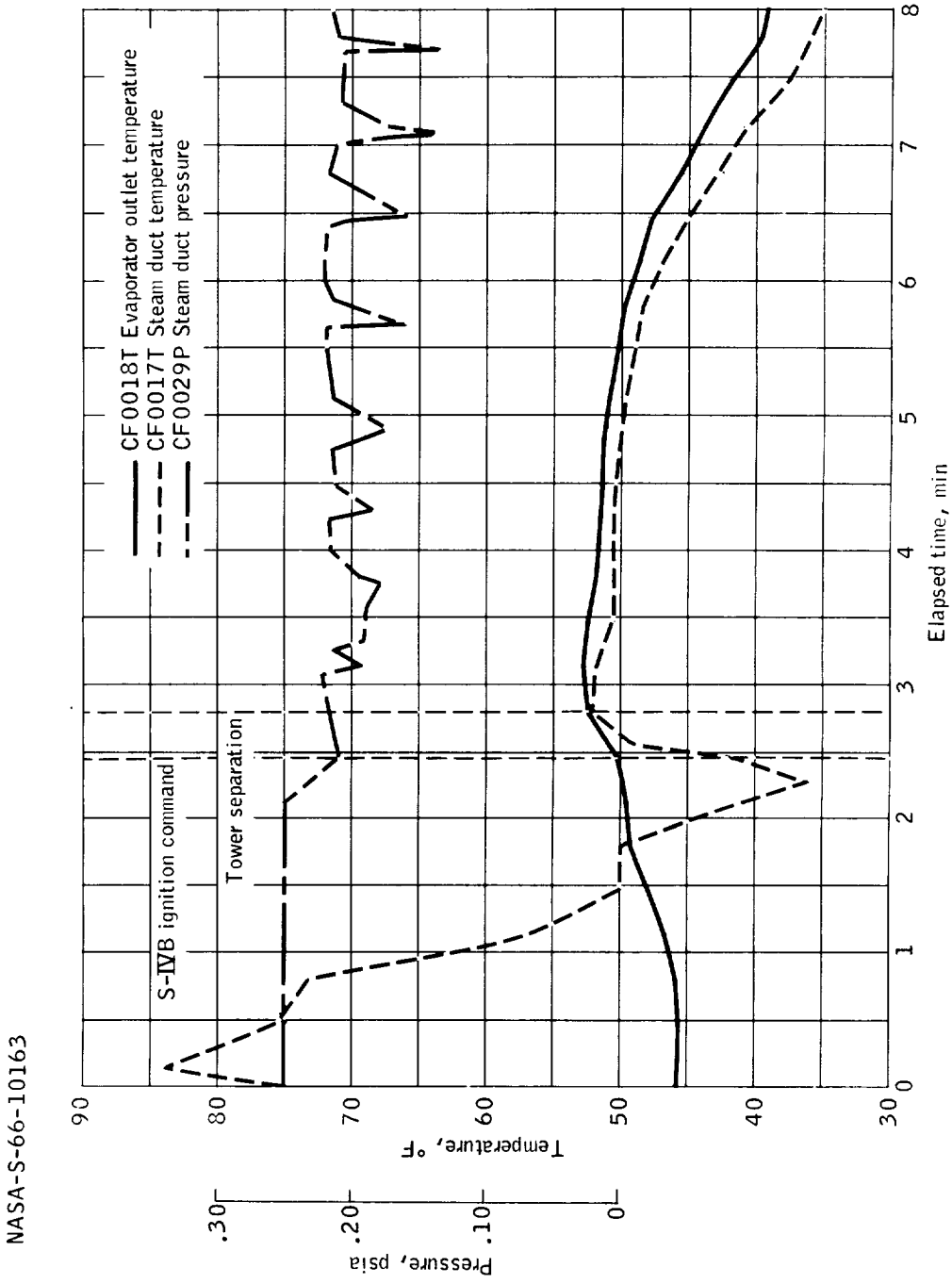

NASA-S-66-10163

(a) 0 to 8 minutes.

Figure 7.17-2.- ECS glycol evaporator performance, Mission AS-202.

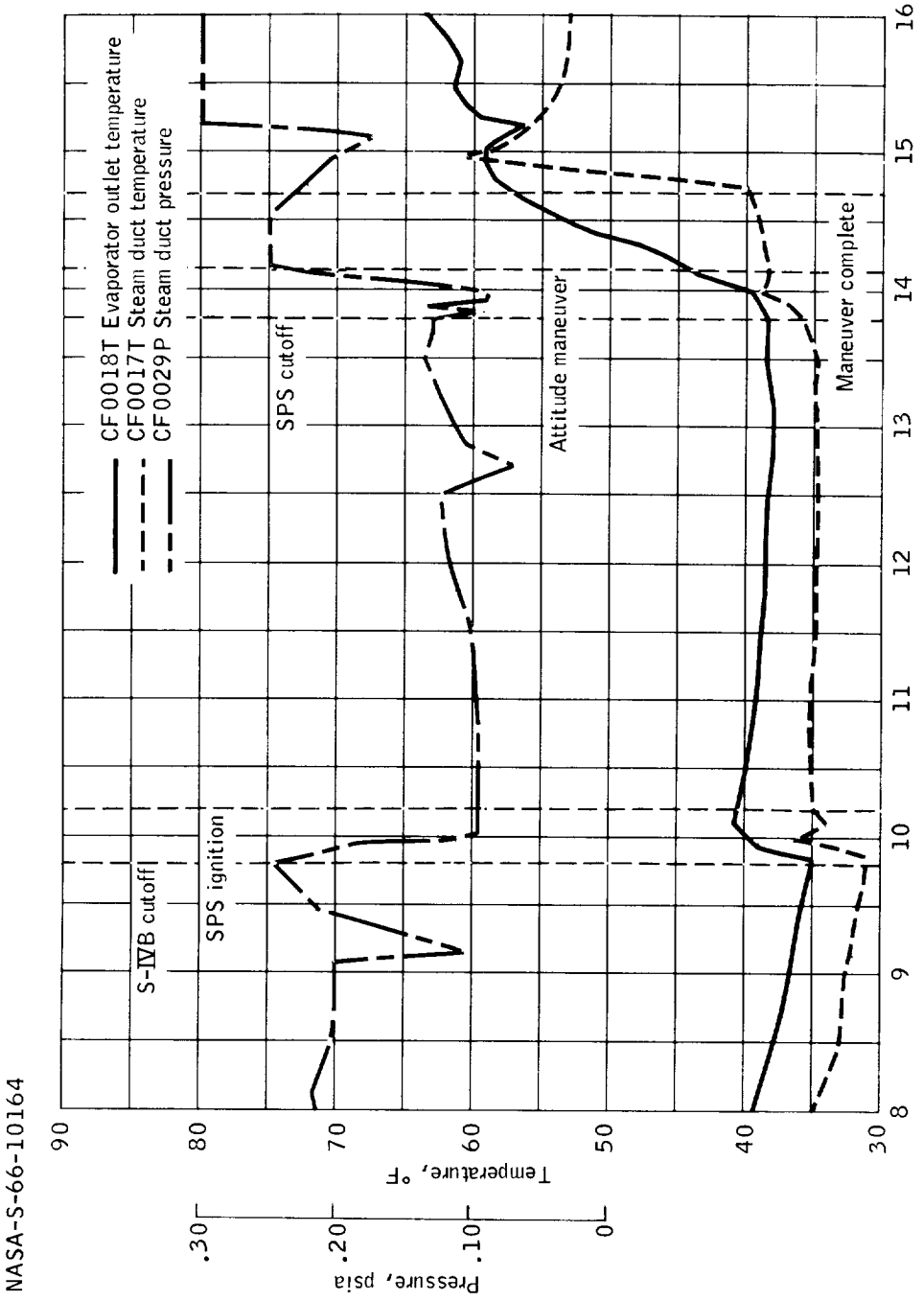

(b) 8 to 16 minutes.

Figure 7.17-2.- Continued.

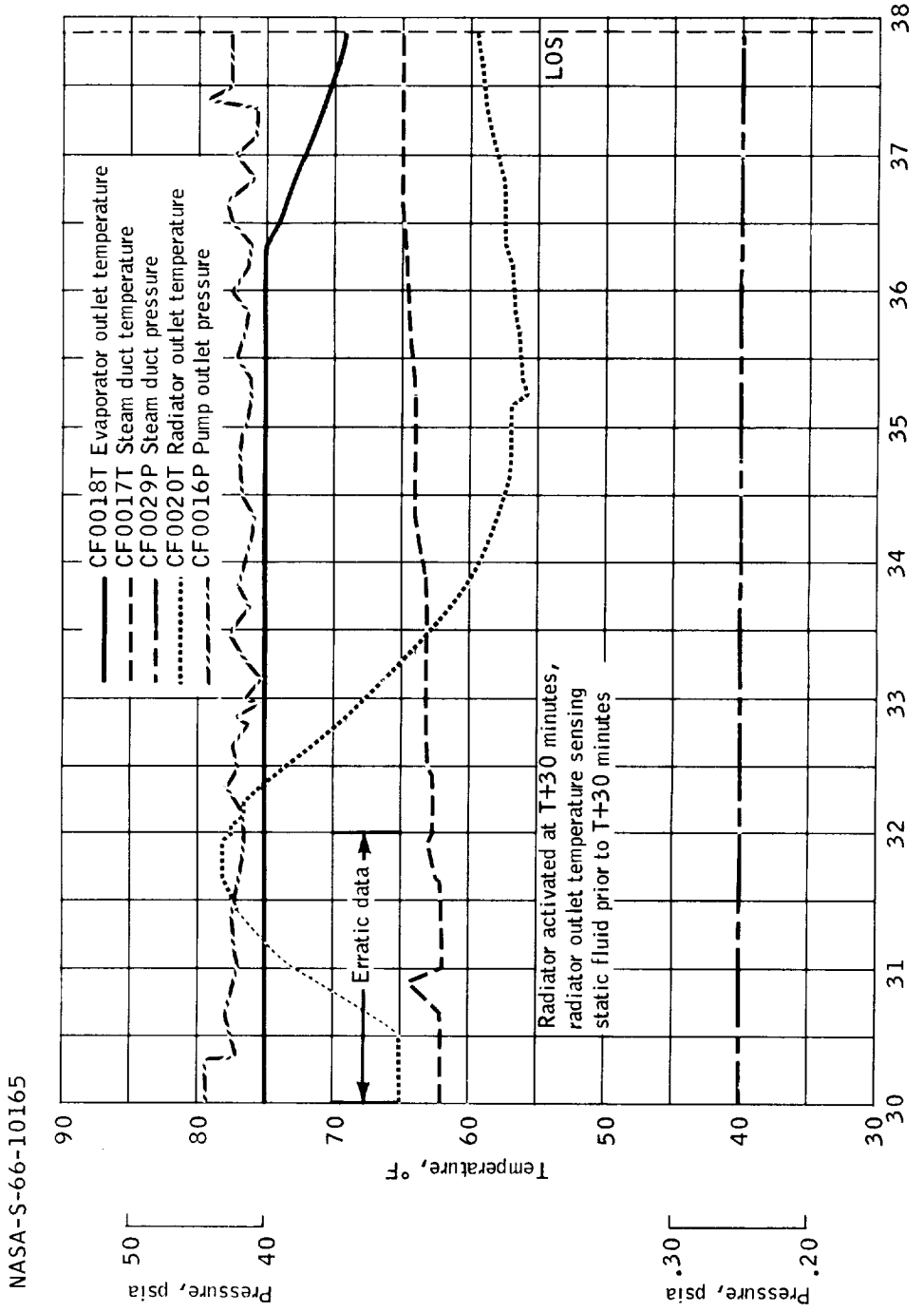

(c) 30 to 38 minutes.

Figure 7.17-2.- Continued.

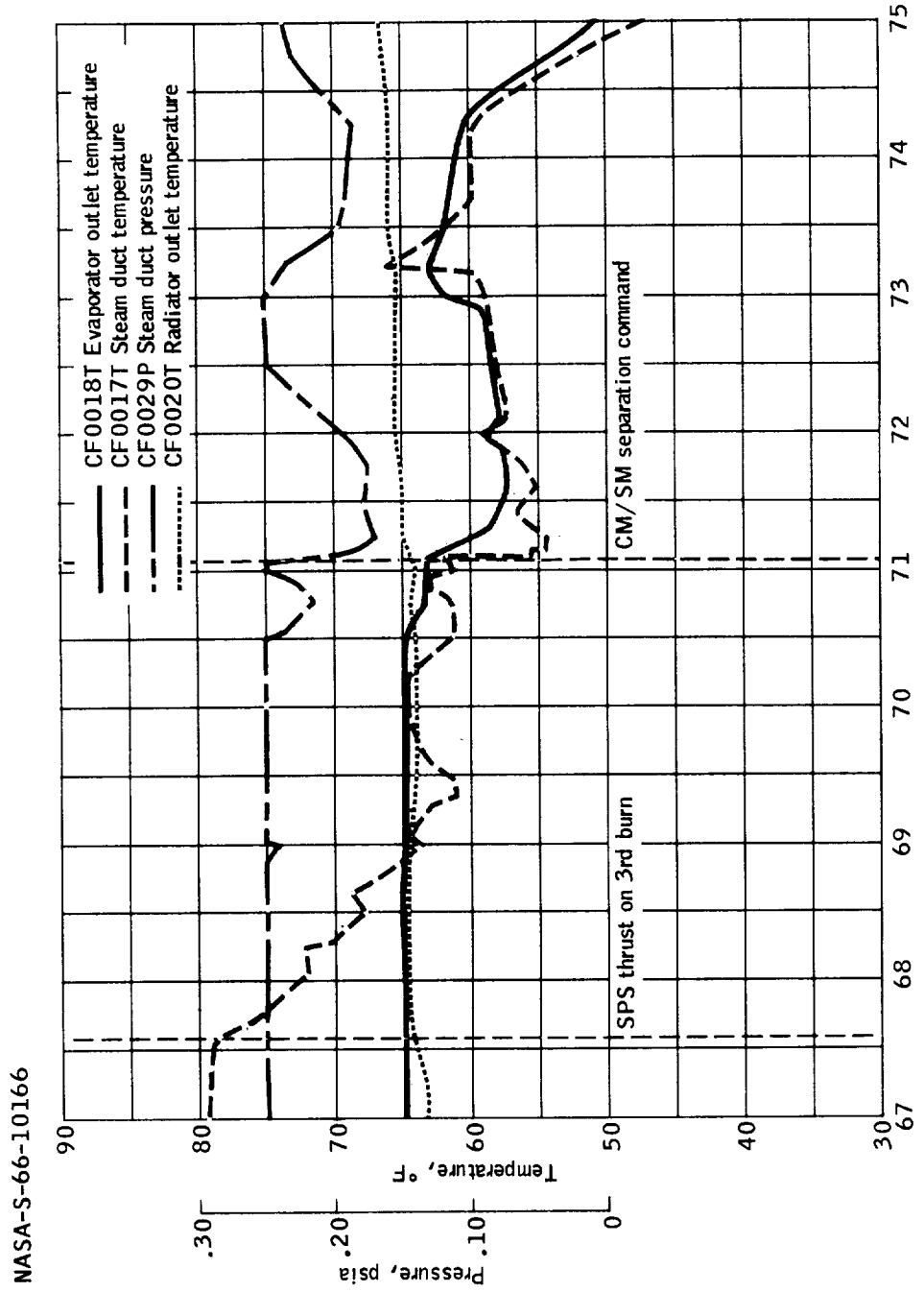

(d) 67 to 75 minutes.

Figure 7.17-2.- Continued.

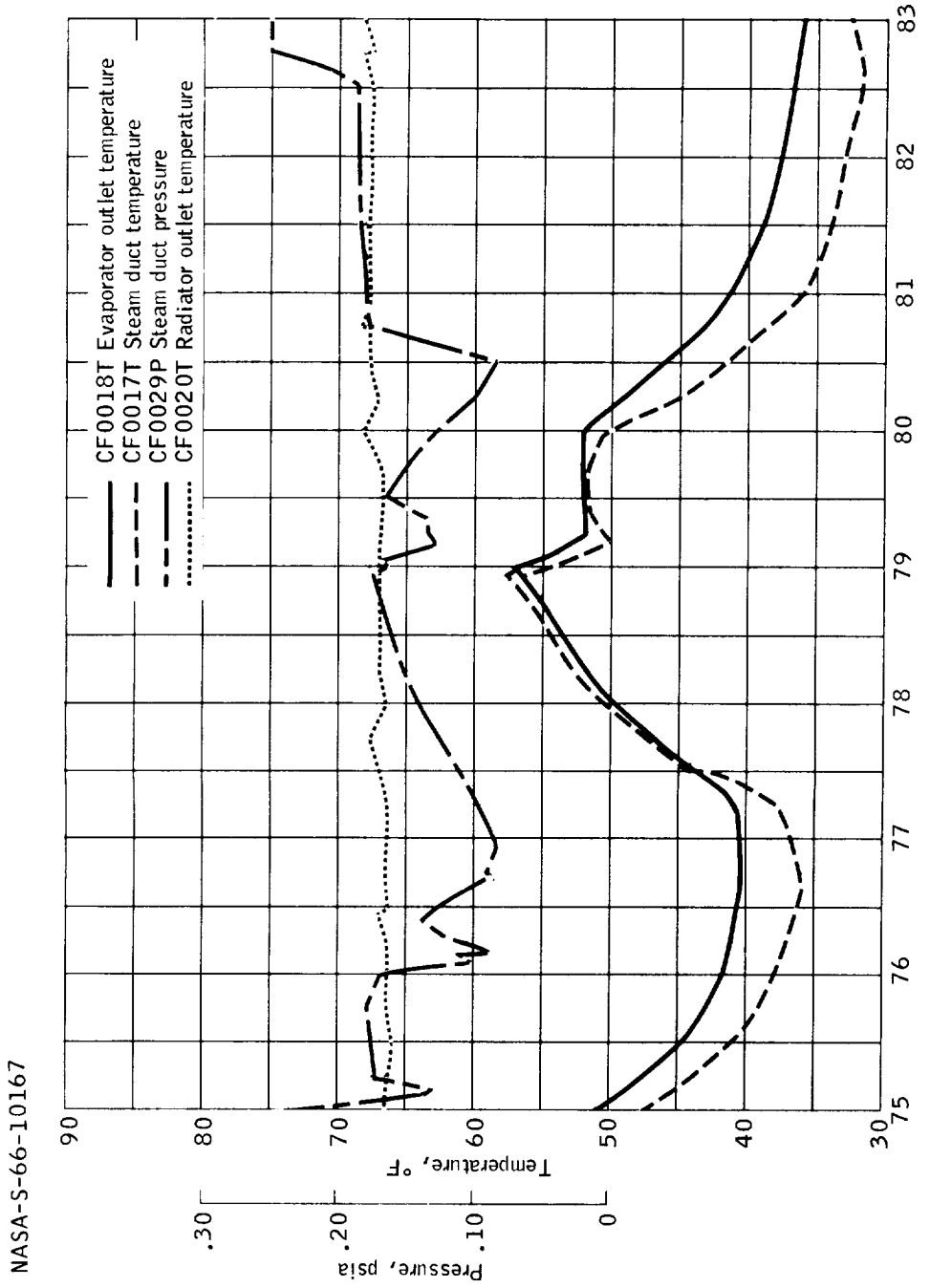

(e) 75 to 83 minutes.

Figure 7.17-2.- Concluded.

NASA-S-66-10168

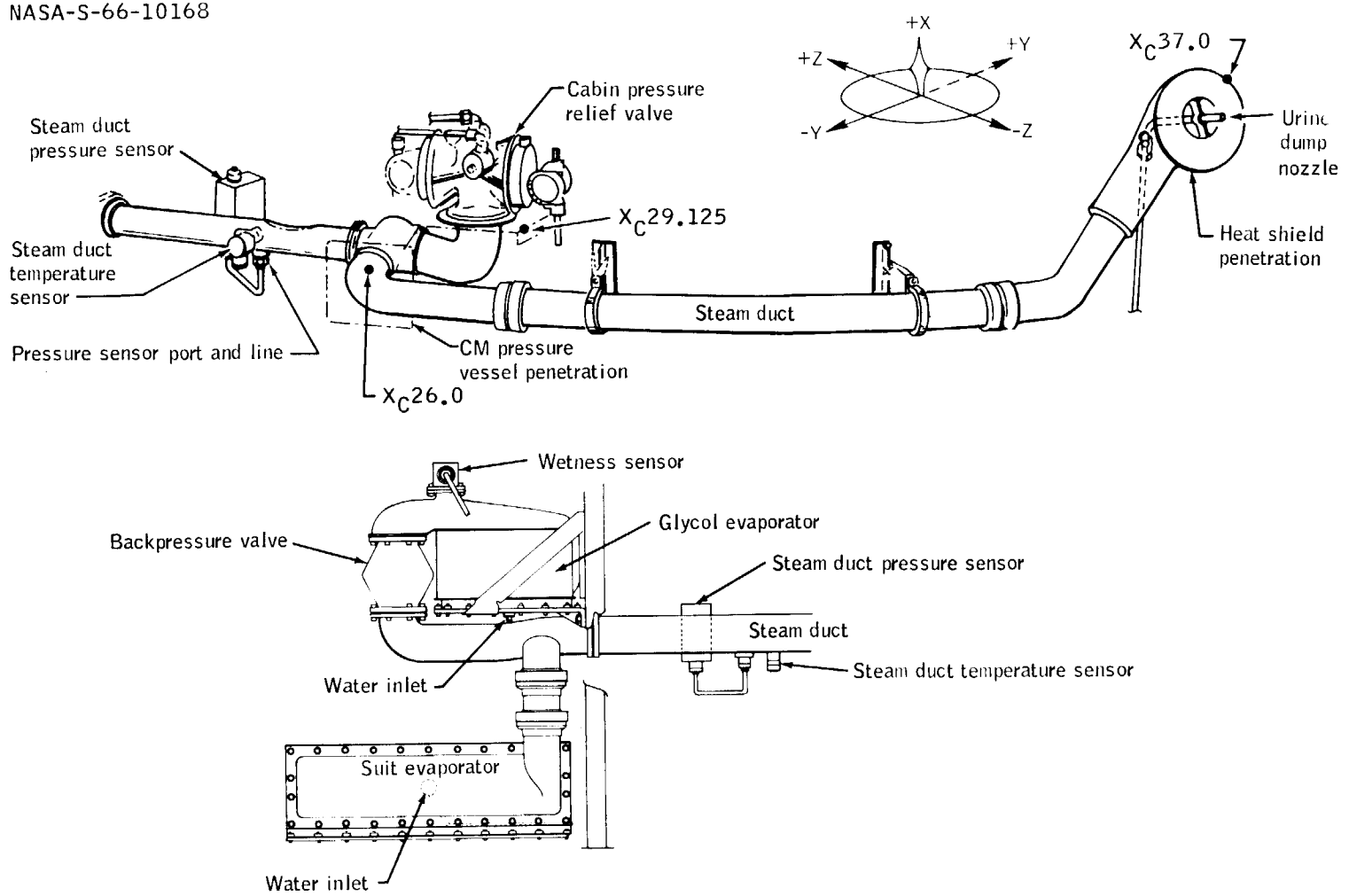

Figure 7.17-3.- ECS evaporator and steam duct installation, Mission AS-202.

NASA-S-66-10169

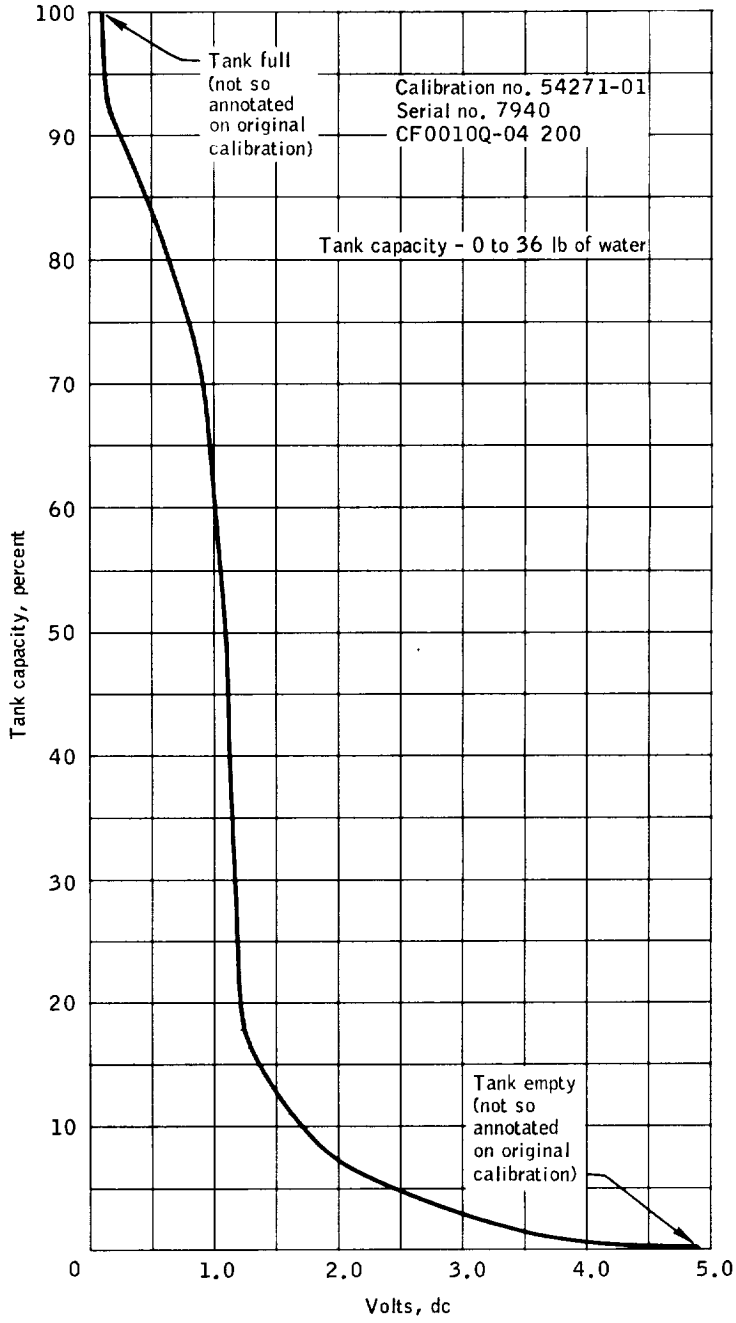

Figure 7.17-4.- Quantity potable water tank calibration curve, Mission AS-202.

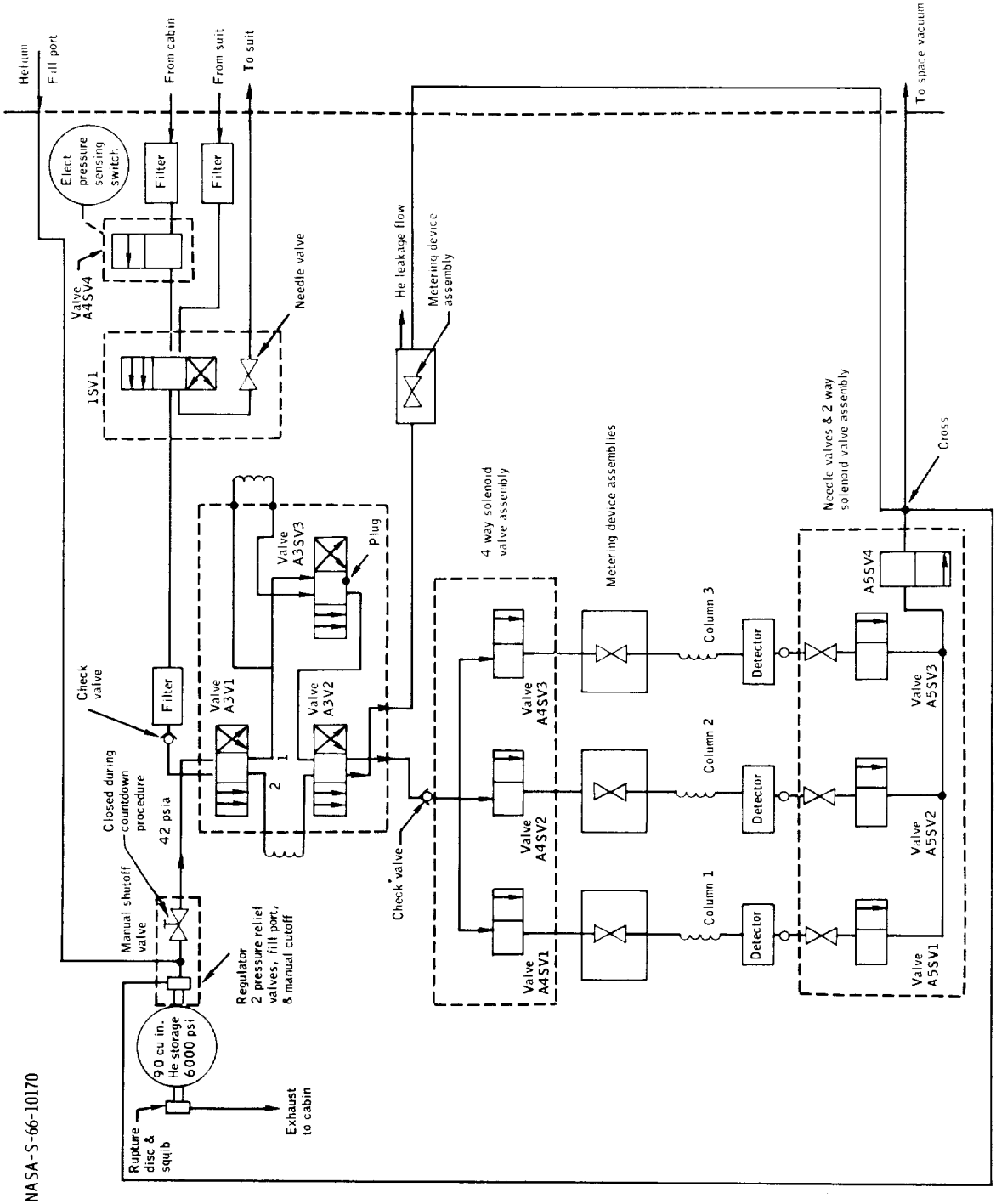

NASA-S-66-10170

Figure 7.17-5.- Gas chromatograph on SC-011, Mission AS-202.

7.18 Crew Station

7.18.1 Displays and controls subsystem.-

Summary: Mission AS-202 was the first flight test of a full set of complete Block I display and control panels. The full complement of displays and controls (D & C) was required to satisfy, in part, mission objectives by supporting the performance evaluation of the G & N, SM RCS, CM RCS, and communications subsystems.

Although it was not feasible to visually monitor the entire main display console, panel areas containing D & C of primary importance were photographed using two 16-mm cine cameras during the launch and entry phases of the mission. In general, performance of the D & C subsystem was nominal.

Description: The spacecraft 011 main display console, shown in figure 7.18.1-1, is basically the same as the spacecraft 012 unit. Notable differences between spacecraft 012 and spacecraft 011 displays and controls are caused primarily by subsystem changes. Panels 8 and 9 on spacecraft 011 were combined to a single panel for spacecraft 012 to allow more efficient use of available space. Changes in quantities of switches, circuit breakers, event indicators, and other smaller components are required on spacecraft 012 to support system changes and manned flight requirements.

Performance analysis: A postflight analysis of the spacecraft 011 displays and controls was completed using inflight panel photographs and telemetry data as a guide. It was concluded that the D & C subsystem functioned correctly. However, several anomalies, detected during the D & C evaluation, were considered significant and are discussed below.

(a) During an analysis of the 16-mm film from onboard cameras, it was evident that the master alarm (master caution and warning) light was illuminated at T+3 seconds and remained on until splashdown. A detailed review of telemetry data revealed intermittent spikes during this time period which indicated an out-of-tolerance condition (less than 155 psia) in the SM RCS quad D helium pressure measurement system (measurement SR5830P). The spiking was gone by T+100, and since the SM RCS system functioned properly and the spiking was too rapid for a pressure change response, this discrepancy was considered to be an instrumentation problem (see sections 7.9 and 7.15).

(b) The caution and warning annunciator for fuel cell number 3 was illuminated prior to launch and remained on throughout the mission. The measurement was waved before flight. Normally this annunciator would have been off until after CM/SM separation. Telemetry data

indicated that the oxygen flow to fuel cell number 3 was below the normal operating range (0.284 lb/hr) prior to launch and during the mission. This abnormal indication was caused by a defective fuel cell number 3, oxygen flow rate sensor, which in turn triggered the caution and warning detection system.

(c) The angle-of-attack (AOA) meter indications were erratic starting at approximately T+93 seconds. Postflight analysis indicated that the Q-ball, the AOA meter sensing unit, was not operating correctly (see section 7.14 and ref. 19).

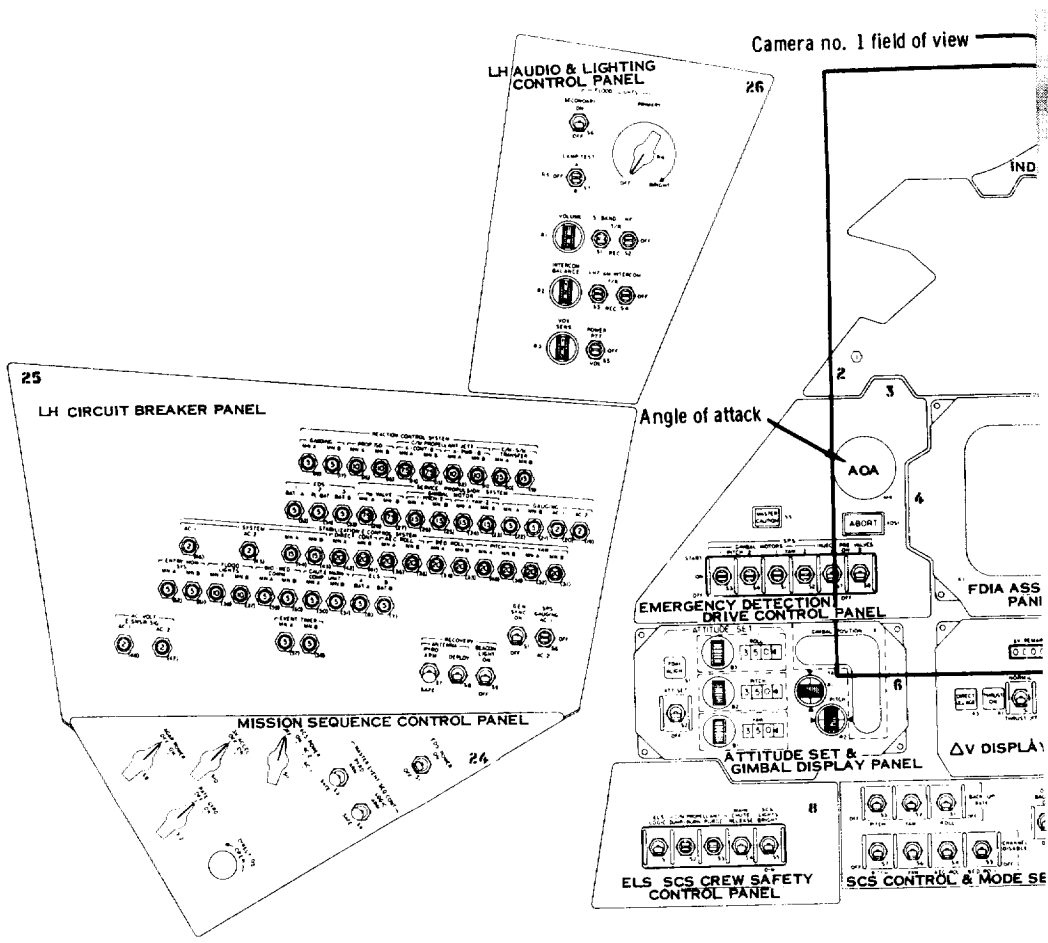

FOLDOUT FRAME

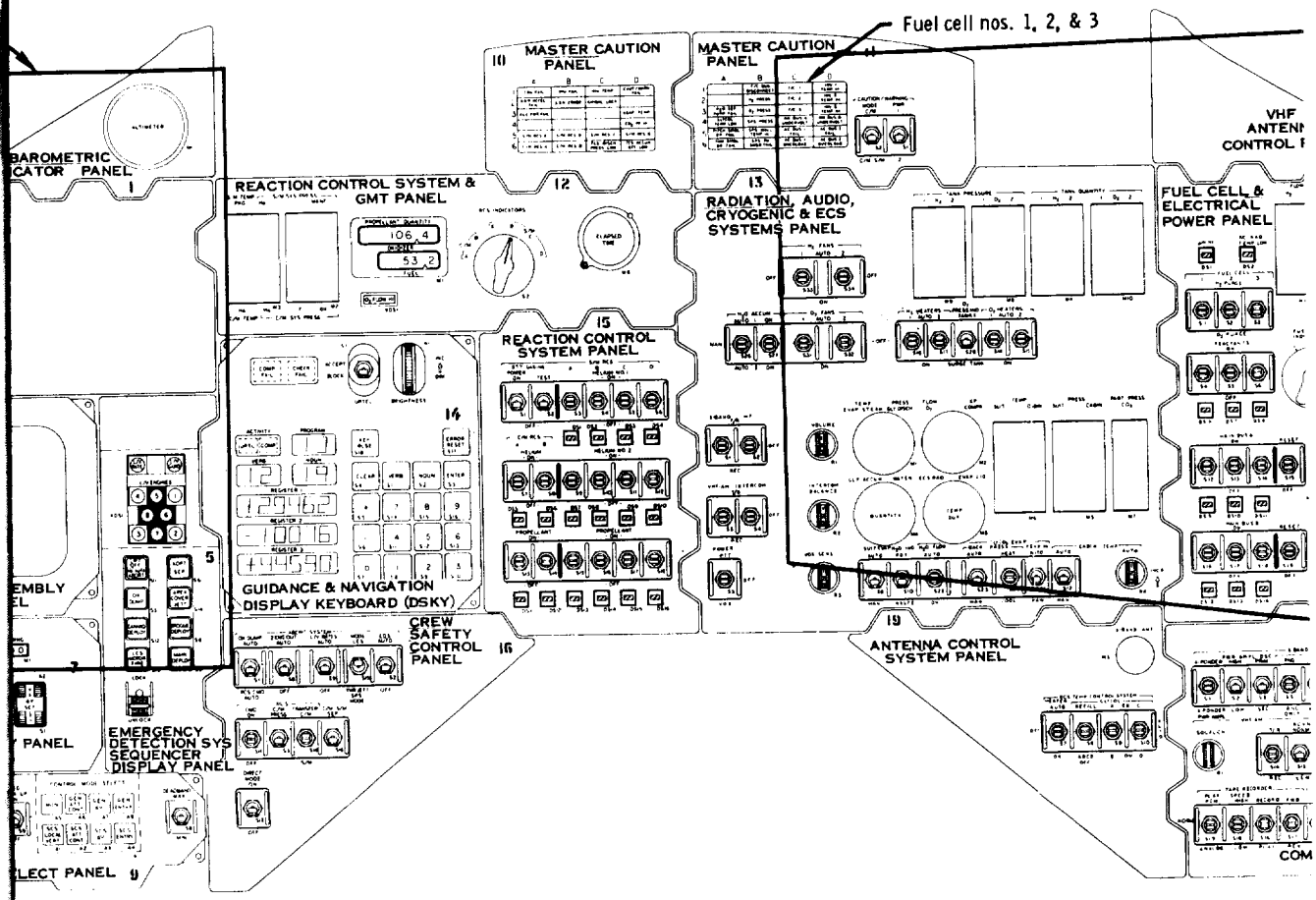

FOLDOUT FRAME 2

NASA-S-66-10171

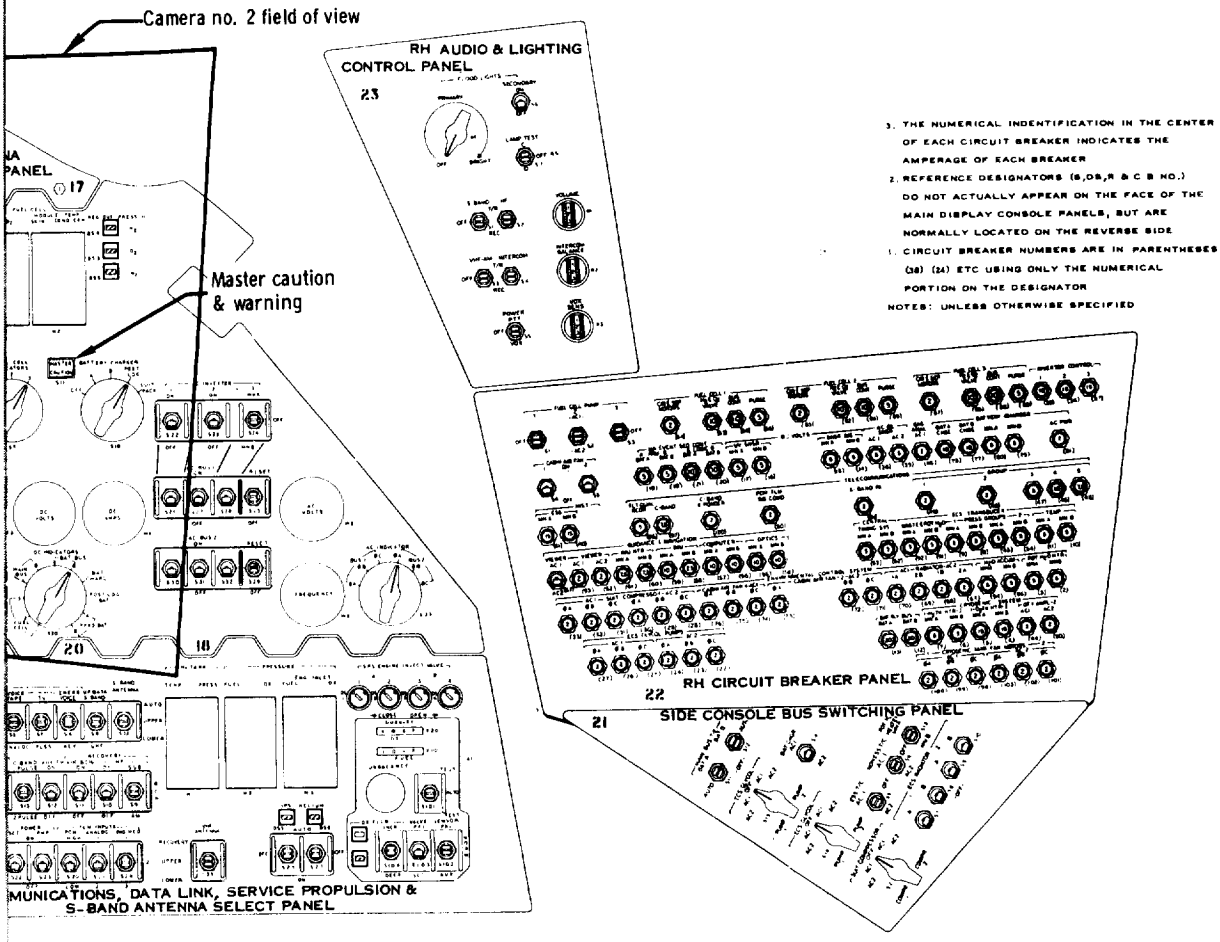

Figure 7.18.1-1.- Main display console, Mission AS-202.

FOLDOUT FRAME 3

7.18.2 Crew visibility.-

Summary: In general, four of the CM windows on spacecraft 011 had the same postflight appearance. The left rendezvous window had a bluish-green discoloration. After landing, a "fog-like" condensation of moisture developed between the outer heat shield pane and the outer pressure cabin window assembly for each window. This is to be expected since the space is vented to the outside. There was no evidence of moisture in the sealed space between the two panes making up the pressure cabin window assembly. A light to moderate density gray film was deposited at random over the outer surface of each of the heat shield windows. Through-the-window incident light transmission was reduced by the contaminant, and visual acuity was degraded, but to a lesser degree than experienced on spacecraft 002 and spacecraft 009.

Description: The CM window installation was a Block I type configuration, and consisted of one hatch window, two side windows, and two rendezvous windows (fig. 7.18.2-1). Each window assembly consisted of three panels: two inner panels, each 0.20-inch thick with a 0.175-inch spacing between them, installed in the pressure cabin structure, and one outer panel, 0.70-inch thick, installed in the CM heat shield structure, approximately 1 inch from the inner window assembly (fig. 7.18.2-2). The space between the two panes installed in the pressure cabin structure was evacuated and refilled with ambient air (as opposed to dry air or a dry inert gas) to 7.5 psia and sealed. The two inner panels were aluminum silicate (Corning Code 1723). The multilayer antireflective coating (HEA) to be applied to both sides of each panel was not included for this unmanned mission. The outer panel was amorphous fused silica (Corning Code 7940) UV grade quartz. Only the left rendezvous window had the magnesium fluoride antireflective coating on the outer surface and the blue-red (UV-IR absorbitive-reflective) coating on the inner surface.

A 16-mm camera, with a 10-mm lens, was installed on the instrument pallet, 16 inches away and perpendicular to the window (section 7.15 and fig. 7.15-4). Figure 7.18.2-1 indicates the bore sight view point location of the window camera. The camera was operated from approximately T+2 minutes to T+14 minutes for the launch phase and from about T+1 hour 14 minutes through splashdown for the descent and landing phase. Postflight review of the film indicated that the film was underexposed. A new copy was made from the optical master, overexposing the copy 3f stops. The new film was useable for photo analysis.

To establish the degree of visibility degradation as the result of window contamination and the additional visual attenuation resulting from vaporization of sea water which left an outer layer of crystallized

salt, a grid-resolution photography procedure was conducted on the spacecraft window system.

The preflight grid-resolution photography was conducted at Kennedy Space Center after installation of the spacecraft inside the altitude chamber. Figures 7.18.2-3 and 7.18.2-4 show the condition of the windows before flight. Postflight grid-resolution photography was conducted twice: the first time was onboard the recovery ship 24 hours after recovery of the spacecraft; the second time was after the spacecraft had been returned to the contractor's facility, Downey. The condition of the windows after shipboard recovery is shown in figures 7.18.2-5 and 7.18.2-6, while figures 7.18.2-7 and 7.18.2-8 show the postflight condition of the windows after the spacecraft arrived at the contractor's facility, Downey.

Postflight inspection: The first postflight inspection of the windows was conducted by the recovery team after the spacecraft had been secured onboard the aircraft carrier. The examination revealed heavy condensation of moisture between the heat shield window and the outer window panel of the pressure cabin assembly of the right side window (figs. 7.18.2-5 and 7.18.2-6). The condensation occluded 80 percent of the total window viewing area. The other windows had a light to moderate condensation of moisture between the heat shield window and the outer panel of the pressure cabin window assembly.

There was evidence of a light to moderate contamination on all spacecraft windows. The right side window had a moderate film around the periphery extending inward 1 inch. The right rendezvous window had a light film and streaked water pattern randomly distributed over the viewing area. The left rendezvous window had a light to moderate density pattern covering the window. "Water-run" patterns were noted across the total window surface. The left side window had a light to heavy film. The heavy film was a 1-inch-wide band around the periphery. The light film was general.

Examination of the spacecraft windows at the contractor's facility, Downey, confirmed the basic report from the recovery team. The right side window had a heavy fog-like condensation between the outer window and inner window assembly. The other three windows had a light to moderate fog-like condensation between the two window structures. The right side window had eight to nine beaded lines where the fog-like condensation had coalesced into water droplets. The condensation on the other three windows had coalesced into water droplets randomly distributed over the window area. The coalesced water droplets were noted to be present on the inner surface of the outer window, as well as on the outer surface of the outer window of the pressure cabin assembly. The condensation was the result of the higher temperature of

of the outer window (over 400° F) and its rapid cooling after landing in the water. The spacecraft was in the water approximately 8 to 9 hours, and the space between the outer window and inner window assembly was vented to ambient conditions. The rapid cooling of the outer window and high moisture laden air between the two window panes resulted in condensation on the window.

There was evidence of some salt crystallization located randomly on the outer surface of the windows. These crystallized areas are more in number but are not as large as was experienced on spacecraft 009. The distribution of a very light to moderate film was noted on the left and right side windows. The moderate film was around the periphery of each window extending inward approximately 0.5 to 1 inch. The very light film was in the form of very small spatters randomly distributed over the surface. Both rendezvous windows had a moderate film in the lower inboard corner. The right window had a general spattered appearance of light film, and the left rendezvous window exhibited a bluish-green discoloration of the total central viewing area. Examination of the scorching pattern on the ablator indicated that the discoloration was the result of scimitar antenna ablation. Close examination of the inner window assembly revealed no water or contamination. There was no definite evidence of the windows being deliberately wiped or abraded, although reports of the recovery team stated that the pararescue team had stepped on one of the rendezvous windows and the left side window had been wiped. However, the contamination had been washed to some degree by the wave-lapping action during the 8 to 9 hours the spacecraft was in the ocean.

Onboard camera film analysis: The window camera started at T-2 minutes and the boost protective cover came off at T+2 minutes 50 seconds. At the time the cover came off there was no evidence of contamination on the right rendezvous window. The horizon appeared in the upper part of the window at T+6 minutes 6 seconds. The area was approximately one third of the total window area. The horizon disappeared at T+7 minutes 3 seconds, returned at T+7 minutes 10 seconds, disappeared again at T+9 minutes 47 seconds, and was not seen until after reentry heating. During the time that the horizon was visible, there was no evidence of heavy contamination on the window.

During reentry, a few carbonized particles appeared to be within the window field of view. The first of these particles appeared at 1 minute 15 seconds after start of reentry and the last observed particle was at 2 minutes 10 seconds. During the skip-out no additional particles were observed. During reentry heating there was evidence of some light film deposit on the lower outboard area of the window. The upper inboard area of the window showed a slightly heavier deposit during the beginning of the second heat pulse.

After the second heat pulse the horizon came into view as the spacecraft continued to descend. The horizon was visible in about one half of the total window area. Again, there was good visibility through the window. During this time clouds came within the window field of view. These clouds had good detail and the sun was noted to be reflecting off an occasional cloud. Forward heat shield jettison was very clear. The jettisoned heat shield and its parachute could be seen through the window after the drogues had been deployed. There was good detail and resolution in the showing of the drogue and main parachutes deploy, of the reefed and unreefed main parachutes, of the main parachutes suspension lines during descent, and of the right rendezvous window being lapped by the sea water action after landing.

Grid-resolution photography analysis: The results of the resolution photography are shown in table 7.18.2-I. The right side window had the greatest reduction in resolution quality. A comparison of the shipboard photographs with the photographs taken after the spacecraft was returned to the contractor's facility, Downey, indicated that the resolution quality had improved. The general increase in resolution was the result of the fog-like condensation coalescing into water droplets.

Comparison of the preflight and postflight grid-resolution photography indicated a general loss in transmitted intensity, a slight decrease in window resolution, and little loss in through-the-window visual acuity.

Postflight analysis: The outer heat shield windows were removed for visual examination, photographing, spectral transmission (direct and scattered), reflection characteristics, and emission spectrographic analyses of the contamination. Visual examination revealed that all the windows had a deposit of crystallized salt. In general, the salt deposits were in the form of small spattered-type areas distributed over the total window area. Dust and dirt which collected on the window surface after arrival at the contractor's plant was taken into account in the analysis of the postflight examination of the window. Close examination of the left rendezvous window revealed that the discoloration was the result of a very thin film of contaminant. Figure 7.18.2-9 shows the condition of the outer windows after their arrival at the subcontractor's facility.

Smears of the contamination from each window were taken for emission spectrographic analysis. Figure 7.18.2-10 gives the location on each window where a smear was taken. The hatch window was sacrificed; the total contaminant being scraped off for quantitative analysis. An emission spectrographic analysis was also conducted on a paint sample taken from the aft heat shield.

Tables 7.18.2-II and 7.18.2-III show the results of the emission spectrographic and quantitative IR analyses. The infrared analysis resulted in small amounts of carbonyl or carboxylic compounds in the form of esters. Silanes and siloxanes were also found in the contaminant taken from the hatch window. All are indicative of decomposed byproducts of complex organic compounds. Also presented is a comparison of the window contaminants found on spacecraft 002 and spacecraft 009. On spacecraft 009 and spacecraft 011 there is a general increase in the amount of sodium, calcium, magnesium, and silicon, due mainly to the recovery environment and ablator system differences from that of spacecraft 002. Comparison of the elements found in the paint sample and those of the hatch window indicate ablator action during reentry attributed the majority of contamination to the window system. All three spacecraft have exhibited window contaminants. The density of the window contamination has decreased with each flight.

Direct spectral transmission was conducted on each window through an area of greatest contaminant density and then through an area of least density. Figure 7.18.2-11 represents the results of the direct spectral transmission through each of the spacecraft windows. For comparison, preflight window transmission characteristics are shown in figure 7.18.2-12. The transmission through a complete window assembly with optical coatings is indicated by the solid line. Also shown is the transmission and reflection characteristics of the virgin outer heat shield window at normal incidence (dotted line). These spectrographic analyses were conducted on a preflight window under controlled laboratory conditions. Conducting transmission tests on random selected window samples could easily result in a 10-percent loss in transmission.

The transmission through the heaviest contamination (fig. 7.18.2-11) was 48 to 51 percent and was located 2 inches from the inbound corner on the right rendezvous window. This area was approximately 1 inch in diameter and was covered with a moderate layer of crystallized salt. Based on preliminary testing with salt-coated window samples, approximately 15 percent of the total transmission loss could be attributed to the layer of salt. The transmission characteristics of the left rendezvous window are caused by the optical coatings. The steep dip at 510 millimicrons is representative of the monolayer of bluish-green contaminant present on this window. The direct light transmission in the visual spectrum through the central viewing area of the windows ranged from 55 percent to 81 percent. The transmission through the contamination area around the periphery of the window was 48 percent to 75 percent.

Plotted for comparison in figure 7.18.2-13 are the general spectral transmission characteristics of the three Apollo flights. The shaded area represents the worst and best postflight Gemini window.

It can be noted that the transmission characteristic of the Apollo windows fall within the same range experiences on the Gemini flights.

Total transmission and back reflection measurements were conducted only on the left rendezvous window. The other windows did not have the optical coatings, therefore light scattering and reflection information would be arbitrary. Figure 7.18.2-14 represents the total transmission, diffuse transmission, and spectral reflection of the left rendezvous window. The diffuse transmission is a measure of the light which is scattered as it is transmitted through the window. The difference between the total transmission and the direct transmission is the diffused transmission. The average total transmittance through the heaviest discoloration was about 78 percent and the average value of diffuse transmittance was about 5 percent, indicating that only 5 percent of the light impinging on the window was being scattered. The reflectance, with the normal incidence light towards the outboard surface, was about 5 percent at 450 to 475 and 540 to 750 millimicrons. Normal reflectivity in the visible range of the window with optical coatings is 4 percent. Note the effects of the contaminant film on total transmission reflection and diffuse transmission at 510 millimicrons. This wave length is representative of the bluish-green color of the film.

Concluding remarks: The postflight measurements of transmittance and reflectance show that a degradation in light transmission and a lesser loss in visual acuity has occurred and that 5 to 10 percent of the light is absorbed by the contaminant film. The transparent characteristics of the contaminant film on spacecraft 011 are indicative of the spectrographic analysis. The transparency of the film on spacecraft 011 is contrary to the translucent film experiences on spacecraft 002 and spacecraft 009, and results in the improved postflight resolution quality of the windows.

Part of the contaminant film was deposited on the windows during the flight and part was deposited as a result of the salt water environment during recovery. Preliminary testing with salt water window samples indicates that about 10 to 15 percent of the transmission loss could be attributed to the crystalled salt. Onboard film analysis indicates that during the major phase of flight there could possibly be a very light uniform density film on the window and that the heavy deposit around the periphery occurs during reentry which is the case for the discolored film on the left rendezvous window. The results of the quantitative IR analysis of the hatch window confirms that the majority of the contaminants are the byproducts of decomposed organic materials.

The amount of contaminant that was washed off the windows by wave lapping is unknown. Based on the amount of detail shown in the drogue and parachute system during descent very little contaminant was removed.

The window condition on spacecraft 011 would not cause degradation to the horizon or ground orientation during a high altitude abort, would be tolerable on a lunar mission, and rendezvous and docking maneuver could be performed. Star magnitude would be lowered but would be well within the apparent equivalent brightness error.

TABLE 7.18.2-I.- SPACECRAFT WINDOW RESOLUTION CHARACTERISTICS

Conditions	Resolution of each window, lines per mm				
	Camera system	Left rendezvous	Right rendezvous	Left side	Right side
Preflight	56	40	40	50	50
Postflight, shipboard	56	20	28	40	5
Postflight, Downey	56	28	34	40	40

TABLE 7.18.2-II.- EMISSION SPECTROGRAPHIC ANALYSIS[a]

Element	SC-002 code	SC-009 code	SC-011 code
Aluminum	Light minor	Major	Light major
Antimony	None	Trace	Base
Barium	None	Trace	None
Bismuth	Trace	None	None
Boron	Light minor	Light minor	Light major
Cadmium	None	Base	None
Calcium	Base	Heavy minor	Major
Chromium	Trace	Light major	Light minor
Copper	Base	Minor	Minor
Iron	Major	Major	Major
Lead	Heavy major	Heavy minor	Heavy minor
Magnesium	Base	Heavy minor	Heavy minor
Manganese	Trace	Base	Light minor
Molybdenum	None	Trace	None
Nickel	Trace	Trace	Base
Silicone	Minor	Heavy major	Heavy major
Silver	None	Trace	Base
Sodium	Major	Heavy major	Heavy major
Tin	Base	Base	Light minor
Titanium	Light major	Light major	Base
Vanadium	None	Base	Minor
Zinc	Heavy minor	Light major	Heavy major
Zirconium	None	Trace	None

[a]Key to weighted code:

1-Heavy major
2-Heavy minor
3-Major
4-Minor
5-Light major
6-Light minor
7-Base
8-Trace

TABLE 7.18.2-III.- RESULTS OF QUANTITATIVE INFRARED ANALYSIS

Element	Paint	Hatch window
Aluminum	Light	Heavy
Antimony	- -	Trace
Barium	- -	Base
Boron	Base	Trace
Calcium	Heavy	Heavy
Chromium	- -	Base
Cobalt	Heavy	Light
Copper	Light	Light
Iron	Light	Heavy
Lead	Heavy	Heavy
Magnesium	Major	Heavy
Manganese	Base	Light
Molybdenum	- -	Base
Silicon	Major	Heavy
Sodium	Major	Major
Tin	Base	Trace
Titanium	Base	Heavy
Zinc	Major	Major

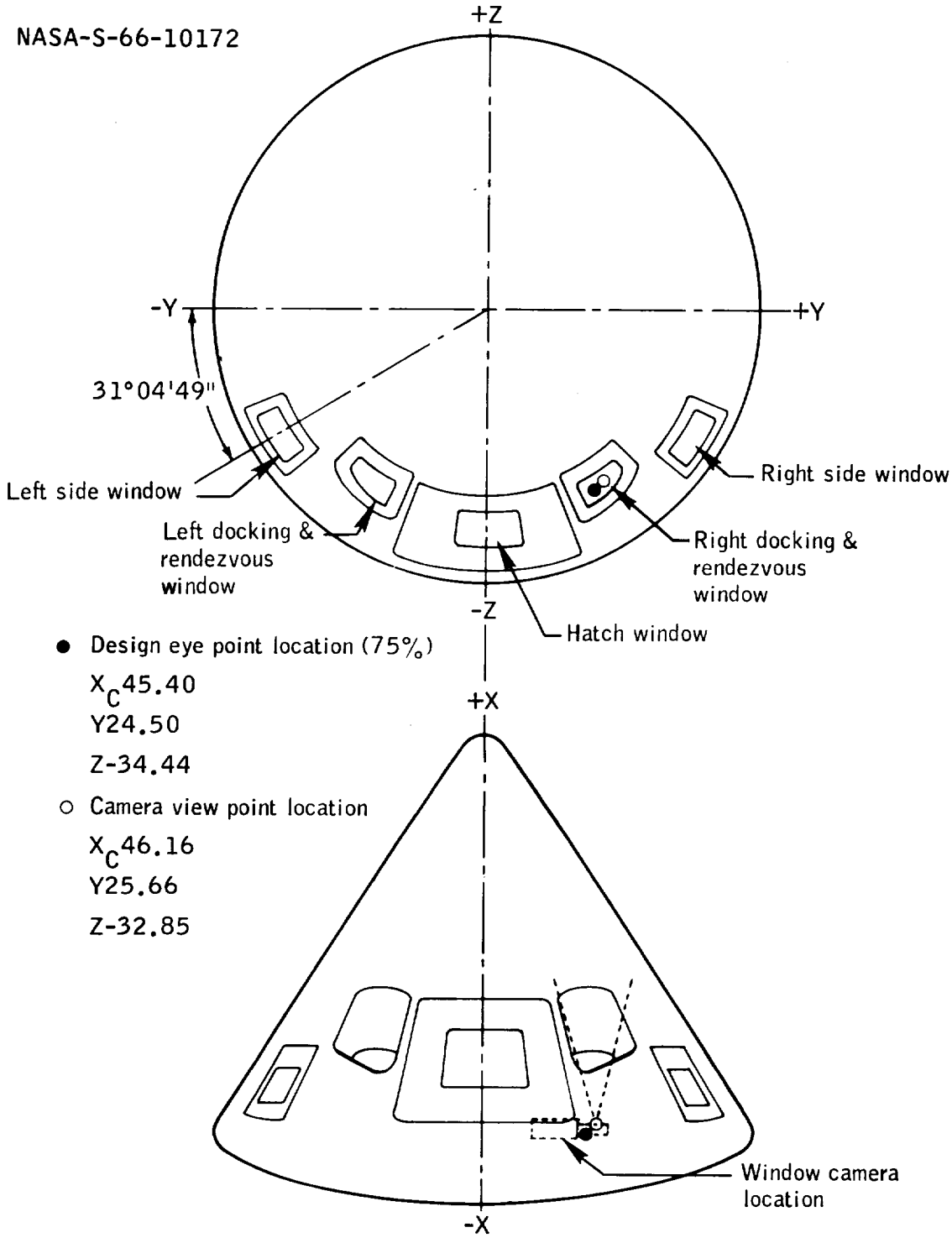

Figure 7.18.2-1.- Right docking window visibility, Mission AS-202.

NASA-S-66-10173

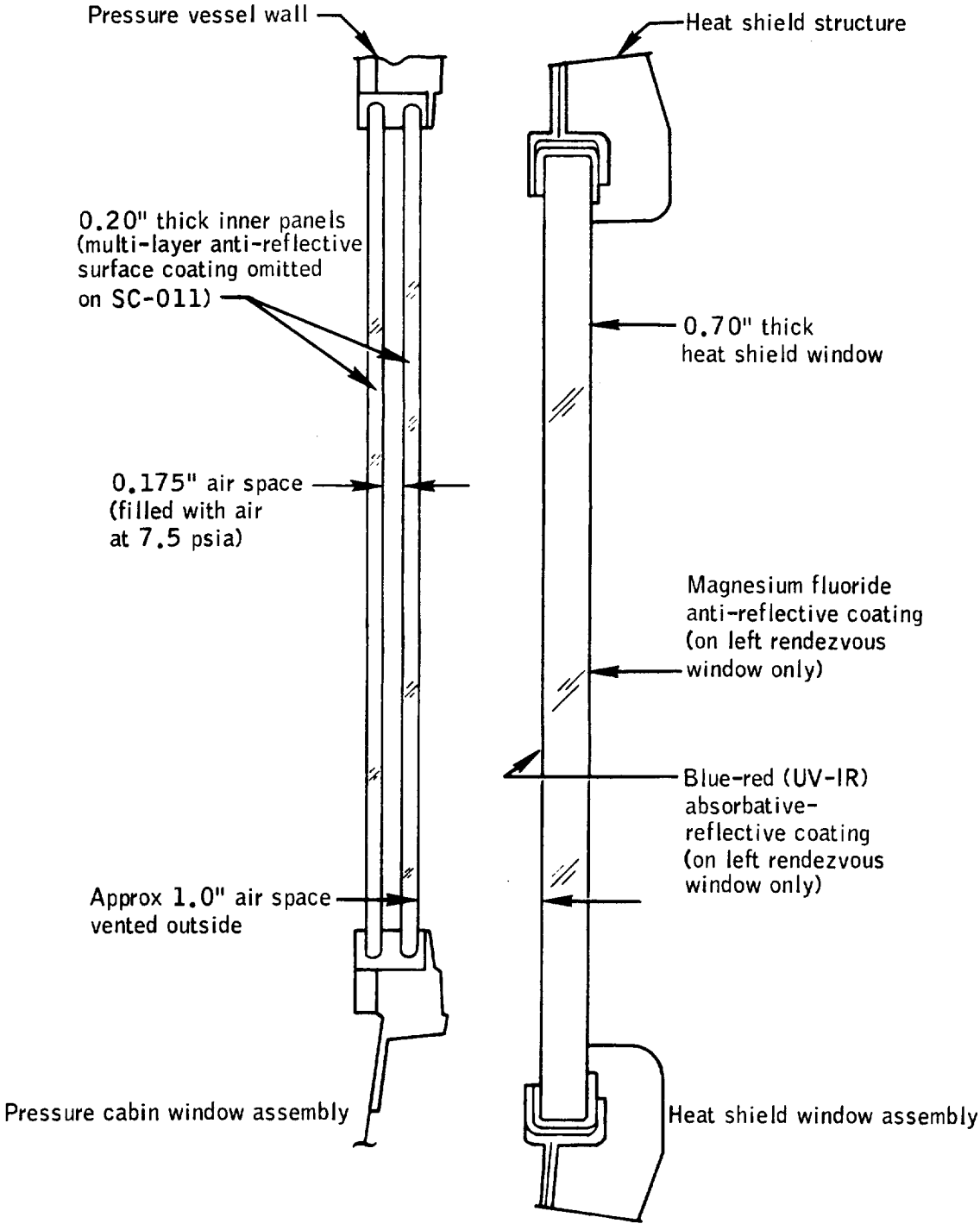

Figure 7.18.2-2.- Command module window assembly, Mission AS-202.

NASA-S-66-10174

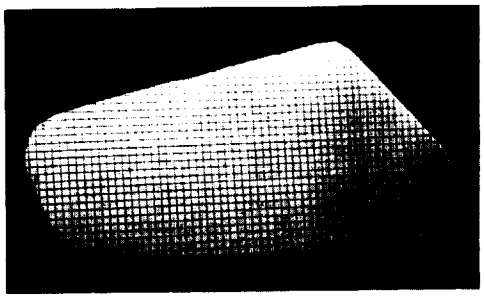

Left rendezvous

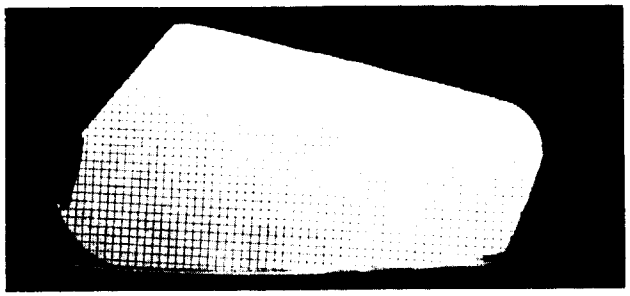

Right rendezvous

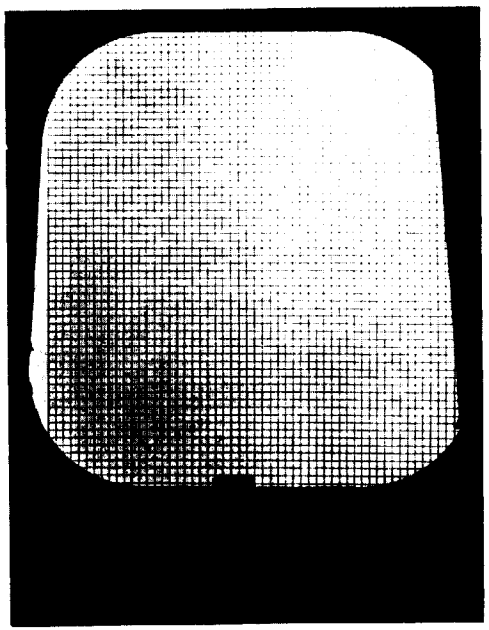

Left side

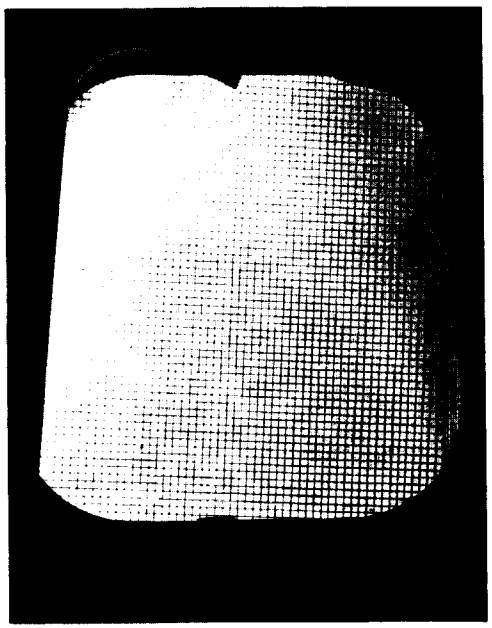

Right side

Figure 7.18.2-3.- Preflight grid photography showing condition of SC-011 windows, Mission AS-202.

NASA-S-66-10175

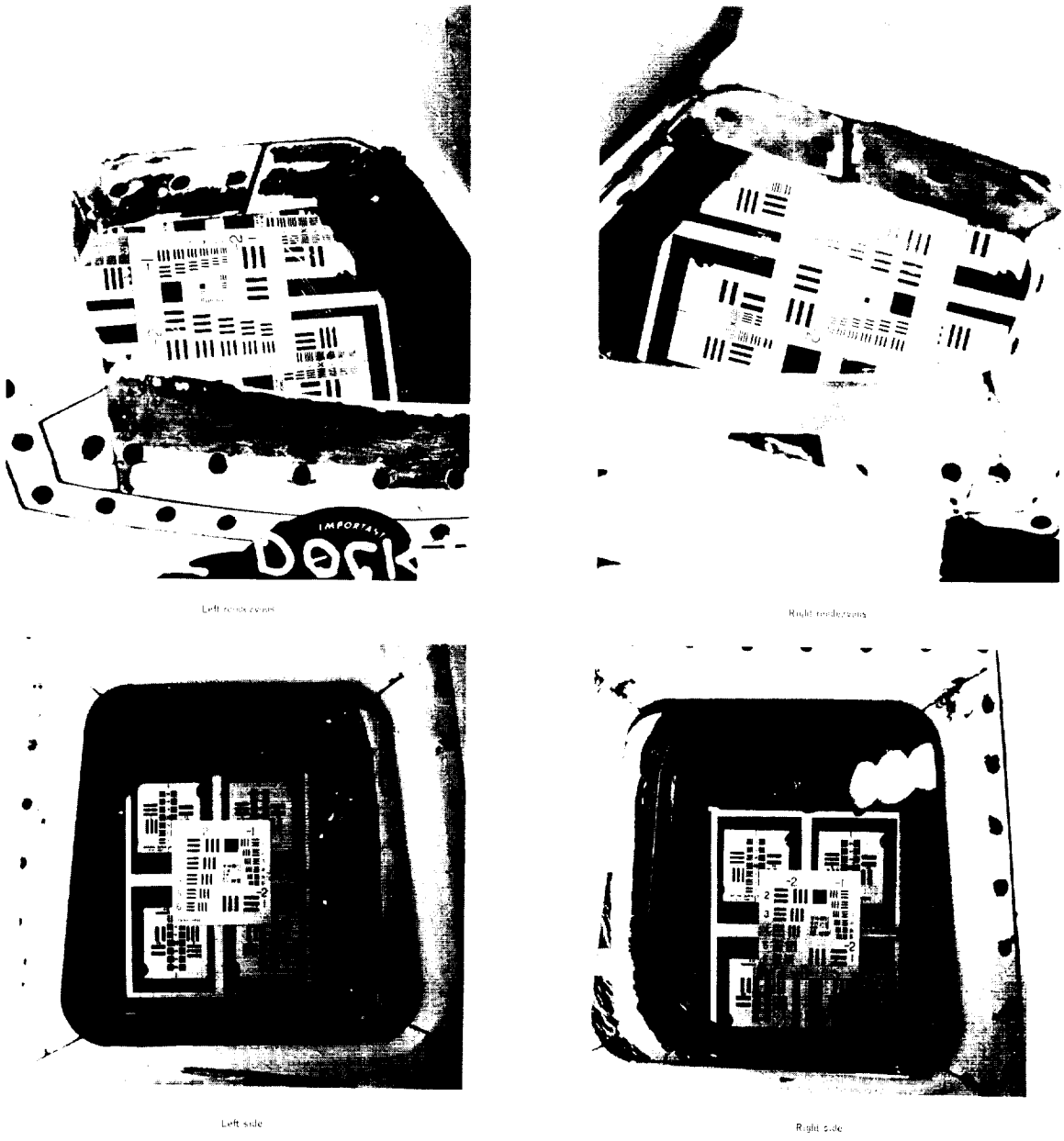

Figure 7.18.2-4.- Preflight resolution photograph showing quality of resolution through SC-011 windows, Mission AS-202.

NASA-S-66-10176

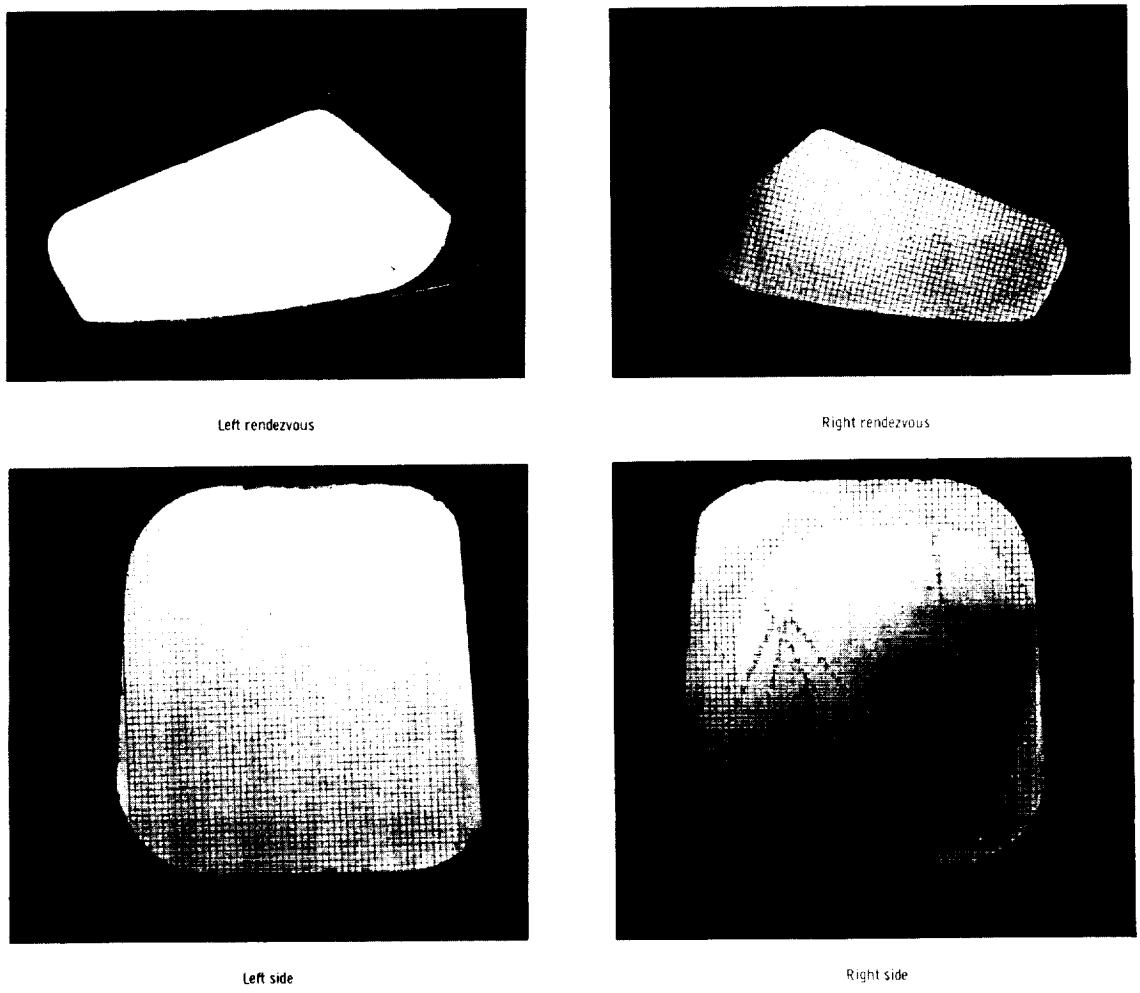

Figure 7.18.2-5.- Shipboard grid photography showing postflight contamination and water condensation on SC-011 windows, Mission AS-202.

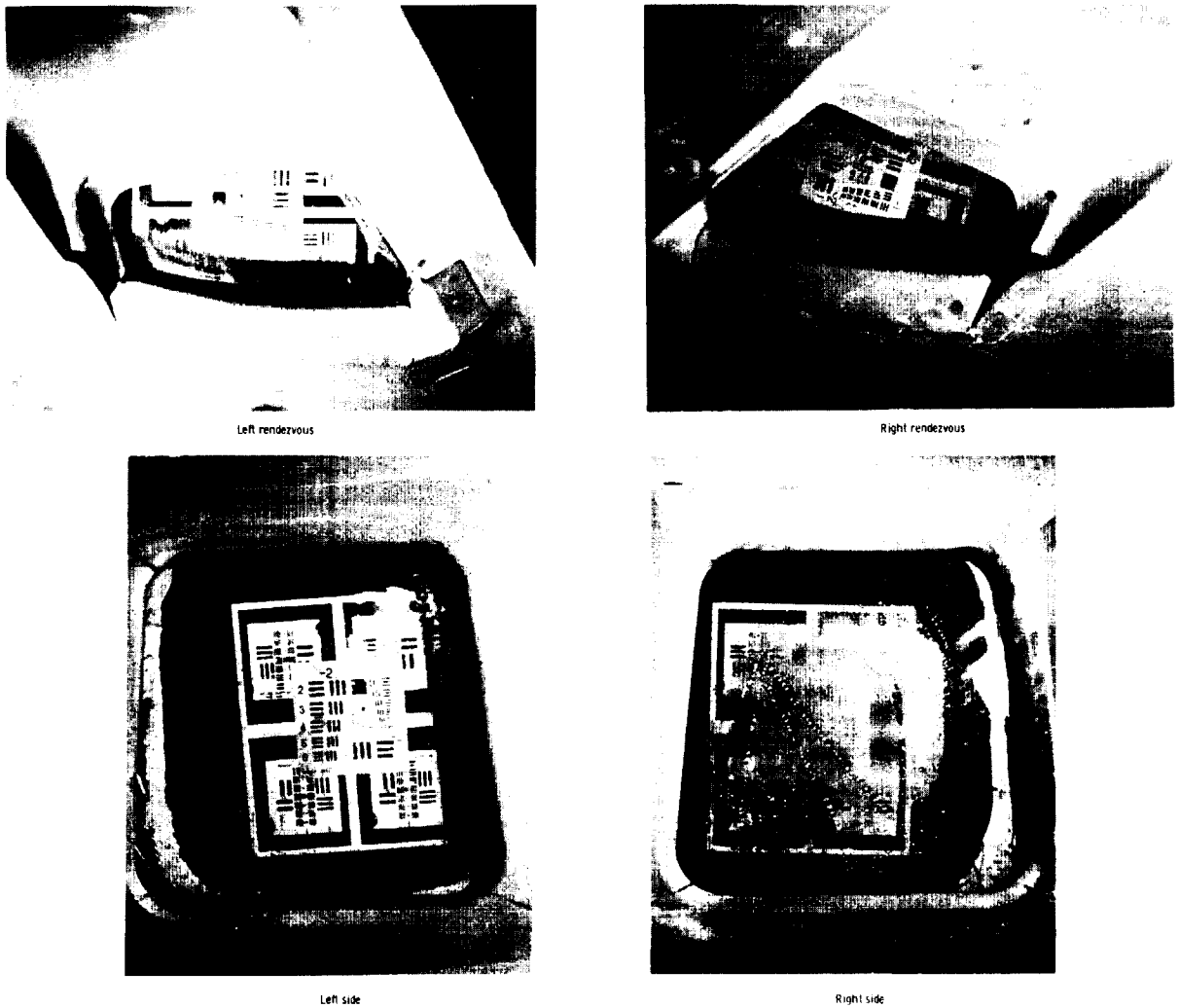

Figure 7.18.2-6.- Shipboard resolution photography showing loss of window resolution due to moisture condensation between window air space on SC-011, Mission AS-202.

NASA-S-66-10178

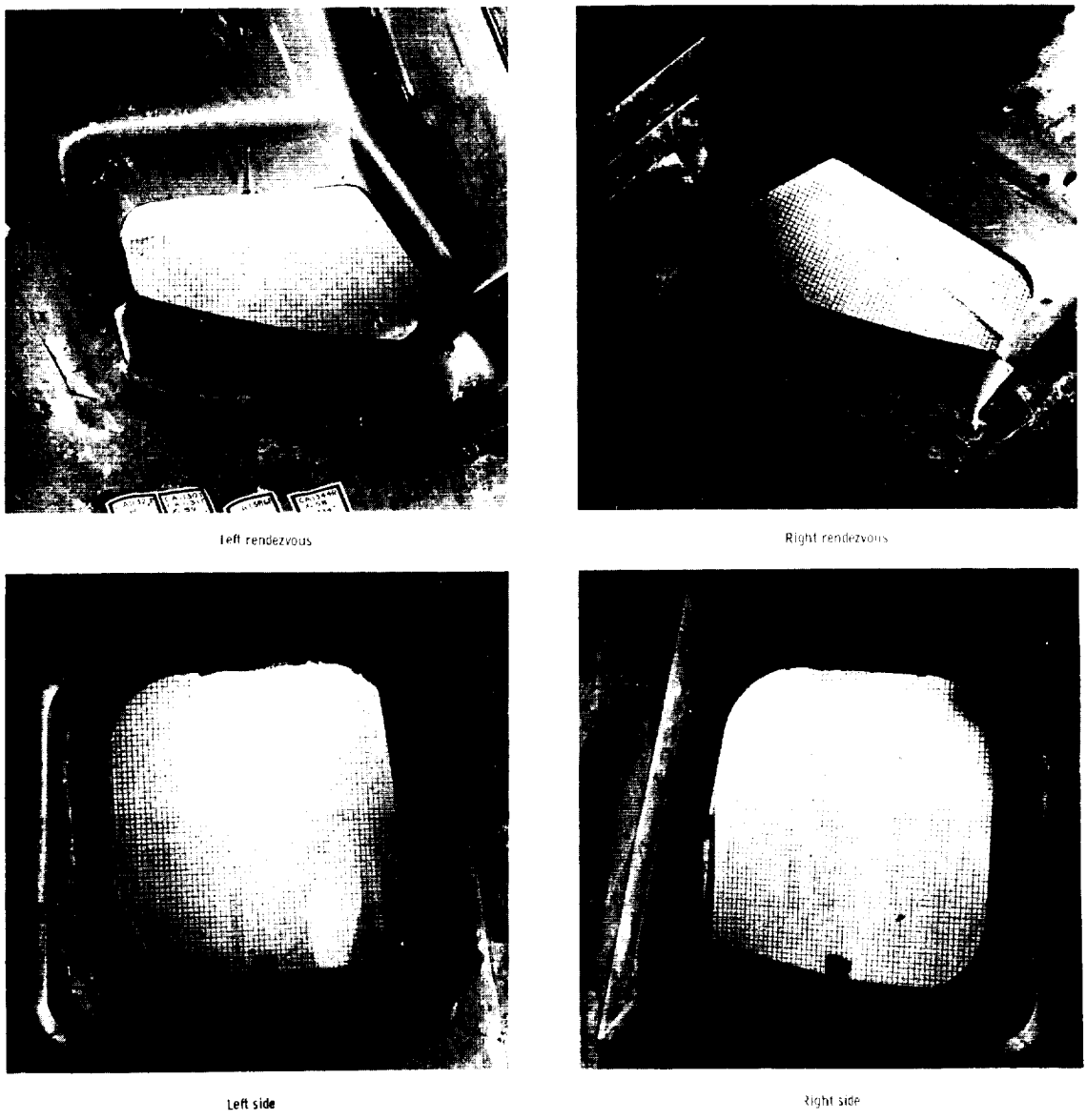

Left rendezvous

Right rendezvous

Left side

Right side

Figure 7.18.2-7.- NAA, grid photography showing condensation on SC-011 windows 10 days after flight, Mission AS-202.

NASA-S-66-10179

Left rendezvous

Right rendezvous

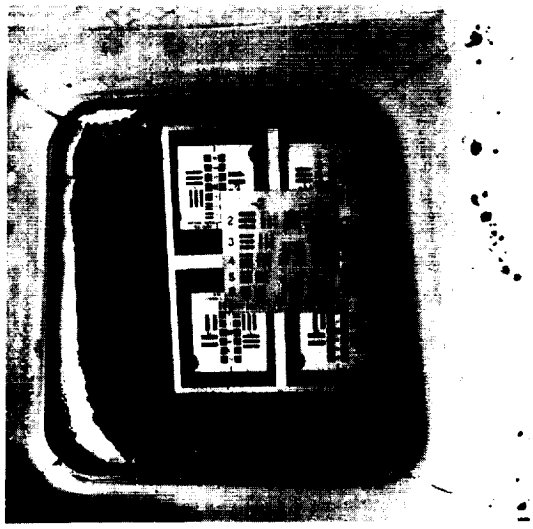

Left side

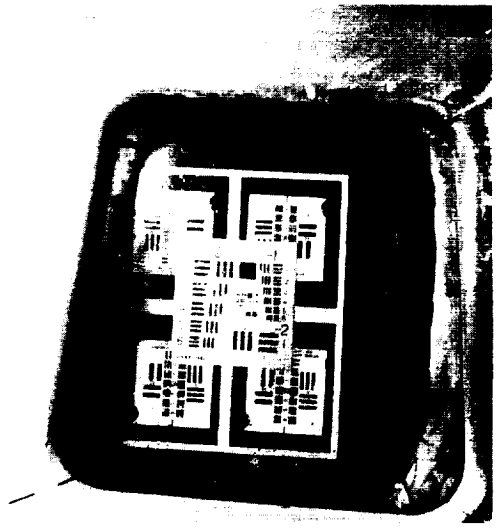

Right side

Figure 7.18.2-8.- NAA, resolution photography showing condensation on SC-011 windows 10 days after flight, Mission AS-202.

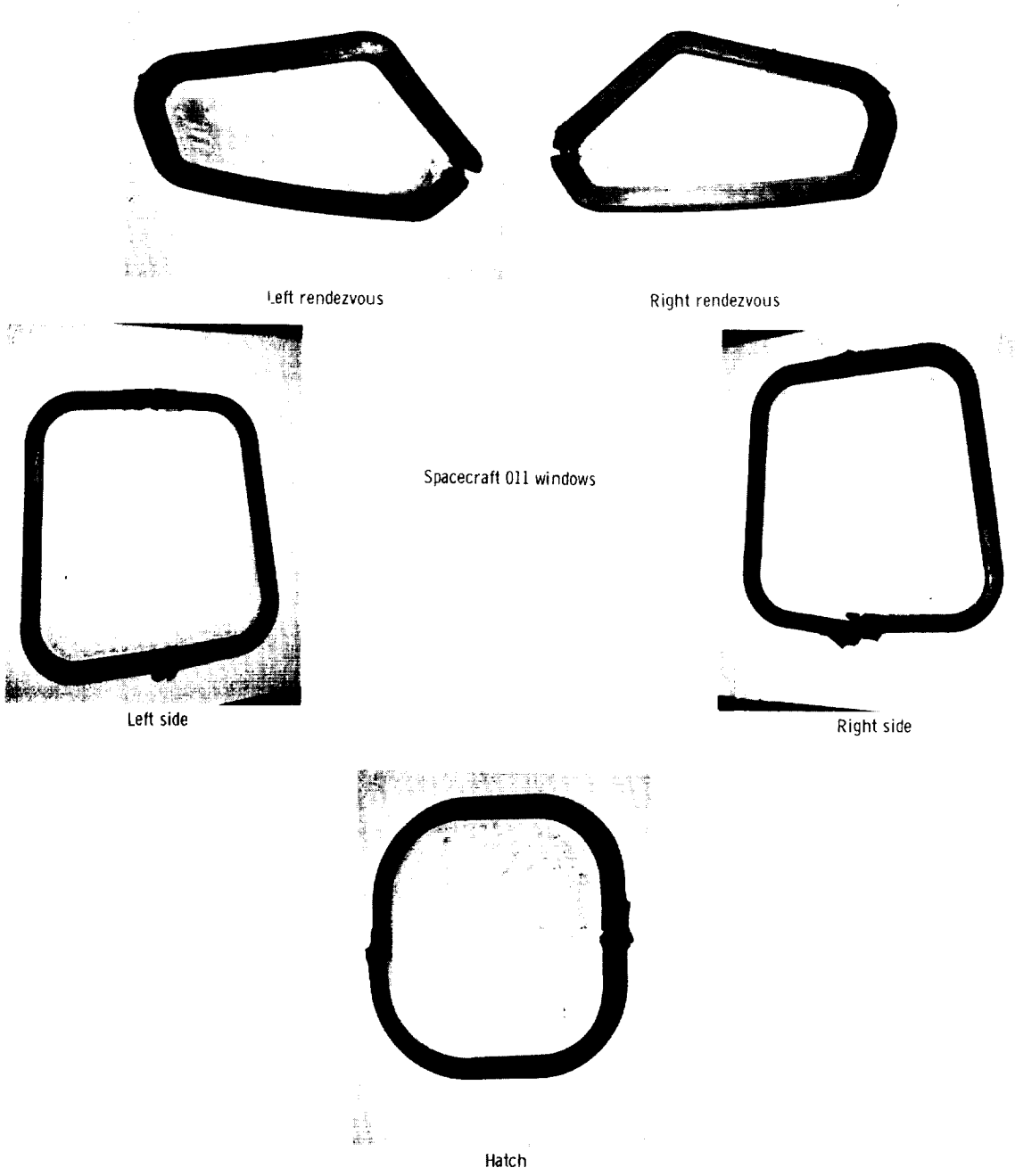

Figure 7.18.2-9. - Photographs of the five outer heat shield windows showing the contamination and crystallized salt formation, Mission AS-202.

NASA-S-66-10181

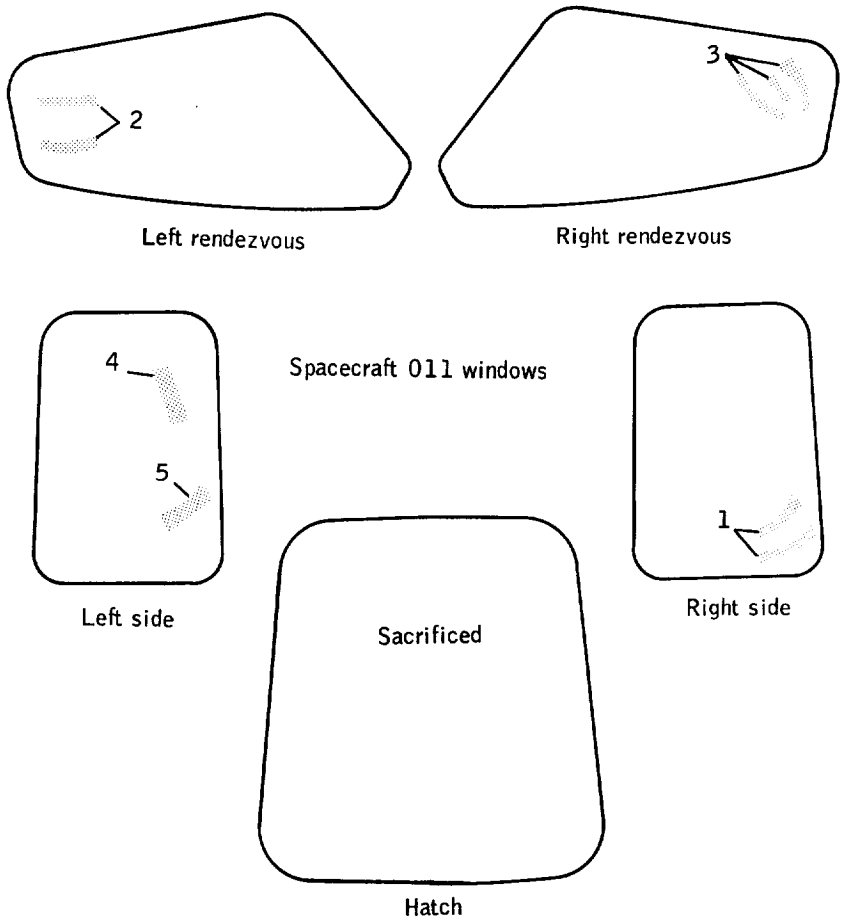

Note: Numbers denote where contamination smears were taken for emission test

Figure 7.18.2-10.- Window contamination smear locations, Mission AS-202.

NASA-S-66-10182

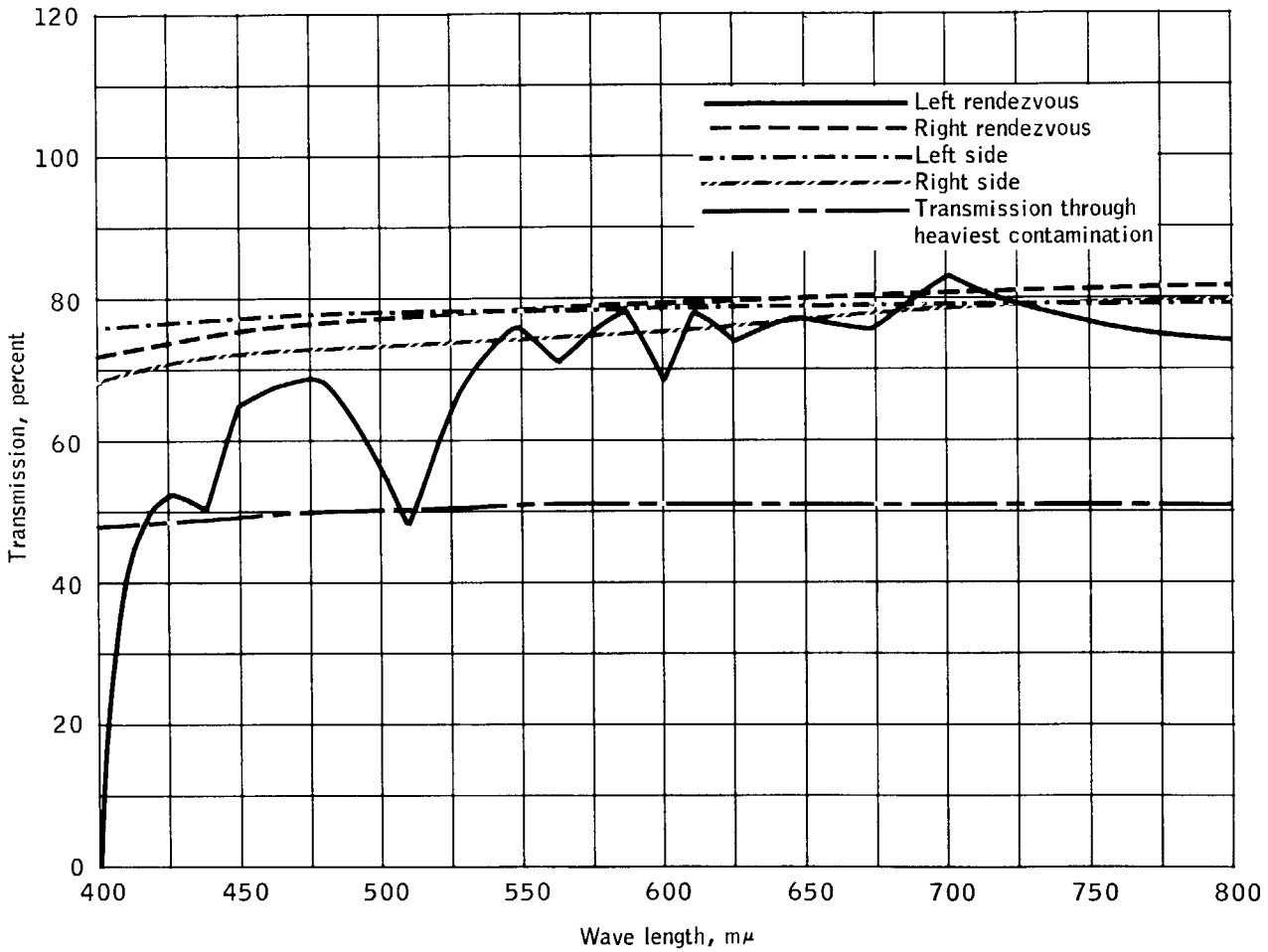

Figure 7.18.2-11.- Postflight SC-011 window transmission characteristics, Mission AS-202.

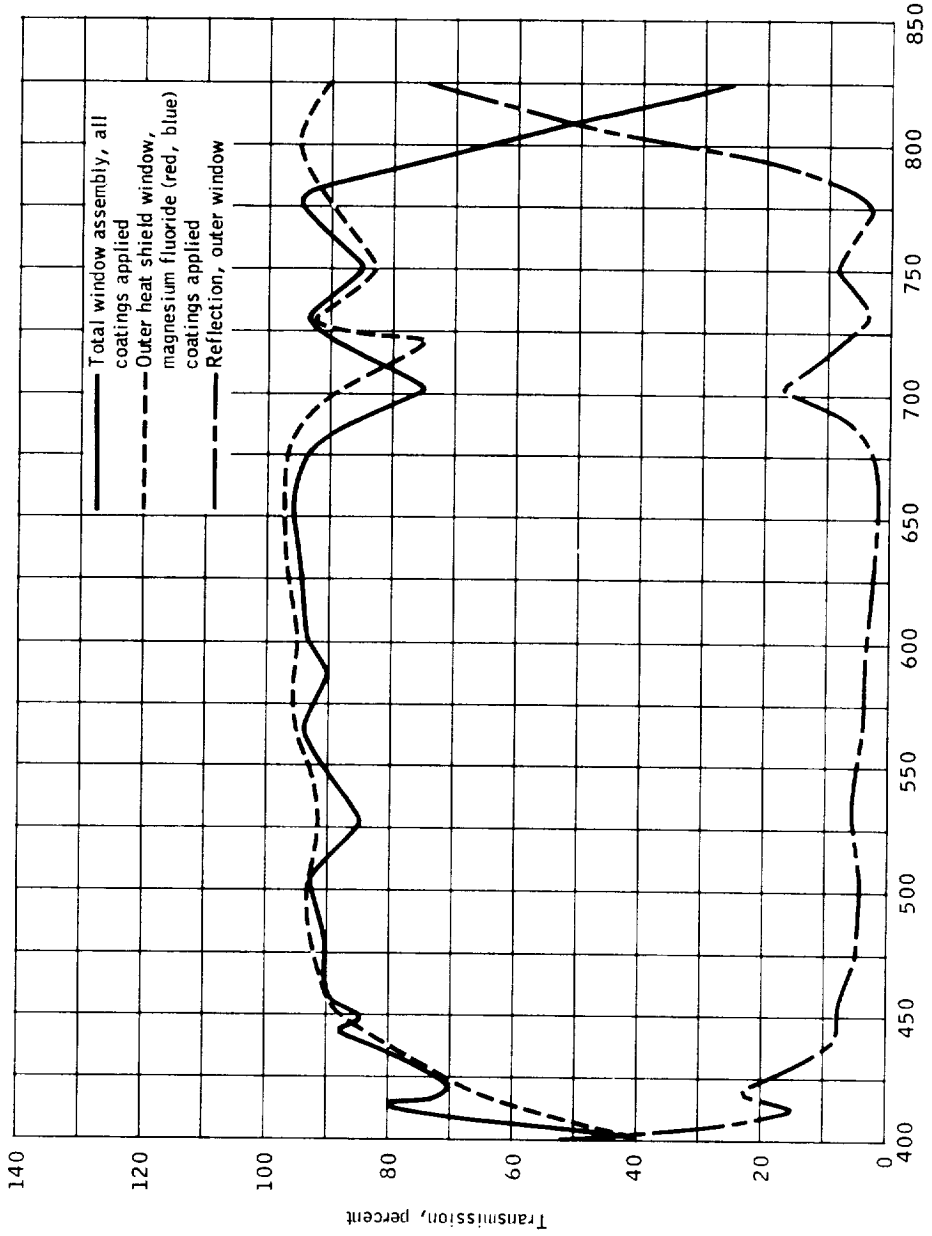

NASA-S-66-10183

Figure 7.18.2-12.- Preflight spectral transmission characteristics of a CM window assembly.

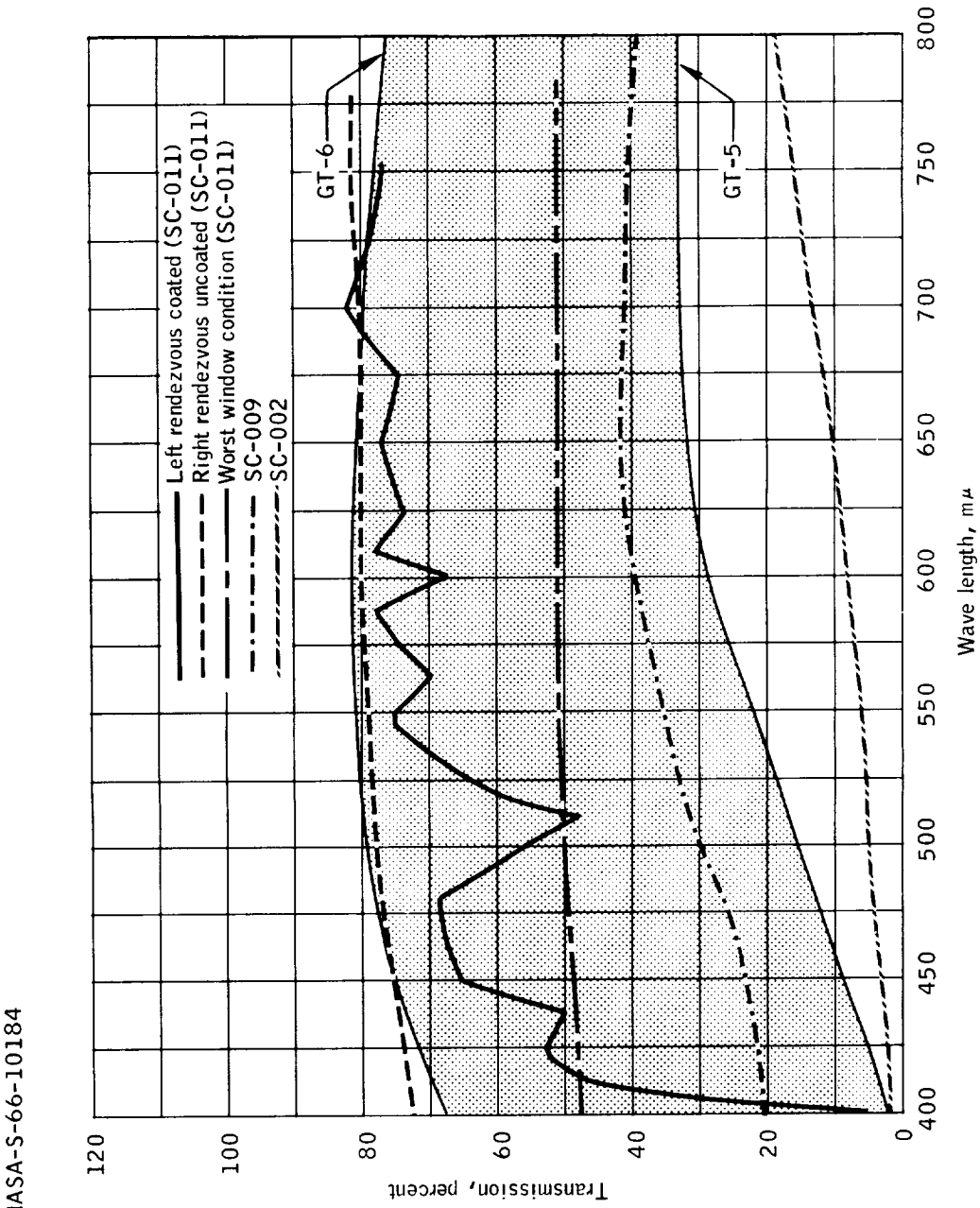

NASA-S-66-10184

Figure 7.18.2-13.- Postflight window spectral transmission characteristics of the three Apollo flights.

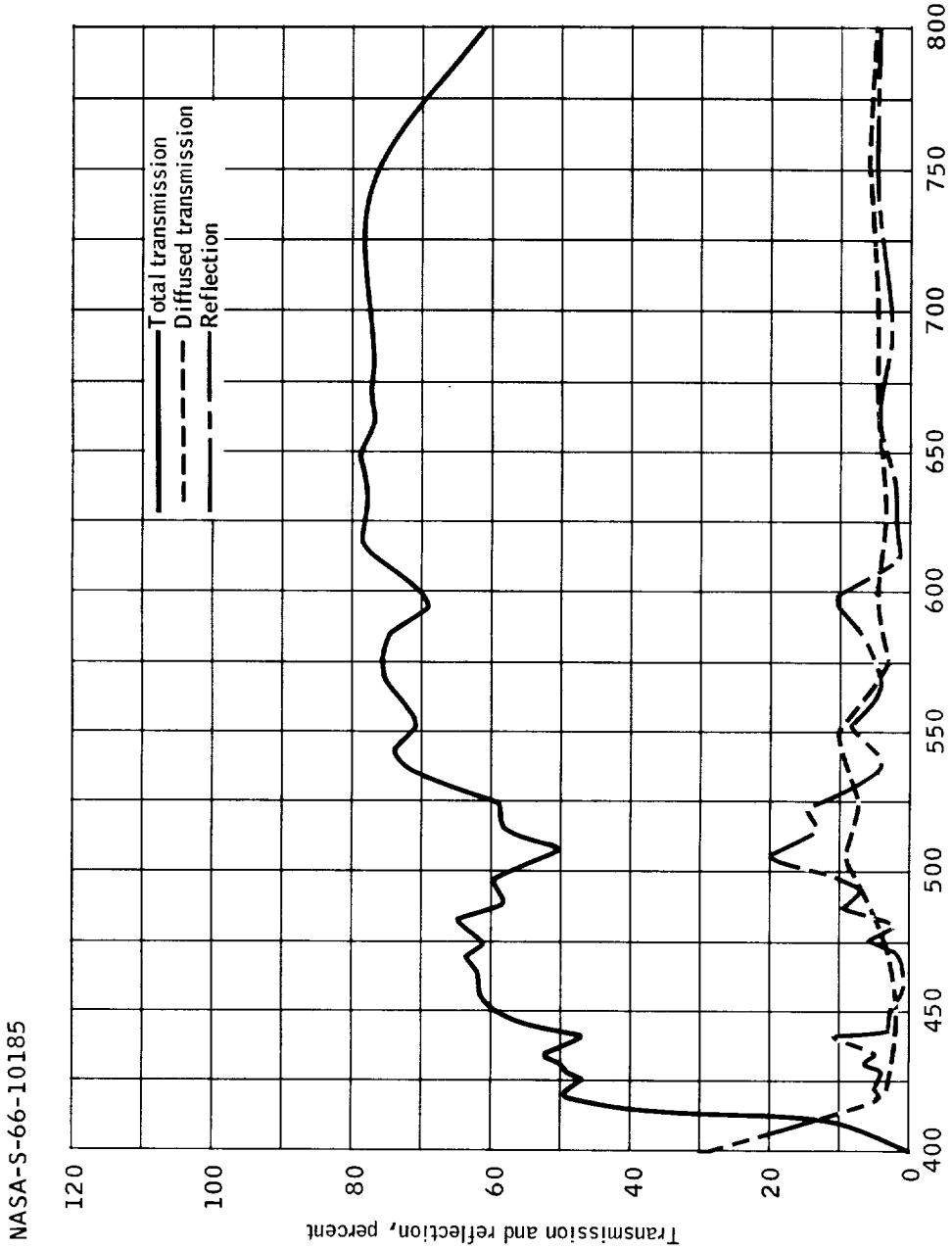

NASA-S-66-10185

Figure 7.18.2-14.- Spectographic characteristics of left rendezvous window, Mission AS-202.

7.18.3 Crew related acoustics.- Two microphones, measurements CK0032Y and CK0033Y, were installed in the command module on the crew couch platform at station X_C35.75, Y_C-6.5, Z_C0, to determine the acoustic environment for the crew during boost and reentry flight. Measurement CK0033Y, with a measurement capability for sound pressures between 100 dB and 140 dB (re: 0.0002 dyne/cm^2) was recorded on the flight tape recorder during the periods between T-10 and T+169 seconds, T+597 and T+835 seconds, and T+3952 and T+5220 seconds. The frequency response of the system was $\pm$1 dB from 20 cps to 5 kcps. Measurement CK0032Y, with a sound pressure range between 70 dB and 110 dB (re: 0.0002 dynes/cm^2), was recorded on the operational tape recorder from T+4000 seconds to splashdown.

Figure 7.18.3-1 gives the rms time history of measurement CK0033Y from T-10 to T+130 seconds. These data show the maximum sound pressure levels during the boost period to occur at lift-off, between T+80 and T+90 seconds, and during the CM pressure relief valve operation. A sound pressure of 112 dB was indicated in the CM at lift-off, due to the acoustic environment generated by the uprated S-IB booster engines. A one-third octave spectrogram is given in figure 7.18.3-2 with an illustrated external environment by adding the attenuation characteristics of the CM. As the vehicle accelerated, the sound pressure level in the crew compartment decreased and became insignificant between T+10 and T+30 seconds. A one-third octave spectrogram is shown in figure 7.18.3-3.

At T+30 seconds, the aerodynamic noise became predominant in the crew compartment and continued to increase until T+90 seconds (Mach 2.1). At approximately T+48 seconds, the CM pressure relief valve opened, causing a flow of air from the CM which increased the internal noise level 11 dB. The pressure relief valve stayed open for approximately 1 second. When the valve closed, the CM internal noise level was reduced to that generated by the aerodynamic noise field. Between T+48 and T+140 seconds, the CM pressure relief valve operated 19 times. Each time the valve opened the internal noise level was increased by 4 to 11 dB, depending on the background noise. Figure 7.18.3-4 shows the differences in sound pressure level when the relief valve was open and when it was closed at a period of minimum aerodynamic background noise. Figure 7.18.3-5 shows the difference in sound pressure level during the pressure relief operation when the aerodynamic background noise was maximum. The difference in sound pressure level between 300 and 2500 cps indicates the influence of relief valve venting on the CM acoustic environment created by aerodynamic noise.

Figure 7.18.3-6 shows a comparison of CM internal noise during a period of maximum sound pressure for SC-011 and SC-002. These data indicate the internal acoustic environment created by the aerodynamic noise with the pressure relief valve closed. A comparison is also given between the external acoustic environment measured on BP-13 and that calculated for SC-011 by adding CM noise attenuation characteristics to the internal noise measurements.

Measurement CK0032Y recorded the CM acoustic environment from T+4000 seconds to splashdown. The most significant increases in CM sound pressure level during this period were reaction control subsystem propellant depletion burn from T+5288 to T+5340 seconds and RCS helium purge from T+5539 to T+5590 seconds. During the RCS burn and helium purge, the CM sound pressure level increased to 98 and 105 dB, respectively (fig. 7.18.3-7).

Conclusion: The sound pressure levels experienced in the spacecraft 011 CM during the boost and reentry periods were lower than expected and will not jeopardize the crew or cause any physical pain. It should be noted, however, that during the boost and reentry periods certain events occur that change the CM noise levels significantly and could cause alarm or distraction for the crew. Some of the major events are pressure relief valve operation, RCS burns, and RCS helium purge.

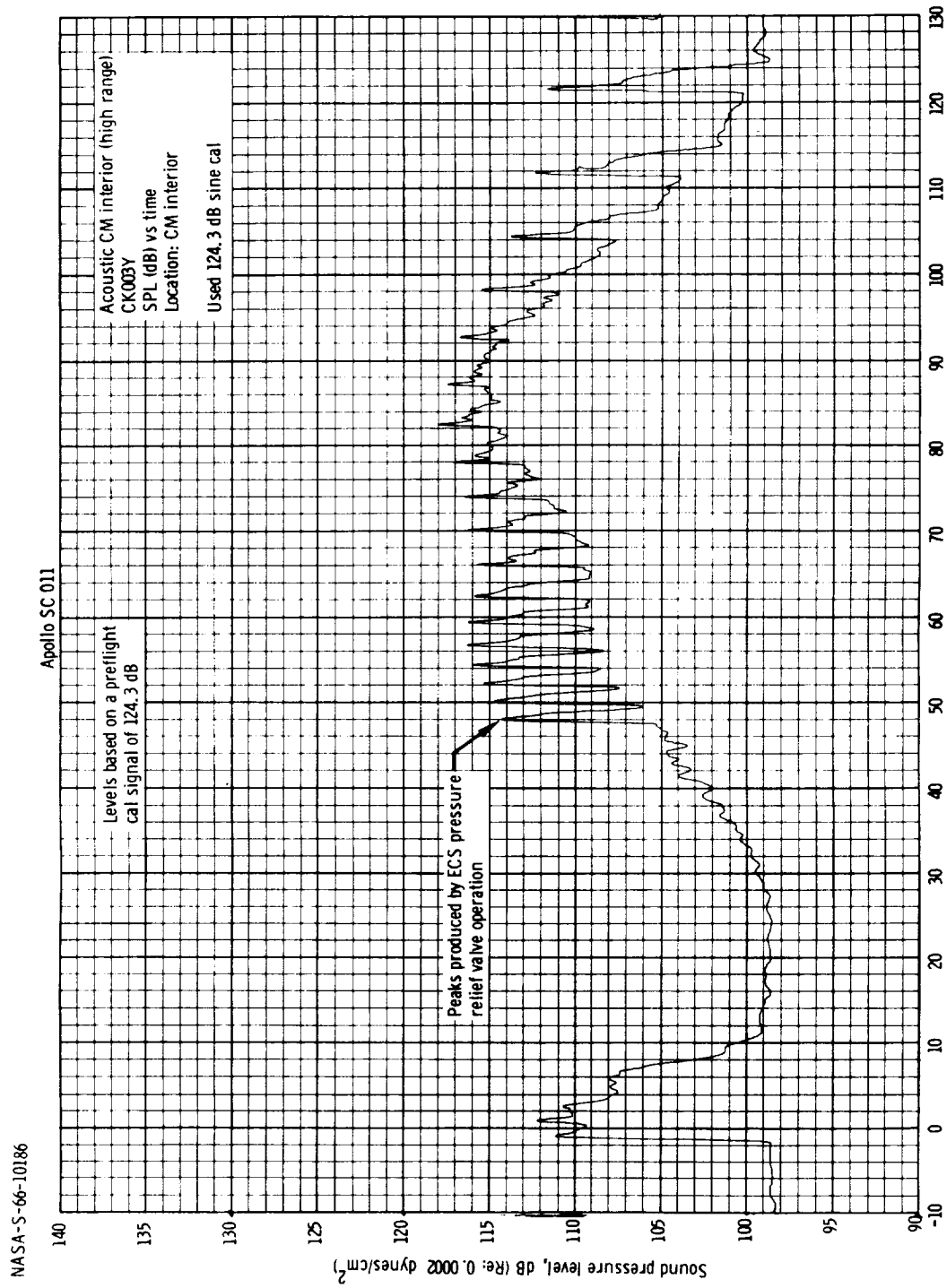

Figure 7.18.3-1.- Command module internal sound pressure level rms time history, measurement CK0033Y, Mission AS-202.

NASA-S-66-10187

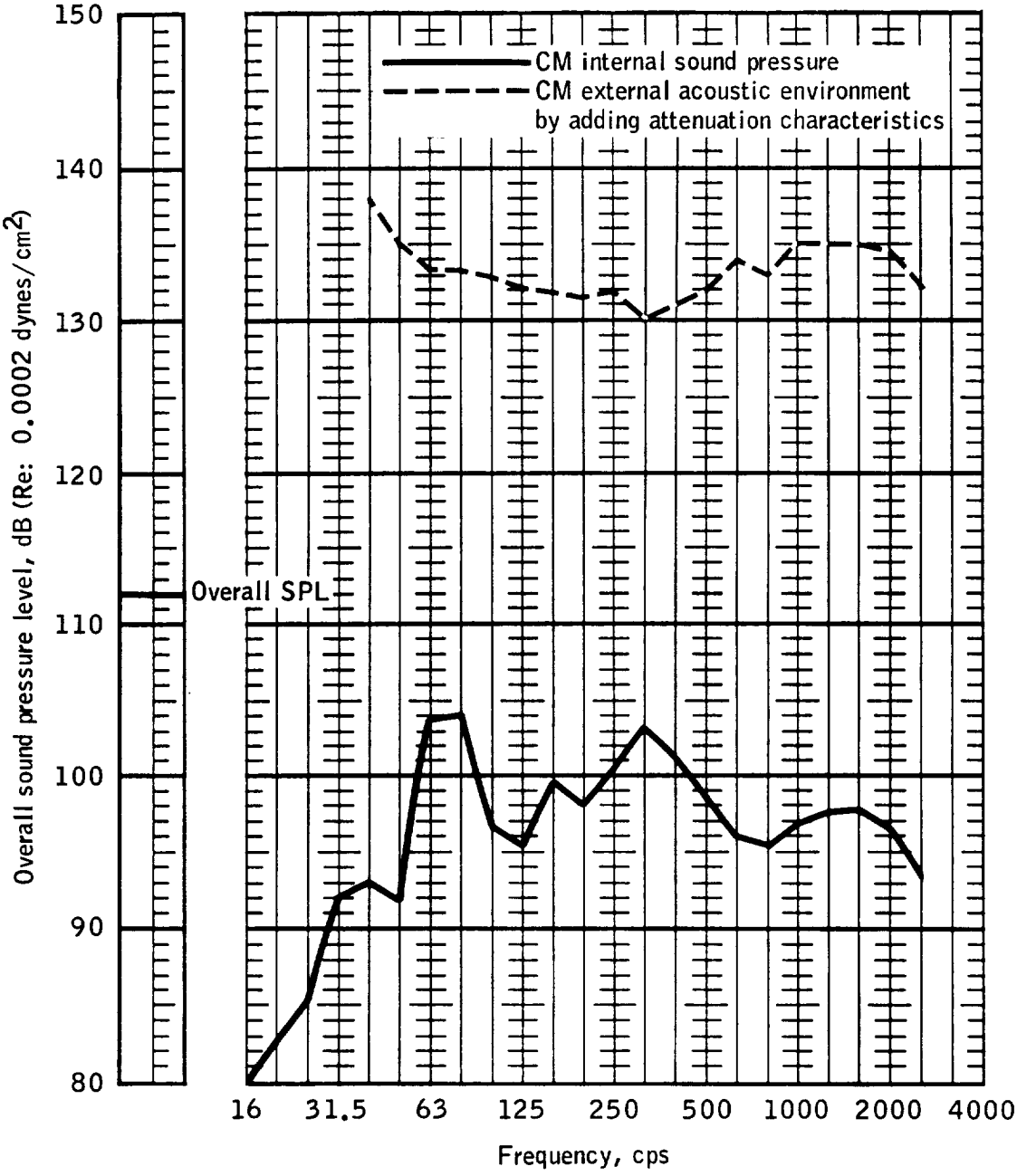

Figure 7.18.3-2.- One-third octave band spectrogram of CM internal sound pressure during lift-off, Mission AS-202.

NASA-S-66-10188

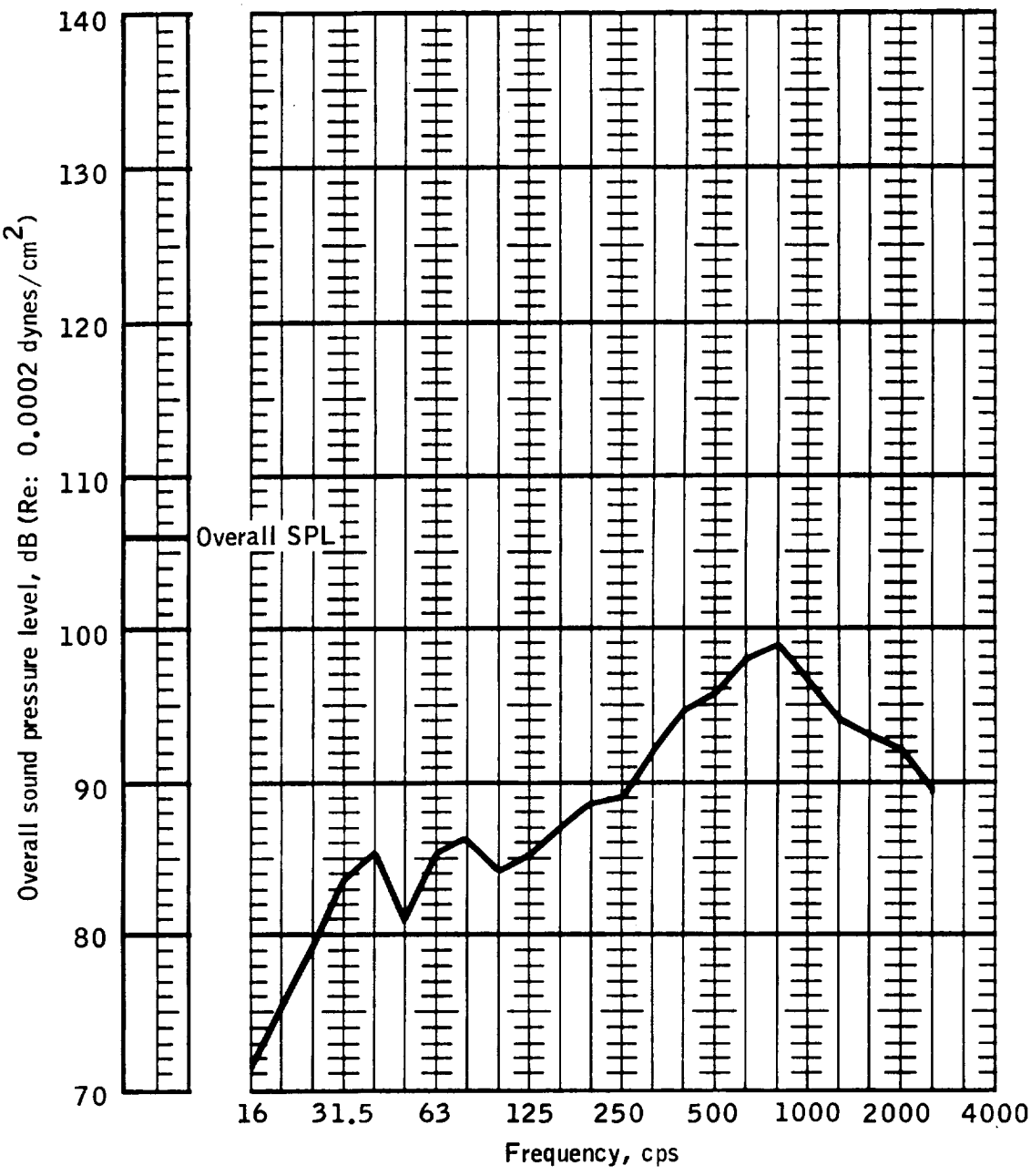

Figure 7.18.3-3.- One-third octave band spectrogram of CM internal sound pressure during a low noise period, Mission AS-202.

NASA-S-66-10189

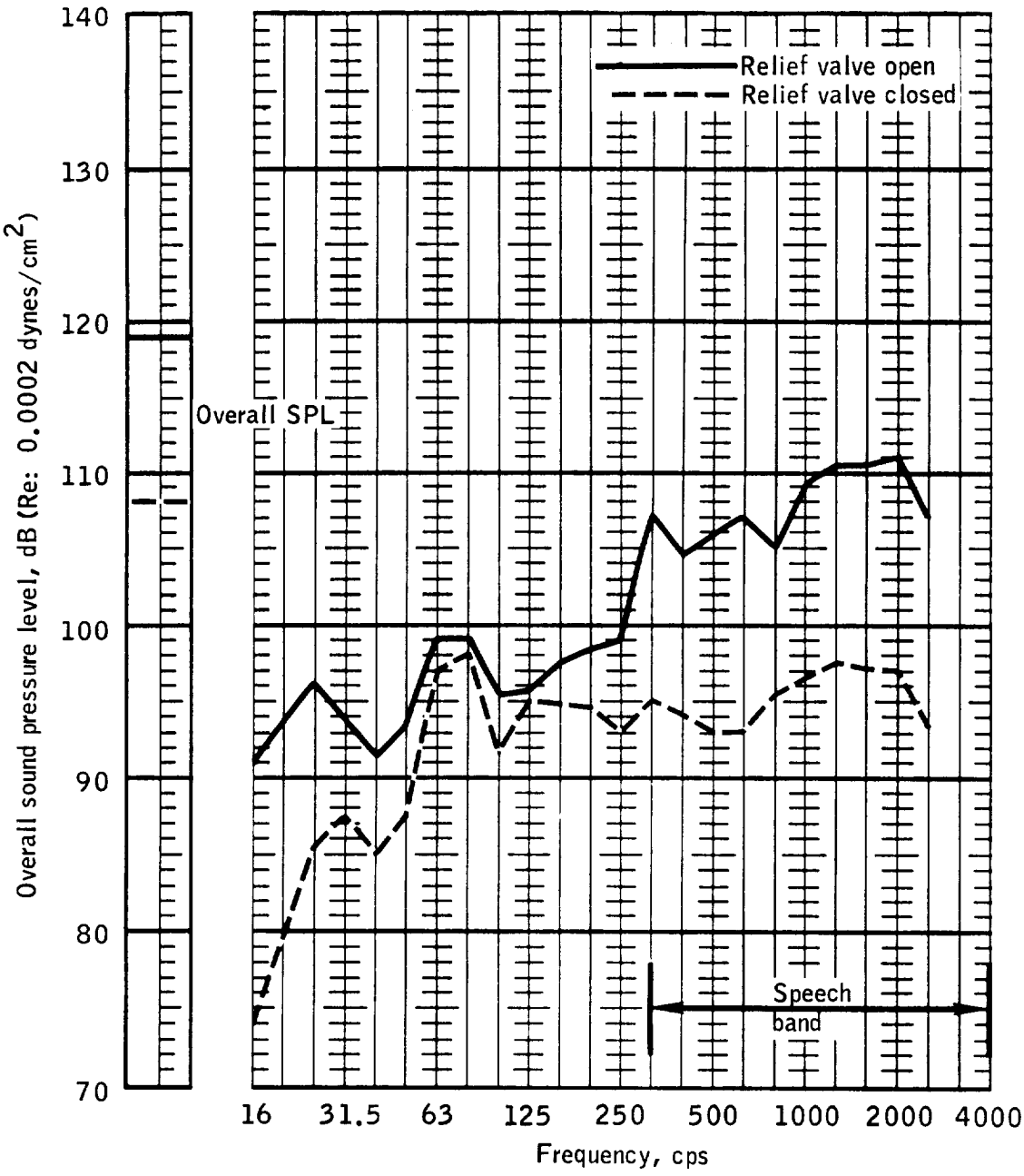

Figure 7.18.3-4.- Comparison of CM internal sound pressure level during CM pressure relief valve operation at minimum aerodynamic noise, measurement CK0033Y, Mission AS-202.

NASA-S-66-10190

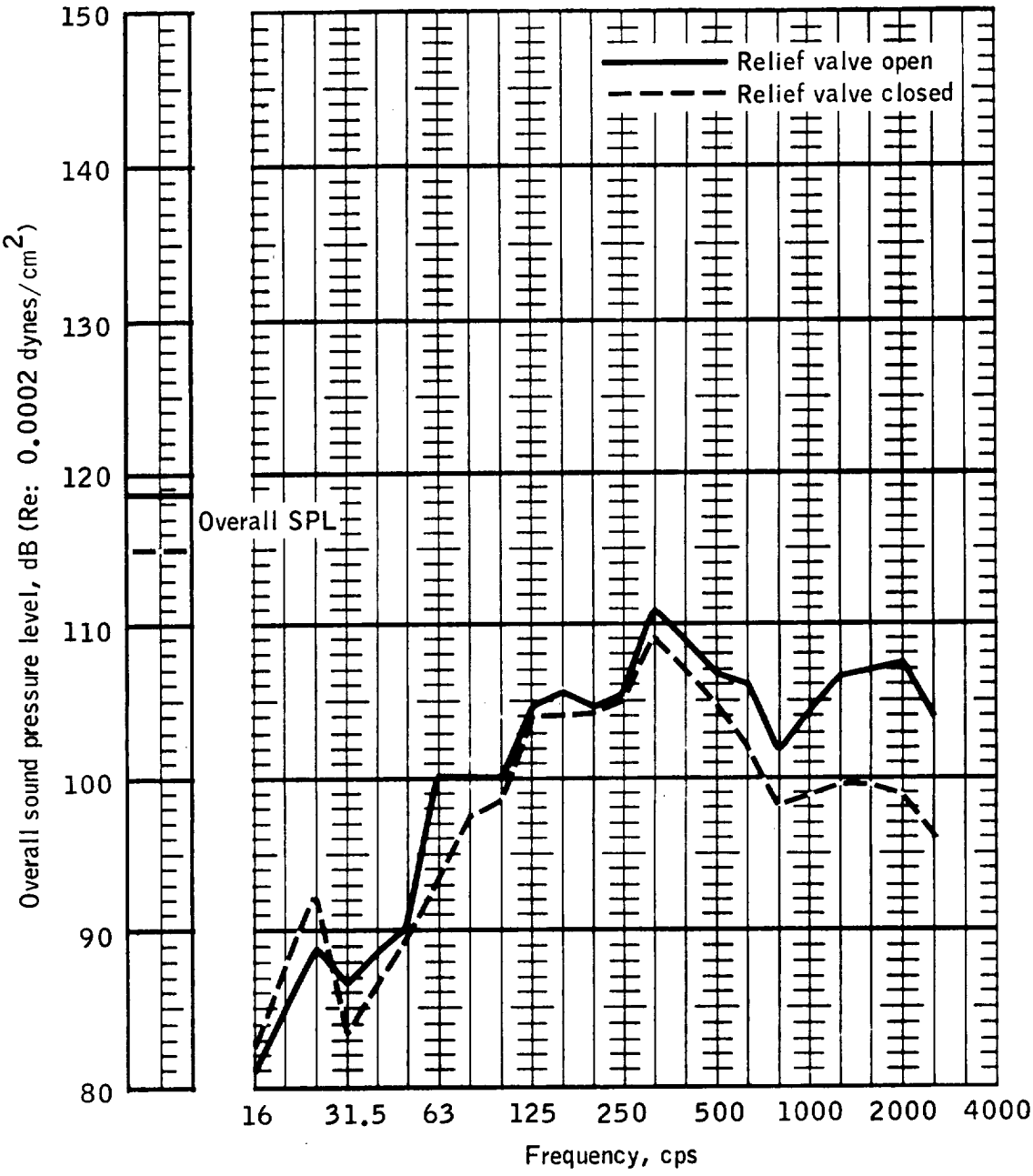

Figure 7.18.3-5.- Comparison of CM internal SPL during pressure relief valve operation at maximum aerodynamic noise, measurement CK0033Y, Mission AS-202.

NASA-S-66-10191

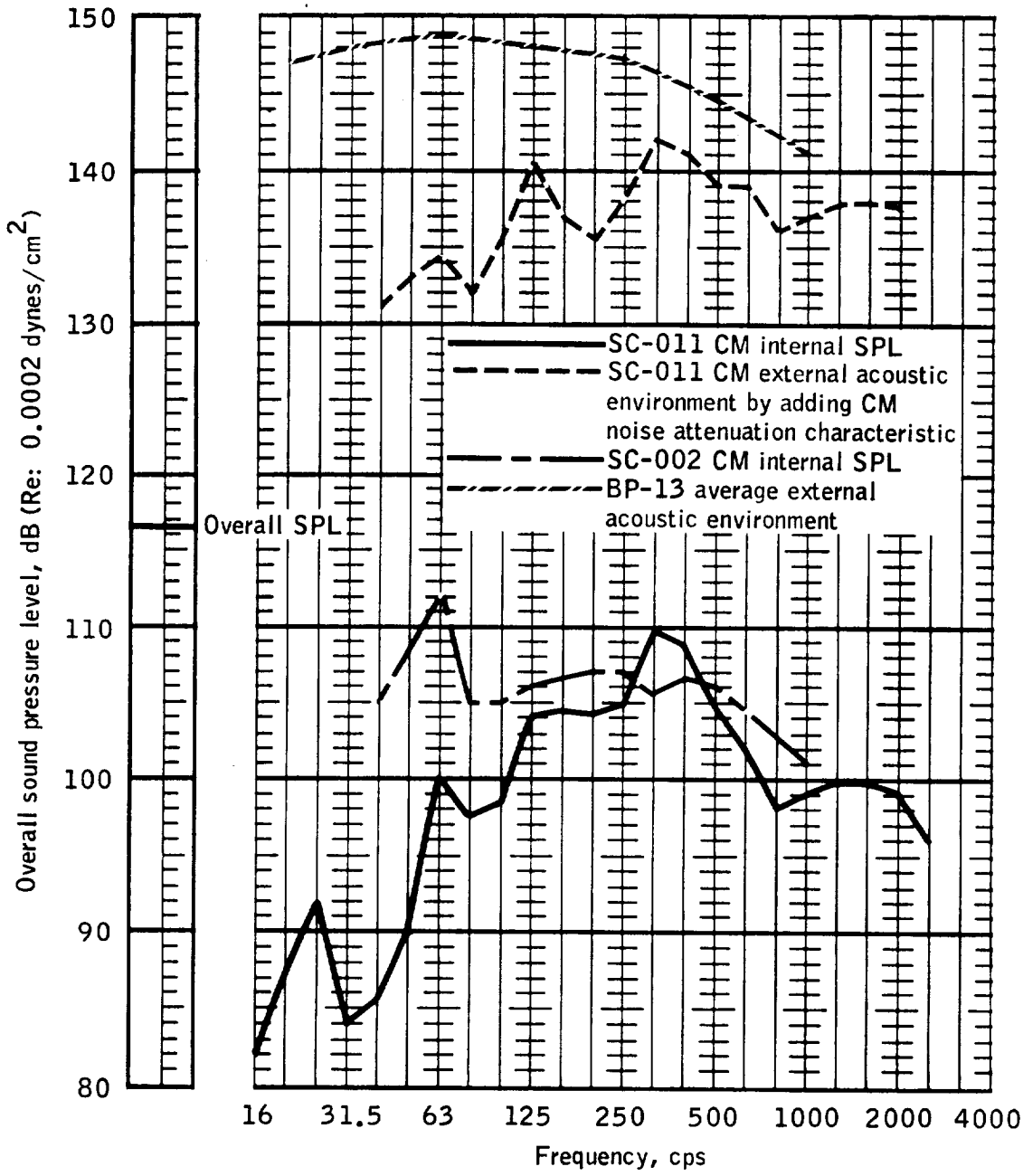

Figure 7.18.3-6.- Comparison of CM internal noise during a period of maximum sound pressure for SC-011, SC-002, and external noise measured on BP-13.

NASA-S-66-10192

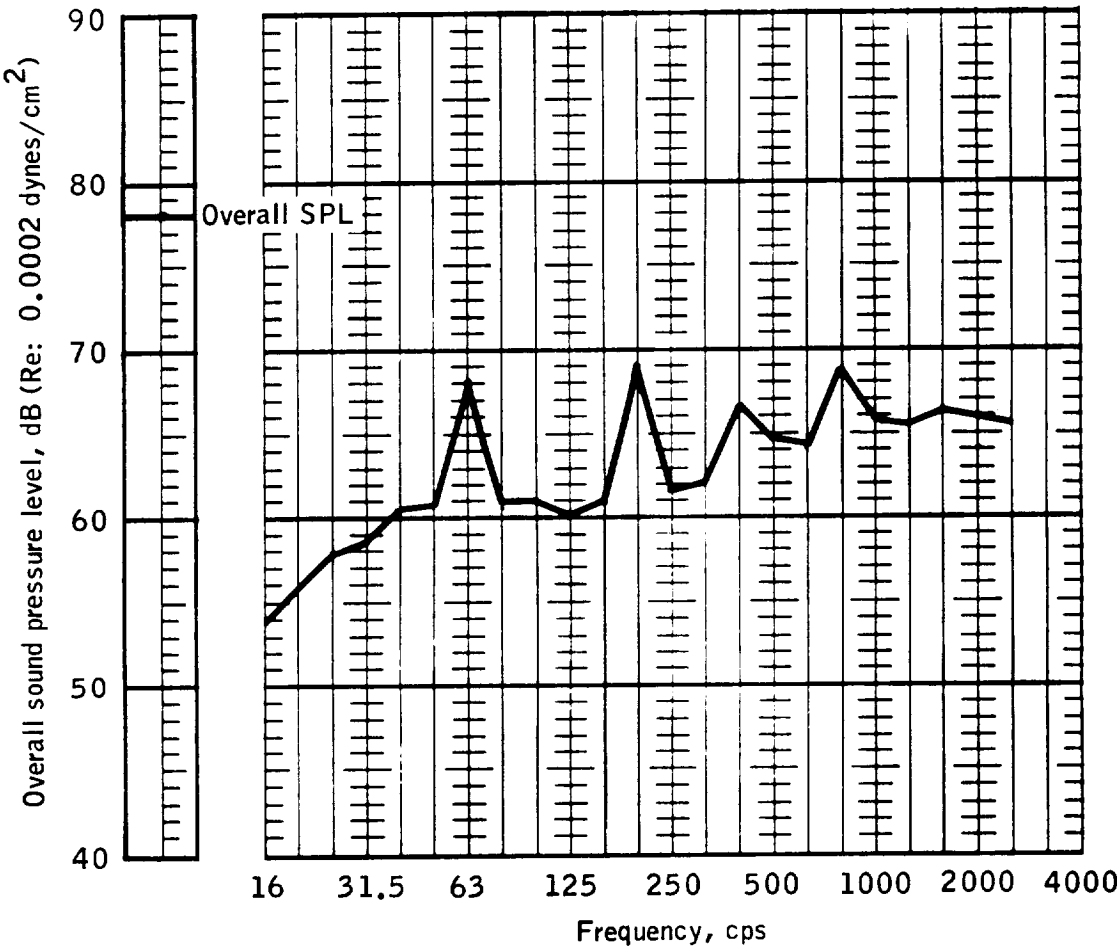

Figure 7.18.3-7.- CM internal sound pressure during midcourse (approximately T+4333), Mission AS-202.

7.18.4 Crew related dynamics.-

Summary: The vibration levels, measured on the crew compartment forward bulkhead, were assumed to represent the vibration environment to which crew members would be exposed during a manned mission. These levels exceeded the Gemini limits for the crew for approximately 3 seconds at lift-off. They were higher than anticipated between T+51 and T+101 seconds.

The vibrations during these periods would not have jeopardized the physical well-being of the crew. Crew members might, however, have experienced a noticeable degradation in visual acuity. They might not be able to monitor instrument panel meters and dials with the same speed and accuracy which they would monitor the same meters and dials if the vibration were not present.

Data: Acceleration measurements CK0004A, CK0005A, and CK0006A (section 7.1 and table 7.1-I) were used to determine the vibration environment.

The vibration levels exceeded the Gemini crew limits for approximately 3 seconds at lift-off, reaching maximum peak-to-peak levels of 1.2g in the X-axis and 1.1g in the Y-axis between T+1.12 and T+1.89 seconds.

The vibration levels between T+51 and T+101 seconds were approximately 30 percent higher on spacecraft 011 than on spacecraft 009. For example, between T+82 and T+85 seconds, the maximum peak-to-peak accelerations were 1.4g on spacecraft 009 and 2.05g on spacecraft 011 in the X-axis, and 1.6g on spacecraft 009 and 1.9g on spacecraft 011 in the Y-axis. Z-axis vibrations on spacecraft 011 were also slightly higher than on spacecraft 009, but again these were negligible. The vibration amplitudes at inboard and outboard engine cutoff appeared smaller on spacecraft 011 than on spacecraft 009.

Spectral analysis of the significant periods of vibration indicated that the majority of the energy was contributed by approximately 2-, 4-, 6-, 8-, and 10-cps longitudinal components and 2-, 3-, 4-, 6-, and 8-cps lateral components (figs. 7.1-3, 7.1-4, 7.1-5, and 7.1-6).

Transmissibility curves, based on the transmission of vibrations from the crew couch strut attach points to the crew couch during the crew support system vibration tests conducted at S and ID (NAA), indicated that longitudinal X-axis vibrations will be amplified less than 1.2 times for frequencies under 30 cps. Lateral Y-axis vibrations will

be attenuated between 2 and 6.5 cps, and amplified by a factor of less than 1.1 between 6.5 and 12 cps. Between 12 and 25 cps, however, the lateral vibration amplification factor rises to approximately 4. Above 25 cps the amplification depends on crew weight. With a 90-percentile crew (192.6 pounds per man) the maximum amplification was 4, and with a 10-percentile crew (138.3 pounds per man) the maximum was 11 (ref. 9). The downward shift in frequencies (spacecraft 009 had very dominant 23- to 26-cps lateral vibration not noted on spacecraft 011) was significant as it indicated that there would have been a minimum amplification of the spacecraft 011 vibrations measured on the forward bulkhead of the crew compartment.

Effect on crew: None of the vibrations observed were of sufficient magnitude or duration to jeopardize the physiological well-being of the crew or cause any physical pain. The vibrations might, however, have noticeably degraded the crew's ability to perform visual tasks. The ability to read a given dial or meter would not have been eliminated. To obtain information from a dial or meter, however, the crew might have to concentrate for a longer period of time than normally required (ref. 25). In addition, the ability to obtain rate information (based on the rate of movement of a needle) might be impaired (ref. 26). These conditions might cause an instrument scan pattern, established during training without vibration, to be interrupted and result in either incomplete or late monitoring of spacecraft systems. During the periods when the crew may be required to make decisions rapidly (lift-off and max. q), their ability to obtain visual data on which to base these decisions might have been degraded.

The inherent damping characteristics of the crew members and their clothing would be expected to reduce the effect of these low frequency vibrations. However, damping will require additional physical effort on the part of the crew members. Potential degradation of performance during these periods should be taken into account in mission preparations

8.0 LAUNCH VEHICLE PERFORMANCE SUMMARY

Vertical flight was maintained until T+10.3 seconds, at which time the launch vehicle began to roll from the the 100-degree east-of-north launch azimuth to the proper flight azimuth of 105-degree east-of-north and completed the maneuver at T+16.6 seconds. At T+10.7 seconds, the time programmed pitch attitude profile was initiated and continued until T+138.1 seconds. Shutdown of the S-IB stage occurred at T+143.5 seconds, 1.1 seconds earlier than nominal. At S-IB cutoff the actual trajectory parameters as compared with nominal were 68.2 ft/sec higher in space-fixed velocity, 1.4 nautical miles higher in altitude, and 0.4 nautical mile greater in range.

Separation of the S-IB stage occurred at T+144.2 seconds, followed by ignition of the S-IVB stage 1.4 seconds later. Active guidance was initiated successfully T+28.2 seconds after separation of the S-IB/S-IVB stages. All ullage rockets functioned as expected and were successfully jettisoned.

S-IVB stage cutoff occurred at T+588.5 seconds, 13.8 seconds earlier than predicted. At S-IVB stage cutoff the actual trajectory parameters as compared with nominal were 2.0 ft/sec greater in space-fixed velocity, 0.05 nautical mile lower in altitude, and 20.7 nautical miles shorter in range. Separation of the spacecraft occurred 10.2 seconds after S-IVB cutoff. At spacecraft separation the trajectory parameters were 5.2 ft/sec greater in space-fixed velocity, 0.05 nautical mile lower in altitude, and 20.8 nautical miles shorter in range.

The overall performance of the S-IB propulsion system was satisfactory. Average thrust and specific impulse were 1.01 percent and 0.44 percent higher, respectively, than predicted. Three of the four retrorockets performed nominally. The other burned out approximately 0.15 second earlier but this had no detrimental effect on separation. Outboard engine cutoff was initiated simultaneously by a fuel depletion sensor activation and LOX starvation.

The over-all performance of the S-IVB propulsion system was satisfactory. Average thrust and specific impulse were 1.97 percent and 0.02 percent higher, respectively, than predicted. The J-2 engine on AS-202 was flown at a mixture ratio of approximately 5.5:1 for the first 350 seconds of burn, at which time the mixture ratio was changed to approximately 4.7:1. Mixture ratio cutback occurred 24 seconds later than predicted. The late cutback contributed to the higher

The GN_2 temperature at the gas bearing heat exchanger exit was maintained within 1.5° F of the methanol/water inlet temperature from launch until spacecraft engine ignition. The GN_2 inlet temperature to the ST-124 gas bearing fell 2° F below the 50° F design minimum. This presented no problem and the design limit has subsequently been lowered to 32° F.

All electrical subsystems on the launch vehicle performed as expected and operated within appropriate limits. However, an intermittent electrical short circuit occurred in the Q-ball, which is an emergency detection subsystem sensor, beginning at 93.6 seconds. A hard short finally occurred at 114.9 seconds. The most likely point of occurrence of the short circuit is in the series transister regulator circuit, either in a capacitor or in the wiring. All other portions of the launch vehicle EDS are deemed to have performed properly. The three EDS busses were energized properly; auto abort enable and disable were commanded at the proper times; and the engine-out measurements indicated ignition, the events of staging, and the cutoff of both stages. The 60-second EDS cutoff enabling timer timed out properly. No angular overrates were sensed. No abort conditions were encountered, and therefore, the auto abort bus was not energized.

The angular rates sensed by the EDS sensors were all within the EDS limits. The maximum rates observed were in the Mach 1 region and were 3.3 deg/sec in pitch, 0.8 deg/sec in yaw, and 5.1 deg/sec in roll. These rates were successfully filtered to 1.5 deg/sec in pitch, 0.2 deg/sec in yaw, and 1.0 deg/sec in roll. The overrate settings for AS-202 were $\pm$5 deg/sec in pitch and yaw, and $\pm$20 deg/sec in roll.

Large torque forces were exerted on the S-IVB when the two SLA panels were displaced from the normal 45-degree deployment position by the plume impingement which resulted from the proximity firing of the SPS engine (see section 7.2). The APS controlled out the disturbances after a maximum attitude excursion of 60 degrees in pitch. Approximately 23 percent of the available APS propellants were used after separation to control out these disturbances.

Launch vehicle telemetered instrumentation performance was very good. Ten launch vehicle measurements were deleted during launch preparation. Of the 1242 active measurements at lift-off, 5 failed completely and 16 were partially successfully. Remaining measurements were successful.

average stage performance. The LH_2 recirculation valve on AS-202 failed to close as scheduled just prior to J-2 engine start. The failure of this valve to close had no effects on the AS-202 mission.

The performance of the guidance system was adequate and control system deviations were about as expected. A velocity error of -1.4 m/sec accumulated in the Z-axis accelerometer output between lift-off and 6 seconds of flight. This resulted from saturation of the servo error signals caused by initial vehicle vibration effects on the ST-124M platform accelerometers. During max. q, the attitude errors were 1.7 degrees nose-up in pitch, 0.6 degree nose-left in yaw, and 0.6 degree counterclockwise (CCW), looking forward, in roll. Maximum angles of attack during max. q were 0.9 degree nose-down in pitch and 0.9 degree nose-right in yaw. Maximum actuator position movements were 0.4 degree in pitch and 0.7 degree in yaw.

Disturbances during S-IB/S-IVB separation were quite small. Maximum S-IVB attitude errors during separation were negligible in pitch, approximately 0.3 degree nose-left in yaw and 0.5 degree clockwise, looking forward, in roll. · Maximum S-IVB actuator response was 0.8 degree in pitch, occurring at the initiation of active guidance.

The steady state roll torque experienced during the S-IVB powered flight was approximately 17 ft-lb CCW looking forward. This torque was in the same direction as on Mission AS-203 and in the opposite direction to that on Mission AS-201. The torque caused a 0.5 degree CCW roll (viewing from the rear), which was well within the 1-degree deadband in the auxiliary propulsion subsystem (APS). Only 4.6 percent of the total APS propellants were used for roll control through S-IVB powered flight.

There were no structural loads of sufficiently high magnitude to threaten the structural integrity of the launch vehicle. The maximum bending moment, 12.2 percent of design bending moment, was experienced at 39.5 seconds. Overall vibration levels were as expected, and acoustic levels were about as expected.

Analysis of telemetry data indicated that both the thermal conditioning subsystem and gas bearing supply subsystem in the Instrument Unit operated satisfactorily. The sublimator showed evidence of cooling after 55 seconds of flight, reaching a maximum cooling rate of 4.6 kilowatts at 125 seconds. It is believed that moisture entering the external vent holes condensed in the sublimator prior to launch. Future vehicles will have inboard vents and a controlled moisture-free environment which should eliminate this premature cooling effect.

Values in this section were subject to change after Oct. 12, 1966.

9.0 FLIGHT OPERATIONS

9.1 Flight Control

Flight control operations were carried out satisfactorily. Flight control personnel were trained by participating in simulations, pad support, and network testing.

During the countdown, the MCC-H and its interfaces, which included the MCC Network Flight Control Operations, were exercised at the proper times. The overall AS-202 mission operation and support plan is presented in figure 9.1-1.

Countdown.- Prior to the flight controller's coming to station at MCC-H, a decision was made at Cape Kennedy to delete all built-in holds. This was done to pick up the time that the count was behind and to allow an on-time launch. The approach of a hurricane to Antigua limited launch time to no later than 1800 G.m.t. This limit was placed by the supervisor of range operations to allow time to dismantle the Antigua antennas, thus preventing wind damage. The count proceeded on schedule until T-20 minutes when a hold was called for a failure in the remote site data processor (RSDP) on the RKV. A decision was made to proceed without a complete RSDP. The count progressed to lift-off with only a momentary hold at T-3 minutes.

Launch phase.- Lift-off occurred at 17:15:32 G.m.t. The booster operated well within the three-sigma envelope, and the trajectory was nominal. Staging occurred on time and all normal events were observed. The tower jettison and guidance initiate functions were on time, and a command to switch the active antenna to the -Z was sent after tower jettison. The second stage flight (S-IVB) was nominal except for a late mixture ratio shift and resultant early cutoff. The mixture ratio shift was 28 seconds late and the cutoff was approximately 13 seconds early. The spacecraft separation was on time, and all events occurred as programmed. The first service propulsion subsystem burn was completely nominal, and cutoff was within 1 second of expected duration. All SPS parameters were in the normal range except propellant gaging which indicated low all through the firing. The RKV reported evaporator outlet temperature as off-scale high. This was confirmed by the MCC-H and diagnosed as a frozen steam vent line (see setion 7.17).

Suborbital flight phase.- The suborbital flight phase of this mission was very close to nominal. The S-IVB initiated a bulkhead reversal test after CSM separation and destroyed itself as expected. The spacecraft continued to perform all functions as planned. All event

indications were noted and occurred within 1 second of the expected time. Telemetry reception was good at all sites with only momentary dropouts.

The G & N state vector from the spacecraft computer was not compared in real time with the state vector from Antigua.

State vector from the Apollo Guidance Computer (AGC) comes down every 2 seconds for 11.3 seconds after the SPS cutoff. The flight controller waited until he was confident that the SPS had been cut off before releasing the state vector into the Mission Control Center Real Time Computer Complex (RTCC). As a result he missed the computation cycle by 0.1 second. Postflight examination of the spacecraft state vector and the state vector from Antigua confirmed that a state vector update from Carnarvon was not required.

The computer program for spacecraft 012 and on is already provisioned to send down state vector continuously.

Entry phase.- The entry phase was as nominal as the rest of the flight. One failure did occur in that the CM/SM physical separation indication was not received by the CSQ. However, the separation was indicated by the loss of all SM telemetry indications. Attempts to command separation (section 7.16.1) were made from the CSQ, attempting to insure that it did occur. These attempts were unsuccessful for an unexplained reason. (See section 7.15 for additional analysis.) The remainder of entry sequence was nominal except for the spacecraft flying to a landing point some 205 nautical miles short of the predicted point.

NASA-S-66-10193

ACR	Auxiliary Computing Room
AFD	Assistant Flight Director
BSE	Booster Systems Engineer
CAPCOM	Capsule Communicator
CSTC	Cape SC Test Conductor
CSQ	Coastal Sentry Quebec (Ship)
CLTC	Cape LV Test Conductor
CRO	Canarvon, Australia
CVTS	Cape Vehicle Test Supervisor
EECOM	Electrical,Environmental, Communications Systems Engineer
ETR	Eastern Test Range
FIDO	Flight Dynamics Officer
GNC	Guidance, Navigation & Control Systems Engineer
HOSC	Huntsville Operations Support Center
KSC	Kennedy Space Center
LIEF	Launch Information Exchange Facility
M & O	Maintenance & Operations Supervisor
MSC	Manned Spacecraft Center
MSR	Mission Support Room
MSFC	Manned Space Flight Center
MSFN	Manned Space Flight Network
MSTC	MILA SC Test Conductor
OPS & PROC	Operations & Procedures Officer
PAO	Public Affairs Officer
RETRO	Retrofire Officer
RKV	Rose Knot Victor (Ship)
RSO	Range Safety Officer
SRO	Superintendent of Range Operations
SSR	Staff Support Room

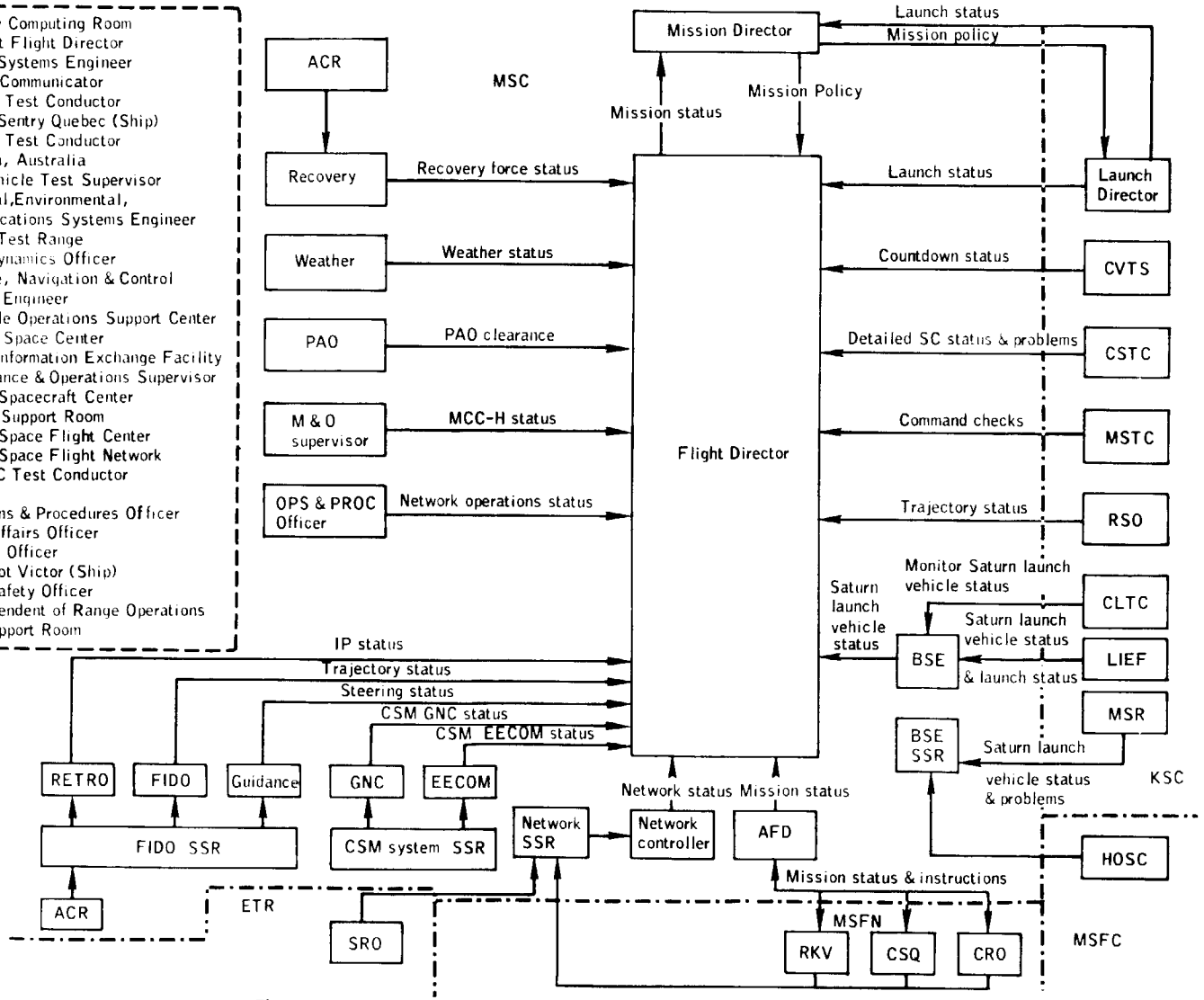

Figure 9.1-1. - Mission AS-202 operation and support plan.

9.2 Network Instrumentation

The Manned Space Flight Network (MSFN) for NCG720 was placed in mission status on August 8, 1966, at F-12 days. Two launch slippages occurred, one on August 10 and one on August 12, resulting in August 25 as launch day. The following major problems occurred on launch day.

Communications.-

(a) At the start of the T-05:30:00 Carnarvon high speed interface, the circuits were in a loop-back configuration to Goddard Space Flight Center (GSFC). These circuits were promptly restored to normal configuration.

(b) One wideband modem on the alternate 40.8 kilo bits/sec circuit to GSFC was not sending properly. Since this was a fourth alternate circuit, it was not restored for the mission.

(c) The ground operational support system (GOSS) 1 was outputting low levels prior to launch. It was restored on GOSS 2. Within 30 minutes, however, normal operation was restored on GOSS 1.

(d) During USNS WHEELING tracking coverage, voice communication was lost due to a rain shower in the WHEELING area. There was no restoration during USNS WHEELING coverage.

Radar.-

(a) Signal strength as received at the Air Force Eastern Test Range (AFETR) ground stations from the S-IVB/IU C-band beacon was much less than prelaunch predictions. Predicted strength was 15 dB above noise; actual measurement was less than 3 dB above noise. AFETR is currently investigating and will submit a report to MSC.

(b) The command and service modules C-band transponder was not seen at all times by all AFETR radars. Modified ground techniques are to be implemented for the CSM antenna patterns on the next missions.

(c) Pretoria tracking was not useable by the mission computer during the mission because the JJ header acceptance characters for low speed radar data had been deleted when received at MCC-K. These data were re-sent post pass with the JJ header.

(d) The USNS WHEELING did not acquire the spacecraft and so did not obtain useable radar tracking data.

Command.- The USNS COASTAL SENTRY QUEBEC received no message acceptance word when real-time command (RTC) 61, Separation Command, was sent. Further analysis of the spacecraft and ship systems is discussed in section 7.16.1.

Computers.-

(a) The real-time computer complex (RTCC) "A" computer on the AFETR was nonoperational for 30 minutes during the minus count. This was due to a parity error. No support was lost and the computer was operational 1 hour prior to launch.

(b) The USNS ROSE KNOT VICTOR (RKV) reported that the remote site data processor (RSDP) was nonoperational due to faulting with the erratta K received the previous day. Erratta K was a program change to allow proper inertial measurement unit (IMU) attitude display. This problem caused a hold of 40 minutes prior to launch. The faulting RSDP problem aboard the USNS RKV is still unresolved. The RKV was unable to further analyze this problem due to reconfiguring for Gemini 11. Operation during Gemini 11 did not reproduce the same problem.

Unified S-band.- The unified S-band subsystem was not used for operational support of the mission. See section 7.16.2 for an evaluation of the test results.

9.3 Recovery Operations

Recovery force deployment.- The planned landing areas designated for Mission AS-202 included the following:

(a) The launch site area, which provided coverage during the period between T-30 minutes, prior to launch, and approximately the first 100 seconds of powered flight.

(b) The launch abort area, which provided coverage for the period between approximately 100 and 520 seconds of powered flight.

(c) The discrete abort area, which provided coverage for the period between approximately 520 and 640 seconds of flight, including the first few seconds of service propulsion subsystem (SPS) burn.

(d) The terminal landing footprint, which provided coverage for landings occurring as the result of mission termination during a portion of the first SPS burn, failures of the guidance subsystem, and failures of the SPS to restart for the second, third, and fourth burns. The landing areas for a ballistic and guided entry were included in this footprint.

A landing occurring outside of a planned landing area was considered to be a contingency landing.

The level of recovery support provided within each of the above areas was dictated by the predicted probabilities of landing occurrence and was distributed such that any point within a given area could be reached within a specified access time.

A total of 6 ships, 18 fixed-wing aircraft, and 7 helicopters, in addition to various special vehicles, was utilized in support of the mission, both in planned and contingency areas. A summary and description of the landing areas and the recovery forces assigned are shown in table 9.3-I and figures 9.3-1 and 9.3-2.

Ships, aircraft, and associated personnel providing recovery support were assigned from operational Department of Defense (DOD) units. Special equipment, such as shipboard spacecraft retrieval cranes, airborne electronic receivers, and spacecraft flotation collars, was furnished to the DOD by NASA.

Location and retrieval.- All recovery force elements were on their assigned stations prior to lift-off with the exception of Wake Rescue 3

in the Pacific, which experienced mechanical difficulties. Additionally, the USS RA OWENS and KINDLEY Rescue 2 were repositioned prior to launch, due to the presence of a tropical storm in the vicinity of their originally assigned stations.

Unified S-band and VHF electronic signals were received by both Atlantic- and Pacific-based recovery aircraft prior to and during the entry sequence and after landing. Inflight visual sightings were also reported by various units located in the terminal landing footprint.

Electronic reception of signals from the VHF recovery aids (243.0 Mc), activated at main parachute deployment, was the first indication that landing had occurred approximately 200 nautical miles short of the nominal aiming point. Times associated with the common reception of these signals indicated that main parachute deployment took place at about 1843 G.m.t. and landing at 1849 G.m.t. Based on four of these electronic bearing reports, an estimated landing position at 15°40'N, 168°20'E was established. Subsequently, two HF/DF network fixes confirmed that spacecraft landing had occurred in this general vicinity. At 1924 G.m.t., a recovery aircraft, having homed on the spacecraft VHF recovery aids, reported visual contact and that its position was 16°07'N, 168°54'E. These coordinates, based on long range navigation (LORAN) fix, are considered to be the best estimate of actual spacecraft landing position. Pararescue personnel were deployed to the spacecraft, and a flotation collar was installed at 2207 G.m.t.

The USS HORNET, the primary recovery ship, arrived on the scene and hoisted the spacecraft aboard at 0317 G.m.t. The position of the HORNET at the time of retrieval was 16°39.0'E.

Preliminary inspection, data collection, and equipment removals were performed during the 3 days following recovery. Subsequently, the spacecraft was delivered to Long Beach, California, for reaction control subsystem deactivation and delivery of the recovered CM to the contractor.

The following is a sequential listing of significant events occurring during the AS-202 recovery. Reference should be made to figures 9.3-1 to 9.3-5 for correlation of reports.

Time, G.m.t.	Events
17:22:00	Kindley Rescue 2 - AOS VHF/TM; no AOS USB.
17:34:14	Ascension Rescue 1 - AOS VHF/TM; AOS USB at 17:35:56; LOS USB at 17:36:00; LOS VHF/TM at 17:44:56.
18:24:36	Guam Rescue 1 - AOS VHF/TM; no AOS USB.

Time, G.m.t.	Events
18:26:24	Guam Rescue 4 - AOS VHF/TM; AOS USB at 18:29:44; LOS USB at 18:30:10; visual at 18:28:00.
--	Visual contact established by USS STODDERT.
--	Guam Rescue 2 - no AOS USB; VHF/TM in blackout.
18:36:32	Guam Rescue 3 - AOS USB; LOS USB at 18:37:36; visual at about 18:36:20; VHF/TM in blackout.
--	Visual contact established by USS SPROSTON.
18:37:40	Wake Rescue 1 - AOS USB; LOS USB at 18:38:06; visual at about 18:37:10; VHF/TM in blackout.
18:39:14	Wake Rescue 2 - AOS VHF/TM (exit from blackout); LOS VHF/TM at 18:44:30.
18:43:15	Search 1 reported weak search, range, and homing beacon (SARAH) contact VHF (243.0 Mc); no bearing.
18:44:15	Search 2 reported SARAH contact VHF (243.0 Mc) at bearing 230 degrees.
18:44:30	Air Boss 1 reported auxiliary recovery antenna (ARA) 25 contact VHF (243.0 Mc) at bearing 240 degrees.
18:44:38	Wake Rescue 2 - AOS VHF (243.0 Mc) at bearing 316 degrees.
18:44:45	Search 1 reported SARAH at bearing 232 degrees.
18:47:15	Search 1 and 2 reported LOS.
18:48	Air Boss 1 bearing erratic.
18:48	Estimated position of spacecraft established as 15°40'N, 168°20'E.
18:49	Estimated time of splashdown.
--	Wake Rescue 2 - homing on electronic signal.
19:03	HF/DF fix received; 15°45'N, 169°54'E.

Time, G.m.t.	Events
19:15	Second HF/DF fix received; 15°55'N, 168°55'E.
19:21:50	Wake Rescue 1 (inbound) - AOS VHF (243.0 Mc) and homing.
19:24	Wake Rescue 2 - reported visual contact at position 16°07'N, 168°54'E. Spacecraft upright; dye marker visibility poor.
19:40	All HORNET aircraft except Relay 1 directed to return to HORNET.
20:02	First pararescue team exited Wake Rescue 2.
20:10	First pararescueman arrived at spacecraft.
20:13	Second and third pararescuemen exited Wake Rescue 2.
20:15	One pararescueman experienced difficulty. Second and third pararescuemen could not reach spacecraft.
20:35	Wake Rescue 1 directed to drop pararescue team.
20:40	HORNET launched two helicopters.
21:09	Wake Rescue 1 began pararescue team drops.
21:42	Wake Rescue 1 reported deploying flotation collar.
21:50	Search 1 arrived at spacecraft; picked up two pararescuemen separated from spacecraft.
21:55	Search 2 arrived at spacecraft.
22:07	Wake Rescue 1 reported flotation collar installed and inflated.
22:15	Search 1 and Search 2 conducted a search for other spacecraft components. Negative results.
03:17	Spacecraft hoisted aboard HORNET at position 16°04.5'N, 168°39.0'E.

Recovery aids performance.- Recovery aircraft attempting to track the spacecraft throughout the entry sequence utilizing VHF/TM and unified S-band reported that, while signals from the VHF transmitter were properly and adequately received, some difficulty with S-band was experienced. This attempt was for aircraft system evaluation only because there was no operational requirement for S-band communication on this mission.

Reports received from aircraft in the vicinity of landing indicated that both the VHF (243.0 Mc) survival radio and VHF (243.0 Mc) recovery beacon were functioning properly. Ranges of acquisition varied between 30 and 235 nautical miles.

Reception of spacecraft HF signals by recovery forces was not distinguishable from those of WWV-H (National Bureau of Standards high frequency standard time signal station, Maui, Hawaii); however, good HF/DF network fixes of the spacecraft location were obtained.

The spacecraft flashing light was functioning upon arrival of recovery forces at the scene of landing; however, range of acquisition was limited, possibly because of the daylight recovery of the spacecraft.

Sea dye marker visibility, before and after disturbance by recovery force personnel, was limited. Wake Rescue 2 reported visual acquisition at a range of 1 to 2 miles. Pararescue reports indicated a trail approximately 3 feet in width and 200 feet in length (see section 7.5).

Postrecovery inspection.- Postrecovery procedures were performed in accordance with the Apollo Recovery Operations Manual, its revisions, and special procedures received after the mission. The following is a summary of observations during recovery and postrecovery activities:

(a) Pararescue inspection prior to flotation collar installation indicated no visible damage to the aft heat shield. Only a discoloration of the paint and some blistering on the +Z-axis was indicated on the crew compartment heat shield.

(b) Significant paint and ablator burning was noted in the vicinity of both sets of RCS roll thrusters and the aft +Y yaw thruster. Burning effects from other thrusters were negligible.

(c) All tension tie bolts were melted but were not burned through. Very little water was draining from the spacecraft while being hoisted aboard the recovery ship as compared to the water draining from the tension tie holes in the spacecraft 009 aft heat shield.

(d) The -Z scimitar antenna was in excellent condition with moderate burning noted on the lower side. The +Z scimitar was almost totally destroyed.

(e) No sign of RCS leaking was noted either prior to or after retrieval.

(f) The dye marker lanyard was cut during retrieval operations, and the dye canister packaged immediately upon retrieval. The lanyard had been chafed at the upper deck edge of the crew compartment heat shield during recovery operations while being used as a tether and swimmer assist.

(g) Neither the drogue nor main parachutes were seen or recovered. A portion of layered, fibrous material was retrieved; however, this was possibly a portion of the forward heat shield.

(h) All parachute disconnects and mortars and forward heat shield jettison thrusters appeared to have functioned normally. No evidence of forward heat shield recontact was noted.

(i) The outer lip of each drogue mortar can was bent.

(j) Condensation was heavy on the inner surface of the right-side outer window, while the remaining four outer windows showed only light and localized condensation.

(k) The HF antenna was in good condition until the spacecraft was hoisted aboard ship, at which time it became fouled in the hoisting gear and was twisted. Subsequently, it was cut about 3 feet above the antenna canister.

(l) Both VHF antennas erected properly, as did the flashing light. The spacecraft uprighting system had not been activated.

(m) The spacecraft hatch assembly appeared normal; no deformations or abnormalities were observed. Outer hatch removal began at about 1700 G.m.t., followed by gas sample extractions prior to removal of the inner hatch. A positive pressure of less than 1 psig was noted within the spacecraft. Maximum hatch torque readings were recorded as follows:

Outer hatch removal - 275 in-lb

Inner hatch removal - 200 in-lb

Inner hatch installation - 175 in-lb

Inner hatch removal - 250 in-lb

Inner hatch reinstallation - 225 in-lb

Outer hatch installation - 500 in-lb

Outer hatch removal - 250 in-lb

Outer hatch reinstallation - 425 in-lb

(n) Switch positions were photographed and recorded, and powering-down procedures were carried out at 2130 G.m.t. These procedures, however, did not deactivate the VHF recovery beacon, which was powered-down some 20 hours later when its continued operation was noted by the ship's receivers.

(o) The data storage and flight qualification tape recorders were removed and packaged. These recorders, in addition to the four onboard cameras, gas sample, switch position data, and other information, were flown from the recovery ship to MSC. The time of departure was 2300 G.m.t. or approximately 20 hours after spacecraft retrieval.

(p) Impact attenuation strut positions were measured and recorded. Measurements indicated no stroking had occurred.

(q) A small amount of water (an estimated quantity of 2 ounces) was found in the spacecraft.

(r) The gas chromatograph was removed, safed, packaged for shipment, and returned to MSC (see section 7.17).

(s) Condition of the ECS components appeared to be undisturbed.

The spacecraft was returned aboard ship to Long Beach, California, for RCS deactivation. It arrived on September 2, 1966. Following receipt of the spacecraft, the landing safing team made the unexpended pyrotechnics safe (CM RCS oxidizer depletion dump pyrotechnics) by replacing the initiator plugs with shorting plugs, and verified that the spacecraft was now in a safe condition for RCS deactivation.

RCS deactivation procedures were performed in accordance with the Apollo RCS Deactivation Procedures Handbook for NASA Landing

Safing Team (SID 66-327). The anomalies noted during deactivation of the RCS are listed below:

(a) In performing propellant bladder leak checks, high leakage rates were indicated in the "A" and "B" oxidizer systems due to incomplete crimping of the tube on the outlet side.

(b) During the initial purge of the helium system, the burst diaphragms in the oxidizer A and fuel B system relief valves were found to be ruptured.

Deactivation was successfully completed the evening of September 6, 1966. The spacecraft was then moved to the contractor's Downey facility the morning of September 7, 1966, for postflight testing and analysis.

TABLE 9.3-I.- AS-202 RECOVERY SUPPORT[a]

Landing area	Access time, hr		Support	Remarks
	Ship	Aircraft		
Launch site	--	0.25	2 CH-3C helicopters 4 LARC's 2 LVTR's 1 range boat 1 LCU 1 bulldozer 1 crane 1 truck	
Launch abort	30	4	2 destroyers 1 HC-97 1 HC-130H	USS JC OWNES and USS RA OWENS Kindley Rescue 1 Kindley Rescue 2
Discrete abort	Not defined		1 oiler 1 HC-130H	USS SALAMONIE Ascension Rescue
Terminal landing footprint	18 to 36	4	2 destroyers 6 HC-130H 1 aircraft carrier 1 destroyer	USS STODDERT and USS SPROSTON Guam Rescue 1, 2, 3, and 4 and Wake Rescue 1 and 2 USS HORNET USS O'BANNON
Guided entry area	2	1	5 SH-3A helicopters 4 E-1B	Search 1 and 2, Swim 1 and 2, and Photo 1 Air Boss 1 and 2 and Relay 1 and 2
Contingency	--	18	5 HC-130H	Ascension Rescue 2, Mauritius Rescue 1 and 2, and Perth Rescue 1 and 2

[a]The recovery support included a total of 6 ships, 18 fixed-wing aircraft, and 7 helicopters.

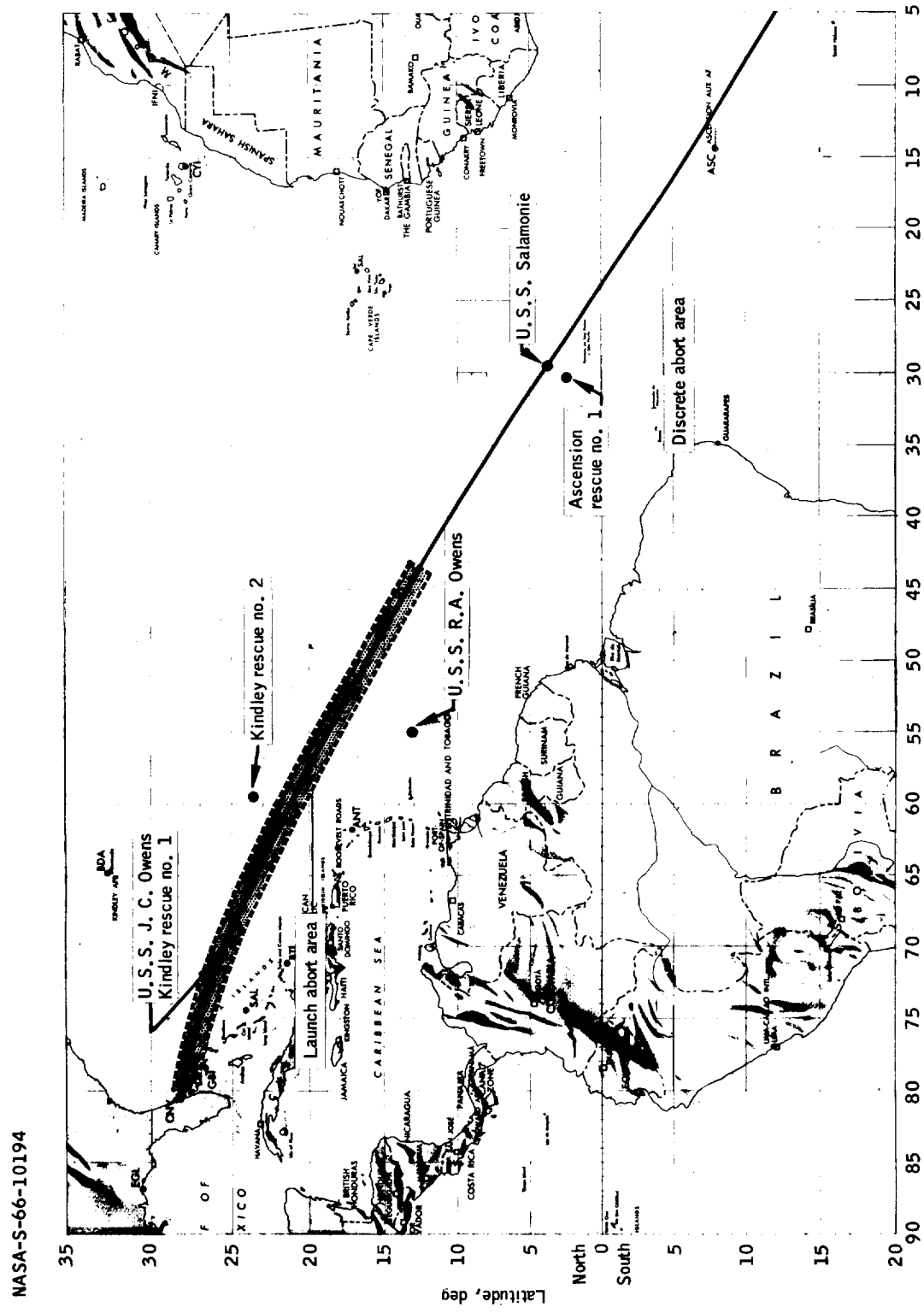

Figure 9.3-1.- Mission AS-202 abort areas and recovery force deployment.

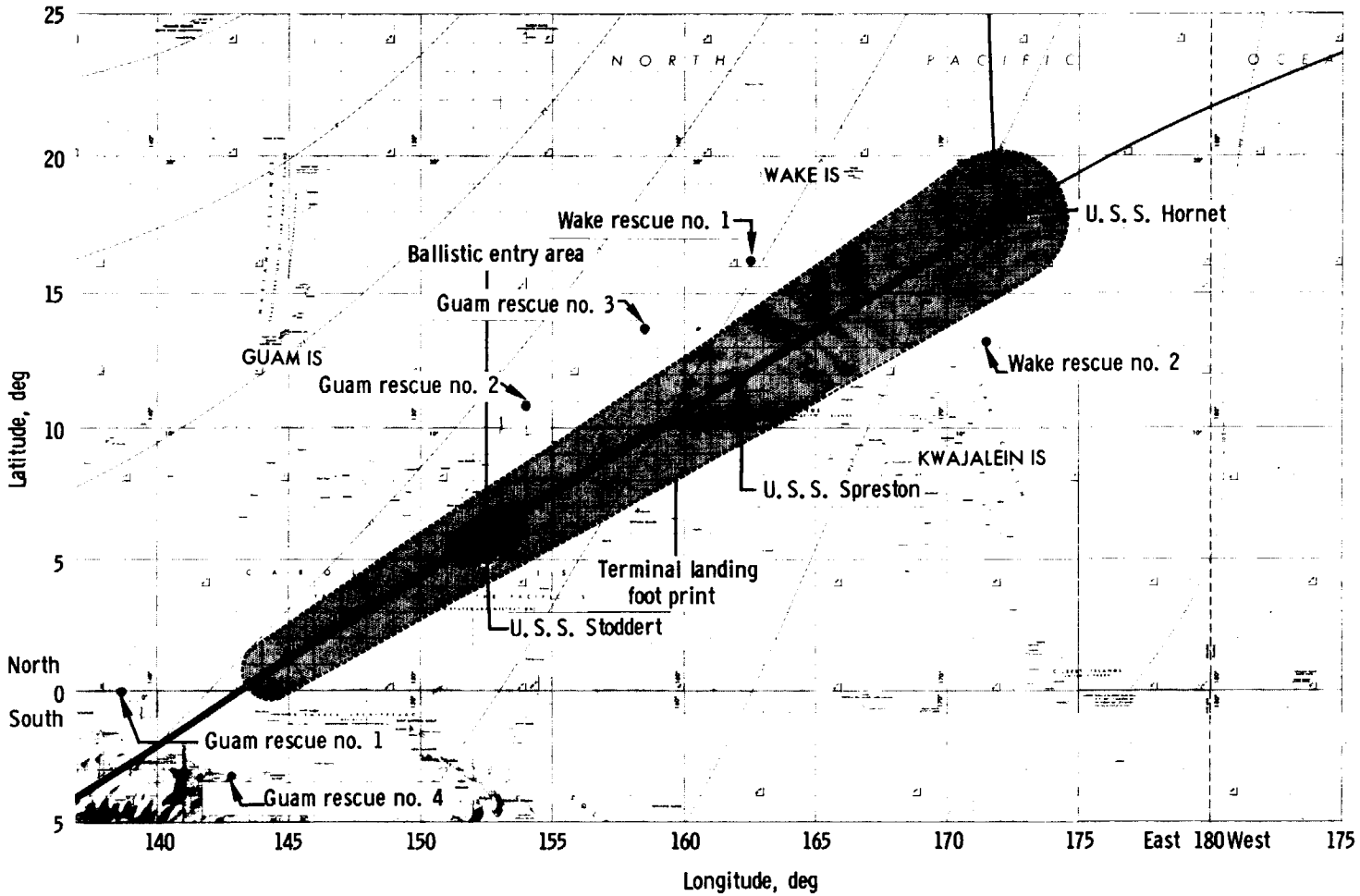

Figure 9.3-2. - Mission AS-202 terminal landing footprint and recovery force deployment.

NASA-S-66-10196

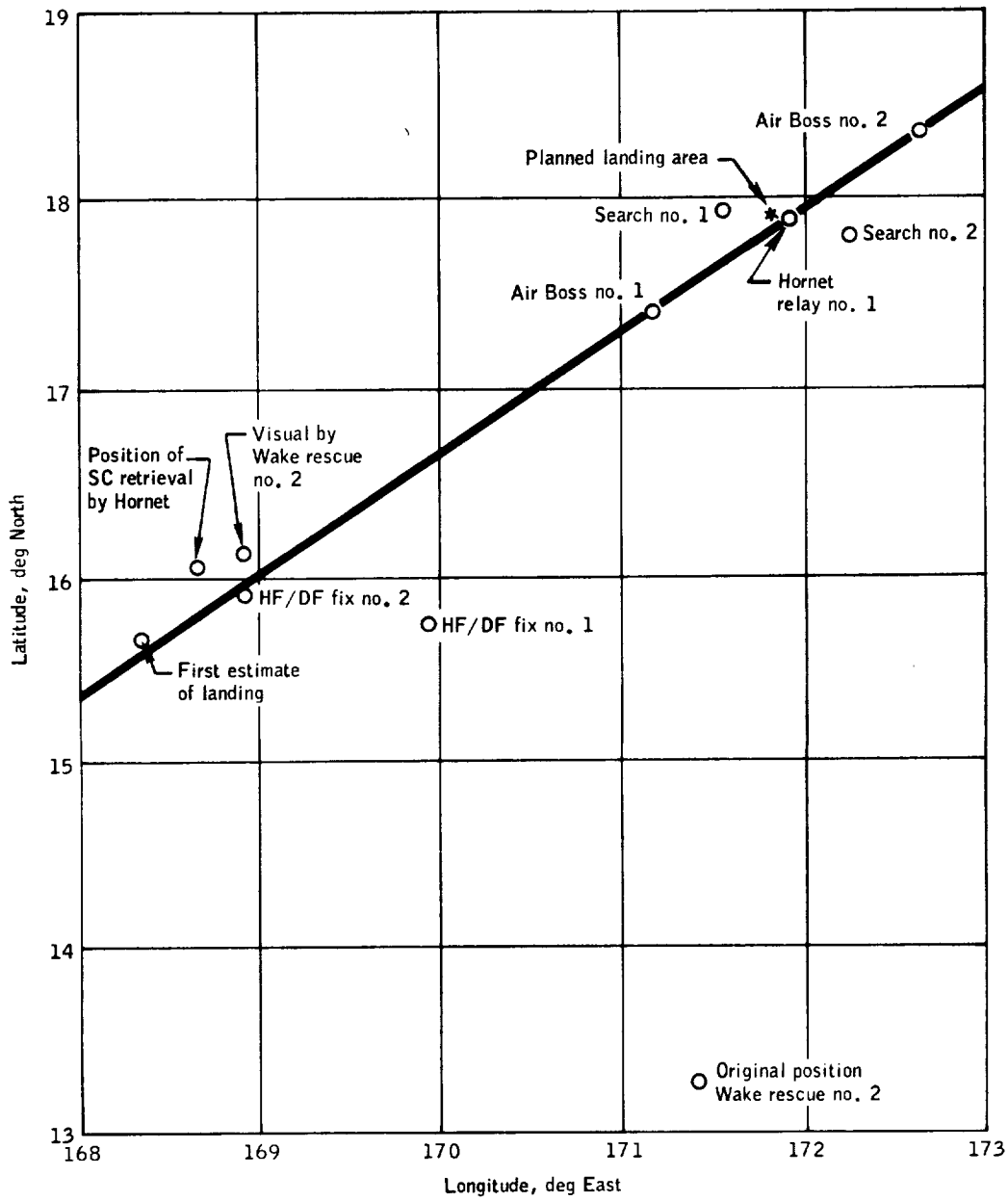

Figure 9.3-3.- Mission AS-202 landing area data and forces.

NASA-S-66-10197

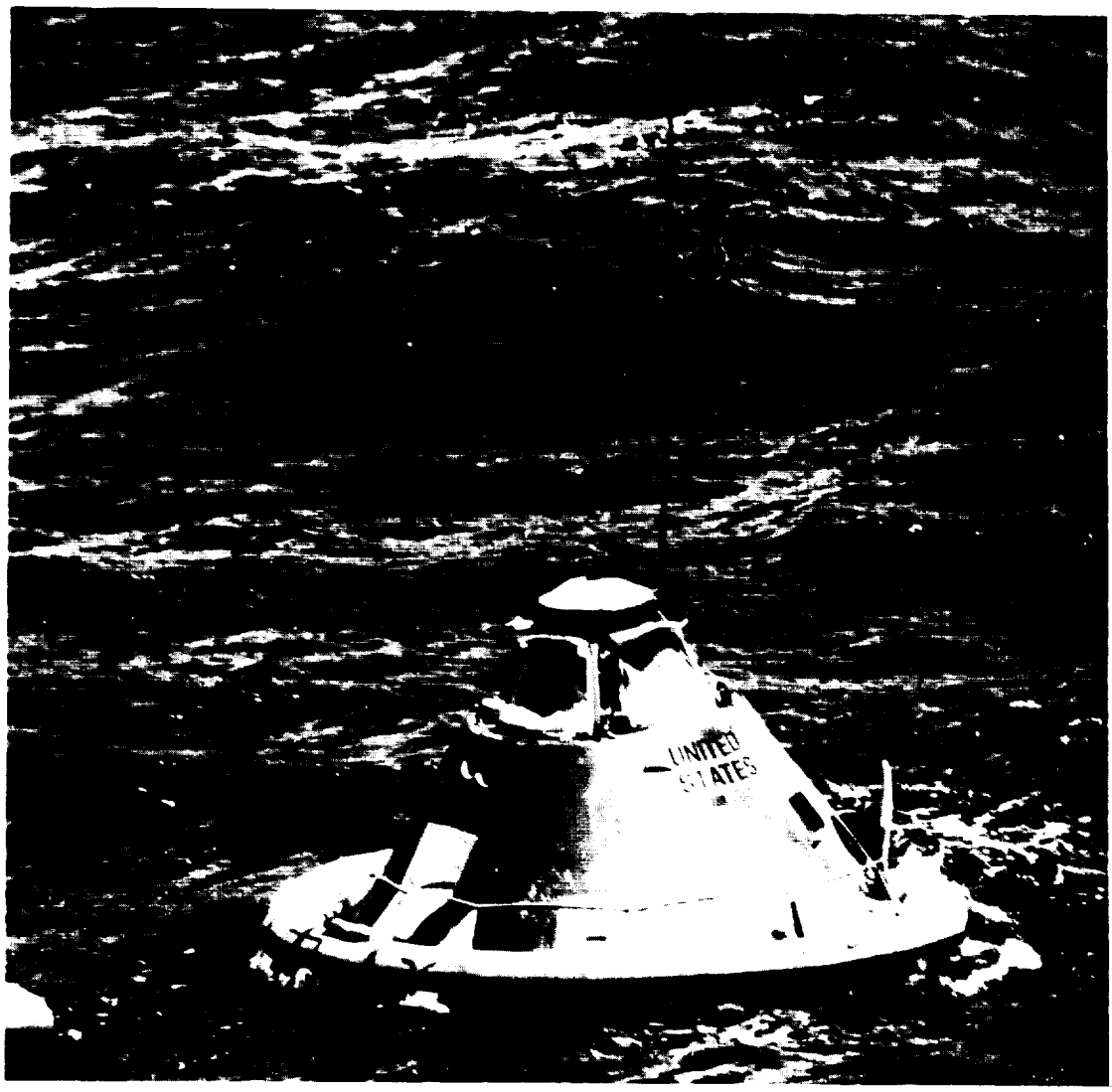

Figure 9.3-4.- Spacecraft with flotation collar installed, Mission AS-202.

NASA-S-66-10198

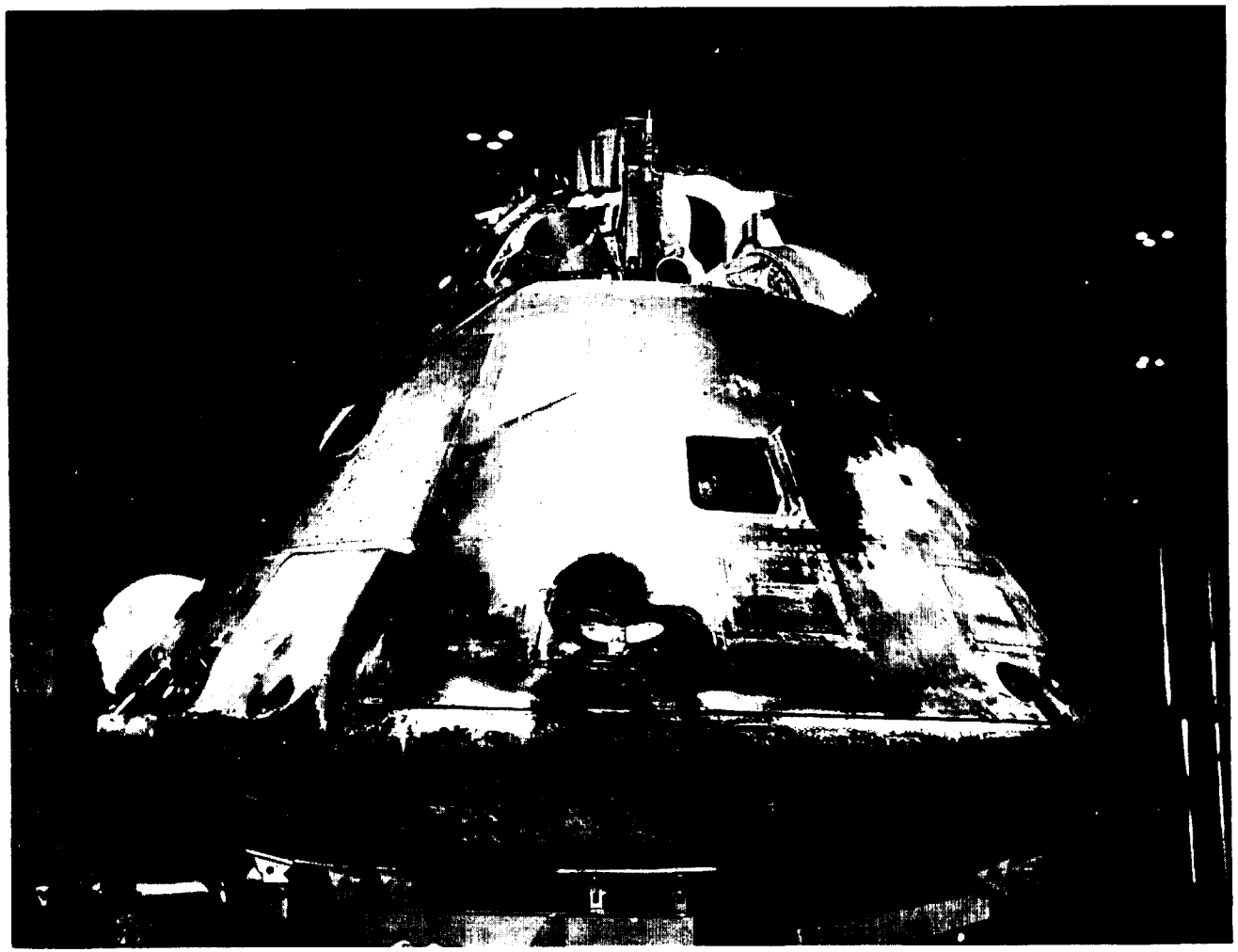

Figure 9.3-5.- Spacecraft aboard U,S.S. Hornet, Mission AS-202.

10.0 POSTFLIGHT TESTING AND ANOMALY SUMMARY

10.1 Postflight Testing

Postflight testing on spacecraft 011 was conducted at the port of entry following recovery, at the contractor's facility, and at MSC. Planned testing was accomplished to support analysis of subsystem performance,formance, as well as special tests necessary in the resolution of mission anomalies. The testing, which included the following, is discussed in detail elsewhere in this report (section sequenced in parentheses).

Heat protection.- Cores were cut from preselected areas of the aft heat shield for study of reentry heating effects. Core samples were cut in half for study and evaluation at the contractor's facility and at MSC. The astrosectant passive thermal protection subsystem was removed and analyzed (section 7.4).

Mechanical subsystem.- The uprighting subsystem was tested for proper operation. Flashing light recovery aid anomaly tests were conducted to evaluate installation characteristics (section 7.5).

Reaction control subsystem (RCS).- The helium isolation valves were tested for contamination, and the propellant relief valve burst diaphragms were leak-checked. Oxidizer and fuel tanks and bladders were removed, leak-checked, and analyzed for contamination (section 7.8).

Guidance and control (G & C).- The Apollo guidance computer (AGC) was removed from the vehicle and forwarded to the vendor for recovery of the stored state vector information. The roll rate gyro package from the stabilization and control subsystem (SCS) was removed and tested for signal variation (section 7.11).

Electrial power subsystem (EPS).- Spacecraft batteries were tested to determine capacity remaining at the end of the flight. The static inverters were subjected to bench maintenance equipment tests. Tests to evaluate the SM fuel cell secondary coolant subsystem anomaly are being conducted at the vendors and at MSC (section 7.12).

Instrumentation.- Cores were removed from the heat shield containing the calorimeters and pressure sensors and subjected to analysis. The heat shield pressure instrumentation was recalibrated to evaluate degradation. Anomaly tests were conducted on the CM/SM separation monitor subsystem and the instrumentation 5-volt reference (section 7.15).

Communications.- A postflight performance evaluation of the unified S-band subsystem was conducted. Anomaly tests consisting of S-band low signal strength, updata link signal reception and response investigations, utilizing tapes of the CSQ signal and further examination of antenna patterns were conducted at the contractor's Downey facility and at MSC (section 7.16).

Environmental control subsystem (ECS).- Potable and waste water, water/glycol, and lithium-hydroxide samples, and the carbon dioxide sensor were removed from the spacecraft and forwarded to MSC for analysis. Anomaly investigations which were conducted included removal of the environmental control unit and performance testing at the vendor's plant, testing of the steam duct instrumentation, simulation of the KSC water servicing operational checjout procedures (OCP), leak check of the water subsystem, and calibration of the potable and waste water tank quantity instrumentation (section 7.17).

Crew windows.- The crew windows were subjected to grid photography and removed from the spacecraft. The windows were also subjected to spectral transmission, reflection, and light scattering analysis, with emission spectrographic analysis of the contamination accomplished (section 7.18).

Acoustics.- The two CM microphones were removed and forwarded to MSC where they were inspected and calibrated (section 7.18).

10.2 Anomalies Listing

The anomalies for Mission AS-202 are listed as follows. All have been resolved. The report section number indicate where the items are discussed.

Instrumentation 5-volt reference variation.- The instrumentation 5-volt reference varied from 5 volts to a low of 3.2 volts between 4511 and 4583 seconds and 4787 and 5091 seconds. The data subsystem was not affected by this voltage drop (section 7.15.1).

State vector update.- The state vector from the spacecraft computer was not compared in real time with the state vector from Antigua (sections 7.11 and 9.1).

Flashing light installation incorrect.- The flashing light recovery aid worked satisfactorily, although the bulb was not properly installed and was therefore loose (section 7.5).

USB lock recognition at Carnarvon.- Although two-way lock was achieved at very nearly the predicted time, it was not recognized by the exciter/main receiver operator because of a malfunction in the AGC voltage meter channel with an intermittent short in the ground station equipment. Considerable Carnarvon USB transmission data were lost because of the multiple ground equipment problems (section 7.16.2).

Swimmer umbilical chafed.- The swimmer telephone umbilical was chafed through to bare wire by the ablator edge at the upper deck (sections 7.5 and 9.3).

CM RCS pressurization.- During CM RCS activation prior to CM/SM separation, the relief valve burst discs in the A oxidizer and B fuel subsystems were ruptured. This anomaly was noted during postflight testing (section 7.9).

Master caution and warning light indication.- Investigation of telemetry data and films from onboard cameras indicates that the master caution and warning light was illuminated at T+3 seconds (sections 7.9, 7.15.1, and 7.18.1).

SLA/SM separation debris.- Television pictures of the SLA/SM separation show a 3-foot strip of material flopping from the base of the SM. There also appears to be smoke and some free-floating debris in certain areas of the SLA (section 7.1).

SM RCS quad C pressurization.- Initial regulated pressure of quad C was approximately 20-psi high until the first RCS burn, when the pressure. It then maintained the proper value for the remainder of the flight (section 7.9).

Fuel cell condenser exit temperatures high.- The power generation subsystem operational performance was found to be normal with the exception of the condenser exit temperatures of fuel cells 1 and 3. This anomaly did not, however, adversely affect the primary objective of the subsystem to supply the spacecraft with electrical power. All bus voltages were within prescribed limits, and load sharing between the fuel cells and batteries was satisfactory. The high condenser exit temperature was evidence that the cooling capacity of the secondary cooling loop was effectively reduced (section 7.12).

Glycol evaporator malfunction.- The glycol evaporator ceased to function from T+14 until T+68 minutes. This was evidenced by the evaporator outlet temperature increasing from 40° to 58° F in approximately 40 seconds at T+14 minutes, and eventually exceeding 75° F at

T+17 minutes. Steam duct pressure also increased to full scale (0.25 psia), during this period of temperature increase. These data indicate that the steam duct became obstructed by ice. No spacecraft subsystems were affected by this problem (section 7.17).

Low USB signal levels at MILA and BDA.- The S-band uplink and downlink received carrier powers were 10 to 30 dB lower than predicted at MILA and BDA. BDA acquired the downlink prior to T+396 seconds, but dropped lock when the signal level decreased 30 dB in less then 50 seconds. Since BDA did not have downlink lock, the handover at T+420 seconds was unsuccessful. BDA acquired late, and obtained less than 1 minute of ranging data prior to the "key-hole" (antenna angle limits) (section 7.16.2).

CM/SM separation command.- The telemetry snip CSQ sent a CM/SM separation backup command to the spacecraft, but did not receive a validity signal from the spacecraft, which would indicate that the separation command was properly received. Examination of the CSQ signal indicated an out-of-tolerance condition in phase and amplitude which would make it unacceptable to the spacecraft (section 7.16.1).

Short range on CM reentry and descent.- The landing point was approximately 205 nautical miles uprange from the predicted point (section 4.1, 5.0, 6.0 and 7.3).

11.0 CONCLUDING REMARKS

Mission AS-202 demonstrated the compatibility and structural integrity of the Block I type Apollo spacecraft 011 with the uprated Saturn I launch vehicle. The structural loading of the spacecraft adapter under the uprated Saturn I launch environment fell within acceptable limits.

The mission demonstrated satisfactory separation of the S-IVB from the S-IB, the launch-escape subsystem and boost protective cover from the command module (CM), the command and service modules from the spacecraft lunar-module adapter (SLA), and the CM from the service module (SM). The launch vehicle propulsion, guidance and control, and electrical subsystems performed adequately throughout the boost phase, with no abort signals generated by the spacecraft emergency detection subsystem. The mission demonstrated the adequacy of the CM for manned entry from a low earth orbit. The service propulsion subsystem was started and operated satisfactorily four times in a space environment. The propellant sump tank standpipe fix was verified with over 200 seconds of satisfactory operation. Stable operation as well as satisfactory startup and shutdown characteristics were obtained for all burns.

The guidance and navigation subsystem, stabilization and control subsystem, SM and CM reaction control subsystems, earth landing subsystem, and the recovery aids performed satisfactorily during Mission AS-202 and demonstrated their adequacy for a manned orbital mission.

Satisfactory operation of the onboard communication subsystem was obtained. However, detailed evaluation of spacecraft/MSFN S-band subsystems performance was only partially accomplished due to low signal strengths during the initial powered flight phase and ground station operational problems at Carnarvon.

The electrical power subsystem performed adequately even though the fuel cell condenser outlet temperatures approached maximum specified limits. The environmental control subsystem performed adequately except that the water evaporator ceased to function with the outlet water/glycol temperatures finally exceeding 75° F. The thermal performance of the CM heat shield ablator and astrosextant thermal protection system was satisfactory with a reentry heat load of approximately 20 000 Btu/sq ft and a reentry velocity of 28 512 ft/sec. Spacecraft splashdown occurred approximately 205 miles short of the planned location due to lower spacecraft lift-to-drag ratio and steeper reentry flight path angle than predicted. In general, the desired flight measurements were obtained during the mission.

Satisfactory operation of the mission support facilities required for launch, mission operations, and spacecraft recovery were demonstrated.

12.0 APPENDIX A

12.1 Spacecraft History

The history of CSM 011 from manufacture through flight and post-flight evaluation is shown in figures 12.1-1 and 12.1-2. Significant events during this period are summarized below.

Design engineering inspection (DEI).- The purpose of the DEI was to access the suitability of the spacecraft design, the checkout procedures, and GSE utilization to support the AS-202 mission requirements. The DEI was conducted during the period of August 30 to September 2, 1965, and actions are summarized in table 12.1-I.

The significant changes were primarily for unmanned configuration electrical power control, sequential subsystems refinements, and G & N software.

Subsystem assessment review (SAR).- The purpose of the SAR was to review the configuration changes since the DEI, the results of subsystems checkout, and the outstanding subsystems problems to assess the acceptability of proceeding with integrated subsystems and simulated flight checkout. The SAR was conducted during the period of March 15 to 16, 1966, and actions are summarized in table 12.1-I. The significant items were for fluid subsystems retest after component replacement, fit check of field-installed items, low ECS coolant flow, and G & N component retrofit due to qualification problems. G & N component replacement was the only constraint to integrated testing.

Customer acceptance readiness review (CARR).- The purpose of the CARR was to review all spacecraft test operations and, pending configuration changes, to verify that the spacecraft was acceptable for shipment to the launch site. The CARR was conducted on April 6, 1966, and actions are summarized in table 12.1-I. The significant items were for ECS modifications and retest to minimize the low coolant flow problem, further study and retest of G & N anomalies, and modification to the MCP to correct functional discrepancies and incorporate new design requirements. No constraints to shipment were imposed, and the SM and CM were shipped to KSC on April 10 and 15, respectively.

Significant preflight configuration changes.- The following significant configuration changes were made to CSM 011 during checkout operations at KSC:

(a) SPS standpipe replacement: modified standpipes were retrofitted into the fuel and oxidizer sump tanks to correct the helium ingestion problem encountered on Mission AS-201.

(b) Astrosextant passive thermal protection system: astrosextant heat shield doors were removed and replaced with a passive ablative subsystem due to qualification failures of the door mechanism.

(c) Forward heat shield (FHS) drag parachute: a drag parachute was added to the FHS to aid separation from the CM when analysis indicated a probable recontact problem.

(d) Photographic cameras: motion picture cameras were added to confirm the operation of the FHS drag parachute and enable study of window sooting and horizon visibility.

(e) Fuel cell loss: during the countdown demonstration test, fuel cell number 2 was accidentally destroyed due to a GSE wiring discrepancy. The fuel cell was not removed but was inoperative through the mission.

Flight readiness review (FRR).- The purpose of the FRR was to review the spacecraft test history and subsystem qualification to assess the readiness of the spacecraft and GSE to support Mission AS-202. The FRR was conducted on August 10 and 11, 1966, and actions are summarized in table 12.1-I. The significant items were for retrofit of particular SCS capacitors, inspection and mission level vibration of G & N components, and voltage-spike suppression on the MCP. Based on the completion of these items, plus planned checkout, the spacecraft and supporting equipment were declared flight-ready.

TABLE 12.1-I.- CSM 011 REVIEW ACTION SUMMARY

Subsystems	Event									Mission anomalies
	DEI			SAR		CARR		Spacecraft FRR		
	Fix	Study	Pro-cedure	Fix	Study	Fix	Study	Fix	Study	
EPS	5	3	1	3	12		3	1	2	1
COMM		1		1	9				2	3
INST			5	1	5	1	4			1
SCS				1	23	1	2	2		
G & N	3	1	4	5	1	4	5	3	1	
SPS	1	2		4	6	1			1	
RCS	1		1	3	5					3
ECS	2	3		5	15	2	3		1	1
SECS	7		4	1	6	1	1	1		
MECH	1	2	1	3	1					2
STRUC	1	4	1	6	8					2
GSE	1			4	3				1	1
Total	22	16	17	37	94	10	18	7	8	14
Reference	NAA Report AP65-75 September 2, 1965			NAA Memo ATO-D-TP-66-TD-099 March 21, 1966		NAA Memo ATO-D-TP-66-TD-124 April 11, 1966		MSC Memo PR6/M66-120 August 22, 1966		MSC 30-day Failure/ Anomalies Report September 23, 1966

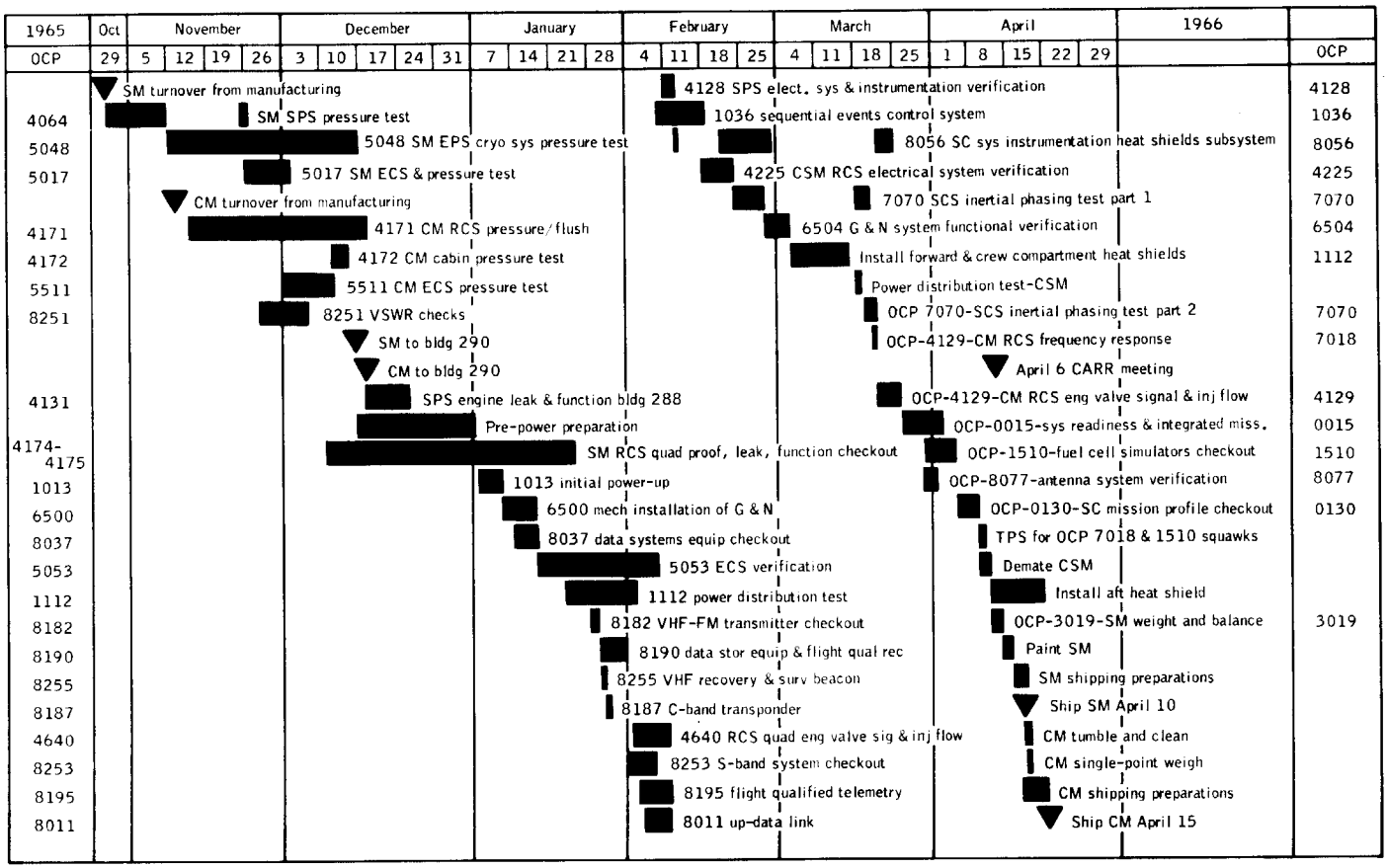

Figure 12.1-1. - Spacecraft 011 at Downey, preflight, Mission AS-202.

NASA-S-66-10200

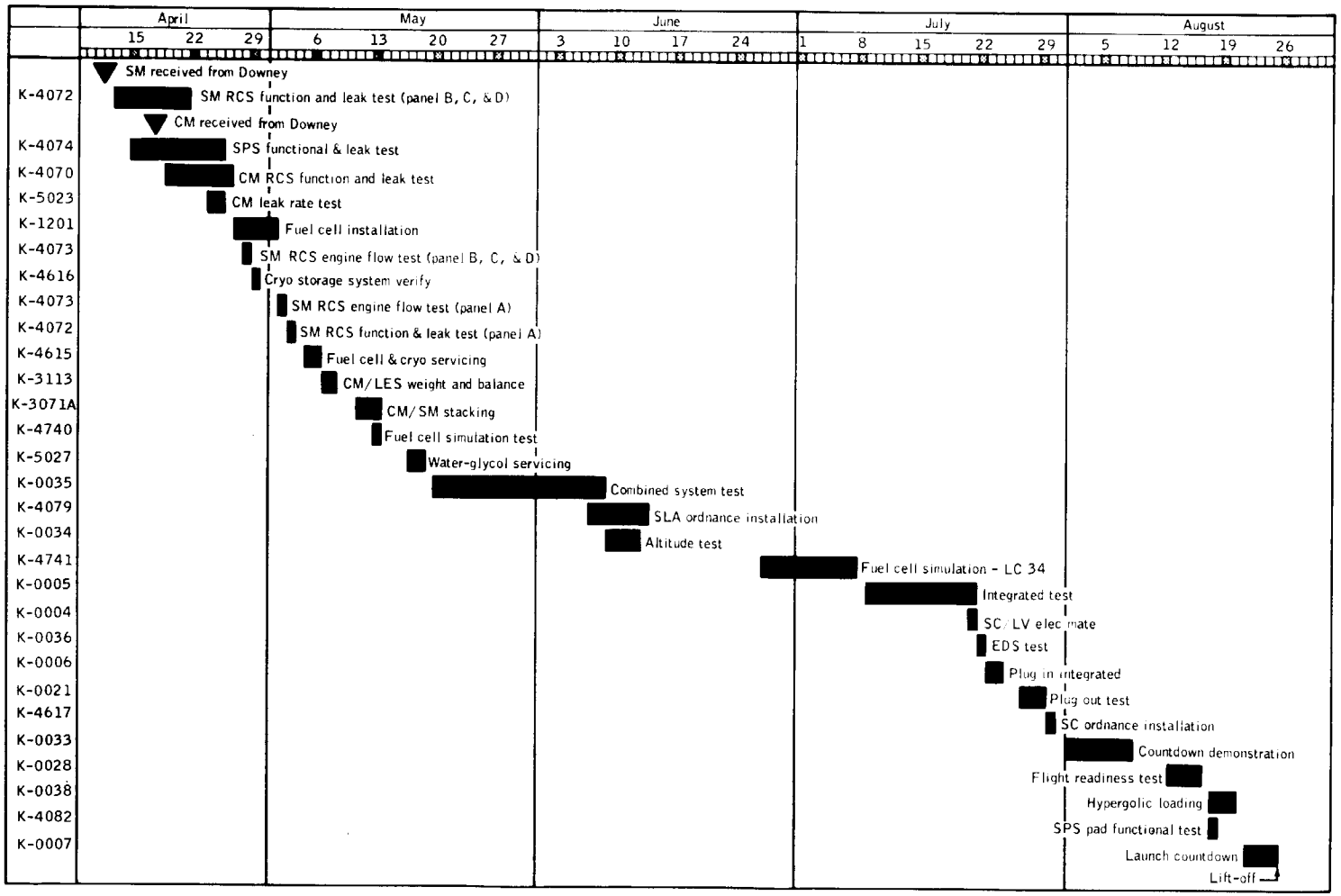

Figure 12.1-2. - Spacecraft 011 at Cape Kennedy, preflight, Mission AS-202.

13.0 APPENDIX B

13.1 Photographic Coverage

The photographic coverage required for the analysis of performance of spacecraft 011 for Apollo Mission AS-202 included still photography, motion picture photography, and a special onboard television coverage of the spacecraft lunar module adapter panel deployment.

The still photography consisted of preflight, recovery, and post-flight views of components, assemblies, and systems which confirmed their configuration and visual condition. The motion picture photography consisted of engineering sequential film, tracking film, and four onboard cameras located in the command and service module.

The locations of the cameras used in covering the launch phase of the mission in relation to the launch pad and the ground track are shown in figures 13.1-1 and 13.1-2. The sequence for defining the coverage, identification, and processing of the engineering sequential and tracking film is shown in figures 13.1-3 and 13.1-4. Table 13.1-I presents a film quality assessment of the engineering sequential and tracking films for this mission. Table 13.1-II presents an assessment of the film quality of the onboard cameras and television coverage.

The 70-mm Roti and Igor tracking films were not available for review (as noted) at the time of this report. The required 70-mm to 16-mm reduction equipment was not available in the MSC photo lab because of delivery delay.

13.1-I.- ACTUAL PHOTOGRAPHIC COVERAGE, MISSION AS-202

[Engineering sequential and tracking films]

Identification (a)	Camera location	Film (all color)		Lens	Focus	Exposure	Orientation	Field of view	Range time (coded)	Required orientation	Comments
		Size, mm	Frame rate, fps								
Item E-43	SC umbilical tower 230 level West Platform	16	400	40 mm	Good	Good	Good	Good	Good	Center umbilical connectors of swing arm No. 4 in frame for detailed study of umbilical disconnect. 1000 pps timing.	Every objective well achieved.
Item E-47	34-1 50-foot tower	16	400	20 in.	Bad	Poor	Good	Good	Poor	Center umbilical connectors of swing arm No. 4 in frame for detailed study of umbilical disconnect. 1000 pps timing.	Bad focus. Ignition clouds field of view completely with smoke. Poor timing - Intermittent. Unuseable.
Item E-77	34-1 50-foot tower	16	200	40 mm	Good	Good	Good	Good	Good	Center the Apollo Systems interface in bottom edge of frame for structure surveillance of the interface area during booster ignition and lift-off. 1000 pps timing.	From this position exhaust obscures lift-off completely. Value negligible.
Item E-78	34-2 50-foot tower	16	200	40 mm	Good	Good	Good	Good	Good	Center the Apollo Systems interface in bottom edge of frame for structure surveillance of the interface area during booster ignition and lift-off. 1000 pps timing.	Every objective well achieved.
Item E-79	34-3 50-foot tower	16	200	40 mm	Good	Good	Good	Good	Good	Center the Apollo Systems interface in bottom edge of frame for structure surveillance of the interface area during booster ignition and lift-off. 1000 pps timing.	Every objective well achieved.
Item E-80	34-4 50-foot tower	16	200	63 mm	Good	Good	Good	Good	Good	Center the Apollo Systems interface in bottom edge of frame for structure surveillance of the interface area during booster ignition and lift-off. 1000 pps timing.	Every objective well achieved. Closer view (than E-79) provides more significant data in area of interest.

[a] Item is KSC identification; E is technical report identification.

13.1-I.- ACTUAL PHOTOGRAPHIC COVERAGE, MISSION AS-202 - Continued

[Engineering sequential and tracking films]

Identification (a)	Camera location	Film (all color)		Lens	Focus	Exposure	Orientation	Field of view	Range time (coded)	Required orientation	Comments
		Size, mm	Frame rate, fps								
Item 1.2-1	U23GL87	35	12	75 mm	Good	Good	Good	Poor	Fair	Fixed: Missile and launcher centered in bottom of frame for area of surveillance during early flight (T-5 sec to T+4 min).	Field of view much too small. Timing marks faint.
Item 1.2-2	U306L213	35	96	40 in.	Poor	Poor	Good	Good	Good	Tracking: Entire vehicle centered for surveillance before lift-off and during early flight (T-30 sec to T+7 sec).	Good field of view and timing marks but so badly underexposed (3 to 4 stops) value is poor. Tracking poor - lost vehicle several times in clouds but hunted for it later.
Item 1.2-3	U286L72	35	96	20 in.	Good	Good	Good	Good	Good	Tracking: Entire vehicle centered for surveillance before lift-off and during early flight (T-30 sec to T+7 sec).	Excellent tracking: Field of view naturally a little larger and therefore not as revealing as 1.2-2. Timing good.
Item 1.2-4	U142L61	35	96	17 in.	Good	Good	Good	Good	Good	Tracking: Entire vehicle centered for surveillance before lift-off and during early flight. (T-30 sec to T+7 sec).	Tracking good. Timing marks good. Again, field of view naturally a little larger than 1.2-3.
Item 1.2-5	U306L213	35	96	80 in.	Bad	Good	Good	Good	Poor	Tracking: First stage centered until entire vehicle is in frame for flight and structure surveillance (T-5 sec to LOV).	Early tracking poor. Lost in clouds several times - had to hunt for it. Poor focus throughout. Timing marks intermittent and very poor. LOV in clouds sometime before shutdown S-IB.
Item 1.2-6	U286L72	35	96	80 in.	Good	Good	Good	Good	Good	Tracking: First stage centered until entire vehicle is in frame for flight and structure surveillance (T-5 sec to LOV).	Tracking good. Objectives well achieved. LOV in clouds again sometime before shutdown S-IB.

[a]Item is DOD identification;) is technicolor identification.

13.1-1.- ACTUAL PHOTOGRAPHIC COVERAGE, MISSION AS-202 - Continued

[Engineering sequential and tracking films]

Identification (a)	Camera location	Film (all color)		Lens	Focus	Exposure	Orientation	Field of view	Range time (coded)	Required orientation	Comments
		Size, mm	Frame rate, fps								
Item 1.2-7	D23L0	35	96	120 in.	Good	Good	Good	Good	Fair	Tracking: First stage centered until entire vehicle is in frame for flight and structure surveillance (T-5 sec to LOV).	Time faint. Early tracking poor, lost in clouds, had to hunt to find vehicle. LOV in clouds again sometime before S-IB shutdown.
Item 1.2-10	U264L17t	16	64	40 in.	Fair	Good	Good	Good	Good	Tracking: Command module and escape tower centered in frame for emergency surveillance (T-150 sec to LOV).	Focus only fair since heat disturbances in air produce wavering picture. Good tracking.
Item 1.2-11	U122L29	16	64	40 in.	Good	Good	Good	Good	Good	Tracking: Command module and escape tower centered in frame for emergency surveillance (T-150 sec to LOV).	Focus better than 1.2-10. Almost no heat wavering from this angle. Tracking poor, lost in clouds several times, hunted for it more than had it.
Item 1.2-12	U435L285 (UC 12)	70	30	360 in.						Tracking: From first acquisition to LOV, first stage centered until entire vehicle is in frame for flight and structural surveillance.	Not available at this date for review. (See note in text.)
Item 1.2-13	RTCB	70	30	400 in.						Same as above, except entire vehicle centered throughout track.	Not available at this date for review. (See note in text.)
Item 1.2-14	IGPA	16	32	360 in.	Poor	Good	Good	Good	None	Tracking: First acquisition to LOV of first stage for flight and structural surveillance. First stage centered until entire vehicle is in frame. At second stage ignition continue to track first stage.	Very poor to poor focus throughout. No timing marks on film.

[a]Item is DOD identification; E is technicolor identification.

13.1-1.- ACTUAL PHOTOGRAPHIC COVERAGE, MISSION AS-202 - Concluded

[Engineering sequential and tracking films]

Identification (a)	Camera location	Film (all color)		Lens	Focus	Exposure	Orientation	Field of view	Range time (coded)	Required orientation	Comments
		Size, mm	Frame rate, fps								
Item 1.2-15	RTMB	70	30	500 in.						Tracking: From first acquisition, but not before T+25 sec, to LOV for flight and structural surveillance, S-IB/S-IVB separation and escape tower separation.	Not available at this date for review. (See note in text.)
Item 1.2-16	RTVB	70	30	500 in.						Tracking: From first acquisition, but not before T+25 sec, to LOV for flight and structural surveillance, S-IB/S-IVB separation and escape tower separation.	Not available at this date for review. (See note in text.)

[a]Item is DOD identification; E is technicolor identification.

TABLE 13.1-II.- ACTUAL PHOTOGRAPHIC AND TELEVISION COVERAGE, MISSION AS-202

Camera number	Camera position	Type of film	Exposed film, ft	Frame rate, fps	Remarks
1	On left-hand couch photographing left-hand panel	Color	538	10	Shot at 10 fps, shown at 24 fps for 15 minutes. Shows eight ball and peripheral indicators. Focus soft enough so that indicators and numbers can be read only if accompanied by a knowledge of timing of events. Shows good eight-ball movement through entire flight to splashdown.
2	On center couch photographing right-hand panel	Color	547	10	Focus comparable to camera no. 1. Can read indications only if accompanied by knowledge of timing of events. Can just see out one very small area of docking window. Can see some sky and some reentry phenomena. Can see some sky during skip between reentries.
3	Through right-hand docking window photographing reentry	Color	533	10	This film was originally underexposed due to difficulties with the lights. However, by overexposing in the processing of the print, it was possible to obtain an acceptable print (see section 7.18.2). In addition to window surface coverage parachute deployment was visible. The film continues to splashdown. Has timing marks on sides of film from onboard signal generator. Good color rendition indication of reentry phenomena.
4	Forward heat shield	Color	--	10	Good shot of nose-cone separation and drogue parachute and main parachute deployments. Forward heat shield separation drogue and main parachute shown clearly.
Television	Bottom of SLA photographing panel deployment	Black and white	--	30	The camera was positioned in the bottom of the SLA pointing into and past a mirror arrangement that allowed monitoring of the panel deployment. The film quality on the whole was good. However, due to the extreme dynamic range of the light, overmodulation occurred intermittently at extremely bright areas, resulting in temporary loss of information at these times in these areas. The panel deployment coverage appears quite good. See section 3.2. The range timing is recorded on the film in digits.

NASA-S-66-10201

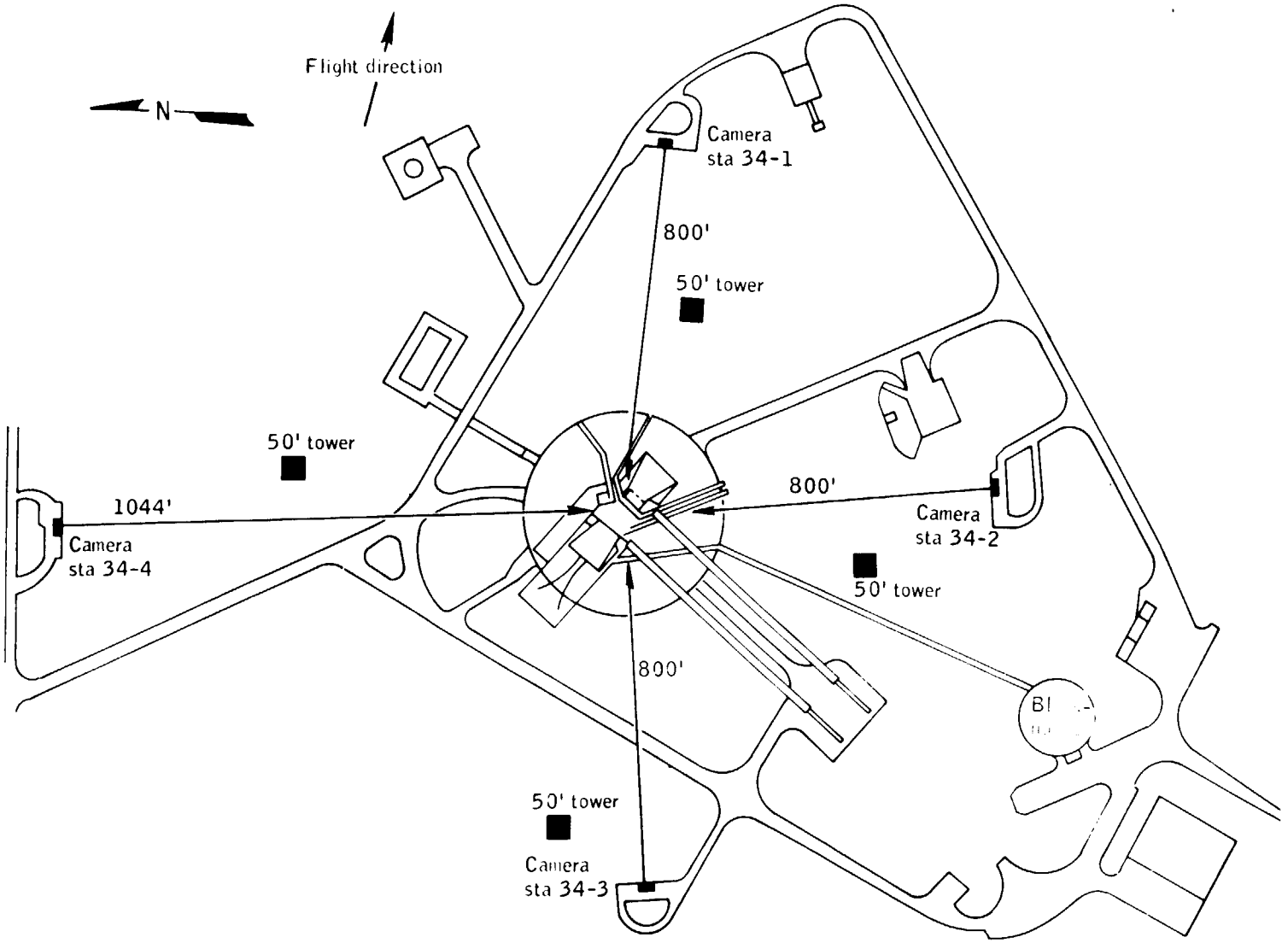

Figure 13.1-1.- Camera locations, Mission AS-202.

NASA-S-66-10202

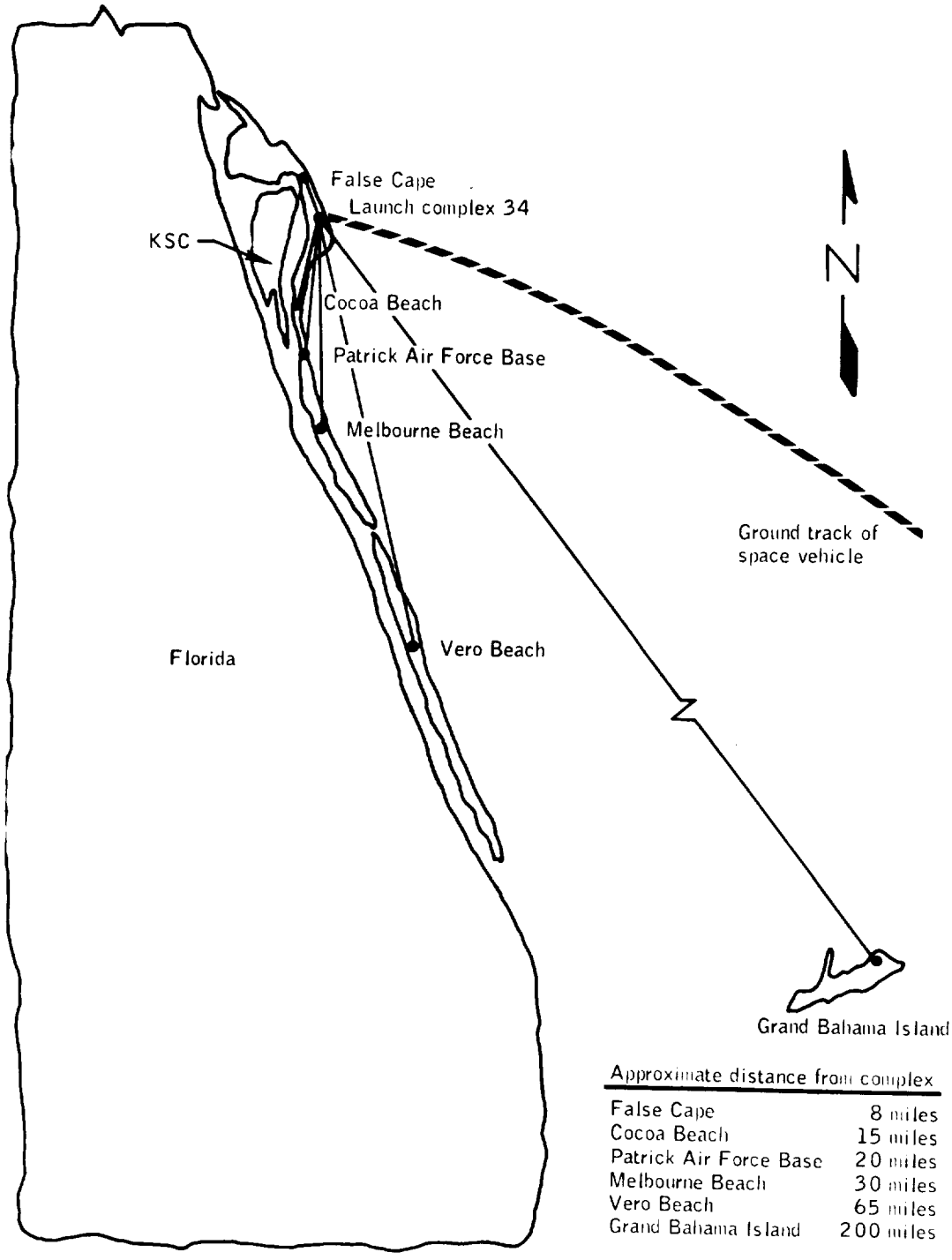

Approximate distance from complex	
False Cape	8 miles
Cocoa Beach	15 miles
Patrick Air Force Base	20 miles
Melbourne Beach	30 miles
Vero Beach	65 miles
Grand Bahama Island	200 miles

Figure 13.1-2.- Long range camera locations, Mission AS-202.

NASA-S-66-10203

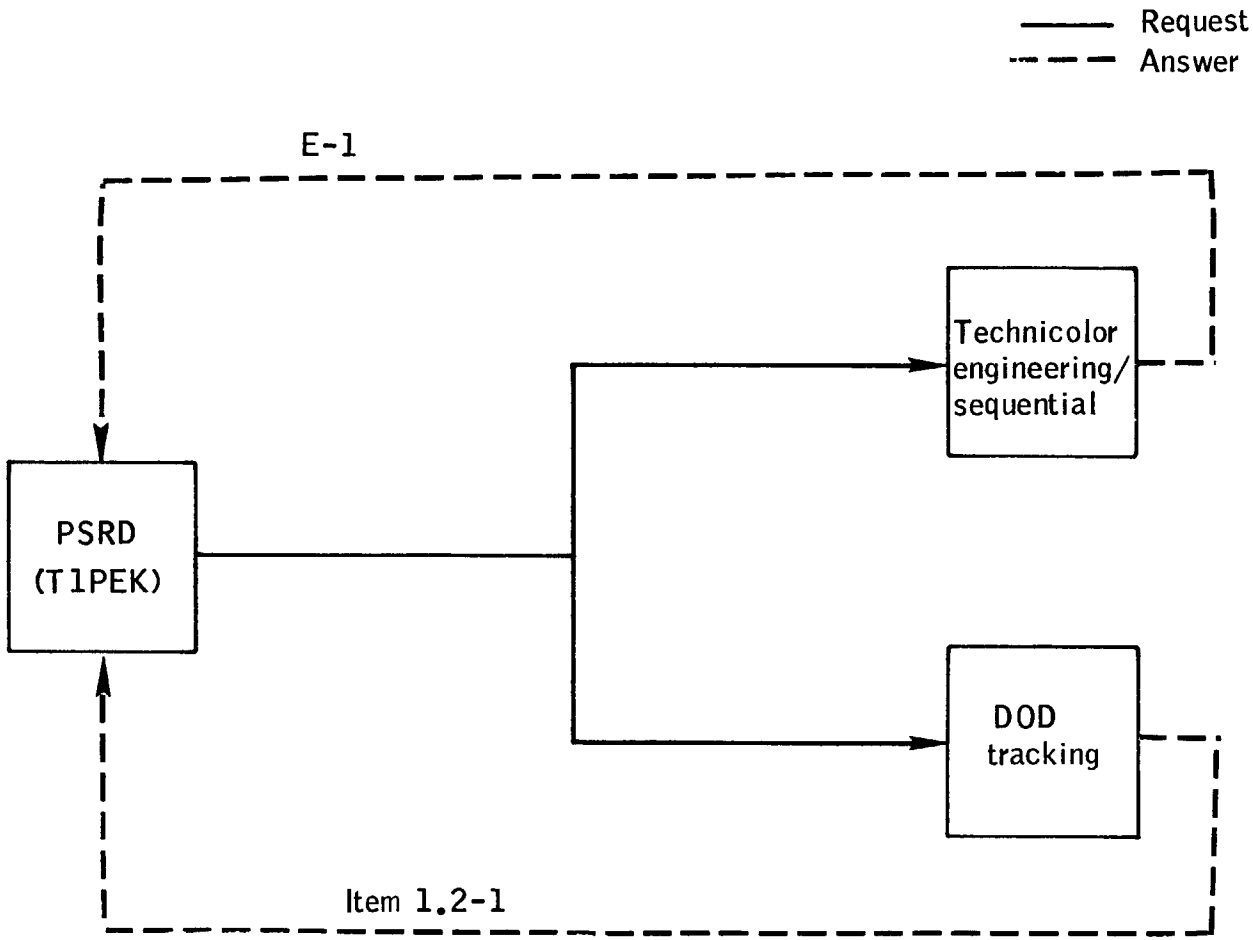

Figure 13.1-3.- Initiating photo identification no. prior to launch, Apollo Mission AS-202

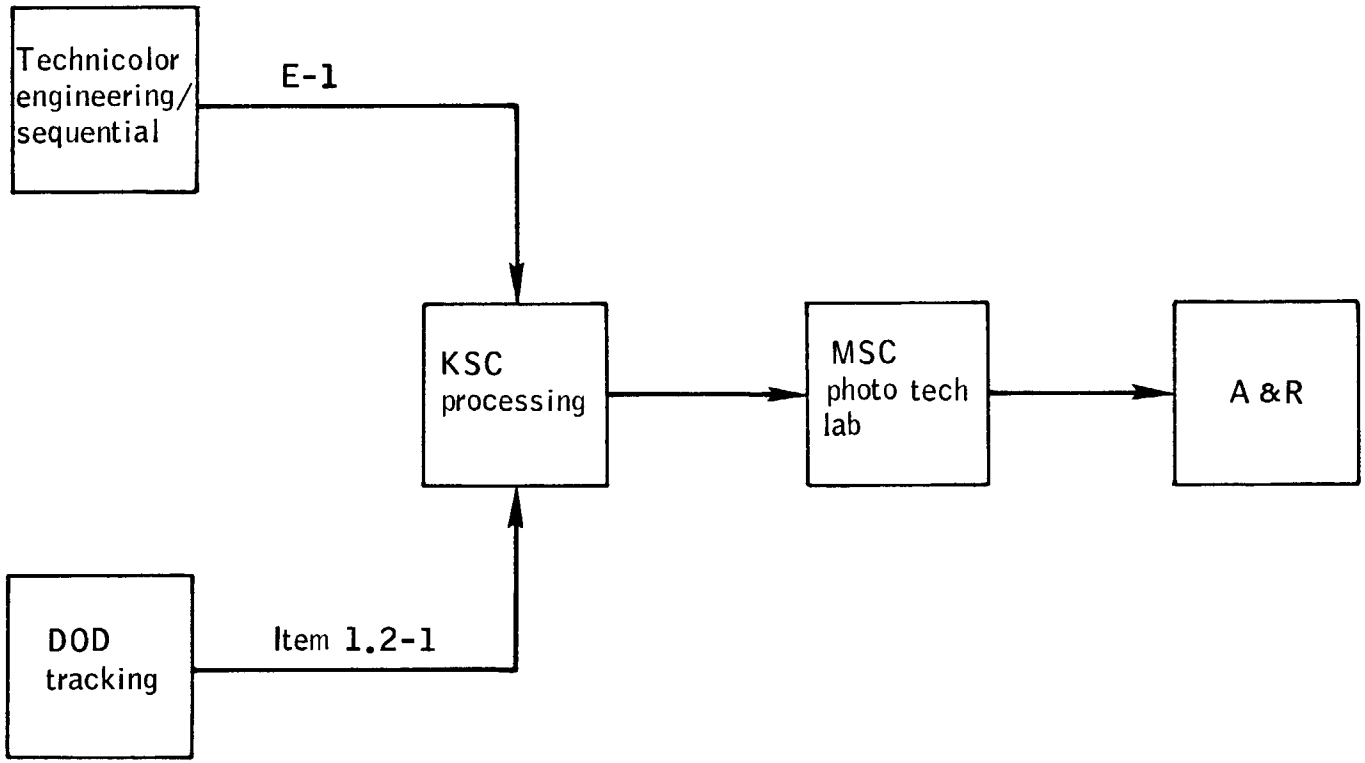

Figure 13.1-4.- Actual film flow from launch site to A & R team, Apollo Mission AS-202.

REFERENCES

1. Staff of Manned Spacecraft Center: Postlaunch Memorandum Report for Apollo Pad Abort I. Nov. 13, 1963.

2. Staff of Manned Spacecraft Center: Postlaunch Report for Apollo Mission A-001 (BP-12). MSC-R-A-64-1, May 28, 1964.

3. Staff of Manned Spacecraft Center: Postlaunch Report for Apollo Mission A-101 (BP-13). MSC-R-A-64-2, June 18, 1964.

4. Staff of Manned Spacecraft Center: Postlaunch Report for Apollo Mission A-102 (BP-15). MSC-R-A-64-3, Oct. 10, 1964.

5. Staff of Manned Spacecraft Center: Postlaunch Report for Apollo Mission A-002 (BP-23). MSC-R-A-65-1, Jan. 22, 1965.

6. Staff of Manned Spacecraft Center: Postlaunch Report for Apollo Mission A-003 (BP-22). MSC-A-R-65-2, June 28, 1965.

7. Staff of Manned Spacecraft Center: Postlaunch Report for Apollo Mission PA-2 (BP-23A). MSC-A-R-65-3, July 29, 1965.

8. Staff of Manned Spacecraft Center: Postlaunch Report for Apollo Mission A-004 (Spacecraft 002). MSC-A-R-66-3, April 15, 1966.

9. Staff of Manned Spacecraft Center: Postlaunch Report for Apollo Mission AS-201 (Spacecraft 009). MSC-A-R-66-4, May 6, 1966.

10. Staff of North American Aviation: GSE End Item Specification for Data Recording Group Model C14-020 (-101 Configuration). SID 63-1237, North American Aviation, Inc., Jan. 16, 1964.

11. Staff of North American Aviation: CSM End Item Specification Part I - Performance and Design Requirements Spacecraft 011. SID 63-703, North American Aviation, Inc., Feb. 22, 1965.

12. Staff of NASA Headquarters: Project Apollo Coordinate System Standard. OMSF Directive SC-008-001-L, June 1965.

13. Staff of North American Aviation: Apollo Technical Manuals. Structural Loads and Criteria. SID 64-183, North American Aviation, Inc., Jan. 1963.

14. Staff of North American Aviation: Apollo Command Module/Service Module Measurement Requirements Spacecraft 011. SID 63-511, North American Aviation, Inc., July 21, 1965.

15. Detra, R. W.; Kemp, N. H.; and Riddell, F. R.: Addendum to Heat Transfer and Satellite Vehicles Reentering the Atmosphere. Jet Propulsion, vol. 27, no. 12, Dec. 1957, pp. 1256-1257.

16. Van Driest, E. R.: On Skin Friction and Heat Transfer Near the Stagnation Point. AL-2267, North American Aviation, Inc., March 1, 1956.

17. Larson, Howard K.: Heat Transfer in Separated Flows. J. of the Aero/Space Sciences, vol. 26, no. 11, Nov. 1959, pp. 731-738.

18. MIT/Instrumentation Lab.: Guidance and Navigation System Operations Plan Apollo Mission AS-202. MIT R-477, MIT/Instrumentation Lab., Oct. 1965.

19. Staff of George C. Marshall Space Flight Center: Results of the Third Saturn IB Launch Vehicle Test Flight, AS-202. MPR-SAT-FE-66-13.

20. Staff of North American Aviation: GFE Communication Equipment Performance and Interface Specification, Block I. SID 65-159, North American Aviation, Inc., Feb. 1965.

21. Apollo SC-011 Flight Onboard Camera Number 1, Left-Hand Panel. NASA MSC Film no. S-66-464.

22. Apollo SC-011 Flight Onboard Camera Number 2, Right-Hand Panel. NASA MSC Film no. S-66-460.

23. Apollo SC-011 Flight Onboard Camera Number 3, Reentry Right-Hand Docking Window. NASA MSC Film no. S-66-465.

24. Apollo SC-011 Flight Onboard Camera Number 4, Apex Cover Separation, Drogue and Main Parachute. NASA MSC Film no. S-66-462.

25. North, Warren; and Shows, James C.: Effect of Simulated Launch Vibrations on Ability of Crew to Monitor Gemini Spacecraft Displays and Controls. Gemini Working Paper 5010, Apr. 16, 1964.

26. Dolkas, Constantine B.; and Stewart, John D.: Effect of Combined Linear and Oscillatory Acceleration on Pilot Attitude-Control Capabilities. NASA TN D-2710, Mar. 1965.

DISTRIBUTION

Addressee	Number of copies
National Aeronautics and Space Administration Washington, D.C. 20546	
Associate Administrator Office of Manned Space Flight, M	1
Apollo Program Director, MA	1
Flight Operations Director, MAO	1
Program Control Director, MAP	1
Reliability and Quality Assurance Director, MAR	2
Systems Engineering Director, MAS	2
Test Director, MAT	8
MSF Field Center Development Director, MC	1
Deputy Director, Saturn-Apollo Applications, ML	1
Test Director, Saturn-Apollo Applications, MLT	1
Deputy Director, Mission Operations, MO-1	1
Advanced Manned Missions Program Director, MT	2
National Aeronautics and Space Administration Manned Spacecraft Center 2101 Webster-Seabrook Road Houston, Texas 77058	
Director, AA	1
Deputy Director, AB	1
Special Assistant to the Director, AC	1
Executive Assistant to the Director, AF	1
Office of Patent Counsel, AL3	1
Public Affairs Office, AP	1

Addressee	Number of copies
Flight Safety Office, AR	2
Assistant Director for Administration, BA	1
Reproduction Services Branch, BF6	1
Forms and Publications Section, BF52	69
Field Test Branch, BH6	1
Security Branch, BM4	1
Technical Information Preparation Branch Records, BM5	4
Technical Information Dissemination Branch, BM6	6
Technical Information Dissemination Branch, BM6 Attention: BM6/M. P. McDonough	10
Assistant Director for Flight Crew Operations, CA	1
Astronaut Office, CB	3
Flight Crew Support Division, CF	7
Chief of Center Medical Programs, DA	3
Chief of Biomedical Research, DB	2
Medical Operations Office, DD	1
Assistant Director for Engineering and Development, EA	2
Information Systems Division, EB	4
Crew Systems Division, EC	5
Computation and Analysis Division, ED	3
Instrumentation and Electronic Systems Division, EE	9
Space Science Office, EF	1
Guidance and Control Division, EG	8

Addressee	Number of copies
Propulsion and Power Division, EP	12
Structures and Mechanics Division, ES	18
Advanced Spacecraft Technology Division, ET	5
Experiments Program Office, EX	3
Assistant Director for Flight Operations, FA	3
Flight Control Division, FC	6
Landing and Recovery Division, FL	5
Mission Planning and Analysis Division, FM	4
Flight Support Division, FS	3
Gemini Program Office, Office of Program Manager, GA	2
Test Operations Manager, GT	1
Apollo Applications Program Office, KA	1
Apollo Spacecraft Program Office, Office of Program Manager, PA	2
NASA-RASPO, PB Grumman Aircraft Engineering Corporation Bethpage, L.I., New York 11714	2
NASA-RASPO, PC North American Aviation 12214 Lakewood Blvd. Downey, California 90240	5
Systems Engineering Division, PD	12
LM Project Engineering and Checkout Division, PE	1
C and SM Project Engineering and Checkout Division, PF	4
Mission Support Division, PK	2
Apollo Analysis and Reporting Team, PK2	35

Addressee	Number of copies
Mission Operations Division, PM	6
Program Control Division, PP	5
Reliability, Quality, and Test Division, PR	2
Resident Liaison Offices	
Goddard Space Flight Center Liaison Office, GSF-L	1
Marshall Space Flight Center Resident Liaison Office, RL	1
Langley Research Center Liaison Office, RAA	1
Libraries	
NASA Headquarters Library, USS-10	6
Ames Research Center Library	6
Flight Research Center Library	6
Goddard Space Flight Center Library	3
John F. Kennedy Space Center Library	6
Lewis Research Center Library	6
Marshall Space Flight Center Library	6
NASA Ames Research Center Moffett Field, California 94035	2
Eastern Test Range Patrick Air Force Base, Florida	2
NASA Electronics Research Center 565 Technology Square Cambridge, Massachusetts 02139	1
NASA Flight Research Center Post Office Box 273 Edwards, California 93523	1

Addressee	Number of copies
NASA Goddard Space Flight Center Greenbelt, Maryland 20771	3
John F. Kennedy Space Center, NASA NASA Kennedy Space Center, Florida 32899	7
NASA Langley Research Center Langley Station Hampton, Virginia 23365	2
NASA Lewis Research Center 2100 Brookpark Road Cleveland, Ohio 44135	1
NASA George C. Marshall Space Flight Center Huntsville, Alabama 35812	2
NASA George C. Marshall Space Flight Center Aero-Astrodynamics Laboratory, R-Aero-F Huntsville, Alabama 35812	4
NASA MSC White Sands Test Facility Office of the Manager, RA P. O. Drawer MM Las Cruces, New Mexico 88001	1
NASA-RASPO Massachusetts Institute of Technology 75 Cambridge Parkway Cambridge, Massachusetts 02142	2
NASA-RASPO AC Electronics Division Company Milwaukee, Wisconsin 53200	2
Arnold Engineering Development Center Arnold Air Force Station, Tennessee 37389	1
Bellcomm Inc. 1100 17th Street NW Washington, D.C.	1
Grumman Aircraft Engineering Corp. Bethpage, L. I., New York 11714	4

Addressee	Number of copies
Jet Propulsion Laboratory Pasadena, California	1
North American Aviation, Inc., S&ID Systems Engineering, Dept. 692 12214 Lakewood Blvd. Downey, California 90240	6
North American Aviation, Inc., S&ID Apollo Program Manager 12214 Lakewood Blvd. Downey, California 90240	1
North American Aviation, Inc., S&ID Spacecraft Design Engineering, Dept. 696 12214 Lakewood Blvd. Downey, California 90240	1
North American Aviation, Inc. AT&O Florida Facilities 5505 North Atlantic Ave. Cocoa Beach, Florida 32899	4